รายงานฉบับสมบูรณ์

โครงการออกแบบระบบผลิตไฮโดรเจนซึ่งใช้วัตถุดิบที่สามารถหาได้ในประเทศไทยเป็นสารตั้งต้นได้อย่างมีประสิทธิภาพเพื่อใช้ประโยชน์ในเซลล์เชื้อเพลิงแบบออกไซด์ของแข็ง

โดย ดร. นวดล เหล่าศิริพจน์ และคณะ

ธันวาคม 2548

สัญญาเลขที่ MRG4780

รายงานฉบับสมบูรณ์

โครงการออกแบบระบบผลิตไฮโดรเจนซึ่งใช้วัตถุดิบที่สามารถหาได้ในประเทศไทยเป็นสารตั้งต้นได้อย่างมีประสิทธิภาพเพื่อใช้ประโยชน์ในเซลล์เชื้อเพลิงแบบออกไซด์ของแข็ง

คณะผู้วิจัย	สังกัด
1. ดร. นวดล เหล่าศิริพจน์	บัณฑิตวิทยาลัยร่วมด้านพลังงานและสิ่งแวดล้อม มหาวิทยาลัยเทคโนโลยีพระจอมเกล้า ธนบุรี
2. รศ.ดร. สุทธิชัย อัสสะบำรุงรัตน์	คณะวิศวกรรมศาสตร์ จุฬาลงกรณ์มหาวิทยาลัย

สนับสนุนโดยสำนักงานคณะกรรมการอุดมศึกษา และสำนักงานกองทุนสนับสนุนการวิจัย

สารบัญ

บทคัดย่อ

งานวิจัยนี้ได้ค้นพบว่า CeO_2 สามารถนำไปใช้ประโยชน์ในกระบวนการรีฟอร์มมิ่งได้อย่างหลากหลายและมีประสิทธิภาพ ซึ่งจากผลการดำเนินงานทดลองพบว่าการใช้สาร CeO_2 เป็นตัวรองรับ (Support) และสารเติมแต่ง (Promoter) สามารถช่วยเพิ่มประสิทธิภาพในการผลิตไฮโดรเจนได้เป็นอย่างดีทั้งในแง่เสถียรภาพและศักยภาพเมื่อเปรียบเทียบกับการใช้ตัวเร่งปฏิกิริยาทั่วไปเช่น Ni/Al_2O_3 [1,2,3,4] สาเหตุดังกล่าวเนื่องมาจากสาร CeO_2 มีคุณสมบัติรีดอกซ์สูงมากดังนั้นระหว่างกระบวนการรีฟอร์มมิ่งนอกจากปฏิกิริยาที่เกิดขึ้นบนผิวของตัวเร่งปฏิกิริยานิเกิลแล้วจะเกิดปฏิกิริยารีดอกซ์ระหว่างสารไฮโดรคาร์บอนและออกซิเจน (lattice oxygen) บนผิวของ CeO_2 ขึ้นด้วย และในบรรดาปฏิกิริยารีดอกซ์เหล่านั้น ปฏิกิริยารีดอกซ์ของมีเทนและคาร์บอนมอนอกไซด์กับออกซิเจนบนผิวของ CeO_2 ($CH_4 + O_x = CO + H_2 + O_{x-1}$ และ $CO + O_x = CO_2 + O_{x-1}$) จะช่วยป้องกันการเกิดการฟอร์มตัวของคาร์บอนที่ผิวของตัวเร่งปฏิกิริยาจากกระบวนการสลายตัวของมีเทน($CH_4 \rightarrow C + 2H_2$) และกระบวนการ ($2CO \rightarrow C + CO_2$) ซึ่งเป็นปฏิกิริยาหลักที่ส่งผลให้ตัวเร่งปฏิกิริยาเสื่อมสภาพโดยเฉพาะอย่างยิ่งเมื่อมีปริมาณของสารออกซิแดนซ์เช่น น้ำหรือคาร์บอนไดออกไซด์ในระบบต่ำ

นอกจากนั้นในงานวิจัยโครงการนี้ยังค้นพบว่า CeO_2 ที่เตรียมขึ้นให้มีอนุภาคระดับนาโนเมตรและมีพื้นที่ผิวสูงกว่าปรกติ (nanocomposite high surface area ceria) จะเป็นตัวเร่งปฏิกิริยาที่ดีสำหรับกระบวนการรีฟอร์มมิ่งด้วยน้ำและคาร์บอนไดออกไซด์ของสารตั้งต้นชนิดต่างๆ เช่นมีเทน ก๊าซหุงต้ม (โพรเพน + บิวเทน) [5] เมทานอล [6] และเอทานอล [7,8] โดยจะสามารถผลิตไฮโดรเจนได้อย่างมีประสิทธิภาพในช่วงอุณหภูมิเดียวกับเซลล์เชื้อเพลิงแบบออกไซด์ของแข็ง [3] ซึ่งงานวิจัยในโครงการนี้ได้ทำการศึกษาจลศาสตร์ (Kinetics) ของกระบวนการรีฟอร์มมิ่งบนตัวเร่งปฏิกิริยา nanocomposite high surface area ceria อย่างละเอียดโดยการเปลี่ยนความเข้มข้นของสารตั้งต้นและตัวออกซิแดนซ์ชนิดต่างๆ ที่อุณหภูมิต่างๆ กัน ซึ่งจากการทดลองพบว่าอัตราการเกิดปฏิกิริยาจะแปรผันตามความเข้มข้นของสารไฮโดรคาร์บอนตั้งต้นแต่จะไม่ขึ้นกับความเข้มเข้นของสารออกซิแดนซ์ ซึ่งจากการค้นพบดังกล่าวทำให้สามารถสรุปได้ว่ากลไกทางเคมี (Chemical Mechanism) ของการรีฟอร์มสารตั้งต้นชนิดต่างๆ บนผิวของ nanocomposite high surface area ceria มีลักษณะใกล้เคียงกันคือการแตกสลายโมเลกุลของสารไฮโดรคาร์บอนอย่างช้าๆ ในขณะที่การออกซิเจน (lattice oxygen) บนผิวของ CeO_2 ที่ถูกใช้ไปในการทำปฏิกิริยากับสารไฮโดรคาร์บอนจะถูกแทนที่ได้อย่างรวดเร็วจากแหล่งของธาตุออกซิเจนที่มาจากภายนอก เช่น น้ำ และคาร์บอนไดออกไซด์

Abstract

Cerium Oxide or ceria (CeO_2) was found to be useful for the reforming processes. By applying this material as support and promoter, the catalyst provides significantly higher reforming reactivity and excellent resistance toward carbon deposition compared to conventional Ni/Al_2O_3 [1,2,3,4]. These enhancements are due to the high redox property of CeO_2. During the reforming processes, in addition to the reaction on metallic catalyst surface, the redox reactions between the gaseous components in the system and the lattice oxygen (Ox) take place on ceria surface. Among these reactions, the rapid redox reactions of carbon compounds such as CH_4, and CO with lattice oxygen ($CH_4 + O_x = CO + H_2 + O_{x-1}$ and $CO + O_x = CO_2 + O_{x-1}$) can prevent the formation of carbon species from the methane decomposition ($CH_4 \rightarrow C + 2H_2$) and Boudard reactions ($2CO \rightarrow C + CO_2$) even at low inlet steam and carbon dioxide concentrations.

Surprisingly, nanocomposite high surface area ceria (CeO_2 (HSA)), synthesized by a surfactant-assisted approach, was observed to be an excellent catalyst for the reforming of methane, LPG [5], methanol [6], and ethanol [7,8] producing H_2 and CO under Solid Oxide Fuel Cells (SOFCs) conditions [3]. Regarding the intrinsic reaction kinetics over CeO_2 (HSA), the reforming rate over this catalyst is proportional to the methane partial pressure and the operating temperature. Carbon dioxide presents weak positive impact on the methane conversion, whereas steam concentration seems to be independent of the rate. The adding of carbon monoxide and hydrogen inhibit the reforming rate. The activation energies and reforming rates under the same methane concentration for CeO_2 toward the dry reforming are almost equal to the steam reforming. This result suggests the similar reaction mechanisms for both the steam reforming and the dry reforming over CeO_2; i.e., the dry reforming rate is governed by the slow reaction of adsorbed methane, or surface hydrocarbon species, with oxygen in CeO_2, and a rapid gas-solid reaction between CO_2 and CeO_2 to replenish the oxygen.

[1] N. Laosiripojana, and S. Assabumrungrat, Methane steam reforming over $Ni/Ce\text{-}ZrO_2$ catalyst: Influences of $Ce\text{-}ZrO_2$ support on reactivity, resistance toward carbon formation, and intrinsic reaction kinetics, **Applied Catalysis A: General**, 290 (2005) 200-211

[2] N. Laosiripojana, W. Sutthisripok, and S. Assabumrungrat, Synthesis gas production from dry reforming of methane over CeO_2 doped Ni/Al_2O_3: Influence of the doping ceria on the resistance toward carbon formation, **Chemical Engineering Journal**, 112 (2005) 13-22

[3] N. Laosiripojana and S. Assabumrungrat, Catalytic Dry Reforming of Methane over High Surface Area Ceria, **Applied Catalysis B: Environmental**, 60 (2005) 109–118

[4] N. Laosiripojana, W. Sangtongkitcharoen and S. Assabumrungrat, "Catalytic steam reforming ethane and propane over CeO_2-doped Ni/Al_2O_3 at SOFC temperature: Improvement of resistance toward carbon formation by the redox properties of doping CeO_2", **Fuel**, 85 (2006) 323-332

[5] N. Laosiripojana and S. Assabumrungrat, "Hydrogen production from the steam and autothermal reforming of LPG over high surface area ceria at SOFC temperature", **Journal of Power Sources**, In Press

[6] N. Laosiripojana and S. Assabumrungrat, "The effect of specific surface area on the activity of nano-scale ceria catalysts for methanol decomposition with and without steam at SOFC operating temperatures", **Chemical Engineering Science**, In Press

[7] N. Laosiripojana and S. Assabumrungrat, "Catalytic steam reforming of ethanol over high surface area CeO_2: The role of CeO_2 as an internal pre-reforming catalyst", **Applied Catalysis B: Environmental**, revised

[8] N. Laosiripojana and S. Assabumrungrat, "Reactivity of high surface area CeO_2 synthesized by surfactant-assisted method to ethanol decomposition with and without steam", Submitted **to Chemical Engineering Journal**

หน้าสรุปโครงการ (Executive Summary)
ทุนเพิ่มขีดความสามารถด้านการวิจัยของอาจารย์รุ่นใหม่ (MRG4780166)

1. **ชื่อโครงการ (ภาษาไทย)** การออกแบบระบบผลิตไฮโดรเจนซึ่งใช้วัตถุดิบที่สามารถหาได้ในประเทศไทยเป็นสารตั้งต้นได้อย่างมีประสิทธิภาพเพื่อใช้ประโยชน์ในเซลล์เชื้อเพลิงแบบออกไซด์แข็ง

(ภาษาอังกฤษ) Design of hydrogen production unit (Reformer) based on the feedstock available in Thailand for application in SOFC

2. **หัวหน้าโครงการ** นายนวดล เหล่าศิริพจน์
(Mr. Navadol Laosiripojana)
คุณวุฒิ ปริญญาเอก (Ph.D.)
ตำแหน่ง อาจารย์
หน่วยงานที่สังกัด บัณฑิตวิทยาลัยร่วมด้านพลังงานและสิ่งแวดล้อม
มหาวิทยาลัยเทคโนโลยีพระจอมเกล้าธนบุรี
91 ถนนประชาอุทิศ บางมด ทุ่งครุ กรุงเทพฯ 10140
โทรศัพท์ (02)-8729014 (4146)
Email navadol_l@jgsee.kmutt.ac.th

3. **หลักการและเหตุผลของงานวิจัย**

ในปัจจุบันปรากฏการณ์เรือนกระจกเป็นปัญหาที่สำคัญอย่างหนึ่งของโลก กระบวนการเผาไหม้ (Combustion Process) ถูกใช้อย่างแพร่หลายเพื่อผลิตพลังงานในรูปแบบต่างๆ ถึงแม้ว่ากระบวนการนี้จะสามารถผลิตพลังงานออกมาได้อย่างมีประสิทธิภาพด้วยต้นทุนที่ต่ำ ข้อเสียสำคัญของการใช้กระบวนการนี้เพื่อผลิตพลังงานคือการมีก๊าซเสียออกจากกระบวนการนี้จำนวนมากเช่น NOx หรือ COx เป็นต้น ซึ่งก๊าซเสียเหล่านี้เองที่ส่งผลต่อปรากฏการณ์เรือนกระจก หนทางที่จะแก้ไขซึ่งมีการพัฒนาอย่างต่อเนื่องและกว้างขวางในปัจจุบันคือการใช้เซลล์เชื้อเพลิง (Fuel Cell) เข้าแทนที่ในการผลิตกระแสไฟฟ้าโดยใช้ไฮโดรเจนซึ่งไม่มีองค์ประกอบของคาร์บอนอยู่เป็นเชื้อเพลิง เซลล์เชื้อเพลิงเป็นเทคโนโลยีสะอาดซึ่งเพิ่งถูกพัฒนามาไม่นานมานี้ การทำงานของเซลล์เชื้อเพลิงนั้นไม่ใช่เกี่ยวข้องกับกระบวนการเผาไหม้ ดังนั้นก๊าซเสียถูกปล่อยออกมาจะมีปริมาณต่ำกว่าก๊าซเสียปล่อยจากเครื่องยนต์สันดาปภายในมาก

งานวิจัยในโครงการนี้เป็นงานที่ทำต่อเนื่องมาจากงานวิทยานิพนธ์ปริญญาเอกของผู้เขียน รวมถึงงานวิจัยที่เคยทำรับทำให้กับบริษัท Rolls-Royce ที่ประเทศอังกฤษ ซึ่งเกี่ยวข้องการการศึกษาการทำงานของเซลล์เชื้อเพลิงแบบออกไซด์แข็ง (Solid Oxide Fuel Cell; SOFC) ซึ่งมีกระบวนการปฏิรูปน้ำด้วยมีเทน (Methane Steam Reforming) เพื่อผลิตไฮโดรเจนอยู่ภายใน (Internal Reforming Operation) การทำงานของเซลล์เชื้อเพลิงออกไซด์แข็งในลักษณะนี้จะทำการรวมหน่วยผลิตไฮโดรเจน (Reformer) ซึ่งปฏิกิริยาภายในเป็นแบบดูดความร้อน กับหน่วยเซลล์เชื้อเพลิงหลักซึ่งมีปฏิกิริยาคายความร้อนอยู่ภายในไว้ด้วยกัน เพื่อประโยชน์ในการแลกเปลี่ยนความร้อนซึ่งกันและกันและลดปริมาณพลังงานที่ต้องป้อนให้ อย่างไรก็ตามการรวมกันของสองหน่วยนี้ไม่ใช่เรื่องง่ายเนื่องจากโดยปรกติแล้วจะเกิดความเหลื่อมล้ำกันระหว่างความต้องการพลังงานที่สูงของหน่วยผลิตไฮโดรเจน กับพลังงานที่สามารถปล่อยออกมาได้ของหน่วยเซลล์เชื้อเพลิงหลัก ความเหลื่อมล้ำของพลังงานนี้ทำให้เกิดไม่คงที่ของอุณหภูมิภายในตัวเซลล์ โดยอุณหภูมิจะต่ำมากในบริเวณทางเข้าของหน่วยผลิตไฮโดรเจน และส่งผลให้เกิดการแตกร้าวของวัสดุที่ใช้ได้ วิธีการแก้ปัญหานี้ทำได้โดยการใช้ตัวเร่งปฏิกิริยาชนิดใหม่ที่มีความว่องไวต่อกระบวนการปฏิรูปน้อยลง เพื่อลดความต้องการพลังงานที่สูงของหน่วยผลิตไฮโดรเจน แต่มีความเสถียรและความต้านทานการเกิดคาร์บอนที่ผิวสูง

สืบเนื่องจากงานวิจัยในช่วงปริญญาเอกซึ่งทำการวิจัยถึงประสิทธิภาพของตัวเร่งปฏิกิริยาแบบออกไซด์ต่อกระบวนการปฏิรูปน้ำโดยใช้มีเทน พบว่าตัวเร่งปฏิกิริยาชนิดนี้เป็นทางเลือกที่ดีสำหรับเซลล์เชื้อเพลิงแบบออกไซด์แข็งซึ่งมีกระบวนการปฏิรูปน้ำเพื่อผลิตไฮโดรเจนอยู่ภายใน เนื่องจากตัวเร่งปฏิกิริยาชนิดนี้ที่มีความว่องไวต่อกระบวนการปฏิรูปต่ำกว่าตัวเร่งปฏิกิริยาที่ใช้กันในเชิงพานิชย์ในปัจจุบัน (เช่น นิเกิล) และมีความต้านทานการเกิดคาร์บอนที่ผิว (Carbon formation) สูงกว่ามาก แต่ปัญหาใหญ่ของการใช้ตัวเร่งปฏิกิริยาแบบออกไซด์หากต้องการแปรรูปเชื้อเพลิงตัวอื่นเป็นไฮโดรเจนแทนมีเทนเช่น ก๊าซธรรมชาติซึ่งมีส่วนประกอบของสารไฮโดรคาร์บอนตัวอื่นๆ อยู่ด้วย (เช่น อีเทน โพรเพน และบิวเทน) เอทานอล หรือ เมทานอลแล้วความว่องไวต่อกระบวนการปฏิรูปอาจจะต่ำเกินไป และส่งผลให้สารไฮโดรคาร์บอนเหล่านี้ที่เหลือจากปฏิกิริยาการปฏิรูป (Reforming) เข้าไปยังส่วนหลักของเซลล์เชื้อเพลิงและส่งผลให้ปริสิทธิภาพการทำงานของเซลล์เชื้อเพลิงลดลง ซึ่งในทางปฏิบัติแล้วเชื้อเพลิงเหล่านี้น่าจะถูกใช้ในงานจริงมากกว่าการใช้มีเทนหรือไฮโดรเจน เนื่องจากสามารถหาได้ทั่วไป และราคาถูก ดังนั้นงานวิจัยนี้จึงดำเนินการขึ้นเพื่อพัฒนาและปรับปรุงชนิดของตัวเร่งปฏิกิริยารวมถึงกระบวนการที่ใช้ในการผลิตไฮโดรเจนจากวัตถุดิบชนิดต่างๆ

อนึ่งประเทศไทยมีข้อได้เปรียบของการใช้เทคโนโลยีเซลล์เชื้อเพลิงคือเรามีเชื้อเพลิงที่สามารถใช้งานร่วมกับเทคโนโลยีดังกล่าวเพื่อผลิตกระแสไฟฟ้ามากมาย อาทิเช่น ก๊าซธรรมชาติ ก๊าซชีวภาพ (Biogas) ก๊าซจากกระบวนการชีวมวล (Synthesis Gas from Biomass Pyrolysis and Gasification) หรือแม้แต่ไบโอเอทานอล หากสามารถสร้างเทคโนโลยีในการเปลี่ยนวัตถุดิบดังกล่าวไปเป็นไฮโดรเจนเพื่อใช้งานในเซลล์เชื้อเพลิงได้ ถึงแม้ในอนาคตเราต้องซื้อเทคโนโลยีเซลล์เชื้อเพลิงจากต่างประเทศเข้ามา จะเป็นการลดต้นทุนของประเทศชาติอย่างมากมาย ในอนาคตอันใกล้ เทคโนโลยีไฮโดรเจน และเซลล์เชื้อเพลิงจะมีการ

พัฒนาจนใช้งานจริงในเชิงพาณิชย์อย่างแพร่หลายแน่นอน โดยมีปัญหาการขาดแคลน Conventional Fuel และปัญหาสิ่งแวดล้อมเป็นแรงผลักดัน แต่เนื่องจากปัญหา สำคัญของประเทศไทยคือศักยภาพของการพัฒนาเทคโนโลยีดังกล่าวในประเทศยังไม่สามารถทัดเทียมได้กับต่างประเทศ สิ่งที่ควรดำเนินการในระยะแรกคือพยายามพัฒนาสิ่งที่น่าจะมี Potential ในการดำเนินการมากที่สุด หรือการใช้ประโยชน์จากสิ่งที่มีอยู่ให้มากที่สุด นั่นคือตัว Resource นั่นเอง การพัฒนาระบบผลิตไฮโดรเจนนั้นจะช่วยให้ประเทศไทยสามารถลดต้นทุนของการใช้เทคโนโลยีลงได้หากมีการใช้งานจริงในอนาคต อีกทั้งประสิทธิภาพการใช้งานของก๊าซธรรมชาติในการผลิตไฮโดรเจน และกระแสไฟฟ้าจะสูงกว่าการนำเทคโนโลยีจากต่างประเทศมาใช้อย่างแน่นอน เนื่องจากคุณสมบัติที่แตกต่างกันของวัตถุดิบในแต่ละประเทศ เช่นในกรณีก๊าซธรรมชาติของประเทศไทยซึ่งมีปริมาณคาร์บอนไดออกไซด์สูงมากเมื่อเทียบกับประเทศอื่นๆ การเลือกสภาวะของระบบผลิตไฮโดรเจน และการเลือกตัวเร่งปฏิกิริยาที่ใช้เพื่อให้สามารถผลิตไฮโดรเจนให้ได้มากที่สุดจะแตกต่างกับเทคโนโลยีการผลิตก๊าซไฮโดรเจนจากก๊าซธรรมชาติที่มีปริมาณคาร์บอนไดออกไซด์อยู่น้อย เป็นต้น

อนึ่งผลที่ได้จากการทดลองในช่วง 2 ปีจึงได้รับการตอบรับให้ตีพิมพ์ในวรสารระดับนานาชาติ (International Journal) 6 ฉบับ และอยู่ในระหว่างการแก้ไข (Revised) 1 ฉบับ อยู่ในระหว่างการพิจารณา (Submitted) 1 ฉบับ นอกจากนั้นยังถูกเผยแพร่ในการประชุมระดับนานาชาติ (International Conference) 7 ฉบับ ดังแสดงรายละเอียดในตอนท้ายของรายงาน

เนื้อหางานวิจัย

<u>บทนำ</u>

วัตถุประสงค์หลักของโครงการนี้คือการพัฒนาตัวเร่งปฏิกิริยาสำหรับกระบวนการผลิตไฮโดรเจนเพื่อใช้ประโยชน์สำหรับเซลล์เชื้อเพลิงแบบอุณหภูมิสูง (High Temperature Fuel Cells) โดยใช้วัตถุดิบที่สามารถหาได้ในประเทศไทยเช่นก๊าซธรรมชาติ ก๊าซชีวภาพ ก๊าซหุงต้ม เอทานอล และเมทานอล ซึ่งการดำเนินงานวิจัยในช่วง 2 ปีที่ผ่านมานั้น ผู้วิจัยได้สร้างหน่วยผลิตไฮโดรเจน (Hydrogen Production Testing Unit) ในระดับ Lab-scale และศึกษาถึงการใช้ตัวเร่งปฏิกิริยาชนิดใหม่ซึ่งใช้เทคโนโลยีนาโน (Nano-technology) เข้าช่วยในการเตรียมนั้นคือ Nano-composite CeO_2 (HSA: High Surface Area) และ Ni/Ce-ZrO_2 รวมถึง CeO_2-doped Ni/Al_2O_3 เพื่อทำการเปรียบเทียบคุณสมบัติกับตัวเร่งปฏิกิริยาที่มีอยู่ในเชิงพาณิชย์เช่น Ni/Al_2O_3 โดยการเปรียบเทียบดังกล่าวได้ทำการเปรียบเทียบถึงเสถียรภาพ (Stability) และศักยภาพ (Activity) ในการผลิตไฮโดรเจนจากกระบวนการรีฟอร์มมิ่งประเภทต่างๆ เช่น Steam Reforming, Dry Reforming, Autothermal Reforming, Partial Oxidation, และ Cracking นอกจากนั้นยังทำการศึกษาถึง Kinetics ของตัวเร่งปฏิกิริยาชนิดใหม่ที่เตรียมขึ้นมาด้วย โดยในช่วง 2 ปีที่ผ่านมาทางผู้วิจัยได้ดำเนินการใช้วัตถุดิบชนิดต่างๆ เพื่อผลิตไฮโดรเจนจากกระบวนการรีฟอร์มมิ่งประเภทต่างๆ ดังนี้

- ใช้มีเทนเป็นสารตั้งต้น และใช้กระบวนการรีฟอร์มมิ่งด้วยน้ำ (Steam Reforming) และกระบวนการ Autothermal Reforming เป็นปฏิกิริยาหลักเพื่อศึกษาถึงคุณสมบัติ Kinetics ของตัวเร่งปฏิกิริยา Ni/Ce-ZrO_2 เปรียบเทียบกับ Ni/Al_2O_3
- ใช้ก๊าซชีวภาพ (มีเทน + คาร์บอนไดออกไซด์) เป็นสารตั้งต้น และใช้กระบวนการรีฟอร์มมิ่งด้วยคาร์บอนไดออกไซด์ (Dry Reforming) เป็นปฏิกิริยาหลัก บนตัวเร่งปฏิกิริยา CeO_2 (HSA) เปรียบเทียบกับ Ni/Al_2O_3
- ใช้อีเทน และโพรเพน (ซึ่งเป็นองค์ประกอบในก๊าซธรรมชาติ) เป็นสารตั้งต้น และใช้กระบวนการรีฟอร์มมิ่งด้วยน้ำ (Steam Reforming) เป็นปฏิกิริยาหลัก บนตัวเร่งปฏิกิริยา CeO_2-doped Ni/Al_2O_3 เปรียบเทียบกับ Ni/Al_2O_3
- ใช้เมทานอลเป็นสารตั้งต้น และใช้กระบวนแตกตัว (Cracking) และกระบวนการออกซิไดซ์บางส่วน (Partial Oxidation) เป็นปฏิกิริยาหลักบนตัวเร่งปฏิกิริยา CeO_2 (HSA) เปรียบเทียบกับ Ni/Al_2O_3
- ใช้ก๊าซหุงต้มเป็นสารตั้งต้นเพื่อผลิตไฮโดรเจนจากกระบวนการรีฟอร์มมิ่งด้วยน้ำและกระบวนการ Autothermal Reforming บนตัวเร่งปฏิกิริยา CeO_2 (HSA)

- ใช้เอทานอลเป็นสารตั้งต้นเพื่อผลิตไฮโดรเจนจากกระบวนการรีฟอร์มมิ่งด้วยน้ำ บนตัวเร่งปฏิกิริยา CeO_2 (HSA) + Ni/Al_2O_3

ซึ่งจากผลการดำเนินงานทดลองพบว่าการใช้สาร CeO_2 เป็นตัวเร่งปฏิกิริยา หรือเป็นตัว Support และตัว Promoter สามารถช่วยเพิ่มประสิทธิภาพในการผลิตไฮโดรเจนได้เป็นอย่างดีเมื่อเปรียบเทียบกับ Ni/Al_2O_3 ซึ่งมีการใช้กันอย่างแพร่หลายในปัจจุบัน ซึ่งการใช้สาร CeO_2 ในกระบวนการรีฟอร์มมิ่งถึงเป็นเรื่องใหม่ ดังนั้นผลที่ได้จากการทดลองในช่วง 2 ปีจึงได้รับการตอบรับให้ตีพิมพ์ในวารสารระดับนานาชาติ (International Journal) 6 ฉบับ และอยู่ในระหว่างการแก้ไข (Revised) 1 ฉบับ อยู่ในระหว่างการพิจารณา (Submitted) 1 ฉบับ นอกจากนั้นยังถูกเผยแพร่ในการประชุมระดับนานาชาติ (International Conference) 7 ฉบับ ดังแสดงรายละเอียดในตอนท้ายของรายงาน

อนึ่งเนื้อหางานวิจัยที่จะนำเสนอประกอบด้วยการรวบรวมข้อมูลด้านงานวิจัยในอดีตที่มีความเกี่ยวข้องกับเทคโนโลยีการผลิตไฮโดรเจน (บทที่ 1) และเทคโนโลยีเซลล์เชื้อเพลิง (บทที่ 2) โดยกระบวนการผลิตไฮโดรเจนจะเน้นหลักไปที่กระบวนการรีฟอร์มมิ่งซึ่งมีการศึกษาวิจัยกันอย่างแพร่หลายเนื่องจากเป็นกระบวนการที่เหมาะสมและมีประสิทธิภาพมากที่สุดในการผลิตก๊าซไฮโดรเจนจากสารประกอบไฮโดรคาร์บอนหรือก๊าซธรรมชาติ หลังจากนั้นจึงนำเสนอขั้นตอนและวิธีการดำเนินการวิจัยอันประกอบด้วยการสร้างระบบที่ใช้ในการทดสอบตัวเร่งปฏิกิริยา (Reforming Catalyst) เพื่อรีฟอร์มสารไฮโดรคาร์บอนไปเป็นไฮโดรเจน (บทที่ 3-4) รวมถึงแสดงผลของการทดลองที่ได้ดำเนินการไปซึ่งจะมุ่งเน้นไปที่การทดสอบเสถียรภาพ และศักยภาพของตัวเร่งปฏิกิริยาที่เลือกขึ้น ความต้านทานต่อการเกิดคาร์บอนที่ผิว และค่า Product Selectivity ที่ผลิตได้เป็นต้น (บทที่ 5-9) และในบทสุดท้าย (บทที่ 10) จะบรรยายถึงการออกแบบระบบรีฟอร์มเมอร์ในรูปแบบใหม่ รวมถึงการนำเมมเบรนมาใช้งานในระบบรีฟอร์มเมอร์

บทที่ 1
ทฤษฎีที่เกี่ยวข้องกับเทคโนโลยีการผลิตไฮโดรเจนเพื่อใช้ประโยชน์ในเซลล์เชื้อเพลิง

1.1 เทคโนโลยีการผลิตไฮโดรเจนเพื่อใช้ประโยชน์ในเซลล์เชื้อเพลิง

ในปัจจุบันปัญหาสภาพแวดล้อม และปรากฏการณ์เรือนกระจกเป็นปัญหาที่สำคัญอย่างหนึ่งของโลก กระบวนการเผาไหม้ (Combustion Process) ถูกใช้อย่างแพร่หลายเพื่อผลิตพลังงานในรูปแบบต่างๆ มาเป็นเวลานาน ถึงแม้ว่ากระบวนการนี้จะได้รับการพัฒนามาเป็นเวลานาน และยังสามารถผลิตพลังงานออกมาได้ด้วยต้นทุนที่ต่ำ ข้อเสียสำคัญของการใช้กระบวนการนี้เพื่อผลิตพลังงานคือการมีก๊าซเสียออกจากกระบวนการนี้จำนวนมาก เช่น NO_x หรือ CO_x เป็นต้น ซึ่งก๊าซเสียเหล่านี้เองที่ส่งผลต่อปรากฏการณ์เรือนกระจก หนทางที่จะแก้ไขซึ่งมีการพัฒนาอย่างต่อเนื่องและกว้างขวางในปัจจุบันคือการใช้เซลล์เชื้อเพลิง (Fuel Cell) ซึ่งเป็นเทคโนโลยีสะอาดที่เพิ่งถูกพัฒนามาไม่นานมานี้เข้าแทนที่ในการผลิตกระแสไฟฟ้า เซลล์เชื้อเพลิงทำงานโดยใช้ไฮโดรเจนเป็นเชื้อเพลิงดังนั้นก๊าซเสียถูกปล่อยออกมาจึงมีปริมาณต่ำกว่าก๊าซเสียปล่อยจากเครื่องยนต์สันดาปภายในมาก ประโยชน์อีกประการหนึ่งของเซลล์เชื้อเพลิงเมื่อเปรียบเทียบกับกระวนการเผาไหม้คือประสิทธิภาพของเซลล์เชื้อเพลิงในการผลิตพลังงานสูงกว่ากระวนการเผาไหม้มาก

เซลล์เชื้อเพลิงชนิดต่างๆ ได้รับความสนใจจากบริษัทต่างๆมากมายทั่วโลก บริษัทผลิตรถยนต์ในหลายประเทศได้ทำการผลิตรถยนต์เซลล์เชื้อเพลิง อาทิเช่น บริษัท Honda และบริษัท Toyota ของประเทศญี่ปุ่น บริษัท Fiat ของประเทศอิตาลี และ บริษัท General Motor และ บริษัท Chrysler-Daimler ของประเทศสหรัฐอเมริกา นอกจากนี้ยังมีบริษัทและโรงงานอุตสาหกรรมอีกมากมายทั้งในอเมริกา ยุโรป และเอเชียกำลังทำการพัฒนาเซลล์เชื้อเพลิงที่ใช้งานที่อุณหภูมิสูงกว่า 500 องศาเซลเซียส (Molten Carbonate Fuel Cell; MCFC, and Solid Oxide Fuel Cell; SOFC) เพื่อผลิตกระแสไฟฟ้าจ่ายให้กับที่อยู่อาศัย รวมไปถึงโรงงานอุตสาหกรรม ในส่วนของงานวิจัยและพัฒนานั้นที่ผ่านมามีงานวิจัยมากมายที่ศึกษาเกี่ยวกับกระบวนการผลิตไฮโดรเจนโดยใช้สารตั้งต้นและกระบวนการผลิตที่แตกต่างกัน วัตถุดิบที่มักนำมาศึกษากันประกอบด้วยผลิตภัณฑ์น้ำมันปิโตรเลียมอันได้แก่ ก๊าซโซลีน และดีเซลเนื่องจากเชื้อเพลิงเหล่านี้มีการใช้กันอย่างแพร่หลายอยู่แล้ว แต่เนื่องจากในปัจจุบันน้ำมันเริ่มมีราคาสูงขึ้นจึงมีการนำวัตถุดิบอื่นมาใช้เพื่อผลิตก๊าซไฮโดรเจนอันได้แก่ ก๊าซธรรมชาติ (Natural Gas), หรือ วัตถุดิบจากแหล่งพลังงานทดแทนต่างๆ อันประกอบด้วย ก๊าซชีวภาพ (Biogas) ที่มีองค์ประกอบหลักเป็นก๊าซมีเทน เมธานอล และเอทานอล เป็นต้น

การเปลี่ยนรูปของไฮโดรเจนไปเป็นกระแสไฟฟ้าโดยใช้เซลล์เชื้อเพลิงนั้นมีความเกี่ยวข้องกับเทคโนโลยีต่างๆมากมาย โดยหลักการแล้วแหล่งพลังงานทดแทนต่างๆเช่นวัสดุชีวมวล จะต้องถูกแปรรูปไปเป็นไฮโดรเจนเสียก่อนจึงจะนำไปใช้ประโยชน์ในเชื้อเพลิงในเซลล์เชื้อเพลิงได้ นอกจากการแปรรูปวัสดุชีว

มวลเป็นไฮโดรเจนแล้ว ไฮโดรเจนสามารถผลิตขึ้นมาด้วยกระบวนการอื่นๆ อีกเช่นกระบวนการแยกน้ำโดยอาศัยไฟฟ้าจากพลังงานแสงอาทิตย์ ลม น้ำ เป็นต้น ซึ่งรายละเอียดของเทคโนโลยีที่เกี่ยวข้องกับการเปลี่ยนรูปของพลังงานทดแทนไปเป็นไฮโดรเจนเพื่อใช้ประโยชน์ในการผลิตกระแสไฟฟ้าโดยเซลล์เชื้อเพลิงมีดังแสดงใน Flowchart ด้านล่างนี้

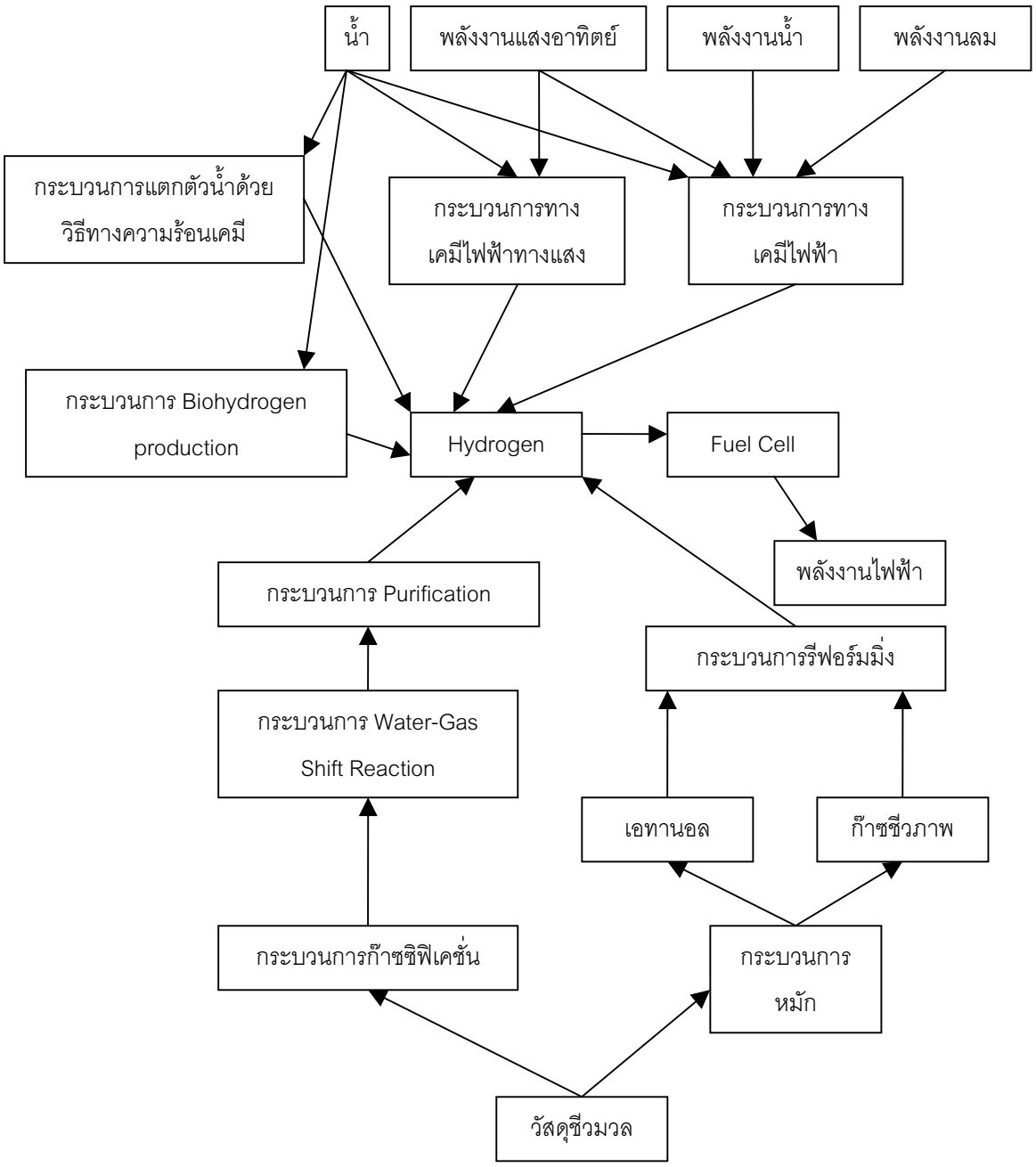

รูปที่ 1.1 แผนภาพแสดงรายละเอียดของเทคโนโลยีที่เกี่ยวข้องกับการผลิตไฮโดรเจนเพื่อใช้ประโยชน์ในการผลิตกระแสไฟฟ้าโดยเซลล์เชื้อเพลิง

1.2. <u>ทฤษฎีและหลักการโดยรวมของเทคโนโลยีการผลิตไฮโดรเจน</u> [1-2]

1.2.1. กระบวนการทางความร้อน (Thermal Process)

การผลิตก๊าซไฮโดรเจนจากแหล่งพลังงานทดแทนโดยกระบวนการทางความร้อน (Thermal Process) มีหลายกระบวนการ กระบวนการหลักๆ ที่รู้จักกันอย่างแพร่หลายคือ กระบวนการปฏิรูปด้วยไอน้ำ (steam reforming) กระบวนการปฏิรูปด้วยก๊าซคาร์บอนไดอ๊อกไซด์ (dry reforming) กระบวนการทำออกซิเดชันบางส่วน (partial oxidation) กระบวนการร่วมของกระบวนการปฏิรูปด้วยไอน้ำกับกระบวนการทำออกซิเดชันบางส่วน (combined partial oxidation-steam reforming) หรือที่เรียกกันว่า autothermal reforming ซึ่งก่อนจะใช้กระบวนการเหล่านี้ผลิตไฮโดรเจนเพื่อใช้ประโยชน์ในเซลล์เชื้อเพลิงแหล่งพลังงานทดแทนต่างๆ จะต้องถูกแปรรูปให้เป็นสารตั้งต้นของปฏิกิริยาเหล่านี้เสียก่อน โดยมากแหล่งพลังงานทดแทนเช่นไม้ ของเหลือใช้ทางการเกษตร และของเสียที่เป็นของแข็งซึ่งเรียกรวมๆกันว่าวัสดุชีวมวล (Biomass) จะต้องผ่านกระบวนการหมัก (Fermentation) หรือกระบวนการ Digestion เพื่อให้ได้ก๊าซชีวภาพ (Biogas) หรือเอทานอลก่อนจะนำสารที่ได้เหล่านี้ผ่านเข้ากระบวนการดังที่กล่าวมา ซึ่งแต่ละกระบวนการต่างมีข้อดีข้อเสียทั้งนี้ขึ้นอยู่กับประเภทของสารตั้งต้น ตัวเร่งปฏิกิริยา และสภาวะการทำงานของระบบในแต่ละกระบวนการมีตัวแปรหลากหลายที่ต้องทำการศึกษา ตลอดจนต้องมีการพัฒนาตัวเร่งปฏิกิริยาให้เหมาะสมเพื่อความคุ้มค่าทางเศรษฐศาสตร์

นอกจากการนำวัสดุชีวมวลเหล่านี้ไปผ่านกระบวนการหมักดังกล่าวมาด้านบนแล้ว วัสดุชีวมวลอาจจะถูกเปลี่ยนเป็นก๊าซไฮโดรเจนโดยตรงได้เลยจากกระบวนการก๊าซซิฟิเคชั่น และอีกกระบวนการหนึ่งซึ่งสามารถสังเคราะห์ไฮโดรเจนได้คือกระบวนการแตกตัวน้ำด้วยวิธีทางความร้อนเคมี กระบวนการต่างๆที่กล่าวมาเหล่านี้มีรายละเอียดดังต่อไปนี้

1.2.1.1. กระบวนการปฏิรูปด้วยไอน้ำ(Steam Reforming)

กระบวนการรีฟอร์มมิ่งหรือกระบวนการปฏิรูปกับไอน้ำเป็นกระบวนการที่ให้ประสิทธิภาพในการผลิตก๊าซไฮโดรเจนสูง เสียค่าใช้จ่ายน้อยกว่าวิธีอื่น และเป็นวิธีที่แพร่หลายและนำมาใช้ทางการค้าแล้ว โดยหลักการของกระบวนการนี้คือ การดึงธาตุไฮโดรเจนจากไฮโดรคาร์บอนและไอน้ำที่เป็นวัตถุดิบ (feedstock) ของกระบวนการออกมาให้กลายเป็นก๊าซไฮโดรเจนให้ได้มากที่สุด ซึ่งกระบวนการผลิตจะประกอบไปด้วย 4 ขั้นตอน คือ 1) การทำให้วัตถุดิบมีความบริสุทธิ์ โดยเน้นที่การกำจัดซัลเฟอร์ออก 2) การเกิดปฏิกิริยาปฏิรูปกับไอน้ำของไฮโดรคาร์บอนซึ่งจะทำให้เกิดก๊าซ H_2 CO และ CO_2 3) การเกิด shift reaction ของ CO ให้กลายเป็นCO_2 และ 4) การทำให้ก๊าซ H_2 บริสุทธิ์ โดยกำจัดเอาก๊าซ CO_2 CO และไฮโดรคาร์บอนอื่นๆ ออก

ในกรณีที่ใช้ก๊าซชีวภาพซึ่งมีองค์ประกอบหลักคือมีเทนเป็นวัตถุดิบจะต้องทำการกำจัดซัลเฟอร์ออกจากก๊าซชีวภาพก่อนทำปฏิกิริยา โดยก๊าซชีวภาพจะถูกส่งผ่านเข้าสู่เบดที่บรรจุด้วยซิงค์ออกไซด์ (ZnO) หลังจากนั้นก๊าซที่ปราศจากซัลเฟอร์จะถูกผสมกับไอน้ำร้อนยิ่งยวด (superheated steam) เกิดปฏิกิริยาปฏิรูปกับไอน้ำขึ้น ปฏิกิริยาปฏิรูปกับไอน้ำนี้เป็นปฏิกิริยาดูดความร้อนที่ต้องการอุณหภูมิสูงถึง 760-925^{o}C และมีความดันอยู่ที่ 2 MPa จึงมีการนำตัวเร่งปฏิกิริยามาใช้เพื่อเพิ่มประสิทธิภาพของปฏิกิริยานี้ ก๊าซที่ผ่านออกมาจากเครื่องรีฟอร์มเมอร์ซึ่งประกอบไปด้วยก๊าซ H_2 และCO จะผ่านเข้าสู่ขั้นตอนการดึงความร้อนออก แล้วป้อนเข้าสู่เครื่องปฏิกรณ์เปลี่ยนสาร (shift conversion) ที่เกิด shift reaction เพื่อผลิต H_2 ให้ได้เพิ่มขึ้น โดยปฏิกิริยานี้เป็นปฏิกิริยาคายความร้อนที่มีอุณหภูมิอยู่ระหว่าง 200-400^{o}C ทำให้ปริมาณ CO ลดลงเหลือประมาณ 0.2-0.4% โดยปริมาตร ก๊าซที่ออกมาจากเครื่องปฏิกรณ์ shift conversion จะถูกส่งผ่านเข้าหน่วยทำให้ก๊าซบริสุทธิ์ (gas purification) เพื่อจะกำจัด CO_2 CO ที่เหลือจาก shift reaction และก๊าซอื่นๆ ออกเพื่อให้ได้ผลิตภัณฑ์ที่เป็นก๊าซ H_2 ที่บริสุทธิ์ วิธีการกำจัดก๊าซ CO_2 สามารถทำได้หลายวิธี วิธีหนึ่งในวิธีเหล่านั้นคือกระบวนการจับแบบเปียก (wet scrubbing) ที่ใช้สารเคมีจำพวกโมโนเอทาโนละมีน (monoethanolamine) ซัลฟินอล (sulfinol) และ โปแทสเซียมคาร์บอเนตร้อน (hot potassium carbonate) ในกรณีที่ยังมีก๊าซ CO และ CO_2 หลงเหลืออยู่ ก๊าซเหล่านี้สามารถถูกกำจัดออกโดยจะถูกเปลี่ยนให้เป็นก๊าซ CH_4 โดยการเกิดปฏิกิริยาเมธาเนชั่น (methanation) กระบวนการทั้งหมดนี้จะทำให้ก๊าซ H_2 ที่ได้ในขั้นตอนสุดท้ายมีความบริสุทธิ์ถึง 97 ถึง 98% กระบวนการปฏิรูปด้วยไอน้ำ (steam reforming) เป็นปฏิกิริยาดูดความร้อนที่ต้องการอุณหภูมิสูงจึงมีการนำตัวเร่งปฏิกิริยามาใช้เพื่อเพิ่มประสิทธิภาพของปฏิกิริยานี้ ตัวเร่งปฏิกิริยาที่ใช้ประกอบด้วยนิกเกิ้ลออกไซด์กับอลูมินาและตัวส่งเสริม โดยคุณสมบัติของตัวเร่งปฏิกิริยาที่ต้องการคือ ความว่องไว เสถียรภาพ ความแข็งแรงทางกล และความต้านทานต่อการเกาะของคาร์บอนที่ดี ในกรณีที่ใช้เอทานอลจากกระบวนการหมักเป็นวัตถุดิบนั้นขั้นตอนการทำให้วัตถุดิบมีความบริสุทธิ์หรือการกำจัดซัล-เฟอร์ออกสามารถตัดทิ้งได้เนื่องจากสารตั้งต้นอยู่ในสภาวะของเหลวจะไม่มีหรือมีสารประกอบซัลเฟอร์ปะปนอยู่น้อยมาก ก๊าซที่ผ่านออกมาจากเครื่องปฏิกรณ์ (reactor) เมื่อใช้เอทานอลเป็นวัตถุดิบส่วนใหญ่จะประกอบด้วย ก๊าซ H_2 และCO โดยมีCO_2 และ CH_4 เป็นผลิตภัณฑ์รอง

1.2.1.2. กระบวนการปฏิรูปด้วยคาร์บอนไดออกไซด์

กระบวนการปฏิรูปสารประกอบไฮโดรคาร์บอนนอกจากจะใช้ไอน้ำเป็นตัวรีดิวซิ่งแล้วยังสามารถใช้สารอื่นได้อีก อาทิเช่น CO_2 ตัวอย่างของปฏิกิริยาปฏิรูปมีเธนด้วย CO_2 สามารถเขียนได้ดังนี้

$$CH_4 + CO_2 \rightarrow 2H_2 + 2CO$$

กระบวนการดังกล่าวจะมีประโยชน์ในการเปลี่ยนก๊าซชีวภาพไปเป็นไฮโดรเจน เนื่องจากก๊าซชีวภาพจะมีส่วนผสมของคาร์บอนไดออกไซด์ปะปนอยู่แล้ว ขอกจากนั้นปฏิกิริยาดังกล่าวข้างต้นถูกนำเสนอเพื่อใช้เป็นวิธีการที่จะใช้กักเก็บแสงอาทิตย์ในเครื่องปฏิกรณ์เคมีที่เรียกว่า Solar driven volumetric receiver/reactor

1.2.1.3. **กระบวนการออกซิเดชันบางส่วน** (Partial Oxidation)

โดยหลักการกระบวนการออกซิเดชันบางส่วนของสารประกอบไฮโดรคาร์บอน คือ การทำปฏิกิริยาระหว่างสารไฮโดรคาร์บอนกับออกซิเจนที่มีปริมาณไม่เพียงพอต่อการเกิดการเผาไหม้อย่างสมบูรณ์ของกระบวนการออกซิเดชันบางส่วน ปฏิกิริยาหลักที่เกิดขึ้นคือ

$$2\,CH_n + O_2 \longrightarrow 2\,CO + nH_2$$

ปฏิกริยาที่เกิดขึ้นนี้เป็นปฏิกิริยาที่ทำลายพันธะระหว่างไฮโดรคาร์บอน-ไฮโดรคาร์บอนซึ่งอาจทำให้เกิดเป็นคาร์บอนที่เกาะอยู่บนตัวเร่งปฏิกิริยาได้ ปฏิกิริยาออกซิเดชันบางส่วนแบบใช้ตัวเร่งปฏิกิริยา (Catalytic Partial Oxidation Process, CPO) ได้รับความสนใจจากนักวิจัยทั่วไปทั้งนี้เพราะกระบวนการที่ใช้ผลิตก๊าซสังเคราะห์นี้มีข้อได้เปรียบที่เหนือกว่ากระบวนการปฏิรูปที่ใช้ไอน้ำดังต่อไปนี้

- ก๊าซสังเคราะห์ที่ผลิตขึ้นได้จะมีค่าสัดส่วน H_2/CO ต่ำจึงเหมาะที่ใช้ผลิตเอธานอลและเชื้อเพลิงสังเคราะห์
- เครื่องปฏิกรณ์เคมีที่ใช้ในกระบวนการ CPO นี้จะง่ายกว่ากระบวนการปฏิรูปโดยใช้ไอน้ำเพราะไม่จำเป็นต้องใช้แหล่งป้อนพลังงานจากภายนอก (externally fired heater)
- กระบวนการ CPO จะมีค่าความไวและการเลือกจำเพาะสำหรับผลิตก๊าซสังเคราะห์สูง
- ไม่มีการปล่อยก๊าซพิษที่เราไม่ต้องการ อาทิเช่น CO_2 NO_x และ SO_x

ตัวเร่งปฏิกิริยาที่ใช้ในกระบวนการ CPO คือตัวเร่งปฏิกิริยาที่ใช้นิกเกิ้ลเป็นตัวหลักกับตัวเร่งปฏิกิริยาที่ใช้ Rh เป็นหลัก ซึ่งสำหรับตัวเร่งปฏิกิริยาประเภทหลังนี้จะมีความไว การเลือกจำเพาะและเสถียรภาพสูง แต่ธาตุ Rh นี้มีปริมาณอยู่น้อยจึงทำให้ตัวเร่งปฏิกิริยาที่ใช้นิกเกิ้ลมี

ความน่าสนใจมากกว่า โดยปกติปริมาณของออกซิเจนที่ป้อนต้องมีค่าสูงกว่าค่าความต้องการตามปริมาณมวลสารสัมพันธ์ ในกรณีของ CH_4 ค่าออกซิเจนต่อมีเธนต้องมากกว่า 0.5

1.2.1.4 กระบวนการร่วมระหว่างการปฏิรูปด้วยไอน้ำกับออกซิเดชันบางส่วน

กระบวนการปฏิรูปด้วยไอน้ำเหมาะสำหรับใช้ในการเปลี่ยนสารประกอบไฮโดรคาร์บอนที่เบาให้เป็นไฮโดรเจนได้ดี แต่ไม่เหมาะสำหรับสารประกอบไฮโดรคาร์บอนที่หนัก จากสารประกอบไฮโดรคาร์บอนหนักมักต้องใช้กระบวนการร่วมระหว่างการทำออกซิเดชันบางส่วนกับกระบวนการปฏิรูป ทั้งนี้เพราะการทำออกซิเดชันบางส่วนของสารประกอบไฮโดรคาร์บอนหนักจะทำให้ได้ผลิตภัณฑ์ที่มีก๊าซคาร์บอนมอนอกไซด์อยู่สูง จากนั้นคาร์บอนมอนนอกไซด์จะทำปฏิกิริยากับไอน้ำเพื่อผลิต CO_2 และ H_2 ก๊าซออกซิเจนที่อุณหภูมิและความดันสูง

$$C_nH_m + n/2\ O_2 \longrightarrow n\ CO + m/2\ H_2 + heat$$
$$C_nH_m + n\ H_2O + heat \longrightarrow n\ CO + (n+m/2)\ H_2$$
$$CO + n\ H_2O \longrightarrow CO_2 + H_2 + heat$$

นอกจากนี้ปฏิกิริยาระหว่างไฮโดรคาร์บอนกับออกซิเจนเป็นปฏิกิริยาคายความร้อน พลังงานที่ได้นี้สามารถนำไปถ่ายเทให้กับปฏิกิริยาปฏิรูประหว่างสารประกอบไฮโดรคาร์บอนกับไอน้ำซึ่งเป็นปฏิกิริยาดูดความร้อน ตัวอย่างหนึ่งของกระบวนการที่ใช้กระบวนการร่วมคือการเปลี่ยน CH_4 ให้กลายเป็นก๊าซสังเคราะห์โดยใช้กระบวนการร่วมทั้งสาม (CO_2 reforming, steam reforming และ partial oxidation) ดังปฏิกิริยาต่อไปนี้

$$CH_4 + H_2O \rightarrow CO + 3H_2 \quad (-\Delta H^o_{298} = -206\ kJ/mol)$$
$$CH_4 + ½\ O_2 \rightarrow CO + 2H_2 \quad (-\Delta H^o_{298} = 38\ kJ/mol)$$
$$CH_4 + CO_2 \rightarrow 2CO + 2H_2 \quad (-\Delta H^o_{298} = -247\ kJ/mol)$$

กระบวนการดังกล่าวข้างต้นสามารถดำเนินการในสองขั้นตอน กล่าวคือ การให้บางส่วนของ CH_4 ทำปฏิกิริยากับ O_2 เกิดเป็น H_2O กับ CO_2 โดยอาศัยการออกซิเดชันอย่างเต็มที่จากนั้น CH_4 ที่เหลือจึงทำปฏิกิริยาปฏิรูปกับ H_2O ร่วมกับ CO_2 ที่ผลิตได้ เกิดเป็น H_2 และ CO ดังปฏิกิริยารวมต่อไปนี้

$$CH_4 + 2/3\ H_2O + 1/3\ CO_2 \rightarrow 4/3\ CO + 8/3\ H_2 \quad (-\Delta H^o_{298} = -219\ kJ/mol)$$

ข้อดีของการทำปฏิกิริยาปฏิรูปร่วม คือจะทำให้สามารถปรับค่าอัตราส่วนของ H_2/CO ให้ได้อยู่ในช่วงตามที่ต้องการ นอกจากนี้ยังเป็นการใช้ผลิตภัณฑ์ข้างเคียง (CO_2) ที่เกิดจากปฏิกิริยา water gas shift reaction (ตามสมการข้างล่าง) ให้เป็นประโยชน์

$$CO + H_2O \rightarrow H_2 + CO_2 \quad (-\Delta H^o_{298} = -41\ kJ/mol)$$

1.2.1.5. กระบวนการแตกโมเลกุลด้วยความร้อน (Thermal Cracking Process)

วิธีนี้เป็นการใช้ความร้อนในการแตกโมเลกุลของไฮโดรคาร์บอนหนักให้ได้โมเลกุลสั้นลง ซึ่งวิธีนี้โรงกลั่นน้ำมันมักนำมาใช้แตกโมเลกุลของน้ำมันหนัก (short residue) ที่ได้จากส่วนล่างของหอกลั่นน้ำมันดิบ (crude) ให้ได้พวกแนฟธา (naphtha) หรือน้ำมันก๊าด (kerosene) มากขึ้น และจากงานวิจัยของอภิชัย เทอดเทียนวงษ์และคณะ [1997] ได้พบว่าปฏิกิริยาแตกสลายโมเลกุลด้วยความร้อนนี้เป็นปฏิกิริยาที่สำคัญอันหนึ่งในการผลิตก๊าซไฮโดรเจน

1.2.1.6. กระบวนการไพโลไลซีส/ก๊าซซิฟิเตชั้น

โฮโดรเจนสามารถผลิตได้จากชีวมวลโดยกระบวนการไพโลไลซีส/ก๊าซซิฟิเตชั้น (Pyrolysis/Gasification) ซึ่งในกระบวนการนี้จะต้องประกอบด้วยการเก็บรวบรวมชีวมวล การขนส่ง และการเตรียมชีวมวล ขั้นตอนของการเตรียมชีวมวลจะเกี่ยวข้องกับการให้ความร้อนแก่สารละลายข้น หรือชีวมวล/น้ำให้ได้อุณหภูมิสูงภายใต้ความดันในเครื่องปฏิกรณ์เคมี การปรับสภาพโดยการให้ความร้อนนี้จะทำให้ชีวมวลเกิดการสลายตัวและเกิดกระบวนการอ็อกซิไดซ์บางส่วน (Partial Oxidation) ก๊าซที่เกิดจากกระบวนการนี้จะประกอบด้วยคาร์บอนมอนออกไซด์ คาร์บอนไดออกไซด์ ไนโตรเจน มีเธน และไฮโดรเจน ส่วนที่ออกทางด้านล่างของเครื่องปฏิกรณ์จะเป็นส่วนที่มีธาตุปนเป็นหลัก ก๊าซที่เกิดในตอนต้นจะถูกป้อนเข้าเครื่องปฏิกรณ์ water-gas shift เพื่อเปลี่ยนผลิตภัณฑ์ก๊าซให้เป็นไฮโดรเจนให้มากที่สุดและมีคาร์บอนมอนออกไซด์ปะปนอยู่เพียงเล็กน้อย กระบวนการทำให้ก๊าซไฮโดรเจนมีความบริสุทธิ์สามารถทำได้โดยกระบวนการดูดซับแบบเปลี่ยนแปลงความดัน

ระบบดังกล่าวนี้จะคล้ายคลึงกับกระบวนการก๊าซซิฟิเคชั่นของถ่านหิน (Coal Gasification) ยกเว้นตรงที่ว่าระบบการปรับสภาพโดยการให้ความร้อนของชีวมวลและการออกแบบเครื่องปฏิกรณ์เคมี หากเปรียบเทียบที่กำลังการผลิตที่เท่ากันแล้วเครื่องมือที่ใช้ในการผลิตไฮโดรเจนจากชีวมวลจะมีขนาดใหญ่กว่าการผลิตจากถ่านหิน ทั้งนี้เพราะคุณค่าทางความร้อนต่อ

หนึ่งหน่วยมวลของชีวมวลมีค่าต่ำกว่าของถ่านหิน และนี่อาจส่งผลทำให้ราคาต้นทุนในการผลิตไฮโดรเจนจากชีวมวลสูงกว่าการผลิตจากถ่านหิน

ในส่วนของการทำให้ก๊าซที่ได้มีความบริสุทธิ์นั้น การกำจัดสารประกอบซัลเฟอร์ที่ปะปนอยู่ในก๊าซที่ได้จากกระบวนการสามารถทำได้โดยใช้ตัวทำละลายจำพวกคาร์บอเนตและเอมีน โดยก๊าซที่ได้จะถูกทำให้เย็นลงมาก่อนที่อุณหภูมิ 130 ถึง 150 องศาเซลเซียส ในทางปฏิบัตินั้นจะมีทางเลือกในการกำจัดสารประกอบซัลเฟอร์ที่ปะปนอยู่ในก๊าซ 2 ระบบคือ ระบบทางเคมี และระบบทางกายภาพ โดยการเลือกใช้จะขึ้นอยู่กับระดับของความบริสุทธิ์ที่ต้องการ ความดันของก๊าซ และแฟคเตอร์อื่นๆ สำหรับวิธีทางเคมี (ตัวทำละลายคาร์โบเนตหรือเอมีน) นั้นจะเกี่ยวข้องกับปฏิกิริยาทางเคมีที่ย้อนกลับได้ของ H_2S และ CO_2 กับตัวทำละลายพวกที่มีขั้ว (Polar group) ซึ่งตัวทำละลายพวกนี้สามารถนำกลับมาใช้ใหม่ได้ (Regenerate) โดยใช้กระบวนการไล่ก๊าซโดยใช้ไอน้ำแบบระบบปิด (Closed Steam Stripping) ที่ความดันที่ต่ำกว่า ระบบที่เป็นที่นิยมอย่างกว้างขวางในกระบวนการก๊าซไฮโดรของปิโตรเลียม (Petroleum Hydroprocessing) คือระบบที่มีการใช้สาร Diisopropyl amine และ methylethyl amine โดย Chow และคณะได้นำเสนอรายละเอียดของระบบคาร์บอเนต ซึ่งโดยทั่วๆไปจะทำการกำจัด H_2S ออกได้ถึง 99% และปริมาณของ COS และ CO_2 ที่สามารถกำจัดได้จะเป็นฟังก์ชั่นของความดันย่อยของ H_2S/CO_2 ตัวทำละลาย และแฟคเตอร์อื่นๆ

ลักษณะทางกายภาพของตัวทำละลายอินทรีย์สามารถดูดซึมก๊าซที่เป็นกรด (H_2S และ CO_2) ได้ที่ความดันสูงโดยตัวทำละลายนี้จะถูกทำให้ดีและนำกลับมาใช้ใหม่โดยการทำ Flashing ที่ความดันที่ต่ำกว่า เนื่องจากความสามารถในการละลายระหว่าง H_2S และ CO_2 มีความแตกต่างกัน หลายๆ ระบบจึงมีการออกแบบแตกต่างกันไปตามกระบวนการดูดซัมของ H_2S

หลังจากที่ H_2S ถูกกำจัดออกจากก๊าซแล้ว H_2S จะถูกแยกซัลเฟอร์ออกอีกครั้งหนึ่งเพื่อเหตุผลทางสิ่งแวดล้อม แต่เนื่องจากวัสดุชีวมวลจะมีปริมาณซัลเฟอร์ต่ำ หน่วยแยกซัลเฟอร์จึงไม่มีความจำเป็นในแง่ของการนำซัลเฟอร์ที่แยกออกมาได้ไปขายเพื่อเพิ่มรายได้

บทที่ 2
เทคโนโลยีเซลล์เชื้อเพลิง

2.1 **เทคโนโลยีเซลล์เชื้อเพลิง** [3-17]

เซลล์เชื้อเพลิง หรือ Fuel Cells เริ่มเป็นที่รู้จักและคุ้นหูคนไทยมากขึ้นจากข่าวสารความก้าวหน้าทางด้านวิทยาการและเทคโนโลยี ในการเป็นเครื่องมือที่ให้กำเนิดไฟฟ้าได้จากกระบวนการทางเคมี การใช้งานของเซลล์เชื้อเพลิงที่เริ่มแพร่หลาย คือ การใช้งานในอุปกรณ์อิเล็กทรอนิกส์แทนที่แบตเตอรี่ดังในปัจจุบัน เช่น เครื่องคอมพิวเตอร์ Notebook โทรศัพท์มือถือ ซึ่งอุปกรณ์เหล่านี้ยังไม่มีวางจำหน่าย เป็นแต่เพียงไอเดีย และเครื่องต้นแบบเท่านั้น นอกจากอุปกรณ์อิเล็กทรอนิกส์แล้ว เซลล์เชื้อเพลิงยังได้มีการกล่าวถึงมากในอุตสาหกรรมยานยนต์ คือ รถยนต์ไฟฟ้าต้นแบบนั้น ส่วนใหญ่แล้ว เป็นรถที่ขับเคลื่อนด้วยไฟฟ้าจากเซลล์เชื้อเพลิง หรือใช้ระบบไฮบริด ระหว่างเซลล์เชื้อเพลิงและแบตเตอรี่เซลล์เชื้อเพลิงให้กำเนิดกระแสไฟฟ้าได้โดยอาศัยปฏิกิริยาไฟฟ้าเคมี ซึ่งคล้ายกับหลักการทำงานของแบตเตอรี่ เพียงแต่แบตเตอรี่มีอายุการใช้งานที่แน่นอน ทำหน้าที่เป็นตัวเก็บประจุ และจ่ายประจุ ในการใช้งานจึงต้องทำการชาร์จไฟก่อนนำไปใช้งาน และต้องชาร์จไฟใหม่เมื่อหมดแรงดัน กระแสไฟฟ้าที่เกิดขึ้นในเซลล์เชื้อเพลิงนั้นมาจากการเกิดออกซิเดชันและรีดักชันที่ขั้วไฟฟ้าแต่ละด้าน เมื่อต่อขั้วไฟฟ้าจะก่อให้เกิดการไหลเวียนของอิเล็กตรอน โดยทั่วไปแล้วเชื้อเพลิง (fuel) ที่เป็นตัวอย่างของปฏิกิริยาเคมีคือ ก๊าซไฮโดรเจน และมีก๊าซออกซิเจนเป็นสารออกซิแดนต์ ปฏิกิริยารีดักชันของก๊าซออกซิเจนนั้นเกิดขึ้นที่ขั้วคาโทดและปฏิกิริยาออกซิเดชันของไฮโดรเจนเกิดขึ้นที่ขั้วอาโนดอิเล็กตรอนจึงไหลจากขั้วอาโนดผ่านวงจรไปที่ขั้วคาโทดเพื่อทำปฏิกิริยาดังแสดงในรูปที่ 2.1

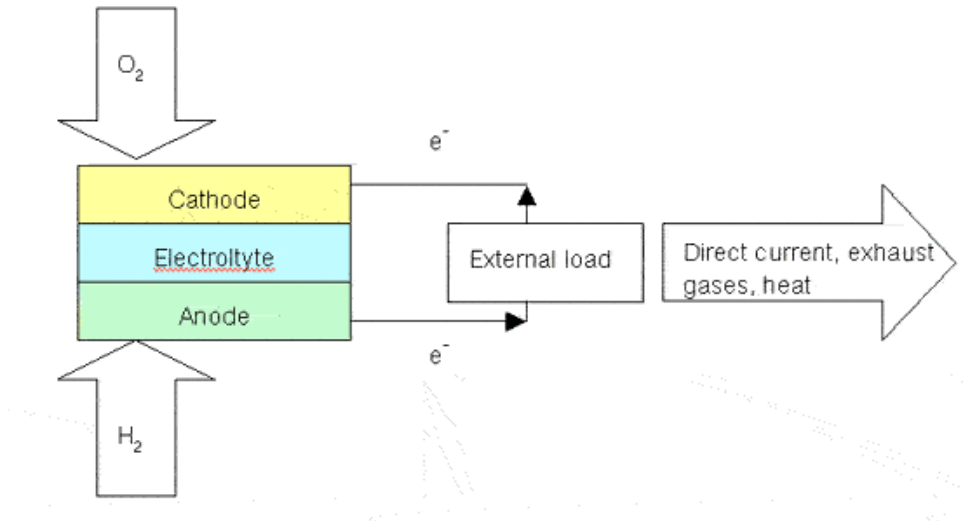

รูปที่ 2.1 ส่วนประกอบหลัก และการทำงานของเซลล์เชื้อเพลิง

ปฏิกิริยาของเซลล์เชื้อเพลิงนั้นมีการรายงานครั้งแรกโดยศาสตราจารย์คริสเตียน เฟรเดอริก เชอนบาย (Christian Friedrich Schoenbein) ในปี ค.ศ.1839 ว่ามีกระแสไฟฟ้าเกิดขึ้นจากปฏิกิริยาระหว่างไฮโดรเจนและออกซิเจน โดยใช้กรดซัลฟุริก และลวดแพลตินัม เซอร์วิลเลียม โกรว์ฟ (Sir William Grove) รายงานในอีก 1 เดือนถัดมาถึง แบตเตอรี่ที่ใช้แพลตินัมและสังกะสี เมื่อใช้กรดซัลฟุริกและไนตริกเป็นอิเล็กโตรไลต์ ซึ่งถือว่าเป็นเซลล์เชื้อเพลิงเครื่องแรกในโลก หลังจากนั้นก็ได้มีการพัฒนาขึ้นมาอย่างรวดเร็วอีกครั้งในกลางศตวรรษที่ 20 ประสิทธิภาพของเซลล์เชื้อเพลิงนั้นได้จากประสิทธิภาพทางเคมี โดยอาศัยหลักการทางเทอร์โมไดนามิก ไม่เกี่ยวข้องกับวัฏจักรคาร์โนต์ (Carnot cycle) ที่เป็นตัวควบคุมประสิทธิภาพการทำงานในเครื่องกำเนิดพลังงานจากความร้อน เช่น ระบบกังหันก๊าซ และเครื่องยนต์สันดาปภายใน เนื่องจากกระแสไฟฟ้าที่ผลิตได้จากปฏิกิริยาเคมีโดยตรง ประสิทธิภาพการทำงานจึงสูงถึง 85 % ในทางทฤษฎี ทั้งนี้เชื้อเพลิงที่นำมาใช้จะต้องนำมาคิดหาค่าประสิทธิภาพที่แท้จริงด้วยหากต้องมีการแปรสภาพก่อนการใช้งาน เซลล์เชื้อเพลิงจำแนกออกได้หลายระบบ ขึ้นอยู่กับอิเล็กโตรไลต์ โดยทั่วไปแล้วจะจำแนกได้เป็น 5 ประเภท คือ

1. Alkaline Fuel Cell (AFC) อิเล็กโตรไลต์ที่ใช้คือ โปแตสเซียมไฮดรอกไซด์เหลว โดยจะต้องใช้ก๊าซออกซิเจนบริสุทธิ์และก๊าซไฮโดรเจนบริสุทธิ์เท่านั้น การใช้งานจำกัดอยู่ในงานทางด้านอวกาศ เช่น ในยานอวกาศอพอลโล อุณหภูมิที่ใช้อยู่ในช่วง 60-120 องศาเซลเซียส

2. Phosphoric Acid Fuel Cell (PAFC) ใช้กรดฟอสฟอริกเป็นอิเล็กโตรไลต์ สามารถทนต่อก๊าซเจือปนได้มากกว่าแบบ AFC แต่ก็ยังใช้เชื้อเพลิงและออกซิแดนต์ชนิดเดียวกัน อุณหภูมิการใช้งานอยู่ที่ประมาณ 200 องศาเซลเซียส ปัญหาของเซลล์เชื้อเพลิงชนิดนี้คือ การกัดกร่อนของกรดที่อุณหภูมิการใช้งาน ในปัจจุบันได้มีการใช้ในเชิงพาณิชย์แล้ว โดยมีขนาดกำลังไฟฟ้า ประมาณ 200 กิโลวัตต์

3. Polymer Membrane Fuel Cell (PMFC) or Polymer Electrolyte Fuel Cell (PEFC) เป็นชนิดที่ใช้โพลิเมอร์เมมเบรนเป็นอิเล็กโตรไลต์ ดังนั้นจึงไม่มีปัญหากับของเหลวอิเล็กโตรไลต์ที่กัดกร่อนเพราะของเหลวชนิดเดียวภายในเซลล์คือ น้ำ เซลล์ชนิดนี้ใช้งานที่อุณหภูมิไม่เกิน 120 องศาเซลเซียส ใช้ก๊าซไฮโดรเจนและออกซิเจนในการทำปฏิกิริยา เป็นเซลล์เชื้อเพลิงที่นำมาใช้กับรถยนต์ไฟฟ้า และอุปกรณ์อิเล็กทรอนิกส์ นอกจากนี้ได้มีการพัฒนาเมมเบรนโพลิเมอร์เพิ่มเติม เพื่อให้สามารถจ่ายกระแสไฟฟ้าได้จากเชื้อเพลิงเมทานอล โดยไม่ต้องเปลี่ยนเป็นไฮโดรเจนก่อน จึงเรียกเซลล์เชื้อเพลิงชนิดใหม่นี้ว่า เซลล์เชื้อเพลิงที่ใช้เมทานอลได้โดยตรง (Direct Methanol Fuel Cell) เพราะอุณหภูมิการใช้งานค่อนข้างต่ำจึงใช้เวลาในการเริ่มเดินเครื่องน้อยกว่าประเภทอื่น บริษัทรถยนต์ต่าง ๆ ตระหนักถึงปัญหาทางด้านสิ่งแวดล้อมที่เกิดจากการเผาไหม้ของเครื่องยนต์ จึงได้มีการพัฒนา PMFC เพื่อใช้ในรถยนต์สำหรับอนาคตซึ่งได้เริ่มทำมาหลายปีแล้ว คาดว่าในอนาคตอันใกล้นี้ จะมี

รถยนต์เซลล์เชื้อเพลิงออกสู่ตลาดในเชิงพานิชย์ ทั้งในรูปของรถยนต์นั่งส่วนบุคคล และรสบัส บริษัทที่มีการพัฒนาเช่น Daimler Chrysler โตโยต้า ฟอร์ด จีเอ็ม ฮอนด้า นิสสัน และมาสด้า เพื่อนำมาใช้ในการขับเคลื่อน เซลล์เชื้อเพลิงชนิดนี้ประกอบด้วยเมนเบรนโพลิเมอร์ของแข็งซึ่งทำหน้าที่เป็นอิเล็กโทรไลท์ ซึ่งจะถูกประกบด้วยขั้วอิเลคโทรดสองขั้วที่มีความพรุนตัวและมีตัวเร่งปฏิกิริยาที่เป็นแพลนทินัม เกาะอยู่ เซลล์เชื้อเพลิงแบบนี้ต้องใช้ก๊าซไฮโดเจนและออกซิเจนที่มีความชื้น ชั้นเมมเบรนโพลิเมอร์ที่ถูกประกบทั้งสองด้านด้วยขั้วอิเลคโทรด อิเล็กโทรดจะถูกเร่งปฏิกิริยาด้วยแพลนทินัม หรือโลหะผสมของแพลนทินัม เพื่อให้ปฏิกิริยาเคมีไฟฟ้าทั้งขั้วแอโนค และขั้วแคโทด **สามารถดำไปอย่างรวดเร็ว** จากการศึกษาของศูนย์วิจัยเคมีไฟฟ้าและ ไฮโดรานของมหาวิทยาลัย TAXAS A&M ได้แสดงให้เห็นว่าโลหะผสมแพลนทีนัมที่เจาะอยู่บนตัวรองรับคาร์บอน (Pt + Fe Pt -Mn Pt - Ni Pt - Co) ช่วยทำให้สมรรถนะการทำงานของอิเล็กโทรดในแง่การเร่งปฏิกิริยาเคมีไฟฟ้าสูงขึ้น ทั้งนี้เนื่องมาจากพฤติกรรมการดูดซับทางเคมี ของออกซิเจนกับแพลทินัมกับโลหะผสมแพลทินัมจะแตกต่างกันที่ค่าความศักดิ์ที่มากกว่า 0.8 V

4. <u>Molten Carbonate Fuel Cell (MCFC)</u> อิเล็กโตรไลต์ที่ใช้เป็นพวกเกลือคาร์บอเนตหลอมของโซเดียม และโปแตสเซียมในเซรามิกเมตริกของ ลิเทียมอลูมิเนต (LiAlO2) โดยอุณหภูมิที่ใช้งานอยู่ที่ประมาณ 650 องศาเซลเซียส ดังนั้นปัญหาจากการกัดกร่อนจึงมีความสำคัญมาก เนื่องจากการใช้งานที่อุณหภูมิค่อนข้างสูง สารไฮโดรคาร์บอนต่าง ๆ จึงสามารถนำมาใช้เป็นเชื้อเพลิงได้ เซลล์เชื้อเพลิงชนิดนี้ นิยมใช้เป็นโรงไฟฟ้าขนาดเมกกะวัตต์จึงจะเหมาะสมกับประสิทธิภาพการทำงานเนื่องจากระบบที่ใช้ค่อนข้างซับซ้อน

5. <u>Solid Oxide Fuel Cell (SOFC)</u> เป็นเซลล์เชื้อเพลิงที่ใช้สารเซรามิกเป็นอิเล็กโตรไลต์ ซึ่งสารที่ใช้มากคือ สารประกอบของเซอร์โคเนีย โดยใช้งานที่อุณหภูมิ 650-1000 องศาเซลเซียส ขึ้นอยู่กับการออกแบบและสารที่ใช้เป็นอิเล็กโตรไลต์ เช่นเดียวกับเซลล์เชื้อเพลิงแบบเกลือคาร์บอเนตหลอม สารไฮโดรคาร์บอนต่าง ๆ สามารถนำมาใช้เป็นเชื้อเพลิงได้ และออกซิเจนในอากาศนำมาใช้เป็นออกซิแดนต์ได้ PMFC นั้นเป็นประเภทที่ถูกเลือกใช้ในด้านยานยนต์ มีเพียง BMW เท่านั้นที่ต้องการใช้เซลล์เชื้อเพลิงแบบออกไซด์ของแข็ง (SOFC) มาใช้เป็นระบบจ่ายไฟโดยไม่ได้ใช้ในการขับเคลื่อน โดยรวมแล้ว SOFC ได้มีการพัฒนาให้ใช้เป็นเครื่องกำเนิดกระแสไฟฟ้าทั้งขนาดเล็กภายในครัวเรือน 1-2 kW โดยบริษัท Sulzer Hexis สวิสเซอร์แลนด์ หรือบริษัท Ceramic Fuel Cells Limited ของออสเตรเลียที่มีขนาดหลายสิบกิโลวัตต์ขึ้นไป เครื่องกำเนิดกระแสไฟฟ้าในชุมชนเช่นของ บริษัท Siemens Westinghouse ของสหรัฐอเมริกา มีแนวโน้มการพัฒนาเซลล์เชื้อเพลิงชนิดนี้เพื่อเป็นโรงไฟฟ้าขนาดย่อม ในช่วงหลักร้อยกิโลวัตต์ ถึงเมกะวัตต์ โดยในอนาคตจะพัฒนาให้ทำงานร่วมกับการผลิตไฟฟ้าด้วยกังหันก๊าซ หรือกังหันไอน้ำด้วยความร้อนที่เหลือจากปฏิกิริยาในเซลล์

ตารางที่ 2.1: Main types of fuel cells

Fuel cell type	Abbreviation	Electrolyte	Operating temperature, °C
Alkaline	AFC	Potassium hydroxide	50–90
Proton Exchange Membrane	PEMFC	Solid proton conducting polymer	50–125
Phosphoric acid	PAFC	Orthophosphoric acid	190–210
Molten carbonate	MCFC	Lithium/potassium carbonate mixture	630–650
Solid oxide	SOFC	Stabilised zirconia	700-1100
Direct methanol	DMFC	Sulphuric acid or solid polymer	50–120

ตารางที่ 2.2: Electrocatalysts in fuel cell systems

Fuel cell	Anode catalyst	Cathode catalyst
AFC	Pt/Au, Pt, Ag	Pt/Au, Pt, Ag
PEMFC	Pt, Pt/Ru	Pt
PAFC	Pt	Pt/Cr/Co, Pt/Ni
MCFC	Ni, Ni/Cr	Li/NiO
SOFC	Ni/ZrO_2	$LaSrMnO_3$

ตารางที่ **2.3**: Anode and cathode reactions and net ion transport in the electrolyte of fuel cells

Fuel cell	Anode reaction	Net ion transport	Cathode reaction
AFC	$H_2 + 2OH^- \rightarrow 2H_2O + 2e^-$	OH^-	$O_2 + 2H_2O + 4e^- \rightarrow 4OH^-$
PEMFC	$H_2 \rightarrow 2H^+ + 2e^-$	H^+	$O_2 + 4H^+ + 4e^- \rightarrow 2H_2O$
PAFC	$H_2 \rightarrow 2H^+ + 2e^-$	H^+	$O_2 + 4H^+ + 4e^- \rightarrow 2H_2O$
MCFC	$H_2 + CO_3^{2-} \rightarrow H_2O + CO_2 + 2e^-$ $CO + CO_3^{2-} \rightarrow 2CO_2 + 2e^-$	CO_3^{2-}	$O_2 + 2CO_2 + 4e^- \rightarrow 2CO_3^{2-}$
SOFC	$H_2 + O^{2-} \rightarrow H_2O + 2e^-$ $CO + O^{2-} \rightarrow CO_2 + 2e^-$	O^{2-}	$O_2 + 4e^- \rightarrow 2\ O^{2-}$

โดยสรุปแล้วการจำแนกประเภทของเซลล์เชื้อเพลิงทั้ง 5 ชนิดนี้ จะแบ่งได้อย่างคร่าวเป็นประเภทที่ใช้งานที่อุณหภูมิต่ำ คือ AFC PAFC และ PMFC ซึ่งต้องใช้แพลตินัมเป็นตัวเร่งปฏิกิริยา และใช้ก๊าซไฮโดรเจนเป็นเชื้อเพลิง ในขณะที่เซลล์เชื้อเพลิงที่ทำงานที่อุณหภูมิสูง MCFC และ SOFC สามารถใช้สารไฮโดรคาร์บอนเป็นเชื้อเพลิงได้ และไม่ต้องใช้แพลตินัมเป็นตัวเร่งปฏิกิริยา จึงสามารถลดค่าใช้จ่ายลงได้

มาก ลักษณะการใช้งานของเซลล์เชื้อเพลิงแต่ละชนิด แตกต่างกันออกไปตามข้อดีและข้อจำกัดโดยได้ยกตัวอย่างในตารางที่ 2.4

ตารางที่ 2.4 ลักษณะการใช้งานของเซลล์เชื้อเพลิงแต่ละประเภทที่ได้มีการใช้งานแล้ว

Type	Capacity	Application
AFC	1.5 kW 12 kW	Apollo Programme Space Shuttle Orbiter
PAFC	200 kW 11 MW	Power Plant (40,000 hours at 40%LHV electric eff., 80% cogeneration) Power Plant
PEMFC	1 kW 200 kW 250 kW 2 MW < 24 W	Gemini Programme Transport bus in Canada Power Plant Power Plant (8 stacks of 125 kW each, 58 %LHV electric eff.) Mobile applications (mobile phone, laptop computer, PDA)
MCFC	2 MW	Power Plant (44% LHV eff.)
SOFC	100 kW 220 kW (180kW)	Power Plant (4000 hours at 45%LHV electric eff.) Power Plant (combined cycle with micro turbine generator 75kW, 55% eff.)

เซลล์เชื้อเพลิงจัดว่าเป็นมิตรกับสิ่งแวดล้อมโดยเฉพาะถ้าใช้ก๊าซไฮโดรเจนเป็นเชื้อเพลิง จะไม่ก่อให้เกิดมลพิษเลยเพราะสิ่งที่ได้ออกมานั้นคือ น้ำบริสุทธิ์ ซึ่งสามารถใช้บริโภคได้ในกรณีของนักบินอวกาศ ก๊าซพิษอื่น ๆ เช่น NOx และ SOxจะมีปริมาณน้อยกว่าที่เกิดจากเครื่องกำเนิดไฟฟ้าจากความร้อน เพราะอุณหภูมิที่ใช้ต่ำกว่ามาก นอกจากเรื่องมลพิษนี้แล้ว ไม่มีส่วนใดในเซลล์ที่เคลื่อนที่จึงไม่ก่อให้เกิดเสียงดังรบกวน สามารถติดตั้งไว้ในเมืองหรือแหล่งชุมชนได้ แม้ในบ้านเรือนที่มีพื้นที่จำกัดก็สามารถนำมาติดตั้งได้ เพราะใช้พื้นที่น้อย และแบ่งการใช้งานเป็นแบบโมดูล จึงช่วยเพิ่มประสิทธิภาพการทำงานแม้ว่าจะใช้กำลังไฟต่างกัน ประสิทธิภาพการทำงานของเซลล์เชื้อเพลิงแบบอุณหภูมิสูงนั้น หากนำมาประกอบการใช้งานกับเครื่องยนต์แบบกังหันก๊าซ จะช่วยเพิ่มประสิทธิภาพได้อีก จนคาดว่าอาจสูงถึง 75 %

ถึงแม้ว่าเซลล์เชื้อเพลิงจะมีข้อดีมากมาย แต่ในขณะนี้รถยนต์เซลล์เชื้อเพลิงยังมีราคาที่สูงมากกว่าเครื่องยนต์สันดาปภายในอยู่หลายเท่า จึงต้องมีการวิจัยและพัฒนาทางด้านวิศวกรรมเพื่อค้นหาวิธีการผลิตและประกอบที่มีประสิทธิภาพดี เหมาะสมที่สุดเพื่อนำมาใช้ในเชิงพานิชย์ ในอนาคตอันใกล้นี้ เซลล์เชื้อ

เพลิงที่จะเข้ามามีบทบาทในชีวิตประจำวันก็คือ ยานยนต์เพื่อสิ่งแวดล้อม และในเวลาต่อไปจึงจะเป็นเครื่องกำเนิดกระแสไฟฟ้า ที่จะค่อย ๆ เข้ามาแทนที่เครื่องกำเนิดกระแสไฟฟ้าประสิทธิภาพต่ำและก่อมลภาวะในปัจจุบัน

2.2. ข้อจำกัดในเชิงเทคนิค และเชิงเศรษฐศาสตร์สำหรับเซลล์เชื้อเพลิง

จากรายงานความก้าวหน้าของเทคโนโลยีเซลล์เชื้อเพลิงของสหรัฐอเมริกาในปีคศ. 2003 (Fuel Cell Report to Congrass 2003) ข้อจำกัดในเชิงเทคนิค และเชิงเศรษฐศาสตร์สำหรับการพัฒนาเซลล์เชื้อเพลิงทุกประเภทเพื่อประโยชน์ในเชิงพานิชย์ซึ่งประกอบด้วยเซลล์เชื้อเพลิงที่ใช้ประโยชน์ในโรงงานอุตสาหกรรมหรืออาคารบ้านเรือน (Stationary Applications) เซลล์เชื้อเพลิงที่ใช้ประโยชน์ในการขับเคลื่อนของเครื่องยนต์ (Transportation Applications) และเซลล์เชื้อเพลิงที่ใช้ประโยชน์ในงานที่พกพาได้ (Portable Applications) มีความสัมพันธ์กันอย่างมาก ข้อจำกัดที่สำคัณทั้งหลายมีดังนี้

2.2.1. ข้อจำกัดเรื่องราคา (Cost)

ราคาเป็นข้อจำกัดของเซลล์เชื้อเพลิงทุกประเภทและทุกการใช้งาน มีรายงานว่าในปัจจุบันราคาค่าไฟฟ้าต่อหน่วยที่ผลิตจากเซลล์เชื้อเพลิงสูงถึง 500 ถึง 10,000 US dollars ต่อ kW ในขณะที่ราคาไฟฟ้าที่ผลิตได้จาก Gas Turbine อยู่ที่ 400 ถึง 600 US dollars ต่อ kW ซึ่งค่อนข้างต่างกันมาก ในปัจจุบันมีความพยายามที่จะลดค่าใช้จ่ายทั้งในการสร้างเซลล์เชื้อเพลิงและในการผลิตกระแสไฟฟ้าจากเซลล์เชื้อเพลิงลงโดยศึกษาถึงการใช้วัสดุราคาถูกลงในการสร้างเซลล์เชื้อเพลิงหรือการลดปริมาณการใช้วัสดุที่มีราคาแพงลง ในส่วนของการผลิตกระแสไฟฟ้าโดยเซลล์เชื้อเพลิงนั้นมีความพยายามมากมายที่จะลดการใช้พลังงานของเซลล์เชื้อเพลิงระหว่างการทำงานลงหรือการทำให้ประสิทธิภาพของเซลล์เชื้อเพลิงในการผลิตกระแสไฟฟ้าดีขึ้นวิธีการที่มีการศึกษากันอยู่ที่สำคัญเช่น การรวมหน่วยผลิตไฮโดรเจน (Reformer) เข้ากับเซลล์เชื้อเพลิงเพื่อให้เกิดการแลกเปลี่ยนความร้อนซึ่งกันและกัน (Internal Reforming) และสามารถลดปริมาณพลังงานที่ต้องจ่ายลง นอกจากนี้ยังมีการศึกษาการออกแบบเซลล์เชื้อเพลิงให้สามารถผลิตกระแสไฟฟ้าได้อย่างมีประสิทธิภาพมากที่สุด

2.2.2. ข้อจำกัดด้านเสถียรภาพ และประสิทธิภาพ

เพื่อจะแข่งขันกับเทคโนโลยีผลิตพลังงานอื่นๆ ประสิทธิภาพและอายุการใช้งานของเซลล์เชื้อเพลิงเป็นปัจจัยที่สำคัญอย่างหนึ่งในเชิงพานิชย์ โดยปรกติแล้วอายุการใช้งานของอุปกรณ์ผลิตไฟฟ้าเพื่อประโยชน์ในโรงงานอุตสาหกรรมหรืออาคารบ้านเรือน (Stationary Applications) ควรจะมีสูงกว่า 40,000 ชั่วโมง ในส่วนของอุปกรณ์เพื่อใช้ประโยชน์ในการขับเคลื่อนของเครื่องยนต์

(Transportation Applications) ควรจะมีสูงกว่า 5,000 ชั่วโมง ซึ่งข้อจำกัดซึ่งทำให้เซลล์เชื้อเพลิงมีอายุการทำงานสั้นลงกว่าที่ควรจะเป็นมีดังนี้

สำหรับเซลล์เชื้อเพลิงแบบ Polymer Membrane Fuel Cell (PMFC) or Polymer Electrolyte Fuel Cell (PEFC) ซึ่งใช้งานที่อุณหภูมิต่ำและใช้แพทตินั่ม (Pt) เป็นตัวเร่งปฏิกิริยามักจะประสบปัญหาการลดประสิทธิภาพของเซลล์เชื้อเพลิงหากมีคาร์บอนมอนอกไซด์ปะปนเข้ามากับก๊าซขาเข้าด้วย นอกจากคาร์บอนมอนออกไซด์แล้วการมีสารประกอบซัลเฟอร์ปะปนเข้ามาก็ส่งผลให้การทำงานของเซลล์เชื้อเพลิงลดลงมากเช่นกัน ในส่วนของเซลล์เชื้อเพลิงแบบ Molten Carbonate Fuel Cell (MCFC) และแบบSolid Oxide Fuel Cell (SOFC) นั้นจะไม่ประสบปัญหาการ Deactivation โดยคาร์บอนมอนออกไซด์มากนัก แต่ซัลเฟอร์กับยังคงเป็นปัญหาหลักที่ทำให้ประสิทธิภาพการทำงานของเซลล์ลดลง นอกจากนั้นการเจือปนของสารประกอบอัลคาไลด์ (Alkali) จะทำให้ประสิทธิภาพในการผลิตกระแสไฟฟ้าของเซลล์เชื้อเพลิงแบบ Molten Carbonate Fuel Cell (MCFC) ลดลงไปมากเช่นกัน ในส่วนของเซลล์เชื้อเพลิงแบบ Solid Oxide Fuel Cell (SOFC) ซึ่งมีช่วงอุณหภูมิของการใช้งานที่สูงนั้นจะประสบปัญหาเกี่ยวกับการขยายตัวของวัสดุที่ใช้ซึ่งอาจทำให้เซลล์แตกได้

2.2.3. ข้อจำกัดของเชื้อเพลิงที่ใช้

ดังที่กล่าวมาแล้ว เซลล์เชื้อเพลิงทำงานโดยใช้ไฮโดรเจนเป็นเชื้อเพลิงหลัก การใช้ประโยชน์จากไฮโดรเจนสำหรับเซลล์เชื้อเพลิงเพื่อใช้งานในเชิงพานิชย์ยังต้องการการศึกษาวิจัยเพื่อพัฒนาทั้งระบบการผลิต การเก็บและการขนส่งเพื่อให้มีราคาที่ถูกลง ปลอดภัย และสามารถนำไปใช้ได้อย่างสะดวกขึ้น โดยรายละเอียดเกี่ยวกับข้อจำกัดต่างๆ ของการใช้ไฮโดรเจนมีดังนี้

2.2.3.1. ข้อจำกัดของระบบการผลิตไฮโดรเจน

ในปัจจุบันราคาต่อหน่วยของไฮโดรเจนที่ผลิตได้จากแหล่งพลังงานฟอสซิลเช่นก๊าซธรรมชาติยังมีราคาสูงกว่าเชื้อเพลิงตัวอื่นๆ ซึ่งทำให้ราคาค่าไฟฟ้าต่อหน่วยที่ผลิตได้จากเซลล์เชื้อเพลิงสูงตามไปด้วย ไฮโดรเจนที่ผลิตได้จากแหล่งพลังงานฟอสซิลจะมาจากกระบวนการรีฟอร์มิ่ง หรือก๊าซซิฟิเคชั่นซึ่งกระบวนการเหล่านี้ยังต้องการการพัฒนาและปรับปรุงอีกมากเพื่อให้สามารถผลิตไฮโดรเจนได้อย่างมีประสิทธิภาพมากกว่าที่เป็นอยู่ในปัจจุบัน

ในส่วนของการผลิตไฮโดรเจนจากแหล่งพลังงานทดแทน (Renewable Energy) เช่นจากแหล่งพลังงานลม เซลล์แสงอาทิตย์หรือจากวัสดุชีวมวลนั้นการพัฒนายังคงอยู่ในระยะเบื้องต้น และต้องการการศึกษาพัฒนาอีกมากเพื่อประโยชน์ในเชิงพานิชย์ อีกปัญหา

หนึ่งทำให้การพัฒนาการผลิตไฮโดรเจนยังไม่ดีเท่าที่ควรคือคือตลาดหรือความต้องการการใช้ไฮโดรเจนในปัจจุบันนี้ยังน้อยอยู่

2.2.3.2. ข้อจำกัดของระบบการขนส่งไฮโดรเจน

การที่จะใช้ประโยชน์จากไฮโดรเจนในเชิงพานิชย์จำเป็นที่จะต้องมีระบบการขนส่งหรือแจกจ่าย (Delivery) ที่ดี ซึ่งระบบและวิธีการขนส่งไฮโดรเจนที่ทำการศึกษาอยู่ในปัจจุบันยังมีราคาแพง และมีความอันตรายค่อนข้างมาก โดยเฉพาะอย่างยิ่งการขนส่งไฮโดรเจนเพื่อใช้ประโยชน์ในงานขนาดเล็ก (Small Scale Application) นั้นยังไม่คุ้มค่าเนื่องจากมีราคาค่าขนส่งที่สูงมาก

2.2.3.3. ข้อจำกัดของระบบกักเก็บไฮโดรเจน

ระบบการกักเก็บไฮโดรเจนยังจำเป็นที่จะต้องมีการศึกษาวิจัยอีกเพื่อให้ประสิทธิภาพในการเก็บดีขึ้น (High Density Storage) และราคาถูกลง การกักเก็บไฮโดรเจนโดยวิธีอัดความดันหรือทำให้เป็นไฮโดรเจนเหลว (Liquid Hydrogen) เป็นวิธีที่เหมาะสมสำหรับการใช้งานในการขับเคลื่อนหรือรถยนต์ (Vehicle Application) แต่ราคาของถังกักเก็บยังคงสูงอยู่มาก ในปัจจุบันนี้มีงานวิจัยด้านวัสดุศาสตร์ที่พยายามเพิ่มประสิทธิภาพในการเก็บไฮโดรเจนให้ดีขึ้นโดยใช้วิธี Hyydrides และ Carbon Adsorption Materials

2.2.3.4. ข้อจำกัดในแง่ของระบบควบคุม

การทำงานของเซลล์เชื้อเพลิงประกอบด้วยส่วนต่างๆ มากมายซึ่งจำเป็นต้องมีระบบการควบคุมที่ดี อาทิเช่นระบบควบคุมเชื้อเพลิงที่ใช้ ระบบควบคุมการทำงานของเซลล์เชื้อเพลิงที่ประกอบกัน (Cell Stacks) และระบบต่างๆ ที่เกี่ยวข้อง (เช่น Compressor, pumps, humidifier, heat exchanger, sensor, control เป็นต้น) ซึ่งในปัจจุบันยังไม่มีการศึกษาและรายงานผลความสำเร็จในเรื่องเหล่านี้มากนัก

ตัวอย่างสำคัญที่จำเป็นต้องมีการศึกษาเพื่อจะใช้เซลล์เชื้อเพลิงในเชิงพานิชย์คือการการศึกษาระบบต่างๆ ที่เกี่ยวข้องกับเซลล์เชื้อเพลิงดังที่กล่าวมา การศึกษาระบบควบคุมความร้อนและการใช้น้ำซึ่งสำคัญมากสำหรับการใช้งานของเซลล์เชื้อเพลิงชนิด Polymer Membrane Fuel Cell (PMFC) ซึ่งทำงานที่อุณหภูมิต่ำ และจำเป็นต้องใช้อากาศและเชื้อเพลิงที่ชื้นเพื่อให้เซลล์สามารถทำงานได้อย่างมีประสิทธิภาพ

2.3. สถานภาพของระดับความก้าวหน้าด้านเทคนิคของ Technology

ดังที่ได้กล่าวมา เซลล์เชื้อเพลิงชนิดต่างๆ ได้รับความสนใจจากบริษัทและโรงงานอุตสาหกรรมต่างๆมากมายทั่วโลก ซึ่งมีบริษัทมากมายนำเซลล์เชื้อเพลิงมาใช้ประโยชน์ในเชิงพาณิชย์แล้ว สถานภาพโดยรวมของการใช้งานเซลล์เพลิงชนิดต่างๆ ในปัจจุบันมีดังนี้

ในส่วนของการใช้เซลล์เชื้อเพลิงเป็นแบตเตอรี่สำหรับคอมพิวเตอร์ขนาดเล็ก และโทรศัพท์มือถือนั้น Fraunhofer Institute, บริษัท Motorola, และบริษัท Sanyo ได้ทำการพัฒนาอยู่ในปัจจุบันและกำลังจะมีวางขายอย่างแพร่หลายในเวลาอันสั้นซึ่งปัญหาหลักของการใช้เซลล์เชื้อเพลิงในงานประเภทนี้คือราคาซึ่งยังสูงมาก สำหรับงานวิจัยและพัฒนาการใช้เซลล์เชื้อเพลิงในงานอาคารซึ่งเน้นหลักไปที่การใช้งานของเซลล์เชื้อเพลิงชนิด Polymer Membrane Fuel Cell (PMFC) และ Solid Oxide Fuel Cell (SOFC) นั้นประสบความสำเร็จแล้วในปัจจุบันและคาดว่าจะมีการติดตั้งใช้งานจริงในเชิงพาณิชย์ในอีก 2-3 ปีข้างหน้า

สำหรับการใช้ประโยชน์ของเซลล์เชื้อเพลิงในเครื่องยนต์นั้น งานวิจัยในปัจจุบันจะมุ่งเน้นไปที่การพยายามที่จะลดราคาต้นทุนการผลิตลง มีการคาดการณ์กับว่าจะต้องมีการผลิตรถยนต์ที่ใช้เซลล์เชื้อเพลิงในการขับเคลื่อนจำนวนมากกว่า 250,000 คันเพื่อจะทำให้ราคาต้นทุนการผลิตลดลงจนสามารถแข่งขันกับรถยนต์ที่ใช้เอยู่ในปัจจุบัน ส่วนการใช้งานของเซลล์เชื้อเพลิงในอุตสาหกรรมขนาดเล็ก และงานผลิตกระแสไฟฟ้าร่วมกับ Microturbine (Cogeneration) นั้นเซลล์เชื้อเพลิงชนิด Phosphoric Acid Fuel Cell (PAFC) มีการใช้งานจริงในเชิงพาณิชย์แล้วแต่ราคาต้นทุนการผลิตก็ยังคงเป็นปัญหาหลักซึ่งยังสูงอยู่ และมีการคาดหมายว่าเซลล์เชื้อเพลิงชนิด Polymer Membrane Fuel Cell (PMFC), Molten Carbonate Fuel Cell (MCFC) และ Solid Oxide Fuel Cell (SOFC) ขนาดเล็กจะถูกนำมาใช้แทนที่สำหรับงานประเภทนี้ในอนาคตอันใกล้

ในส่วนของงานวิจัยการใช้เซลล์เชื้อเพลิงเพื่อผลิตกระแสไฟฟ้าสำหรับงานอุตสาหกรรมขนาดใหญ่ (1-20 MW) นั้นยังคงต้องการการศึกษาวิจัย และพัฒนาอยู่เพื่อให้มีอายุการใช้งานได้นานกว่าที่ทำได้ในปัจจุบัน (มากกว่า 40,000 ชั่วโมง) โดยมีการคาดการณ์ว่าเซลล์เชื้อเพลิงจะพร้อมสำหรับการใช้งานประเภทนี้ในเชิงพาณิชย์ในอีก 5-10 ปีข้างหน้า

บทที่ 3
ตัวเร่งปฏิกิริยาสำหรับกระบวนการรีฟอร์มมิ่ง

3.1 ตัวเร่งปฏิกิริยาสำหรับกระบวนการรีฟอร์มมิ่ง

คุณสมบัติที่สำคัญสำหรับตัวเร่งปฏิกิริยาของกระบวนการรีฟอร์มมิ่งคือความสามารถในการทำปฏิกิริยา และความต้านทานต่อการเกิดคาร์บอนบนพื้นผิว นอกจากนั้นแล้วตัวเร่งปฏิกิริยาที่ดีความมีเสถียรภาพสูงเมื่อถูกใช้งานที่อุณหภูมิสูง (High Thermal Stability) และมีความต้านทานต่อการเสื่อมสภาพเนื่องจากสารปนเปื้อนบางชนิด (Poisoning) ในแง่คุณสมบัติทางกายภาพของตัวเร่งปฏิกิริยานั้นตัวเร่งปฏิกิริยาที่ดีควรมีความคงทนต่อการเสียดสี และไม่เกิดการเสียรูปเช่นการหัก หรือแตกเมื่อใช้งานซึ่งจะนำมาซึ่งการเปลี่ยนแปลงในเรื่องของคุณสมบัติการการถ่ายเทความร้อน และมวลสาร (Heat and Mass Transfer Behaviour) ได้ ในการใช้งานจริงนั้นรูปทรงของตัวเร่งปฏิกิริยาที่ดีหลังการขึ้นรูปแล้วควรจะมีพื้นที่ผิวต่อน้ำหนัก หรือปริมาตรสูง และทำให้เกิด Pressure Drop ภายในเครื่องปฏิกรณ์น้อยที่สุด [18]

สำหรับตัวเร่งปฏิกิริยาที่ใช้ในกระบวนการรีฟอร์มมิ่งเพื่อผลิตไฮโดรเจนนั้น พบว่าธาตุกรุ๊ป VIII อันประกอบด้วย Fe, Co, Ni, Rd, Ru, Pd, Os, Ir and Pt [19, 20, 21, 22] สามารถเป็นตัวเร่งปฏิกิริยาของกระบวนการดังกล่าวได้ อย่างไรก็ตามได้มีรายงานมากมายเกี่ยวข้องกับการเสื่อมศักยภาพ (Deactivation) ของตัวเร่งปฏิกิริยาเหล่านี้เมื่อใช้งานภายใต้กระบวนการดังกล่าว ซึ่งปัญหาหลักที่ทำให้ตัวเร่งปฏิกิริยาเกิดการเสื่อมศักยภาพคือการเกิดคาร์บอนบริเวณผิวของตัวเร่งปฏิกิริยา (Carbon Formation) ผ่านกระบวนการ Boudouard Reaction หรือกระบวนการ Thermal Cracking การที่สารปนเปื้อนบางชนิดเช่น Sulphur ทำปฏิกิริยากับตัวเร่งปฏิกิริยา (Catalyst Poisoning) เป็นต้น

สำหรับกระบวนการผลิตฮโดรเจนเพื่อใช้ประโยชน์ในเซลล์เชื้อเพลิงนั้นโดยทั่วไปกระบวนการผลิตไฮโดรเจนจะเกิดที่เครื่องรีฟอร์มเมอร์ (Reformer) ซึ่งมักจะเกิดคาร์บอนบริเวณผิวของตัวเร่งปฏิกิริยาและทำให้ตัวเร่งปฏิกิริยาเสื่อมศักยภาพเสมอๆ โดยเฉพาะอย่างยิ่งบริเวณทางเข้า หรือบริเวณปากทางเข้าของเครื่องรีฟอร์มเมอร์เนื่องจากมีปริมาณไฮโดรเจนบริเวณนั้นค่อนข้างต่ำ และยิ่งถ้าสารตั้งต้นที่ใช้ในการผลิตไฮโดรเจนเป็นสารประกอบไฮโดรคาร์บอนใหญ่ๆ (High Hydrocarbon) แล้วโอกาสที่จะเกิดการฟอร์มตัวของคาร์บอนบริเวณพื้นผิวของตัวเร่งปฏิกิริยาก็จะยิ่งมากขึ้น

โดยทั่วไปแล้วเพื่อป้องกันปัญหาดังกล่าวในกระบวนการผลิตไฮโดรเจนจะต้องมีกระบวนการรีฟอร์มมิ่งบางส่วนก่อนที่จะเข้าเครื่องรีฟอร์มเมอร์หลัก (Pre-Reforming unit) เพื่อใช้เปลี่ยนสารประกอบไฮโดรคาร์บอนใหญ่ๆ (High Hydrocarbon) ทั้งหมดให้กล่าวเป็นมีเทนก่อนที่จะถูกป้อนเข้าเครื่องรีฟอร์มเมอร์หลัก ซึ่งส่วน Pre-reformer ดังกล่าวจะต้องทำงานที่อุณหภูมิค่อนข้างต่ำประมาณ 250-500^{o}C [18]

เพื่อไม่ให้เกิดปัญหาการฟอร์มตัวของคาร์บอนได้ นอกจากนั้นการเติมไฮโดรเจนบางส่วนเข้าไปในเครื่องรีฟอร์มเมอร์ก็ช่วยลดปัญหาดังกล่าวได้เช่นกัน

นอกจากปัญหาการเกิดคาร์บอนที่ผิวของตัวเร่งปฏิกิริยาแล้ว การเจือปนของสารไฮโดรเจน ซัลไฟด์ (H_2S) และสาร Alkali ในสารตั้งต้นก็ทำให้ตัวเร่งปฏิกิริยาเสื่อมสภาพได้อย่างรวดเร็วเช่นกัน ดังนั้นในการใช้งานจริงนั้นมีการกำหนดไว้ว่าปริมาณไฮโดรเจร ซัลไฟด์ต้องมีค่าต่ำกว่า 0.2-wt ppm [18] ซึ่งโดยทั่วไปแล้วต้องมีระบบกำจัดไฮโดรเจน ซัลไฟด์ก่อนที่จะปล่อยก๊าซเข้าสู่ระบบรีฟอร์มเมอร์ (Desulpherization) ในการใช้งานจริง ในส่วนของสาร Alkali ที่ปนเข้ามานั้นจะมีผลกระทบต่อการเกิดปฏิกิริยารีฟอร์มมิ่งโดยสารเหล่านี้จะจับตัวบริเวณพื้นผิวของตัวเร่งปฏิกิริยา ทำให้ปฏิกิริยาที่เกิดขึ้นลดลง [23] ดังที่แสดงในตารางต่อไปนี้

ตารางที่ 3.1 Steam reforming of methane activity of alkali-promoted metal catalysts. Rates referred to unit metal surface area (turnover frequency 1.000 = 0.70 molecules/s), (H_2O/CH_4 = 4.0, H_2O/H_2 = 10)

Catalyst	Relative rate (500°C)	Activation Energy (kcal/mole)
Ni (9.1)	1.0	26
Ni (7.1), Li (1.6)	0.6	24
Ni (8.3), Na (1.3)	0.3	21
Ni (8.5), K (1.0)	0.2	25
Ru (0.4)	5.0	23
Ru (0.5), Li (1.1)	2.0	17
Ru (0.3), Na(1.3)	2.0	25
Ru (0.4), K (1.3)	0.3	24
Rh (0.5)	17	29
Rh (0.4), Li(0.2)	16	24
Rh (0.4), Na(1.3)	8.0	23
Rh (0.4), K(1.0)	0.5	34
Pt (0.5)	1.8	
Pt (0.3), Na (1.4)	0.2	

ดังที่ได้กล่าวมาในข้างต้น ธาตุกรุ๊ป VIII อันประกอบด้วย Fe, Co, Ni, Rd, Ru, Pd, Os, Ir and Pt [19, 20, 21, 22] สามารถเป็นตัวเร่งปฏิกิริยาของกระบวนการรีฟอร์มมิ่งได้ โดยจากการศึกษาในอดีตนั้น Rh และ Rd มีความทนทานต่อการเกิดคาร์บอนบริเวณพื้นผิวสูงกว่าธาตุตัวอื่นๆ แต่ราคาของสารเหล่านี้ก็ค่อนข้างแพงเช่นกันเนื่องจากเป็นสารจำพวก Noble Metal Materials ในอดีตที่ผ่านมามีการศึกษากระบวนการรีฟอรมิ่งของสารจำพวกนี้อยู่บ้าง Rostrup-Nielsen and Hansen [20] ระบุว่า Rh และ Rd มีความทน

ทานต่อการเกิดคาร์บอนบริเวณพื้นผิวสูงกว่าธาตุตัวอื่นๆ ดังแสดงในรูปที่ 3.1 จากรูปดังกล่าวพบว่าสารที่มีโอกาสเกิดคาร์บอนบริเวณพื้นผิวสูงที่สุดคือนิเกิล ซึ่งจะเกิดการฟอร์มตัวของคาร์บอนบริเวณพื้นผิวที่อุณหภูมิ 500 องศาเซลเซียส

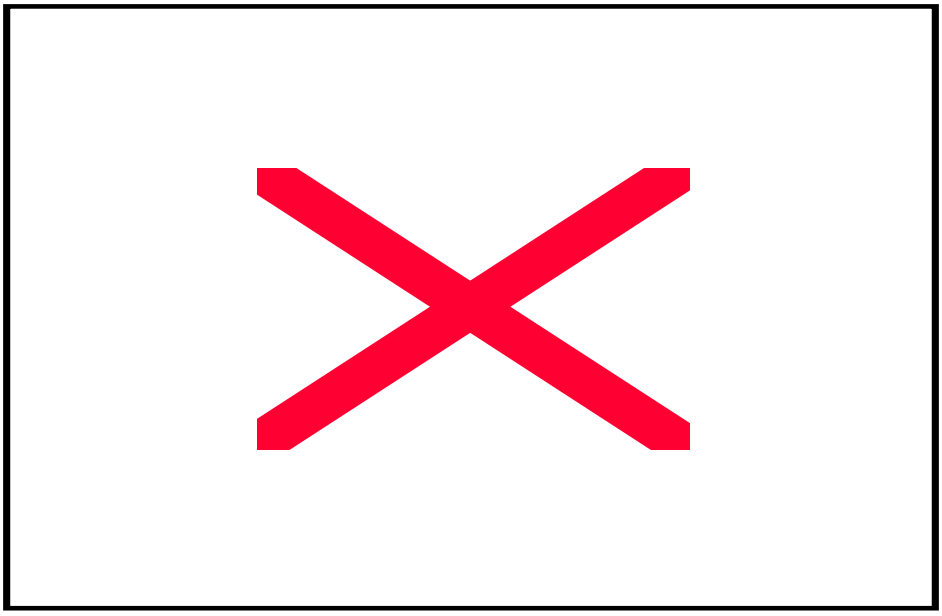

รูปที่ 3.1 Carbon formation rate over several metal catalysts at 500, and 650°C

ในอดีตที่ผ่านมามีการศึกษาผลกระทบของตัว Support ต่อกระบวนการรีฟอร์มมิ่งค่อนข้างน้อย Green and co-workers [24, 25] ศึกษากระบวนการอ๊อกซิไดซ์บางส่วน (partial oxidation) เพื่อผลิตไฮโดรเจนบนตัวเร่งปฏิกิริยา Ni, Ru, Rh, Pd, Ir, and Pt โดยจากการศึกษาได้ระบุว่าการใช้ตัว supported จำพวกอลูมินา (alumina) ทำให้ปฏิกิริยานี้เกิดได้ดีที่อุณหภูมิ 800 องศาเซลเซียส Erdohelyi et al. [26, 27] ระบุว่าชนิดของตัว Support ไม่มีผลกับการเกิดปฏิกิริยารีฟอร์มมิ่งมีเทนด้วยคาร์บอนไดออกไซด์ (Dry Reforming) บนตัวเร่งปฏิกิริยา Rh ในทางกลับกัน Nakamura et al. [28] and Zhang et al. [29] ระบุว่าชนิดของตัว Support มีผลกับการเกิดปฏิกิริยารีฟอร์มมิ่งมีเทนด้วยคาร์บอนไดออกไซด์ (Dry Reforming) อย่างมาก โดยได้มีการศึกษาชนิดของตัว Support 2 กลุ่มต่อการเกิดปฏิกิริยารีฟอร์มมิ่งมีเทนด้วยคาร์บอนไดออกไซด์ (Dry Reforming)บนตัวเร่งปฏิกิริยา Rh [29] โดยตัว Support ทั้ง 2 กลุ่มประกอบด้วยตัว Support แบบ reducible (CeO_2, Nb_2O_5, Ta_2O_5, TiO_2, and ZrO_2), และตัว Support แบบ irreducible (Al_2O_3, La_2O_3, MgO, SiO_2, and Y_2O_3) ซึ่งผลของการทดลองดังแสดงในรูปที่ 3.2 ในบรรดาตัว Support แบบ irreducible metal oxide นั้น Al_2O_3, La_2O_3 และ MgO เป็นตัว Support ที่ทำให้ปฏิกิริยารีฟอร์มมิ่งมีเทนด้วยคาร์บอนไดออกไซด์เกิดอย่างมีเสถียรภาพมากที่สุด และปฏิกิริยาดังกล่าวบนตัวเร่งปฏิกิริยา Rh บนตัว Support Al_2O_3 และ MgO จะมีค่าสูงกว่าตัวเร่งปฏิกิริยา Rh บนตัว Support La_2O_3 มาก. ส่วน

เสถียรภาพของปฏิกิริยาสำหรับ Rh บนตัว Support SiO_2 และ Y_2O_3 มีค่าต่ำกว่า Al_2O_3, La_2O_3 และ MgO มาก. ในส่วนของตัวเร่งปฏิกิริยา Rh บนตัว Support แบบ Reducible นั้นจะมีศักยภาพต่อกระบวนการรีฟอร์มมิ่งต่ำกว่าการใช้ Support แบบ Irreducible

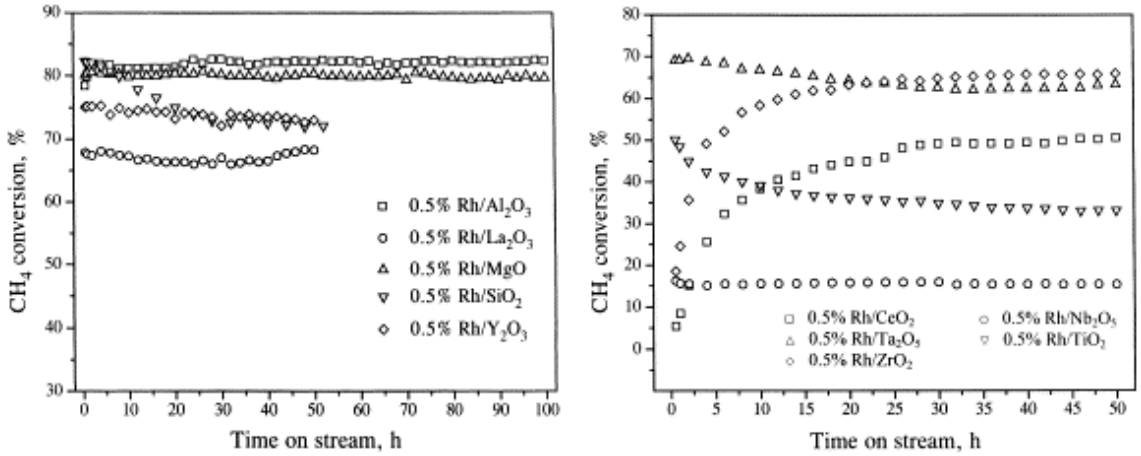

รูปที่ 3.2 Carbon dioxide reforming activity over Rh catalyst with several supports [29]

บทที่ 4
ขั้นตอนการทดลอง

4.1. การเตรียมระบบที่ใช้ในการทดลอง

ระบบการทดลองดังรูปที่ 4.1 ได้ถูกสร้างขึ้นเพื่อทำการศึกษากระบวนการรีฟอร์มมิ่งมีเทนด้วยน้ำและกระบวนการอื่นๆ ที่เกี่ยวข้อง ระบบดังกล่าวถูกออกแบบให้สามารถใช้งานเพื่อการศึกษาได้ทั้งในสภาวะระบบคงที่ (Steady State Study) และในสภาวะที่ระบบเปลี่ยนแปลงตามเวลา (Transient Study) จากรูปดังกล่าว ท่อที่ใช้ทั้งหมดทำด้วย Stainless Steel ขนาด 1/8 หรือ 1/16 นิ้ว และประกอบต่อกันด้วย non-return valves, three-way valves, elbows, reductions, expansions และ on-off valves จากบริษัท Swagelok

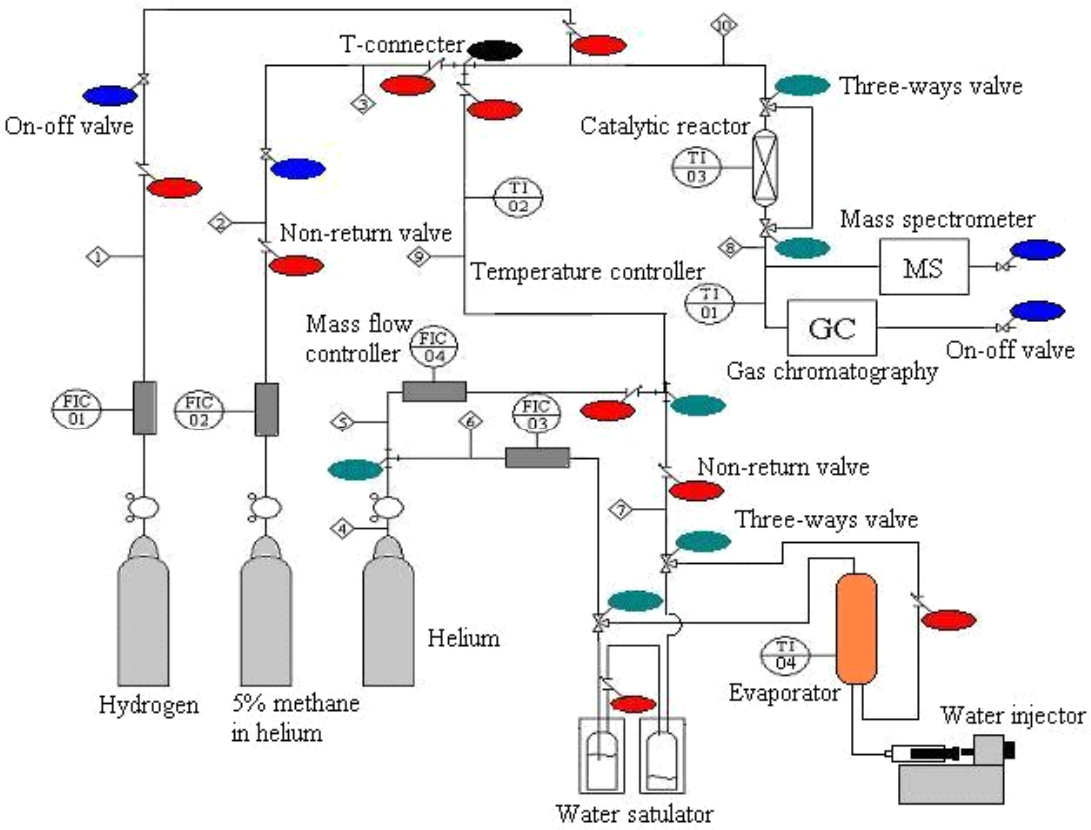

รูปที่ 4.1 ระบบที่ใช้ในการทดลอง

ระบบดังกล่าวประกอบด้วย 3 ส่วนใหญ่ๆ คือส่วน Feed สารหรือก๊าซที่ต้องการศึกษาเข้าสู่ระบบ ส่วนที่เกิดปฏิกิริยา และส่วนการวิเคราะห์ผลที่เกิดปฏิกิริยา ในส่วนแรกนั้นก๊าซแต่ละชนิดที่เกี่ยวข้องกับการทดลองซึ่งประกอบด้วยก๊าซมีเทน ไฮโดรเจน ฮีเลียม คาร์บอนไดออกไซด์ และออกซิเจนจะถูกส่งเข้าสู่ระบบโดยมี Mass Flow Controllers เป็นตัวควบคุมการไหลของก๊าซแต่ละชนิด ซึ่งก่อนการทดลองทุกครั้งต้องทำการ Calibrate เครื่อง Mass Flow Controller เหล่านี้เพื่อป้องกนความผิดพลาดที่อาจจะเกิดขึ้นเช่นการรั่วของระบบ หรือการเกิด Pressure Drop เป็นต้น

นอกจากการใช้ Mass Flow Controller ป้อนก๊าซต่างๆ เข้าสู่ระบบแล้ว ระบบนี้มีอุปกรณ์เพื่อทำการป้อนน้ำ หรือไอน้ำเข้าสู่ระบบเช่นกันเพื่อทำการศึกษากระบวนการรีฟอร์มมิ่งด้วยน้ำ โดยอุปกรณ์ดังกล่าวมี 2 ชนิดแล้วแต่ลักษณะของงานที่ทำการทดลอง ประกอบด้วยเครื่อง Saturator/Condenser และเครื่อง Evaporator ข้อดีของเครื่อง Evaporator คือสามารถป้อนไอน้ำเข้าสู่ระบบได้ในปริมาณที่คงที่และแน่นอนกว่าเครื่อง Saturator/Condenser แต่ข้อเสียของเครื่องดังกล่าวคือสามารถทำการป้อนน้ำได้เพียง 6-7 ชั่วโมงเท่านั้น (หลังจากนั้นต้องทำการเติมน้ำอีกครั้ง) ดังนั้นในการทดลองที่ต้องใช้ระยะเวลานาน เครื่อง Saturator/Condenser จะถูกใช้แทนที่ รูปที่ 4.2 และ 4.3 แสดงเครื่องมือทั้ง 2 ชนิดดังกล่าว

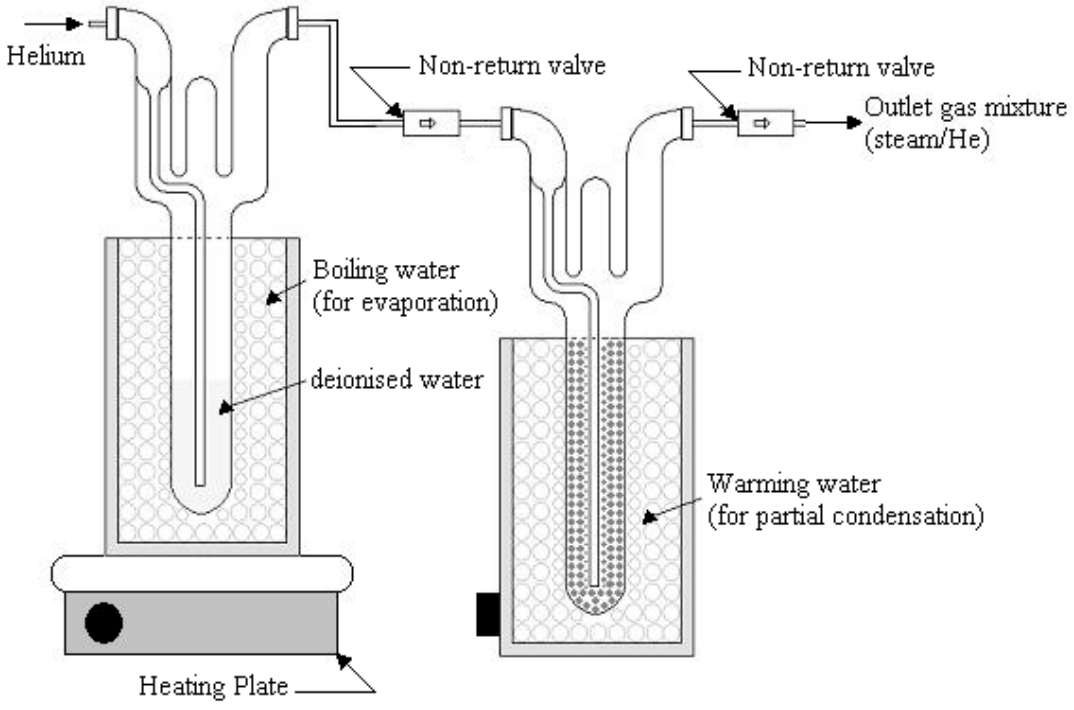

รูปที่ 4.2 Saturator/condenser system

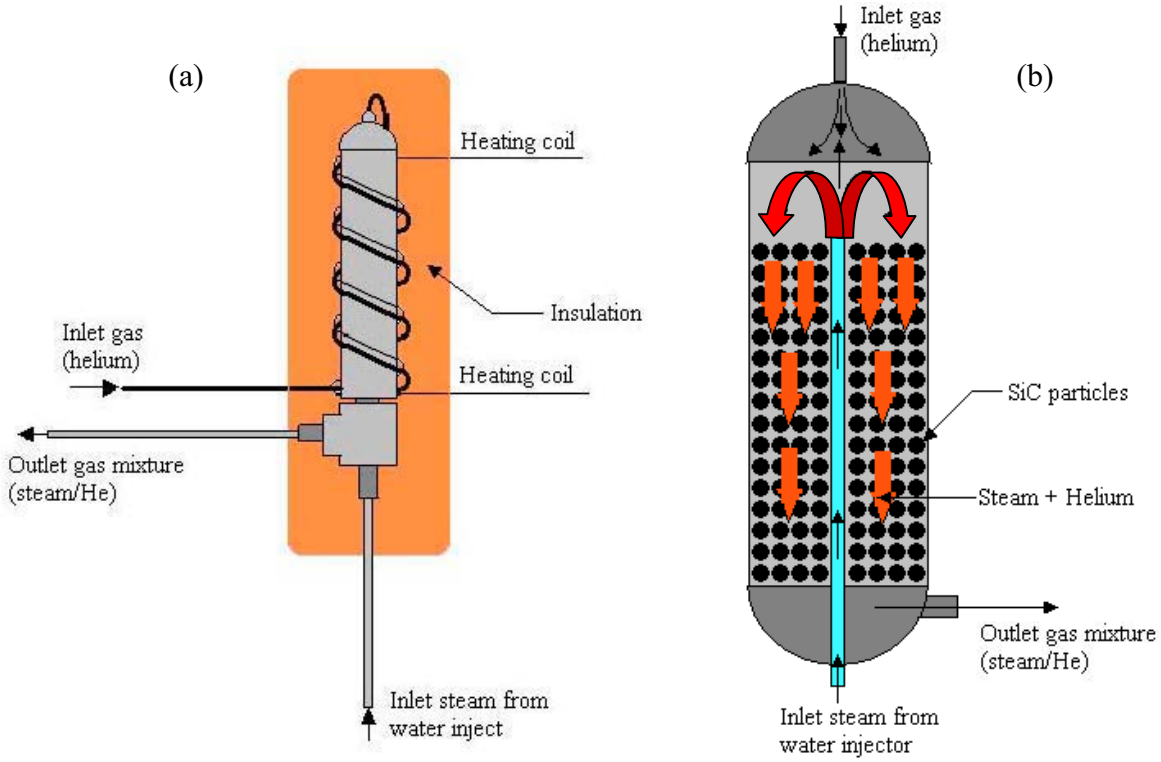

รูปที่ 4.3 Evaporator system

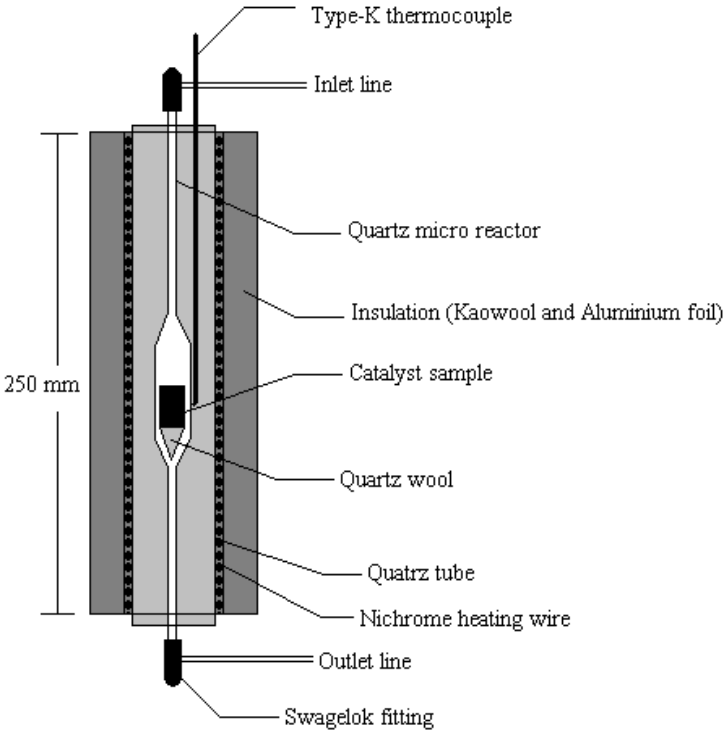

รูปที่ 4.4 Catalytic Reactor

ในส่วนที่ 2 ของระบบ หรือส่วนที่เกิดปฏิกิริยาขึ้นนั้นจะประกอบด้วยเครื่องปฏิกรณ์ (Catalytic Reactor) ซึ่งอยู่ภายในเตาเผา (Furnace) รูปที่ 4.4 แสดงระบบดังกล่าว ซึ่งเครื่องปฏิกรณ์ที่ใช้ทำจาก Quartz มีขนาดยาว 30 เซนติเมตร ซึ่งเหตุผลที่เลือกใช้ Quartz แทนที่จะใช้ Stainless Steel เพื่อป้องกันการเกิดคาร์บอนบริเวณผิวด้านในของท่อ เนื่องจากอุณหภูมิที่ใช้สูงถึง 800 องศาเซลเซียส

ในส่วนสุดท้ายหรือส่วนวิเคราะห์ผลนั้นจะใช้เครื่องมือ 2 ชนิดศึกษาผลของปฏิกิริยาคือ Gas Chromatography และ Mass Spectometer โดยเครื่อง Gas Chromatography จะใช้วิเคราะห์ผลในงานที่สภาวะของระบบคงที่ (Steady State Condition) ส่วน Mass Spectrometer จะใช้วิเคราะห์ผลในงานที่สภาวะของระบบมีการเปลี่ยนแปลงตลอดเวลา (Transient Condition) และเครื่อง Mass Spectrometer ยังถูกใช้เพื่อทำการศึกษาปริมาณของคาร์บอนที่เกิดขึ้นบริเวณผิวของตัวเร่งปฏิกิริยาเช่นกันโดยใช้กระบวนการ Temperature Program Oxidation (TPO)

เครื่อง Gas Chromatography ที่ใช้เป็นเครื่อง Shimadzu 14B มีคอลัมน์ชนิด Porapak Q อยู่ภายใน และมี Detector 2 ชนิดคือ Thermal Conductivity Detector (TCD) และ Frame Ionized Detector (FID) การคำนวณปริมาณของก๊าซในท่อที่เข้าสู่ Gas Chromatography จะใช้ความสัมพันธ์ระหว่างพื้นที่ใช้กราฟกับปริมาณก๊าซที่เข้ามา โดยอาศัย Internal Standardization Method ในการคำนวณความสัมพันธ์ซึ่งจะอยู่ในรูปของค่า Response Factor (RF) ดังแสดงในสมการด้านล่าง

$$RF = \frac{concentration\ (atm)}{peak\ area}$$

จากการทดลองค่า Response Factor ของก๊าซแต่ละชนิดมีดังนี้

Gas	RF	RF relative to O_2	Retention time (min)
H_2	0.45	1.40	0.50
O_2	0.32	1.0	1.01
CO	0.26	0.81	1.03
CH_4	0.12	0.37	1.43
CO_2	0.29	0.90	2.44
H_2O	0.21	0.65	6.51

ในส่วนของเครื่อง Mass Spectrometer ที่ใช้นั้นเป็นเครื่อง QMS ของบริษัท ESS การคำนวณหาปริมาณก๊าซแต่ละชนิดในท่อจะอาศัยความสัมพันธ์ระหว่างปริมาณก๊าซกับความสูงของสัญญาณที่ได้รับโดยใช้หลักการ External Standardization

นอกจากนั้นแล้ว เพื่อให้สามารถดำเนินการทดลองได้อย่างมีประสิทธิภาพ การดำเนินการในขั้นต่อมาคือการปรับปรุง และต่อเติมระบบที่ใช้ในการทดลองโดยเพิ่มเครื่องปฏิกรณ์ (Catalytic Reactor) เป็น 2 เครื่องจากเดิมที่มีเพียงเครื่องเดียว รูปที่ 5 ด้านล่างแสดงระบบที่ถูกออกแบบ และสร้างขึ้นมา โดยระบบดังกล่าวจะถูกต่อเข้ากับเครื่อง Gas Chromatography / Mass Spectrometer (GC-MS) เพื่อให้สามารถทำการวิเคราะห์ได้ทั้งแบบ Steady State Condition และ Transient Condition ในส่วนของการวัดปริมาณคาร์บอนบนผิวของตัวเร่งปฏิกิริยานั้นสามารถดำเนินการได้โดยใช้เครื่อง TGA-MS ดังแสดงในรูปที่ 6

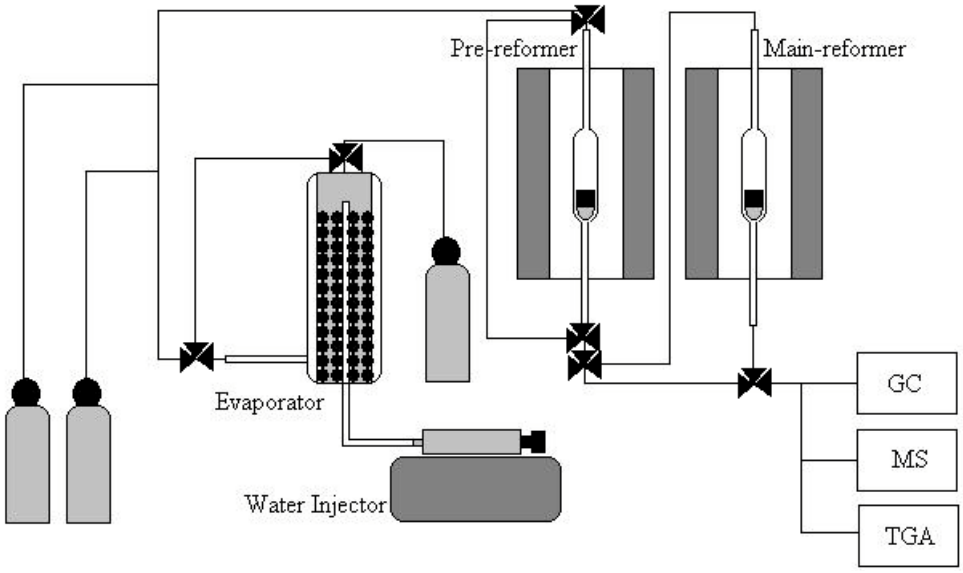

รูปที่ 4.5 ระบบที่ปรับปรุงขึ้นเพื่อใช้ในการทดลอง

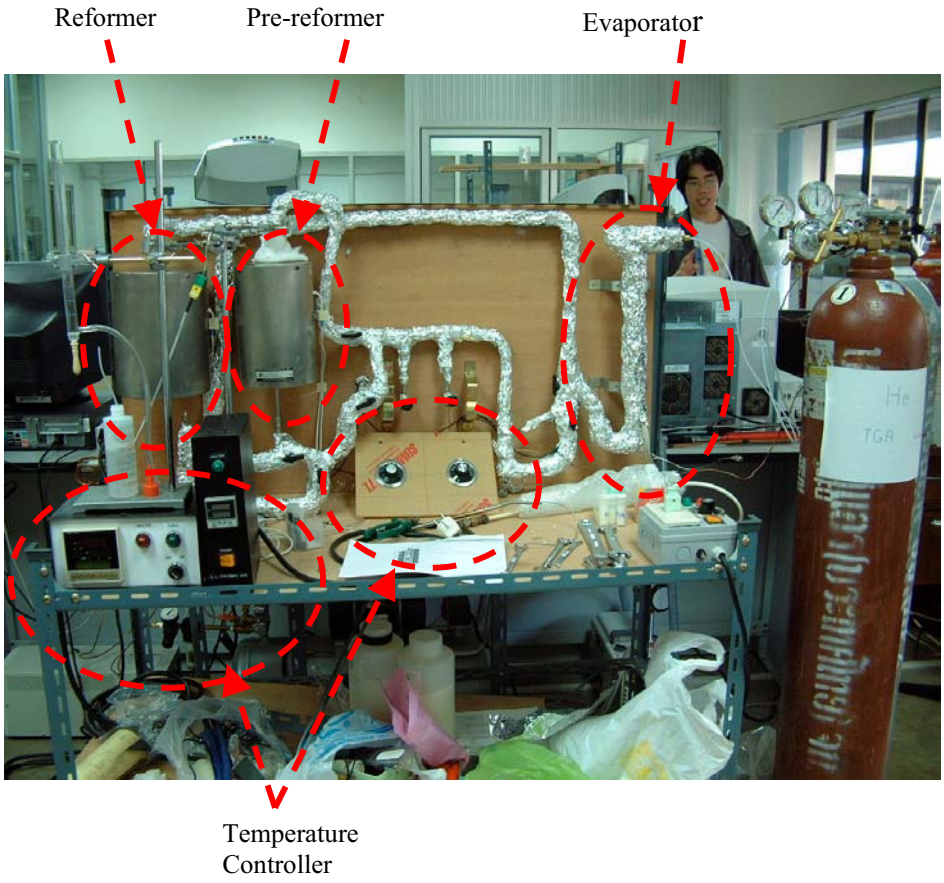

รูปที่ 4.6 ระบบที่ปรับปรุงขึ้นเพื่อใช้ในการทดลอง

4.2 กระบวนการในการทดลอง

ดังที่ได้กล่าวมาในข้างต้น การทดลองสามารถแบ่งเป็น 2 ส่วนใหญ่คือการทดลองที่ Steady State Condition และการทดลองที่ Transient Condition

การทดลองในสภาวะ Steady State Condition จะมีขั้นตอนทั้งสิ้น 5 ขั้นประกอบด้วยการใส่ตัวเร่งปฏิกิริยาเข้าไปในเครื่องปฏิกรณ์ การปรับสภาพของตัวเร่งปฏิกิริยาให้พร้อมก่อนการทดลอง (Pre-Treatment) การส่งผ่านก๊าซทั้งหลายเขาสู่ระบบ การเปลี่ยนความเข้มข้นของก๊าซแต่ละชนิดเพื่อทำการศึกษา และการวิเคราะห์ผลที่ได้รับ ในขั้นตอนแรกคือการใส่ตัวเร่งปฏิกิริยาเข้าสู่ระบบนั้นต้องมีการทำการทดลองก่อนการทดลองจริง (Preliminary Experiment) เพื่อหาสภาวะของตัวเร่งปฏิกิริยา และระบบที่เหมาะสมแก่การศึกษาที่สุดนั่นคือไม่ให้เกิดสภาวะ Mass and Heat Transfer Limitation โดยสภาวะดังกล่าวประกอบด้วยขนาดของตัวเร่งปฏิกิริยา อัตราการไหลของก๊าซเข้าสู่เครื่องปฏิกรณ์เป็นต้น ซึ่งผลการทดลองดังกล่าวจะปรากฏอยู่ในบทถัดไป

ในส่วนที่ 2 หรือการปรับสภาพของตัวเร่งปฏิกิริยาก่อนการทดลองนั้น ตัวเร่งปฏิกิริยาแบบ Metallic จะต้องถูก Reduced ด้วยไฮโดรเจนก่อนทำการทดลองจริง ทั้งนี้เพื่อกำจัดสภาวะ Oxidized State ของตัวเร่งปฏิกิริยาให้หมดไป เนื่องจาก Oxidized Metallic Material จะไม่เป็นตัวเร่งปฏิกิริยาต่อกระบวนการรีฟอร์มมิ่งที่ดี ในการ Reduce ตัวเร่งปฏิกิริยานั้น ตัวเร่งปฏิกิริยาแต่ละชนิดจะใช้สภาวะการ Reduce ที่ไม่เหมือนกันซึ่งจำเป็นต้องทำการทดลองเพื่อหาสภาวะที่เหมาะสมที่สุดเช่นกัน ในส่วนถัดมาคือการป้อนก๊าซที่สนใจเข้าสู่ระบบนั้น สำหรับกระบวนการรีฟอร์มมิ่งมีเทนด้วยน้ำนั้น ก๊าซสำคัญที่จำเป็นต้องใส่เข้าไปสู่ระบบมี 3 ชนิดคือ มีเทน ไอน้ำ และไฮโดรเจนในปริมาณเล็กน้อย สาเหตุที่ต้องมีการใส่ไฮโดรเจนเข้าไปในปริมาณเล็กน้อยเนื่องจากได้มีการรายงานจากการศึกษากระบวนการนี้ในอดีตที่ผ่านมาว่าการป้อนไฮโดรเจนในปริมาณเล็กน้อยเข้าสู่ระบบสามารถเพิ่มอัตราการเกิดปฏิกิริยารีฟอร์มมิ่งได้อย่างดี และจาก Chemical Mechanism ของกระบวนการดังกล่าวดังแสดงด้านล่างจะพบว่ามีเทนจะไม่สามารถถูกรีฟอร์มเพื่อเปลี่ยนไปไฮโดรเจนได้เลย หรือเปลี่ยนได้น้อยมากหากไม่มีการใส่ไฮโดรเจนเริ่มต้นเข้าสู่ระบบเนื่องจากการ Adsorption ของน้ำในปฏิกิริยาที่ 2 เกิดเร็วก่อนการ Adsorption ของมีเทนในปฏิกิริยาที่ 1 มาก

$$CH_4 + n^* \rightarrow CH_x\text{-}^*n + (4\text{-}x)/2H_2 \quad (1)$$

$$H_2O + * \Leftrightarrow O\text{-}^* + H_2 \quad (2)$$

$$CHx\text{-}^*n + O\text{-}^* \rightarrow CO + x/2H_2 + (n+1)^* \quad (3)$$

$$H_2 + 2^* \Leftrightarrow 2H\text{-}^* \quad (4)$$

ในการทดลองเพื่อหาศึกษาเสถียรภาพ (Stability) **และศักยภาพ** (Activity) **ของตัวเร่งปฏิกิริยานั้นความเข้มข้นของมีเทนเข้าสู่ระบบคือ** 4% **ความเข้มข้นของไอน้ำเข้าสู่ระบบคือ** 10% **และความเข้มข้นของก๊าซไฮโดรเจนที่ใช้คือ** 1% **ส่วนอุณหภูมิที่ใช้ในการศึกษาคือ** 800 **องศาเซลเซียส เนื่องจากเป็นอุณหภูมิที่เหมาะสมสำหรับการใช้งานของเซลล์เชื้อเพลิงแบบอุณหภูมิสูงทั้ง** MCFC **และ** SOFC **ซึ่งการศึกษากระบวนการรีฟอร์มมิ่งที่อุณหภูมิดังกล่าวสามารถใช้ประโยชน์ในการศึกษานี้เพื่อประยุกต์ใช้งานแบบ** Internal Reforming **ได้ง่ายขึ้น**

สำหรับการทดลองในสภาวะ Transient Condition จะมีขั้นตอนทั้งสิ้น 5 ขั้นเช่นกันประกอบด้วย การใส่ตัวเร่งปฏิกิริยาเข้าไปในเครื่องปฏิกรณ์ การปรับสภาพของตัวเร่งปฏิกิริยาให้พร้อมก่อนการทดลอง (Pre-Treatment) การส่งผ่านก๊าซทั้งหลายเขาสู่ระบบ การเพิ่มอุณหภูมิตามที่ได้โปรแกรมไว้ (Temperature Program) ซึ่งจะใช้ในงาน Temperature Program Reduction (TPR), Temperature Program Reaction (TPRx), Temperature Program Hydrogenation (TPH), Temperature Program Oxidation (TPO) เพื่อศึกษาการเกิดคาร์บอนที่ผิวของตัวเร่งปฏิกิริยา และการวิเคราะห์ผลที่ได้รับ ในงาน Temperature Program (TP) นั้นแต่ละปรเภทจะมีการใช้ก๊าซต่างชนิดกันโดยจะใช้ 5% ไฮโดรเจนในงาน TPR และ TPH ใช้ 5% มีเทนในงาน TPRx และใช้ 10% อ็อกซิเจนในงาน TPO โดยจะสั่งให้อุณหภูมิของระบบสูงขึ้นจากที่อุณหภูมิห้องขึ้นไปที่ 900 องศาเซลเซียสโดยใช้อัตราการเพิ่มของอุณหภูมิ 10 องศาเซลเซียสต่อนาที

4.3 การคำนวณผลที่ได้จากการทดลอง

เมื่อได้ผลการทดลองจาก Gas Chromatography แล้วการหาค่า Methane Conversion (X_{CH4}) จะสามารถคำนวณได้จากความสัมพันธ์ของพื้นที่ใต้กราฟใน Chromatogram (A_x) กับค่า Response Factor (RF) ของแต่ละ Component โดยใช้สมการดังแสดงด้านล่าง

$$X_{CH_4} = \frac{\left(RF_{CO} * A_{CO}\right) + \left(RF_{CO_2} * A_{CO_2}\right)}{\left(RF_{CH_4} * A_{CH_4}\right) + \left(RF_{CO} * A_{CO}\right) + \left(RF_{CO_2} * A_{CO_2}\right)}$$

โดยสมการดังกล่าวสามารถใช้ได้บนสมมุติฐานที่คาร์บอนของมีเทนทั้งหมดเปลี่ยนไปเป็นคาร์บอนมอนออกไซด์ และคาร์บอนไดออกไซด์ ส่วนค่า Rate ของการเกิดปฏิกิริยาจะใช้ผลของค่า Methane Conversion ที่คำนวณได้ในการหา ดังแสดงในสมการด้านล่าง

$$Rate = \frac{F_{CH_4} * X_{CH_4}}{W_{Cat}}$$

4.4 การเตรียมตัวเร่งปฏิกิริยาที่ใช้ในการทดลอง

ตัวเร่งปฏิกิริยาที่เลือกใช้ในการทดอลงนี้ประกอบด้วยสาร Metallic Material คือ Rh, Pd, Pt และ Ni ส่วนตัว Support ซึ่งเป็น Oxide Material ประกอบด้วย Al_2O_3, MgO, ZrO_2, CeO_2, CeO_2-ZrO_2 และ TiO_2 ซึ่งสาร Support เหล่านี้ยกเว้น CeO_2 และ CeO_2-ZrO_2 สามารถหาซื้อได้ทั่วไป (Commercial Grade) ส่วนสารเริ่มต้นที่จะใช้เตรียม Metallic Catalyst นั้นจะใช้สาร Metal Chloride ($MtCl_x$) โดย Mt คือ Rh, Pd, Pt และ Ni นั่นเอง ทำการละลายในน้ำในอัตราส่วนที่เหมาะสม และทำการ Impregnate สาร Metal เหล่านี้บนตัว Commercial Support ต่างๆ โดยนำมาผสมกันและใช้อัตราการกวน 100 rpm เป็นเวลา 6 ชั่วโมง จากนั้นให้ความร้อนเพื่อให้เกิดการระเหยอย่างช้าๆ นำไปอบที่อุณหภูมิ 110 องศาเซลเซียสเป็นเวลา 6 ชั่วโมง และนำไปเผา (Calcination) ที่อุณหภูมิ 900 องศาเซลเซียส

ส่วนตัว Support CeO_2 และ CeO_2-ZrO_2 ที่ใช้ในการทดลองนั้นจะทำการเตรียมขึ้นมาเองโดยอาศัยกระบวนการ Co-Precipitation ซึ่งในการเตรียม CeO_2 นั้นสารเริ่มต้นที่ใช้คือสารประกอบไนเตรท ($Ce(NO_3)_3 \cdot 6H_2O$ (99.0%)) เมื่อผสมสารนี้เข้ากับ Ammonium Hydroxide แล้วสารประกอบ Cerium Hydroxide ($Ce(OH)_4$) จะตกตะกอนออกมา ทำการกวนติดต่อกัน 3 ชั่วโมงเพื่อให้ปฏิกิริยาที่เกิดขึ้นสมบูรณ์ จากนั้นก็กรองสารดังกล่าวออกมา ทำการล้างด้วยน้ำ และเอทานอลเพื่อป้องกันการเกิด Agglomeration ของแต่ละโมเลกุล นำไปอบที่อุณหภูมิ 110 องศาเซลเซียสเป็นเวลา 6 ชั่วโมง และนำไปเผา (Calcination) ที่อุณหภูมิ 900 องศาเซลเซียสเพื่อรอการใช้งานต่อไป

สำหรับการเตรียมตัว Support CeO_2-ZrO_2 นั้นจะมีกระบวนการคล้ายกับการเตรียม CeO_2 แต่ก่อนการผสม Ammonium Hydroxide เข้าไปนั้นจะทำการผสม$Ce(NO_3)_3 \cdot 6H_2O$ (99.0%) ด้วย $ZrOCl_2 \cdot 8H_2O$ (99.0%) ในอัตราส่วนที่เหมาะสมก่อน

4.5 การทดสอบคุณสมบัติทางกายภาพของตัวเร่งปฏิกิริยา (Physical Characterization)

ตัวเร่งปฏิกิริยาทั้งก่อนและหลังการทดลองจะถูกนำไปทดสอบคุณสมบัติทางกายภาพเพื่อศึกษาการเปลี่ยนแปลงอันเนื่องมาจากปฏิกิริยา โดยการทดสอบดังกล่าวจะประกอบด้วยการใช้ Brunauer-Emmett-Teller (BET) method เพื่อหาพื้นที่ผิวต่อน้ำหนักของตัวเร่งปฏิกิริยา การใช้ X-ray powder diffraction (XRPD) เพื่อศึกษาองค์ประกอบของตัวเร่งปฏิกิริยาหลังการทดลอง การใช้ X-ray photoelectron spectroscopy (XPS) เพื่อศึกษาการเปลี่ยนเฟสของตัวเร่งปฏิกิริยาหลังการทดลอง และการใช้ electron microscopy (SEM, and EDX) เพื่อศึกษาโครงสร้างบริเวณพื้นผิวของตัวเร่งปฏิกิริยาก่อนและหลังกระบวนการรีฟอร์มมิ่ง

บทที่ 5
การผลิตไฮโดรเจนจากสารตั้งต้นที่มีองค์ประกอบเป็นมีเทน

5.1 การทดลองเบื้องต้นเพื่อหาสภาวะที่เหมาะสมสำหรับกระบวนการรีฟอร์มมิ่ง

ดังที่ได้กล่าวมาแล้ว อุณหภูมิการใช้งานของเซลล์เชื้อเพลิงแบบอุณหภูมิสูงอยู่ที่ประมาณ 700-900 องศาเซลเซียส ดังนั้นในการศึกษากระบวนการรีฟอร์มมิ่งนั้นอุณหภูมิที่ทำการศึกษาก็ควรจะอยู่ในช่วงนี้ด้วย และเพื่อให้ผลที่ได้จากการศึกษาไม่มีผลกระทบของ Mass และ Heat Transfer Limitations เข้ามาเกี่ยวข้องด้วย การเลือกใช้อัตราการไหลของก๊าซ ขนาดของตัวเร่งปฏิกิริยาจึงเป็นสิ่งสำคัญยิ่งซึ่งต้องมีการทดลองเพื่อเลือกสภาวะที่เหมาะสมที่สุดดังแสดงต่อไปนี้

เพื่อหาอัตราการไหลของก๊าซเข้าสู่เครื่องปฏิกรณ์ที่เหมาะสมที่สุด อัตราการไหลรวมของก๊าซถูกเปลี่ยนค่าตั้งแต่ 20 ถึง 200 ml/min โดยตัวเร่งปฏิกิริยาภายในเครื่องปฏิกรณ์ที่ใช้คือ Ni/Al_2O_3 มีน้ำหนัก 50 mg และใช้มีเทน 5% น้ำ 10% ไฮโดรเจน 1% ทำการทดลองที่อุณหภูมิ 800 องศาเซลเซียส จากผลการทดลองเปลี่ยนค่าอัตราการไหลของก๊าซภายในดังแสดงในรูปที่ 6.1 พบว่าที่อัตราการไหลต่ำกว่า 80 ml/min นั้นอัตราการเกิดปฏิกิริยามีค่าแปรผันตามอัตราการไหลซึ่งเนื่องมาจากการเกิด Mass Transfer ระหว่างก๊าซโดยรอบ (Bulk Gas) กับก๊าซบริเวณพื้นผิวของตัวเร่งปฏิกิริยาขึ้น แต่ถ้าอัตราการไหลของก๊าซสูงกว่า 80 ml/min แล้วค่าอัตราการเกิดปฏิกิริยาจะไม่เปลี่ยนแปลงตามอัตราการไหลซึ่งเป็นช่วงที่ควรใช้ในการทดลอง ดังนั้นในการทดลองทุกครั้ง อัตราการไหลของก๊าซรวมจะถูกกำหนดให้คงที่ที่ 100 ml/min

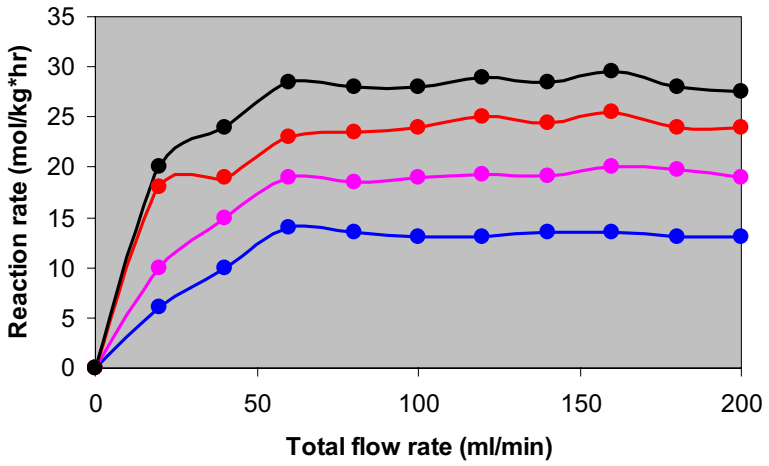

รูปที่ 5.1 ความสัมพันธ์ระหว่างอัตราการเกิดปฏิกิริยารีฟอร์มมิ่งกับอัตราการไหลโดยรวมของก๊าซผ่านระบบบนตัวเร่งปฏิกิริยา Ni/Al_2O_3 ที่อุณหภูมิ 800 องศาเซลเซียส

นอกจากผลของอัตราการไหลโดยรวมแล้ว ขนาดของตัวเร่งปฏิกิริยาก็มีผลต่อกระบวนการเช่นกัน เพื่อหาขนาดของตัวเร่งปฏิกิริยาที่เหมาะสมที่สุด กระบวนการรีฟอร์มมิ่งโดยใช้ขนาดของตัวเร่งปฏิกิริยาที่แตกต่างกันระหว่าง 100 ถึง 500 μm จึงถูกดำเนินการภายในสภาวะการทดลองเดียวกับการศึกษาผลของอัตราการไหล ซึ่งจากการทดลองพบว่าเมื่อขนาดของตัวเร่งปฏิกิริยาอยู่ระหว่าง 100-200 μm ค่าอัตราการเกิดปฏิกิริยาค่อนข้างจะคงที่ ดังนั้นขนาดของตัวเร่งปฏิกิริยาในช่วงดังกล่าวจึงถูกใช้ในการทดลอง

เมื่อใช้สภาวะดังกล่าวในการทดลองแล้ว อัตราการเกิดปฏิกิริยาที่หาได้จากการทดลองน่าจะเป็นอัตราการเกิดปฏิกิริยาจริง (Intrinsic Rate) ซึ่งการเปลี่ยนแปลงต่างๆ ที่เกิดขึ้นน่าจะเป็นผลมาจากชนิดของตัวเร่งปฏิกิริยาเท่านั้น

5.2 การศึกษาศักยภาพของตัวเร่งปฏิกิริยาต่อกระบวนการรีฟอร์มมิ่งมีเทนด้วยน้ำ

ในระยะเริ่มต้นตัวเร่งปฏิกิริยาที่น่าสนใจเช่น Ni/Al_2O_3 หรือ $Ni/Ce\text{-}ZrO_2$ ถูกเลือกเพื่อศึกษาคุณสมบัติต่อกระบวนการรีฟอร์มมิ่งอย่างละเอียด โดยการดำเนินการทดลองจะประกอบด้วยการศึกษาคุณสมบัติต่อกระบวนการรีฟอร์มมิ่งอย่างละเอียดเช่นการหาผลของการเติมน้ำ หรือการเติมไฮโดรเจนมากขึ้นในสายป้อนต่ออัตราการเกิดปฏิกิริยาดังกล่าว รวมถึงการศึกษาเพื่อหาค่า Chemical Mechanism ของตัวเร่งปฏิกิริยาดังกล่าวเพื่อใช้ประโยชน์ต่อไป หลังจากนั้นตัวเร่งปฏิกิริยาชนิดใหม่เช่น CeO_2 ก็จะถูกศึกษาในระดับลึกเช่นกัน ถึงแม้สารดังกล่าวจะมีอัตราการเกิดปฏิกิริยารีฟอร์มมิ่งต่ำเมื่อเทียบกับ Metallic Catalyst แต่สารดังกล่าวมีประโยชน์ในแง่ที่มีความต้านทานต่อการเกิดคาร์บอนที่ผิวสูงมาก ซึ่งถ้าทำการศึกษาและเลือกใช้สารดังกล่าวอย่างถูกวิธีจะมีประโยชน์ต่อกระบวนการผลิตไฮโดรเจนมาก

5.2.1 ผลของมีเทนต่อกระบวนการรีฟอร์มมิ่ง

ในการทดลองนี้ความเข้มข้นของก๊าซมีเทนในสายป้อนจะถูกเปลี่ยนค่าโดยควบคุมความเข้มข้นของสารชนิดอื่นๆ ให้คงที่ ซึ่งผลที่ได้ดังแสดงในรูปที่ 5.1 โดยอัตราการเกิดปฏิกิริยาของตัวเร่งปฏิกิริยาทั้ง 2 ชนิดมีค่าเพิ่มขึ้นตามความเข้มข้นของมีเทน ซึ่งจากการคำนวณพบว่าค่า Reaction Order ของมีเทนสำหรับตัวเร่งปฏิกิริยาทั้ง 2 ชนิดมีค่าเท่ากับ 1 เสมอ การคำนวนหา Reaction Order สามารถทำได้จากสมการด้านล่างนี้

$$Rate = k' P_X{}^n P_{CH_4}{}^m$$

$$Rate = (k' P_X{}^n) * P_{CH_4}{}^m$$

$$Rate = k * P_{CH_4}{}^m$$

$$\ln(Rate) = \ln(k) + m(\ln P_{CH_4})$$

$$K = Ae^{-\frac{E}{RT}}$$

$$\ln(K) = \ln(A) - \frac{E}{R}(\frac{1}{T})$$

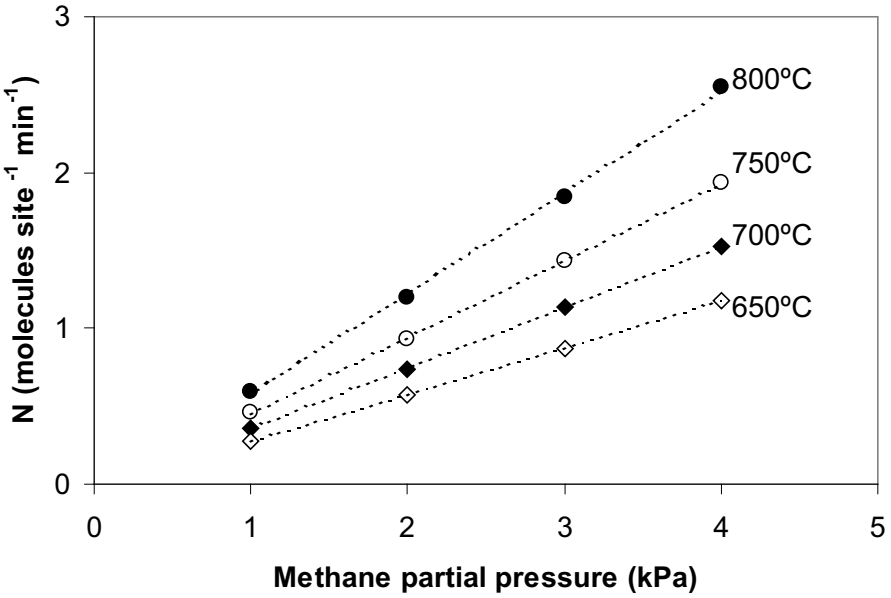

รูปที่ 5.1 ผลของมีเทนต่ออัตราการเกิดไฮโดรเจนสำหรับ Ni/Ce-ZrO_2 ที่อุณหภูมิต่างๆ

5.2.2 ผลของน้ำต่อกระบวนการรีฟอร์มมิ่ง

การทดลองนี้จะคล้ายคลึงกับการศึกษาผลของมีเทนต่อกระบวนการรีฟอร์มมิ่ง แต่จะเปลี่ยนค่าความเข้มข้นของไอน้ำเข้าสู่ระบบไปเรื่อยๆ โดยควบคุมให้ความเข้มข้นของมีเทนมีค่าคงที่ ผลของการเปลี่ยนความเข้มข้นของน้ำดังแสดงในรูปที่ 5.2 ซึ่งอัตราการเกิดปฏิกิริยาจะมีค่าเพิ่มขึ้นเมื่อความเข้มข้นของไอน้ำมีค่าเพิ่มขึ้นในช่วงแรกๆ แต่จากนั้นอัตราการเกิดปฏิกิริยาจะลดลงเมื่อเพิ่มปริมาณของไอน้ำเข้าสู่ระบบไปเรื่อยๆ

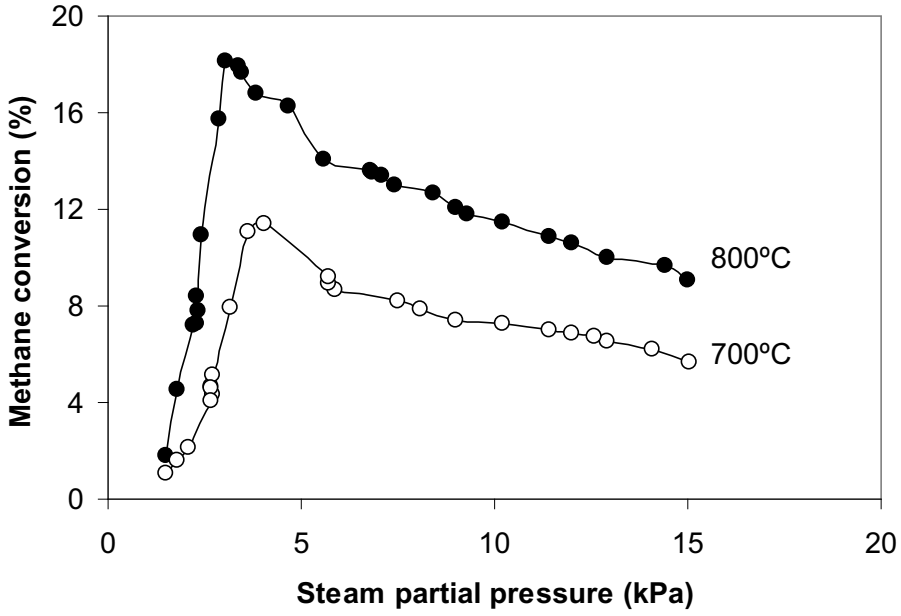

รูปที่ 5.2 ผลของปริมาณน้ำต่ออัตราการเกิดไฮโดรเจนสำหรับ Ni/Ce-ZrO_2 ที่อุณหภูมิต่างๆ

สาเหตุดังกล่าวสามารถอธิบายได้จากกระบวนการเกิดปฏิกิริยารีฟอร์มมิ่งของมีเทนด้วยน้ำดังแสดงด้านล่าง

$$CH_4 + n^* \rightarrow CH_x\text{-}^*n + (4\text{-}x)/2H_2 \quad (5.1)$$

$$H_2O + * \Leftrightarrow O\text{-}^* + H_2 \quad (5.2)$$

$$CH_x\text{-}^*n + O\text{-}^* \rightarrow CO + x/2H_2 + (n+1)^* \quad (5.3)$$

$$H_2 + 2^* \Leftrightarrow 2H\text{-}^* \quad (5.4)$$

การที่เพิ่มความเข้มข้นของน้ำในช่วงแรก น้ำจะถูกดูดซึมบนผิวของตัวเร่งปฏิกิริยา (*) เพื่อฟอร์ม O-* และทำปฏิกิริยากับมีเทนที่ถูกดูดซึมบนผิวของตัวเร่งปฏิกิริยา (CH_x-*n) ในสมการที่ 5.3 แต่เมื่อมีปริมาณน้ำมากเกินไปการดูดซึมน้ำบนผิวของตัวเร่งปฏิกิริยาจะขัดขวางการดูดซึมมีเทนบนตัวเร่งปฏิกิริยาในสมการที่ 5.1 และทำให้อัตราการเกิดปฏิกิริยาลดลง

5.2.3 ผลของไฮโดรเจนต่อกระบวนการรีฟอร์มมิ่ง

ในการทดลองนี้ จะมีการเติมก๊าซไฮโดรเจนด้วยความเข้มข้นต่างๆ เข้าไปในสายป้อน และควบคุมความเข้มข้นของสารชนิดอื่นๆ ให้คงที่ ซึ่งผลที่ได้ดังแสดงในรูปที่ 5.3 โดยอัตราการเกิดปฏิกิริยาของตัวเร่งปฏิกิริยาทั้ง 2 ชนิดจะมีค่าเข้าใกล้ 0 มากเมื่อไม่มีการเติมไฮโดรเจนเข้าสู่สายป้อนเลย และอัตราการเกิดปฏิกิริยาจะมีค่าเพิ่มขึ้นเรื่อยๆ เมื่อความเข้มข้นของไฮโดรเจนมีค่าเพิ่มขึ้น การที่ไฮโดรเจนสามารถเพิ่มอัตรา

การเกิดปฏิกิริยารีฟอร์มมิ่งได้เนื่องมาจากการที่ไฮโดรเจนช่วยยับยั้งการดูดซึมของน้ำที่มากเกินไปบนผิวของตัวเร่งปฏิกิริยานั่นเอง

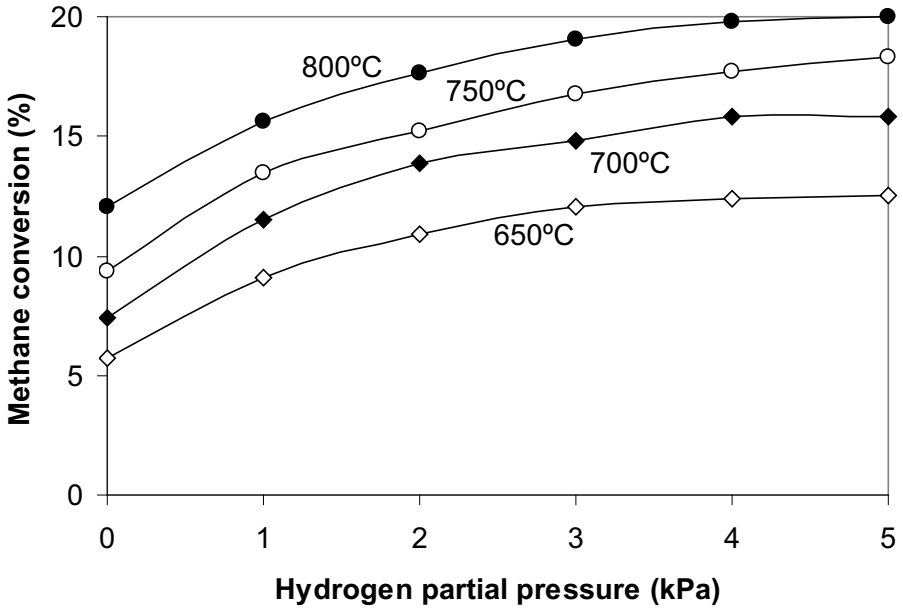

รูปที่ 5.3 ผลของปริมาณไฮโดรเจนต่ออัตราการเกิดปฏิกิริยาของ Ni/Ce-ZrO_2 ที่อุณหภูมิต่างๆ

5.2.4 ผลของออกซิเจนต่อกระบวนการรีฟอร์มมิ่ง

ในการทดลองนี้ จะมีการเติมก๊าซออกซิเจนด้วยความเข้มข้นต่างๆ เข้าไปในสายป้อน และควบคุมความเข้มข้นของสารชนิดอื่นๆ ให้คงที่ซึ่งผลที่ได้ดังแสดงใน รูปที่ 5.4

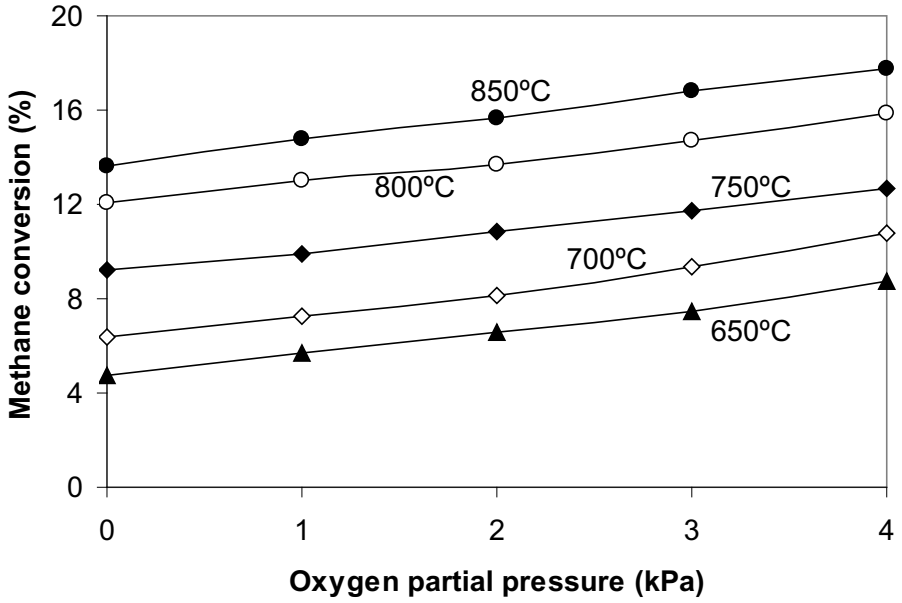

รูปที่ 5.4 ผลของปริมาณออกซิเจนต่ออัตราการเกิดปฏิกิริยาของ Ni/Ce-ZrO_2 ที่อุณหภูมิต่างๆ

อัตราการเกิดปฏิกิริยาของตัวเร่งปฏิกิริยา Ni/Ce-ZrO_2 จะมีค่าเพิ่มขึ้นเรื่อยๆ เมื่อความเข้มข้นของออกซิเจนมีค่าเพิ่มขึ้น แต่ความเข้มข้นของไฮโดรเจน และคาร์บอน มอนออกไซด์ซึ่งสามารถใช้ประโยชน์ในเซลล์เชื้อเพลิงได้จะมีค่าลดลงดังแสดงในรูปที่ 5.5 เนื่องจากคาร์บอนมอนออกไซด์ถูกออกซิไดซ์โดยออกซิเจนที่เติมเข้ามาและเปลี่ยนสภาพกลายเป็นคาร์บอนไดออกไซด์ ส่วนไฮโดรเจนก็จะถูกเปลี่ยนรูปไปเป็นน้ำ

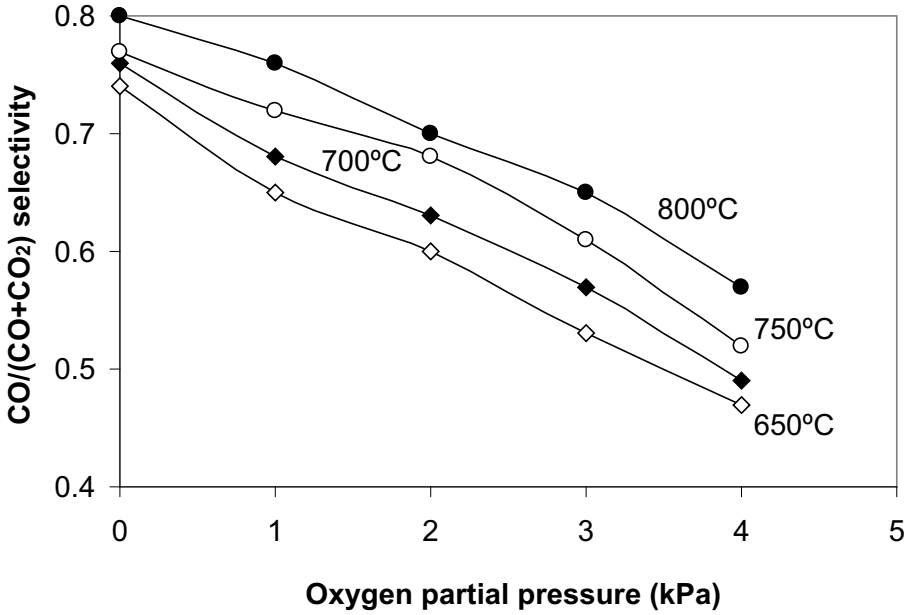

รูปที่ 5.5 ผลของปริมาณ CO/(CO+CO_2) ต่ออัตราการเกิดไฮโดรเจนสำหรับ Ni/Ce-ZrO_2

ตารางที่ 5.1 ในหน้าถัดไปแสดงค่า Reaction Order เปรียบเทียบระหว่าง Ni/Al_2O_3 และ Ni/Ce-ZrO_2 ของก๊าซทุกชนิดที่ดำเนินการทดลอง

Table 5.1
Reaction orders for the components of interest (CH_4, H_2O, and H_2) from methane steam reforming over Ni/Ce-ZrO_2 (Ce/Zr = 3/1) and Ni/Al_2O_3 at different operating conditions

Components of interest	Temperature (°C)	Other inlet compositions	Reaction order for components of interest	
			Ni/Ce-ZrO_2 (Ce/Zr=3/1)	Ni/Al_2O_3
Methane	650-800	9kPa H_2O / 0 kPa H_2	1.0 ± 0.04	1.0 ± 0.01
(1-4 kPa)		12kPa H_2O / 0 kPa H_2	1.0 ± 0.05	1.0 ± 0.01
		15kPa H_2O / 0 kPa H_2	1.0 ± 0.02	1.0 ± 0.02
		9kPa H_2O / 1 kPa H_2	1.0 ± 0.02	1.0 ± 0.01
		9kPa H_2O / 3 kPa H_2	1.0 ± 0.01	1.0 ± 0.03
		9kPa H_2O / 5 kPa H_2	1.0 ± 0.03	1.0 ± 0.01
Hydrogen	650	9kPa H_2O / 3 kPa CH_4	0.18	0.31
(1-4 kPa)	700	9kPa H_2O / 3 kPa CH_4	0.20	0.28
	750	9kPa H_2O / 3 kPa CH_4	0.18	0.34
	800	9kPa H_2O / 3 kPa CH_4	0.19	0.33
	700	9kPa H_2O / 1 kPa CH_4	0.18	0.29
	700	9kPa H_2O / 5 kPa CH_4	0.20	0.32
	700	12kPa H_2O / 3 kPa CH_4	0.25	0.39
	700	15kPa H_2O / 3 kPa CH_4	0.28	0.42
Hydrogen	650	9kPa H_2O / 3 kPa CH_4	- 0.31	- 0.15
(12-18 kPa)	700	9kPa H_2O / 3 kPa CH_4	- 0.30	- 0.16
	800	9kPa H_2O / 3 kPa CH_4	- 0.34	- 0.15
Steam	650	0kPa H_2 / 3 kPa CH_4	- 0.39	- 0.37
(5-15 kPa)	700	0kPa H_2 / 3 kPa CH_4	- 0.40	- 0.39
	750	0kPa H_2 / 3 kPa CH_4	- 0.38	- 0.41
	800	0kPa H_2 / 3 kPa CH_4	- 0.42	- 0.40
	700	1kPa H_2 / 3 kPa CH_4	- 0.31	- 0.31
	700	2kPa H_2 / 3 kPa CH_4	- 0.25	- 0.24
	700	3kPa H_2 / 3 kPa CH_4	- 0.22	- 0.19

5.3 การใช้ CeO_2 ในกระบวนการรีฟอร์มมิ่ง

นอกจากตัวเร่งปฏิกิริยา Metallic Catalysts ที่กล่าวมาแล้ว สาร CeO_2 ก็ถูกศึกษาเช่นกัน โดยกระบวนการที่เลือกศึกษาคือกระบวนการ Dry Reforming ซึ่งถึงแม้สารดังกล่าวจะมีอัตราการเกิดปฏิกิริยารีฟอร์มมิ่งต่ำเมื่อเทียบกับ Metallic Catalysts แต่สารดังกล่าวมีประโยชน์ในแง่ที่มีความต้านทานต่อการเกิดคาร์บอนที่ผิวสูงมาก ซึ่งถ้าทำการศึกษาและเลือกใช้สารดังกล่าวอย่างถูกวิธีจะมีประโยชน์ต่อกระบวนการผลิตไฮโดรเจนมาก

5.3.1 ผลของมีเทนต่อกระบวนการรีฟอร์มมิ่งของ CeO_2

เช่นเดียวกับการทดลองสำหรับตัวเร่งปฏิกิริยา Metallic Catalysts ในการทดลองนี้ ความเข้มข้นของก๊าซมีเทนในสายป้อนจะถูกเปลี่ยนค่าโดยควบคุมความเข้มข้นของสารชนิดอื่นๆ ให้คงที่ ซึ่งผลที่ได้ดังแสดงในรูปที่ 5.6 โดยอัตราการเกิดปฏิกิริยาของตัวเร่งปฏิกิริยา CeO_2 มีค่าเพิ่มขึ้นตามความเข้มข้นของมีเทนเช่นเดียวกับตัวเร่งปฏิกิริยาทั้ง 2 ชนิดที่ได้กล่าวมาแล้ว แต่จากการคำนวณพบว่าค่า Reaction Order ของมีเทนสำหรับตัวเร่งปฏิกิริยา CeO_2 มีค่าเท่ากับ 0.5 ซึ่งน้อยกว่าตัวเร่งปฏิกิริยา Metallic Catalysts

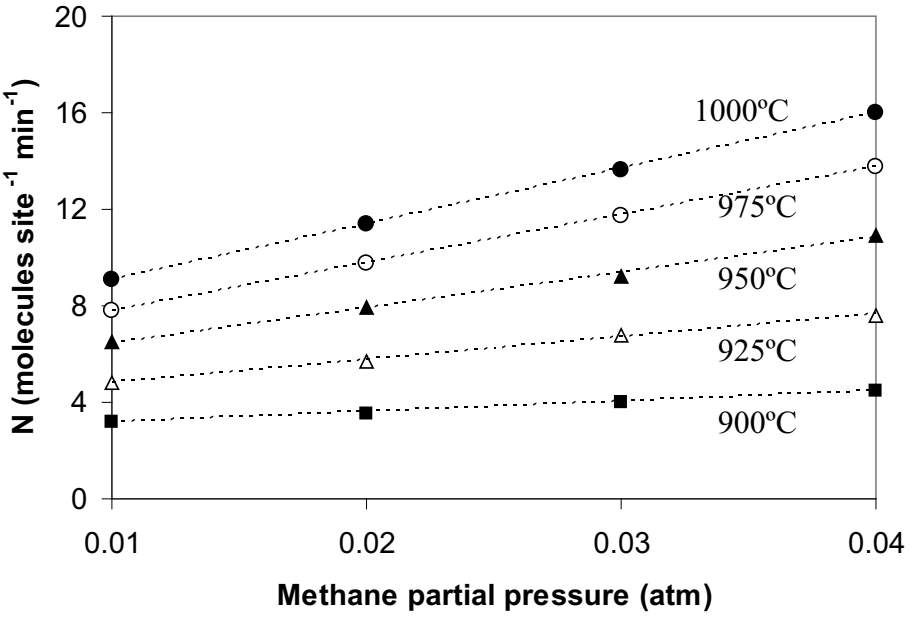

รูปที่ 5.6 ผลของปริมาณมีเทนต่ออัตราการเกิดไฮโดรเจนสำหรับ CeO_2 ที่อุณหภูมิต่างๆ

5.3.2 ผลของคาร์บอนไดออกไซด์ต่อกระบวนการรีฟอร์มมิ่งของ CeO_2

ความเข้มข้นของคาร์บอนไดออกไซด์เข้าสู่ระบบจะถูกเปลี่ยนไปเรื่อยๆ โดยควบคุมให้ความเข้มข้นของมีเทนมีค่าคงที่ ผลของการเปลี่ยนความเข้มข้นของน้ำดังแสดงในรูปที่ 5.7 ซึ่งอัตราการเกิดปฏิกิริยาจะมีค่าคงที่ไม่ขึ้นกับความเข้มข้นของคาร์บอนไดออกไซด์มีค่าเพิ่มขึ้น

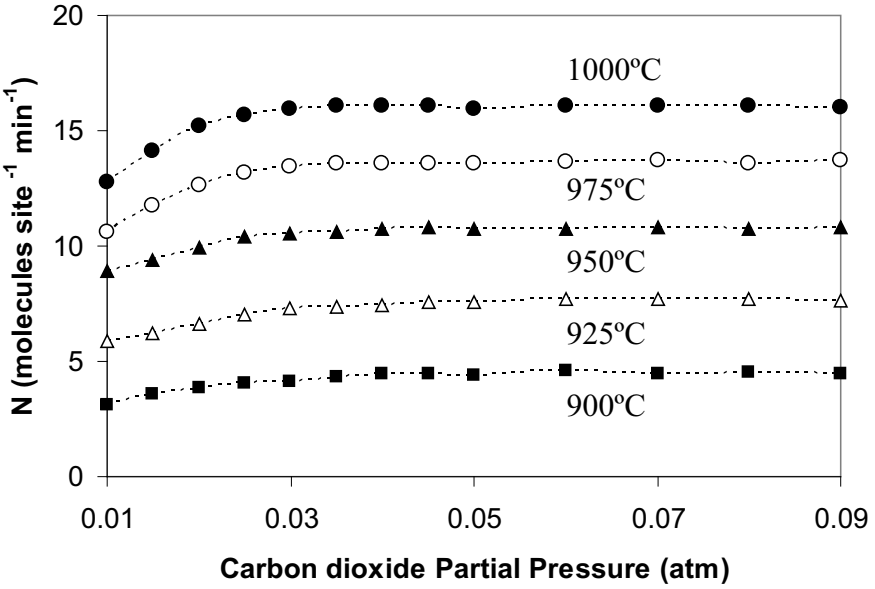

รูปที่ 5.7 ผลของปริมาณคาร์บอนไดออกไซด์ต่ออัตราการเกิดไฮโดรเจนสำหรับ CeO_2 ที่อุณหภูมิต่างๆ

5.3.3 ผลของไฮโดรเจนต่อกระบวนการรีฟอร์มมิ่งของ CeO_2

เมื่อก๊าซไฮโดรเจนที่ความเข้มข้นต่างๆ ถูกป้อนเข้าไปสู่ระบบ โดยควบคุมความเข้มข้นของสารชนิดอื่นๆ ให้คงที่ ผลที่ได้ดังแสดงในรูปที่ 5.8 พบว่าอัตราการเกิดปฏิกิริยาของตัวเร่งปฏิกิริยา CeO_2 จะมีค่าลดลงเมื่อความเข้มข้นของไฮโดรเจนมีค่าเพิ่มขึ้น

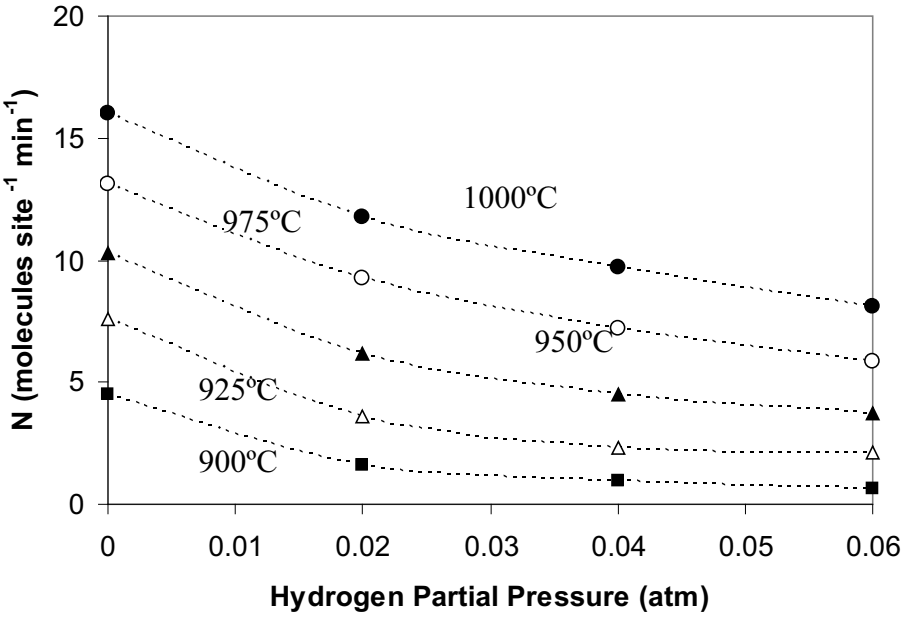

รูปที่ 5.8 ผลของปริมาณไฮโดรเจนต่ออัตราการเกิดไฮโดรเจนสำหรับ CeO_2 ที่อุณหภูมิต่างๆ

5.3.4 ผลของการเติมคาร์บอนมอนอกไซด์ต่อกระบวนการรีฟอร์มมิ่งของ CeO_2

การเติมก๊าซคาร์บอนมอนอกไซด์ด้วยความเข้มข้นต่างๆ เข้าไปในสายป้อนจะลดอัตราการเกิดปฏิกิริยารีฟอร์มมิ่งของ CeO_2 ดังแสดงในรูปที่ 5.9 เนื่องจากคาร์บอนมอนอกไซด์ที่ถูกเติมเข้าไปจะทำปฏิกิริยากับ CeO_2 และเปลี่ยนเป็น CeO_{2-n}

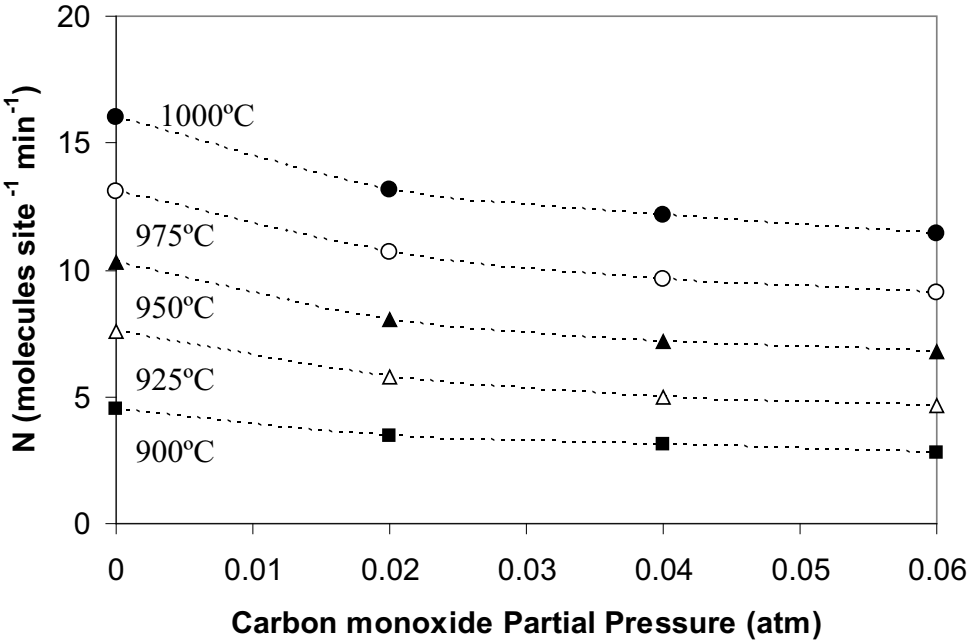

รูปที่ 5.9 ผลของการเติม CO ต่ออัตราการเกิดไฮโดรเจนสำหรับ CeO_2 ที่อุณหภูมิต่างๆ

5.3.5 ผลของออกซิเจนต่อกระบวนการรีฟอร์มมิ่งของ CeO_2

การเติมก๊าซออกซิเจนด้วยความเข้มข้นต่างๆ เข้าไปในสายป้อนจะทำให้อัตราการเกิดปฏิกิริยารีฟอร์มมิ่งของ CeO_2 มีค่าเพิ่มขึ้นเช่นเดียวกับการเติมคาร์บอนไดออกไซด์ เนื่องจากออกซิเจนสามารถออกซิไดซ์ CeO_{2-n} ให้กลายเป็น CeO_2 ได้ดังสมการด้านล่าง แต่ความเข้มข้นของไฮโดรเจน และคาร์บอน มอนออกไซด์ซึ่งสามารถใช้ประโยชน์ในเซลล์เชื้อเพลิงได้จะมีค่าลดลงเมื่อเติมออกซิเจนเข้าสู่ระบบ

$$CeO_{2-n} + nO_2 \Leftrightarrow CeO_2$$

ตารางที่ 5.2 ในหน้าถัดไปแสดงค่า Reaction Order ของก๊าซทุกชนิดที่ดำเนินการทดลองบนตัวเร่งปฏิกิริยา CeO_2

Table 5.2 Reaction orders for the components of interest (CH_4, CO_2, CO, and H_2) from the dry reforming over CeO_2 (HSA) at different operating conditions

Components of interest	Temperature (ºC)	Other inlet compositions (atm)				Reaction order for components of interest
		CH_4	CO_2	H_2	CO	
CH_4	900-1000		0.05	0	0	0.52 ± 0.02
(0.01-0.04 atm)	900		0.10	0	0	0.50
	900		0.15	0	0	0.51
	900-950		0.05	0.02	0	0.54 ± 0.01
	900-950		0.05	0	0.02	0.53 ± 0.02
CO_2	900-1000	0.04		0	0	0.10 ± 0.02
(0.01-0.09 atm)	900	0.02		0	0	0.10
	900	0.07		0	0	0.08
	900-925	0.04		0.02	0	0.10 ± 0.02
	900-950	0.04		0	0.02	0.11 ± 0.01
H_2	900-1000	0.04	0.05		0	–0.31 ± 0.03
(0.02-0.06 atm)	900	0.04	0.10		0	-0.28
	900	0.02	0.05		0	-0.34
	900	0.04	0.05		0.02	-0.30
CO	900-1000	0.04	0.05	0		-0.11 ± 0.01
(0.02-0.06 atm)	900	0.04	0.10	0		-0.12
	900	0.02	0.05	0		-0.15
	900	0.04	0.05	0.02		-0.10

บทที่ 6
การศึกษาผลของชนิดเชื้อเพลิงที่ป้อนต่อการเสื่อมสภาพของตัวเร่งปฏิกิริยา

ดังที่ได้กล่าวมา นิกเกิลเป็นสารที่ใช้กันแพร่หลายเนื่องจากให้ประสิทธิภาพที่ดีในทุกช่วงของอุณหภูมิและสามารถทำหน้าที่เป็นตัวเร่งปฏิกิริยาที่ดี แต่สารนิกเกิลก็มีข้อเสียที่สำคัญคือ การเสื่อมสภาพของอันสืบเนื่องมาจากการฟอร์มตัวของคาร์บอนที่ผิว ดังนั้นงานวิจัยนี้จึงดำเนินการทดลองเพื่อแสดงผลการเสื่อมสภาพของ Ni บนตัวรองรับหลายๆ ชนิด เมื่อมีการใช้เชื้อเพลิงประเภทต่างๆ ป้อนเข้ามา เช่น ก๊าซไฮโดรเจน, ก๊าซไฮโดรเจนผสมก๊าซคาร์บอนมอนอกไซด์, ก๊าซมีเทน, ก๊าซมีเทนผสมไอน้ำ ($CH_4 + H_2O$), เมทานอลผสมไอน้ำ ($CH_3OH + H_2O$) และเอทานอลผสมไอน้ำ($C_2H_5OH + H_2O$)

รูปที่ 6.1 แสดงรูปแบบการต่อชุดทดลอง ซึ่งประกอบด้วยสามส่วนหลักคือ ชุดป้อนก๊าซ, ชุดปฏิกรณ์ และ ชุดเครื่องมือวัด ชุดป้อนก๊าซจะเพิ่มระบบ evaporator เพื่อใช้กับเชื้อเพลิงเมทานอล และ เอทานอล เชื้อเพลิงที่ป้อนอาทิ เช่น ก๊าซไฮโดรเจน ก๊าซไฮโดรเจนผสมกับก๊าซคาร์บอนมอนอกไซด์ ก๊าซมีเทน ก๊าซมีเทนผสมไอน้ำ เมทานอลผสมไอน้ำและเอทานอลผสมไอน้ำจะถูกป้อนเข้าไปที่ชุดปฏิกรณ์ซึ่งบรรจุอยู่ภายในเตาปฏิกรณ์ Ni ปริมาณ150มิลลิกรัมจะถูกบรรจุเข้าไปในชุดปฏิกรณ์โดยรองด้วquartz-wool เพื่อป้องกันการเคลื่อนที่ของสารประกอบ Ni/ZrO_2 ความเร็วของการป้อน 20-200-มิลลิลิตรต่อนาที และทำการติดตั้ง type K เทอร์โมคัปเปิ้ล ในชุดปฏิกรณ์เพื่อทำการวัดอุณหภูมิของระบบ ก๊าซผลิตภัณฑ์ที่เกิดจากการทำปฏิกิริยาจะถูกป้อนเข้าไปยังเครื่อง Mass Spectrometer (MS) เพื่อทำการวิเคราะห์องค์ประกอบของก๊าซผลิตภัณฑ์ที่เกิดขึ้น ขั้นตอนการทดลองจะเริ่มต้นจากการรีดิวซ์สารประกอบ Ni/ZrO_2 ด้วยก๊าซฮีเลียมผสมกับก๊าซไฮโดรเจน 7เปอร์เซ็นต์เป็นเวลาสามชั่วโมงที่อุณหภูมิ 400 ˚C แล้วลดอุณหภูมิลงมาที่100˚C หลังจากนั้นป้อนก๊าซเชื้อเพลิงโดยเริ่มที่ก๊าซมีเทนที่ความดัน 0.05 atm จากนั้นค่อยๆเพิ่มอุณหภูมิขึ้นไปจนถึง900˚C เพื่อจะให้เชื้อเพลิงป้อนเกิดการสลายตัวของสารประกอบคาร์บอน กระบวนการนี้เรียกว่ากระบวนการ Temperature Program Methane Absorption (TPMA) หลังจากนั้นก็ใช้กระบวนการ Temperature Program Oxidation (TPO) เพื่อหาปริมาณคาร์บอนฟอร์มเมชั่นที่เกิดบนสารประกอบ Ni หลังจากนั้นทำการทดลองโดยเปลี่ยนอุณหภูมิจาก 900˚C เป็น 925, 950, 975 และ 1000˚C ตามลำดับ โดยเชื้อเพลิงป้อนจะป้อนหลังจากที่อุณหภูมิถึงค่าที่กำหนด หลังจากนั้นทำการเปลี่ยนชนิดของเชื้อเพลิงชนิดอื่นๆ

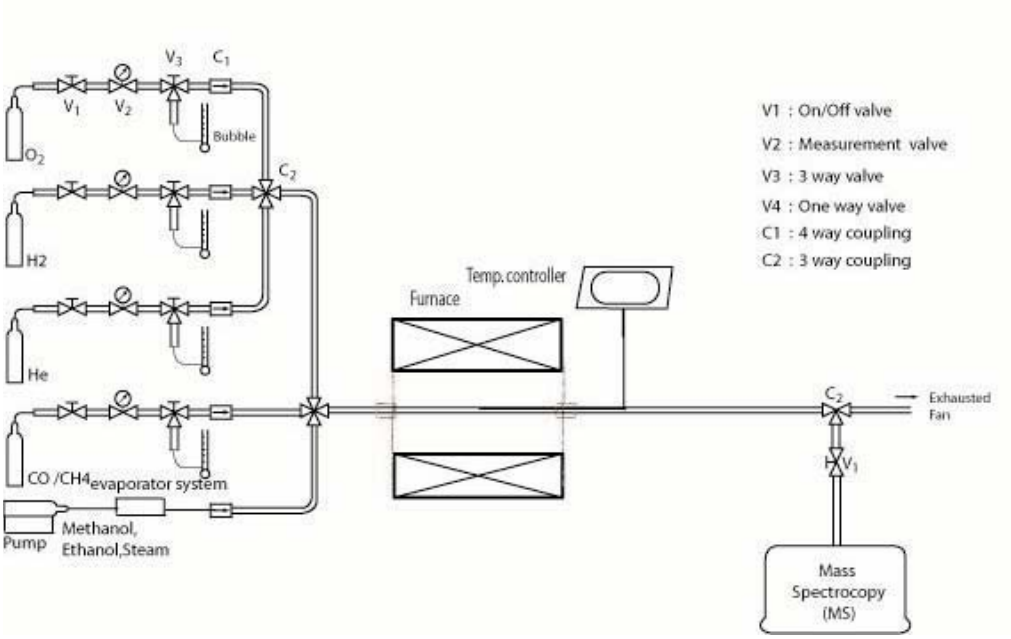

รูปที่ 6.1 ภาพแสดงการต่อชุดทดลอง

6.1 <u>การศึกษาผลการดูดซับก๊าซมีเทนโดยใช้กระบวนการ Temperature Program Methane Absorption (TPMA)</u>

การดำเนินการเริ่มต้นจากการรีดิวซ์ Ni ด้วยก๊าซฮีเลียมผสมกับก๊าซไฮโดรเจน 7 เปอร์เซ็นต์เป็นเวลาสามชั่วโมงที่อุณหภูมิ400 ˚C แล้วลดอุณหภูมิลงมาที่100 ˚C หลังจากนั้นป้อนก๊าซมีเทนที่ความดัน 0.05 atm จากนั้นค่อยๆเพิ่มอุณหภูมิขึ้นไปจนถึง900˚C ผลการทดลองแสดงดังรูป 6.2

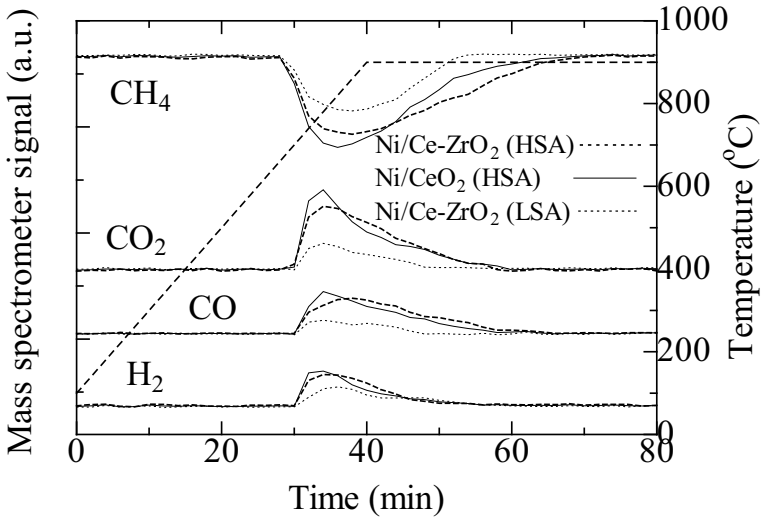

รูปที่ 6.2 กราฟแสดงผลของการดูดซับก๊าซมีเทนของสารประกอบ Ni/ZrO_2 จากกระบวนการ Temperature Program Methane Absorption (TPMA)

จากรูปดังกล่าวพบว่าค่าปริมาณก๊าซมีเทน (CH_4) จะลดต่ำลงและในขณะเดียวกันค่าของปริมาณก๊าซ H_2 จะมีปริมาณเพิ่มขึ้น จากนั้นปริมาณก๊าซมีเทนค่อยๆเพิ่มกลับไปยังค่าปกติ และค่าของปริมาณก๊าซ H_2 จะมีปริมาณลดลง แสดงว่ามีการสลายตัวของก๊าซมีเทนไปเป็นก๊าซ H_2 และเกิดคาร์บอนฟอร์มเมชันบน Ni

6.2 การศึกษาหาปริมาณการเกิด Carbon formation โดยกระบวนการ Temperature Program Oxidation (TPO)

หลังจากกระบวนการTemperature Program Methane Absorption (TPMA) เสร็จสิ้นแล้วทำการลดอุณหภูมิลงมาที่100 ˚C หลังจากนั้นป้อนก๊าซฮีเลียมเพื่อไล่ก๊าซเชื้อเพลิงที่ค้างอยู่ออกแล้วทำการป้อนก๊าซออกซิเจนที่ความดัน 0.05 atm และค่อยๆเพิ่มอุณหภูมิขึ้นไปจนถึง900˚C ผลจากการทดลอง แสดงดังรูป 6.3 หลังจากป้อนก๊าซออกซิเจนค่าปริมาณออกซิเจนจะลดต่ำลงและในขณะเดียวกันค่าของปริมาณก๊าซ CO และ CO_2 จะมีปริมาณเพิ่มขึ้น ปริมาณก๊าซออกซิเจนค่อยๆเพิ่มกลับไปยังค่าปกติ และค่าของปริมาณก๊าซ CO และ CO_2 จะมีปริมาณลดลง แสดงว่ามีการสลายตัวของคาร์บอนที่เกาะอยู่บน Ni ไปเป็นก๊าซ CO และ CO_2

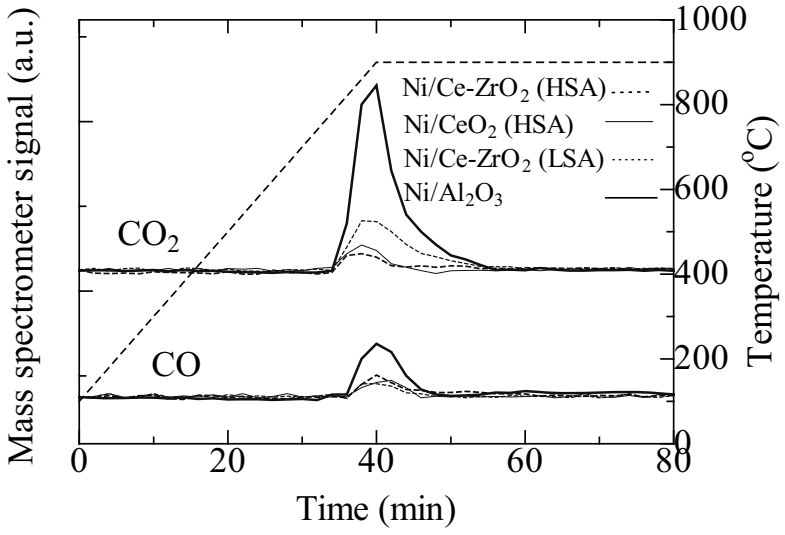

รูปที่ 6.3 Temperature Program Methane Absorption (TPMA) ของ Ni/ZrO_2

6.3 การศึกษาผลของอุณหภูมิที่มีต่อการเกิด Carbon formation

การดำเนินการจะคล้ายเดิมคือทำการรีดิวซ์ด้วยก๊าซฮีเลียมผสมกับก๊าซไฮโดรเจน 7 เปอร์เซ็นต์เป็นเวลาสามชั่วโมงที่อุณหภูมิ 400˚C หลังจากนั้นป้อนเฉพาะก๊าซฮีเลียมและเพิ่มอุณหภูมิจนถึง900˚C และทำการป้อนก๊าซมีเทนที่ความดัน 0.05 atm เป็นเวลา1ชั่วโมง และทำการทดลองโดยการเปลี่ยนอุณหภูมิจาก 900˚C เป็น 925, 950, 975 และ 1000˚Cตามลำดับ ผลจากการทดลองแสดงดังรูป 6.4 จะพบว่ามีการ

สลายตัวของก๊าซมีเทนไปเป็นก๊าซH_2 เพิ่มมากขึ้นตามอุณหภูมิที่สูงขึ้น ดังนั้นปริมาณคาร์บอนที่ฟอร์มตัวบนผิวของสารประกอบ Ni/Ce-ZrO_2 จะเกิดในปริมาณมากขึ้นตามอุณหภูมิที่สูงขึ้นด้วย

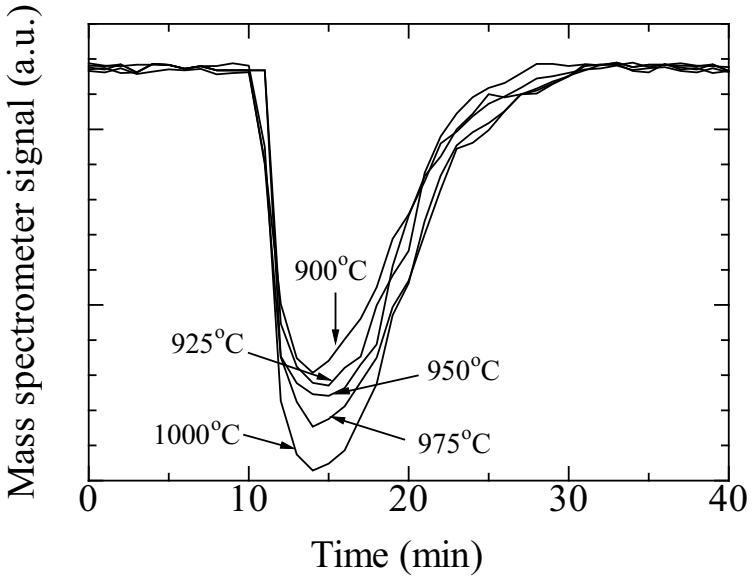

รูปที่ 6.4 กราฟแสดงผลของอุณหภูมิต่อการดูดซับก๊าซมีเทนของสารประกอบ Ni/Ce-ZrO_2 จากกระบวนการ Temperature Program Methane Absorption (TPMA) ที่อุณหภูมิต่าง ๆ

6.4 การศึกษาการเกิด Carbon formation เมื่อใช้เชื้อเพลิงป้อนชนิดต่าง ๆ กัน

ทำการทดลองตามกระบวนการในหัวข้อ 6.1 และ 6.2 เพื่อทำการหาปริมาณการเกิดคาร์บอนฟอร์มเมชัน โดยทำการเปลี่ยนเชื้อเพลิงชนิดต่าง ๆ กัน ได้แก่ ก๊าซไฮโดรเจน, ก๊าซไฮโดรเจนผสมก๊าซคาร์บอนมอนอกไซด์, มีเทนผสมไอน้ำ เมทานอลผสมไอน้ำ และเอทานอลผสมไอน้ำ ในการผสมน้ำจะผสมน้ำในอัตราส่วน 3:1 การเกิดคาร์บอนฟอร์มเมชันบน Ni จะแสดงได้ดังรูป 6.5 โดยเมื่อทำการป้อนก๊าซคาร์บอนมอนอกไซด์ผสมกับก๊าซไฮโดรเจน และก๊าซมีเทนผสมไอน้ำ จะเกิดคาร์บอนฟอร์มเมชันในอัตราส่วนไม่สูงเมื่อเทียบกับการป้อนด้วยก๊าซไฮโดรเจนบริสุทธิ์ ส่วนการป้อนด้วยก๊าซมีเทน, เมทานอลผสมไอน้ำ และเอทานอลผสมไอน้ำ จะเกิดคาร์บอนฟอร์มเมชันในอัตราส่วนที่สูง และหลังจากการป้อนเป็นเวลา60 นาทีการเกิดคาร์บอนฟอร์มเมชันของทุกชนิดเชื้อเพลิงป้อนจะเริ่มคงที่ ค่าปริมาณคาร์บอนฟอร์มเมชันจากผลการทดลองจะมีค่าตามตารางที่ 6.1

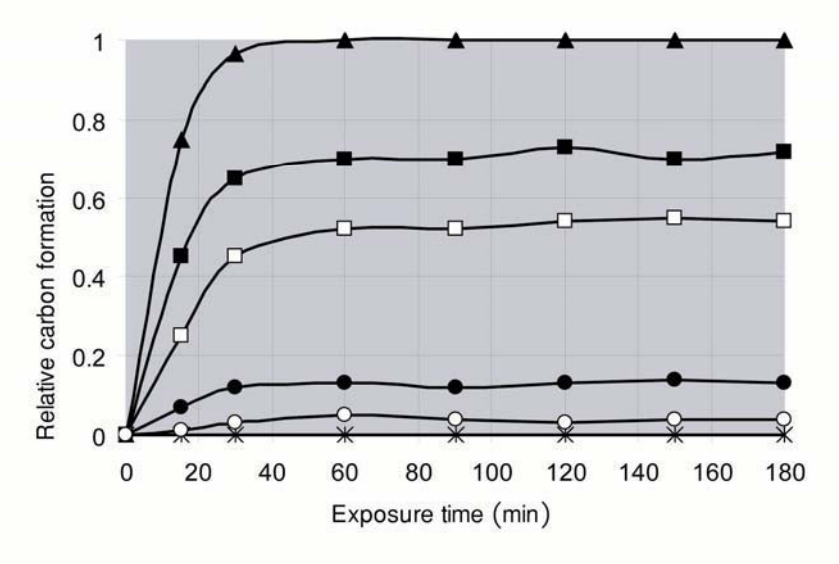

รูปที่ 6.5 ปริมาณการเกิดคาร์บอนจากการป้อนเชื้อเพลิงชนิดต่างๆ (H_2(✳), $CO+H_2$(○), CH_4+H_2O (●), CH_4(□), CH_3OH+H_2O(■), และ$C_2H_5OH+H_2O$(▲))ที่อุณหภูมิ 900°C

ตารางที่ 6.1 แสดงปริมาณของคาร์บอนฟอร์มเมชันที่อุณหภูมิ900˚C สำหรับการป้อนเชื้อเพลิงชนิดต่าง ๆ

ชนิดเชื้อเพลิงป้อน	ปริมาณของคาร์บอนฟอร์มเมชันที่ 900ºC (mmol/g)
H_2	0.0
$CO + H_2$	0.17
$CH_4 + H_2O$	0.55
CH_4	2.31
$CH_3OH + H_2O$	3.08
$C_2H_5OH + H_2O$	4.27

เมื่อทำการทดลองโดยการเปลี่ยนอุณหภูมิจาก 900˚C เป็น 925, 950, 975 และ 1000˚Cตามลำดับ ผลจากการทดลองแสดงดังรูปที่ 6.6 การป้อนก๊าซคาร์บอนมอนอกไซด์ผสมกับก๊าซไฮโดรเจน และก๊าซมีเทนผสมไอน้ำ จะเกิดคาร์บอนฟอร์มเมชันในอัตราส่วนไม่สูงเมื่อเทียบกับการป้อนด้วยก๊าซไฮโดรเจนบริสุทธิ์ตลอดช่วงอุณหภูมิ 900˚Cถึง 1000˚C ส่วนการป้อนด้วยก๊าซมีเทน, เมทานอลผสมไอน้ำ และเอทานอลผสมไอน้ำ จะเกิดคาร์บอนฟอร์มเมชันในอัตราส่วนที่สูงมากเมื่ออุณหภูมิเพิ่มสูงขึ้น

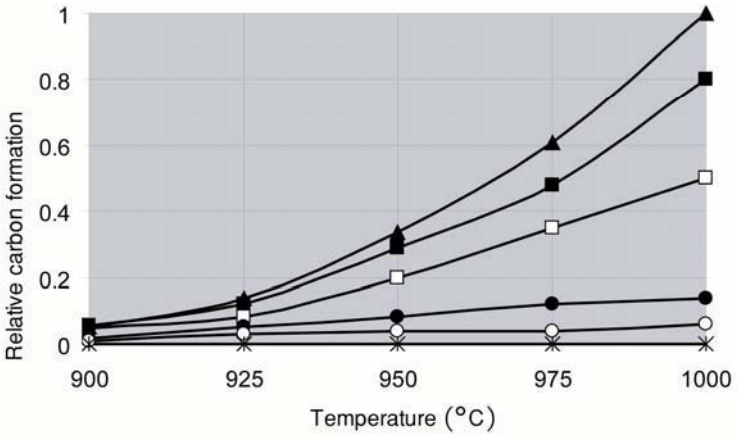

รูปที่ 6.6 ปริมาณการเกิดคาร์บอนฟอร์มเมชันของเชื้อเพลิงป้อนชนิดต่างๆ (H_2(✳), $CO+H_2$(○), CH_4+H_2O(●), CH_4(□), CH_3OH+H_2O(■), และ$C_2H_5OH+H_2O$(▲))ที่อุณหภูมิ 900,925, 950, 975 และ 1000 ๐C

6.5 ผลของอัตราส่วนน้ำต่อเชื้อเพลิงไฮโดรคาร์บอน (CH_4 , CH_3OH และ C_2H_5OH) ที่มีผลต่อการเกิด Carbon formation

เมื่อทำการเปลี่ยนอัตราส่วนของไอน้ำต่อเชื้อเพลิงไฮโดรคาร์บอน (CH_4, CH_3OH และ C_2H_5OH) จากอัตราส่วน 3:1 เป็น 4:1 และ 5:1 ตามลำดับ ปริมาณของ Carbon formation ที่ได้ดังแสดงในตารางที่ 6.2

ตารางที่ 6.2 แสดงปริมาณของ Carbon formation โดยใช้อัตราส่วนของไอน้ำต่อเชื้อเพลิงต่างกัน

ชนิดเชื้อเพลิงป้อน	ปริมาณของ Carbon formation ที่ 900ºC (mmol/g)		
	ไอน้ำ/เชื้อเพลิง = 3:1	ไอน้ำ/เชื้อเพลิง = 4:1	ไอน้ำ/เชื้อเพลิง = 5:1
CH_4+H_2O	0.55	0.42	0.27
CH_3OH+H_2O	3.08	2.86	2.54
$C_2H_5OH+H_2O$	4.27	4.20	4.09

จากตารางที่ 6.2 จะพบว่าเมื่อเพิ่มอัตราส่วนของไอน้ำต่อเชื้อเพลิงมีเทน ค่าของคาร์บอนฟอร์มเมชันจะลดลงในอัตราส่วนที่สูง แต่สำหรับเชื้อเพลิงเมทานอลและเอทานอลค่าของคาร์บอนฟอร์มเมชันลดลงในปริมาณไม่มาก

บทที่ 7
กระบวนการรีฟอร์มมิ่งเอทานอลด้วยน้ำ (Ethanol Steam Reforming)

กระบวนการรีฟอร์มมิ่งเอทานอลด้วยน้ำจะมีปฏิกิริยาที่เกี่ยวข้องอยู่ 4 ปฏิกิริยาใหญ่ซึ่งแต่ละปฏิกิริยาจะเกิดขึ้นที่สภาวะอุณหภูมิต่างกัน โดยที่อุณหภูมิต่ำ (200-350 ºC) ปฏิกิริยาที่เกิดขึ้นคือปฏิกิริยาการสลายตัวของเอทานอล (Ethanol dehydration) กลายเป็นสารประกอบ Acetaldehyde (CH_3CHO) จากนั้นสารประกอบดังกล่าวจะเกิดการแตกตัวเป็นมีเทน (CH_4) และคาร์บอนมอนออกไซด์ (CO) ได้เช่นกัน ดังแสดงในปฏิกิริยาที่ 1 และ 2

$$C_2H_5OH \rightarrow CH_3CHO + H_2 \quad (1)$$

$$CH_3CHO \rightarrow CH_4 + CO \quad (2)$$

ที่อุณหภูมิสูงขึ้นจะมีปฏิกิริยาอีก 2 ปฏิกิริยาเกิดขึ้นคือปฏิกิริยารีฟอร์มมิ่งของมีเทนด้วยน้ำ (Methane steam reforming) และปฏิกิริยา Water-Gas shift reaction ดังแสดงในปฏิกิริยาที่ 3 และ 4 ด้านล่าง

$$CH_4 + H_2O \rightarrow CO + 3H_2 \quad (3)$$

$$CO + H_2O \rightarrow CO_2 + H_2 \quad (4)$$

คุณสมบัติที่สำคัญสำหรับตัวเร่งปฏิกิริยาของกระบวนการรีฟอร์มมิ่งคือความสามารถในการทำปฏิกิริยา และความต้านทานต่อการเกิดคาร์บอนบนพื้นผิว นอกจากนั้นแล้วตัวเร่งปฏิกิริยาที่ดีควรมีเสถียรภาพสูงเมื่อถูกใช้งานที่อุณหภูมิสูง (High thermal stability) และมีความต้านทานต่อการเสื่อมสภาพเนื่องจากสารปนเปื้อนบางชนิด (Poisoning) ในแง่คุณสมบัติทางกายภาพของตัวเร่งปฏิกิริยานั้นตัวเร่งปฏิกิริยาที่ดีควรมีความคงทนต่อการเสียดสี และไม่เกิดการเสียรูปเช่นการหัก หรือแตกเมื่อใช้งานซึ่งจะนำมาซึ่งการเปลี่ยนแปลงในเรื่องของคุณสมบัติการถ่ายเทความร้อน และมวลสารได้ ในการใช้งานจริงนั้นรูปทรงของตัวเร่งปฏิกิริยาที่ดีหลังการขึ้นรูปแล้วควรจะมีพื้นที่ผิวต่อน้ำหนัก หรือปริมาตรสูง และทำให้เกิดการลดลงของความดัน (Pressure drop) ภายในเครื่องปฏิกรณ์น้อยที่สุด สำหรับตัวเร่งปฏิกิริยาที่ใช้ในกระบวนการรีฟอร์มมิ่งเพื่อผลิตไฮโดรเจนนั้น พบว่าธาตุในหมู่ VIII อันประกอบด้วย Fe, Co, Ni, Rd, Ru, Pd, Os, Ir and Pt สามารถเป็นตัวเร่งปฏิกิริยาของกระบวนการดังกล่าวได้ อย่างไรก็ตามได้มีรายงานมากมายเกี่ยวข้องกับการเสื่อมศักยภาพ (Deactivation) ของตัวเร่งปฏิกิริยาเหล่านี้เมื่อใช้งานภายใต้กระบวนการดัง

กล่าว ซึ่งปัญหาหลักที่ทำให้ตัวเร่งปฏิกิริยาเกิดการเสื่อมศักยภาพคือการเกิดคาร์บอนบริเวณผิวของตัวเร่งปฏิกิริยา (Carbon formation) ผ่านกระบวนการ Boudouard reaction หรือกระบวนการ สลายตัวด้วยความร้อน (Thermal cracking) การที่สารปนเปื้อนบางชนิดเช่น กำมะถัน (Sulphur) ทำปฏิกิริยากับตัวเร่งปฏิกิริยา (Catalyst poisoning) เป็นต้น ในปัจจุบันตัวเร่งปฏิกิริยานิเกิล (Ni) ถูกนำมาใช้กันอย่างแพร่หลายเนื่องจากปัจจัยด้านราคา และปริมาณ (Availability) ของสารชนิดนี้ ดังนั้นในงานวิจัยนี้จึงใช้ตัวเร่งปฏิกิริยา Ni/Al_2O_3 และ ตัวเร่งปฏิกิริยาชนิด Ni/CeO_2 ที่สังเคราะห์หาอัตราส่วนที่เหมาะสมขึ้นเองในการทดลอง

7.1 การดำเนินการทดลองเพื่อศึกษากระบวนการรีฟอร์มมิ่งเอทานอลด้วยน้ำ

เพื่อดำเนินการศึกษากระบวนการรีฟอร์มมิ่งเอทานอลด้วยน้ำ จึงมีการสร้างระบบที่ใช้ในการทดลองโดยส่วนประกอบหลักคือเครื่องปฏิกรณ์ (Catalytic reactor) นอกจากนี้ยังนำระบบ Evaporator เข้ามาใช้เพื่อให้สามารถควบคุมอัตราการป้อนของเอทานอล และน้ำเข้าสู่ระบบได้อย่างมีประสิทธิภาพ โดยระบบดังกล่าวจะถูกต่อเข้ากับเครื่อง Gas Chromatography/Mass Spectrometer (GC-MS) เพื่อให้สามารถทำการวิเคราะห์องค์ประกอบของก๊าซผลิตภัณฑ์จากกระบวนการรีฟอร์มมิ่งว่าสามารถผลิตก๊าซชนิดใดออกมาได้ และปริมาณของสารตั้งต้นที่คงเหลือ ทั้งแบบ Steady state condition และ Transient condition ในส่วนของการวัดปริมาณคาร์บอนบนผิวของตัวเร่งปฏิกิริยานั้นดำเนินการโดยใช้เครื่อง Thermogravimetric Analyzer/ Mass Spectrometer (TGA-MS)

ในส่วนของการดำเนินการทดลองนั้นได้ทำการศึกษาในสภาวะที่ไม่มีตัวเร่งปฏิกิริยา (Homogeneous reaction) และมีตัวเร่งปฏิกิริยา ในกรณีของการศึกษาด้วยตัวเร่งปฏิกิริยา เมื่อทำการบรรจุตัวเร่งปฏิกิริยาชนิด Ni/Al_2O_3 หรือ Ni/CeO_2 แล้วป้อนเอทานอล และน้ำเข้าสู่ระบบ จะทำการวัดอัตราการสลายตัวของเอทานอล (Conversion) รวมถึงอัตราการเกิดไฮโดรเจนที่อุณหภูมิต่างๆ กัน (700–1000 °C) เพื่อศึกษาผลของอุณหภูมิต่ออัตราเร็วในการเกิดปฏิกิริยา นอกจากการศึกษาผลของอุณหภูมิแล้ว ก็ทำการวัดอัตราการเกิดไฮโดรเจน (H_2 Selectivity) วัดเสถียรภาพของตัวเร่งปฏิกิริยา (Stability) โดยการทำการทดลองต่อเนื่องเป็นเวลา 600 นาที รวมถึงวัดปริมาณการเกิดคาร์บอนที่ผิวของตัวเร่งปฏิกิริยาโดยวิธี Temperature Programmed Oxidation (TPO)

7.1.1 การรีฟอร์มมิ่งเอทานอลด้วยน้ำ โดยปราศจากตัวเร่งปฏิกิริยา (Homogeneous reaction)

ก่อนทำการศึกษากระบวนการรีฟอร์มมิ่งด้วยน้ำบนตัวเร่งปฏิกิริยา Ni/Al_2O_3 และ Ni/CeO_2 ได้ทำการศึกษาปฏิกิริยาของการรีฟอร์มมิ่งด้วยน้ำโดยปราศจากตัวเร่งปฏิกิริยาที่อุณหภูมิต่าง ๆ เพื่อใช้เปรียบเทียบกับแบบที่มีตัวเร่งปฏิกิริยา ผลที่ได้แสดงในรูปที่ 7.1 พบว่า ที่ช่วงอุณหภูมิต่ำ (200-550°C) จะเกิด Acetaldehyde (CH_3CHO) และจะถูกเปลี่ยนไปเป็นสารอื่นในอุณหภูมิที่สูงขึ้นซึ่งที่อุณหภูมิช่วงนั้น เอทานอลจะสามารถแตกตัว (Cracking) เป็นมีเทน (CH_4), ไฮโดรเจน (H_2) คาร์บอนมอนออกไซด์ (CO), และ

คาร์บอนไดออกไซด์(CO_2)ได้ และค่าการสลายตัว (Conversion) ของเอทานอล (C_2H_5OH) จะแปรผันโดยตรงกับอุณหภูมิ

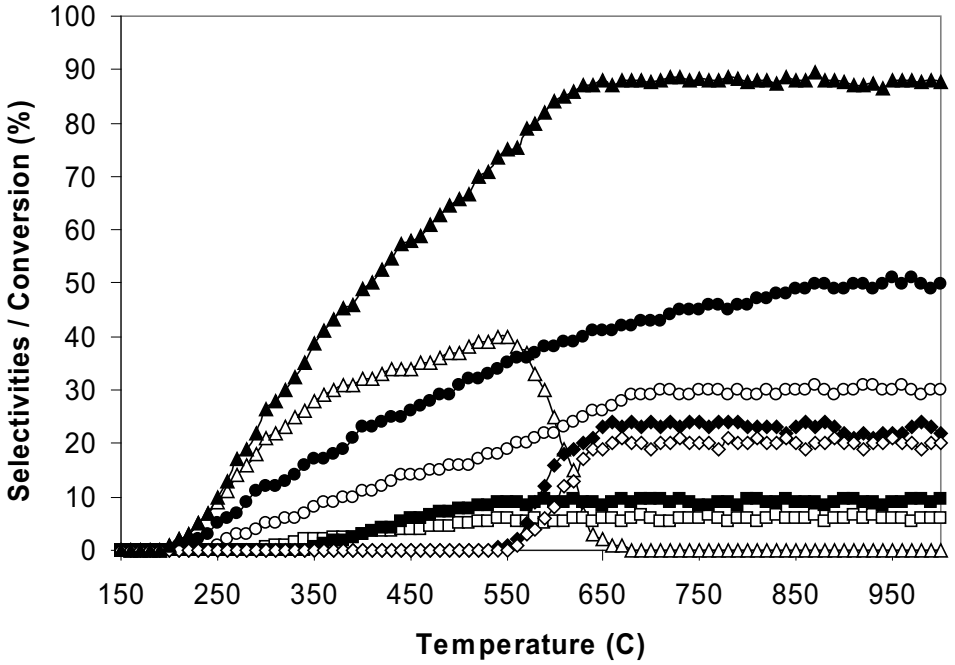

รูปที่ 7.1 ค่า Selectivities ของสารต่างๆ ที่ได้จากกระบวนการรีฟอร์มมิ่งเอทานอลด้วยน้ำที่อุณหภูมิระหว่าง 200 ถึง 1000 °C โดยปราศจากตัวเร่งปฏิกิริยา (EtOH (▲), H_2 (●), CO (○), CO_2 (■), CH_4 (□), CH_3CHO (△), C_2H_6 (◇), and C_2H_4 (◆)).

7.1.2 ศักยภาพในการผลิตไฮโดรเจนจากกระบวนการรีฟอร์มมิ่งเอทานอลด้วยน้ำ โดยใช้ตัวเร่งปฏิกิริยา Ni/Al_2O_3 และตัวเร่งปฏิกิริยา Ni/CeO_2

การทดลองเริ่มต้นโดยการศึกษาถึงศักยภาพในการผลิตไฮโดรเจนจากกระบวนการรีฟอร์มมิ่งเอทานอลด้วยน้ำที่อุณหภูมิต่างๆ กันบนตัวเร่งปฏิกิริยา Ni/Al_2O_3 (Lab grade) ผลที่ได้ดังแสดงในรูปที่ 7.2 พบว่าเมื่ออุณหภูมิสูงขึ้นเอทานอลสามารถรีฟอร์ม และผลิตไฮโดรเจนออกมาได้มากขึ้น จากนั้นศึกษาศักยภาพในการผลิตไฮโดรเจนจากกระบวนการรีฟอร์มมิ่งเอทานอลด้วยน้ำ ที่อุณหภูมิต่างๆ กันบนตัวเร่งปฏิกิริยา Ni/CeO_2 ผลที่ได้ดังแสดงในรูปที่ 7.3

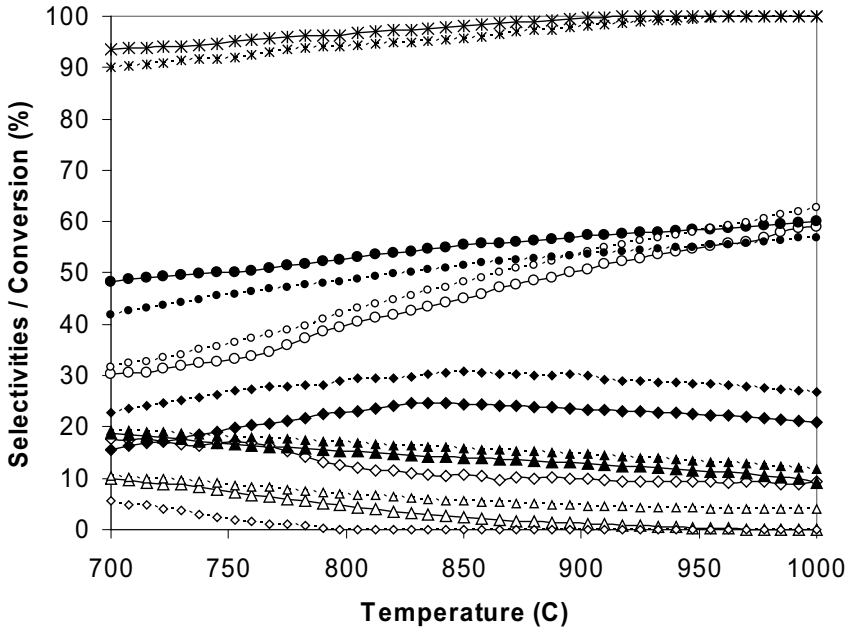

รูปที่ 7.2 ค่า Selectivities ของสารต่างๆ (EtOH (✕), H_2 (●), CO (○), CO_2 (◇), CH_4 (◆), C_2H_6 (△), and C_2H_4 (▲)) ที่ได้จากกระบวนการรีฟอร์มมิ่งเอทานอลด้วยน้ำที่อุณหภูมิระหว่าง 700 ถึง 1000 ° C บน Ni/Al_2O_3

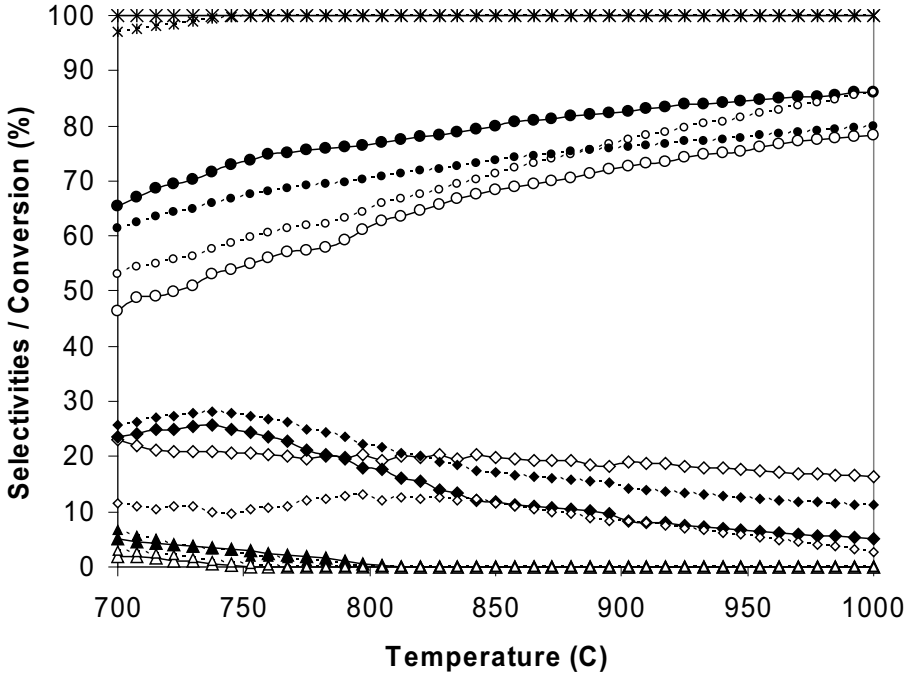

รูปที่ 7.3 ค่า Selectivities ของสารต่างๆ (EtOH (✕), H_2 (●), CO (○), CO_2 (◇), CH_4 (◆), C_2H_6 (△), and C_2H_4 (▲)) ที่ได้จากกระบวนการรีฟอร์มมิ่งเอทานอลด้วยน้ำที่อุณหภูมิระหว่าง 700 ถึง 1000 ° C บน Ni/CeO_2

นอกจากนี้ยังได้ศึกษาเสถียรภาพ (Stability) ของตัวเร่งปฏิกิริยาทั้ง 2 ชนิด โดยการดำเนินการต่อเนื่องเป็นเวลา 600 นาที พบว่า ตัวเร่งปฏิกิริยาชนิด Ni/CeO_2 นั้น มีเสถียรภาพสูงกว่า Ni/Al_2O_3 ดังแสดงในรูปที่ 7.4

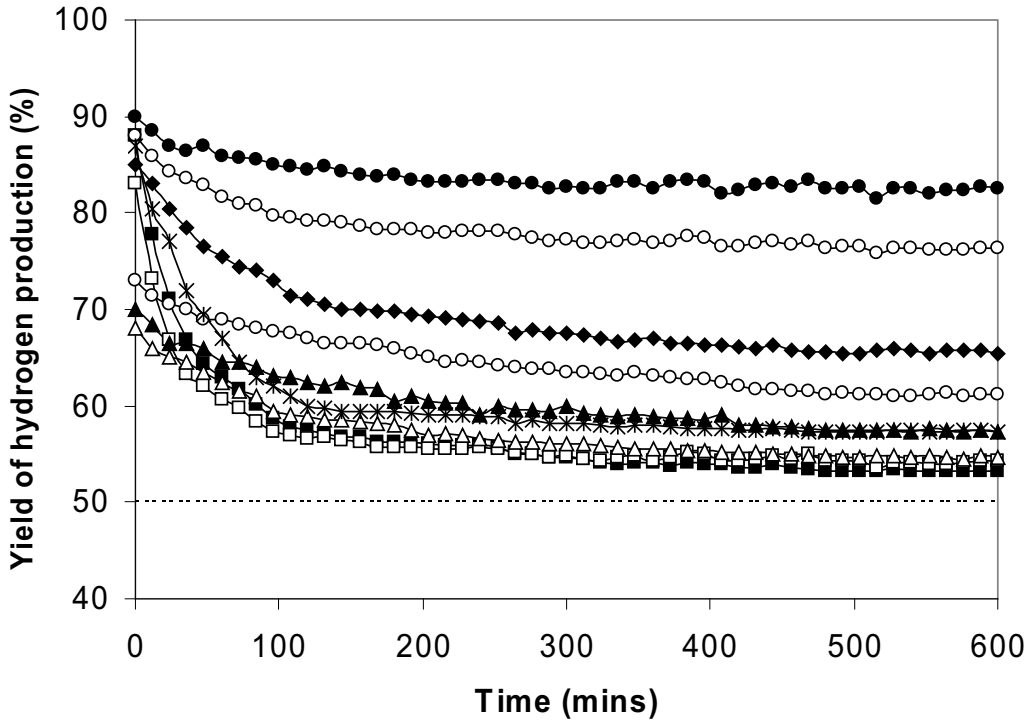

รูปที่ 7.4 แสดงเสถียรภาพของตัวเร่งปฏิกิริยาทั้งสองชนิด จากการดำเนินการรีฟอร์มมิ่งที่ 900 °C ต่อเนื่องถึง 600 นาที (Ni/CeO_2 (HSA) with 1/3 of $EtOH/H_2O$ (●), Ni/CeO_2 (HSA) with 1/2 of $EtOH/H_2O$ (○),Ni/CeO_2 (HSA) with 1/1 of $EtOH/H_2O$ (◆), Ni/CeO_2 (LSA) with 1/3 of $EtOH/H_2O$ (◇), Ni/CeO_2 (LSA) with 1/2 of $EtOH/H_2O$ (▲), Ni/CeO_2 (LSA) with 1/1 of $EtOH/H_2O$ (△),Ni/Al_2O_3 with 1/3 of $EtOH/H_2O$ (✕), Ni/Al_2O_3 with 1/2 of $EtOH/H_2O$ (□), and Ni/Al_2O_3 with 1/1 of $EtOH/H_2O$ (■)

จากนั้นได้ใช้วิธี Temperature Programmed Oxidation (TPO) เพื่อหาปริมาณการเกิดคาร์บอนบนพื้นผิวของตัวเร่งปฏิกิริยาทั้งสอง หลังจากการใช้งานรีฟอร์มมิ่งเป็นเวลา 600 นาที ดังแสดงผล ในรูปที่ 7.5 พบว่าการเกิดคาร์บอนที่พื้นผิวของตัวเร่งปฏิกิริยา Ni/CeO_2 นั้น มีปริมาณน้อยกว่า การเกิดคาร์บอนบนพื้นผิวของตัวเร่งปฏิกิริยา Ni/Al_2O_3 ซึ่งสอดคล้องกับผลการวิเคราะห์ปริมาณคาร์บอนของเครื่อง TGA-MS ดังแสดงผลในตารางที่ 7.1

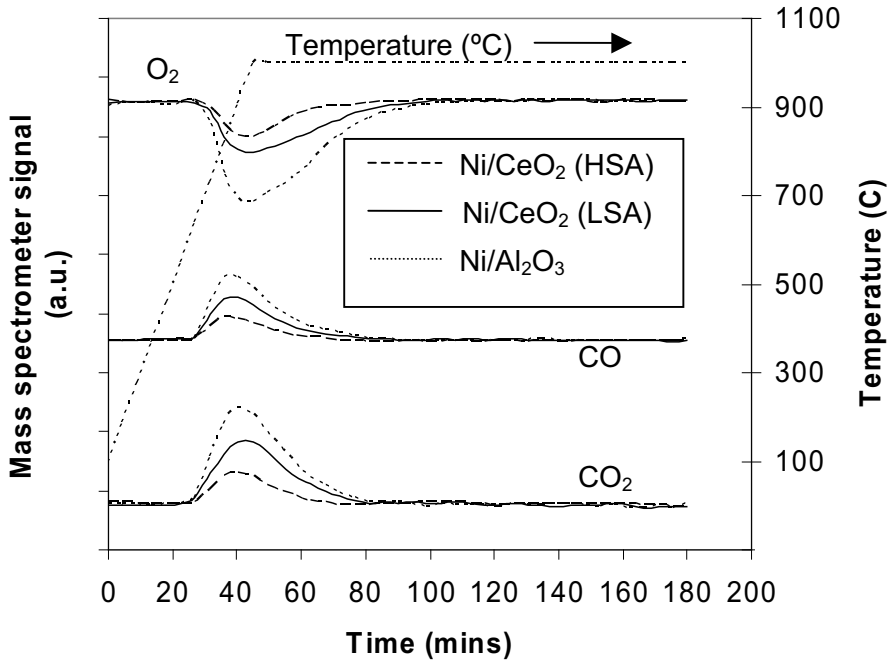

รูปที่ 7.5 แสดงผลของการทำ Temperature Programmed Oxidation ของตัวเร่งปฏิกิริยา Ni/Al_2O_3 เทียบกับ $Ni/Ce\text{-}ZrO_2$ หลังจากผ่านการใช้งานเป็นเวลา 600 นาที

Table 7.1
The dependence of inlet C_2H_5OH/H_2O ratio on the amount of carbon formation remaining on the catalyst surface

C_2H_5OH/H_2O ratio	Total carbon formation (monolayers)		
	Ni/CeO_2 (HSA)	Ni/CeO_2 (LSA)	Ni/Al_2O_3
1.0/3.0	1.08[a] (1.08)[b]	2.17 (2.15)	4.52 (4.54)
1.0/2.0	1.19 (1.17)	2.23 (2.21)	4.76 (4.78)
1.0/1.0	1.24 (1.26)	2.31 (2.34)	4.81 (4.79)

[a] Calculated using CO and CO_2 yields from temperature-programmed oxidation (TPO) with 10% oxygen.
[b] Calculated from the balance of carbon in the system.

บทที่ 8
กระบวนการรีฟอร์มมิ่งเมทานอลด้วยน้ำ (Methanol Steam Reforming)

8.1 กระบวนการรีฟอร์มมิงเมทานอลด้วยน้ำ (Methanol Steam Reforming Process)

ปฏิกิริยาหลักที่เกี่ยวข้องกับกระบวนการรีฟอร์มมิ่งเมทานอลด้วยน้ำประกอบด้วย (1) ปฏิกิริยารีฟอร์มมิ่งเมทานอลด้วยน้ำ (Methanol Steam Reforming), (2) ปฏิกิริยาการแตกตัวของเมทานอล (Methanol decomposition), และ (3) ปฏิกิริยา Water Gas Shift reaction

$$CH_3OH + H_2O \leftrightarrow CO_2 + 3H_2 \quad (1)$$

$$CH_3OH \leftrightarrow CO + 2H_2 \quad (2)$$

$$CO + H_2O \leftrightarrow CO_2 + H2 \quad (3)$$

ตามทฤษฎีแล้วร้อยละ 75 ของไฮโดรเจนที่ผลิตได้ทั้งหมดในกระบวนการนี้มาจากปฏิกิริยารีฟอร์มมิ่งเมทานอลด้วยน้ำ อย่างไรก็ตามกระบวนการนี้เกิดที่อุณหภูมิสูง ดังนั้นจึงต้องให้ความสำคัญกับปฏิกิริยาการแตกตัวของเมทานอล ซึ่งเป็นสาเหตุหลักในการเกิดคาร์บอนบนผิวของตัวเร่งปฏิกิริยา ส่งผลให้ประสิทธิภาพของตัวเร่งปฏิกิริยาลดลง เมื่อเร็วๆนี้ คณะทำงานของ Y.Choi [3] ได้เสนอกลไกการแตกตัวอย่างง่ายของเมทานอล โดยสารประกอบที่เกิดขึ้นมีดังต่อไปนี้ Dimethylether $(CH_3O)_2$, Methoxy (CH_3O), Formaldehyde (CH_2O), MethylFormate (CH_3OCHO) ท้ายที่สุดแล้ว นอกจากสารประกอบเหล่านี้จะแตกตัวกลายให้ผลิตภัณฑ์ดังปฏิกิริยาที่(2) แล้วยังมี ก๊าซมีเทน(CH_4) เกิดขึ้นด้วย เมื่อคาร์บอนมอนอกไซด์และมีเทนแตกตัว จะทำให้เกิดคาร์บอนบนผิวตัวเร่งปฏิกิริยาดังแสดงในปฏิกิริยาที่ (4) ปฏิกิริยา Boudouard และ (5) ปฏิกิริยาการแตกตัวของมีเทน (Methane decomposition)

$$2CO \leftrightarrow CO_2 + C \quad (4)$$

$$CH_4 \leftrightarrow 2H_2 + C \quad (5)$$

ตัวเร่งปฏิกิริยาที่เลือกใช้ในกระบวนการนี้คือ CeO_2 (HSA; High Surface Area) โดยจะทำการเปรียบเทียบกับ CeO_2 (LSA) ทั่วไป ส่วนระบบที่ใช้ในการศึกษากระบวนการรีฟอร์มมิ่งเมทานอลด้วยน้ำมีส่วนประกอบหลักคือ ระบบ Evaporator ใช้เพื่อควบคุมอัตราการป้อนเมทานอลและน้ำเข้าสู่ ระบบเครื่องปฏิกรณ์ (Catalytic Reactor) ปฏิกิริยาที่ต้องการศึกษาจะเกิดขึ้นในเครื่องนี้ อีกด้านหนึ่งเครื่องปฏิกรณ์ต่อเข้ากับเครื่องGas-Chromatography/Mass- Spectrometer (GC-MS) เพื่อวิเคราะห์องค์ประกอบของก๊าซ

จากกระบวนรีฟอร์มมิ่งว่ามีส่วนประกอบของสารตั้งต้นเหลือจากการทำปฏิกิริยาหรือไม่ และหลังจากเกิดปฏิกิริยาแล้ว เกิดก๊าซชนิดใดขึ้น สภาวะในการทดลองมีทั้งแบบ Steady State และ Transient ในส่วนของปริมาณคาร์บอนที่เกิดขึ้นบนผิวของตัวเร่งปฏิกิริยานั้น สามารถวิเคราะห์ได้โดยใช้เครื่อง TGA-MS หลังจากติดตั้งอุปกรณ์เรียบร้อยแล้ว จึงเริ่มทำการ ศึกษาการแตกตัวของเมทานอลโดยไม่ใช้ตัวเร่งปฏิกิริยา (Homogenous reaction) โดย ป้อนน้ำและเมทานอล (อัตราส่วนของน้ำต่อเมทานอลท คือ 1:3) เข้าสู่ระบบแล้ววัดอัตราการสลายตัวของเมทานอลและอัตราการเกิดไฮโดรเจนที่อุณหภูมิ 700 – 1000 ^{o}C เพื่อศึกษาผลของอุณหภูมิที่มีต่ออัตราการเกิดปฏิกิริยา หลัง จากนั้นจึงบรรจุตัวเร่งปฏิกิริยาลงในเครื่องปฏิกรณ์และทำการ ศึกษาเสถียรภาพทางความร้อน (Thermal stability)ของตัวเร่งปฏิกิริยาโดยการวัดอัตราการสลายตัวของเมทานอลที่อุณหภูมิ 900 ^{o}C เป็นเวลา 100 ชั่วโมง ต่อจาก นั้นจึงวิเคราะห์ปริมาณคาร์บอนที่เกิดขึ้นที่ผิวของตัวเร่งปฏิกิริยาในเครื่อง TGA-MS โดยการป้อน ออกซิเจนเข้าไปทำปฏิกิริยากับคาร์บอนบนผิวตัวเร่งปฏิกิริยา เรียกวิธีการนี้ว่า Temperature Program Oxidation (TPO) ปริมาณคาร์บอนบนผิวตัวเร่งปฏิกิริยาสามารถคำนวนได้จากสมดุลมวลรอบเครื่องปฏิกรณ์(mass balance) ซึ่งทางทฤษฎีนั้น จะเท่ากับผลต่างระหว่าง คาร์บอนในองค์ประกอบของสารที่ป้อนเข้าทั้งหมด (CH_3OH) กับคาร์บอนในองค์ประกอบของสารที่ออกจากเครื่องปฏิกรณ์ (CO, CO_2, และ CH_4) ทำการทดลองแบบนี้กับตัวเร่งปฏิกิริยาทั้ง 2 ชนิด เพื่อที่จะเปรียบเทียบประสิทธิภาพของตัวเร่งปฏิกิริยา CeO_2 (HSA; High Surface Area) กับตัวเร่งปฏิกิริยา CeO_2 (LSA)

8.2 <u>ผลการทดลองเพื่อศึกษากระบวนการรีฟอร์มมิงเมทานอลด้วยน้ำ</u>

จากการศึกษาการแตกตัวของเมทานอลโดยไม่ใช้ตัวเร่งปฏิกิริยาพบว่าเมทานอลสามารถผลิตไฮโดรเจนได้ที่อุณหภูมิสูง แต่ปริมาณไฮโดรเจนที่ได้มีปริมาณน้อย ดังแสดงในรูปที่ 8.1 ซึ่งอาจเป็นผลมาจากปฏิกิริยามี Selectivity ต่ำ ดังนั้นจึงต้องใช้ตัวเร่งปฏิกิริยาเพื่อเพิ่มอัตราการผลิตไฮโดรเจนของปฏิกิริยา อย่างไรก็ตามตัวเร่งปฏิกิริยาที่ใช้อยู่ในปัจจุบัน (Ni/Al_2O_3) มีปัญหาเรื่องการเกิดคาร์บอนที่ผิวส่งผลให้ความสามารถในการเร่งปฏิกิริยาลดลง จึงได้มีความพยายามในการหาตังเร่งปฏิกิริยาที่สามารถต้านทานการเกิดคาร์บอนที่ผิวได้มากกว่าซึ่งในงานวิจัยนี้เลือกใช้ตัวเร่งปฏิกิริยา CeO_2 เพื่อเป็นอีกทางเลือกหนึ่ง ซึ่งเมื่อทำการศึกษาเสถียรภาพต่อกระบวนการ (stability) และปริมาณของคาร์บอนที่เกิดที่ผิวของตัวเร่งปฏิกิริยาพบว่าอัตราการสลายตัวของเมทานอลบนตัวเร่งปฏิกิริยา CeO_2 ค่อนข้างคงที่ตลอดการใช้งาน ดังแสดงในรูปที่ 8.2 และเมื่อวิเคราะห์ปริมาณของคาร์บอนที่ผิวของตัวเร่งปฏิกิริยาพบว่าปริมาณคาร์บอนที่ผิวของตัวเร่งปฏิกิริยา CeO_2 มีค่าค่อนข้างต่ำดังผลที่แสดงในรูปที่ 8.3 ทั้งนี้เป็นผลมาจากความสามารถในการให้และรับออกซิเจนของ CeO_2 (Oxygen Storage Capacity; OSC) นั่นเอง

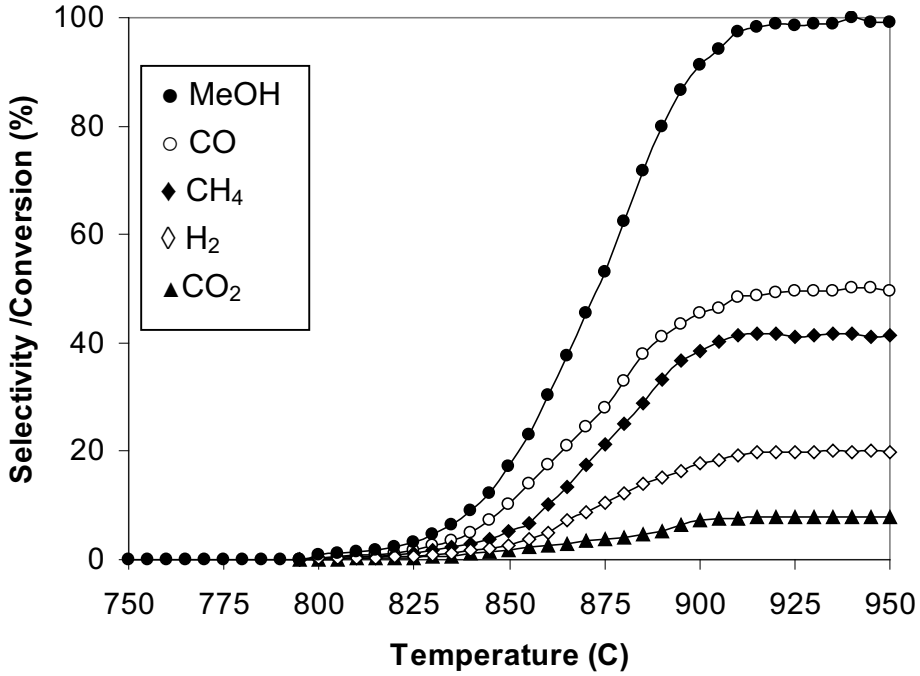

รูปที่ 8.1 ผลจากปฏิกิริยาการแตกตัวของเมทานอล โดยไม่ใช้ตัวเร่งปฏิกิริยา (1 kPa เมทานอล และ 3 kPa น้ำ)

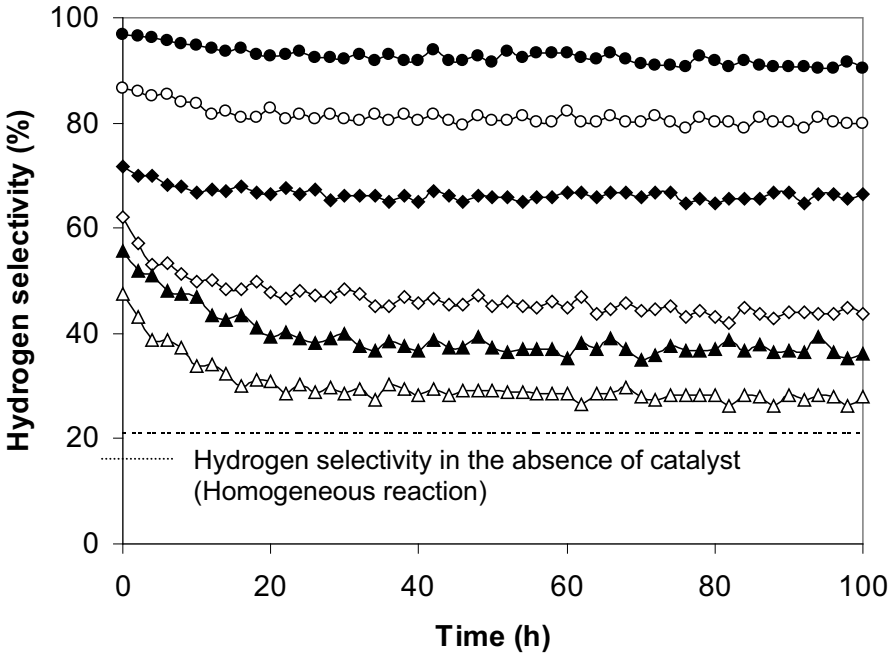

รูปที่ 8.2 เสถียรภาพต่อกระบวนการของตัวเร่งปฏิกิริยา CeO_2 ที่อุณหภูมิ 900 °C นาน 100 ชั่วโมง CeO_2 (HSA) with H_2O/CH_3OH of 3.0 (●),CeO_2 (HSA) with H_2O/CH_3OH of 1.0 (○),CeO_2 (HSA) with H_2O/CH_3OH of 0.0 (♦),CeO_2 (LSA) with H_2O/CH_3OH of 3.0 (◊),CeO_2 (LSA) with H_2O/CH_3OH of 1.0 (▲), and CeO_2 (LSA) with H_2O/CH_3OH of 0.0 (Δ)

เมื่อเปรียบเทียบปริมาณไฮโดรเจนที่ผลิตได้จากขบวนการรีฟอร์มมิ่งด้วยน้ำพบว่าเมื่อใช้ตัวเร่งปฏิกิริยา ปริมาณไฮโดรเจนที่ผลิต (ที่อุณหภูมิเดียวกัน) สูงขึ้น เพราะ ตัวเร่งปฏิกิริยาจะช่วยลดพลังงานกระตุ้น ส่งผลให้ขบวนการรีฟอร์มมิ่งเกิดง่ายขึ้น ขณะเดียวกันก็จะช่วยให้ selectivity ของกระบวนการมีค่าสูงขึ้นเช่นกัน

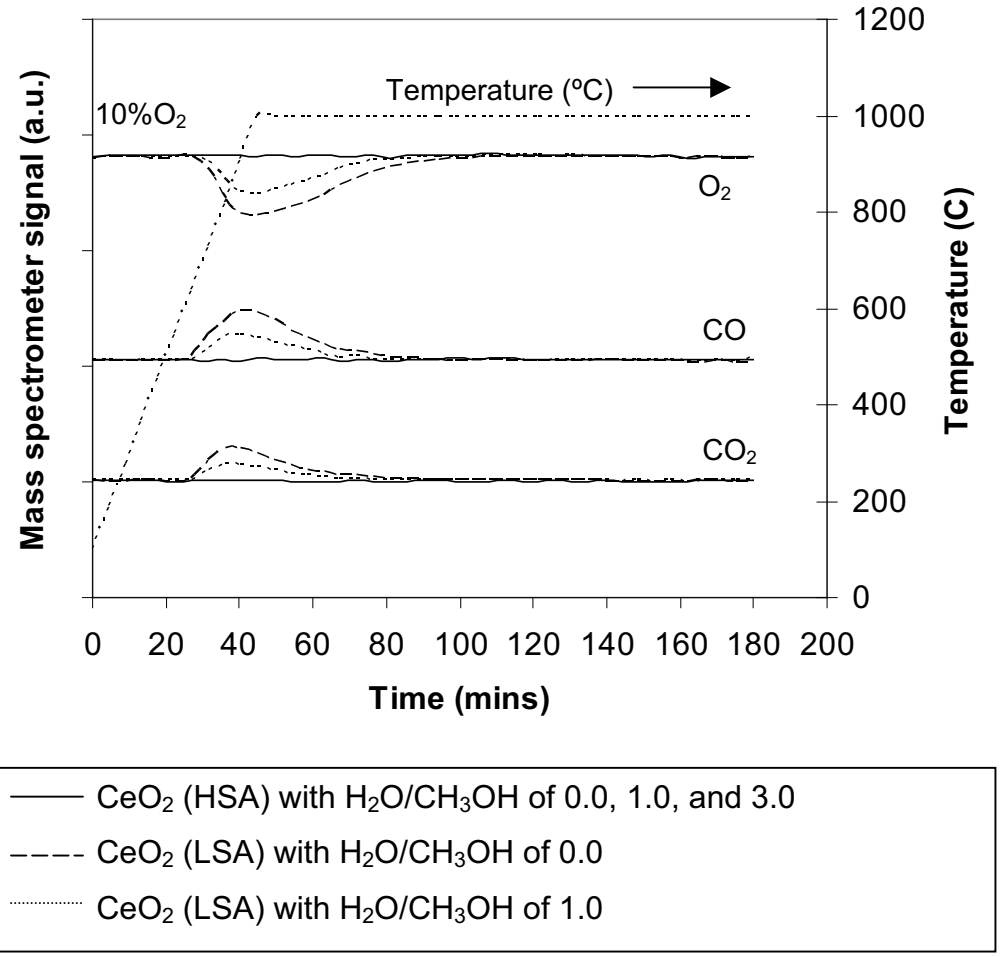

รูปที่ 8.3 TPO ของ CeO_2 หลังจากผ่านการใช้งานที่อุณหภูมิ 900 $^{\circ}C$ เป็นเวลา 100 ชั่วโมง

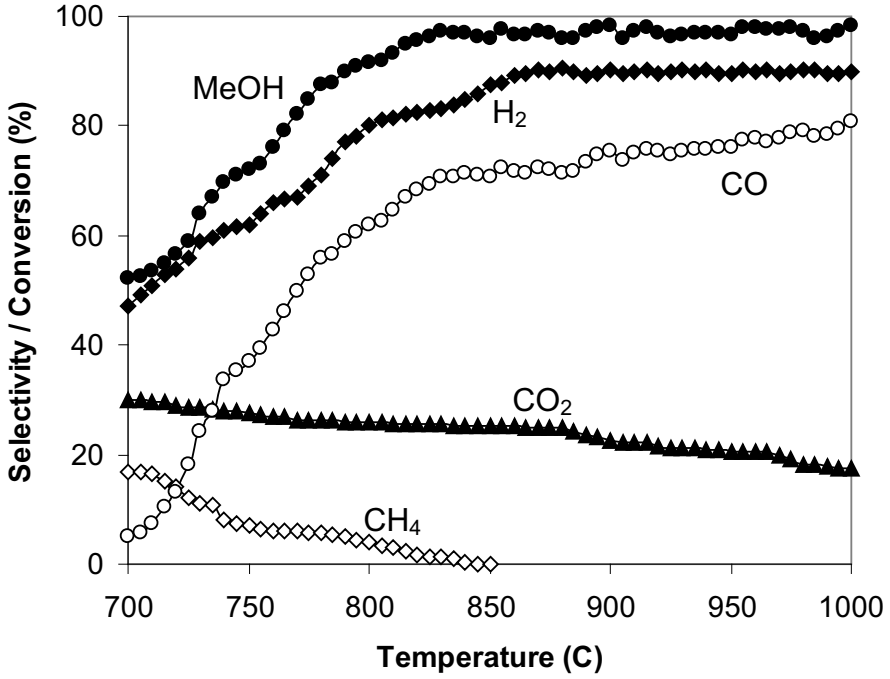

รูปที่ 8.4 ผลของอุณหภูมิที่มีต่อ การสลายตัวของเมทานอลและ Selectivity ของปฏิกิริยาเมทานอลรีฟอร์มมิ่งด้วยน้ำบนตัวเร่งปฏิกิริยา CeO_2 (HSA)

Table 8.1 Deactivation percentages, steady state hydrogen selectivities, specific surface area, and amount of carbon deposition on the surface of catalysts after exposure in methanol decomposition conditions (various inlet H_2O/CH_3OH ratios) at 900ºC for 100 h

Catalyst	H_2O/CH_3OH ratio	Deactivation (%)	Hydrogen selectivity (%) at steady state	C formation[a] (monolayers)	BET surface ($m^2\ g^{-1}$)
CeO_2 (LSA)[b]	0.0	40.9	28.0	0.35	6.0
	1.0	34.9	36.2	0.17	6.0
	3.0	29.7	43.6	0.06	6.1
CeO_2 (HSA)[c]	0.0	7.4	66.5	~ 0	22.0
	1.0	7.6	80.0	~ 0	22.2
	3.0	6.5	90.4	~ 0	22.1

[a] Calculated using CO and CO_2 yields from temperature-programmed oxidation (TPO) with 10% oxygen
[b] conventional CeO_2 prepared by precipitation method
[c] nanocomposite high surface area CeO_2

บทที่ 9
กระบวนการรีฟอร์มมิ่งก๊าซหุงต้มด้วยน้ำ

9.1 ศึกษาศักยภาพของ CeO_2 ต่อกระบวนการรีฟอร์มมิ่ง LPG ด้วยน้ำ

การทดลองดำเนินการโดยการป้อนน้ำพร้อมกับก๊าซโพรเพน และบิวเทน เข้าสู่ระบบซึ่งบรรจุตัวเร่งปฏิกิริยา CeO_2 ไว้ โดยในการทดลองจะป้อน LPG และไอน้ำด้วยอัตราส่วนคงที่ที่ 1.0 ต่อ 5.0 เข้าสู่ระบบ และทำการศึกษาเสถียรภาพ (Stability) ของ CeO_2 (เปรียบเทียบกับ Ni/Al_2O_3) จากรูปที่ 9.1 พบว่ากระบวนการรีฟอร์มมิ่งด้วยน้ำบนตัวเร่งปฏิกิริยา CeO_2 จะมีเสถียรภาพสูงกว่ากระบวนการดังกล่าวบน Ni/Al_2O_3 มากเนื่องจาก CeO_2 มีความต้านทานต่อการเกิดคาร์บอนที่ผิวสูง ซึ่งสามารถยืนยันข้อสรุปนี้ได้จากการทำ TPO (Temperature Programmed Oxidation) ดังแสดงในรูปที่ 9.2

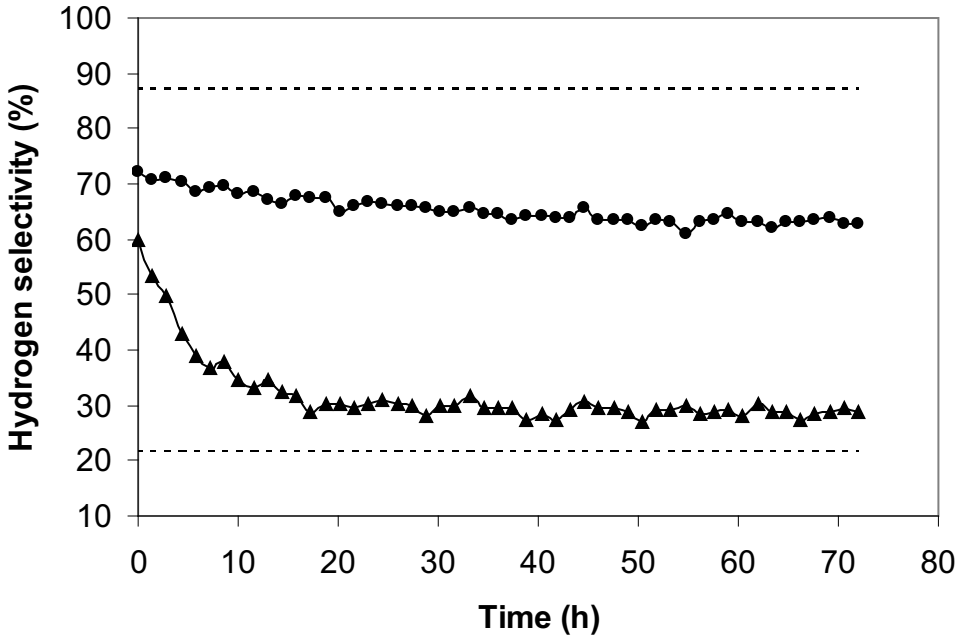

รูปที่ 9.1 เสถียรภาพของการผลิตไฮโดรเจนจากกระบวนการรีฟอร์มมิ่งของ LPG ด้วยน้ำบนตัวเร่งปฏิกิริยา CeO_2 (●) และ Ni/Al_2O_3 (▲) ที่อุณหภูมิ 900 องศาเซลเซียส

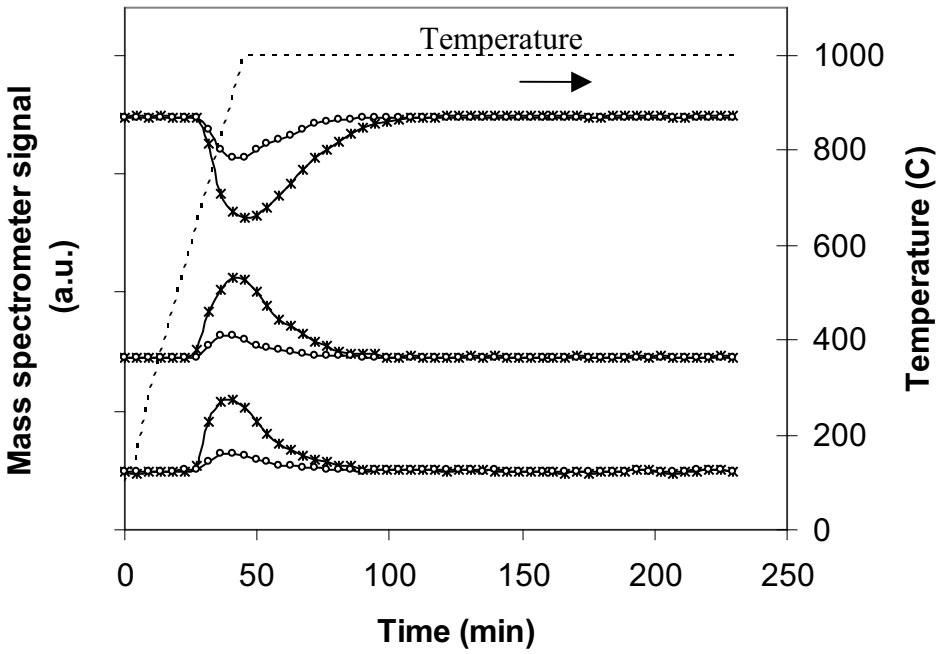

รูปที่ 9.2 กระบวนการ Temperature programmed oxidation จากกระบวนการรีฟอร์มมิ่งของ LPG ด้วยน้ำโดยใช้ตัวเร่งปฏิกิริยา CeO_2 (○) และ Ni/Al_2O_3 (×)

หลังจากระบบเข้าสู่สภาวะสมดุล (Steady state) แล้ว การดำเนินการในขั้นถัดมาคือการศึกษาผลของอุณหภูมิต่อปริมาณผลิตภัณฑ์ที่ผลิตได้ ซึ่งทำการทดลองโดยการเปลี่ยนอุณหภูมิของระบบจาก 700 ถึง 900 องศาเซลเซียส ผลการทดลองดังกล่าวแสดงในรูปที่ 9.3 ด้านล่าง ซึ่งพบว่าปริมาณไฮโดรเจนที่ผลิตได้มีค่าเพิ่มขึ้นตามอุณหภูมิที่ใช้ เช่นเดียวกันกับปริมาณคาร์บอน มอนออกไซด์ ในทางกลับกันสัดส่วนของก๊าซคาร์บอนไดออกไซด์ที่ผลิตได้จะมีค่าลดลงตามอุณหภูมิที่ใช้ สำหรับสัดส่วนของมีเทนที่ออกจากระบบนั้นจะมีค่าสูงขึ้นเมื่อเพิ่มอุณหภูมิจาก 700 ไปเป็น 850 องศาเซลเซียส จากนั้นสัดส่วนของมีเทนที่ได้ก็จะลดลง นอกจากนั้นยังพบว่าเกิดการฟอร์มตัวของเอทีลีน (C_2H_4) ในช่วงอุณหภูมิดังกล่าวด้วย โดยปริมาณเอทีลีนที่ได้จะมีค่าสูงที่อุณหภูมิต่ำ และที่อุณหภูมิต่ำกว่า 775 องศาเซลเซียสจะพบการฟอร์มตัวของก๊าซอีเทนอีกด้วย ดังที่ได้กล่าวมา สารไฮโดรคาร์บอนเหล่านี้จะเป็นตัวก่อให้เกิดปัญหาการฟอร์มตัวของคาร์บอนที่ผิวของตัวเร่งปฏิกิริยาได้ง่ายถึงแม้จะใช้ CeO_2 ซึ่งมีความต้านทานต่อการเกิดคาร์บอนที่ผิวสูงก็ตาม

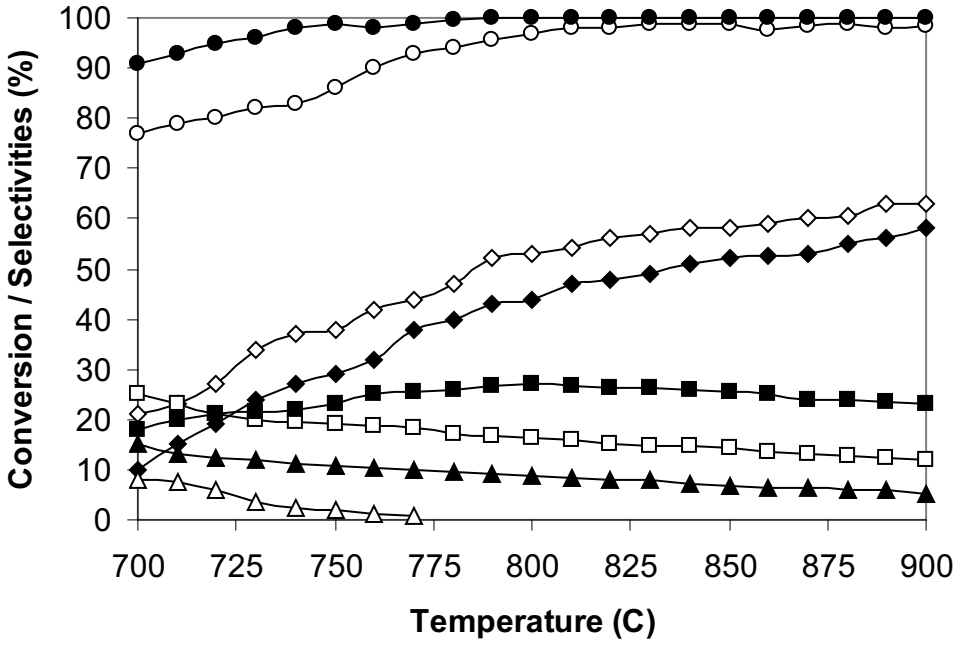

รูปที่ 9.3 อัตราการสลายตัว (Conversion) ของโพรเพนและบิวเทน รวมถึงสัดส่วนของผลิตภัณฑ์ที่ผลิตได้ (Selectivities) จากกระบวนการรีฟอร์มมิ่งของ LPG ด้วยน้ำบนตัวเร่งปฏิกิริยา CeO_2 ที่อุณหภูมิต่างๆ (conversion of C_4H_{10} (●), conversion of C_3H_8 (○), and the selectivities of H_2 (◇), CO (◆), CO_2 (□), CH_4 (■), C_2H_6 (△), and C_2H_4 (▲))

การทดลองถัดมาคือการศึกษาผลของน้ำที่ป้อนเข้าสู่ระบบต่อปริมาณคาร์บอนที่เกิดขึ้น และสัดส่วนของผลิตภัณฑ์ที่ได้รับ โดยการเปลี่ยนอัตราส่วนของ LPG ต่อน้ำจาก 1.0/3.0 เป็น 1.0/4.0, 1.0/50., 1.0/6.0, และ 1.0/70.0 ตามลำดับ ดังแสดงในรูป 9.4 พบว่าการเพิ่มน้ำเข้าสู่ระบบช่วยลดอัตราการเกิดเอทีลีน และปริมาณอีเทนได้เล็กน้อย อย่างไรก็ดียังมีสารไฮโดรคาร์บอนเหล่านี้ออกจากระบบอยู่ในปริมาณที่ค่อนข้างมาก อีกทั้งปริมาณคาร์บอนที่ผิวของ CeO_2 ก็ลงลงเพียงเล็กน้อยเท่านั้นดังแสดงในตารางที่ 9.1

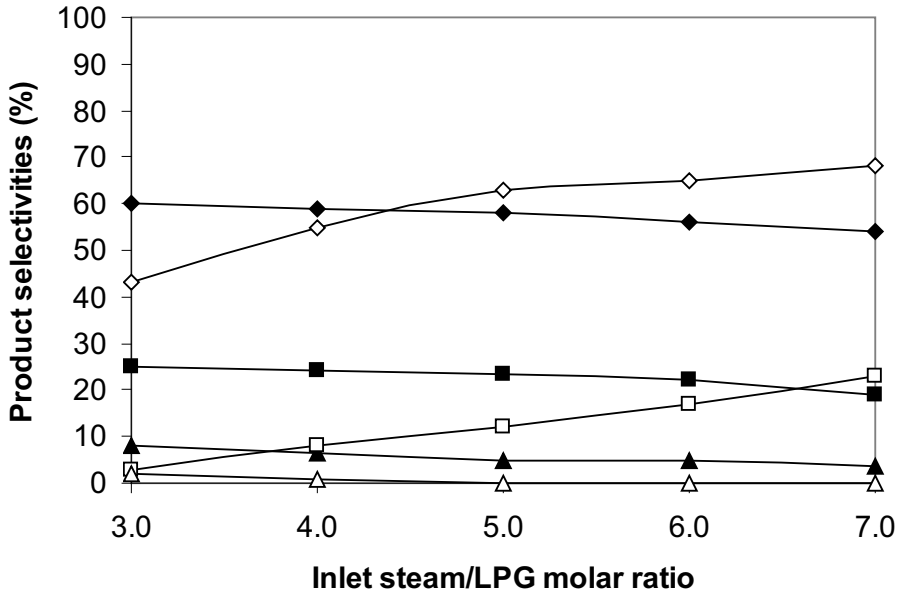

รูปที่ 9.4 ผลของปริมาณน้ำขาเข้าต่อสัดส่วนของผลิตภัณฑ์ที่ผลิตได้ (Selectivities) จากกระบวนการรีฟอร์มมิ่งของ LPG ด้วยน้ำบนตัวเร่งปฏิกิริยา CeO_2 ที่อุณหภูมิ 900 องศาเซลเซียส (selectivities of H_2 (◇), CO (◆), CO_2 (□), CH_4 (■), C_2H_6 (△), and C_2H_4 (▲))

ตารางที่ 9.1

ผลของปริมาณน้ำขาเข้าต่อปริมาณไฮโดรเจนที่ผลิตได้ และปริมาณคาร์บอนที่เกิดขึ้นที่ผิวของตัวเร่งปฏิกิริยา CeO_2 จากกระบวนการ Steam reforming of LPG

H_2O/LPG ratio	Hydrogen selectivity (%) at steady state	Total carbon formation (monolayers)
3.0	43.1	0.82[a] (0.84)[b]
4.0	55.0	0.67 (0.65)
5.0	62.9	0.51 (0.48)
6.0	65.3	0.44 (0.44)
7.0	68.0	0.41 (0.39)

[a] Calculated using CO and CO_2 yields from temperature-programmed oxidation (TPO) with 10% oxygen.
[b] Calculated from the balance of carbon in the system.

จากการทดลองสามารถสรุปได้ว่า CeO_2 มีศักยภาพในการรีฟอร์มก๊าซหุงต้มเช่นเดียวกับก๊าซธรรมชาติ ซึ่งกลไกการเกิดปฏิกิริยา (Chemical mechanism) ของ Steam reforming of LPG บนตัวเร่งปฏิกิริยา CeO_2 สามารถอธิบายได้ด้วยกระบวนการรีด๊อกซ์ (Redox) ดังแสดงในสมการด้านล่าง

$C_4H_{10} + 4S_{Ce} \Leftrightarrow 2(CH_3\text{-}S_{Ce}) + 2(CH_2\text{-}S_{Ce})$

$C_3H_8 + 3S_{Ce} \Leftrightarrow 2(CH_3\text{-}S_{Ce}) + CH_2\text{-}S_{Ce}$

$C_2H_6 + 2S_{Ce} \Leftrightarrow 2(CH_3\text{-}S_{Ce})$

$C_2H_4 + 2S_{Ce} \Leftrightarrow 2(CH_2\text{-}S_{Ce})$

$CH_4 + 2S_{Ce} \Leftrightarrow CH_3\text{-}S_{Ce} + H\text{-}S_{Ce}$

$CH_3\text{-}S_{Ce} + S_{Ce} \Leftrightarrow CH_2\text{-}S_{Ce} + H\text{-}S_{Ce}$

$CH_2\text{-}S_{Ce} + S_{Ce} \Leftrightarrow CH\text{-}S_{Ce} + H\text{-}S_{Ce}$

$CH\text{-}S_{Ce} + S_{Ce} \Leftrightarrow C\text{-}S_{Ce} + H\text{-}S_{Ce}$

$C\text{-}S_{Ce} + O_O^{x} \Leftrightarrow CO + V_O^{\bullet\bullet} + 2\,e' + S_{Ce}$

$2H\text{-}S_{Ce} \Leftrightarrow H_2 + 2S_{Ce}$

$H_2O + V_O^{\bullet\bullet} + 2\,e' \Leftrightarrow O_O^{x} + H_2$

9.2 <u>ศึกษาศักยภาพของ CeO_2 ต่อกระบวนการ Autothermal reforming of LPG</u>

การดำเนินการขั้นต่อมาเพื่อลดปริมาณคาร์บอนที่ผิว CeO_2 รวมถึงปรับปรุงสัดส่วนของก๊าซผลิตภัณฑ์คือการป้อนน้ำและออกซิเจนเข้าสู่ระบบด้วยพร้อมกับก๊าซโพรเพน และบิวเทน (กระบวนการ Autothermal reforming) ซึ่งการทดลองจะเริ่มต้นจากการศึกษาหาสัดส่วนของออกซิเจนต่อน้ำ และ LPG ที่เหมาะสมเสียก่อน โดยการป้อนออกซิเจนต่อ LPG ที่สัดส่วนความเข้มข้นตั้งแต่ 0, 0.2, 0.4, 0.6, 0.8, และ 1.0 เข้าสู่ระบบและทำการเปรียบเทียบปริมาณไฮโดรเจนที่ได้ ดังแสดงในรูป 9.5 พบว่าสัดส่วนระหว่างออกซิเจนต่อ LPG ที่เหมาะสมที่สุดคือ 0.6 ซึ่งที่สัดส่วนดังกล่าวจะสามารถผลิตไฮโดรเจนได้ถึง 77% และจากการศึกษาปริมาณคาร์บอนที่ผิวของ CeO_2 ด้วยกระบวนการ Temperature programmed oxidation (TPO) พบว่าเมื่อสัดส่วนของการป้อนออกซิเจนต่อ LPG สูงกว่า 0.6 จะไม่เกิดการฟอร์มตัวของคาร์บอนที่ผิวของ CeO_2

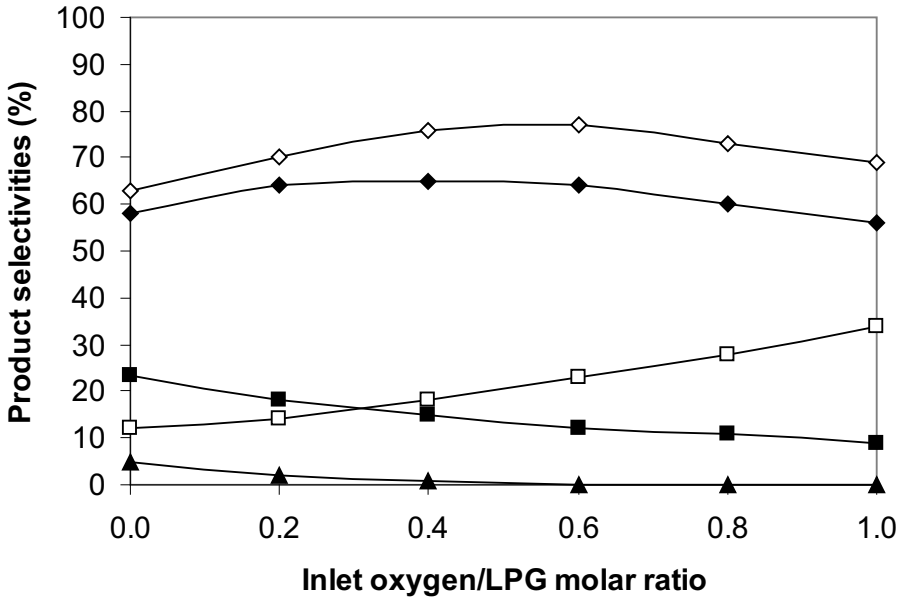

รูปที่ 9.5 ผลของปริมาณออกซิเจนขาเข้าต่อสัดส่วนของผลิตภัณฑ์ที่ผลิตได้ (Selectivities) จากกระบวนการรีฟอร์มมิ่งของ LPG ด้วยน้ำบนตัวเร่งปฏิกิริยา CeO_2 ที่อุณหภูมิ 900 องศาเซลเซียส (selectivities of H_2 (◇), CO (◆), CO_2 (□), CH_4 (■),and C_2H_4 (▲))

ตารางที่ 9.2 แสดงปริมาณคาร์บอนบนผิวของตัวเร่งปฏิกิริยา CeO_2 ที่วัดได้จากตัวเร่งปฏิกิริยา CeO_2 เมื่อผ่านกระบวนการ Autothermal reforming โดยป้อนออกซิเจนในปริมาณต่างๆ กัน ซึ่งจากตารางดังกล่าวพบว่าเมื่อมีการป้อนออกซิเจนต่อ LPG ในสัดส่วนมากกว่า 0.6 จะไม่พบการฟอร์มตัวของคาร์บอนบนผิวของตัวเร่งปฏิกิริยา CeO_2

ตารางที่ 9.2

ผลของปริมาณน้ำขาเข้าต่อปริมาณไฮโดรเจนที่ผลิตได้ และปริมาณคาร์บอนที่เกิดขึ้นที่ผิวของตัวเร่งปฏิกิริยา CeO_2 จากกระบวนการ Autothermal reforming of LPG

Oxygen/LPG ratio	Hydrogen selectivity (%) at steady state	Total carbon formation (monolayers)
0.0	62.9	0.51[a] (0.48)[b]
0.2	69.8	0.19 (0.21)
0.4	76.1	0.07 (0.06)
0.6	77.0	~0.0 (~0.0)
0.8	72.8	~0.0 (~0.0)
1.0	69.0	~0.0 (~0.0)

[a] Calculated using CO and CO_2 yields from temperature-programmed oxidation (TPO) with 10% oxygen.

[b] Calculated from the balance of carbon in the system.

หลังทราบสัดส่วนของออกซิเจนที่เหมาะสมแล้ว การดำเนินการต่อมาคือการศึกษาผลของอุณหภูมิต่ออัตราการสลายตัวของโพรเพน และบิวเทน รวมถึงสัดส่วนของก๊าซต่างๆ ที่เกิดขึ้นดังแสดงในรูป 9.6 ซึ่งพบว่าที่อุณหภูมิสูงกว่า 800 องศาเซลเซียสจะไม่มีเอทีลีนเกิดขึ้นจากกระบวนการ Autothermal reforming of LPG

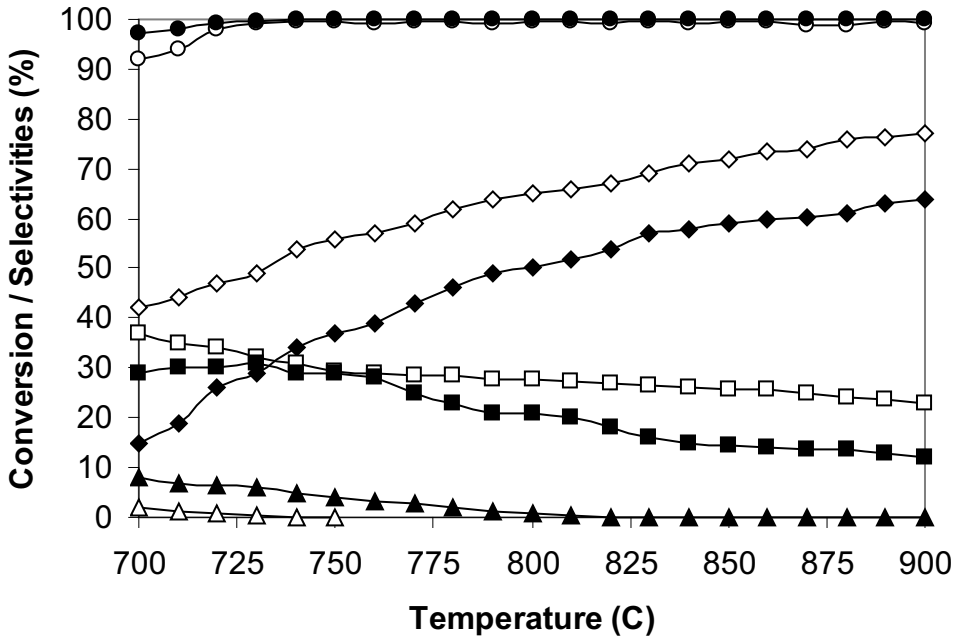

รูปที่ 9.6 อัตราการสลายตัว (Conversion) ของโพรเพนและบิวเทน รวมถึงสัดส่วนของผลิตภัณฑ์ที่ผลิตได้ (Selectivities) จากกระบวนการ Autothermal reforming ของ LPG บนตัวเร่งปฏิกิริยา CeO_2 ที่อุณหภูมิต่างๆ (conversion of C_4H_{10} (●), conversion of C_3H_8 (○), and the selectivities of H_2 (◇), CO (◆), CO_2 (□), CH_4 (■), C_2H_6 (△), and C_2H_4 (▲))

บทที่ 10
การออกแบบระบบรีฟอร์มเมอร์รูปแบบใหม่

10.1 การออกแบบระบบรีฟอร์มเมอร์

ระบบรีฟอร์มเมอร์ซึ่งใช้ CeO_2 เป็นตัวเร่งปฏิกิริยาเบื้องต้น (Pre-reforming element) ได้ถูกออกแบบในลักษณะของ Annular reactor ซึ่งมีท่อซ้อนกันอยู่ 2 ชั้น ท่อด้านในมีขนาดเส้นผ่าศูนย์กลาง 1/4นิ้ว ส่วนท่อด้านนอกมีขนาดเส้นผ่าศูนย์กลาง 1/2 นิ้ว และท่อทั้งสองมีความยาว 40 เซนติเมตร โดยก๊าซธรรมชาติจะถูกป้อนเข้าสู่ท่อขนาดเล็กชั้นในก่อน แล้วจึงย้อนกลับเข้าสู่ท่อขนาดใหญ่ด้านนอกภายหลังดังแสดงในรูปที่ 10.1

จากการออกแบบดังกล่าว CeO_2 จะถูกบรรจุไว้ในท่อชั้นใน ซึ่งวัตถุดิบจากภายนอกจะเข้ามาสัมผัสและทำปฏิกิริยาบนตัวเร่งปฏิกิริยาดังกล่าวก่อน (Pre-reforming) จากนั้นก๊าซผลิตภัณฑ์ที่ได้จะไหลวกกลับเข้าสู่ท่อชั้นนอกซึ่งบรรจุตัวเร่งปฏิกิริยา Ni/Al_2O_3 อยู่เพื่อเกิดปฏิกิริยารีฟอร์มมิ่งอีกครั้ง และสามารถผลิตไฮโดรเจนออกมาได้อย่างมีประสิทธิภาพ

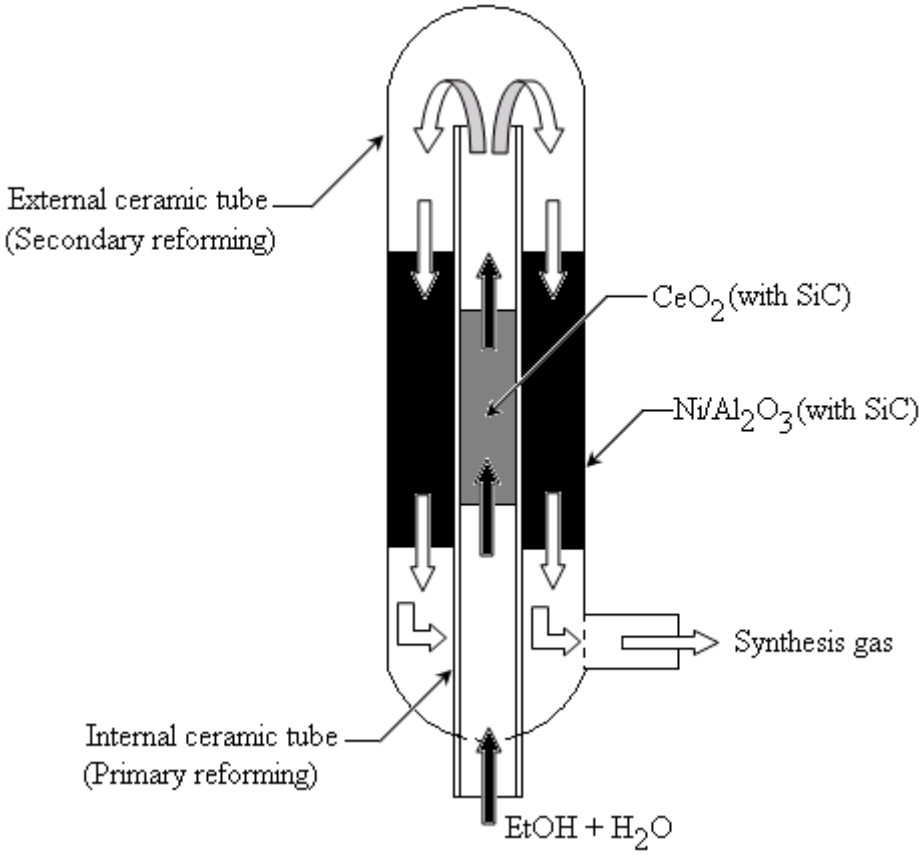

รูปที่ 9.1 ระบบ Annular reactor ที่สร้างขึ้น

ระบบดังกล่าวจะถูกต่อเข้ากับระบบรวมแทนที่ Catalytic packed-bed reactor เดิมซึ่งไอน้ำที่เกิดขึ้นจะเกิดจากการระเหยน้ำโดยใช้ระบบ Evaporator ส่วน Hydrogen-rich gas ที่ได้จากกระบวนการจะถูกนำไปวิเคราะห์โดยเครื่อง Gas chromatography และ Mass spectrometer ต่อไป

10.2 การดำเนินการเพื่อศึกษาผลของการใช้เมมเบรนในระบบรีฟอร์มเมอร์

เพื่อศึกษาผลของการติดเมมเบรนในระบบรีฟอร์มเมอร์ งานวิจัยนี้จึงดำเนินการพัฒนาโมเดลทางคณิตศาสตร์ของระบบเมมเบรนขึ้นมาเพื่อทำการเปรียบเทียบกับระบบรีฟอร์มเมอร์ปรกติ โดยมีรายละเอียดของงานดังนี้

10.2.1 การพัฒนาโมเดลของระบบรีฟอร์มเมอร์ปรกติ (Fixed bed model)

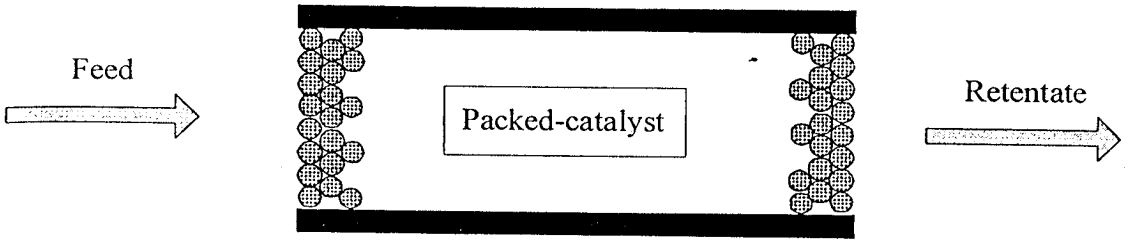

รูปที่ 10.2: ระบบรีฟอร์มเมอร์ปรกติ

Material balance:

$$\frac{d\overline{M}_i}{dL} = c_1 r_i \qquad (10.1)$$

Energy balance:

$$\sum\left(M_i C_{p,i}\right)\frac{d\overline{T}}{dL} = c_2\left(\overline{T}_{SS} - \overline{T}\right) + c_3 \sum\left(r_i \times \Delta H_{R,i}\right) \qquad (10.2)$$

Heat transfer through stainless steel

Heat of reaction

โดย

$$c_1 = \frac{\rho_c A_c l_0}{M_{T,0}}$$

$$c_2 = U_{SS} 2\pi r_1 l_0$$

$$c_3 = \pi r_1^2 l_0 \rho_c$$

$$\overline{M}_i = \left(\frac{M_i}{M_{T,0}}\right) \; ; \qquad \overline{T} = \frac{T}{T_0} \; ; \qquad \overline{T}_{SS} = \frac{T_{ss}}{T_0}$$

10.2.2 การพัฒนาโมเดลของระบบรีฟอร์มเมอร์ที่ใช้เมมเบรน

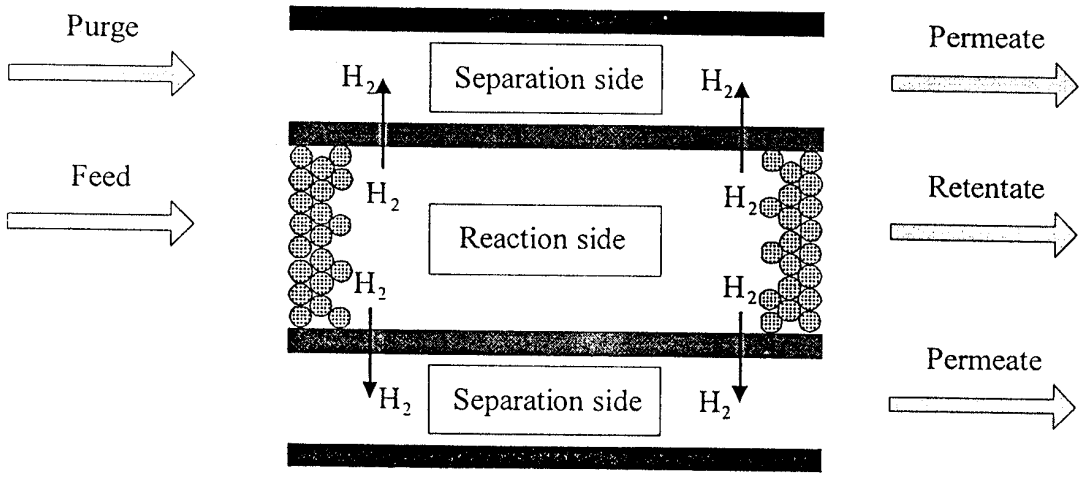

รูปที่ 10.3: ระบบรีฟอร์มเมอร์ที่ใช้เมมเบรน

Material balance:

Reaction side:

$$\frac{d\overline{M}_i^S}{dL} = a_1 r_i - a_2 Q_H \tag{10.3}$$

Permeation side:

$$\frac{d\overline{M}_i^T}{dL} = a_7 Q_H \tag{10.4}$$

Energy balance:

Reaction side:

$$\sum\left(M_i^S C_{p,i}^S\right)\frac{d\overline{T}^S}{dL} = a_3\left(\overline{T}_{SS} - \overline{T}^S\right) + a_4\left(\overline{T}^T - \overline{T}^S\right) + a_5\sum\left(r_i \times \Delta H_{R,i}\right) + a_6 H_m^S Q_H \tag{3.8}$$

Heat transfer through stainless steel | Heat transfer through membrane | Heat of reaction | Heat transfer by permeation gas

Permeation side:

$$\sum\left(M_i^T C_{p,i}\right)\frac{d\overline{T}^T}{dL} = -a_8\left(\overline{T}^T - \overline{T}^S\right) + a_9 H_m^T Q_H \tag{10.5}$$

Heat transfer through membrane | Heat transfer by mass permeation

$$a_1 = \frac{\rho_c A_c^S l_0}{M_{T,0}^S} \;;\; a_2 = \frac{l_0}{M_{T,0}^S} \;;\; a_3 = U_{SS} 2\pi r_3 l_0 \;;\; a_4 = U_m 2\pi r_1 l_0$$

$$a_5 = \frac{\rho_c A_c l_0}{T_0^S} \;;\; a_6 = \frac{l_0}{T_0^S} \;;\; a_7 = \frac{l_0}{M_{T,0}^T} \;;\; a_8 = U_m 2\pi r_1 l_0 \;;\; a_9 = \frac{l_0}{T_0^T}$$

$$\overline{M}_i^S = \left(\frac{M_i^S}{M_{T,0}^S}\right) \;;\; \overline{M}_i^T = \left(\frac{M_i^T}{M_{T,0}^T}\right) \;;\; \overline{T}^S = \frac{T^S}{T_0^S} \;;\; \overline{T}^T = \frac{T^T}{T_0^S} \;;\; \overline{T}_{SS} = \frac{T_{ss}}{T_0^S}$$

$$A_c^S = \pi\left(r_3^2 - r_2^2\right)$$

จากรูปที่ 10.3 มีการตั้งสมมุติฐานคือก๊าซที่แพร่ผ่านเมมเบรนคือไฮโดรเจนเท่านั้น โดยสามารถคำนวณอัตราการแพร่ได้จากสมการด้านล่าง

$$\frac{J\Delta Z}{P_{1s}^{0.5} - P_{2s}^{0.5}} = \frac{DN_b}{K_s} \qquad (10.6)$$

J = Hydrogen atom flux or permeation rate of hydrogen

N_b = bulk metal Pd atom concentration (0.113 mol Pd/cm^2)

The diffusion coefficient (D) สามารถคำนวณได้จากสมการด้านล่าง

$$D = D_o \exp\left(\frac{-E_{diff}}{RT}\right) \qquad (10.7)$$

E_{diff} = the activation energy for hydrogen atom diffusion (5.3 kcal/mol H)

$D_o = 2.9\times10^{-3}$ cm^2/s

E_{diff} = 5.3 kcal/mol H

$$K_s = 351.6 \exp\left(\frac{-1007}{T}\right) \qquad (10.8)$$

รูปที่ 10.4 แสดงผลของปริมาณไฮโดรเจนที่ผลิตได้จากกระบวนการรีฟอร์มมิ่งของมีเทนด้วยน้ำเมื่อมีการนำเอาเมมเบรนมาใช้ในระบบรีฟอร์มเมอร์ โดยรูปดังกล่าวแสดงถึงผลของความหนาของเมมเบรนต่อปริมาณไฮโดรเจนที่สามารถผลิตได้จากกระบวนการดังกล่าว ซึ่งจากการคำนวณพบว่าการติดตั้งเมมเบรนจะช่วยให้สามารถผลิตไฮโดรเจนได้ในปริมาณที่สูงขึ้น แต่ความหนาของเมมเบรนเป็นปัจจัยที่สำคัญหนึ่งที่สำคัญซึ่งจะเป็นตัวกำหนดว่าปริมาณไฮโดรเจนที่ผลิตได้จะมีมากน้อยเพียงใด

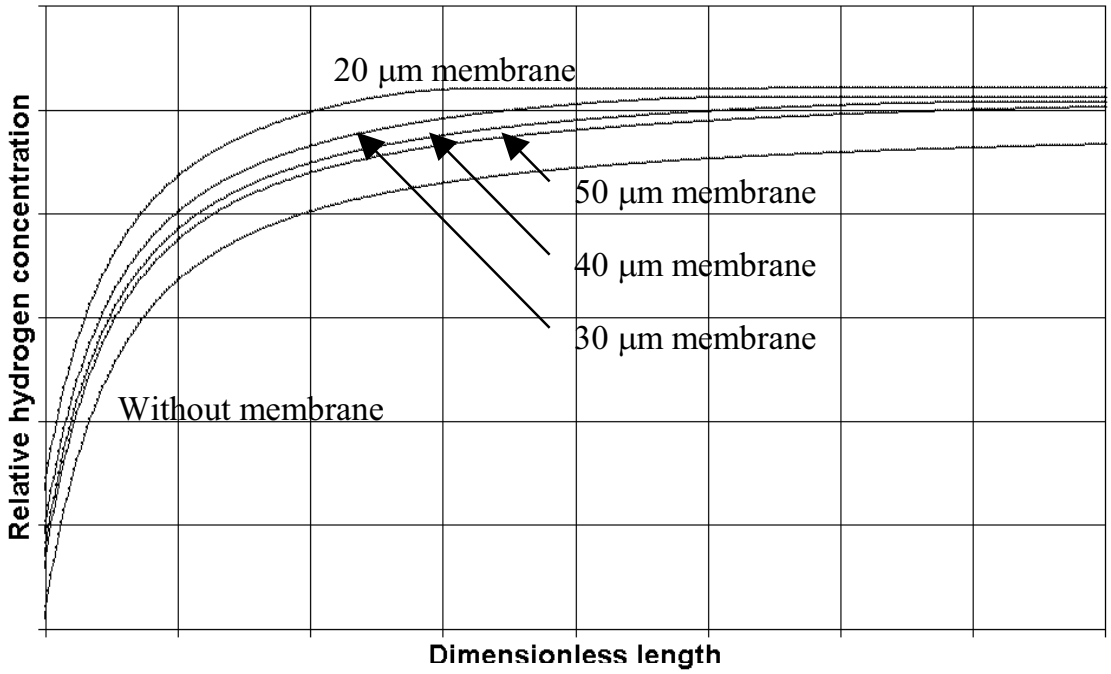

รูปที่ 10.4: ผลของความหนาของเมมเบรนต่อปริมาณไฮโดรเจนที่สามารถผลิตได้จากกระบวนการรีฟอร์มมิ่งของมีเทนด้วยน้ำที่อุณหภูมิ 900 องศาเซลเซียส

เอกสารอ้างอิง

[1] การศึกษาเบื้องต้นความเป็นไปได้ และศักยภาพในการพัฒนาก๊าซไฮโดรเจนเพื่อเป็นพลังงานทดแทน โดยสถาบันพัฒนาและฝึกอบรมโรงงานต้นแบบ มหาวิทยาลัยพระจอมเกล้าธนบุรี

[2] โครงการจัดทำสถานภาพ ภาพฉายอนาคต และแผนที่นำทางการพัฒนาเทคโนโลยีชีวภาพของประเทศไทย สาขาพลังงานและสิ่งแวดล้อม โดยบัณฑิตวิทยาลัยร่วมด้านพลังงานและสิ่งแวดล้อม

[3] เซลล์เชื้อเพลิง: พลังงานสะอาดทางเลือกแห่งอนาคต โดย ดร. สุมิตรา จรสโรจน์กุล ศูนย์เทคโนโลยีโลหะและวัสดุแห่งชาติ

[4] An Introduction to fuel cell technology and economics, Nigel Brandon and David Hart, 1999

[5] N.Q. Minh, and T. Takahashi, Science and Technology of Ceramic Fuel Cells, Elsevier, 1995.

[6] U. Bossel, The Birth of the Fuel Cell, European Fuel Cell Forum, 2000.

[7] Fuel Cell Handbook: 4th Edition, DOE/FETC-99/1076, edited by J.H. Hirschenhofer, D.B. Stauffer, R.R. Engleman, and M.G. Klett, U.S. Department of Energy, Federal Energy Technology Center, 1998.

[8] http://www.daimlerchrysler.com/index_e.htm?/products/products_e.htm

[9] http://www.hexis.ch/english/frhexis.htm

[10] http://www.fe.doe.gov/

[11] http://www.pg.siemens.com/en/fuelcells

[12] http://www.cfcl.com.au/

[13] http://www.nec.com/

[14] http://www.ford.com/

[15] http://www.gm.com/

[16] http://www.h2cars.de/

[17] Laosiripojana, N., 2003. Reaction engineering of indirect internal steam reforming of methane for application in solid oxide fuel cells. Ph.D. Thesis, University of London, England

[18] J.R. Rostrup-Nielsen, Steam Reforming Catalysts, (1975)

[19] D. Grenoble, J. Catal., 51, (1978), 203

[20] J.R. Rostrup-Nielsen and J.-H. Bak-Hansen., J. Catal., 144, (1993), 38

[21] A. Guerrero-Ruiz, I. Rodríguez-Ramos, A. Sepúlveda-Escribano, J. Chem. Soc., Chem. Commun., (1993), 487

[22] H. Papp, P. Schuler and Q. Zhang., Topics in Catalysis, 3, (1996), 299

[23] J.R. Rostrup-Nielsen, L.J. Christiansen, Applied Catalysis A, 126, (1995), 381-390

[24] A.T. Ashcroft, A.K. Cheetham, J.S. Foord, M.L.H. Green, C.P. Grey, A.J. Murrel and P.D.F. Vernon., Nature, 344, (1990), 319

[25] S.C. Tsang, J.B. Claridge and M.L.H. Green., Catal. Today, 23, (1995), 3

[26] A. Erdöhelyi, J. Cserényi and F. Solymosi., J. Catal., 141, (1993), 287

[27] A. Erdöhelyi, J. Cserényi, E. Rapp and F. Solymosi., Appl. Catal. A: Gen., 108, (1994), 205

[28] J. Nakamura, K. Aikawa, K. Sato and T. Uchijima., Catal. Lett., 25, (1994), 265

[29] H. Y. Wang and E. Ruckenstein, Applied Catalysis A: General, 204, (2000), 143-152

สิ่งที่ได้รับ (Output) จากโครงการ

<u>วารสารระดับนานาชาติที่มี Impact Factor (International Journal with impact factor)</u>

1) **N. Laosiripojana** and S. Assabumrungrat, "Catalytic Dry Reforming of Methane over High Surface Area Ceria", Appl. Cat.-B, 60 (2005) 107-116 **(IF-2004 = 4.06)**
   <u>(Sciencedirect Top 25 hottest articles of the year 2005, range 18th)</u>*
2) **N. Laosiripojana** and S. Assabumrungrat, "Methane steam reforming over Ni/Ce-ZrO_2 catalyst: Influences of Ce-ZrO_2 support on reactivity, resistance toward carbon formation, and intrinsic reaction kinetics", Appl. Cat.-A, 290 (2005) 200-211 **(IF-2004 = 2.31)**
3) **N. Laosiripojana**, W. Sutthisripok and S. Assabumrungrat, "Synthesis gas production from dry reforming of methane over CeO_2 doped Ni/Al_2O_3: Influence of the doping ceria on the resistance toward carbon formation", Chem. Eng. J., 112 (2005) 13-22 **(IF-2004 = 1.38)**
4) **N. Laosiripojana**, W. Sangtongkitcharoen and S. Assabumrungrat, "Catalytic steam reforming ethane and propane over CeO_2-doped Ni/Al_2O_3 at SOFC temperature: Improvement of resistance toward carbon formation by the redox properties of doping CeO_2", accepted by Fuel, June 2005 **(IF-2003 = 1.368)**
5) **N. Laosiripojana** and S. Assabumrungrat, "Hydrogen production from the steam and autothermal reforming of LPG over high surface area ceria at SOFC temperature", J. Power Sources, In Press, October 2005 **(IF-2004 = 2.513)**
6) **N. Laosiripojana** and S. Assabumrungrat, "The effect of specific surface area on the activity of nano-scale ceria catalysts for methanol decomposition with and without steam at SOFC operating temperatures", Chem. Eng. Sci., accepted, October 2005 **(IF-2004 = 1.65)**
7) **N. Laosiripojana** and S. Assabumrungrat, "Catalytic steam reforming of ethanol over high surface area CeO_2: The role of CeO_2 as an internal pre-reforming catalyst", Appl. Cat.-B, revised **(IF-2004 = 4.06)**
8) **N. Laosiripojana** and S. Assabumrungrat, "Reactivity of high surface area CeO_2 synthesized by surfactant-assisted method to ethanol decomposition with and without steam", Submitted to Chemical Engineering Journal

International Conference

1) **Laosiripojana, N.**, Assabumrungrat S., et al. (2004). Catalytic Cracking of Methane, Methanol, and Ethanol by Ceria. The Third Regional Conference on Energy Technology towards a Clean Environment "Sustainable Energy and Environment (SEE)", December 1-3, 2004, Hilton Hua Hin Resort & Spa, Hua Hin, Thailand.
2) **Laosiripojana, N.**, Watcharathamrongkul K., et al. (2004). Methane Steam Reforming Performance on Selective Hydrogen Permeable Menbrane Reformer Using CeO_2 as a Reforming Catalyst. The Third Regional Conference on Energy Technology towards a Clean Environment "Sustainable Energy and Environment (SEE)", December 1-3, 2004, Hilton Hua Hin Resort & Spa, Hua Hin, Thailand.
3) **Laosiripojana, N.** and Assabumrungrat S. (2004). Hydrogen Production from Dry Reforming over CeO_2 Fueled by Biogas. Regional Symposium on Chemical Engineering (RSCE 2004), December 2004.
4) **Laosiripojana, N.** and Assabumrungrat S. (2004). Methane Steam Reforming Performance and the Resistance toward Carbon Formation of Ni on High Surface Area CeO_2 Support. Regional Symposium on Chemical Engineering (RSCE 2004), December 2004.
5) **Laosiripojana, N.**, Watcharathamrongkul K., et al. (2004). Hydrogen Production from Pd Membrane Reformer using Ni/Al_2O_3 as Methane Steam Reforming Catalyst. Regional Symposium on Chemical Engineering (RSCE 2004), December 2004.
6) **Laosiripojana N.**, Assabumrungrat S., Sutthisripok W., (2005) Catalytic Steam Reforming of Ni on High Surface Area CeO_2 and Ce-ZrO_2, PSU-UNS Conference, July 2005.
7) **Laosiripojana N.**, Assabumrungrat S., (2005) Catalytic Steam Reforming of Ethane on CeO_2-doped Ni/Al_2O_3: Improvement of Reactivity and Resistance toward Carbon Deposition by the Doping of CeO_2, International Hydrogen Energy Conference, Turkey, July 2005.

รางวัลที่ได้รับระหว่างโครงการ

1. รางวัลนักวิจัยรุ่นใหม่ดีเด่น สกว. ประจำปี 2548
2. รางวัลเสนอผลงานวิจัยดีเด่น สกว. ประจำปี 2548
3. Sciencedirect Top 25 hottest articles of the year 2005 for the journal "Applied Catalysis B: Environmental", (Impact factor: 4.04), range 18th

ภาคผนวก

LIST OF INTERNATIONAL JOURNALS

1. N. Laosiripojana and S. Assabumrungrat, Appl. Cat.-B, 60 (2005) 107-116
2. N. Laosiripojana and S. Assabumrungrat, Appl. Cat.-A, 290 (2005) 200-211
3. N. Laosiripojana, W. Sutthisripok and S. Assabumrungrat, Chem. Eng. J., 112 (2006) 13-22
4. N. Laosiripojana, W. Sangtongkitcharoen and S. Assabumrungrat, Fuel, 85 (2006) 323-332
5. N. Laosiripojana and S. Assabumrungrat, J. Power Sources, In Press
6. N. Laosiripojana and S. Assabumrungrat, Chem. Eng. Sci., In Press
7. N. Laosiripojana and S. Assabumrungrat, Appl. Cat.-B, revised
8. N. Laosiripojana and S. Assabumrungrat, Submitted to Chemical Engineering Journal

LIST OF INTERNATIONAL CONFERENCES

1. Laosiripojana, N., Assabumrungrat S., et al. (2004), Sustainable Energy and Environment (SEE)", December 1-3, 2004, Hilton Hua Hin Resort & Spa, Hua Hin, Thailand.
2. Laosiripojana, N., Watcharathamrongkul K., et al. (2004), Sustainable Energy and Environment (SEE)", December 1-3, 2004, Hilton Hua Hin Resort & Spa, Hua Hin, Thailand.
3. Laosiripojana, N. and Assabumrungrat S. (2004), Regional Symposium on Chemical Engineering (RSCE 2004), December 2004.
4. Laosiripojana, N. and Assabumrungrat S. (2004), Regional Symposium on Chemical Engineering (RSCE 2004), December 2004.
5. Laosiripojana, N., Watcharathamrongkul K., et al. (2004), Regional Symposium on Chemical Engineering (RSCE 2004), December 2004.
6. Laosiripojana N., Assabumrungrat S., Sutthisripok W., (2005), PSU-UNS Conference, July 2005.
7. Laosiripojana N., Assabumrungrat S., (2005), International Hydrogen Energy Conference, Turkey, July 2005

N. Laosiripojana and S. Assabumrungrat

"Catalytic Dry Reforming of Methane over High Surface Area Ceria"

Applied Catalysis B: Environmental, 60 (2005) 107-116

(IF-2004 = 4.06)

(Sciencedirect Top 25 hottest articles of the year 2005, range 18th)*

Available online at www.sciencedirect.com
SCIENCE DIRECT
Applied Catalysis B: Environmental 60 (2005) 107–116
APPLIED CATALYSIS B: ENVIRONMENTAL
www.elsevier.com/locate/apcatb

Catalytic dry reforming of methane over high surface area ceria

N. Laosiripojana [a,*], S. Assabumrungrat [b]

[a] *The Joint Graduate School of Energy and Environment, King Mongkut's University of Technology Thonburi, Bangkok 10140, Thailand*

[b] *Center of Excellence on Catalysis and Catalytic Reaction Engineering, Department of Chemical Engineering, Chulalongkorn University, Bangkok 10330, Thailand*

Received 6 October 2004; received in revised form 28 February 2005; accepted 1 March 2005
Available online 31 March 2005

Abstract

High surface area ceria (CeO_2 (HSA)), synthesized by a surfactant-assisted approach, was found to have useful dry reforming activity for H_2 and CO production under solid oxide fuel cells (SOFCs) conditions. The catalyst provides significantly higher reforming reactivity and excellent resistance toward carbon deposition compared to Ni/Al_2O_3 and conventional low surface area ceria (CeO_2 (LSA)) under dry reforming conditions. These enhancements are due to the high redox property of CeO_2 (HSA). During the dry reforming process, the redox reactions between the gaseous components in the system and the lattice oxygen (O_x) take place on ceria surface. Among these reactions, the rapid redox reactions of carbon compounds such as CH_4, and CO with lattice oxygen ($CH_4 + O_x \rightarrow CO + H_2 + O_{x-1}$ and $CO + O_x = CO_2 + O_{x-1}$) can prevent the formation of carbon species from the methane decomposition and Boudard reactions even at low inlet carbon dioxide concentration.

In particular, the dry reforming rate over CeO_2 (HSA) is proportional to the methane partial pressure and the operating temperature. Carbon dioxide presents weak positive impact on the methane conversion, whereas both carbon monoxide and hydrogen inhibit the reforming rate. The activation energies and reforming rates under the same methane concentration for CeO_2 toward the dry reforming are almost equal to the steam reforming as previously reported [1–4]. This result suggests the similar reaction mechanisms for both the steam reforming and the dry reforming over CeO_2; i.e., the dry reforming rate is governed by the slow reaction of adsorbed methane, or surface hydrocarbon species, with oxygen in CeO_2, and a rapid gas–solid reaction between CO_2 and CeO_2 to replenish the oxygen.

Keywords: Ceria; Dry reforming; High surface area; Hydrogen; SOFC

1. Introduction

Cerium oxide or ceria is an important material for a variety of catalytic reactions involving oxidation of hydrocarbons (e.g., automobile exhaust catalysts). This material contains a high concentration of highly mobile oxygen vacancies, which act as local sources or sinks for oxygen involved in reactions taking place on its surface.

Nowadays, a potential application of ceria is in solid oxide fuel cells (SOFCs) application as a reforming catalyst for in-stack (called indirect internal) reforming of methane [1]. Conventional Ni catalysts have been reported to provide too high endothermic reforming reactivity for in-stack reforming in SOFCs [5]. The rapid endothermic reaction can lead to local temperature gradients especially close to the entrance of the reformer, which consequently cause the possible mechanical failure due to thermally induced stresses [6,7]. In addition, the carbon deposition was easily formed on the surface of Ni catalyst under SOFC operating conditions, resulting in the rapid catalyst deactivation [8]. Thus, a less active and high resistant toward carbon formation catalyst is desirable to give better control of the coupled heat flows and chemical reactions. Ceria is a candidate catalyst for this application since it is much less active and more resistant toward carbon deposition

* Corresponding author. Tel.: +66 2 8729014; fax: +66 2 8726736.
E-mail address: navadol_l@jgsee.kmutt.ac.th (N. Laosiripojana).

0926-3373/$ – see front matter © 2005 Elsevier B.V. All rights reserved.
doi:10.1016/j.apcatb.2005.03.001

compared to Ni [3]. Recently, the successful tests of ceria for the 'dry methane' and 'methane steam reforming' reactions have been reported [1–3].

Due to the high resistance toward carbon formation, ceria should also be a good candidate for use in the dry reforming process. Both the steam and dry reforming reactions have similar thermodynamic characteristics except that the carbon formation in the dry reforming is more severe than in the steam reforming due to the lower H/C ratio of this reaction [9]. The attractive feature of the dry reforming reaction is the utilization of CO_2, which is a greenhouse effect gas. In general, the dry reforming reaction (Eq. (1)) is typically accompanied by the simultaneous occurrence of the reverse water–gas shift reaction (RWGS) (Eq. (2)).

$$CH_4 + CO_2 = 2CO + 2H_2 \Delta H = 247\text{kJ/mol} \quad (1)$$

$$CO_2 + H_2 = CO + H_2O \Delta H = 41.1\text{kJ/mol} \quad (2)$$

The hydrogen to carbon monoxide production ratio from the dry reforming reaction is, therefore, less than 1. Sodesawa et al. [10] studied the dry reforming reaction at a stoichiometric feed ratio over several catalysts. They found that the activities of most catalysts deactivated rapidly due to the carbon deposition. Previously, no researcher has investigated the dry reforming over ceria before.

As described, ceria has a great potential to be used as the reforming catalyst for the indirect internal reforming solid oxide fuel cells (IIR-SOFCs); however, the main weaknesses of this material are its low specific surface area and high deactivation due to the thermal sintering when operated under SOFC stack conditions. It was reported that after exposure in methane steam reforming conditions at 900 °C for 18 h, the reforming reactivity over ceria deactivated 30% and the steady-state methane conversion was less than 10% [3]. The use of high surface area ceria (CeO_2 (HSA)) would be a good alternative method to minimize the sintering impact and consequently improve the stability and steady-state activity. Several methods have recently been described for the preparation of CeO_2 (HSA) solid solution. Most interest is focused on the preparation via templating pathways [11–13]. Several meso-structured surfactant–oxide composites have been synthesized by this approach. However, a few of these composites showed a regular pore structure after calcination [14–16]. Terribile et al. [17] synthesized CeO_2 (HSA) with improved textural, structural and chemical properties for environmental applications by using a surfactant-assisted approach. The materials with good homogeneity and stability especially after thermal treatments were achieved.

In the present work, CeO_2 (HSA) was synthesized by the surfactant-assisted approach. The stability and activity toward the dry reforming of CeO_2 (HSA) were studied and compared to the conventional low surface area ceria (CeO_2 (LSA)), and Ni/Al_2O_3. The resistance toward carbon formation and the kinetics of the reactions on CeO_2 (HSA) were also determined.

2. Experimental

2.1. Catalyst preparations and characterizations

CeO_2 (LSA) was prepared by the precipitation of cerium chloride ($CeCl_3 \cdot 7H_2O$) from Aldrich. The starting solution was prepared by mixing 0.1 M of this metal salt solution with 0.4 M of ammonia at a 2:1 volumetric ratio. This solution was stirred by magnetic stirring (100 rpm) for 3 h, then sealed and placed in a thermostatic bath maintained at 90 °C for 3 days. The precipitate was filtered and washed with deionised water and acetone to remove the free surfactant. It was dried overnight in an oven at 110 °C, and then calcined in air at 1000 °C for 6 h.

Following to the work from Terribile et al. [17], CeO_2 (HSA) were prepared by adding an aqueous solution of the appropriate cationic surfactant, 0.1 M cetyltrimethylammonium bromide solution from Aldrich, to a 0.1 M cerium chloride. The molar ratio of ([Ce])/[cetyltrimethylammonium bromide] was kept constant at 0.8. The mixture was stirred and then aqueous ammonia was slowly added with vigorous stirring until the pH was 11.5 [17]. The mixture was continually stirred for 3 h, then sealed and placed in the thermostatic bath maintained at 90 °C for 3 days. After that, the mixture was cooled and the resulting precipitate was filtered and washed repeatedly with water and acetone. The filtered powder was then treated under the same procedures as CeO_2 (LSA). For comparison, Ni/Al_2O_3 (5 wt.% Ni) was also prepared by impregnating α-Al_2O_3 (from Aldrich) with $NiCl_3$. After stirring, the solution was dried and calcined at 1000 °C for 6 h. The catalyst powder was reduced with 10%H_2/Ar at 700 °C for 6 h before use.

BET measurements of CeO_2 were carried out before and after calcination at different temperatures in order to determine the decrease in surface area by the thermal sintering. As presented in Table 1, after drying in the oven, surface areas of 105 and 55 $m^2\ g^{-1}$ were observed for CeO_2 (HSA) and CeO_2 (LSA), respectively and, as expected, the surface area decreased at high calcination temperatures. However, the value for CeO_2 (HSA) is still appreciable after calcination at 1000 °C and it is almost three times of that for the general CeO_2 (LSA). The homogeneity and morphology of CeO_2 (HSA) was also investigated. All samples have a

Table 1
Specific surface area of the catalysts after drying and calcinations at different temperatures

Catalyst	BET surface area ($m^2\ g^{-1}$) after drying or calcination at (°C)						
	100	200	400	600	800	900	1000
CeO_2 (LSA)[a]	55	49	36	21	15	11	8.5
CeO_2 (HSA)[b]	105	97	69	48	35	29	24

[a] Conventional low surface area CeO_2 prepared by the precipitation method.
[b] Nanocomposite high surface area CeO_2 prepared by the surfactant-assisted approach.

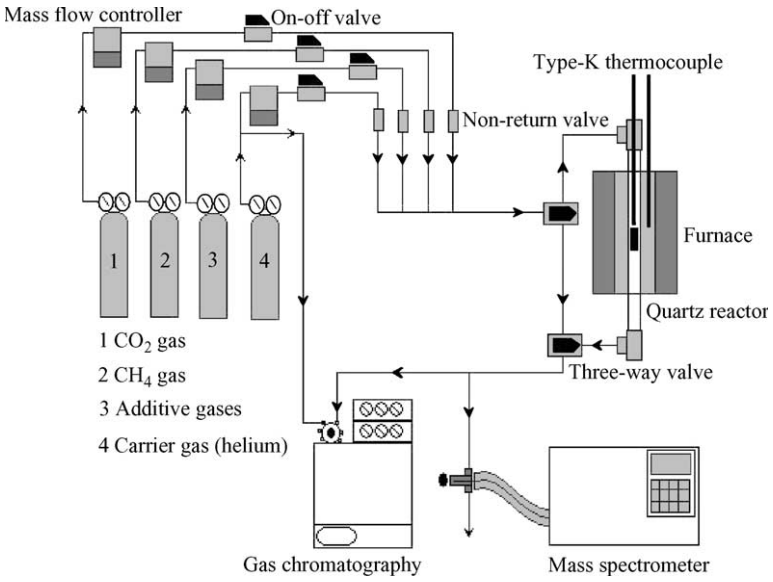

Fig. 1. Schematic diagram of the experimental set-up.

similar morphology and exhibit a very narrow particle-size histogram. As expected, samples treated at 1000 °C showed a larger particle size than those treated at lower temperatures. The mean particle size for CeO_2 (HSA) after calcination at 1000 °C was 30–100 nm.

2.2. Experimental set-up

In order to investigate the dry reforming reaction, an experimental reactor system was constructed as shown in Fig. 1. This system consists of three main sections: feed, reaction, and analysis sections. The main obligation of the feed section is to supply the components of interest including CH_4, CO_2, H_2, and CO to the reaction section, where an 8 mm internal diameter and 40 cm length quartz reactor was mounted vertically inside a furnace. The gas mixture was flowed though this quartz reactor, in which the catalyst was filled inside. A small amount of quartz wool was used to prevent the catalyst from moving. The weight of catalyst loading was 50 mg, while a typical range of total gas flow was 20–200 $cm^3\ min^{-1}$ depending on the desired space velocity. A Type-K thermocouple was placed into the annular space between the reactor and the furnace. This thermocouple was mounted on the tubular reactor in close contact with the catalyst bed to minimize the temperature difference between the catalyst bed and the thermocouple. Another Type-K thermocouple was inserted in the middle of the quartz tube in order to re-check the possible temperature gradient. The record showed that the maximum temperature fluctuation during the reaction was always within ±0.75 °C or less from the temperature specified for the reaction.

After reaction, the gas mixture was transferred via trace-heated lines to the analysis section, which consists of a Porapak Q column Shimadzu 14B gas chromatograph (GC) and a mass spectrometer (MS). The gas chromatography was applied in order to investigate the steady-state condition experiments, whereas the mass spectrometer was used for the transient carbon formation experiments.

In the present work, the outlet of the GC column was directly connected to a thermal conductivity detector (TCD). In order to satisfactorily separate CH_4, CO, CO_2, and H_2, the temperature setting inside the GC column was programmed varying with time. In the first 3 min, the column temperature was constant at 60 °C, it was then increased steadily by the rate of 15 °C per min until 120 °C. Finally, the temperature was decreased to 60 °C. The analytical method applied is an internal standardization in which the peak area is related to the molar concentration through the response factor (RF).

$$\mathrm{RF} = \frac{\text{concentration (ppm)}}{\text{peak area}} \tag{3}$$

Table 2 presents the absolute response factor (RF) for all components concerned in this research. In order to study the formation of carbon species on catalyst surface, the transient exhaust gas from the catalytic reactor was analyzed using the mass spectrometer. Sampling of the exhaust gas was done by a quartz capillary and differential pumping. The calibration of CO and CO_2 were performed by injecting a known amount of these calibration gases from a loop, in an injection valve in the bypass line. The response factors were obtained by dividing the number of moles for each component over the respective areas under peaks. This process was

Table 2
Absolute response factors and retention time of each component

Gas	Response factor (RF)	Retention time (min)
H_2	0.35	0.70
CO	0.19	1.15
CH_4	0.09	1.59
CO_2	0.21	2.65

performed before each experiment to achieve maximum accuracy in the quantitative carbon analysis.

2.3. Temperature programmed techniques (TP)

Temperature programmed technique (TP) was applied for studying the resistance toward carbon formation. The temperature programmed oxidation (TPO) was carried out by introducing 10% oxygen in helium with the total flow rate of 100 $cm^3\ min^{-1}$ into the system. The temperature was increased from room temperature to 900 °C at the rate of 10 °C/min. The amount of carbon formations on the surface of catalysts were determined by measuring the CO and CO_2 yields from the TPO results and assuming a value of 0.026 nm^2 for the area occupied by a carbon atom in a surface monolayer of the basal plane in graphite [18]. In addition to the TPO method, the amount of carbon deposition was confirmed by calculating carbon balance of the system. The amount of carbon deposited on the surface of catalyst would theoretically be equal to the difference between the inlet carbon containing components (CH_4 and CO_2) and the outlet carbon containing components (CO, CH_4, and CO_2). The amount of carbon deposited per gram of catalyst is given by the following equation:

$$C_{deposition} = \frac{mole_{carbon(in)} - mole_{carbon(out)}}{m_{catalyst}} \quad (4)$$

3. Results

3.1. Preliminary test

Preliminary experiments were carried out to find a suitable condition in which internal and external mass transfer effects are not predominant. Considering the effect of external mass transfer, the total gas flow rate was varied between 10 and 200 $cm^3\ min^{-1}$ under a constant residence time of 5×10^{-4} g min cm^{-3}. As shown in Fig. 2, the

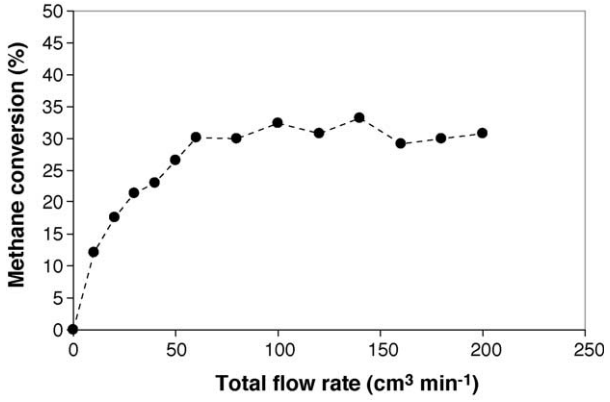

Fig. 2. Effect of the total gas flow rate on the methane conversion from the dry reforming (CH_4/CO_2 = 1.0/3.0) at 900 °C with the constant resident time of 5×10^{-4} g min cm^{-3}.

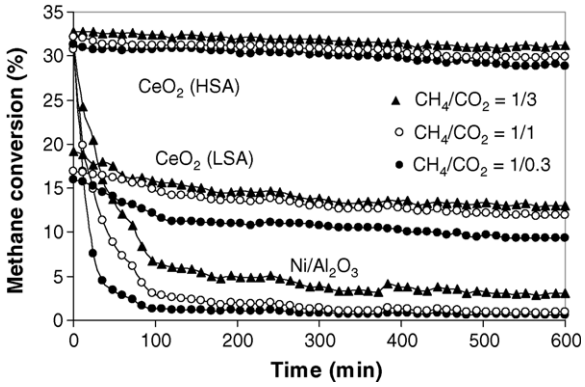

Fig. 3. Dry reforming of methane at 900 °C for different catalysts using different inlet CH_4/CO_2 ratios.

reforming rate was found to be independent of the gas velocity when the gas flow rate was higher than 60 $cm^3\ min^{-1}$, indicating the absence of external mass transfer effects at this high velocity.

The reaction on different average sizes of catalysts (up to 500 μm) were carried out in order to confirm that the experiments were performed within the region of intrinsic kinetics. It was observed that the catalysts with the particle size less than 200 μm showed no intraparticle diffusion limitation in the range of conditions studied. Therefore, in the following studies, the total flow rate was kept constant at 100 $cm^3\ min^{-1}$ whereas the catalyst diameters were kept within the above-mentioned range in all experiments.

3.2. Stability and activity toward the dry reforming

Synthesized CeO_2 (HSA), CeO_2 (LSA), and 5% Ni/Al_2O_3 were studied in the dry reforming at 900 °C. The feed was CH_4/CO_2 in helium with different CH_4/CO_2 molar ratios of 1.0/0.3, 1.0/1.0, and 1.0/3.0. The main products from this reaction were H_2 and CO with some H_2O. The observed H_2/CO production ratios were less than 1.0 in all conditions indicating a contribution from the reverse water–gas shift reaction at this operating temperature. The reforming rate was measured as a function of time in order to indicate the stability and the deactivation rate. The variations in the methane conversion with time at 900 °C for the different inlet CH_4/CO_2 ratios are shown in Fig. 3.

Significant deactivations were detected for Ni/Al_2O_3 catalyst in all conditions especially at high inlet CH_4/CO_2 ratio, whereas much lower deactivations were detected for both CeO_2 (HSA), and CeO_2 (LSA). At steady-state, the dry reforming over CeO_2 (HSA) with inlet CH_4/CO_2 of 1.0/3.0 showed the best performance in terms of stability, and activity. Catalyst stabilities expressed as deactivation percentages are given in Table 3. It should be noted that, in order to determine whether the observed deactivation is due to the carbon formation, the post-reaction temperature-programmed oxidation (TPO) experiments were carried out. From the TPO results shown in Fig. 4, the huge peaks of

Table 3
Deactivation percentages, specific surface area, and the amount of carbon deposition on the surface of catalysts after exposure in dry reforming conditions (various inlet CH_4/CO_2 ratios) at 900 °C for 10 h

Catalyst	CH_4/CO_2 ratio	Deactivation (%)	BET surface ($m^2\ g^{-1}$)	Surface area reduction (%)	C formation[a] (monolayers)
CeO_2 (HSA)[b]	1.0/3.0	4.5	23	4.2	~0
	1.0/1.0	6.9	22	8.3	~0
	1.0/0.3	7.7	22	8.3	~0
CeO_2 (LSA)[c]	1.0/3.0	28	6.2	27	0.08
	1.0/1.0	30	6.2	27	0.11
	1.0/0.3	41	6.0	30	0.15
Ni/Al_2O_3[d]	1.0/3.0	90	~40	~0	3.9
	1.0/1.0	96	~40	~0	5.2
	1.0/0.3	97	~40	~0	5.8

[a] Calculated using CO and CO_2 yields from temperature-programmed oxidation (TPO) with 10% oxygen.
[b] High surface area CeO_2 prepared by surfactant-assisted approach.
[c] Conventional low surface area CeO_2 prepared by precipitation method.
[d] Ni/Al_2O_3 prepared by impregnation method with the specific surface area of 40 $m^2\ g^{-1}$ after calcinations.

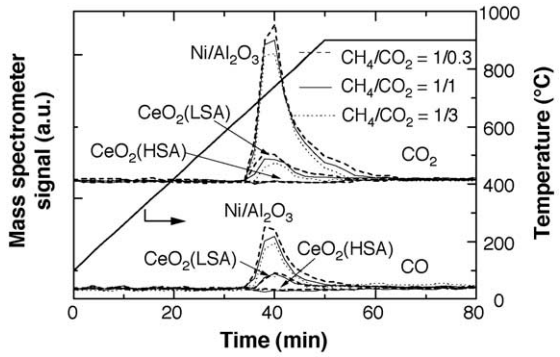

Fig. 4. Temperature programmed oxidation (TPO) over several catalysts after exposure in dry reforming conditions.

carbon dioxide and carbon monoxide were observed for Ni/Al_2O_3 at 600 °C, while small peaks of carbon dioxide and carbon monoxide were detected for CeO_2 (LSA). No peak of either carbon dioxide or carbon monoxide was detected for CeO_2 (HSA) in all conditions. The amount of carbon formations on the surface of Ni/Al_2O_3 with different inlet CH_4/CO_2 ratios were determined by measuring the CO and CO_2 yields from the TPO results (using Microcal Origin Software). Using a value of 0.026 nm^2 for the area occupied by a carbon atom in a surface monolayer of the basal plane in graphite [18], the quantities of carbon deposited over Ni/Al_2O_3 were observed to be approximately 5.8, 5.2, and 3.9 monolayers, while those over CeO_2 (LSA) were 0.15, 0.11, and 0.08 monolayers for the inlet CH_4/CO_2 ratios of 1.0/0.3, 1.0/1.0, and 1.0/3.0, respectively. The total amounts of carbon deposited were ensured by calculating the carbon balance of the system. Regarding the calculations, for the inlet CH_4/CO_2 ratios of 1.0/0.3, 1.0/1.0, and 1.0/3.0, the moles of carbon deposited per gram of CeO_2 (LSA) were 0.19, 0.12, and 0.09 mmol g^{-1}. By the same assumption for the area occupied by a carbon atom [18], these values are equal to 0.16, 0.10, and 0.07 monolayers, respectively, which is in good agreement with the values observed from the TPO method described above. The results clearly indicated that the deactivations observed for Ni/Al_2O_3 were mainly due to the carbon deposition on the surface of catalyst, and CeO_2 presented significantly stronger resistance toward carbon formation compared to Ni/Al_2O_3.

The BET measurements were carried out to observe the surface area reduction percentages of all catalysts. As shown in Table 3, it was suggested that the deactivations of ceria are mainly due to the thermal sintering. In addition, the surface area reduction percentage of CeO_2 (HSA) is much lower than CeO_2 (LSA), indicating its better stability toward the thermal sintering.

3.3. Kinetics of the dry reforming on CeO_2 (HSA)

The kinetics of the dry reforming over CeO_2 (HSA) was studied by varying inlet CH_4, and CO_2 partial pressures at different operating temperatures. The effects of CO and H_2 in feed on the reforming rate over this catalyst were also investigated, as both components are the main products from the dry reforming.

The inlet methane partial pressure was varied from 0.01 to 0.04 atm, while the operating temperature range was 900–1000 °C. The activity of CeO_2 (HSA) increased with increasing methane partial pressure as well as the operating temperature as shown in Fig. 5. In the present work, the dry reforming rate was represented in term of the turnover frequencies (N), calculated from the below equation [1].

$$N = \frac{rN_A A_{N_2}}{m_c S} \quad (5)$$

It is assumed that all surface sites accessible by nitrogen adsorption (area per molecule 16.2×10^{-20} m^2 [1,18]) were active. Here, r is the moles of CH_4 changing per unit time ($mol_{CH_4}\ min^{-1}$), N_A the Avagadro's number, A_{N_2} the area occupied by an adsorbed nitrogen molecule (16.2×10^{-20} m^2), m_c the weight of catalyst used (0.05 g), and S the specific surface area of the catalyst ($m^2\ g^{-1}$).

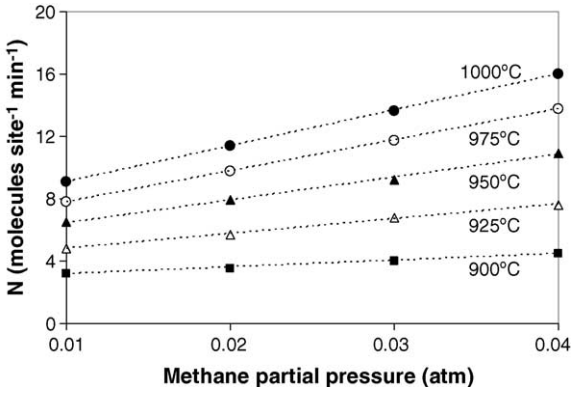

Fig. 5. Effect of methane partial pressure on the turnover frequencies (N) for CeO_2 (HSA) at different temperatures (inlet CO_2 = 0.05 atm).

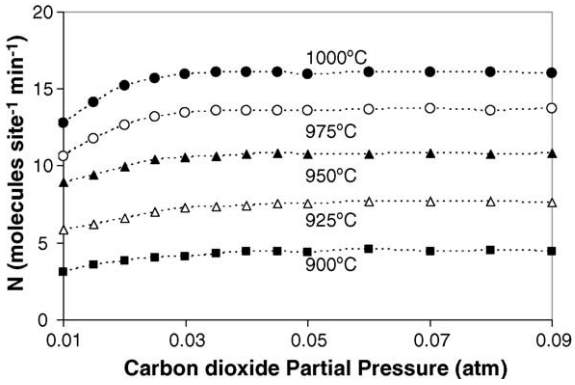

Fig. 6. Effect of carbon dioxide partial pressure on the turnover frequencies (N) for CeO_2 (HSA) at different temperatures (inlet CH_4 of 0.04 atm).

The reaction order in methane (n) for this catalyst was observed to be between 0.50 and 0.55, and seemed to be essentially independent of the operating temperature and carbon dioxide partial pressure for the range of conditions studied. These values n were obtained experimentally by plotting ln(N) versus ln P_{CH_4}. The reaction orders in other components (CO_2, H_2, and CO) were achieved using the same approach by varying the inlet partial pressure of the component of interest while keeping other inlet component partial pressures constant.

The H_2/CO ratio in the products increased with increasing inlet CH_4/CO_2 ratio, whereas it strongly decreased with increasing temperature, as presented in Table 4.

Several inlet carbon dioxide partial pressures, from 0.01 to 0.09 atm, were then introduced to the feed with constant methane partial pressure in order to investigate the influence of CO_2 on the dry reforming rate. Carbon dioxide presented slight positive effect on the dry reforming rate at high inlet CH_4/CO_2 ratios as shown in Fig. 6. The experiments yielded non-linear positive carbon dioxide trend. When the inlet carbon dioxide partial pressure was greater than 0.03 atm, the carbon dioxide influence on the dry reforming rate became less pronounced. At high inlet CH_4/CO_2 ratios, the reaction order in carbon dioxide for this catalyst was observed to be a small positive value between 0.08 and 0.12, and seemed to be independent of the inlet methane partial pressure and the operating temperature for the range of conditions studied. The proportion of H_2/CO in the products reduced from 0.94 to 0.89 as the CH_4/CO_2 ratio was decreased from 3.0/1.0 to 3.0/5.0 (Table 4). This is as expected from an increasing contribution from the RWGS reaction.

Table 4
Effect of inlet compositions on H_2/CO ratio from the dry reforming over CeO_2 (HSA) at different temperatures

Temperature (°C)	Inlet compositions (atm)	H_2/CO production ratio from the dry reforming over CeO_2 (HSA)
900	0.03 CH_4/0.03 CO_2	0.93
925	0.03 CH_4/0.03 CO_2	0.90
950	0.03 CH_4/0.03 CO_2	0.88
975	0.03 CH_4/0.03 CO_2	0.85
1000	0.03 CH_4/0.03 CO_2	0.81
900	0.01 CH_4/0.03 CO_2	0.90
	0.02 CH_4/0.03 CO_2	0.91
	0.03 CH_4/0.03 CO_2	0.93
	0.04 CH_4/0.03 CO_2	0.95
	0.05 CH_4/0.03 CO_2	0.96
900	0.03 CH_4/0.01 CO_2	0.94
	0.03 CH_4/0.02 CO_2	0.93
	0.03 CH_4/0.03 CO_2	0.93
	0.03 CH_4/0.04 CO_2	0.91
	0.03 CH_4/0.05 CO_2	0.89

The dry reforming in the presences of carbon monoxide and hydrogen were then investigated by adding either carbon monoxide or hydrogen to the feed gas at several operating temperatures. The results show that the reforming rates are also dependent on both carbon monoxide and hydrogen concentrations. Unlike CH_4 and CO_2, both components inhibited the dry reforming rate over CeO_2 as shown in Figs. 7 and 8. The reaction order in carbon monoxide was in the range of −0.15 to −0.10, while the reaction order in hydrogen was between −0.34 to −0.28 in the range of

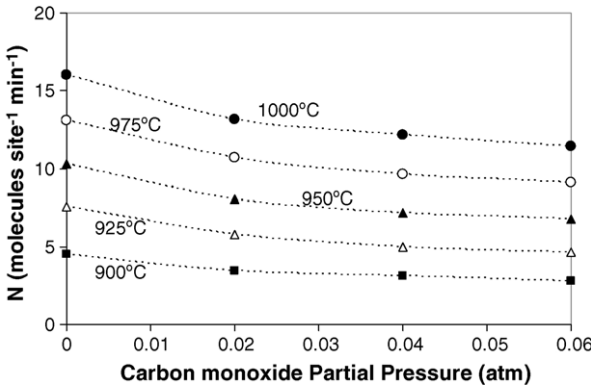

Fig. 7. Effect of carbon monoxide partial pressure on the turnover frequencies (N) for CeO_2 (HSA) at different temperatures (inlet CH_4 of 0.04 atm).

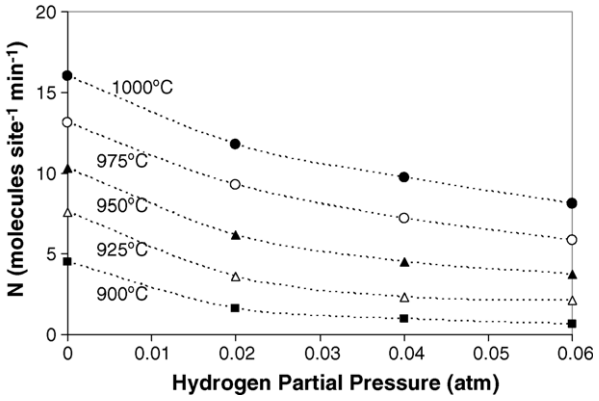

Fig. 8. Effect of hydrogen partial pressure the turnover frequencies (N) for CeO_2 (HSA) at different temperatures (inlet CH_4 of 0.04 atm).

conditions studied. These negative impacts are due to the inhibition of redox property on ceria surface, which will be discussed in the next section. Table 5 presents the summary of observed reaction orders in each component (CH_4, CO_2, CO, and H_2) for CeO_2 (HSA) at different inlet conditions.

According to the influences of CH_4, CO_2, CO, and H_2 as described above, the experimental data can be fitted well to a simple rate Eq. (6), which captures the essential features and could also easily be used in the simulation of indirect internal reforming over CeO_2 (HSA) in SOFCs.

$$-r_{CH_4} = \frac{k(T)(P_{CH_4})^n}{1 + K_1 \frac{P_{CO}}{P_{CO_2}} + K_2(P_{H_2})^m} \quad k(T) = A\exp\left(\frac{-E}{RT}\right)$$

$$\text{and} \quad K_i(T) = B_i \exp\left(\frac{-\Delta H_i}{RT}\right) \tag{6}$$

where P_i is the partial pressure of chemical component i, and K_1 and K_2 are adsorption parameters, obtained from Van't Hoff equation. The positive effect of methane on the dry reforming rate was a consequence of the presence of the $k(T)(P_{CH_4})^n$ term, whereas both positive and negative effects of carbon dioxide and carbon monoxide were a consequence of the $K_1(T)P_{CO}/P_{CO_2}$ term in the denominator. According to the fitting, when n and m were taken as 0.5, a good fit to the data was observed in the range of conditions studied. The value of $k(T)$ increased from 23.98 molecules site^{-1} min^{-1} atm$^{-0.5}$ at 900 °C to 83.76 molecules site^{-1} min^{-1} atm$^{-0.5}$ at 1000 °C, while $K_1(T)$ and $K_2(T)$, also temperature dependent parameters, were in the range of 0.35–0.50 and 8.5–15.2 atm$^{-0.5}$, respectively. The parameters of the rate expression can be summarized in Table 6. It should be noted that the activation energy for this reaction, which were achieved by the Arrhenius plots as shown in Fig. 9, was approximately 154 kJ/mol.

4. Discussion

It has been widely reported that the gas–solid reaction between ceria and CH_4 can generate CO and H_2 at high temperature [19,20]. In addition, the reduced state, CeO_{2-n}, can react with CO_2 to produce CO [21]. Therefore, the dry reforming of methane over CeO_2 can be presented as follows:

$$CeO_2 + nCH_4 \rightarrow CeO_{2-n} + nCO + 2nH_2 \tag{7}$$

$$CeO_{2-n} + nCO_2 = CeO_2 + nCO \tag{8}$$

$$CeO_2 + nH_2 = CeO_{2-n} + nH_2O \tag{9}$$

The positive effect of CH_4 and CO_2 on the dry reforming reactivity is due to the forward of Eqs. (7) and (8), respectively, while the reverse of Eq. (8) results in the negative effect of CO. Hydrogen presented negative effect on the dry

Table 5
Reaction orders for the components of interest (CH_4, CO_2, CO, and H_2) from the dry reforming over CeO_2 (HSA) at different operating conditions

Components of interest	Temperature (°C)	Other inlet compositions (atm)				Reaction order for components of interest
		CH_4	CO_2	H_2	CO	
CH_4 (0.01–0.04 atm)	900–1000		0.05	0	0	0.52 ± 0.02
	900		0.10	0	0	0.50
	900		0.15	0	0	0.51
	900–950		0.05	0.02	0	0.54 ± 0.01
	900–950		0.05	0	0.02	0.53 ± 0.02
CO_2 (0.01–0.09 atm)	900–1000	0.04		0	0	0.10 ± 0.02
	900	0.02		0	0	0.10
	900	0.07		0	0	0.08
	900–925	0.04		0.02	0	0.10 ± 0.02
	900–950	0.04		0	0.02	0.11 ± 0.01
H_2 (0.02–0.06 atm)	900–1000	0.04	0.05		0	−0.31 ± 0.03
	900	0.04	0.10		0	−0.28
	900	0.02	0.05		0	−0.34
	900	0.04	0.05		0.02	−0.30
CO (0.02–0.06 atm)	900–1000	0.04	0.05	0		−0.11 ± 0.01
	900	0.04	0.10	0		−0.12
	900	0.02	0.05	0		−0.15
	900	0.04	0.05	0.02		−0.10

Table 6
Summary of Pre-exponential factors for Arrhenius and Van't Hoff equations for dry reforming over CeO_2 (HSA)

A (molecules site^{-1} min^{-1} atm$^{-0.5}$)	E (kJ mol^{-1})	B_1	ΔH_1 (kJ mol^{-1})	B_2 (atm$^{-0.5}$)	ΔH_2 (kJ mol^{-1})
1.9×10^8	154	5.3×10^{-3}	−44.28	9.29×10^{-3}	−72.15

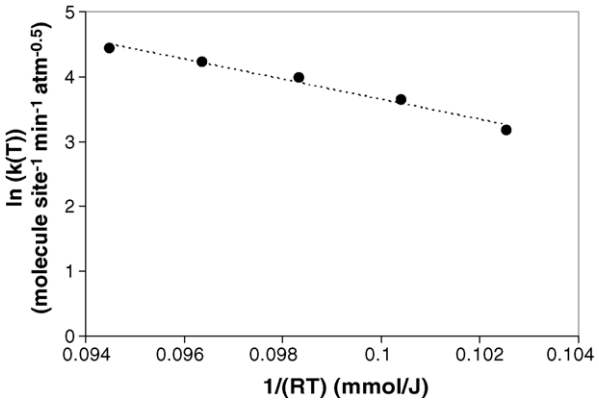

Fig. 9. The Arrhenius-type plot for dry reforming reaction over CeO_2 (HSA).

reforming, as this component reduced Ce^{4+} to Ce^{3+} via Eq. (9) and, consequently, results in the inhibition of methane conversion via Eq. (7). It should be noted that the inhibitory effect of hydrogen is the main disadvantage of using CeO_2 industrially, therefore, the removal of hydrogen during the reforming process might be required.

In the present work, the observed activation energy for the dry reforming over CeO_2 (HSA) is 154 kJ mol^{-1}. This value is in the same range as the activation energies previously observed for the methane steam reforming over CeO_2 (HSA) [4], CeO_2 (LSA) [3], and Gd–CeO_2 (LSA) [1]. Aguiar et al. [22] reported the methane steam reforming rate equation over conventional CeO_2 (LSA) in the form of $-r_{CH_4} = k(T)P_{CH_4}^{0.5}/(1 + K_H P_{H_2}^{0.5})$. The activation energy obtained by the Arrhenius plots of $k(T)$ was 133 kJ mol^{-1}. Laosiripojana and Chadwick [4] studied the methane steam reforming over CeO_2 (HSA) and presented the well-fitting of their experimental data to this form of rate equation. Their corresponding activation energy was 150 kJ mol^{-1}. Ramirez-Cabrera et al. [1] studied the methane steam reforming reaction over Gd–CeO_2 and compared the results with the dry methane reaction over the same catalyst. They reported that the observed activation energies from both reactions are in the same range of 153–165 kJ mol^{-1}. In addition, in the excess of inlet CO_2, the observed methane conversion for the dry reforming of 5% methane at 900 °C in the present work is approximately equal to that for the steam reforming of 5% methane [4]. These observations indicate that the rate-controlling step for the steam and dry reforming reactions for CeO_2 is similar. Hence, the methane steam reforming reaction mechanism for CeO_2 as proposed by Ramirez-Cabrera et al. [1] should also be applied to explain the dry reforming of methane over this material. The dry reforming mechanism for CeO_2 involves the reaction between methane, or an intermediate surface hydrocarbon species, with the lattice oxygen (O_x) at CeO_2 surface, as illustrated schematically below.

$$CH_4 + 2S_{Ce} = CH_3{-}S_{Ce} + H{-}S_{Ce} \quad (10)$$

$$CH_3{-}S_{Ce} + S_{Ce} = CH_2{-}S_{Ce} + H{-}S_{Ce} \quad (11)$$

$$CH_2{-}S_{Ce} + S_{Ce} = CH{-}S_{Ce} + H{-}S_{Ce} \quad (12)$$

$$CH{-}S_{Ce} + S_{Ce} = C{-}S_{Ce} + H{-}S_{Ce} \quad (13)$$

$$C{-}S_{Ce} + O_x = CO + O_{x-1} + S_{Ce} \quad (14)$$

$$CO_2 + O_{x-1} = O_x + CO \quad (15)$$

$$H_2 + O_x = O_{x-1} + H_2O \quad (16)$$

$$2H{-}S_{Ce} = H_2 + 2S_{Ce} \quad (17)$$

There are two possibilities for this scheme depending on what is assumed for the catalyst surface site, S_{Ce}. It can be a unique site, or can also be considered to be the same site as the catalyst oxidised site (O_x) [3]. During the dry reforming, methane is adsorbed on either a unique site, S_{Ce}, or the catalyst oxidized site, O_x, whereas CO_2 is always reacted with the catalyst reduced site, O_{x-1}. The steady-state reforming rate is mainly due to the continuous supply of the oxygen source by CO_2. It should be noted that the measured value of the oxygen diffusion coefficient for ceria is high and the reaction rate is controlled by a surface reaction and not by diffusion of oxygen from the bulk of the solid particles to ceria surfaces [23]. The stronger linear dependence of the reforming rate on methane partial pressure, and the weaker positive of CO_2 provide the evidence that the controlling step is the reaction of methane with the CeO_2 surface, and that oxygen is replenished by a significantly rapid surface reaction of the reduced state CeO_2 with CO_2.

The high resistance toward carbon deposition for ceria, which has been widely reported by several researchers [1–5,24], is mainly due to the high oxygen storage capacity (OSC) of this material. As described, carbon formation is one major problem for the dry reforming of methane. We also observed high amount of carbon formation on the surface of Ni/Al_2O_3 after exposure in a dry reforming condition. Regarding the possible carbon formation during the reforming processes, the following reactions are theoretically the most probable reactions that could lead to carbon formation:

$$2CO = CO_2 + C \quad (18)$$

$$CH_4 = 2H_2 + C \quad (19)$$

$$CO + H_2 = H_2O + C \quad (20)$$

$$CO_2 + 2H_2 = 2H_2O + C \quad (21)$$

At low temperature, reactions (20) and (21) are favorable, while reaction (18) is thermodynamically unflavored [25]. The Boudard reaction (Eq. (18)) and the decomposition of methane (Eq. (19)) are the major pathways for carbon formation at such a high temperature as they show the largest change in Gibbs energy [26]. According to the range of temperature in this study, carbon formation would be formed via the decomposition of methane and Boudard reactions especially at high inlet CH_4/CO_2 ratio (1.0/0.3 and 1.0/1.0). By applying CeO_2, both reactions (Eqs. (20) and (21)) could be inhibited by the redox reactions between methane and carbon monoxide (produced during the dry reforming process) with the lattice oxygen (O_x) at CeO_2 surface (Eqs. (22) and (23)) forming hydrogen and carbon dioxide, which is thermodynamically unflavored to form carbon species in this range of conditions. Therefore, significant lower amount of carbon deposition were observed for ceria even at low inlet carbon dioxide concentration.

$$CH_4 + O_x \rightarrow CO + H_2 + O_{x-1} \quad (22)$$

$$CO + O_x = CO_2 + O_{x-1} \quad (23)$$

Although CeO_2 (LSA) also provides high resistance toward carbon formation, the major weaknesses of CeO_2 (LSA) are its nature low specific surface area and also high size reduction due to the thermal sintering impact, resulting in its low redox property and consequently low reforming reactivity. In the present work, the specific surface area of CeO_2 (HSA) after calcination at 1000 °C was almost three times higher than the conventional one. Moreover, the size reduction percentage for CeO_2 (HSA) was significantly lower. These enhancements were also reported by Terrible et al. [17], who prepared Ce–ZrO_2 by the same procedure. They reported that the achievement of high surface area material by the surfactant-assisted procedure is mainly due to the interaction of hydrous oxide with cationic surfactants under basic conditions during the preparation [17]. At high pH value, conducting the precipitation of hydrous oxide in the presence of cationic surfactant allows the cation exchange process between H^+ and the surfactant, resulting in a developed pore structure with an increase in surface area [17]. Regarding the thermal stability at high temperature, Terrible et al. [17] explained that the incorporation of surfactants during preparation could reduce the interfacial energy and eventually decrease the surface tension of water contained in the pores. This could reduce the shrinkage and collapse of the catalyst during heating up, which consequently help the catalyst maintaining high surface area after calcination [17].

Our previous work on Ni/CeO_2 (HSA) and Ni/Ce–ZrO_2 (HSA) [24] for the steam reforming of methane also indicated the same improvement as described above. We previously studied the resistance of metal catalyst on ceria-based supports toward the carbon formation. Under methane steam reforming conditions with the H_2O/CH_4 ratio of 3.0, Ni/CeO_2 (HSA) exhibited high steady-state steam reforming activity and no carbon species was detected on the surface [24]. However, at steam to methane ratios less than 1, significant carbon deposition was formed. Thus, the use of Ni always increases the risk of carbon deposition even when CeO_2 (HSA) was applied as the support.

5. Conclusions

CeO_2 is a good candidate catalyst for the dry reforming of methane due to its extreme resistance toward the deactivation from carbon formation. The use of high surface area CeO_2 (CeO_2 (HSA)) significantly reduces the degree of deactivation by thermal sintering compared to general low surface area CeO_2.

The dry reforming rate over CeO_2 (HSA) is proportional to the methane partial pressure and the operating temperature. Carbon dioxide presents slight positive impact on the methane conversion, whereas carbon monoxide inhibits the reforming rate. Addition of hydrogen was found to have a significant inhibitory effect on the conversion of methane. This inhibitory effect is the main disadvantage of using CeO_2 as the dry reforming catalyst, and the removal of hydrogen during the reforming process might be required.

The activation energies and reforming rates at the same methane concentration for the dry reforming are equal to those for the steam reforming. These results suggest the similar reaction mechanisms for both the steam reforming and the dry reforming over CeO_2 in which the reforming rate is governed by the slow reaction of adsorbed methane, or surface hydrocarbon species, with oxygen in CeO_2, and a rapid gas–solid reaction between CO_2 and CeO_2 to replenish the oxygen.

Acknowledgement

The financial support from The Thailand Research Fund (TRF) throughout this project is gratefully acknowledged. The first author like to acknowledge Professor David Chadwick from Department of Chemical Engineering and Chemical Technology, Imperial College London for his valuable suggestion.

References

[1] E. Ramírez-Cabrera, A. Atkinson, D. Chadwick, Appl. Catal. B 47 (2004) 127–131.
[2] E. Ramírez-Cabrera, N. Laosiripojana, A. Atkinson, D. Chadwick, Catal. Today 78 (2003) 433–438.
[3] N. Laosiripojana 2003, Reaction engineering of indirect internal steam reforming of methane for application in solid oxide fuel cells. Ph.D. Thesis, University of London, England.

[4] N. Laosiripojana, D. Chadwick, Catalytic methane steam reforming of high surface area CeO_2, International Hydrogen Energy Congress & Exhibition 2005, in press.
[5] P. Aguiar, E. Ramírez-Cabrera, N. Laosiripojana, A. Atkinson, L.S. Kershenbaum, D. Chadwick, Stud. Surf. Sci. Catal. 145 (2003) 387.
[6] P. Aguiar, N. Lapena-Rey, D. Chadwick, L. Kershenbaum, Chem. Eng. Sci. 56 (2001) 652.
[7] P. Aguiar, D. Chadwick, L. Kershenbaum, Chem. Eng. Sci. 57 (2002) 1665.
[8] J.R. Rostrup-Nielsen, L.J. Christiansen, Appl. Catal. A 126 (2) (1995) 381–390.
[9] J.H. Edwards, A.M. Maitra, Fuel Process. Technol. 42 (1995) 269.
[10] T. Sodesawa, A. Dobashi, F. Nozaki, React. Kinet. Catal. Lett. 12 (1979) 107.
[11] C.T. Kresge, M.E. Leonowicz, W.J. Roth, J.C. Vartuli, J.S. Beck, Nature 359 (1992) 710.
[12] Q. Huo, D.I. Margolese, U. Ciesla, P. Feng, T.E. Gier, P. Sieger, R. Leon, P.M. Petroff, B. Schüth, G.D. Stucky, Nature 368 (1994) 317.
[13] P.T. Tanev, T.J. Pinnavaia, Science 267 (1995) 865.
[14] U. Ciesla, S. Schacht, G.D. Stucky, K.K. Unger, F. Schüth, Angew. Chem. Int. Ed. Engl. 35 (1996) 541.
[15] D.M. Antonelli, J.Y. Ying, Angew. Chem. Int. Ed. Engl. 35 (1996) 426.
[16] Q. Huo, D.I. Margolese, U. Ciesla, D.G. Demuth, P. Feng, T.E. Gier, P. Sieger, A. Firouzi, B.F. Chmelka, B. Schüth, G.D. Stucky, Chem. Mater. 6 (1994) 1176.
[17] D. Terribile, A. Trovarelli, J. Llorca, C. de Leitenburg, G. Dolcetti, Catal. Today 43 (1998) 79–88.
[18] E. Ramirez, A. Atkinson, D. Chadwick, Appl. Catal. B 36 (2002) 193–206.
[19] K. Otsuka, T. Ushiyama, I. Yamanaka, Chem. Lett. (1993) 1517.
[20] K. Otsuka, M. Hatano, A. Morikawa, J. Catal. 79 (1983) 493.
[21] K. Otsuka, M. Hatano, A. Morikawa, Inorganica Chim. Acta 109 (1985) 193.
[22] P. Aguiar, D. Chadwick, L. Kershenbaum, Chem. Eng. Sci. 59 (2004) 87–97.
[23] B.C.H. Steele, J.M. Floyd, Proc. Br. Ceram. Soc. 19 (1971) 55.
[24] N. Laosiripojana, S. Assabumrungrat, Catalytic steam reforming of methane over Ni on high surface area CeO_2 and Ce–ZrO_2 supports, PSU-UNS International Conference on Engineering and Environment (ICEE) 2005, in press.
[25] Y. Lwin, W.R.W. Daud, A.B. Mohamad, Z. Yaakob, Int. J. Hydrogen Energy 25 (1) (2000) 47–53.
[26] J.N. Amor, Appl. Catal. A 176 (1999) 159–176.

N. Laosiripojana and S. Assabumrungrat

"Methane steam reforming over Ni/Ce-ZrO_2 catalyst: Influences of Ce-ZrO_2 support on reactivity, resistance toward carbon formation, and intrinsic reaction kinetics"

Applied Catalysis A: General, 290 (2005) 200-211

(IF-2004 = 2.31)

Available online at www.sciencedirect.com
SCIENCE DIRECT®
Applied Catalysis A: General 290 (2005) 200–211
APPLIED CATALYSIS A: GENERAL
www.elsevier.com/locate/apcata

Methane steam reforming over Ni/Ce–ZrO_2 catalyst: Influences of Ce–ZrO_2 support on reactivity, resistance toward carbon formation, and intrinsic reaction kinetics

N. Laosiripojana [a,*], S. Assabumrungrat [b]

[a] *The Joint Graduate School of Energy and Environment, King Mongkut's University of Technology Thonburi, 91 Prachauthit Road, Bangmod, Tungkru, Bangkok 10140, Thailand*
[b] *Center of Excellence on Catalysis and Catalytic Reaction Engineering, Department of Chemical Engineering, Faculty of Engineering, Chulalongkorn University, Bangkok 10330, Thailand*

Received 21 December 2004; received in revised form 17 May 2005; accepted 25 May 2005
Available online 6 July 2005

Abstract

Ni/Ce–ZrO_2 showed good methane steam reforming performance in term of stability toward the deactivation by carbon deposition. It was first observed that the catalyst with Ce/Zr ratio of 3/1 showed the best activity among Ni/Ce–ZrO_2 samples with the Ce/Zr ratios of 1/0, 1/1, 1/3, and 3/1. Temperature-programmed oxidation (TPO) experiments indicated the excellent resistance toward carbon formation for this catalyst, compared to conventional Ni/Al_2O_3; the requirement of inlet H_2O/CH_4 to operate without the formation of carbon species is much lower. These benefits are related to the high oxygen storage capacity (OSC) of Ce–ZrO_2. During the steam reforming process, in addition to the reactions on Ni surface (*), the redox reactions between the gaseous components present in the system and the lattice oxygen (O_x) on Ce–ZrO_2 surface also take place. Among these reactions, the redox reactions between the high carbon formation potential compounds (CH_4, CH_x-*n and CO) and the lattice oxygen (O_x) can prevent the formation of carbon species from the methane decomposition and Boudard reactions, even at low inlet H_2O/CH_4 ratio (1.0/1.0).

Regarding the intrinsic kinetic studies in the present work, the reaction order in methane over Ni/Ce–ZrO_2 was observed to be approximately 1.0 in all conditions. The dependence of steam on the rate was non-monotonic, whereas addition of oxygen as an autothermal reforming promoted the rate but reduced CO and H_2 production selectivities. The addition of a small amount of hydrogen increased the conversion of methane, however, this positive effect became less pronounced and the methane conversion was eventually inhibited when high hydrogen concentration was added. Ni/Ce–ZrO_2 showed significantly stronger negative impact of hydrogen than Ni/Al_2O_3. The redox mechanism on ceria proposed by Otsuka et al. [K. Otsuka, T. Ushiyama, I. Yamanaka, Chem. Lett. (1993) 1517; K. Otsuka, M. Hatano, A. Morikawa, J. Catal. 79 (1983) 493; K. Otsuka, M. Hatano, A. Morikawa, Inorg. Chim. Acta 109 (1985) 193] can explain this high inhibition.

1. Introduction

The methane steam reforming is a widely practiced technology for production of hydrogen or synthesis gas for later utilization in fuel cells. Three main reactions are always carried out as presented in the following equations:

$$CH_4 + H_2O \Leftrightarrow CO + 3H_2 \quad (1)$$

$$CO + H_2O \Leftrightarrow CO_2 + H_2 \quad (2)$$

$$CH_4 + 2H_2O \Leftrightarrow CO_2 + 4H_2 \quad (3)$$

Both water–gas shift reaction (Eq. (2)) and reverse methanation (Eq. (3)) are associated with the steam reforming over a catalyst at elevated temperatures. The reverse methanation (Eq. (3)) is thermodynamically linearly dependent on methane steam reforming and water–gas shift reaction, but it is kinetically independent [4–8]. Due to the

* Corresponding author. Tel.: +662 8729014; fax: +662 8726736.
E-mail address: navadol_1@jgsee.kmutt.ac.th (N. Laosiripojana).

0926-860X/$ – see front matter © 2005 Elsevier B.V. All rights reserved.
doi:10.1016/j.apcata.2005.05.026

overall high endothermic nature of the reactions, they are carried out at high temperature (700–900 °C). In recent years, many researchers have also investigated the addition of oxygen together with methane and steam in a single process, calling an autothermal reforming. This reaction is an economical process, in which the steam reforming of methane (1) is combined with the partial oxidation of methane, as presented in the following equation:

$$CH_4 + (1/2)\,O_2 \Leftrightarrow CO + 2H_2 \quad (4)$$

By this combination, exothermic heat from the partial oxidation can directly supply the energy required for the endothermic steam reforming reaction. Therefore, it is considered to be thermally self-sustaining and consequently more attractive than the steam reforming. However, the main disadvantage of this reaction is the lower production of synthesis gas (H_2 and CO) from this reaction compared to the steam reforming. Currently, the commercial process for the production of hydrogen and synthesis gas is still based on the steam reforming reaction using nickel catalyst on supports such as Al_2O_3, MgO, $MgAl_2O_4$ or their mixtures. Worldwide efforts are in progress to develop a novel catalyst with higher activity and stability for the reforming reactions. Various precious metals such as Pt, Rh and Ru have been reported to be active for the reforming reactions and resistant to the carbon formation [9,10]. However, the current prices of these metals are very high for commercial uses, and the availability of some precious metals such as ruthenium was too low to have a major impact on the total reforming catalyst market [11].

Selection of a support material is another important issue as there was some evidence that metal catalysts are not very active for the steam reforming when supported on inert oxides [12]. Various supports have been investigated, for example, α-Al_2O_3 [13], γ-Al_2O_3 and γ-Al_2O_3 with alkali metal oxide and rare earth metal oxide [14], $CaAl_2O_4$ [15] and Ce–ZrO_2 [16]. A promising catalyst system for the reforming reactions appeared to be a metal on Ce–ZrO_2 support, where the metal can be Ni, Pt or Pd [17–25]. Ni/Ce–ZrO_2 has been successfully applied to the partial oxidation and the autothermal reforming of methane [26]. It is well established that ceria and metal oxide (e.g. Gd, Nb, and Zr) doped cerias provide high oxygen storage capacity, which is beneficial in oxidation processes [27]. Moreover, it has been reported that the gas–solid reaction between CeO_2 and CH_4 produces synthesis gas with a H_2/CO ratio of two, while the reduced ceria, CeO_{2-n}, can react with CO_2 and H_2O to produce CO and H_2, respectively, according to the following reactions [1–3]:

$$CeO_2 + nCH_4 \rightarrow CeO_{2-n} + nCO + 2nH_2 \quad (5)$$

$$CeO_{2-n} + CO_2 \Leftrightarrow CeO_2 + CO \quad (6)$$

$$CeO_{2-n} + H_2O \Leftrightarrow CeO_2 + H_2 \quad (7)$$

The addition of zirconium oxide (ZrO_2) to cerium oxide (CeO_2) has been reported to improve the oxygen storage capacity, redox property, thermal stability and catalytic activity [28–37]. This high oxygen storage capacity was associated with enhanced reducibility of cerium(IV) in Ce–ZrO_2, which is a consequence of the high O^{2-} mobility inside the fluorite lattice. One possible reason for the increasing mobility might be related to the lattice strain, which is generated by the introduction of a smaller isovalent Zr cation into the CeO_2 lattice (Zr^{4+} has a crystal ionic radius of 0.84 Å, which is smaller than 0.97 Å for Ce^{4+} in the same co-ordination enviroment) [38]. Due to the high thermal stability of this material, Ce–ZrO_2 would be a good candidate to be used as the catalyst support for high temperature steam reforming reactions.

Apart from the efforts devoted to catalyst selection, a number of works have been focused on the kinetic study of methane steam reforming. There is a general agreement that the reaction order in methane is always 1.0. However, there is less agreement with the other kinetic parameters, such as dependence on H_2O, and H_2. This could be due to the use of different catalysts and experimental conditions. Moreover, the impact of diffusion limitation could affect the experimental results also. In a study at conditions similar to SOFC, Dicks et al. [39] observed that the product partial pressures from the methane steam reforming on Ni/ZrO_2 could significantly affect the reforming rate, in particular that of hydrogen. The first order reaction in methane was obtained, while a positive effect of hydrogen partial pressure and a negative effect of steam partial pressure on the rate of reforming were observed. The researchers also indicated that hydrogen must be added as the feed gas together with methane and steam, because the steam reforming rate in pure methane/steam gas mixture was low. Xu and Froment [4–6] presented a rate model for the methane steam reforming together with the water–gas shift reaction over Ni/$MgAl_2O_4$ catalyst and also derived intrinsic rate equations. They reported the non-monotonic dependence of steam on the rate of reforming due to the competition of the catalyst active sites. A similar result was observed by Elnashaie et al. [7,8]. Xu and Froment [4–6] also presented the inhibitory effect of hydrogen on the methane steam reforming rate due to the promotion of the reverse reactions of Eqs. (1)–(3).

In the present work, we aimed to study the intrinsic reaction kinetics of an alternative reforming catalyst, which provides high methane steam reforming activity and high resistance toward carbon formation. According to the economical point of view, Ni was selected as a catalyst rather than other precious metals such as Pt, Rh and Ru although Ni is more sensitive to carbon formation. Ni/Ce–ZrO_2 catalysts with different ratios of Ce/Zr were first investigated to determine a suitable ratio. The intrinsic reaction kinetics for the selected catalyst were then studied by varying inlet CH_4, and H_2O concentrations, and by adding H_2, and O_2 in order to evaluate the possible use of Ni/Ce–ZrO_2 industrially.

2. Experimental

2.1. Catalyst preparations and characterizations

$Ce_{1-x}Zr_xO_2$ supports with different Ce/Zr molar ratios were prepared by co-precipitation of cerium nitrate ($Ce(NO_3)_3{\cdot}H_2O$), and zirconium oxychloride ($ZrOCl_2{\cdot}H_2O$) H_2O) (from Aldrich). The starting solution was prepared by mixing 0.1 M of metal salt solution with 0.4 M of urea at a 2/1 volumetric ratio. The ratio between each metal salt was altered to achieve nominal Ce/Zr molar ratios: $Ce_{1-x}Zr_xO_2$, where $x = 0.25$, 0.50, and 0.75, respectively. This solution was stirred by magnetic stirring (100 rpm) for 3 h, and the precipitate was filtered and washed with deionised water and ethanol to prevent an agglomeration of the particles. It was dried overnight in an oven at 110 °C, and then calcined in air at 1000 °C for 6 h.

Ni/Ce–ZrO_2 was prepared by impregnating Ce–ZrO_2 with a $Ni(NO_3)_2$ solution (from Aldrich). The catalyst was reduced with 10%H_2/Ar for 6 h before use. For comparison, Ni/Al_2O_3 and Ni/CeO_2 (5 wt.% Ni) were also prepared by impregnating α-Al_2O_3 (from Aldrich) and CeO_2 with $Ni(NO_3)_2$. After reduction, the catalysts were characterized by several physicochemical methods. The weight content of Ni in Ni/Al_2O_3, Ni/Ce–ZrO_2 (with different Ce/Zr ratio), and Ni/CeO_2 were determined by X-ray fluorescence (XRF) analysis. The reducibility and dispersion percentages of nickel were measured from temperature-programmed reduction (TPR) with 5% H_2 in Ar and temperature-programmed desorption (TPD), respectively. The catalyst specific surface areas were obtained from BET measurement. All physicochemical properties of the synthesized catalysts are presented in Table 1.

2.2. Apparatus and procedures

In order to investigate the methane steam reforming and its associated reactions, we constructed an experimental reactor system as shown in Fig. 1. The feed gases including the components of interest such as CH_4, H_2O, H_2, or O_2 were introduced to the reaction section, in which an 8 mm internal diameter and 40 cm length quartz reactor was mounted vertically inside a furnace. The catalyst was loaded in the quartz reactor, which was packed with a small amount of quartz wool to prevent the catalyst from moving. The weight of catalyst loading was 50 mg, while a typical range of total gas flow was 20–200 $cm^3\ min^{-1}$ depending on the desired space velocity. A type-K thermocouple was placed into the annular space between the reactor and the furnace. This thermocouple was mounted on the tubular reactor in close contact with the catalyst bed to minimize the temperature difference between the catalyst bed and the thermocouple. Another type-K thermocouple was inserted in the middle of the quartz tube in order to re-check the possible temperature gradient, especially when O_2 was added along with CH_4 and H_2O as the autothermal reforming. The record showed that the maximum temperature fluctuation during the reaction was always ± 0.75 °C or less from the temperature specified for the reaction.

After the reactions, the exit gas mixture was transferred via trace-heated lines to the analysis section, which consists of a Porapak Q column Shimadzu 14B gas chromatograph (GC) and a mass spectrometer (MS). The gas chromatography was applied in order to investigate the steady state condition experiments, whereas the mass spectrometer in which the sampling of the exit gas was done by a quartz capillery and differential pumping was used for the transient and carbon formation experiments.

A temperature-programmed technique (TP) was applied in order to study the formation of carbon species on catalyst surface. Temperature-programmed methane adsorption (TPMA) was firstly carried out in order to investigate the reaction of methane with the surface of catalyst and to form the carbon species on catalyst surface. A 5% methane in helium was introduced into the system, while the operating temperature was increased from room temperature to 1000 °C at the rate of 10 °C/min. After the system was purged with helium, TPMA was followed by temperature-programmed oxidation (TPO) in order to quantify the deposited carbon on the catalyst surface. A 10% oxygen in helium was introduced into the system and, similar to TPMA, the temperature was increased from room temperature to 1000 °C at the rate of 10 °C/min. The calibrations of CO and CO_2 productions were performed by injecting a known amount of these calibration gases from a loop, in an injection valve in the bypass line. The response factors were obtained by dividing the number of moles for each component over the respective areas under the peaks. This process was performed before each experiment to achieve maximal accuracy in the quantitative carbon analysis. In

Table 1
Physicochemical properties of the catalysts after reduction

Catalyst	Ce/Zr ratio	Ni-load[a] (wt.%)	BET surface area ($m^2\ g^{-1}$)	Ni-reducibility[b] (Ni%)	Ni-dispersion[c] (Ni%)
Ni/CeO_2		4.8	8.5	84.7	3.17
Ni/Ce–ZrO_2	1/3	5.0	20	90.4	4.24
Ni/Ce–ZrO_2	1/1	4.7	18	89.8	4.13
Ni/Ce–ZrO_2	3/1	4.8	19	88.1	4.37
Ni/Al_2O_3		4.9	40	92.1	4.87

[a] Measured from X-ray fluorescence analysis.
[b] Measured from temperature-programmed reduction (TPR) with 5% hydrogen.
[c] Measured from temperature-programmed desorption (TPD) of hydrogen after TPR measurement.

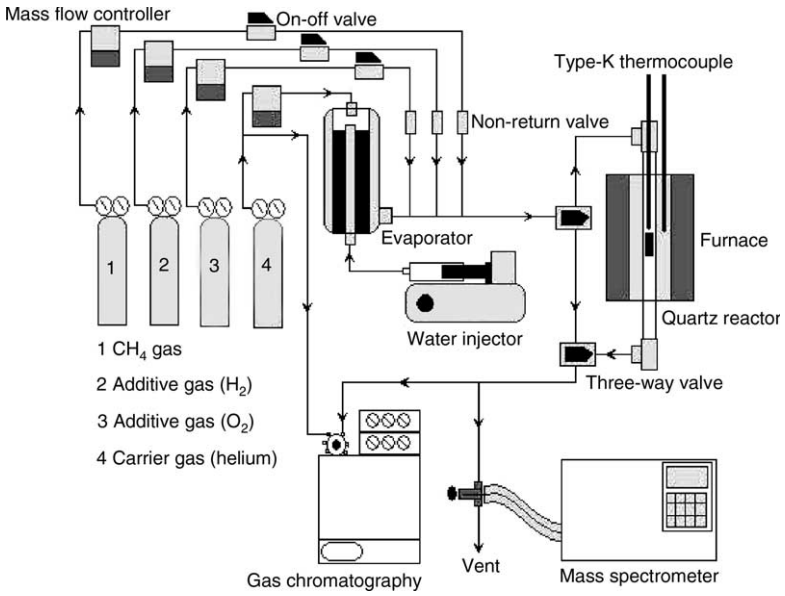

Fig. 1. Schematic diagram of the experimental set-up.

addition to the TPO method, the amount of carbon deposition was confirmed by calculating the carbon balance of the system. The amount of carbon formation would theoretically be equal to the difference between the inlet carbon containing component (CH_4) and the outlet carbon containing components (CO, CH_4, and CO_2). The amount of carbon deposited per gram of catalyst is calculated by the following equation:

$$C_{\text{deposition}} = \frac{\text{mole}_{\text{carbon(in)}} - \text{mole}_{\text{carbon(out)}}}{m_{\text{catalyst}}} \quad (8)$$

3. Results

3.1. Preliminary testing

In order to avoid any limitations by intraparticle diffusion, we checked the impact of the total flow rate before the formal investigations. The total flow rate was varied between 20 and 200 $cm^3\,min^{-1}$ under a constant residence time of 5×10^{-4} g min cm^{-3}. When the total flow rate was below 60 $cm^3\,min^{-1}$, the methane steam reforming rate increased with increasing the gas flow rate, suggesting that the mass transfer between the bulk gas and the catalyst particles is the rate-determining step. The steam reforming rate was almost constant in the range where the gas flow rate was higher than 80 $cm^3\,min^{-1}$, indicating that the mass transfer effect is unimportant in this flow rate range. The total flow rate was therefore kept constant at 100 $cm^3\,min^{-1}$ in all experiments. Fig. 2 shows the effect of the total gas flow rate on the reforming rate over Ni/Ce–ZrO_2.

The reactions on different average sizes (from 100 to 500 μm) of catalysts were carried out in order to guarantee that the experiments were carried out within the region of intrinsic kinetics. It was observed that there were no significant changes in the methane conversion for the catalyst with the particle size between 100 and 200 μm, which indicated that the intraparticle diffusion limitation was negligible in this range of operating conditions. Consequently, the catalyst diameter was kept between 100 and 200 μm in all experiments. Using these conditions, the steam reforming rate observed from the experiments should represent the intrinsic kinetics.

3.2. Stability and activity of Ni/Ce–ZrO_2 with different Ce/Zr ratios toward methane steam reforming

The steam reforming of methane over Ni/CeO_2 and Ni/Ce–ZrO_2 (with different Ce/Zr ratios) were studied at 900 °C by introducing CH_4/H_2O in helium with the inlet ratio of 1.0/1.0 in order to select the most suitable catalyst for further studies. The variations in methane conversion with time at

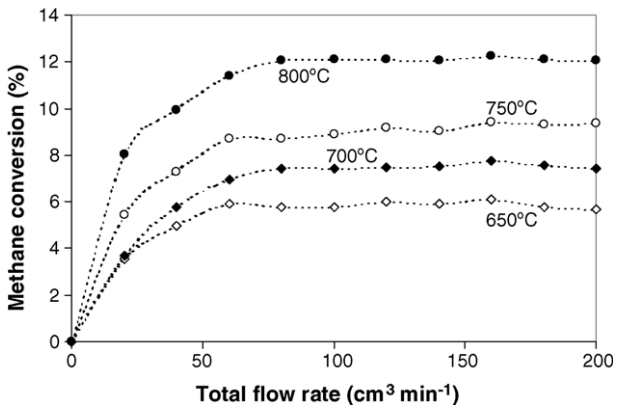

Fig. 2. Effect of the total gas flow rate on the reforming rate over Ni/Ce–ZrO_2 at different temperatures (3 kPa CH_4, 3 kPa H_2O).

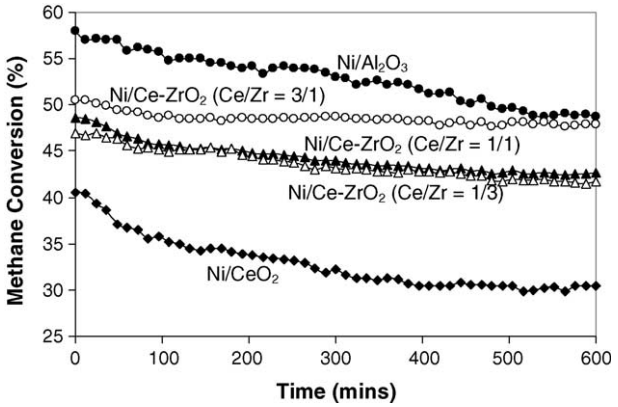

Fig. 3. Steam reforming of methane at 900 °C for different catalysts (3 kPa CH_4, 3 kPa H_2O).

900 °C for different catalysts are shown in Fig. 3. At steady state, the Ni/Ce–ZrO_2 with Ce/Zr ratio of 3/1 shows the best activity among Ni on ceria-based supports, its activity on a weight basis was slightly lower than that over Ni/Al_2O_3 due to the lower specific surface area. The steady state reforming rates of Ni/Ce–ZrO_2 (Ce/Zr = 3/1) and Ni/Al_2O_3 at 900 °C were 81.31 and 82.77 mol kg^{-1} h^{-1}, respectively.

As one can see from Fig. 3, the activities of Ni/Al_2O_3 and Ni/CeO_2 declined with time before reaching a significantly lower steady-state rate, while the activity of Ni/Ce–ZrO_2 declined slightly. Catalyst stabilities expressed as a deactivation percentage are given in Table 2. The post-reaction temperature-programmed oxidation (TPO) experiments were carried out after a helium purge by introducing 10% oxygen in helium in order to determine whether the observed deactivation is due to the carbon formation. TPO experiments detected no carbon formation on the surface of Ni on ceria-based supports. In contrast, the carbon species were observed on the surface of Ni/Al_2O_3. Using a value of 0.026 nm^2 for the area occupied by a carbon atom in a surface monolayer of the basal plane in graphite [27], the total quantities of carbon deposited formed on Ni/Al_2O_3 were 1.39 monolayers. This amount of carbon deposited was ensured by calculating the carbon balance of the system. Regarding the calculations, the molar amount of carbon deposited per gram of Ni/Al_2O_3 was 1.62 mmol g^{-1}. By the same assumption for the area occupied by a carbon atom [18], these values are equal to 1.37 monolayers, which is in good agreement with the value observed from the TPO method. More investigations about resistance toward carbon formation will be presented in the next section.

The BET measurement results as shown in Table 2 suggest that the deactivation of Ni on ceria-based supports could be mainly due to the sintering and the slight decrease of the catalyst dispersion. The % size reduction of these catalysts agreed well with the degree of catalyst deactivation. Regarding these experimental results, Ni/Ce–ZrO_2 with a Ce/Zr ratio of 3/1 was selected for further investigations.

3.3. Resistance toward carbon formation

The resistance of Ni/Ce–ZrO_2 (with Ce/Zr ratio of 3/1) toward the formation of carbon species was investigated and compared to that of Ni/Al_2O_3. Carbon species were firstly formed on the catalyst surface by introducing 5% methane in helium (TPMA). The amount of carbon formation on the surface of each catalyst was then investigated by temperature-programmed oxidation (TPO). Figs. 4 and 5 present the comparison of TPMA and TPO respectively over both Ni/Ce–ZrO_2 and Ni/Al_2O_3.

According to Fig. 4, only hydrogen was produced from the cracking of methane on Ni/Al_2O_3, whereas carbon monoxide and carbon dioxide were also generated along with hydrogen from the cracking of methane on Ni/Ce–ZrO_2. The formations of CO and CO_2 are due to the gas-solid reaction of CH_4 on Ce–ZrO_2 surface (Eq. (5)). After the system was purged with helium, the amount of carbon formation on the surface of each catalyst can be determined by measuring the CO and CO_2 yield from TPO experiment (Fig. 5). Using a value of 0.026 nm^2 for the area occupied by a carbon atom in a surface monolayer of the basal plane in graphite [27], the quantities of carbon deposited on the surface of Ni/Ce–ZrO_2 were approximately 1.29 monolayers, whereas the quantities of carbon deposited over Ni/Al_2O_3 were 2.35 monolayers. Regarding the calculation of carbon balance, the values of carbon deposited from the calculation are also in good agreement with the values observed from the TPO (1.31 monolayers for Ni/Ce–ZrO_2, and 2.34 monolayers for Ni/Al_2O_3).

When a small amount of steam was added during TPMA, the amount of carbon formation was observed to decrease significantly as the steam reforming takes place. The requirements of inlet steam to eliminate all carbon formation on the surface of Ni/Ce–ZrO_2 and Ni/Al_2O_3 were compared, as presented in Table 3. Ni/Ce–ZrO_2 required inlet H_2O/CH_4 ratio of 1.0 in order to prevent the formation of carbon species on catalyst surface, whereas Ni/Al_2O_3 required a higher H_2O/

Table 2
Catalyst deactivations and some characterization results after running the reaction at 900 °C for 10 h

Catalyst	Ce/Zr ratio	Deactivation (%)	BET after reaction (m^2 g^{-1})	Surface area reduction (%)	Ni-load (wt.%)	Ni-dispersion (Ni%)
Ni/CeO_2		24	6.2	27	4.8	3.02
Ni/Ce–ZrO_2	1/3	11	18	10	4.9	4.21
Ni/Ce–ZrO_2	1/1	12	15	13	4.7	4.12
Ni/Ce–ZrO_2	3/1	5.1	18	4.5	4.8	4.32
Ni/Al_2O_3		16	40	~0	4.8	4.80

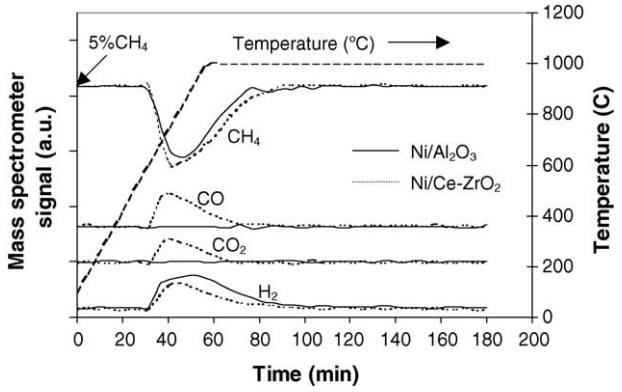

Fig. 4. Temperature-programmed methane adsorption (TPMA) of Ni/Ce–ZrO_2 (5 kPa CH_4).

CH_4 ratio to reduce the carbon formation. According to the table, the minimum requirement of inlet H_2O/CH_4 ratio to avoid the carbon formation for Ni/Al_2O_3 is 3.0.

3.4. Intrinsic reaction kinetic studies

3.4.1. Effects of temperature and methane

The inlet methane partial pressure was varied from 1 to 4 kPa, while the inlet steam was kept constant at 9 kPa. The operating temperature range was 650–850 °C. At steady state, the main products from this reaction were H_2 and CO with a small amount of CO_2, indicating a small contribution from the water–gas shift reaction, Eq. (2), and the reverse methanation (Eq. (3)). Fig. 6 showed the influences of temperature on the $CO/(CO + CO_2)$ production selectivity for both Ni/Ce–ZrO_2 and Ni/Al_2O_3. This selectivity increased with increasing operating temperature. At the same temperature, this selectivity for Ni/Al_2O_3 was observed to be higher than that over Ni/Ce–ZrO_2, which is due to the lower reactivity toward the water–gas shift reaction of Ni/Al_2O_3. The water–gas shift reaction (WGS) for each support was tested in order to ensure the influence of this reaction by using TPRx in CO/H_2O/He gas mixture (5 kPa CO, and 10 kPa H_2O). Fig. 7 shows the activities of

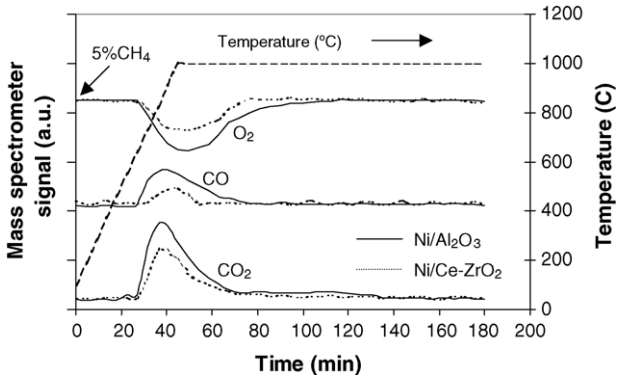

Fig. 5. Temperature-programmed oxidation (TPO) of Ni/Ce–ZrO_2 (10 kPa O_2).

Table 3
The dependence of inlet H_2O/CH_4 ratio on the amount of carbon formation remaining on the catalyst surface (calculated from CO and CO_2 yields during TPO)

H_2O/CH_4 ratio	Total carbon formation (monolayers)	
	Ni/Ce–ZrO_2	Ni/Al_2O_3
0	1.29[a] (1.31)[b]	2.35 (2.34)
0.2	0.47 (0.45)	2.26 (2.28)
0.4	0.39 (0.39)	1.97 (1.99)
0.6	0.21 (0.24)	1.66 (1.61)
0.8	0.11 (0.09)	1.33 (1.30)
1.0	~0 (0.005)	0.79 (0.81)
2.0	~0 (~0)	0.30 (0.27)
3.0	~0 (~0)	~0 (0.01)

[a] Calculated using CO and CO_2 yields from temperature-programmed oxidation (TPO) with 10% oxygen.
[b] Calculated from the balance of carbon in the system.

both supports toward this reaction. Clearly, the activity toward this reaction over Ce–ZrO_2 was significantly higher than that over Al_2O_3 at the same operating conditions.

Fig. 8 illustrates the influence of the inlet methane partial pressure on the turnover frequencies (N) for methane steam reforming over Ni/Ce–ZrO_2 at different operating temperatures. Turnover frequencies were calculated from the methane conversion following the given equation by assuming that all surface sites accessible by nitrogen adsorption (area per molecule 16.2×10^{-20} m^2 [40]) were active:

$$N = \frac{rN_A A_{N_2}}{m_c S} \tag{9}$$

Here r is the moles CH_4 per unit time, N_A the Avogadro's number, A_{N_2} the area occupied by an adsorbed nitrogen molecule (16.2×10^{-20} m^2), m_c the weight of catalyst used (50 mg), and S is the specific surface area of the catalyst (18 m^2 g^{-1}). The activities of each catalyst increased with increasing inlet methane partial pressure as well as operating temperature. Fig. 9 shows an Arrhenius-type plot for methane steam reforming over Ni/Ce–ZrO_2 with various

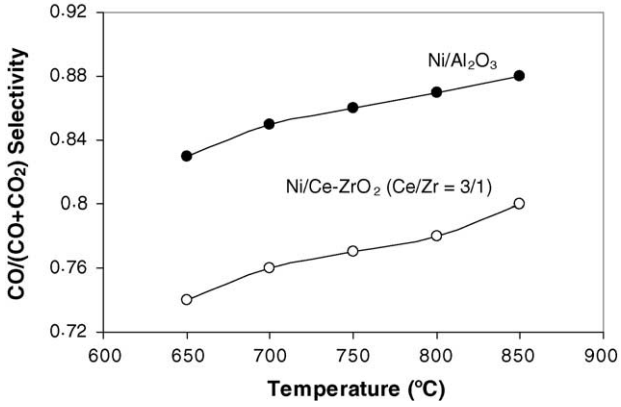

Fig. 6. Influence of temperature on $CO/(CO + CO_2)$ selectivity from methane steam reforming over Ni/Ce–ZrO_2 and Ni/Al_2O_3 (3 kPa CH_4, 9 kPa H_2O).

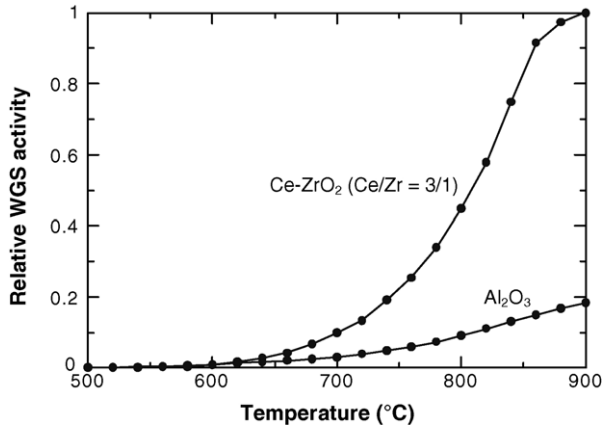

Fig. 7. The activities of Ce–ZrO_2 and Al_2O_3 toward the water-gas shift reaction using TPRx in CO/H_2O/He gas mixture (5 kPa CO, and 10 kPa H_2O).

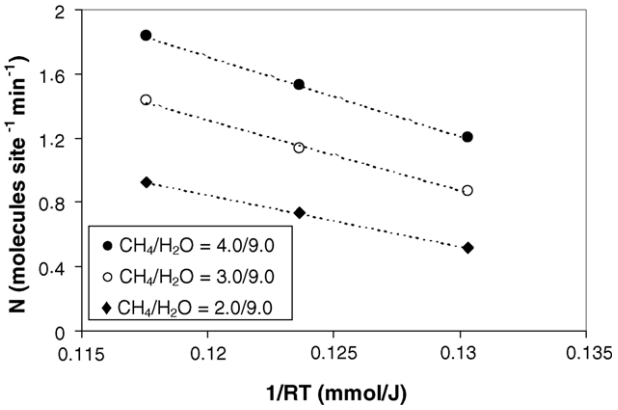

Fig. 9. Arrhenius plot of turnover frequencies (N) for methane steam reforming over Ni/Ce–ZrO_2 (Ce/Zr = 3/1) with different inlet methane/steam ratios.

methane/steam ratios over the temperature range of 650–750 °C. The corresponding activation energy observed for this catalyst is 142 ± 15 kJ mol^{-1}, slightly depending on the gas composition. The composition-dependence of activation energies from the Arrhenius plots has often been observed. The literature values, reviewed by Pointon [41] and Dicks et al. [39], were reported to be 35–287 and 154–253 kJ mol^{-1}, respectively.

The reaction orders in methane for both catalysts were observed to be 1.0 in all conditions. These values (n) were obtained experimentally by plotting $\ln(N)$ versus $\ln P_{CH_4}$ according to the equation below:

$$\ln(N) = \ln(k) + n(\ln P_{CH_4}) \quad (10)$$

The reaction order in methane seemed to be independent of the operating temperature in the range of conditions studied. By varying inlet steam partial pressure (9, 12, and 15 kPa) and adding hydrogen (1, 3, and 5 kPa), we found that the reaction order in methane was also independent of both components in this range of conditions.

3.4.2. Effect of hydrogen

Several inlet hydrogen concentrations (1–18 kPa) were added to the methane/steam in order to investigate the influence of this component on the steam reforming rate. Firstly, the inlet hydrogen partial pressure was varied from 0 to 5 kPa, while the inlet methane and steam partial pressure were kept constant at 3 and 9 kPa, respectively. In this range of conditions, hydrogen promoted the methane conversion as shown in Fig. 10. The reaction orders in hydrogen for Ni/Ce–ZrO_2 at this range of conditions studied were observed to be positive values between 0.18 and 0.20, while the reaction order in hydrogen for Ni/Al_2O_3 was in the range of 0.28–0.34. These values seemed to be independent of the inlet methane partial pressure and the operating temperature. However, they depended on the inlet steam partial pressure. The reaction order in hydrogen became slightly higher with increasing inlet steam partial pressure. This result is in good agreement with Dicks et al. [39] Fig. 11 showed the influences of hydrogen on the CO/(CO + CO_2) production selectivity. This selectivity increased with increasing inlet hydrogen partial pressure due to the promotion of the reverse water–gas shift reaction.

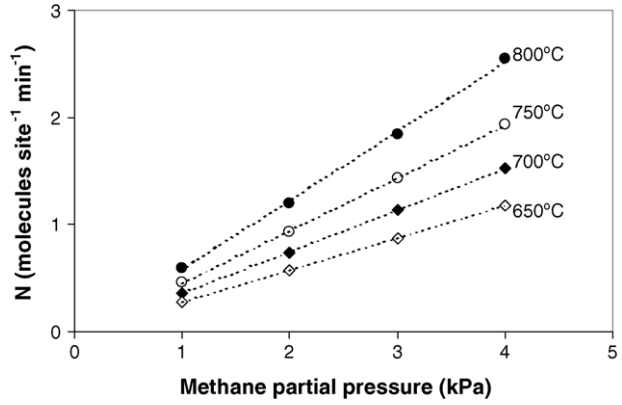

Fig. 8. Effect of methane partial pressure on the turnover frequencies (N) for steam reforming over Ni/Ce–ZrO_2 (Ce/Zr = 3/1) at different temperatures (9 kPa inlet H_2O).

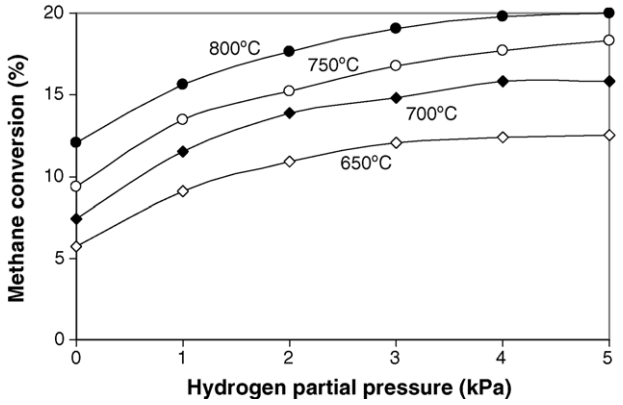

Fig. 10. Effect of hydrogen partial pressure on steam reforming rate over Ni/Ce–ZrO_2 (Ce/Zr = 3/1) at different temperatures (3 kPa CH_4, 9 kPa H_2O).

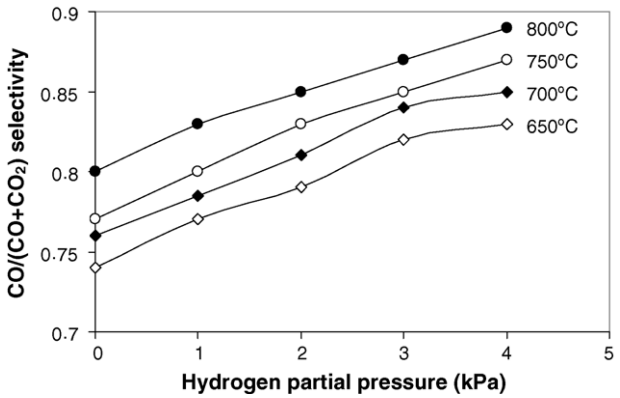

Fig. 11. Influence of hydrogen addition on CO/(CO + CO_2) selectivity from methane steam reforming over Ni/Ce–ZrO_2 at different temperatures (3 kPa CH_4, 9 kPa H_2O).

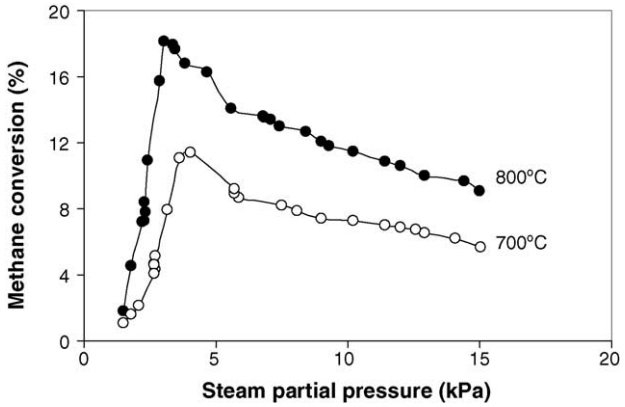

Fig. 13. Effect of steam partial pressure on steam reforming rate over Ni/Ce–ZrO_2 (Ce/Zr = 3/1) at 700 and 800 °C (3 kPa CH_4).

The steam reforming rates at higher inlet hydrogen partial pressures were then measured. The experiments yielded a non-linear positive hydrogen trend. When the inlet hydrogen partial pressure was greater than 8 kPa, the hydrogen influence on the steam reforming rate became much less pronounced. Moreover, the decrease in methane conversion was observed when the inlet hydrogen partial pressure was greater than 10 kPa (Fig. 12). Clearly, the negative effect of hydrogen for Ni/Ce–ZrO_2 was observed to be much stronger than that over Ni/Al_2O_3.

3.4.3. Effect of steam

In order to investigate the effect of inlet H_2O/CH_4 ratio on the steam reforming rate, this ratio was varied from 0.5 to 5.0 by changing the inlet steam partial pressure from 1.5 to 15 kPa. Two temperature levels of 700 and 800 °C were considered. As shown in Fig. 13, the dependence of steam on the rate of reforming is non-monotonic. The steam reforming rate increased with increasing inlet H_2O/CH_4 ratio until this ratio reached approximately 1.0–2.0. Then, steam presented a negative effect on the reforming rate at higher inlet H_2O/CH_4 ratio values. At the inlet H_2O partial pressure of 5–15 kPa, the reaction order related to steam decreased from −0.40 to −0.31 and −0.25 when the inlet hydrogen partial pressure increased from 0 to 1 and 2 kPa, respectively. This could be due to the decrease in the catalyst's oxidized state caused by a small addition of inlet hydrogen.

Unlike the effect of hydrogen, the reaction order in steam for the methane steam reforming over Ni/Al_2O_3 was close to that over Ni/Ce–ZrO_2 at the same operating conditions, indicating the same influence of steam on both Al_2O_3 and Ce–ZrO_2. This result was supported by the works of Laosiripojana [42], who reported the independence of inlet steam partial pressure on the methane steam reforming rate over ceria-based materials. Fig. 14 shows the influences of steam on the CO/(CO + CO_2) production selectivity. This selectivity decreased with increasing inlet steam partial pressure due to the promotion of the water–gas shift reaction in the forward direction. Table 4 presents the summary of observed reaction orders in each component (CH_4, H_2O, and H_2) for both Ni/Ce–ZrO_2 and Ni/Al_2O_3 at different temperatures and inlet compositions.

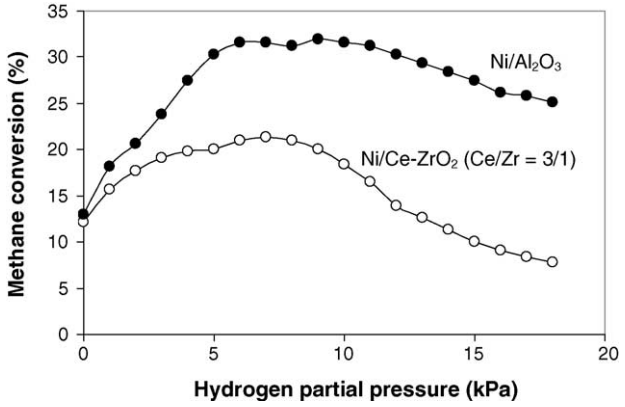

Fig. 12. Effect of hydrogen partial pressure on steam reforming rate over Ni/Ce–ZrO_2 (Ce/Zr = 3/1) and Ni/Al_2O_3 at high presence of hydrogen (0–18 kPa) at 800 °C.

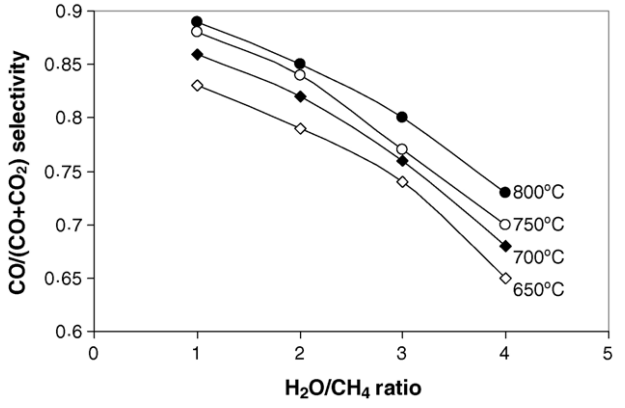

Fig. 14. Influence of inlet steam/methane ratio on CO/(CO + CO_2) selectivity from methane steam reforming over Ni/Ce–ZrO_2 at different temperatures (3 kPa CH_4).

Table 4
Reaction orders for the components of interest (CH_4, H_2O, and H_2) from methane steam reforming over Ni/Ce–ZrO_2 (Ce/Zr = 3/1) and Ni/Al_2O_3 at different operating conditions

Components of interest	Temperature (°C)	Other inlet compositions	Reaction order for components of interest	
			Ni/Ce–ZrO_2 (Ce/Zr = 3/1)	Ni/Al_2O_3
Methane (1–4 kPa)	650–800	9 kPaH_2O/0 kPaH_2	1.0 ± 0.04	1.0 ± 0.01
		12 kPa H_2O/0 kPa H_2	1.0 ± 0.05	1.0 ± 0.01
		15 kPaH_2O/0 kPa H_2	1.0 ± 0.02	1.0 ± 0.02
		9 kPaH_2O/1 kPa H_2	1.0 ± 0.02	1.0 ± 0.01
		9 kPa H_2O/3 kPa H_2	1.0 ± 0.01	1.0 ± 0.03
		9 kPaH_2O/5 kPa H_2	1.0 ± 0.03	1.0 ± 0.01
Hydrogen (1–4 kPa)	650	9 kPa H_2O/3 kPa CH_4	0.18	0.31
	700	9 kPa H_2O/3 kPa CH_4	0.20	0.28
	750	9 kPaH_2O/3 kPa CH_4	0.18	0.34
	800	9 kPa H_2O/3 kPa CH_4	0.19	0.33
	700	9 kPaH_2O/1 kPa CH_4	0.18	0.29
	700	9 kPa H_2O/5 kPa CH_4	0.20	0.32
	700	12 kPa H_2O/3 kPa CH_4	0.25	0.39
	700	15 kPa H_2O/3 kPa CH_4	0.28	0.42
Hydrogen (12–18 kPa)	650	9 kPaH_2 O/3 kPa CH_4	−0.31	−0.15
	700	9 kPa H_2O/3 kPa CH_4	−0.30	−0.16
	800	9 kPa H_2O/3 kPaCH_4	−0.34	−0.15
Steam (5–15 kPa)	650	0 kPa H_2/3 kPaCH_4	−0.39	−0.37
	700	0 kPa H_2/3 kPa CH_4	−0.40	−0.39
	750	0 kPa H_2/3 kPa CH_4	−0.38	−0.41
	800	0 kPaH_2/3 kPaCH_4	−0.42	−0.40
	700	1 kPa H_2/3 kPaCH_4	−0.31	−0.31
	700	2 kPaH_2/3 kPaCH_4	−0.25	−0.24
	700	3 kPa H_2/3 kPa CH_4	−0.22	−0.19

3.4.4. *Effect of oxygen*

As described earlier, autothermal reforming seems to be a promising reaction in order to produce hydrogen in the near future, as it is currently the most economical process. Methane steam reforming in the presence of oxygen or the autothermal reforming was then carried out by adding different oxygen partial pressures into the feed gas at several operating temperatures. The inlet methane and steam partial pressures were kept constant at 3 and 9 kPa, respectively, while the inlet oxygen partial pressure was varied from 0 to 4 kPa. At steady state, the methane steam reforming rate increased with increasing the inlet oxygen partial pressure as shown in Fig. 15. However, the CO/(CO + CO_2) production selectivity strongly decreased with increasing oxygen concentration due to the CO oxidation by O_2, as shown in Fig. 16. Hydrogen production also decreased with increasing oxygen concentration as shown in Fig. 17, which could be due to the inhibition of steam adsorption on the catalyst surface active sites by this component and also due to the combustion of H_2 production by inlet O_2.

4. Discussion

The steam reforming of methane over synthesized Ni/Ce–ZrO_2 was compared to conventional Ni/Al_2O_3 in the conditions where the influences of mass and heat transfer limitations could be considered negligible. Improvement of methane steam reforming performance in term of stability toward the deactivation by carbon deposition was achieved for Ni/Ce–ZrO_2. Compared to conventional Ni/Al_2O_3, Ni on Ce–ZrO_2 support provided higher resistance toward carbon formation and required significantly lower inlet H_2O/CH_4 ratio to prevent the formation of carbon species. These improvements are mainly related to the high redox property of Ce–ZrO_2 support.

Regarding the well known methane steam reforming mechanism over conventional Ni catalyst proposed by Dicks et al. [39], methane only adsorbs on the active surface site of Ni (*) and forms CH_x-*n. Simultaneously, the adsorption of

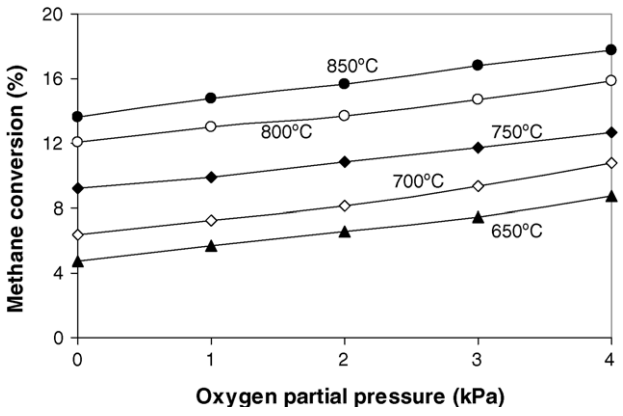

Fig. 15. Effect of oxygen partial pressure on steam reforming rate over Ni/Ce–ZrO_2 (Ce/Zr = 3/1) at different temperatures (3 kPa CH_4, 9 kPa H_2O).

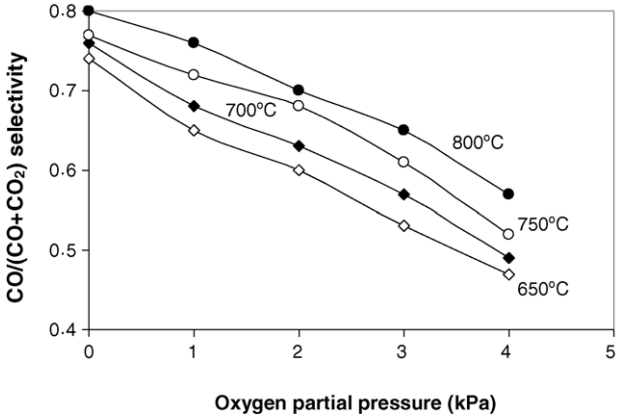

Fig. 16. Influence of oxygen addition on CO/(CO + CO_2) selectivity from methane steam reforming over Ni/Ce–ZrO_2 at different temperatures (3 kPa CH_4, 9 kPa H_2O).

inlet steam also takes place on the surface sites of Ni catalyst, forming O-*. These elements, O-* and CH_x-*n, eventually react with each other, producing CO and H_2, and the active surface site of Ni (*) also recovers as illustrated below:

$$CH_4 + n^* \rightarrow CH_x\text{-}*n + (4-x)/2H_2 \quad (11)$$

$$H_2O + * \Leftrightarrow O\text{-}* + H_2 \quad (12)$$

$$CH_x\text{-}*n + O\text{-}* \rightarrow CO + (x/2)H_2 + (n+1)^* \quad (13)$$

For the steam reforming of methane over Ni/Ce–ZrO_2, in addition to the reactions on Ni surface, the redox reaction between inlet CH_4 and the lattice oxygen (O_x) on Ce–ZrO_2 surface also takes place, producing H_2 and CO (Eq. (5)). Moreover, the reduced Ce–ZrO_2 can react with inlet H_2O to produce more H_2 and to recover O_x [42]. The proposed mechanism for these redox reactions, involving the reactions between methane and/or an intermediate surface hydrocarbon species with the lattice oxygen (O_x) on Ce–ZrO_2 surface and the recovery of O_x by steam, is presented

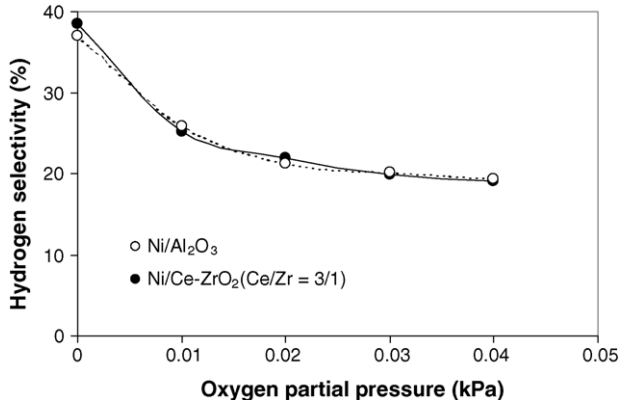

Fig. 17. Effect of oxygen on hydrogen selectivity (%) from methane steam reforming over Ni/Ce–ZrO_2 at 800 °C (3 kPa CH_4, 9 kPa H_2O).

schematically below:

$$CH_4 + 2S \Leftrightarrow CH_3\text{–}S + H\text{–}S \quad (14)$$

$$CH_3\text{–}S + S \Leftrightarrow CH_2\text{–}S + H\text{–}S \quad (15)$$

$$CH_2\text{–}S + S \Leftrightarrow CH\text{–}S + H\text{–}S \quad (16)$$

$$CH\text{–}S + S \Leftrightarrow C\text{–}S + H\text{–}S \quad (17)$$

$$C\text{–}S + O_x \Leftrightarrow CO + O_{x-1} + S \quad (18)$$

$$CO + O_x \Leftrightarrow CO_2 + O_{x-1} \quad (19)$$

$$2H\text{–}S \Leftrightarrow H_2 + 2S \quad (20)$$

$$H_2O + O_{x-1} \Leftrightarrow O_x + H_2 \quad (21)$$

The surface site (S) can be either a unique site, or it can also be considered to be the same site as the catalyst-oxidised site (O_x) [42]. It has been reported [43] that the controlling step of these redox reactions is the reaction of methane on the Ce–ZrO_2 surface; in addition, the lattice oxygen is replenished by a significant rapid surface reaction of the reduced state Ce–ZrO_2 with H_2O.

According to the possible formation of carbon species on the surface of catalyst during the steam reforming process, the following reactions are theoretically the most probable reactions that could lead to carbon formation:

$$2CO = CO_2 + C \quad (22)$$

$$CH_4 = 2H_2 + C \quad (23)$$

$$CO + H_2 = H_2O + C \quad (24)$$

$$CO_2 + 2H_2 = 2H_2O + C \quad (25)$$

C is the carbonaceous deposits. Reactions (24) and (25) are favorable at low temperature, while reaction (22) is thermodynamically unfavored [44]. At such a high temperature, the Boudard reaction (Eq. (22)) and the decomposition of methane (Eq. (23)) are the major pathways for carbon formation, as they show the largest change in Gibbs energy [45]. According to the range of temperature in this study, carbon formation would be formed via the decomposition of methane and Boudard reactions, especially at low inlet H_2O/CH_4 ratio. In the present work, we also observed a high amount of carbon formation on the surface of Ni/Al_2O_3 after exposure in methane steam reforming condition with the inlet H_2O/CH_4 ratio less than 3.0. By applying Ce–ZrO_2 as support, the formation of carbon species via Eqs. (22) and (23) could be inhibited by the redox reactions of methane and carbon monoxide (produced during the steam reforming process) with the lattice oxygen (O_x) at Ce–ZrO_2 surface (Eqs. (14)–(19)) forming hydrogen and carbon dioxide, which is thermodynamically unfavored to form carbon species in this range of conditions. Therefore, significant lower amounts of carbon deposition were consequently observed for Ni/Ce–ZrO_2 even at low inlet H_2O/CH_4 ratios. In addition, the reaction between the lattice oxygen (O_x) at

Ce–ZrO_2 surface with the adsorbed methane on Ni surface (CH_x-*n) and the rapid recovery of the lattice oxygen by the simultaneous supply of oxygen from H_2O also result in the higher resistance toward carbon formation and less inlet H_2O/CH_4 requirement for Ni/Ce–ZrO_2:

$$CH_x\text{-}*n + O_x \rightarrow CO + (x/2)H_2 + n^* + O_{x-1} \quad (26)$$

Many previous researchers have reported the excellent resistance toward carbon formation from methane cracking at high temperature for ceria-based materials including CeO_2 [27], Gd-doped CeO_2 [27], Nb-CeO_2 [46], and CeO_2-ZrO_2 [42]. One of them [42] also proposed that the addition of a small amount of H_2O to the inlet feed can eliminate all carbon species on the surface of CeO_2. The previous reports therefore agree well with the results in this work.

Regarding the kinetic studies over Ni/Ce–ZrO_2 in the present work, similar to the general metal catalysts as reported by previous researchers, the reaction orders in methane were observed to be approximately 1.0 in all conditions. The experiments yielded a non-linear positive hydrogen trend over this catalyst (Fig. 12). The positive effect at the low hydrogen appearance could be due to the reduction of oxidized state on the surface active site of nickel ($H_2 + O\text{-}* \Leftrightarrow H_2O + *$), while the inhibitory effect at high hydrogen partial pressure could be due to the promotion of the methanation, the reverse water–gas shift reactions and the reverse methane steam reforming [4-6]. In addition, the occupying of hydrogen atoms on some active sites of nickel particles ($H_2 + 2^* \Leftrightarrow 2H\text{-}*$) could also lead to the decrease in methane conversion, as explained by Xu and Froment [4–6].

Clearly, the negative effect of hydrogen for Ni/Ce–ZrO_2 was observed to be much stronger than that over Ni/Al_2O_3. This is due to the reduction of lattice oxygen (O_x) by hydrogen via the reverse of Eq. (21) ($O_x + H_2 \Leftrightarrow H_2O + O_{x-1}$) and consequently inhibits the reaction of the lattice oxygen (O_x) with the surface hydrocarbon species (both C–S and CH_x-n) in Eqs. (18) and (26) (C–S + $O_x \Leftrightarrow$ CO + O_{x-1} + S and CH_x-*n + $O_x \rightarrow$ CO + (x/2)H_2 + n^* + O_{x-1}). This explanation is in good agreement with the previous studies [42,43,46] which studied kinetics parameters for the methane steam reforming on ceria-based materials and reported the negative effect of hydrogen on methane conversion over these materials due to the change of Ce^{4+} to Ce^{3+}.

The dependence of steam on the rate of reforming is non-monotonic due to adsorption competition between CH_4 and H_2O on the catalyst active sites. Previous works [4,5] also reported the same results and explanation on Ni/ZrO_2. Furthermore, the study of autothermal reforming over this catalyst found that methane steam reforming rate increased with increasing the inlet oxygen partial pressure. However, the CO/(CO + CO_2) production selectivity and hydrogen production rates strongly decreased with increasing oxygen partial pressure. This is due to the inhibition of steam adsorption on the catalyst surface active sites and the oxidation of hydrogen by oxygen in the feed.

5. Conclusion

Methane steam reforming over Ni catalyst supported on Ce–ZrO_2 was studied at 650–900 °C in the conditions where the influence of mass transfer limitations could be considered negligible. At 900 °C, Ni/Ce–ZrO_2 with Ce/Zr ratio of 3/1 showed the best performance in term of activity and stability. The resistance toward carbon formation over this catalyst was higher than that over conventional Ni/Al_2O_3 at the same operating conditions regarding its high redox property; however, slight deactivation due to the sintering was observed over Ni/Ce–ZrO_2 at these high temperature conditions.

Similar to the conventional Ni/Al_2O_3, the reaction order in methane for Ni/Ce–ZrO_2 was always observed to be 1.0. The dependence of steam on the rate was non-monotonic, and the addition of oxygen promoted the rate but reduced CO and H_2 production selectivity. At high hydrogen appearance, Ni/Ce–ZrO_2 showed a stronger negative impact of hydrogen compared to Ni/Al_2O_3, due to the possible reduction of Ce–ZrO_2. This strong negative effect of hydrogen would be a major concern in applying Ni/Ce–ZrO_2 industrially. Although Ni/Ce–ZrO_2 is a good reforming catalyst in term of the high resistance toward the carbon formation, methane conversion could be significantly reduced at high hydrogen appearance, and the removal of hydrogen during the reforming process might be required.

Acknowledgements

The financial support from The Thailand Research Fund (TRF) throughout this project is gratefully acknowledged. The first author would like to acknowledge Professor David Chadwick from the Department of Chemical Engineering and Chemical Technology, Imperial College London, for his valuable suggestions.

References

[1] K. Otsuka, T. Ushiyama, I. Yamanaka, Chem. Lett. (1993) 1517.
[2] K. Otsuka, M. Hatano, A. Morikawa, J. Catal. 79 (1983) 493.
[3] K. Otsuka, M. Hatano, A. Morikawa, Inorg. Chim. Acta 109 (1985) 193.
[4] J. Xu, PhD Thesis, Laboratorium Voor Petrochemische Techniek, Rijkuniversiteit, Gent, Belgium, 1986.
[5] J. Xu, G.F. Froment, AIChE 35 (1989) 88.
[6] J. Xu, G.F. Froment, AIChE 35 (1989) 97.
[7] S.S.E.H. Elnashaie, A.M. Adris, A.S. Al-Ubaid, M.A. Soliman, Chem. Eng. Sci. 45 (1990) 491.
[8] S.S.E.H. Elnashaie, S.S. Elshishini, Modeling, Simulation and Optimization of Industrial Fixed Bed Catalytic Reactors, Gordon and Breach Science Publishers, UK, 1993.
[9] L.V. Mattos, E. Rodino, D.E. Resasco, F.B. Possos, F.B. Noronha, Fuel Proc. Technol. 83 (2003) 147.
[10] H.S. Roh, K.W. Jun, S.E. Park, Appl. Catal. A 251 (2003) 275.
[11] J.R. Rostrup-Nielsen, J.-H. Bak-Hansen, J. Catal. 144 (1993) 38.
[12] X. Wang, R.J. Gorte, Appl. Catal. A 224 (2002) 209.

[13] H.S. Roh, K.W. Jun, W.S. Dong, J.S. Chang, S.E. Park, Y.I. Joe, J. Mol. Catal. A 181 (2002) 137.
[14] Q. Miao, G. Xiong, S. Sheng, W. Cui, L. Xu, X. Guo, Appl. Catal. A 154 (1987) 17.
[15] A.A. Lemonidou, M.A. Goula, I.A. Vasalos, Catal. Today 46 (1987) 175.
[16] W.S. Dong, H.S. Roh, K.W. Jun, S.E. Park, Y.S. Oh, Appl. Catal. A 226 (2002) 63.
[17] M. Mamak, N. Coombs, G. Ozin, Adv. Mater. 12 (2000) 198.
[18] M. Mamak, N. Coombs, G. Ozin, J. Am. Chem. Soc. 122 (2000) 8932.
[19] M. Mamak, N. Coombs, G.A. Ozin, Chem. Mater. 13 (2001) 3564.
[20] P. Bera, S. Mitra, S. Sampath, M.S. Hegde, Chem. Commun. (2001) 927.
[21] A. Martinez-Arias, J.M. Coronado, R. Cataluna, J.C. Conesa, J.C. Soria, J. Phys. Chem. B 102 (1998) 4357.
[22] D. Skarmoutsos, F. Tietz, P. Nikolopoulos, Fuel Cells 1 (2001) 243.
[23] T. Takeguchi, S.N. Furukawa, M. Inoue, J. Catal. 202 (2001) 14.
[24] J. Sfeir, P.A. Philippe, P. Moseki, N. Xanthopoulos, R. Vasquez, J.M. Hans, V.H. Jan, K.R. Thampi, J. Catal. 202 (2001) 229.
[25] N. Kiratzis, P. Holtappels, C.E. Hatchwell, M. Mogensen, J.T.S. Irvine, Fuel Cells 1 (2001) 211.
[26] H.S. Roh, W.S. Dong, K.W. Jun, S.E. Park, Chem. Lett. 88 (2001).
[27] E. Ramirez, A. Atkinson, D. Chadwick, Appl. Catal. B 36 (2002) 193.
[28] M. Ozawa, M. Kimura, A. Isogai, J. Alloys Compd. 193 (1993) 73.
[29] G. Balducci, J. Kaspar, P. Fornasiero, M. Graziani, M.S. Islam, J. Phys. Chem. B 102 (1998) 557.
[30] G. Vlaic, P. Fornasiero, S. Geremia, J. Kaspar, M. Graziani, J. Catal. 168 (1997) 386.
[31] G.R. Rao, J. Kaspar, S. Meriani, R. Dimonte, M. Graziani, Catal. Lett. 24 (1994) 107.
[32] P. Fornasiero, R. Dimonte, G.R. Rao, J. Kaspar, S. Meriani, A. Trovarelli, M. Graziani, J. Catal. 151 (1995) 168.
[33] M. Haneda, K. Miki, N. Kakuta, A. Ueno, S. Tani, S. Matsura, M. Sato, Nihon Kagaku Kaishi (1990) 820.
[34] T. Ohata, Rare Earths 17 (1990) 37.
[35] J.G. Nunan, W.B. Williamson, H.J. Robota, SAE Paper 960768, 1996.
[36] S. Otsuka-Yao, H. Morikawa, N. Izu, K. Okuda, J. Jpn. Inst. Met. 59 (1995) 1237.
[37] M.H. Yao, T.E. Hoost, R.J. Baird, F.W. Kunz, J. Catal. 166 (1997) 67.
[38] D. Kim, J. Am. Ceram. Soc. 72 (1989) 1415.
[39] A.L. Dicks, K.D. Pointon, A. Siddle, J. Power Sources 86 (2000) 523.
[40] P.A. Webb, C. Orr, Analytical Methods in Fine Particle Technology, Micromeritics Instrument Corporation, USA, 1997.
[41] K.D. Pointon, Review of Work on Internal Reforming in the Solid Oxide Fuel Cell, ETSU Report F/01/00121/REP, 1997.
[42] N. Laosiripojana, Reaction engineering of indirect internal steam reforming of methane for application in solid oxide fuel cells, PhD Thesis, University of London, UK, 2003.
[43] E. Ramírez-Cabrera, A. Atkinson, D. Chadwick, Appl. Catal. B 47 (2004) 127.
[44] Y. Lwin, W.R.W. Daud, A.B. Mohamad, Z. Yaakob, Int. J. Hydrogen Energy 25 (1) (2000) 47.
[45] J.N. Amor, Appl. Catal. A 176 (1999) 159.
[46] E. Ramírez-Cabrera, N. Laosiripojana, A. Atkinson, D. Chadwick, Catal. Today 78 (2003) 433.

N. Laosiripojana, W. Sutthisripok and S. Assabumrungrat

"Synthesis gas production from dry reforming of methane over CeO_2 doped Ni/Al_2O_3: Influence of the doping ceria on the resistance toward carbon formation"

Chemical Engineering Journal, 112 (2005) 13-22

(IF-2004 = 1.38)

ELSEVIER

Chemical Engineering Journal 112 (2005) 13–22

Chemical Engineering Journal

www.elsevier.com/locate/cej

Synthesis gas production from dry reforming of methane over CeO_2 doped Ni/Al_2O_3: Influence of the doping ceria on the resistance toward carbon formation

N. Laosiripojana [a,*], W. Sutthisripok [b], S. Assabumrungrat [c]

[a] *The Joint Graduate School of Energy and Environment, King Mongkut's University of Technology Thonburi, Bangkok 10140, Thailand*
[b] *Department of Mining and Materials Engineering, Faculty of Engineering, Prince of Songkla University, Songkhla, Thailand*
[c] *Center of Excellence on Catalysis and Catalytic Reaction Engineering, Department of Chemical Engineering, Faculty of Engineering, Chulalongkorn University, Bangkok 10330, Thailand*

Received 17 January 2005; received in revised form 4 June 2005; accepted 9 June 2005

Abstract

Doping of CeO_2 as an additive promoter on Ni/Al_2O_3 was found to improve dry reforming activity for H_2 and CO productions at solid oxide fuel cell (SOFC) operating temperature (800–900 °C). The catalyst provides significantly higher reforming reactivity and resistance toward carbon deposition compared to conventional Ni/Al_2O_3. These enhancements are mainly due to the influence of the redox property of ceria. During dry reforming process, in addition to the reactions on Ni surface, the gas–solid reactions between the gaseous components presented in the system (CH_4, CO_2, CO, H_2O, and H_2) and the lattice oxygen (O_x) on ceria surface also take place. The reactions of adsorbed methane and carbon monoxide (produced during dry reforming process) with the lattice oxygen (O_x) on ceria surface ($CH_4 + O_x \rightarrow CO + H_2 + O_{x-1}$ and $CO + O_x \Leftrightarrow CO_2 + O_{x-1}$) can prevent the formation of carbon species on Ni surface from methane decomposition reaction and Boudard reaction.

In particular, CeO_2 doped Ni/Al_2O_3 with 8% ceria content showed the best reforming activity among those with the ceria content between 0 and 14%. The amount of carbon formation decreased with increasing Ce content. However, Ni was oxidized when more than 10% of ceria was doped. According to the post-XPS measurement, a small formation of Ce_2O_3 was observed after exposure in dry methane reforming conditions with low inlet CH_4/CO_2 ratio (1.0/0.3). The intrinsic reaction kinetics of 8% CeO_2 doped Ni/Al_2O_3 was studied by varying inlet CH_4 and CO_2 concentrations, and by adding H_2 and CO to the system at different temperatures. The dry reforming rate increased with increasing methane partial pressure and the operating temperature. The reaction orders in methane were always closed to 1.0 in all conditions. Carbon dioxide also presented weak positive impact on the methane conversion, whereas adding of carbon monoxide and hydrogen inhibited the reforming rate.

Keywords: Hydrogen; Synthesis gas; Carbon formation; Dry reforming; CeO_2

1. Introduction

Solid oxide fuel cell (SOFC) with an indirect internal reforming operation (IIR), called IIR-SOFC, is expected to be an important technology for energy generation in the near future due to the high efficiency and its low environmental impact. Regarding this operation, the endothermic reforming reaction takes place at the reformer, which is in close thermal contact with the anode side of fuel cell where the exothermic electrochemical reaction takes place (Fig. 1). IIR gives the advantage on eliminating the requirement for a separate fuel reformer and providing good heat transfer between the reformer and the fuel cell. In addition, the reformer part and the anode side for IIR operation can be operated separately. Therefore, the catalyst for reforming reaction at the reformer part and the material for electrochemical reactions at the anode side of fuel cell can be different

* Corresponding author.
E-mail address: navadol_l@jgsee.kmutt.ac.th (N. Laosiripojana).

1385-8947/$ – see front matter © 2005 Elsevier B.V. All rights reserved.
doi:10.1016/j.cej.2005.06.003

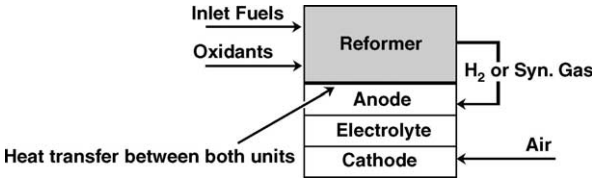

Fig. 1. Diagram of IIR-SOFC operation.

and optimized individually. This operation is expected to simplify the overall system design, making SOFC more attractive and efficient for producing electrical power [1].

The aim of the reformer unit is to reform and maximize the yield of hydrogen production and supply this component to the anode side of SOFC. Theoretically, hydrogen can be produced from several natural hydrocarbon sources including natural gas, bio-ethanol, coal, biomass, and biogas. Biogas consists mainly of methane and carbon dioxide is expected to be the attractive raw material for hydrogen production in the near future due to its economic availability. Due to the rich CO_2 for biogas, carbon dioxide (or dry) reforming reaction would be one of the most suitable processes to convert biogas to hydrogen or synthesis gas (CO and H_2). Compared to the steam reforming, both steam and dry reforming reactions have similar thermodynamic characteristics except that the carbon formation in the dry reforming is more severe than in the steam reforming due to the lower H/C ratio of this reaction [2]. The attractive feature of the dry reforming reaction is the utilisation of CO_2, which is a greenhouse effect gas. In general, the dry reforming reaction (Eq. (1)) is typically accompanied by the simultaneous occurrence of the reverse water-gas shift reaction (RWGS) (Eq. (2)).

$$CH_4 + CO_2 \Leftrightarrow 2CO + 2H_2 \qquad \Delta H = 247\,\text{kJ/mol} \qquad (1)$$

$$CO_2 + H_2 \Leftrightarrow CO + H_2O \qquad \Delta H = 41.1\,\text{kJ/mol} \qquad (2)$$

The hydrogen to carbon monoxide production ratio (H_2/CO ratio) from the dry reforming reaction is always less than 1. Vannice and Bradford [3] presented the apparent activation energies for the consumption of methane and carbon dioxide, as well as the production of carbon monoxide, hydrogen, and water in order to investigate the influence of the RWGS reaction. They observed that the apparent activation energy for hydrogen formation is greater than that for the formation of carbon monoxide, in which supported the influence of the reverse water-gas shift reaction on the reaction mechanism. Sodesawa et al. [4] studied the dry reforming reaction at a stoichiometric feed ratio over several catalysts. They found that the activities of most catalysts deactivated rapidly due to the carbon deposition. Topor et al. [5] suggested that the use of excess carbon dioxide could avoid carbon formation. Chubb et al. [6,7] studied the carbon dioxide reforming using an excess of carbon dioxide with carbon dioxide to methane ratios of 3:1 and 5:1 over Ni/Al_2O_3. They reported that the rate of disintegration is smaller for the higher one. Rostrup-Nielsen and Bak Hansen [8] investigated the activity toward dry reforming over several metals. Their order of reactivity for this reaction was Ru > Rh > Ni ∼ Ir > Pt > Pd, in which similar to their proposed order for steam reforming. They also observed that the replacing of steam with carbon dioxide gave similar activation energies, which indicated a similar rate-determining step in these two reactions. In addition, low levels or no carbon formation was detected from dry reforming over Rh metal at low temperature and CO_2 content [9]. Erdöhelyi et al. [10,11] studied the influence of the catalyst support on the dry reforming of rhodium-based catalyst, and reported that the support had no effect on the activity of Rh. In contrast, Nakamura et al. [12] and Zhang et al. [13] observed that the initial turnover frequency (specific activity) of Rh crystallities was significantly affected by their supports. Zhang et al. [13] also reported that the deactivation of Rh crystallities was strongly dependent on their supports.

In this present study, it is aimed at the development of an alternative catalyst for dry methane reforming reaction, which provided high stability, and activity toward this reaction at such a high temperature (800–900 °C) for later application in IIR-SOFC. According to the economical point of view, Ni/Al_2O_3 was selected as a based catalyst rather than the precious metals. Cerium oxide (CeO_2) was chosen as an additive promoter. This material (called ceria) is an important material for a variety of catalytic reactions involving oxidation of hydrocarbons (e.g. automobile exhaust catalysts). It contains a high concentration of highly mobile oxygen vacancies, which act as local sources or sinks for oxygen involved in reactions taking place on its surface. Nowadays, a potential application of ceria is in solid oxide fuel cells application as a reforming catalyst for in-stack (called indirect internal) reforming of methane, since it is high resistant toward carbon deposition compared to Ni [14]. Recently, the successful test of ceria for the methane steam reforming reaction has been reported [15–17]. Due to the high resistance toward carbon formation, ceria should be a good additive promoter for dry reforming process.

Recently, the use of ceria-based materials as the support and promoter for the catalytic reforming reaction has been reported by several researchers. As the support, it has been reported to be promising support among α-Al_2O_3 [18], γ-Al_2O_3, and γ-Al_2O_3 with alkali metal oxide and rare earth metal oxide [19] and $CaAl_2O_4$ [18–21], while the selected metals were Ni, Pt, or Pd [22–31]. As the promoter, ceria was also reported to be a good promoter for the dry methane reforming at intermediate temperature [32]. Wang and Lu [32] prepared CeO_2 doped Ni/Al_2O_3 by adding CeO_2 on γ-Al_2O_3 powder before impregnated Ni on CeO_2–Al_2O_3 support and tested the dry methane reforming reactivity at 500–800 °C. They found that the doping of CeO_2 significantly improved the resistance of catalyst toward the carbon deposition.

In this work, various amounts of cerium oxide were firstly doped on the surface of Ni/Al_2O_3 in order to determine the suitable doping ratio. The reactivity toward dry reforming and the resistance toward carbon formation over CeO_2 doped Ni/Al_2O_3 was studied and compared to conventional

Ni/Al_2O_3 at the temperature range of 800–900 °C. In addition, the intrinsic kinetics of the dry methane reforming reaction over this catalyst was also studied by varying inlet CH_4, CO_2, and by adding CO and H_2 at different temperatures. The reaction orders in each component and the possible rate isotherm with the fitting parameters were determined. These kinetic informations are important in order to determine the behavior of the catalyst toward this reaction for the large scale or industrial application. By fitting the rate isotherm and parameters in the modeling, the behavior of the whole reformer and the IIR-SOFC system can be predicted.

2. Experimental

2.1. Catalyst preparations

Ni/Al_2O_3 (5 wt.% Ni) was prepared by impregnating α-Al_2O_3 (from Aldrich) with $NiCl_3$ solution at room temperature. This solution was stirred by magnetic stirring (100 rpm) for 6 h, dried overnight in an oven at 110 °C, and calcined in air at 900 °C for 6 h. The catalyst powder was then reduced with 10% H_2/Ar at 700 °C for 6 h. CeO_2 doped Ni/Al_2O_3 was prepared by impregnate different concentration of cerium nitrate ($Ce(NO_3)_3{\cdot}6H_2O$ (99.0%), Fluka) on Ni/Al_2O_3 powder. Similarly, this solution was stirred by magnetic stirring (100 rpm) for 6 h before filtered and washed with deionised water and ethanol to prevent an agglomeration. The sample was dried and calcined in air at 1000 °C for 6 h. It was reduced with 10% H_2/Ar at 700 °C for 6 h before use.

2.2. Apparatus and procedures

In order to investigate the dry reforming and its associated reactions, an experimental reactor system was constructed. The feed gases including the components of interest such as CH_4, CO_2, H_2, or CO were introduced to the reaction section, in which an 8-mm internal diameter and 40-cm length quartz reactor was mounted vertically inside a furnace. The catalyst (50 mg) was loaded in the quartz reactor, which was packed with a small amount of quartz wool to prevent the catalyst from moving. In order to observe the intrinsic reaction kinetics, the methane conversions from dry reforming were always kept below 20% in all experiments.

In the present work, the desired space velocity and suitable catalyst particle size were achieved from several preliminary tests, which were carried out to avoid any limitations by intraparticle diffusion in the experiments. Regarding to these testing, the total flow rate was varied between 20 and 200 $cm^3\ min^{-1}$ under a constant residence time of 5×10^{-4} g min cm^{-3}. When the total flow rate was below 60 $cm^3\ min^{-1}$, the reforming rate increased with increasing the gas flow rate, suggesting that the mass transfer between the bulk gas and the catalyst particles is the rate-determining step. The reforming rate was almost constant in the range where the gas flow rate was higher than 80 $cm^3\ min^{-1}$, indicating that the mass transfer effect is unimportant in this flow rate range. Fig. 2 shows the effect of the total gas flow rate on the reforming rate over 8% CeO_2 doped Ni/Al_2O_3 at different temperatures. The reactions on different average sizes (from 100 to 500 μm) of catalysts were also carried out. It was observed that there were no significant changes in the methane conversion for the catalyst with the particle size between 100 and 200 μm, which indicated that the intraparticle diffusion limitation was negligible in this range of operating conditions. Consequently, the weight of catalyst loading was 50 mg, while the total gas flow was kept constant at 100 $cm^3\ min^{-1}$. The catalyst particle size diameter was between 100 and 200 μm in all experiments.

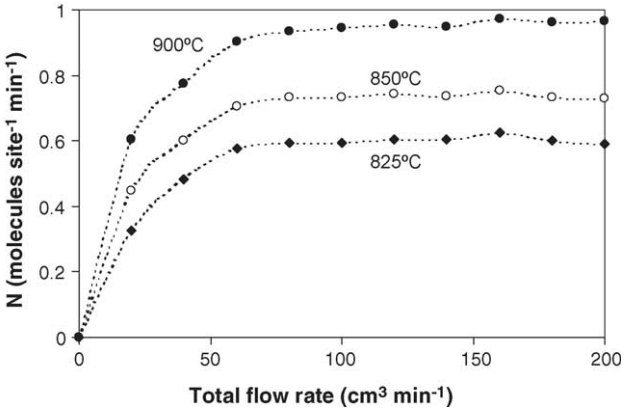

Fig. 2. Effect of the total gas flow rate on the turnover frequencies (*N*) for dry reforming over 8% CeO_2 doped Ni/Al_2O_3 at different temperatures (4 kPa CH_4 and 12 kPa CO_2).

A type-K thermocouple was placed into the annular space between the reactor and the furnace. This thermocouple was mounted on the tubular reactor in close contact with the catalyst bed to minimize the temperature difference between the catalyst bed and the thermocouple. Another type-K thermocouple was inserted in the middle of the quartz tube in order to re-check the possible temperature gradient. The record showed that the maximum temperature fluctuation during the reaction was always ±0.75 °C or less from the temperature specified for the reaction.

After the reactions, the exit gas mixture was transferred via trace-heated lines to the analysis section, which consists of a Porapak Q column Shimadzu 14B gas chromatograph (GC) and a mass spectrometer (MS). The gas chromatography was applied in order to investigate the steady state condition experiments, whereas the mass spectrometer in which the sampling of the exit gas was done by a quartz capillary and differential pumping was used for the transient and carbon formation experiments. In order to study the formation of carbon species on catalyst surface, temperature-programmed oxidation (TPO) was applied by introducing 10% oxygen in helium into the system, after purged with helium. The operating temperature increased from room temperature to 1000 °C by the rate of 10 °C/min. The calibrations of CO and CO_2 productions were performed by injecting a known amount of

these calibration gases from a loop, in an injection valve in the bypass line. The response factors were obtained by dividing the number of moles for each component over the respective areas under peaks. In addition to the TPO method, the amount of carbon deposition was confirmed by the calculation of carbon balance in the system. The amount of carbon deposited on the surface of catalyst would theoretically be equal to the difference between the inlet carbon containing components (CH_4 and CO_2) and the outlet carbon containing components (CO, CO_2, and CH_4). The amount of carbon deposited per gram of catalyst is given by the following equation:

$$C_{\text{deposition}} = \frac{\text{mole}_{\text{carbon (in)}} - \text{mole}_{\text{carbon (out)}}}{m_{\text{catalyst}}} \quad (3)$$

3. Results and discussion

3.1. Catalyst characterizations

After reduction, the catalysts were characterized with several physicochemical methods. The weights content of Ni and Ce loadings were determined by X-ray fluorescence (XRF) analysis. The reducibility and dispersion percentages of nickel were measured from temperature-programmed reduction (TPR) with 5% H_2 in Ar and temperature-programmed desorption (TPD), respectively. The catalyst specific surface areas were obtained from BET measurement. All physicochemical properties of the synthesized catalysts are presented in Table 1. The catalyst specific surface areas slightly increased by the doping of Ce.

3.2. Selection of suitable Ce doping content

After reduction, various Ce contents (from 2 to 14%) doped on Ni/Al_2O_3 were studied in dry reforming at 900 °C. The feed was CH_4/CO_2 in helium with the CH_4/CO_2 ratio of 1.0/0.3. Fig. 3 presents the steady state turnover frequencies (N) for CeO_2 doped Ni/Al_2O_3 with different CeO_2 contents. The turnover frequencies were calculated from the methane conversion following the below equation by assuming that all surface sites accessible by nitrogen adsorption (area per molecule 16.2×10^{-20} m^2 [14]) were active.

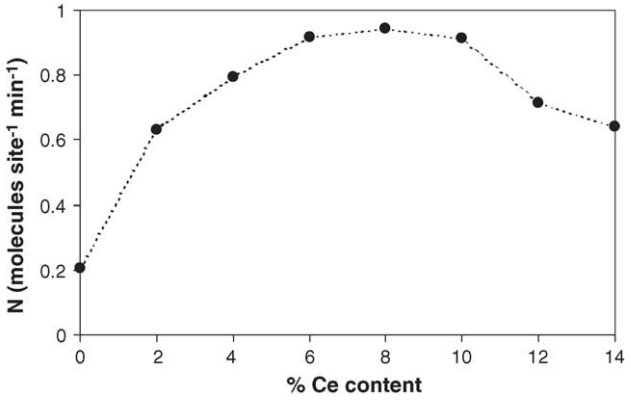

Fig. 3. Effect of Ce doping content on the turnover frequencies (N) for dry reforming (900 °C, 4 kPa CH_4, and 12 kPa CO_2).

$$N = \frac{rN_A A_{N_2}}{m_c S} \quad (4)$$

where r is the reaction rate (moles CH_4 per unit time), N_A the Avagadro's number, A_{N_2} the area occupied by an adsorbed nitrogen molecule (16.2×10^{-20} m^2), m_c the weight of catalyst used (50 mg), and S is the specific surface area of the catalyst. The figure indicates that 8% CeO_2 doping on Ni/Al_2O_3 presents the highest turnover frequencies.

The post-reaction temperature-programmed oxidation experiments were then carried out after a helium purge by introducing of 10% oxygen in helium in order to determine the degree of carbon deposition on the surface of each sample. Table 2 presents the important physicochemical properties of the spent catalysts after exposure in dry reforming conditions for 10 h. According to TPO, the amount of carbon formation decreased with increasing Ce content. No carbon species was observed when the Ce doping content was higher than 8%. The decreasing in the reactivity when more than 10% CeO_2 was doped could be due to the oxidized of Ni, as the reducibility of Ni reduced after exposure in dry reforming for 10 h, regarding to the TPR experiments.

It should also be noted that, at steady state, the main products from this reaction were H_2 and CO with H_2/CO always less than 1, indicating a contribution of the reverse water-

Table 1
Physicochemical properties of the catalysts after reduction at 700 °C

Catalyst	Ni load[a] (wt.%)	Ce load[a] (wt.%)	BET surface area ($m^2\ g^{-1}$)	Ni-reducibility[b] (Ni%)	Ni-dispersion[c] (Ni%)
Ni/Al_2O_3	4.91	0.0	40.2	92.1	4.87
2% Ce-Ni/Al_2O_3	4.84	1.87	40.8	93.5	4.54
4% Ce-Ni/Al_2O_3	4.93	4.02	42.7	91.4	5.12
6% Ce-Ni/Al_2O_3	5.01	5.94	46.5	90.6	4.54
8% Ce-Ni/Al_2O_3	4.96	8.03	49.1	91.1	4.65
10% Ce-Ni/Al_2O_3	4.88	9.86	49.8	89.9	4.77
12% Ce-Ni/Al_2O_3	4.93	12.1	50.4	90.3	4.64
14% Ce-Ni/Al_2O_3	4.92	13.9	50.9	91.0	4.20

[a] Measured from X-ray fluorescence analysis.
[b] Measured from temperature-programmed reduction (TPR) with 5% hydrogen.
[c] Measured from temperature-programmed desorption (TPD) of hydrogen after TPR measurement.

Table 2
Methane conversions, H_2/CO production ratio, and physicochemical properties of the catalysts after exposure in dry reforming (4 kPa CH_4 and 12 kPa CO_2) at 900 °C

Catalyst	CH_4 conversions (%) at steady state	H_2/CO ratio	Ni and Ce load[a] (wt.%)	Carbon formation[b] (monolayers)	BET surface ($m^2\ g^{-1}$)	Ni reducibility[c] (Ni%)	Ni dispersion[d] (Ni%)
Ni/Al_2O_3	3.32	0.89	4.89/0.0	3.48	40.0	92.1	4.84
2% Ce-Ni[e]	9.43	0.88	4.86/1.87	3.01	40.8	93.2	4.48
4% Ce-Ni	12.2	0.84	4.96/4.00	1.62	42.0	91.0	5.07
6% Ce-Ni	14.7	0.81	4.97/5.98	0.43	43.9	90.0	4.52
8% Ce-Ni	15.3	0.80	4.98/8.01	∼0	44.4	90.4	4.60
10% Ce-Ni	14.9	0.77	4.83/9.93	∼0	44.7	87.3	4.71
12% Ce-Ni	11.8	0.75	4.87/11.9	∼0	45.1	70.1	4.55
14% Ce-Ni	10.7	0.71	4.94/14.0	∼0	45.6	67.6	4.14

[a] Measured from X-ray fluorescence analysis.
[b] Calculated using CO and CO_2 yields from temperature-programmed oxidation (TPO) with 10% oxygen.
[c] Nickel reducibility (measured from temperature-programmed reduction (TPR) with 5% hydrogen).
[d] Nickel dispersion (measured from temperature-programmed desorption (TPD) after TPR).
[e] CeO_2 dopedNi/Al_2O_3.

gas shift reaction. Small amount of steam was also observed from the reaction. The H_2/CO ratio decreased with increasing Ce doping content indicated the high reactivity toward the reverse water-gas shift reaction of ceria (Table 2). The reactivities toward the reverse water-gas shift reaction for CeO_2 doped Ni/Al_2O_3 (with several Ce contents) and Ni/Al_2O_3 were tested in order to ensure the above explanation by using TPRx in CO_2/H_2/He gas mixture (5 kPa CO_2 and 10 kPa H_2). Fig. 4 shows the activities of all catalysts toward this reaction. Clearly, the activity toward the RWGS reaction over CeO_2 doped Ni/Al_2O_3 with high Ce content was significantly higher than that over Ni/Al_2O_3 at the same operating conditions.

3.3. Reactivity toward dry reforming

Ni/Al_2O_3 and 8% CeO_2 doped Ni/Al_2O_3 were further studied in dry reforming at 900 °C. The feed was CH_4/CO_2 in helium with different CH_4/CO_2 ratios of 1.0/0.3, 1.0/1.0, and 1.0/3.0. The reforming rate was measured as a function of time in order to indicate the stability and the deactivation rate.

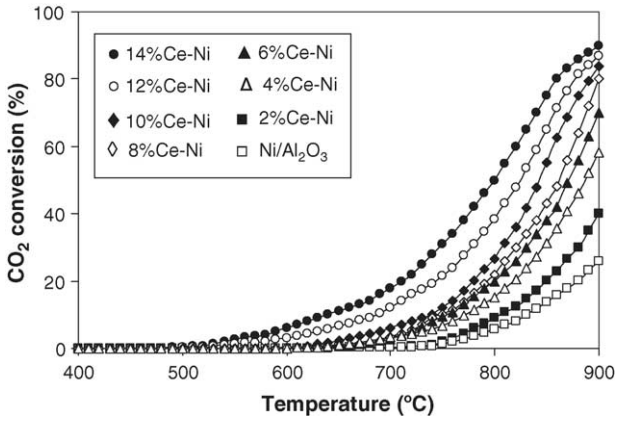

Fig. 4. The activities of Ni/Al_2O_3 and CeO_2 doped Ni/Al_2O_3 (with different Ce contents) toward the reverse water-gas shift reaction using TPRx in CO_2/H_2/He gas mixture (5 kPa CO_2 and 10 kPa H_2).

The variations in turnover frequencies (N) with time at 900 °C for different catalysts and different inlet CH_4/CO_2 ratio are shown in Fig. 5. The significant deactivations were detected for Ni/Al_2O_3 catalyst in all conditions especially at high inlet CH_4/CO_2 ratio, whereas considerable lower deactivations were detected for 8% CeO_2 doped Ni/Al_2O_3. At steady state, the dry reforming over 8% CeO_2 doped Ni/Al_2O_3 with inlet CH_4/CO_2 of 1.0/3.0 showed the best activity. Catalyst stabilities expressed as deactivation percentages are given in Table 3.

The characterization of these spent catalysts by X-ray diffraction (XRD) and X-ray photoelectron spectroscopy (XPS) were then carried out to determine the formation or the changing of chemical states in the spent catalysts, compared to the fresh one after reduction. X-ray diffraction was performed using X-ray defractometer with Cu Kα radiation (λ = 1.54060 Å) and operating parameters of 40 kV and 40 mA. Diffraction patterns were acquired by a step-scanning technique, using a step size ($\Delta 2\theta$) of 0.020°. The XPS spectra were acquired on spectrometer with a hemispherical electron analyser detector, operated in a constant threshold pass energy mode (50 eV), and using a non-monochromatic Al

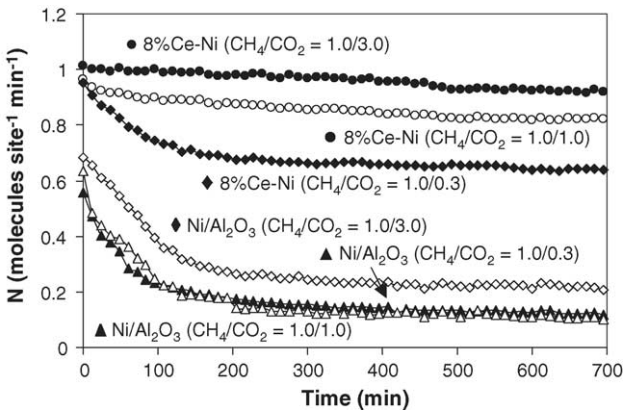

Fig. 5. Dry reforming of methane at 900 °C for several catalysts and various inlet CH_4/CO_2 ratios.

Table 3
Methane conversions, stabilities, and physicochemical properties of the catalysts after exposure in dry reforming conditions at 900 °C for 12 h

Catalyst	CH_4/CO_2 ratio	CH_4 conversions (%) at steady state	Deactivation (%)	Carbon formation[a] (monolayers)	BET after reaction ($m^2\ g^{-1}$)	Ni reducibility[b] (Ni%)
Ni/Al_2O_3	1.0/0.3	1.64	84.2	4.26	40.0	91.0
	1.0/1.0	2.01	78.4	3.97	39.5	93.2
	1.0/3.0	3.32	69.9	3.48	40.0	92.1
8% Ce-Ni[c]	1.0/0.3	10.6	33.1	0.85	44.0	90.0
	1.0/1.0	13.6	14.8	0.34	44.5	89.3
	1.0/3.0	15.3	9.08	~0	44.4	90.4

[a] Calculated using CO and CO_2 yields from temperature-programmed oxidation (TPO) with 10% oxygen.
[b] Nickel reducibility (measured from temperature-programmed reduction (TPR) with 5% hydrogen).
[c] CeO_2 doped Ni/Al_2O_3.

Kα (1.4866 eV) radiation source, which operated at 12 kV and 20 mA. Fig. 6 presents the XRD patterns of the spent and fresh Ni/Al_2O_3 and CeO_2 doped Ni/Al_2O_3. From the XRD results, Ni and $NiAl_2O_4$ reflectance were found in both Ni/Al_2O_3 and CeO_2 doped Ni/Al_2O_3. It is clearly seen that the intensities of $NiAl_2O_4$ peaks for CeO_2 doped Ni/Al_2O_3 were lower than that for Ni/Al_2O_3. This implies that the interaction between NiO and Al_2O_3 was prevented by the doping of CeO_2. A significant carbon peak was observed for the spent Ni/Al_2O_3, indicated the high formation of carbon species on the catalyst surface, whereas a smaller peak of carbon was detect for the spent CeO_2 doped Ni/Al_2O_3.

Table 4 presents the Ce^{3+}/Ce^{4+} ratio for CeO_2 doped Ni/Al_2O_3 before and after exposure in dry methane reforming conditions, determined from XPS. It is seen that no Ce^{3+} (Ce_2O_3) formation was observed for the fresh CeO_2 doped Ni/Al_2O_3 after reduction. Regarding the spent CeO_2 doped Ni/Al_2O_3, no Ce^{3+} formation was detect after exposure in dry methane reforming with the inlet CH_4/CO_2 ratios of 1.0/3.0 and 1.0/1.0, however, a small formation of Ce_2O_3 was observed over CeO_2 doped Ni/Al_2O_3 catalyst after exposure in dry methane reforming with the inlet CH_4/CO_2 ratio of 1.0/0.3. This Ce_2O_3 formation is obviously due to the remaining non-oxidation CeO_2, which will be explained at the end of this section.

Table 4
Ce^{3+}/Ce^{4+} ratio observed from the XPS measurement over CeO_2 doped Ni/Al_2O_3 after reduction and after exposure in dry methane reforming conditions

	Ce^{3+}/Ce^{4+} ratio
After reduction	0
After exposure in dry methane reforming; with CH_4/CO_2 of	
1.0/3.0	0
1.0/1.0	0
1.0/0.3	0.21

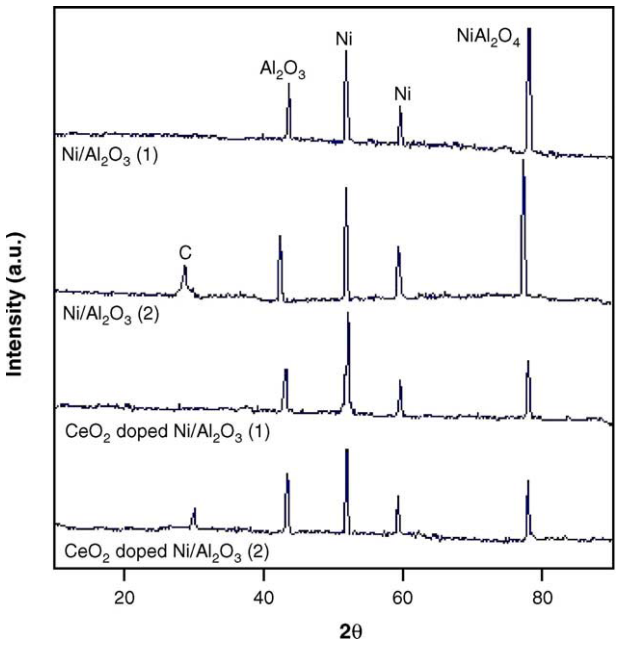

Fig. 6. XRD patterns of the catalysts after reduction (1) and after exposure in dry methane reforming at 900 °C with the inlet CH_4/CO_2 of 1.0/1.0 (2).

The post-reaction temperature-programmed oxidation experiments were then carried out after a helium purge by introducing of 10% oxygen in helium in order to determine whether the observed deactivation is due to the carbon formation. From the TPO results shown in Fig. 7, the huge peaks of carbon dioxide and carbon monoxide were observed for Ni/Al_2O_3 at 600 °C, while smaller peaks of both components were detected for 8% CeO_2 doped Ni/Al_2O_3. The amount of carbon formations on the surface of these catalysts with

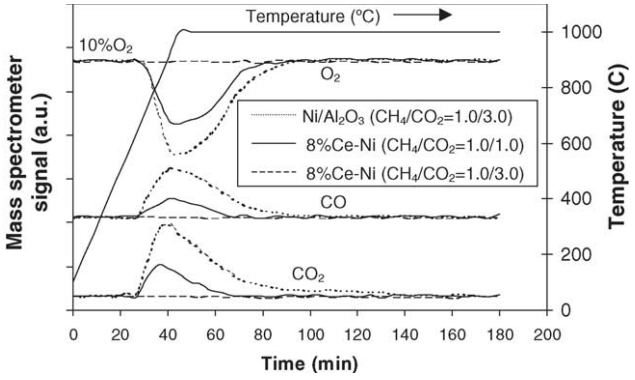

Fig. 7. Temperature-programmed oxidation (TPO) of Ni/Al_2O_3 and 8% CeO_2 doped Ni/Al_2O_3 (10 kPa O_2) after exposure in dry reforming conditions for 10 h.

different inlet CH_4/CO_2 ratios were determined by measuring the CO and CO_2 yields from the TPO results (using Microcal Origin Software). Using a value of 0.026 nm^2 for the area occupied by a carbon atom in a surface monolayer of the basal plane in graphite [17], the quantities of carbon deposited over Ni/Al_2O_3 were observed to be approximately 4.26, 3.97, and 3.48 monolayers, while those over 8% CeO_2 doped Ni/Al_2O_3 were 0.85, 0.34, and ~0 monolayers for the inlet CH_4/CO_2 ratios of 1.0/0.3, 1.0/1.0, and 1.0/3.0, respectively. The total amounts of carbon deposited were ensured by the calculation of carbon balance in the system. Regarding to the calculation for the inlet CH_4/CO_2 ratios of 1.0/0.3, 1.0/1.0, and 1.0/3.0, the moles of carbon deposited per gram of 8% CeO_2 doped Ni/Al_2O_3 were 1.34, 0.49, and ~0 mmol g^{-1}. By the same assumption for the area occupied by a carbon atom [17], these values are equal to 0.87, 0.32, and 0 monolayers, respectively, which is in good agreement with the values observed from the TPO method described above. The results clearly indicated the strong resistance toward carbon formation for 8% CeO_2 doped Ni/Al_2O_3 compared to Ni/Al_2O_3. The BET measurements, as presented in Table 3, indicated that deactivations of 8% CeO_2 doped Ni/Al_2O_3 are also due to the slight sintering of CeO_2. Several researchers also reported the high thermal sintering rate of ceria-based materials at high operating temperature [15,16].

The improvement of dry reforming reactivity and resistance toward carbon formation for CeO_2 doped Ni/Al_2O_3 could be mainly due to the redox property of ceria. During the dry reforming, in addition to the reactions on Ni surface, the solid–gas reaction between CeO_2 and CH_4 also produces synthesis gas with a H_2/CO ratio of two, while the reduced ceria, CeO_{2-x}, can react with CO_2 to produce CO [33–35]. This solid–gas mechanism involves the reactions between methane and/or an intermediate surface hydrocarbon species with the lattice oxygen (O_x) at CeO_2 surface, as illustrated schematically below [36].

$$CH_4 + 2S \Leftrightarrow CH_3{-}S + H{-}S \quad (5)$$

$$CH_3{-}S + S \Leftrightarrow CH_2{-}S + H{-}S \quad (6)$$

$$CH_2{-}S + S \Leftrightarrow CH{-}S + H{-}S \quad (7)$$

$$CH{-}S + S \Leftrightarrow C{-}S + H{-}S \quad (8)$$

$$C{-}S + O_x \Leftrightarrow CO + O_{x-1} + S \quad (9)$$

$$2H{-}S \Leftrightarrow H_2 + 2S \quad (10)$$

During the dry reforming, methane is adsorbed on either a unique site (S) or the lattice oxygen (O_x), whereas CO_2 can react with the reduced site of ceria, O_{x-1}. The steady state reforming rate is mainly due to the continuous supply of the oxygen source by CO_2 (Eq. (11)). Therefore, the Ce_2O_3 formation observed by XPS measurement in Table 4 over spent CeO_2 doped Ni/Al_2O_3 after exposure in dry methane reforming with high inlet CH_4/CO_2 ratio is due to the insufficient supply of inlet CO_2.

$$CO_2 + O_{x-1} \Leftrightarrow O_x + CO \quad (11)$$

Regarding the possible carbon formation during the reforming processes, the following reactions are the most probable reactions that could lead to carbon formation:

$$2CO \Leftrightarrow CO_2 + C \quad (12)$$

$$CH_4 \Leftrightarrow 2H_2 + C \quad (13)$$

$$CO + H_2 \Leftrightarrow H_2O + C \quad (14)$$

$$CO_2 + 2H_2 \Leftrightarrow 2H_2O + C \quad (15)$$

At low temperature, reactions (14) and (15) are favorable, while reaction (12) is thermodynamically unflavored [37]. The Boudard reaction (Eq. (12)) and the decomposition of methane (Eq. (13)) are the major pathways for carbon formation at such a high temperature as they show the largest change in Gibbs energy [38]. According to the range of temperature in this study, 800–900 °C, carbon formation would be formed via the decomposition of methane and Boudard reactions. By doping CeO_2 as the promoter, both reactions (Eqs. (12) and (13)) could be inhibited by the gas–solid reactions between methane and carbon monoxide with the lattice oxygen (O_x) at CeO_2 surface forming hydrogen and carbon dioxide, which is thermodynamically unflavored to form carbon species.

3.4. Effects of temperature and inlet components

The inlet methane partial pressure was varied from 1 to 4 kPa, while inlet carbon dioxide partial pressure was kept constant at 12 kPa. The operating temperature range was 825–900 °C. Fig. 8 illustrates the influence of the inlet methane partial pressure on the turnover frequencies (N) for dry reforming over 8% CeO_2 doped Ni/Al_2O_3 at different operating temperatures. The activities of catalyst increased with increasing inlet methane partial pressure as well as operating temperature. Fig. 9 shows an Arrhenius-type plot

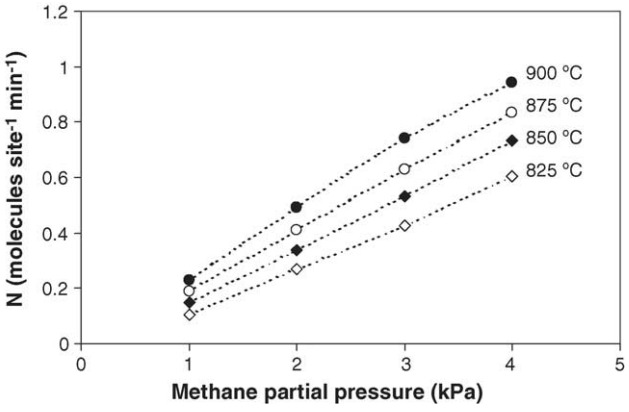

Fig. 8. Effect of methane partial pressure on the turnover frequencies (N) for dry reforming over 8% CeO_2 doped Ni/Al_2O_3 at different temperatures (12 kPa inlet CO_2).

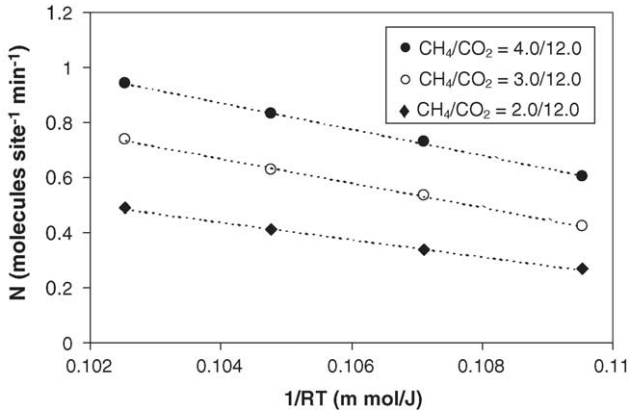

Fig. 9. Arrhenius plot of turnover frequencies (N) for dry reforming of methane over 8% CeO_2 doped Ni/Al_2O_3 with different inlet methane/carbon dioxide ratio.

for dry reforming over CeO_2 doped Ni/Al_2O_3 with various methane/carbon dioxide ratios over the temperature range 825–900 °C. The corresponding activation energy observed for this catalyst is 178 ± 9 kJ/mol, slightly depending on the gas composition.

The reaction order in methane (n) for CeO_2 doped Ni/Al_2O_3 was observed to be 0.96–1.04, and seemed to be essentially independent of the operating temperature and other inlet compositions in the range of conditions studied. These values n were obtained experimentally by plotting $\ln(-r_{CH_4})$ versus $\ln(P_{CH_4})$ according to the equation below.

$$\ln(-r_{CH_4}) = \ln(k) + n\ \ln(P_{CH_4}) \quad (16)$$

where $-r_{CH_4}$ is the dry reforming rate (mol kg_{cat}^{-1} h^{-1}), while P_{CH_4} the methane partial pressure. k is the apparent reaction rate constant and n is the reaction order in methane. The reaction orders in other components (CO_2, H_2, and CO) were achieved using the same approach by varying the inlet partial pressure of the component of interest and keeping other inlet component partial pressures constant.

In order to investigate the influence of CO_2 on the dry reforming rate, several inlet carbon dioxide partial pressures, from 9 to 12 kPa, were introduced to the feed with constant methane partial pressure (3 kPa). Carbon dioxide presented slight positive effect on the dry reforming rate as shown in Fig. 10. The reaction order in carbon dioxide was observed to be a positive value between 0.44 and 0.54, and seemed to be independent of the operating temperature for the range of conditions studied. At 900 °C, the proportion of H_2/CO in the products reduced from 0.80 to 0.67 as the CO_2/CH_4 ratio was increased from 3.0 to 12.0 (Fig. 11). This is as expected from an increasing contribution from the reverse water-gas shift (RWGS) reaction.

The dry reforming in the presences of carbon monoxide and hydrogen were then investigated by adding either carbon monoxide or hydrogen to the feed gas at several operating temperatures. The results show that the reforming rates are also dependent on both carbon monoxide and hydrogen

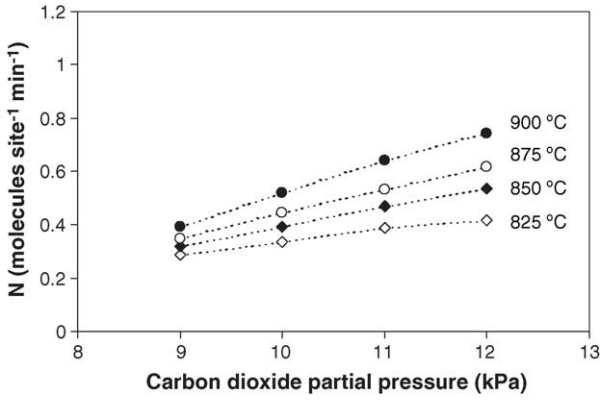

Fig. 10. Effect of carbon dioxide partial pressure on the turnover frequencies (N) for dry reforming over 8% CeO_2 doped Ni/Al_2O_3 at different temperatures (3 kPa CH_4).

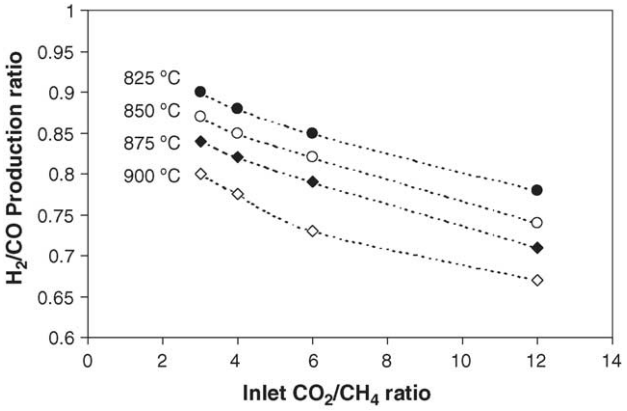

Fig. 11. Influence of inlet carbon dioxide/methane ratio on H_2/CO production ratio from dry reforming of methane over 8% CeO_2 doped Ni/Al_2O_3 at different temperatures (12 kPa CO_2).

concentrations. Unlike CH_4 and CO_2, both components inhibited the dry reforming rate as shown in Figs. 12 and 13. The reaction order in carbon monoxide was in the range of −0.42 to −0.37, while the reaction order in hydrogen was between −0.55 and −0.45 in the range of conditions studied.

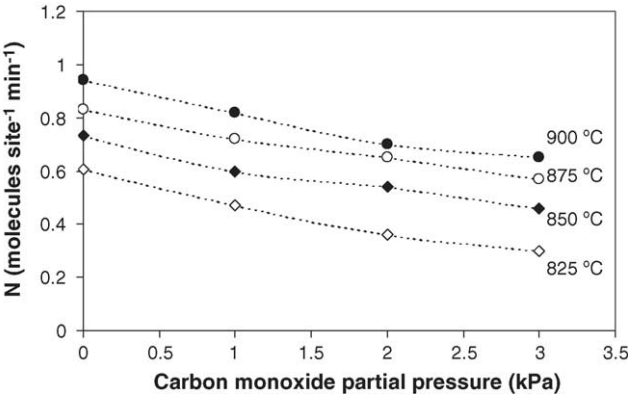

Fig. 12. Effect of carbon monoxide partial pressure on the turnover frequencies (N) for dry reforming of methane over 8% CeO_2 doped Ni/Al_2O_3 at different temperatures (4 kPa CH_4 and 12 kPa CO_2).

Table 5
Reaction orders for the components of interest (CH_4, CO_2, CO, and H_2) from dry reforming over 8% CeO_2 doped Ni/Al_2O_3 at different operating conditions

Components of interest	Temperature (°C)	Other inlet compositions	Reaction order for components of interest
Methane (1–4 kPa)	825	12 kPa CO_2	1.00
	850	12 kPa CO_2	0.97
	900	12 kPa CO_2	0.98
	850	15 kPa CO_2	1.01
	850	17 kPa CO_2	0.99
	825–900	12 kPa CO_2/1 kPa H_2	1.01 ± 0.03
	825–900	12 kPa CO_2/3 kPa H_2	0.98 ± 0.01
	825–900	12 kPa CO_2/1 kPa CO	0.99 ± 0.03
Carbon dioxide (9–12 kPa)	825	3 kPa CH_4	0.44
	850	3 kPa CH_4	0.54
	900	3 kPa CH_4	0.50
	850	3 kPa CH_4/3 kPa H_2	0.48
Hydrogen (1–3 kPa)	825–900	3 kPa CH_4/12 kPa CO_2	-0.49 ± 0.04
	825–850	1 kPa CH_4/12 kPa CO_2	-0.48 ± 0.03
	825–850	3 kPa CH_4/15 kPa CO_2	-0.52 ± 0.03
Carbon monoxide (1–3 kPa)	825–900	3 kPa CH_4/12 kPa CO_2	-0.40 ± 0.01
	825–850	3 kPa CH_4/15 kPa CO_2	-0.38 ± 0.01
	825–850	3 kPa CH_4/17 kPa CO_2	-0.40 ± 0.02

Table 5 presents the summary of observed reaction orders in each component (CH_4, CO_2, CO, and H_2) for CeO_2 doped Ni/Al_2O_3 at different inlet conditions.

Regarding to the above experiments, the experimental data can be fitted well to a simple relative rate coefficient, in which captures the essential features.

$$-r_{CH_4} = \frac{k(T)(P_{CH_4})^n(P_{CO_2})^m}{1 + K_1(T)P_{CO}^a + K_2(T)P_{H_2}^b} \quad (17)$$

where P_i is the partial pressure of chemical component i. The positive effects of methane and carbon dioxide on the dry reforming rate were a consequence of the presence of the $k(T)(P_{CH_4})^n(P_{CO_2})^m$ term, whereas negative effects of carbon monoxide and hydrogen were a consequence of the $K_1(T)P_{CO}^a$ and $K_2(T)P_{H_2}^b$ terms in the denominator. According to the fitting, when n, m, a, and b were taken as 1.0, 0.5, 0.4, and 0.5, a good fit to the data was observed in the range of conditions studied. $k(T)$ increased from 649.0 mol kg^{-1} h^{-1} atm$^{-1.5}$ at 825 °C to 954.3 mol kg^{-1} h^{-1} atm$^{-1.15}$ at 900 °C, while $K_1(T)$ and $K_2(T)$, also temperature dependent parameters, were in the range of 1.68–4.43 atm$^{-0.4}$ and 0.93–3.94 atm$^{-0.5}$, respectively. It should be noted that the apparent activation energy for this reaction, which were achieved by the Arrhenius plots, was approximately 150 kJ/mol.

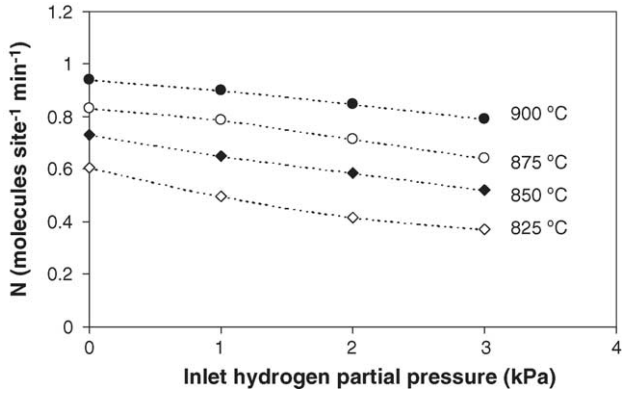

Fig. 13. Effect of hydrogen partial pressure on the turnover frequencies (N) for dry reforming of methane over 8% CeO_2 doped Ni/Al_2O_3 at different temperatures (4 kPa CH_4 and 12 kPa CO_2).

4. Conclusion

8% CeO_2 doped Ni/Al_2O_3 is a good candidate catalyst for the dry reforming of methane due to the high resistance toward the deactivation from carbon formation. During dry reforming process, the gas–solid reaction on ceria surface takes place simultaneously with the reactions on the surface of Ni, in which reduces the degree of carbon deposition on catalyst surface from methane decomposition and Boudard reactions. However, it should also be noted that the doping of too high ceria content results in the oxidation of Ni, which could reduce the reforming reactivity.

The intrinsic kinetic reaction of 8% CeO_2 doped Ni/Al_2O_3 was studied in the conditions where the intraparticle diffusion limitation was negligible. The dry reforming rate increased with increasing methane and carbon dioxide partial pressures as well as the operating temperature. In contrast, the methane conversion was inhibited when hydrogen and carbon monoxide were added to the system during dry reforming process. It can be concluded from the present work that CeO_2 doped Ni/Al_2O_3 seems to be a promise catalyst for the indirect internal reforming solid oxide fuel cells (IIR-SOFC) operation.

Acknowledgement

The financial support from The Thailand Research Fund (TRF) throughout this project is gratefully acknowledged.

References

[1] P. Aguiar, D. Chadwick, L. Kershenbaum, Chem. Eng. Sci. 57 (2002) 1665.
[2] J.H. Edwards, A.M. Maitra, Fuel Process. Technol. 42 (1995) 269.
[3] M.A. Vannice, M.C.J. Bradford, Appl. Catal. A: Gen. 142 (1) (1996) 97–122.
[4] T. Sodesawa, A. Dobashi, F. Nozaki, React. Kinet. Catal. Lett. 12 (1979) 107.
[5] L. Topor, L. Bejan, E. Ivana, N. Georgescu, Rev. Chim. Bucharest 30 (1979) 539.
[6] T.A. Chubb, Sol. Energy 24 (1980) 341.
[7] T.A. Chubb, J.H. McCrary, G.E. McCrary, J.J. Nemecek, D.E. Simmons, Proc. Meet. Am. Sect. Int. Sol. Eng. Soc. 4 (1981) 166.
[8] J.R. Rostrup-Nielsen, J.H. Bak Hansen, J. Catal. 144 (1993) 38.
[9] P. Gronchi, C. Mazzocchia, E. Tempesti, R. Del Rosso, in: G. Centi, et al. (Eds.), Enviromental Catalysis, SCI Publication, Roma, 1995, p. 627.
[10] A. Erdöhelyi, J. Cserényi, F. Solymosi, J. Catal. 141 (1993) 287.
[11] A. Erdöhelyi, J. Cserényi, E. Rapp, F. Solymosi, Appl. Catal. A: Gen. 108 (1994) 205.
[12] J. Nakamura, K. Aikawa, K. Sato, T. Uchijima, Catal. Lett. 25 (1994) 265.
[13] Z.L. Zhang, V.A. Tsipouriari, A.M. Efstathiou, X.E. Verykios, J. Catal. 158 (1996) 51.
[14] E. Ramírez-Cabrera, A. Atkinson, D. Chadwick, Appl. Catal. B 47 (2004) 127–131.
[15] E. Ramírez-Cabrera, N. Laosiripojana, A. Atkinson, D. Chadwick, Catal. Today 78 (2003) 433–438.
[16] N. Laosiripojana, Reaction engineering of indirect internal steam reforming of methane for application in solid oxide fuel cells, Ph.D. Thesis, University of London, England, 2003.
[17] E. Ramirez, A. Atkinson, D. Chadwick, Appl. Catal. B 36 (2002) 193–206.
[18] X. Wang, R.J. Gorte, Appl. Catal. A 224 (2002) 209–218.
[19] H.S. Roh, K.W. Jun, W.S. Dong, J.S. Chang, S.E. Park, Y.I. Joe, J. Mol. Catal. A 181 (2002) 137–142.
[20] Q. Miao, G. Xiong, S. Sheng, W. Cui, L. Xu, X. Guo, Appl. Catal. A 154 (1987) 17–27.
[21] A.A. Lemonidou, M.A. Goula, I.A. Vasalos, Catal. Today 46 (1987) 175–183.
[22] W.S. Dong, H.S. Roh, K.W. Jun, S.E. Park, Y.S. Oh, Appl. Catal. A 226 (2002) 63–72.
[23] M. Mamak, N. Coombs, G. Ozin, Adv. Mater. 12 (2000) 198–202.
[24] M. Mamak, N. Coombs, G. Ozin, J. Am. Chem. Soc. 122 (2000) 8932.
[25] M. Mamak, N. Coombs, G.A. Ozin, Chem. Mater. 13 (2001) 3564.
[26] P. Bera, S. Mitra, S. Sampath, M.S. Hegde, Chem. Commun. (2001) 927.
[27] A. Martinez-Arias, J.M. Coronado, R. Cataluna, J.C. Conesa, J.C. Soria, J. Phys. Chem. B 102 (1998) 4357.
[28] D. Skarmoutsos, F. Tietz, P. Nikolopoulos, Fuel Cells 1 (2001) 243.
[29] T. Takeguchi, S.N. Furukawa, M. Inoue, J. Catal. 202 (2001) 14.
[30] J. Sfeir, P.A. Philippe, P. Moseki, N. Xanthopoulos, R. Vasquez, J.M. Hans, V.H. Jan, K.R. Thampi, J. Catal. 202 (2001) 229.
[31] N. Kiratzis, P. Holtappels, C.E. Hatchwell, M. Mogensen, J.T.S. Irvine, Fuel Cells 1 (2001) 211.
[32] S. Wang, G.Q. Lu, Appl. Catal. B 19 (1998) 267.
[33] K. Otsuka, T. Ushiyama, I. Yamanaka, Chem. Lett. (1993) 1517.
[34] K. Otsuka, M. Hatano, A. Morikawa, J. Catal. 79 (1983) 493.
[35] K. Otsuka, M. Hatano, A. Morikawa, Inorg. Chim. Acta 109 (1985) 193.
[36] N. Laosiripojana, S. Assabumrungrat, Appl. Catal. B 60 (2005) 109–118.
[37] Y. Lwin, W.R.W. Daud, A.B. Mohamad, Z. Yaakob, Int. J. Hydrogen Energy 25 (1) (2000) 47–53.
[38] J.N. Amor, Appl. Catal. A 176 (1999) 159–176.

N. Laosiripojana, W. Sangtongkitcharoen, S. Assabumrungrat

"Catalytic steam reforming ethane and propane over CeO_2-doped Ni/Al_2O_3 at SOFC temperature: Improvement of resistance toward carbon formation by the redox properties of doping CeO_2"

Fuel, 85 (2006), 323-332

(IF-2003 = 1.368)

Available online at www.sciencedirect.com
SCIENCE DIRECT
Fuel 85 (2006) 323–332
FUEL
www.fuelfirst.com

Catalytic steam reforming of ethane and propane over CeO_2-doped Ni/Al_2O_3 at SOFC temperature: Improvement of resistance toward carbon formation by the redox property of doping CeO_2

N. Laosiripojana[a,*], W. Sangtongkitcharoen[b], S. Assabumrungrat[b]

[a]*The Joint Graduate School of Energy and Environment, King Mongkut's University of Technology Thonburi, Bangkok 10140, Thailand*
[b]*Center of Excellence on Catalysis and Catalytic Reaction Engineering, Department of Chemical Engineering, Faculty of Engineering, Chulalongkorn University, Bangkok 10330, Thailand*

Received 21 January 2005; received in revised form 2 June 2005; accepted 28 June 2005
Available online 28 July 2005

Abstract

Ni/Al_2O_3 with the doping of CeO_2 was found to have useful activity to reform ethane and propane with steam under Solid Oxide Fuel Cells (SOFCs) conditions, 700–900 °C. CeO_2-doped Ni/Al_2O_3 with 14% ceria doping content showed the best reforming activity among those with the ceria content between 0 and 20%. The amount of carbon formation decreased with increasing Ce content. However, Ni was easily oxidized when more than 16% of ceria was doped. Compared to conventional Ni/Al_2O_3, 14%CeO_2-doped Ni/Al_2O_3 provides significantly higher reforming reactivity and resistance toward carbon deposition. These enhancements are mainly due to the influence of the redox properties of doped ceria. Regarding the temperature programmed reduction experiments (TPR-1), the redox properties and the oxygen storage capacity (OSC) for the catalysts increased with increasing Ce doping content. In addition, it was also proven in the present work that the redox of these catalysts are reversible, according to the temperature programmed oxidation (TPO) and the second time temperature programmed reduction (TPR-2) results.

During the reforming process, in addition to the reactions on Ni surface, the gas–solid reactions between the gaseous components presented in the system (C_2H_6, C_3H_8, C_2H_4, CH_4, CO_2, CO, H_2O, and H_2) and the lattice oxygen (O_x) on ceria surface also take place. The reactions of adsorbed surface hydrocarbons with the lattice oxygen (O_x) on ceria surface ($C_nH_m + O_x \rightarrow nCO + m/2(H_2) + O_{x-n}$) can prevent the formation of carbon species on Ni surface from hydrocarbons decomposition reaction ($C_nH_m \Leftrightarrow nC + m/2H_2$). Moreover, the formation of carbon via Boudard reaction ($2CO \Leftrightarrow CO_2 + C$) is also reduced by the gas–solid reaction of carbon monoxide (produced from steam reforming) with the lattice oxygen ($CO + O_x \Leftrightarrow CO_2 + O_{x-1}$).

Keywords: Hydrogen; Ethane; Propane; Carbon formation; Steam reforming; CeO_2

1. Introduction

Solid Oxide Fuel Cell (SOFC) is generally operated at high temperature between 700 and 1100 °C [1,2]. Due to its high-operating temperature, fuels such as methane can be in-stack or internal reformed by catalytic steam reforming to produce a H_2/CO rich gas, which is eventually used to generate electrical energy and heat. The operation, called indirect internal reforming (IIR), is expected to simplify the overall system design [3].

Currently, one of the most interesting fuels for SOFC is natural gas consisting mainly of methane. Normally, natural gas also contains significant amounts of higher hydrocarbons such as ethane and propane. When natural gas is reformed internally (IIR) without any pre-treatments, the carbon formation can be easily formed on the catalyst surface due to the decompositions of these hydrocarbons at high temperature. SOFC fueled by natural gas therefore requires a small external pre-reformer unit, where the high hydrocarbon components are reformed readily before introducing to the main part of the system [4]. The pre-reforming unit is normally operated at relatively lower temperature, 300–500 °C, in which the carbon formation is

* Corresponding author.
E-mail address: navadol_l@jgsee.kmutt.ac.th (N. Laosiripojana).

0016-2361/$ - see front matter © 2005 Elsevier Ltd. All rights reserved.
doi:10.1016/j.fuel.2005.06.013

thermodynamically unflavored. The disadvantage of this installation is the extra-requirement of the heat supplied into this unit, which can reduce the fuel cell efficiency [5].

The approach to this problem in this work is developing of an alternative catalyst that is enable to reform high hydrocarbon components with low degree of carbon deposition at SOFC temperature, 700–900 °C. The successful development of this catalyst would help eliminate the requirement of the external pre-reformer, as these high hydrocarbon elements can be simultaneously reformed together with methane at high temperature. In this study, ethane and propane were chosen as the inlet fuels, because they are the main high hydrocarbon components presented in natural gas. According to the economical point of view, Ni/Al_2O_3 was selected as a based catalyst rather than the precious metals such as Pt, Rh and Ru although it is more sensitive to carbon formation. Cerium oxide (CeO_2) was chosen as an additive promoter. This material (called ceria) is an important material for a variety of catalytic reactions involving oxidation of hydrocarbons (e.g. automobile exhaust catalysts). Recently, the use of ceria-based catalysts has shown a rapid increase [6]. A high oxygen mobility [7], high oxygen storage capacity [8–13], strong interaction with the supported metal (strong metal-support interaction) [14] and the modifiable ability [15] render the ceria-based materials very interesting for catalysis and as a support and promoter. It has widely been reported, regarding the above properties, that cerias can promote the action of various metals in the reactions in which hydrogen is involved as a reactant or product [16–20]. According to the catalytic steam reforming reaction, ceria-based materials have been reported by several researchers to be promising supports among α-Al_2O_3 [21], γ-Al_2O_3 and γ-Al_2O_3 with alkali metal oxide and rare earth metal oxide [22], and $CaAl_2O_4$ [21–24]. One of the most promising ceria-based supports for the reforming reactions appeared to be Ce-ZrO_2, where the metal can be Ni, Pt or Pd [25–34].

It has been reported that the gas–solid reaction between CeO_2 and CH_4 produces synthesis gas with a H_2/CO ratio of two according to the following reactions [35,36]. Moreover, the reduced ceria, CeO_{2-x}, can react with CO_2 and steam to produce CO and H_2, respectively [37].

$$CeO_2 + nCH_4 \rightarrow CeO_{2-n} + nCO + 2nH_2 \quad (1)$$

$$CeO_{2-x} + CO_2 \Leftrightarrow CeO_2 + CO \quad (2)$$

$$CeO_{2-x} + H_2O \Leftrightarrow CeO_2 + H_2 \quad (3)$$

Nowadays, a potential application of ceria is in Solid Oxide Fuel Cells (SOFCs) application as a reforming catalyst for in-stack (called indirect internal) reforming of methane, since it is high resistant toward carbon deposition compared to Ni [38]. Recently, the successful tests of ceria for the methane steam reforming reaction have been reported [39,40]. Due to the high resistance toward carbon formation, ceria should be a good additive promoter for the reforming of ethane and propane. In this work, various amounts of ceria were doped on the surface of Ni/Al_2O_3 in order to determine the suitable doping ratio. The reactivity toward steam reforming of ethane and propane, as well as the resistance toward carbon formation of CeO_2-doped Ni/Al_2O_3 were studied and compared to those of conventional Ni/Al_2O_3. The influence of inlet steam content on the product selectivity from this reaction at various temperatures was also determined.

2. Experimental

2.1. Catalyst preparations and characterizations

CeO_2-doped Ni/Al_2O_3 was prepared by impregnating different concentration of cerium nitrate ($Ce(NO_3)_3 \cdot 6H_2O$ (99.0%), Fluka) on Ni/Al_2O_3 powder. Ni/Al_2O_3 (10 wt% Ni) was prepared by impregnating α-Al_2O_3 (from Aldrich) with $NiCl_3$ solution at room temperature. This solution was stirred by magnetic stirring (100 rpm) for 6 h, dried overnight in an oven at 110 °C, and calcined in air at 900 °C for 6 h before use.

After reduction, the catalysts were characterized with several physicochemical methods. The weight contents of Ni and Ce loadings were determined by X-ray fluorescence (XRF) analysis. The reducibility and dispersion percentages of nickel were measured from temperature-programmed reduction (TPR) using 5% H_2 in Ar with the total flow rate of 100 $cm^3\ min^{-1}$ and temperature-programmed desorption (TPD) respectively. The catalyst specific surface areas were obtained from BET measurement. All physicochemical properties of the synthesized catalysts are presented in Table 1.

In addition to the above characterizations, the redox properties and redox reversibilities of the catalysts with different Ce doping contents were determined by the temperature programmed reduction (TPR-1) at high temperature and the temperature programmed oxidation (TPO) following with temperature programmed reduction (TPR-2), respectively. Regarding these experiments, 5% H_2/Ar and 5% O_2/He were used for the TPR and TPO, respectively, while the temperature of the system increased from room temperature to 900 °C and 1000°C, respectively.

2.2. Apparatus and procedures

An experimental reactor system was constructed as shown in Fig. 1. The feed gases including the components of interest (ethane, propane, and steam from the evaporator) and the carrier gas (helium) were introduced to the reaction section, in which a 10-mm diameter quartz reactor was mounted vertically inside a furnace. In the present work, the ethane/propane feed ratio was kept constant at 0.65/0.35, regarding to the approximate ratio of these components presented in natural gas (this information is based on the compositions of natural gas from PTT Company (Thailand)

Table 1
Physicochemical properties of the catalysts after reduction at 700 °C

Catalyst	Ni-load[a] (wt.%)	Ce-load[a] (wt.%)	BET Surface Area ($m^2\ g^{-1}$)	Ni-reducibility[b] (Ni%)	Ni-dispersion[c] (Ni%)
Ni/Al_2O_3	4.91	0.0	40.2	92.1	4.87
$2\%Ce\text{-}Ni/Al_2O_3$	4.84	1.87	40.8	93.5	4.54
$4\%Ce\text{-}Ni/Al_2O_3$	4.93	4.02	42.7	91.4	5.12
$6\%Ce\text{-}Ni/Al_2O_3$	5.01	5.94	46.5	90.6	4.54
$8\%Ce\text{-}Ni/Al_2O_3$	4.96	8.03	49.1	91.1	4.65
$10\%Ce\text{-}Ni/Al_2O_3$	4.88	9.86	49.8	89.9	4.77
$12\%Ce\text{-}Ni/Al_2O_3$	4.93	12.1	50.4	90.3	4.64
$14\%Ce\text{-}Ni/Al_2O_3$	4.92	13.9	50.9	91.0	4.20
$16\%Ce\text{-}Ni/Al_2O_3$	5.00	16.1	51.4	89.7	5.09
$18\%Ce\text{-}Ni/Al_2O_3$	4.94	17.9	51.0	90.1	4.13
$20\%Ce\text{-}Ni/Al_2O_3$	4.98	19.9	52.0	90.3	4.37

[a] Measured from X-ray fluorescence analysis.
[b] Measured from temperature-programmed reduction (TPR) with 5%hydrogen.
[c] Measured from temperature-programmed desorption (TPD) of hydrogen after TPR measurement.

containing 67%CH_4, 8.3%C_2H_6, 4.5%C_3H_8, 2.0%C_4H_{10}, 0.5%C_5H_{12}, and 14.5%CO_2). The catalyst was loaded in the quartz reactor, which was packed with a small amount of quartz wool to prevent the catalyst from moving. The weight of catalyst loading was 50 mg, while a typical range of total gas flow was 20–200 $cm^3\ min^{-1}$ depending on the desired space velocity. A Type-K thermocouple was placed into the annular space between the reactor and the furnace. This thermocouple was mounted on the tubular reactor in close contact with the catalyst bed to minimize the temperature difference between the catalyst bed and the thermocouple. Another Type-K thermocouple was inserted in the middle of the quartz tube in order to re-check the possible temperature gradient. The record showed that the maximum temperature fluctuation during the reaction was always ± 0.75 °C or less from the temperature specified for the reaction. Before the reaction, the catalyst was reduced under 5% H_2 in helium with the flow rate of 100 $cm^3\ min^{-1}$ for 6 h.

During the reactions, the exit gas mixture was transferred via trace-heated lines to the analysis section, which consists of a Porapak Q column Shimadzu 14B gas chromatograph (GC) and a mass spectrometer (MS). The gas chromatography was applied in order to investigate the steady state condition experiments, whereas the mass spectrometer in which the sampling of the exit gas was done by a quartz capillary and differential pumping was used for the transient and carbon formation experiments. In order to study the formation of carbon species on catalyst surface, Temperature programmed Oxidation (TPO) was applied by introducing 10% oxygen in helium into the system, after purged with helium. The operating temperature increased from room temperature to 1000 °C by the rate of 10 °C/min.

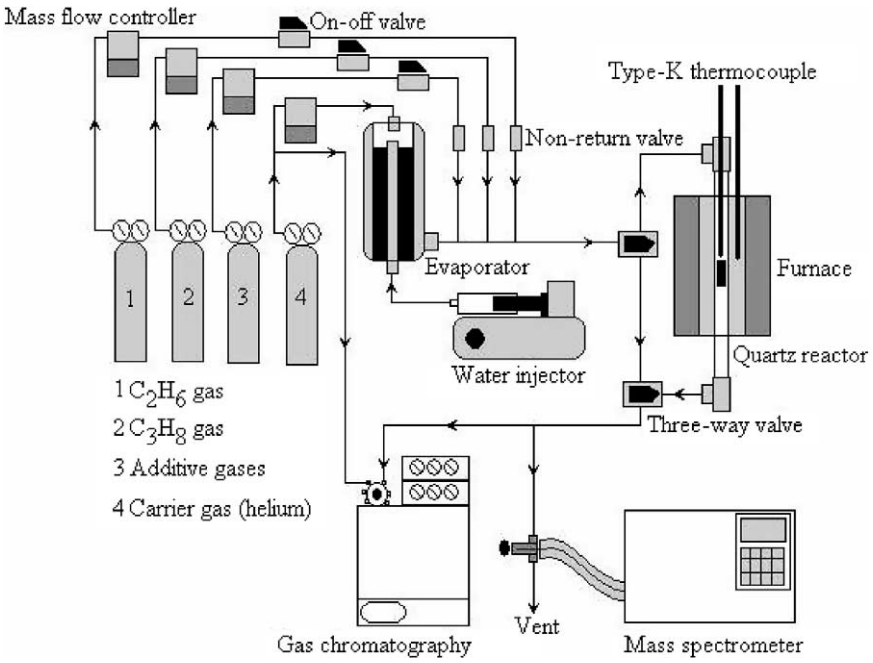

Fig. 1. Schematic diagram of the experimental set-up.

The calibrations of CO and CO_2 productions were performed by injecting a known amount of these calibration gases from a loop, in an injection valve in the bypass line. The response factors were obtained by dividing the number of moles for each component over the respective areas under peaks. The amount of carbon formations on the surface of catalysts were determined by measuring the CO and CO_2 yields from the TPO results (using Microcal Origin Software) assuming a value of 0.026 nm^2 for the area occupied by a carbon atom in a surface monolayer of the basal plane in graphite [38]. In addition to the TPO method, the amount of carbon deposition was confirmed by the calculation of carbon balance in the system. The amount of carbon deposited on the surface of catalyst would theoretically be equal to the difference between the inlet carbon containing components (C_2H_6, and C_3H_8) and the outlet carbon containing components (C_2H_6, C_3H_8, CO, CO_2, CH_4, and C_2H_4). The amount of carbon deposited per gram of catalyst is given by the following equation:

$$C_{\text{deposition}} = \frac{\text{mole}_{\text{carbon(in)}} - \text{mole}_{\text{carbon(out)}}}{m_{\text{catalyst}}} \quad (4)$$

The steam reforming reactivity was defined in terms of the conversions and selectivities. Hydrocarbon conversions (ethane and propane) denoted as $X_{\text{hydrocarbon}}$, and the products selectivity (hydrogen, carbon monoxide, carbon dioxide, methane, and ethylene), denoted as S_{product}, are calculated according to Eqs. (5)–(11):

$$X_{\text{Ethane}} = \frac{100(\%\text{Ethane}_{\text{in}} - \%\text{Ethane}_{\text{out}})}{\%\text{Ethane}_{\text{in}}} \quad (5)$$

$$X_{\text{Propane}} = \frac{100(\%\text{Propane}_{\text{in}} - \%\text{Propane}_{\text{out}})}{\%\text{Propane}_{\text{in}}} \quad (6)$$

$$S_{\text{H}_2} = \frac{100(\%\text{H}_2)}{3(\%\text{Ethane}_{\text{in}} - \%\text{Ethane}_{\text{out}}) + 4(\%\text{Propane}_{\text{in}} - \%\text{Propane}_{\text{out}}) + (\%\text{H}_2\text{O}_{\text{in}} - \%\text{H}_2\text{O}_{\text{out}})} \quad (7)$$

$$S_{\text{CO}} = \frac{100(\%\text{CO})}{2(\%\text{Ethane}_{\text{in}} - \%\text{Ethane}_{\text{out}}) + 3(\%\text{Propane}_{\text{in}} - \%\text{Propane}_{\text{out}})} \quad (8)$$

$$S_{\text{CO}_2} = \frac{100(\%\text{CO}_2)}{2(\%\text{Ethane}_{\text{in}} - \%\text{Ethane}_{\text{out}}) + 3(\%\text{Propane}_{\text{in}} - \%\text{Propane}_{\text{out}})} \quad (9)$$

$$S_{\text{CH}_4} = \frac{100(\%\text{CH}_4)}{2(\%\text{Ethane}_{\text{in}} - \%\text{Ethane}_{\text{out}}) + 3(\%\text{Propane}_{\text{in}} - \%\text{Propane}_{\text{out}})} \quad (10)$$

$$S_{\text{C}_2\text{H}_4} = \frac{100(\%\text{C}_2\text{H}_4)}{(\%\text{Ethane}_{\text{in}} - \%\text{Ethane}_{\text{out}}) + 1.5(\%\text{Propane}_{\text{in}} - \%\text{Propane}_{\text{out}})} \quad (11)$$

3. Results and discussion

3.1. Preliminary tests

The desired space velocity and suitable catalyst particle size were achieved from several preliminary tests, which were carried out to avoid any limitations by intraparticle diffusion in the experiments. The total flow rate was varied between 20 and 200 $cm^3\ min^{-1}$ under a constant residence time of 5×10^{-4} g $min\ cm^{-3}$. When the total flow rate was below 60 $cm^3\ min^{-1}$, the reforming rate increased with increasing the gas flow rate, suggesting that the mass transfer between the bulk gas and the catalyst particles is the rate-determining step. The reforming rate was almost constant in the range where the gas flow rate was higher than 80 $cm^3\ min^{-1}$, indicating that the mass transfer effect is unimportant in this flow rate range. Fig. 2 shows the effect of the total gas flow rate on the reforming rate over 14%CeO_2-doped Ni/Al_2O_3 at different temperatures. The reactions on different average sizes (from 100 to 500 μm) of catalysts were also carried out. It was observed that there were no significant changes in the methane conversion for the catalyst with the particle size between 100 and 200 μm, which indicated that the intraparticle diffusion limitation was negligible in this range. Consequently in this study, the weight of catalyst loading was 50 mg, while the total gas flow was kept constant at 100 $cm^3\ min^{-1}$. The catalyst particle size diameter was between 100 and 200 μm in all experiments.

Before studying the catalyst performance, homogeneous (non-catalytic) steam reforming of ethane and propane was investigated. Inlet $C_2H_6/C_3H_8/H_2O$ in helium with the molar ratio of 0.65/0.35/3.0 was introduced to the system, while the temperature increased from room temperature to 900 °C. From Fig. 3, it was observed that both ethane and propane were converted to methane, ethylene, and hydrogen at

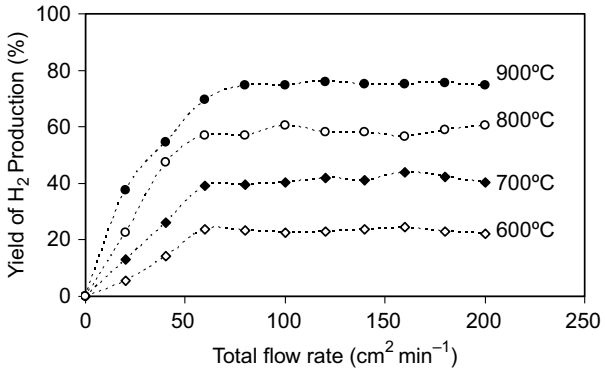

Fig. 2. Effect of the gas flow rate on the yield of H_2 production (%) for steam reforming over 14% CeO_2-doped Ni/Al_2O_3 at different temperatures (2.6 kPa C_2H_6, 1.4 kPa C_3H_8, 12 kPa H_2O).

the temperature above 700 °C. Significant amount of carbons was also detected in the blank reactor after exposure for 10 h. These components were formed via the decomposition of ethane and propane as shown in the equations below [41].

$$C_2H_6 \rightarrow C_2H_4 + H_2 \quad (12)$$

$$C_3H_8 \rightarrow 3/2(C_2H_4) + H_2 \quad (13)$$

$$C_2H_4 \rightarrow 2H_2 + 2C \quad (14)$$

$$C + 2H_2 \rightarrow CH_4 \quad (15)$$

There was no change in steam concentration, and no carbon monoxide and carbon dioxide was produced in the system, indicating that the non-homogenous reforming reaction between steam and hydrocarbon elements took place at this range of conditions studied.

3.2. Investigation of the redox properties and redox reversibility of the catalysts

As described earlier, the oxygen storage capacities and the degree of redox properties for catalysts with different Ce

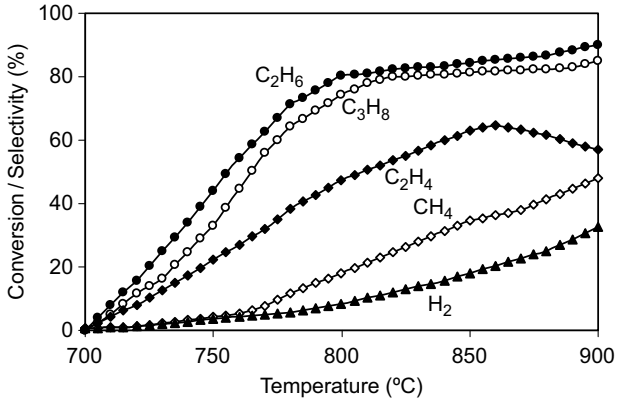

Fig. 3. Homogenous (in the absence of catalyst) reactivity of ethane and propane in the presence of steam (2.6 kPa C_2H_6, 1.4 kPa C_3H_8, and 12 kPa H_2O).

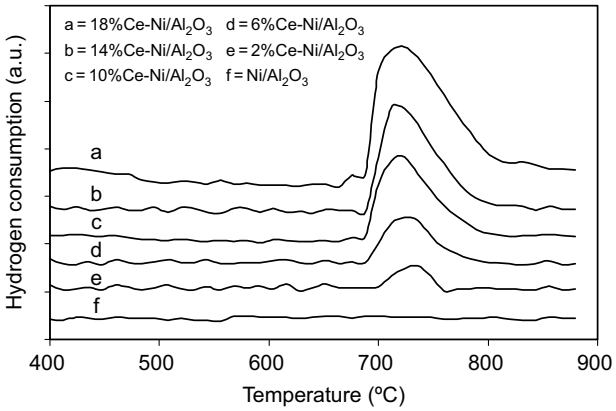

Fig. 4. Temperature Programmed Reduction (TPR-1) of the catalysts with different Ce doping content (0–18% Ce).

doping contents (0–18%) were investigated using temperature programmed reduction (TPR-1), in which performed by heating the reduced catalysts up to 900 °C in 5%H_2 in argon. As shown in Fig. 4, significant amount of hydrogen uptakes were detected from Ni/Al_2O_3 with the doping of CeO_2 at the temperature above 650 °C. The amount of hydrogen uptakes increased with increasing Ce doping content, suggesting the reduction of bulk oxygen ions on ceria surface. In contrast, no hydrogen consumption was observed from the TPR over conventional Ni/Al_2O_3. These results indicated the occurrence of redox properties for Ni/Al_2O_3 with CeO_2 doping at high temperature (650–900 °C), in which increased with increasing Ce content. This redox property provides a great benefit toward the reforming of ethane and propane, which will be presented in Section 3.4.

After purged with helium, the redox reversibility for each catalyst was then determined by applying temperature programmed oxidation (TPO) following with the second time temperature programmed reduction (TPR-2). The TPO was carried out by heating the catalyst up to 1000 °C in 10%O_2 in helium; the amounts of oxygen chemisorbed were then measured, Fig. 5 and Table 2. Regarding the TPR-2 results as shown in Fig. 6 and Table 2, the amount of

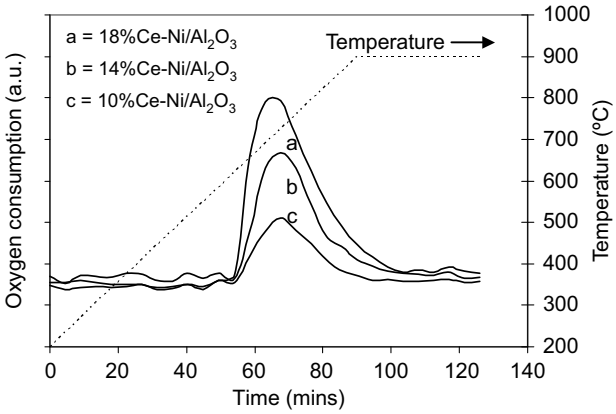

Fig. 5. Temperature Programmed Oxidation (TPO) of CeO_2-doped Ni/Al_2O_3 after TPR-1.

Table 2
Results of TPR(1), TPO, TPR(2) analyses of CeO_2 doped Ni/Al_2O_3 at high temperature

Catalyst	Total H_2 Uptake from TPR(1)[a] ($\mu mol/g_{cat}$)	Total O_2 Uptake from TPO[b] ($\mu mol/g_{cat}$)	Total H_2 Uptake from TPR(2)[c] ($\mu mol/g_{cat}$)
2%Ce-Ni/Al_2O_3	523	271	520
6%Ce-Ni/Al_2O_3	840	402	840
10%Ce-Ni/Al_2O_3	1078	540	1075
14%Ce-Ni/Al_2O_3	1350	691	1350
18%Ce-Ni/Al_2O_3	1505	784	1503

[a] Temperature Programmed Reduction of the reduced catalysts (Relative Standard Deviation = ±3%).
[b] Temperature Programmed Oxidation after TPR (1) (Relative Standard Deviation = ±1%).
[c] Re-Temperature Programmed Reduction after TPO (Relative Standard Deviation = ±2%).

hydrogen uptakes for each catalyst were approximately similar to those from TPR-1, indicated the redox reversibility for these catalysts.

3.3. Selection of suitable Ce doping content for the steam reforming of ethane/propane

After reduction of CeO_2-doped Ni/Al_2O_3, the steam reforming of ethane/propane was performed at 900 °C. The feed was $C_2H_6/C_3H_8/H_2O$ in helium with the molar ratio of 0.65/0.35/3.0. Fig. 7 presents the steady state yield of H_2 production (%) for CeO_2-doped Ni/Al_2O_3 with various CeO_2 contents (0–20%) at 900 °C. It was found that 14% CeO_2 doping on Ni/Al_2O_3 presents the highest hydrogen production yield.

The post-reaction temperature-programmed oxidation (TPO) experiments were then carried out after a helium purge by introducing 10% oxygen in helium in order to determine the degree of carbon deposition on the surface of each sample. Table 3 presents the important physicochemical properties of the spent catalysts after exposure in the steam reforming conditions for 10 h. According to TPO, the amount of carbon formation decreased with increasing Ce content. This is due to the increasing of redox properties by doping more CeO_2, which can inhibit the formation of carbon species on Ni surface. However, as seen from Fig. 7, slight decrease in reforming rate was observed when the Ce doping contents were higher than 14%. This decreasing in reactivity could be due to the possible oxidised of Ni because the reducibility of the catalysts (with 16, 18, and 20% Ce doping) reduced after exposure in the steam reforming for 10 h, according to the TPR experiment. Therefore, 14% CeO_2 doping on Ni/Al_2O_3 is the optimum content, which provides the highest resistance toward carbon deposition and is enable to operate without the oxidised of Ni.

3.4. Reactivity toward steam reforming of ethane/propane

The steam reforming of C_2H_6/C_3H_8 over Ni/Al_2O_3 and 14%CeO_2 doped Ni/Al_2O_3 were studied at 900 °C. After reducing with 5% hydrogen for 6 h, the catalysts were heated up under helium flow to 900 °C. At the isothermal condition, $C_2H_6/C_3H_8/H_2O$ in helium with different $C_2H_6/C_3H_8/H_2O$ molar ratios of 0.65/0.35/1.0, 0.65/0.35/2.0, and 0.65/0.35/3.0 were introduced in order to compare the reforming rates. The variations in hydrogen production yield with time at 900 °C for different catalysts and different inlet $C_2H_6/C_3H_8/H_2O$ ratio are shown in Fig. 8. The significant deactivations were detected for Ni/Al_2O_3 catalyst in all conditions especially at high inlet $C_2H_6/C_3H_8/H_2O$ ratio, whereas considerable lower deactivations were detected for 14%CeO_2 doped Ni/Al_2O_3. Catalyst stabilities expressed as deactivation percentages are given in Table 4.

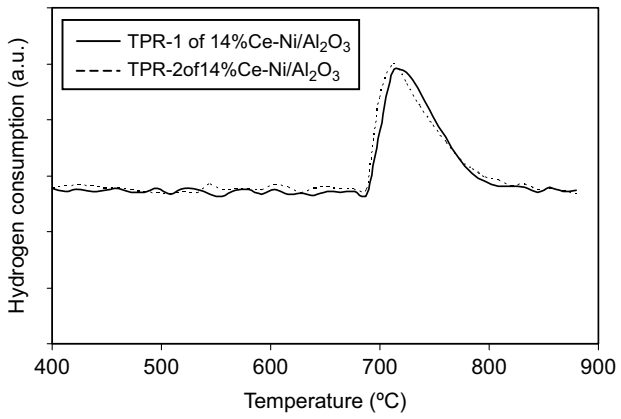

Fig. 6. Second time Temperature Programmed Reduction (TPR-2) of 14% CeO_2-doped Ni/Al_2O_3 compared to that of TPR-1.

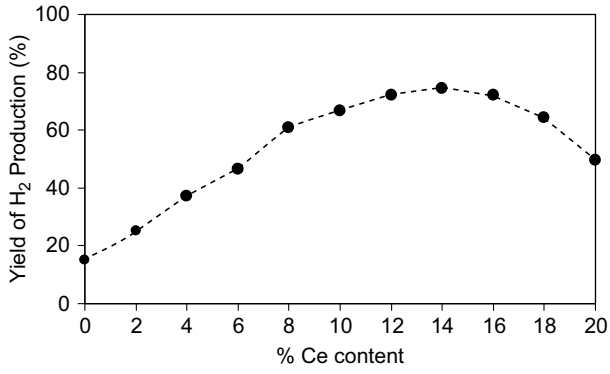

Fig. 7. Effect of Ce doping content on the yield of H_2 production (%) for steam reforming (900 °C, 2.6 kPa C_2H_6, 1.4 kPa C_3H_8, and 12 kPa H_2O).

Table 3
Yield of H_2 production (%), and physicochemical properties of the catalysts after exposure in steam reforming (2.6 kPa C_2H_6, 1.4 kPa C_3H_8, and 12 kPa H_2O) at 900 °C

Catalyst	Yield of H_2 production (%) at steady state	Ni and Ce load[a] (wt.%)	C formation[b] (monolayers)	BET surface ($m^2\ g^{-1}$)	Ni-red.[c] (Ni%)	Ni-disp.[d] (Ni%)
Ni/Al_2O_3	15.2	4.87/0.0	4.85	40.0	92.0	4.80
2%Ce-Ni/Al_2O_3	25.1	4.80/1.84	4.28	40.0	92.6	4.51
4%Ce-Ni/Al_2O_3	36.9	4.91/4.01	4.04	41.4	91.4	5.11
6%Ce-Ni/Al_2O_3	46.2	5.00/5.95	3.21	43.6	90.1	4.49
8%Ce-Ni/Al_2O_3	60.8	4.96/8.00	3.09	45.4	91.9	4.64
10%Ce-Ni/Al_2O_3	66.6	4.87/9.89	2.76	45.2	88.7	4.73
12%Ce-Ni/Al_2O_3	71.8	4.89/12.0	1.98	45.8	90.1	4.59
14%Ce-Ni/Al_2O_3	74.5	4.91/13.9	1.07	45.6	90.4	4.17
16%Ce-Ni/Al_2O_3	72.1	4.98/16.0	1.06	45.5	80.8	4.99
18%Ce-Ni/Al_2O_3	64.3	4.95/17.9	1.02	46.0	71.7	4.10
20%Ce-Ni/Al_2O_3	49.4	4.97/19.9	1.11	46.2	68.5	4.29

[a] Measured from X-ray fluorescence analysis.
[b] Calculated using CO and CO_2 yields from temperature-programmed oxidation (TPO) with 10% oxygen.
[c] Nickel reducibility (measured from temperature-programmed reduction (TPR) with 5%hydrogen).
[d] Nickel dispersion (measured from temperature-programmed desorption (TPD) after TPR).

After operated for 100 h, the steam reforming over 14%CeO_2 doped Ni/Al_2O_3 with inlet $C_2H_6/C_3H_8/H_2O$ of 0.65/0.35/3.0 showed the best activity. The influences of operating temperature and the inlet steam to ethane/propane ratio on the product selectivity were also studied by varying temperature from 700–900 °C and changing the inlet steam to carbon ratio from 1.0/1.0 to 5.0/1.0. As shown in Fig. 9, it was found that, at steady state, the main products from this reaction over 14%CeO_2 doped Ni/Al_2O_3 were H_2, CO, CO_2, and CH_4, with small amount of C_2H_4 depending on the operating temperature. For comparison, the conversions and the product selectivities at equilibrium level were calculated using AspenPlus10.2 simulation program, Fig. 10. Regarding the simulation, the conversions of C_2H_6 and C_3H_8 at equilibrium level are 100% in the range of temperature between 700 and 900 °C. The yields of hydrogen production at equilibrium are slightly higher than those achieved from the experiments, in addition, no C_2H_4 formation was observed at the equilibrium level in this range of temperature due to the complete reforming of this component to CH_4, CO, and CO_2.

Regarding the influence of inlet steam, hydrogen and carbon dioxide selectivity increased with increasing inlet steam concentration, whereas carbon monoxide selectivity decreased, Fig. 11. These are mainly due to the influence of water–gas shift reaction ($CO + H_2O \rightarrow CO_2 + H_2$). Moreover, the appearances of methane and ethylene in the system were found to decrease with increasing steam content, as these components were further reformed to CO, CO_2, and H_2 by the excess steam.

The post-reaction temperature-programmed oxidation (TPO) experiments were carried out after a helium purge by introducing of 10% oxygen in helium in order to determine whether the observed deactivation is due to the carbon formation. From the TPO results shown in Fig. 12, the huge peaks of carbon dioxide and carbon monoxide were observed for Ni/Al_2O_3, while smaller peaks of both components were detected for 14%CeO_2 doped Ni/Al_2O_3. The amount of carbon formations on the surface of these catalysts with different inlet $C_2H_6/C_3H_8/H_2O$ ratios were determined by measuring the CO and CO_2 yields from the TPO results. Using a value of 0.026 nm^2 for the area occupied by a carbon atom in a surface monolayer of the basal plane in graphite [38], the quantities of carbon deposited over Ni/Al_2O_3 were observed to be approximately 5.98, 5.41, and 4.85 monolayers, while those over 14%CeO_2 doped Ni/Al_2O_3 were 2.19, 1.48, and 1.07 monolayers for the inlet $C_2H_6/C_3H_8/H_2O$ ratios of 0.65/0.35/1.0, 0.65/0.35/2.0, and 0.65/0.35/3.0, respectively. The total amounts of carbon deposited were ensured by the calculation of carbon balance in the system. Regarding the calculations, for the inlet $C_2H_6/C_3H_8/H_2O$ ratios of 0.65/0.35/1.0, 0.65/0.35/2.0, and 0.65/0.35/3.0, the moles of carbon deposited per gram of 14%CeO_2 doped Ni/Al_2O_3 were 3.32, 2.33, and 1.68 mmol g^{-1}. By the same assumption for the area

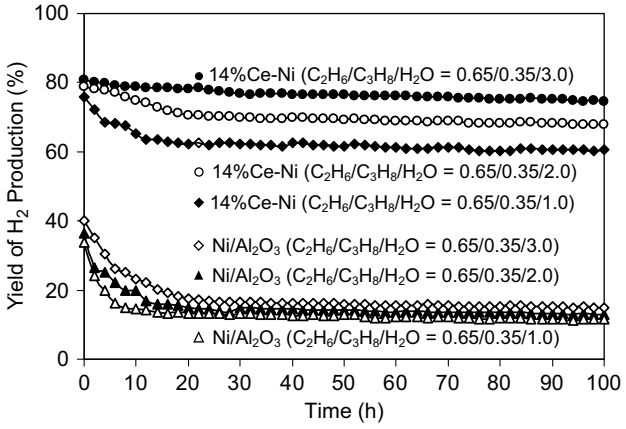

Fig. 8. Steam reforming of ethane/propane at 900 °C for several catalysts and various inlet $C_2H_6/C_3H_8/H_2O$ ratios.

Table 4
Yield of H_2 production (%), deactivation percentages, and physicochemical properties of the catalysts after exposure in steam reforming conditions (various inlet steam/carbon ratio) at 900 °C for 100 h

Catalyst	H_2O/C ratio	Yield of H_2 production (%) at steady state	Deactivation (%)	C formation[a] (monolayers)	BET surface (m^2 g^{-1})	Ni-red.[b] (Ni%)
Ni/Al_2O_3	1.0/1.0	11.5	65.8	5.98	40.0	91.9
	2.0/1.0	12.9	64.6	5.41	39.7	91.8
	3.0/1.0	15.1	62.5	4.85	40.0	92.0
14%Ce-Ni[c]	1.0/1.0	60.2	20.0	2.19	45.4	92.0
	2.0/1.0	67.8	13.6	1.48	45.1	91.8
	3.0/1.0	74.5	7.41	1.07	45.6	90.4

[a] Calculated using CO and CO_2 yields from temperature-programmed oxidation (TPO) with 10% oxygen.
[b] Nickel reducibility (measured from temperature-programmed reduction (TPR) with 5%hydrogen).
[c] CeO_2-doped Ni/Al_2O_3.

occupied by a carbon atom [38], these values are equal to 2.15, 1.51, and 1.09 monolayers, respectively, which are in good agreement with the values observed from the TPO method described above.

The results clearly indicated the strong resistance toward carbon formation for 14%CeO_2 doped Ni/Al_2O_3 compared to Ni/Al_2O_3. The BET measurements, as presented in Table 4, indicated that deactivations of 14%CeO_2 doped Ni/Al_2O_3 are also due to the slight sintering of CeO_2. The improvement of reforming reactivity and resistance toward carbon formation for CeO_2-doped Ni/Al_2O_3 could be mainly due to the redox property of ceria. During the reforming of C_2H_6/C_3H_8, the carbon formation could occur due to several reactions, the following reactions are the most probable reactions that could lead to carbon formation:

$$C_3H_8 \Leftrightarrow 4H_2 + 3C \quad (16)$$

$$C_2H_6 \Leftrightarrow 3H_2 + 2C \quad (17)$$

$$CH_4 \Leftrightarrow 2H_2 + C \quad (18)$$

$$C_2H_4 \Leftrightarrow 2H_2 + 2C \quad (19)$$

$$2CO \Leftrightarrow CO_2 + C \quad (20)$$

$$CO + H_2 \Leftrightarrow H_2O + C \quad (21)$$

$$CO_2 + 2H_2 \Leftrightarrow 2H_2O + C \quad (22)$$

where C is the carbonaceous deposits. At low temperature, Eqs. (21) and (22) are favorable, while Eqs. (16)–(19) are thermodynamically unflavored [42]. The Boudard reaction (Eq. (20)) and the decomposition of hydrocarbons (Eqs. (16)–(19)) are the major pathways for carbon formation at such a high temperature as they show the largest change in Gibbs energy [43]. According to the high temperature in this study, 900 °C, carbon formation would be formed via the decomposition of hydrocarbons and Boudard reactions. With the increase of steam to carbon ratio, the equilibrium of water-gas shift reaction moves forward and produces more CO_2 rather than CO. Therefore, high steam feed can avoid carbon deposition via the Boudouard reaction. However, significant amount of carbon remains detected on the surface of Ni/Al_2O_3 due to the decomposition of ethane, propane, ethylene, and methane (Eqs. (16)–(19)). By doping CeO_2 as the promoter, these reactions could be inhibited by the gas–solid reactions between hydrocarbons

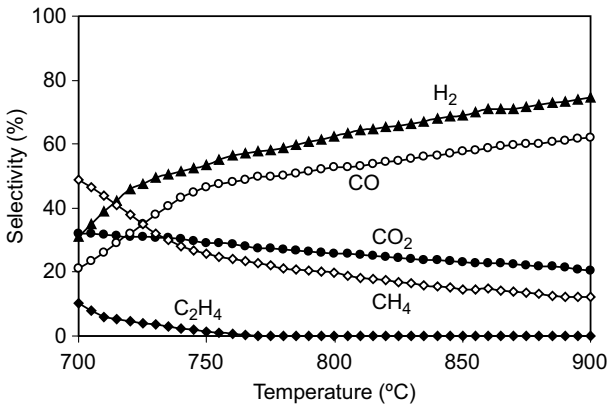

Fig. 9. Effect of reaction temperature on the selectivities of product elements (H_2, CO, CO_2, CH_4, and C_2H_4) from steam reforming over 14%CeO_2-doped Ni/Al_2O_3 (2.6 kPa C_2H_6, 1.4 kPa C_3H_8, and 12 kPa H_2O).

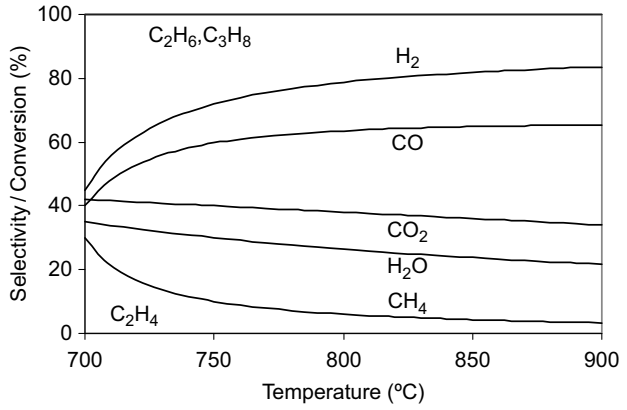

Fig. 10. Conversions of C_2H_6 and C_3H_8, and the selectivities of H_2, CO, CO_2, C_2H_4, and CH_4 at equilibrium level (Inlet conditions of 2.6 kPa C_2H_6, 1.4 kPa C_3H_8, and 12 kPa H_2O).

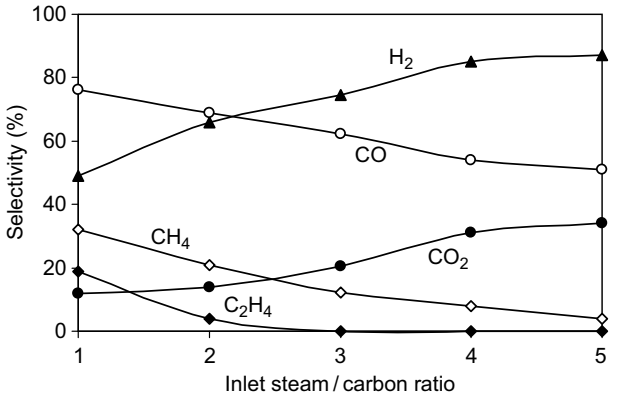

Fig. 11. Effect of inlet steam/carbon molar ratio on the selectivities of product elements (H_2, CO, CO_2, CH_4, and C_2H_4) from steam reforming over 14%CeO_2-doped Ni/Al2O_3 at 900 °C (2.6 kPa C_2H_6, 1.4 kPa C_3H_8, and 12 kPa H_2O).

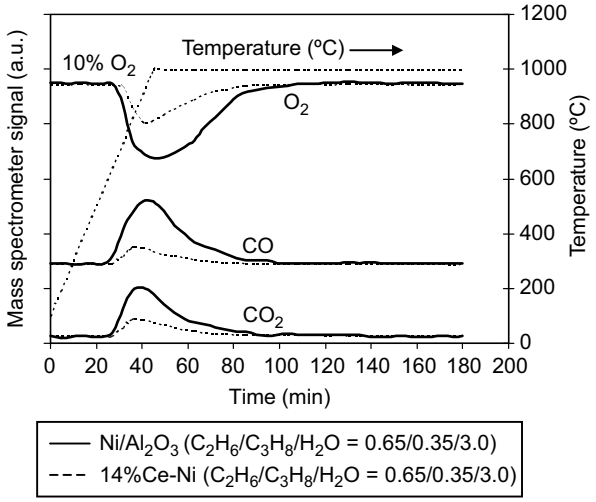

Fig. 12. Temperature Programmed Oxidation (TPO) of Ni/Al_2O_3 and 14%CeO_2-doped Ni/Al_2O_3 (10 kPa O_2) after exposure in steam reforming of ethane/propane (2.6 kPa C_2H_6, 1.4 kPa C_3H_8, and 12 kPa H_2O) for 100 h.

with the lattice oxygen (O_x) at CeO_2 surface forming hydrogen and carbon dioxide, which are thermodynamically unflavored to form carbon species.

Theoretically, the solid–gas reaction between CeO_2 and CH_4 produces synthesis gas, while the reduced ceria, CeO_{2-x}, can react with steam to produce H_2 [35–37]. In the present work, the solid–gas mechanism involves the reactions between hydrocarbons (C_2H_6, C_3H_8, CH_4, and C_2H_4) and/or an intermediate surface hydrocarbon species with the lattice oxygen (O_x) at CeO_2 surface, as illustrated schematically below.

$$C_3H_8 + 3S \Leftrightarrow 2(CH_3-S) + CH_2-S \quad (23)$$

$$C_2H_6 + 2S \Leftrightarrow 2(CH_3-S) \quad (24)$$

$$CH_4 + 2S \Leftrightarrow CH_3-S + H-S \quad (25)$$

$$C_2H_4 + 2S \Leftrightarrow 2(CH_2-S) \quad (26)$$

$$CH_3-S + S \Leftrightarrow CH_2-S + H-S \quad (27)$$

$$CH_2-S + S \Leftrightarrow CH-S + H-S \quad (28)$$

$$CH-S + S \Leftrightarrow C-S + H-S \quad (29)$$

$$C-S + O_x \Leftrightarrow CO + O_{x-1} + S \quad (30)$$

$$2H-S \Leftrightarrow H_2 + 2S \quad (31)$$

where *S* is the catalyst surface site. It can be considered to be a unique site, or the same site as the lattice oxygen (O_x) [40]. During the steam reforming, hydrocarbons are adsorbed on either a unique site (S) or the lattice oxygen (O_x), whereas H_2O can react with the reduced site of ceria, O_{x-1}. The steady state reforming rate is mainly due to the continuous supply of the oxygen source by H_2O.

$$H_2O + O_{x-1} \Leftrightarrow O_x + H_2 \quad (32)$$

It should be noted that the solid–gas reaction on the surface of ceria could also reduce the formation of carbon via Boudouard reaction, as carbon monoxide can adsorb and react with the lattice oxygen (O_x) on the surface of ceria forming carbon dioxide ($CO + O_x \Leftrightarrow O_{x-1} + CO_2$), which is less flavored to form carbon species at high temperature.

4. Conclusion

14%CeO_2-doped Ni/Al_2O_3 is a good candidate catalyst for the reforming of ethane and propane at SOFC temperature (900 °C) due to the high resistance toward the deactivation from carbon formation at high temperature. During reforming process, the gas–solid redox reactions on ceria surface take place simultaneously with the reforming reactions on the surface of Ni, and they reduce the degree of carbon deposition on catalyst surface from hydrocarbons decomposition and Boudard reactions. Regarding the TPR measurement, the redox properties increased with increasing Ce doping content. In addition, this oxygen storage property was proven to be reversible. However, it should also be noted that the doping of too high ceria content on the catalyst results in the oxidation of Ni, which could reduce the reforming reactivity.

In particular, at the temperature above 800 °C and the inlet steam/carbon ratio higher than 3.0, all ethylene formation in which occurs homogenously (non-catalytic) from the thermal cracking of ethane and propane was converted by the steam reforming over this catalyst. By increasing inlet steam content, hydrogen and carbon dioxide selectivities increased, whereas carbon monoxide selectivity decreased. Moreover, the conversions of methane and ethylene were found to increase with increasing steam content in the system.

Acknowledgements

The financial support from The Thailand Research Fund (TRF) throughout this project is gratefully acknowledged.

References

[1] W.L. Lundberg, S.E. Veyo, Conceptual design and performance analysis of a 300 MWel LNG-fuelled pressurised SOFC/Gas turbine power plant, in: Yokohawa, S.C. Singhal (Eds.), Proceeding of the 7th International Symposium Solid Oxide Fuel Cells VII, 2001, 78-87.
[2] Aguiar P, Chadwick D, Kershenbaum L. Chem. Eng. Sci. 2002;57: 1665.
[3] Aguiar P, Lapena-Rey N, Chadwick D, Kershenbaum L. Chemical Engineering Science 2001;56:652.
[4] Peters R, Dahl R, Kluttgen U, Palm C, Stolten D, Power J. Sources 2002;106:238.
[5] N. Laosiripojana, 6th European Solid Oxide Fuel Cell Forum, 28 June - 2 July 2004.
[6] Trovareli A, Leitenburg C, Dolcetti G. Chemtech 1997;32.
[7] Fornasiero P, Balducci G, Monte RD, Kaspar J, Sergo V, Gubitosa G, Ferrero A. M. Graziani. J. Catal. 1996;164:173.
[8] Miki T, Ogawa T, Haneda M, Kakuta N, Ueno A, Tateishi S, Matsuura S. M. Sato, J. Phys. Chem. 1990;94:339.
[9] Padeste C, Cant NW, Trimm L. Catal. Lett. 1993;18:305.
[10] Kacimi S, Barbier Jr. J, Taha R. D. Duperz, Catal. Lett. 1993;22:343.
[11] Zafiris GS, Gorte J. J. Catal. 1993;143:86.
[12] Zafiris GS, Gorte J. J. Catal. 1993;139:561.
[13] Imamura S, Shono M, Okamoto N, Hamada R. S. Ishida, Appl. Catal. A 1996;142:279.
[14] Fan L. K. Fujimoto. J. Catal. 1997;172:238.
[15] Pijolat M, Prin M. M. Soustelle. J. Chem. Soc., Faraday Trans. 1995; 91:3941.
[16] Imamura S, Higashihara T, Saito Y, Aritani H, Kanai H, Matsumura Y. N. Tsuda, Catal. Today 1999;50:369.
[17] Imamura S, Denpo K, Utani K, Matsumura Y. H. Kanai, React. Kinet. Catal. Lett. 1999;67:163.
[18] Imamura S, Denpo K, Kanai K, Yamane H, Saito Y, Utani K. Y. Matsumura, Sekiyu Gakkaishi 2001;44:293.
[19] Imamura S, Yamane H, Kanai H, Shibuta T, Utani K. K. Hamada, J. Jpn. Petrol. Inst. 2002;45:187.
[20] Imamura S, Taniguchi Y, Ikeda Y, Hosokawa S, Kanai H. H. Ando, React. Kinet. Catal. Lett. 2002;76:201.
[21] Roh HS, Jun KW, Dong WS, Chang JS, Park SE, Joe YI. J. Mol. Catal. A 2002;181:137–42.
[22] Miao Q, Xiong G, Sheng S, Cui W, Xu L. Guo. Appl. Catal. A 1987; 154:17–27.
[23] Lemonidou AA, Goula MA, Vasalos IA. Catal. Today 1987;46: 175–83.
[24] Dong WS, Roh HS, Jun KW, Park SE, Oh YS. Appl. Catal. A 2002; 226:63–72.
[25] Mamak M, Coombs N, Ozin G. Adv. Mater. 2000;12:198–202.
[26] Mamak M, Coombs N, Ozin G. J. Am. Chem. Soc. 2000;122:8932.
[27] Mamak M, Coombs N, Ozin GA. Chem. Mater. 2001;13:3564.
[28] Bera P, Mitra S, Sampath S, Hegde MS. Chem. Commun. 2001;927.
[29] Martinez-Arias A, Coronado JM, Cataluna R, Conesa JC, Soria JC. J. Phys. Chem. B 1998;102:4357.
[30] Skarmoutsos D, Tietz F, Nikolopoulos P. Fuel Cells 2001;1:243.
[31] Takeguchi T, Furukawa SN, Inoue M. J. Catal. 2001;202:14.
[32] Sfeir J, Philippe PA, Moseki P, Xanthopoulos N, Vasquez R, Hans JM, Jan VH, Thampi KR. J. Catal. 2001;202:229.
[33] Kiratzis N, Holtappels P, Hatchwell CE, Mogensen M, Irvine JTS. Fuel Cells 2001;1:211.
[34] Roh HS, Dong WS, Jun KW, Park SE. Chem. Lett. 2001;88.
[35] Otsuka K, Ushiyama T. I. Yamanaka, Chemistry Letters 1993;1517.
[36] Otsuka K, Hatano M. A. Morikawa, J. Catalysis 1983;79:493.
[37] Otsuka K, Hatano M. A. Morikawa, Inorganica Chimica Acta 1985; 109:193.
[38] Ramírez-Cabrera E, Atkinson A. D. Chadwick, Applied Catalysis B 2004;47:127–31.
[39] Ramírez-Cabrera E, Laosiripojana N, Atkinson A. D. Chadwick, Catalysis Today 2003;78:433–8.
[40] N. Laosiripojana 2003, Reaction engineering of indirect internal steam reforming of methane for application in solid oxide fuel cells. Ph.D. Thesis, University of London, England.
[41] M.V. Twigg, Catalyst Handbook, 2nd Edition, Wolfe Publishing, London, (1989).
[42] Lwin Y, Daud WRW, Mohamad AB. Z. Yaakob, Int. J. Hydrogen Energy 2000;25(1):47–53.
[43] Amor JN. Appl. Catal. A 1999;176:159–76.

N. Laosiripojana and S. Assabumrungrat

"Hydrogen production from the steam and autothermal reforming of LPG over high surface area ceria at SOFC temperature"

Journal of Power Sources, In Press

(IF-2004 = 2.513)

Available online at www.sciencedirect.com
SCIENCE DIRECT®
Journal of Power Sources xxx (2005) xxx–xxx
JOURNAL OF POWER SOURCES
www.elsevier.com/locate/jpowsour

Hydrogen production from steam and autothermal reforming of LPG over high surface area ceria

N. Laosiripojana [a,*], S. Assabumrungrat [b]

[a] *The Joint Graduate School of Energy and Environment, King Mongkut's University of Technology Thonburi, Bangkok 10140, Thailand*
[b] *Center of Excellence in Catalysis and Catalytic Reaction Engineering, Department of Chemical Engineering, Faculty of Engineering, Chulalongkorn University, Bangkok 10330, Thailand*

Received 22 September 2005; received in revised form 18 October 2005; accepted 18 October 2005

Abstract

Steam and autothermal reforming reactions of LPG (propane/butane) over high surface area CeO_2 (CeO_2 (HSA)) synthesized by a surfactant-assisted approach were studied under solid oxide fuel cell (SOFC) operating conditions. The catalyst provides significantly higher reforming reactivity and excellent resistance toward carbon deposition compared to the conventional Ni/Al_2O_3. These benefits of CeO_2 are due to the redox property of this material. During the reforming process, the gas–solid reactions between the hydrocarbons present in the system (i.e. C_4H_{10}, C_3H_8, C_2H_6, C_2H_4, and CH_4) and the lattice oxygen (O_O^x) take place on the ceria surface. The reactions of these adsorbed surface hydrocarbons with the lattice oxygen ($C_nH_m + O_O^x \rightarrow nCO + m/2(H_2) + V_O^{\bullet\bullet} + 2e'$) can produce synthesis gas (CO and H_2) and also prevent the formation of carbon species from hydrocarbons decomposition reactions ($C_nH_m \Leftrightarrow nC + 2mH_2$). Afterwards, the lattice oxygen (O_O^x) can be regenerated by reaction with the steam present in the system ($H_2O + V_O^{\bullet\bullet} + 2e' \Leftrightarrow O_O^x + H_2$). It should be noted that $V_O^{\bullet\bullet}$ denotes as an oxygen vacancy with an effective charge 2^+.

At 900 °C, the main products from steam reforming over CeO_2 (HSA) were H_2, CO, CO_2, and CH_4 with a small amount of C_2H_4. The addition of oxygen in autothermal reforming was found to reduce the degree of carbon deposition and improve product selectivities by completely eliminating C_2H_4 formation. The major consideration in the autothermal reforming operation is the O_2/LPG (O/C molar ratio) ratio, as the presence of a too high oxygen concentration could oxidize the hydrogen and carbon monoxide produced from the steam reforming. A suitable O/C molar ratio for autothermal reforming of CeO_2 (HSA) was 0.6.

Keywords: LPG; Steam reforming; Autothermal reforming; Ceria; Solid oxide fuel cell

1. Introduction

A fuel cell is an energy conversion device that produces electrical energy with greater conversion efficiency and lower pollutant emissions than combustion processes. Among the various types of fuel cells, the solid oxide fuel cell (SOFC) has attracted considerable interest as it offers the widest range of applications, flexibility in the choice of fuel, and high system efficiency. The waste heat for SOFC can also be utilized in co-generation applications and bottoming cycles to improve the overall system efficiency. Moreover, unlike low-temperature fuel cells, the SOFC anode is not affected by carbon monoxide poisoning. Although, hydrogen is the major fuel for a SOFC, the use of other fuels such as methane, methanol, ethanol, liquefied petroleum gas (LPG), gasoline and other oil derivatives are also possible via internal or in-stack reforming. Since an SOFC is operated at such a high temperature, these hydrocarbons can be internally reformed producing a H_2/CO rich gas, which is eventually used to generate the electrical energy and heat. This operation, called indirect internal reforming (IIR-SOFC), is expected to simplify the overall SOFC system design [1].

Among the above hydrocarbon fuels, liquefied petroleum gas (LPG) is a commercial gas that is easily transported and stored on-site. This gas was proposed to be an attractive fuel for SOFC systems in remote areas where pipeline natural gas is not available [2]. LPG can also be used for auxiliary power units (APU) based on SOFC systems. Typically, the main components of

* Corresponding author. Tel.: +66 2 8729014; fax: +66 2 8726736.
E-mail address: navadol_l@jgsee.kmutt.ac.th (N. Laosiripojana).

0378-7753/$ – see front matter © 2005 Elsevier B.V. All rights reserved.
doi:10.1016/j.jpowsour.2005.10.058

LPG are propane and butane. According to the Australian LPG Association, the composition of LPG in Australia ranges from pure propane to a 40:60 mixture of propane and butane [2]. The steam reforming process has widely been used to produce hydrogen from LPG. The main products from the steam reforming of LPG are hydrogen, carbon monoxide, and carbon dioxide, however, the formation of ethane, ethylene, and methane are usually observed due to the decomposition of LPG and methanation reactions. The major difficulty in reforming LPG is the degradation of the reforming catalyst due to the possible carbon deposition from the decomposition of hydrocarbons, particularly at high temperature. Previously, steam reforming of LPG has been studied by a few researchers [2–8], and most of them have investigated the reforming of LPG over noble metal catalysts (e.g. Rh, Ru, and Pt) on oxide supports. Recupero et al. [8] reported that Pt/CeO_2 provides high reforming reactivity with low carbon formation. Suzuki et al. [3] found that Ru/CeO_2-Al_2O_3 can reform LPG with a low inlet steam requirement at 450 °C. Adding oxygen together with LPG and steam as an autothermal reforming process was reported to provide great benefits in terms of catalyst stability and low coke formation [4,5], however, the yield of hydrogen production could be reduced due to the oxidation of hydrogen by oxygen added. The attractive benefit of this operation is that the exothermic heat from the partial oxidation can directly supply the energy required for the endothermic steam reforming reaction, and so it is considered to be thermally self-sustaining process.

This work is aimed at the development of a catalyst for steam and autothermal reforming of LPG, which provides high stability and activity at a high temperature (700–900 °C) for later application in an IIR-SOFC. Although the precious metals such as Pt, Rh and Ru have been reported by several researchers to provide high activity for the reforming reactions and excellent resistant to carbon formation [9,10], the current prices of these metals are too high for commercial usage, and the availability of some precious metals such as ruthenium was too low to have a major impact on the total reforming catalyst market [11]. In view of these economical considerations, an alternative catalyst was developed and studied instead. Cerium oxide or ceria has been reported to be a catalyst in a wide variety of reactions involving oxidation or partial oxidation of hydrocarbons (e.g. automotive catalysis). A high oxygen mobility (redox property) [12], high oxygen storage capacity [13–18], strong interaction with the supported metal (strong metal–support interaction) [19] and a modifiable capability [20] render this material very interesting for catalysis. It has widely been reported, regarding the above properties, that ceria can promote the action of various metals in the reactions in which hydrogen is involved as a reactant or product [21–25]. According to the catalytic steam reforming reaction, ceria-based materials have been reported by several researchers to be promising supports among α-Al_2O_3 [26], γ-Al_2O_3 and γ-Al_2O_3 with alkali metal oxide and rare earth metal oxide [27], and $CaAl_2O_4$ [26–29]. One of the most promising ceria-based supports for the reforming reactions appeared to be Ce-ZrO_2, where the metal can be Ni, Pt or Pd [30–39]. Recently, a high resistance toward carbon deposition over ceria has been observed [40].

Importantly, CeO_2 has been reported to have reactivity toward methane decomposition at a high temperature (800–1000 °C) [41,42]. It was demonstrated that the gas–solid reaction between CeO_2 and CH_4 produces H_2 and CO, according to Eq. (1). Moreover, the reactions of the reduced ceria (CeO_{2-n}) with carbon dioxide and steam produce more CO and H_2 and regenerate the CeO_2 surface, Eqs. (2) and (3) [43–45]:

$$CH_4 + O_O{}^x = 2H_2 + CO + V_O{}^{\bullet\bullet} + 2e' \quad (1)$$

$$V_O{}^{\bullet\bullet} + 2e' + CO_2 = O_O{}^x + CO \quad (2)$$

$$V_O{}^{\bullet\bullet} + 2e' + H_2O = O_O{}^x + H_2 \quad (3)$$

$V_O{}^{\bullet\bullet}$ denotes an oxygen vacancy with an effective charge 2^+, $O_O{}^x$ is lattice oxygen, e′ is an electron which can either be more or less localized on a cerium ion or delocalized in a conduction band [46].

The major limitation for CeO_2 in high temperature applications is its low specific surface area due to the significant size reduction on thermal sintering [42] and, consequently, the reforming reactivity over CeO_2 was much lower than the conventional metallic catalysts [42]. It was reported that the methane conversion from CeO_2 after exposure in methane steam reforming conditions at 900 °C for 10 h was less than 10%. In addition, the corresponding post-reaction specific surface area for this material after exposure in methane steam reforming conditions was 1.9 $m^2\,g^{-1}$, and the observed size reduction percentage was 23% [42]. Therefore, the use of high surface area ceria (CeO_2 (HSA)) would be a good procedure to improve its catalytic performance at high operating temperatures. Several methods have recently been described for the preparation of a CeO_2 (HSA) solid solution. Among these methods, the surfactant-assisted approach was employed to prepare high surface area CeO_2 with improved textural, structural, and chemical properties [47]. Our previous publication [48] reported the achievement of CeO_2 with a high surface area and good stability after thermal treatment by this preparation method. Regarding the surfactant-assisted method, CeO_2 (HSA) is prepared by reacting a cationic surfactant with a hydrous oxide produced by co-precipitation under basic conditions. At a high pH value, conducting the precipitation of hydrous oxide in the presence of a cationic surfactant allows the cation exchange process between H^+ and the surfactant, resulting in a developed pore structure with an increase in surface area [47]. The achievement of high thermal stability for CeO_2 (HSA) is due to the incorporation of surfactants during preparation, which can reduce the interfacial energy and eventually decrease the surface tension of water contained in the pores. This could reduce the shrinkage and collapse of the catalyst during heating, which consequently helps the catalyst maintain a high surface area after calcination [47].

In the present work, the stability and activity toward steam reforming of LPG over high surface area CeO_2 (CeO_2 (HSA)) was studied and compared to those over the conventional low surface area CeO_2 (CeO_2 (LSA)), and also conventional Ni/Al_2O_3. The resistance towards carbon formation and the influence of the inlet H_2O/LPG molar ratio and temperature on product selectivities over these catalysts were determined. In

Table 1
Specific surface area of CeO_2 (HSA and LSA) after drying and calcinations at different temperatures

Catalyst	BET surface area ($m^2\ g^{-1}$) after drying or calcination at						
	100 °C	200 °C	400 °C	600 °C	800 °C	900 °C	1000 °C
CeO_2 (LSA)[a]	55	49	36	21	15	11	8.5
CeO_2 (HSA)[b]	105	97	69	48	35	29	24

[a] Conventional low surface area CeO_2 prepared by the precipitation method.
[b] Nanocomposite high surface area CeO_2 prepared by the surfactant-assisted approach.

addition, autothermal reforming of LPG was also investigated by adding oxygen at the inlet feed. The improvement in the resistance to carbon deposition by the presence of oxygen and a suitable inlet O_2/LPG molar ratio were determined. It should be noted that the contents of desulpherized LPG used in this work are 60% C_3H_8 and 40% C_4H_{10} (based on the compositions of LPG from PTT Company (Thailand)).

2. Experimental

2.1. Catalyst preparation and characterization

Conventional CeO_2 (CeO_2 (LSA)) was prepared by the precipitation of cerium chloride ($CeCl_3 \cdot 7H_2O$) from Aldrich. The starting solution was prepared by mixing 0.1 M of this metal salt solution with 0.4 M of ammonia in a 2:1 volumetric ratio. This solution was stirred by magnetic stirring (100 rpm) for 3 h, then sealed and placed in a thermostatic bath maintained at 90 °C for 3 days. The precipitate was filtered and washed with deionised water and acetone to remove the free surfactant. It was dried overnight in an oven at 110 °C, and then calcined in air at 1000 °C for 6 h.

High surface area CeO_2 (CeO_2 (HSA)) was prepared by adding an aqueous solution of the appropriate cationic surfactant, 0.1 M cetyltrimethylammonium bromide solution from Aldrich, to a 0.1 M cerium chloride. The molar ratio of ([Ce])/[cetyltrimethylammonium bromide] was kept constant at 0.8. The mixture was stirred and then aqueous ammonia was slowly added with vigorous stirring until the pH was 11.5 [47]. The mixture was continually stirred for 3 h, then sealed and placed in the thermostatic bath maintained at 90 °C for 3 days. After that, the mixture was cooled and the resulting precipitate was filtered and washed repeatedly with water and acetone. The filtered powder was then treated under the same procedures as CeO_2 (LSA). BET measurements of CeO_2 (both LSA and HSA) were carried out at different calcination temperatures in order to determine the loss of specific surface area due to the thermal sintering. As presented in Table 1, after drying, surface areas of 82 and 55 $m^2\ g^{-1}$ were observed for CeO_2 (HSA) and conventional CeO_2, respectively, and as expected, the surface area dramatically decreased at high calcination temperatures. However, the value for CeO_2 (HSA) is still appreciable after calcination at 1000 °C and it is almost three times that of the conventional CeO_2.

The redox properties and redox reversibilities of these synthesized CeO_2 (both LSA and HSA) were then determined by the temperature-programmed reduction (TPR) and temperature-programmed oxidation (TPO). TPR and TPO experiments were conducted in the presence of 5% H_2/Ar and 5% O_2/He, respectively, while the temperature of the system increased from room temperature to 900 °C for both experiments.

For comparison, Ni/Al_2O_3 (5 wt.% Ni) was also prepared by impregnating α-Al_2O_3 (from Aldrich) with $NiCl_3$. After stirring, the solution was dried and calcined at 1000 °C for 6 h. The catalysts were also reduced with 10%H_2/Ar at 500 °C for 6 h before use. After reduction, the catalysts were characterized by several physicochemical methods. The weight content of Ni in Ni/Al_2O_3 was determined by X-ray fluorescence (XRF) analysis. The reducibility and dispersion percentages of nickel were measured from temperature-programmed reduction (TPR) with 5% H_2 in helium and temperature-programmed desorption (TPD), respectively. The catalyst specific surface areas were obtained from BET measurement. All physicochemical properties of the synthesized Ni/Al_2O_3 are presented in Table 2.

2.2. Apparatus and procedures

An experimental reactor system was constructed as shown in Fig. 1. The feed gases including the components of interest (e.g. LPG, steam from the evaporator, and oxygen) and the carrier gas (helium) were introduced to the reaction section, in which a 10 mm diameter quartz reactor was mounted vertically inside a furnace. The reactivities of the catalyst toward steam reforming of LPG were determined by loading the catalyst in this quartz reactor, which was packed with a small amount of quartz wool to prevent the catalyst from moving. The inlet LPG concentration was kept constant at 5 kPa (C_3H_8/C_4H_{10} ratio of 0.6/0.4), while the inlet steam concentrations were varied depending on the inlet H_2O/LPG molar ratio requirement for each experiment (3.0, 4.0, 5.0, 6.0, and 7.0). Regarding the results in our previous publications [48], to avoid any limitations by intraparticle diffusion, the weight of catalyst was always kept constant at 50 mg, while the total gas flow was 100 $cm^3\ min^{-1}$ with a constant residence time of 5×10^{-4} g min cm^{-3} in all experiments. A Type-K

Table 2
Physicochemical properties of synthesized Ni/Al_2O_3 after reduction

Catalyst	Ni-load[a] (wt.%)	BET surface area ($m^2\ g^{-1}$)	Ni-reducibility[b] (Ni%)	Ni-dispersion[c] (Ni%)
Ni/Al_2O_3	4.9	40	92.1	4.87

[a] Measured from X-ray fluorescence analysis.
[b] Measured from temperature-programmed reduction (TPR) with 5% hydrogen.
[c] Measured from temperature-programmed desorption (TPD) of hydrogen after TPR measurement.

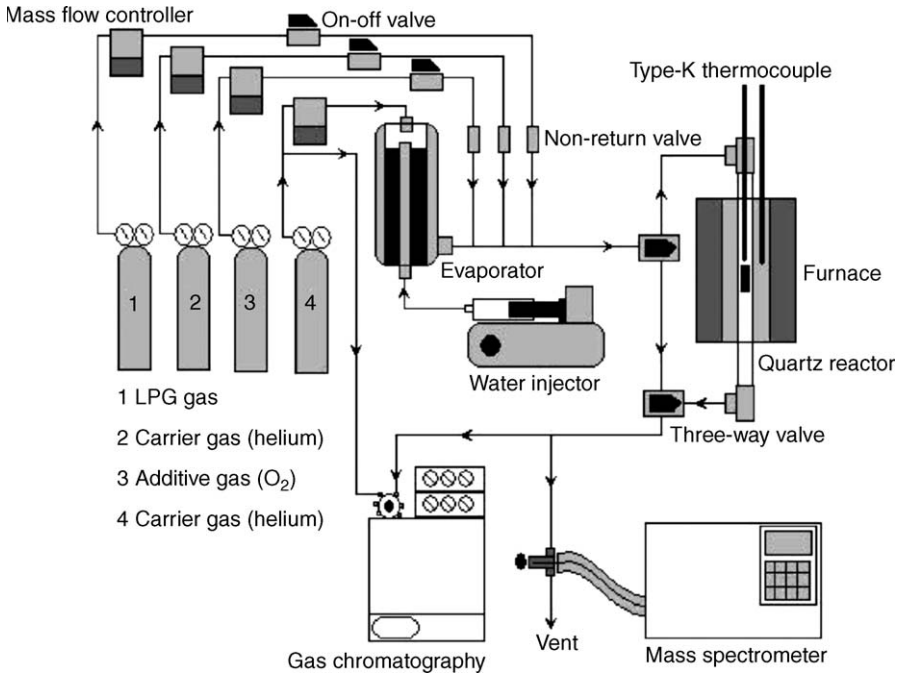

Fig. 1. Schematic diagram of the experimental set-up.

thermocouple was placed in the annular space between the reactor and the furnace. This thermocouple was mounted on the tubular reactor in close contact with the catalyst bed to minimize the temperature difference between the catalyst bed and the thermocouple. Another Type-K thermocouple was inserted in the middle of the quartz tube in order to re-check the possible temperature gradient, especially when O_2 was added along with LPG and H_2O in autothermal reforming. The recorded values showed that the maximum temperature fluctuation during the reaction was always $\pm 0.75\,^{\circ}C$ or less from the temperature specified for the reaction.

After the reactions, the exit gas mixture was transferred via trace-heated lines to the analysis section, which consisted of a Porapak Q column Shimadzu 14B gas chromatograph (GC) and a mass spectrometer (MS). Gas chromatography was used in order to investigate the steady state condition experiments, whereas the mass spectrometer, in which the sampling of the exit gas was done by a quartz capillary and differential pumping, was used in the transient carbon formation experiment. In order to study the formation of carbon species on catalyst surface, temperature-programmed oxidation (TPO) was applied by introducing 5% oxygen in helium into the system, after being purged with helium. The operating temperature was increased from room temperature to 900 °C at a rate of 10 °C min^{-1}. The calibration of CO and CO_2 were performed by injecting a known amount of the gases from a sample loop into an injection valve in the bypass line. The response factors were obtained by dividing the number of moles for each component over the respective areas under peaks. The amount of carbon formed on the surface of catalysts was determined by measuring the CO and CO_2 yields from the TPO results (using Microcal Origin Software) assuming a value of 0.026 nm^2 for the area occupied by a carbon atom in a surface monolayer of the basal plane in graphite [49]. In addition to the TPO method, the amount of carbon deposition was confirmed by the calculation of carbon balance in the system. The amount of carbon deposited on the surface of catalyst would theoretically be equal to the difference between the inlet carbon containing components (C_3H_8 and C_4H_{10}) and the outlet carbon containing components (CO, CO_2, CH_4, C_2H_6, and C_2H_4). The amount of carbon deposited per gram of catalyst is given by the following equation:

$$C_{\text{deposition}} = \frac{\text{mole}_{\text{carbon(in)}} - \text{mole}_{\text{carbon(out)}}}{m_{\text{catalyst}}} \tag{4}$$

The steam reforming reactivity was defined in terms of the conversions and selectivities. Hydrocarbon conversions (propane and butane) denoted as $X_{\text{hydrocarbon}}$, and the products selectivity (hydrogen, carbon monoxide, carbon dioxide, methane, and ethylene), denoted as S_{product}, are calculated according to Eqs. (5)–(12):

$$X_{\text{butane}} = \frac{100(\%\text{butane}_{\text{in}} - \%\text{butane}_{\text{out}})}{\%\text{butane}_{\text{in}}} \tag{5}$$

$$X_{\text{propane}} = \frac{100(\%\text{propane}_{\text{in}} - \%\text{propane}_{\text{out}})}{\%\text{propane}_{\text{in}}} \tag{6}$$

$$S_{H_2} = \frac{100(\%H_2)}{3(\%\text{butane}_{\text{in}} - \%\text{butane}_{\text{out}}) + 4(\%\text{propane}_{\text{in}} - \%\text{propane}_{\text{out}}) + (\%H_2O_{\text{in}} - \%H_2O_{\text{out}})} \tag{7}$$

$$S_{\text{CO}} = \frac{100(\%\text{CO})}{2(\%\text{butane}_{\text{in}} - \%\text{butane}_{\text{out}}) + 3(\%\text{propane}_{\text{in}} - \%\text{propane}_{\text{out}})} \tag{8}$$

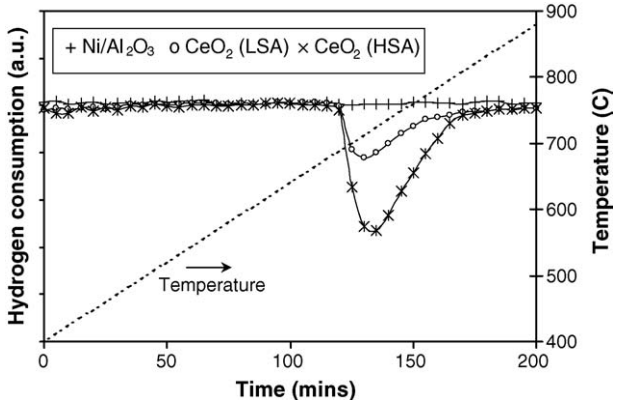

Fig. 2. Temperature-programmed reduction (TPR-1) of fresh catalysts after reduction.

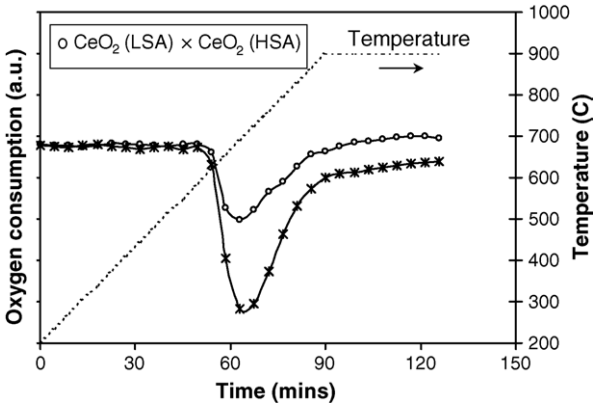

Fig. 3. Temperature-programmed oxidation (TPO) of CeO_2 (HSA and LSA) after TPR-1.

$$S_{CO_2} = \frac{100(\%CO_2)}{2(\%\text{butane}_{in} - \%\text{butane}_{out}) + 3(\%\text{propane}_{in} - \%\text{propane}_{out})} \quad (9)$$

$$S_{CH_4} = \frac{100(\%CH_4)}{2(\%\text{butane}_{in} - \%\text{butane}_{out}) + 3(\%\text{propane}_{in} - \%\text{propane}_{out})} \quad (10)$$

$$S_{C_2H_6} = \frac{100(\%C_2H_6)}{(\%\text{butane}_{in} - \%\text{butane}_{out}) + 1.5(\%\text{propane}_{in} - \%\text{propane}_{out})} \quad (11)$$

$$S_{C_2H_4} = \frac{100(\%C_2H_4)}{(\%\text{butane}_{in} - \%\text{butane}_{out}) + 1.5(\%\text{propane}_{in} - \%\text{propane}_{out})} \quad (12)$$

3. Results

3.1. Redox property and redox reversibility of the synthesized CeO_2

The oxygen storage capacities (OSC) and the redox properties of CeO_2 (both LSA and HSA) were investigated using temperature-programmed reduction (TPR-1) which was performed by heating the reduced catalysts up to 900 °C in 5%H_2 in argon. A test over Ni/Al_2O_3 was also performed for comparison. As shown in Fig. 2, hydrogen uptake was detected from both types of CeO_2 at the temperature above 650 °C. The amount of hydrogen uptake over CeO_2 (HSA) is significantly higher than that over CeO_2 (LSA), suggesting that the OSC and the redox properties strongly depend on the specific surface area of CeO_2. In contrast, no hydrogen consumption was observed from the TPR over Ni/Al_2O_3, indicating the absence of redox properties for this catalyst. The benefit of having a redox property in the reforming of LPG will be presented in Section 4. After being purged with helium, the redox reversibility for each type of CeO_2 was then determined by conducting temperature-programmed oxidation (TPO) following by a second temperature-programmed reduction (TPR-2). The TPO was carried out by heating the catalyst up to 900 °C in 5%O_2 in helium; the amount of oxygen chemisorbed was then measured, as shown in Fig. 3 and Table 3. Regarding the TPR-2 results as shown in Fig. 4 and Table 3, the amount of hydrogen uptake for CeO_2 (both LSA and HSA) were approximately similar to those from TPR-1, indicating the redox reversibility of these synthesized versions of CeO_2.

3.2. Homogenous (non-catalytic) reactions

Before studying the catalyst performance, homogeneous (non-catalytic) steam reforming of LPG was investigated. A

Table 3
Results of TPR(1), TPO, TPR(2) analyses of CeO_2 (both HSA and LSA)

Catalyst	Total H_2 uptake from TPR(1)[a] (μmol g_{cat}^{-1})	Total O_2 uptake from TPO[b] (μmol g_{cat}^{-1})	Total H_2 uptake from TPR(2)[c] (μmol g_{cat}^{-1})
CeO_2 (HSA)	2159	1044	2155
CeO_2 (LSA)	1784	867	1781

[a] Temperature-programmed reduction of the reduced catalysts (relative standard deviation = ±3%).
[b] Temperature-programmed oxidation after TPR(1) (relative standard deviation = ±1%).
[c] Re-temperature-programmed reduction after TPO (relative standard deviation = ±2%).

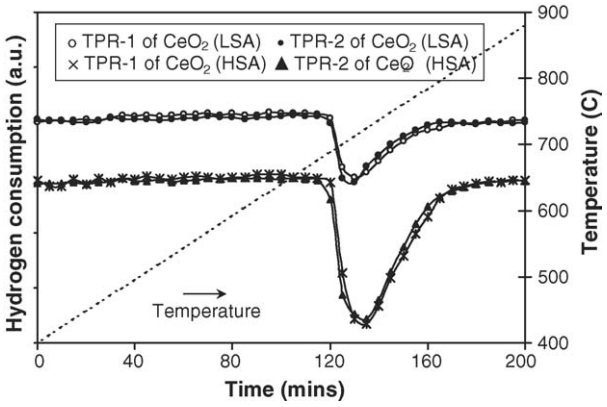

Fig. 4. Second time temperature-programmed reduction (TPR-2) of CeO_2 (HSA and LSA) compared to that of TPR-1.

feed stream consisting a LPG/H_2O at a molar ratio of 1.0/5.0 was introduced into the system, while the temperature increased from ambient to 900 °C. Both propane and butane were converted to methane, ethane, ethylene, and hydrogen at the temperature above 700 °C, as shown in Fig. 5. A significant amount of carbon was also detected in the blank reactor after exposure for 10 h. These components were formed via the decomposition of butane and propane as shown in the equations below.

$$C_4H_{10} \rightarrow C_2H_6 + C_2H_4 \quad (13)$$

$$C_3H_8 \rightarrow 3/2(C_2H_4) + H_2 \quad (14)$$

$$C_2H_6 \rightarrow C_2H_4 + H_2 \quad (15)$$

$$C_2H_4 \Leftrightarrow CH_4 + C \quad (16)$$

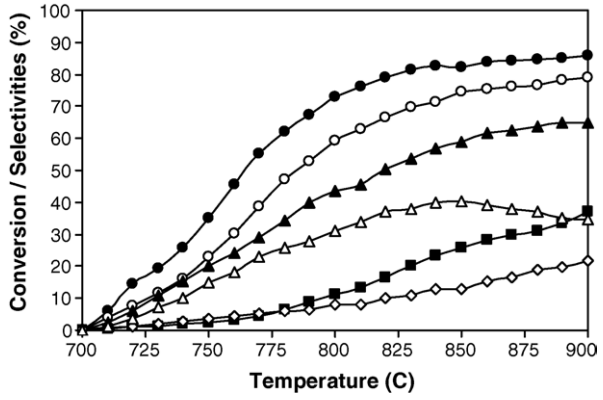

Fig. 5. Homogeneous (in the absence of a catalyst) reactivity of LPG in the presence of steam (with the inlet H_2O/LPG of 5.0) (C_4H_{10} (●), C_3H_8 (◯), C_2H_4 (▲), C_2H_6 (△), CH_4 (■), and H_2 (◇)).

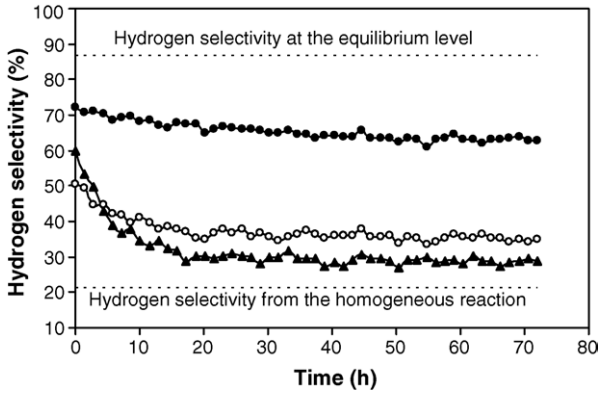

Fig. 6. Hydrogen selectivity from the steam reforming of LPG over CeO_2 (HSA) (●), CeO_2 (LSA) (◯), and Ni/Al_2O_3 (▲) at 900 °C compared to that from the homogeneous reaction and at the equilibrium level.

There was no change in the steam concentration, and no carbon monoxide and carbon dioxide were produced in the system, indicating that the non-homogenous reforming reaction between steam and hydrocarbons did not take place at this range of conditions studied.

3.3. Stability and activity toward the steam reforming of LPG

The synthesized CeO_2 (HSA), CeO_2 (LSA), and Ni/Al_2O_3 were studied in the steam reforming of C_3H_8/C_4H_{10} at 900 °C. The feed was H_2O/LPG in helium with the molar ratio of 5.0 (H_2O/C ratio of 1.45). The reforming rate was measured as a function of time in order to determine the stability and the deactivation rate. The variations in the hydrogen selectivity with time at 900 °C are shown in Fig. 6. Significant deactivation was detected with Ni/Al_2O_3 catalyst, whereas much lower deactivations were observed for CeO_2 (HSA). Catalyst stabilities expressed as deactivation percentages are given in Table 4. It should be noted that, in order to determine whether the observed deactivation is due to the carbon formation, the post-reaction temperature-programmed oxidation (TPO) experiments were carried out.

From the TPO results shown in Fig. 7, a huge amount of carbon deposition was observed on Ni/Al_2O_3, whereas significantly less carbon formation was detected on CeO_2 (LSA) and CeO_2 (HSA) after exposure to the steam reforming conditions for 72 h. The amount of carbon formation (monolayer) on the surface of catalysts was determined by measuring the CO and CO_2 yields (using Microcal Origin Software). Using a value of 0.026 nm^2 for the area occupied by a carbon atom in a surface mono-

Table 4
Physicochemical properties of catalysts after exposure in the steam reforming of LPG at 900 °C for 72 h.

Catalyst	Deactivation (%)	C formation (monolayers)	BET surface (m^2 g^{-1})	Ni-load (wt.%)	Ni-red. (Ni%)	Ni-disp. (Ni%)
CeO_2 (HSA)	12.8	0.51[a] (0.48)[b]	22.0	–	–	–
CeO_2 (LSA)	30.6	0.92 (0.92)	7.1	–	–	–
Ni/Al_2O_3	52.3	4.73 (4.71)	~40.0	4.9	92.1	4.82

[a] Calculated using CO and CO_2 yields from temperature-programmed oxidation (TPO) with 5% oxygen.
[b] Calculated from the balance of carbon in the system.

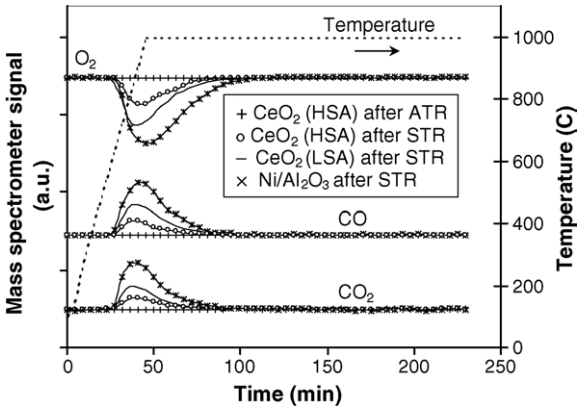

Fig. 7. Temperature-programmed oxidation (TPO) of CeO_2 (HSA), CeO_2 (LSA), and Ni/Al_2O_3 after exposure in the steam reforming (STR) and autothermal reforming (ATR) of LPG (H_2O/LPG of 5.0 for STR and O_2/LPG of 0.6 for ATR) for 72 h.

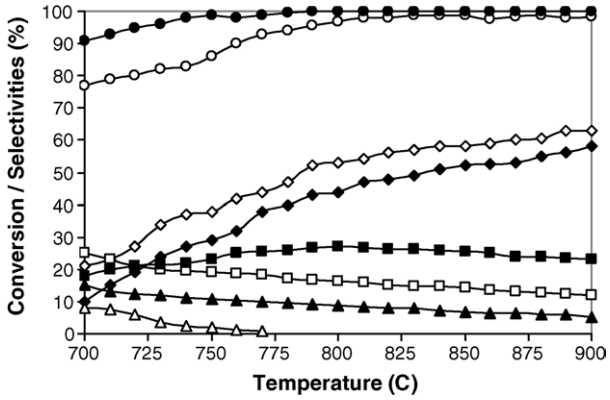

Fig. 8. Effect of reaction temperature on the conversions of C_4H_{10} (●) and C_3H_8 (○), and the selectivities of H_2 (◊), CO (♦), CO_2 (□), CH_4 (■), C_2H_6 (△), and C_2H_4 (▲) from steam reforming over CeO_2 (HSA) (with the inlet H_2O/LPG of 5.0).

layer of the basal plane in graphite [49], the quantities of carbon deposited for each catalyst were observed as in Table 4. The total amounts of carbon deposited were then verified by calculating the carbon balance of the system. Regarding the calculations, the moles of carbon deposited per gram of CeO_2 (HSA), CeO_2 (LSA), and Ni/Al_2O_3 were 0.54, 0.97, and 4.76 mmol g^{-1}. By the same assumption for the area occupied by a carbon atom [49], the values shown in Table 4 are in good agreement with the values observed from the TPO method described above. These results clearly indicate that the deactivation observed on Ni/Al_2O_3 was mainly due to carbon deposition on the surface of catalyst, and CeO_2 especially the high surface area had a significant resistance toward carbon formation as compared to Ni/Al_2O_3. BET measurements were then carried out to observe the percentage decrease in surface area of all catalysts. It should be noted that the BET measurement for Ni/Al_2O_3 was carried out after reducution of the catalyst (after TPO) with hydrogen in order to eliminate all NiO from the TRO experiment, which could affect the catalyst surface area. Results shown in Table 4 suggest that the deactivation of ceria is mainly due to the thermal sintering. However, the surface area reduction percentage of CeO_2 (HSA) is much lower than CeO_2 (LSA), indicating a higher stability toward the thermal sintering.

It should be noted that, the steady-state hydrogen selectivity observed from all catalysts (62.9% for CeO_2 (HSA), 35.0% for CeO_2 (LSA), and 28.6% for Ni/Al_2O_3) was lower than that at equilibrium state, which is approximately 87% (according to the simulation using AspenPlus 10.2), due to the incomplete decomposition of LPG to H_2, CO, and CO_2.

3.4. Effects of temperature and inlet reactants

The influences of operating temperature and the inlet steam content on the conversion of butane and propane, and the product selectivities from the steam reforming of LPG over CeO_2 (HSA) and CeO_2 (LSA) were studied by varying the operating temperature from 700 to 900 °C and changing the inlet H_2O/LPG ratio from 3.0 to 7.0 (H_2O/C ratio from 0.87 to 2.02) as represented in Figs. 8 and 9.

At 900 °C, the main products from the steam reforming reaction over CeO_2 (HSA) were CH_4, H_2 CO, and CO_2. Some formation of C_2H_4 was also observed. Hydrogen and carbon monoxide selectivities increased with increasing temperature, whereas carbon dioxide and ethylene production selectivities decreased. The dependence of methane selectivity on the operating temperature was non-monotonic, the maximum production of methane occurred at approximately 800 °C. Regarding the effect of steam, hydrogen and carbon dioxide selectivities increased with increasing inlet steam concentration, whereas carbon monoxide, methane, and ethylene selectivities decreased. These changes in product selectivities are due to the influence of the exothermic water-gas shift reaction ($CO + H_2O \rightarrow CO_2 + H_2$), whereas the decreased methane and ethylene selectivities could be due to further reforming which would generate more carbon monoxide and hydrogen. Temperature-programmed oxidations of CeO_2 (HSA) after exposure in steam reforming with different inlet H_2O/LPG ratios were then carried out to determine the effect of the inlet steam concentration on the degree of carbon formation. From the TPO results, the amount of carbon deposited slightly decreased with increasing inlet steam concentration, however, a

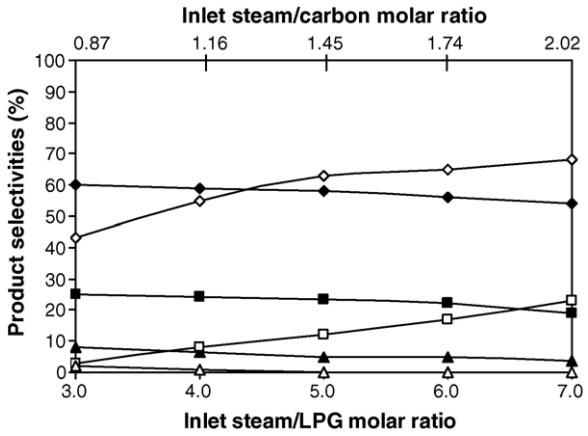

Fig. 9. Effect of inlet steam/LPG molar ratio on the selectivities of H_2 (◊), CO (♦), CO_2 (□), CH_4 (■), C_2H_6 (△), and C_2H_4 (▲) from the steam reforming of LPG over CeO_2 (HSA) at 900 °C.

Table 5
The dependence of hydrogen yield on the H_2O/LPG molar ratio and the amount of carbon formation on CeO_2 (HSA) after exposure in the steam reforming condition for 72 h

H_2O/LPG ratio	Hydrogen selectivity (%) at steady state	Total carbon formation (monolayers)
3.0	43.1	0.82[a] (0.84)[b]
4.0	55.0	0.67 (0.65)
5.0	62.9	0.51 (0.48)
6.0	65.3	0.44 (0.44)
7.0	68.0	0.41 (0.39)

[a] Calculated using CO and CO_2 yields from temperature-programmed oxidation (TPO) with 5% oxygen.
[b] Calculated from the balance of carbon in the system.

significant amount of carbon was detected even at a H_2O/LPG molar ratio of 7.0 (0.39–0.41 monolayers, Table 5).

3.5. Reactivity toward autothermal reforming

In order to reduce the degree of carbon formation and improve the product selectivities, autothermal reforming of LPG over CeO_2 (HSA) was studied by adding oxygen along with LPG and steam. The inlet H_2O/C molar ratio was kept constant at 1.45 (H_2O/LPG molar ratio of 5.0), while the inlet O/C molar ratios were varied at 0.2, 0.4, 0.6, 0.8 and 1.0. It should be noted that, while varying the ratios of H_2O/LPG and O_2/LPG, the overall space velocity was always maintained at a constant value by adjusting the flow rate of carrier gas (helium) to keep the total flow rate constant.

The effect of oxygen concentration on the product selectivities (%) at 900 °C is shown in Fig. 10. The effect of oxygen on the yields of hydrogen and carbon monoxide productions were non-monotonic. Hydrogen selectivity increased with increasing O/C molar ratio until the ratio reached 0.6. The positive effect of oxygen on the hydrogen selectivity in this range is due to the assistance of this component to reform hydrocarbons. However, higher O/C ratios showed a negative effect on the hydrogen selectivity, as too high an oxygen concentration resulted in the oxidation of the hydrogen produced from the steam reforming.

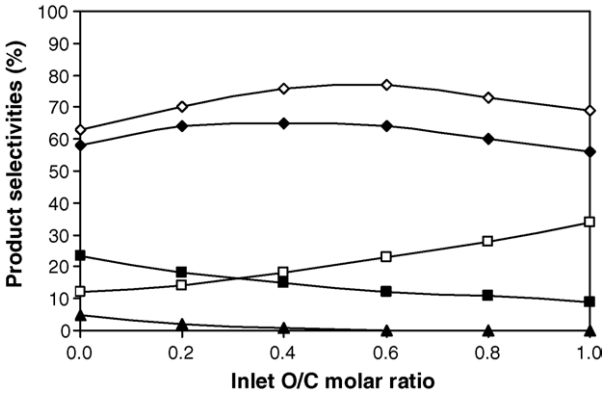

Fig. 10. Effect of inlet oxygen/carbon molar ratio on the selectivities of H_2 (◊), CO (♦), CO_2 (□), CH_4 (■), and C_2H_4 (▲) from the autothermal reforming of LPG over CeO_2 (HSA) at 900 °C.

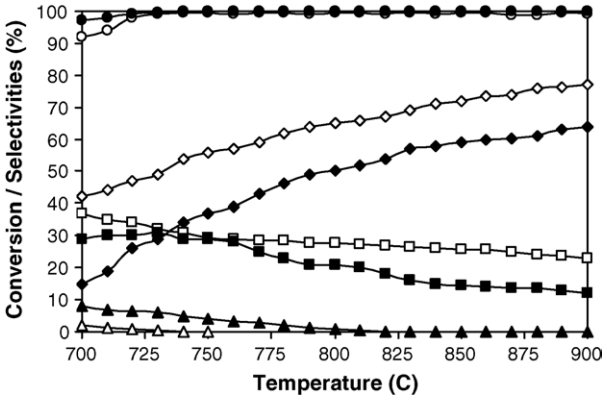

Fig. 11. Effect of reaction temperature on the conversions of C_4H_{10} (●) and C_3H_8 (●), and the selectivities of H_2 (◊), CO (♦), CO_2 (□), CH_4 (■), C_2H_6 (△), and C_2H_4 (▲) from the autothermal reforming over CeO_2 (HSA) (inlet O_2/C molar ratio of 0.6).

Table 6
The dependence of hydrogen yield on the O/C molar ratio and the amount of carbon formation on CeO_2 (HSA) after exposure in the reforming for 72 h

O/C ratio	Hydrogen selectivity (%) at steady state	Total carbon formation (monolayers)
0.0	62.9	0.51[a] (0.48)[b]
0.2	69.8	0.19 (0.21)
0.4	76.1	0.07 (0.06)
0.6	77.0	∼0.0 (∼0.0)
0.8	72.8	∼0.0 (∼0.0)
1.0	69.0	∼0.0 (∼0.0)

[a] Calculated using CO and CO_2 yields from temperature-programmed oxidation (TPO) with 5% oxygen.
[b] Calculated from the balance of carbon in the system.

Fig. 11 presents the product selectivities from the autothermal reforming of LPG (with the O/C molar ratio of 0.6) over CeO_2 (HSA) at different temperatures (700 °C to 900 °C). It was found that the main products from the autothermal reforming are similar to the steam reforming (e.g. H_2, CO, CO_2, and CH_4). Higher H_2, CO, and CO_2 selectivities were observed from autothermal reforming, whereas less CH_4, C_2H_6, and C_2H_4 were found compared to steam reforming under the same operating conditions. At 900 °C, neither C_2H_6 nor C_2H_4 formation was observed from the reaction due to the complete decomposition of these high hydrocarbons by the addition of oxygen. The benefits of the oxygen addition along with LPG and steam are presented in Section 4.

Temperature-programmed oxidation was carried out on the spent catalysts in order to determine the degree of carbon formation on the catalyst surface after exposure to the autothermal reforming reaction. From the TPO results, significantly lower quantities of deposited carbon was observed over CeO_2 (HSA) surface, and no carbon formation was detected when the inlet O/C molar ratio reached 0.6, shown in Fig. 7 and Table 6.

4. Discussion

High surface area ceria (CeO_2 (HSA)), synthesized by a surfactant-assisted approach, provided a high LPG reforming

reactivity and excellent resistance toward carbon deposition compared to conventional Ni/Al_2O_3. Carbon formation during LPG reforming could occur due to the reactions listed below:

$$C_4H_{10} \Leftrightarrow 5H_2 + 4C \quad (17)$$

$$C_3H_8 \Leftrightarrow 4H_2 + 3C \quad (18)$$

$$C_2H_4 \Leftrightarrow 2H_2 + 2C \quad (19)$$

$$CH_4 \Leftrightarrow 2H_2 + C \quad (20)$$

$$2CO \Leftrightarrow CO_2 + C \quad (21)$$

$$CO + H_2 \Leftrightarrow H_2O + C \quad (22)$$

$$CO_2 + 2H_2 \Leftrightarrow 2H_2O + C \quad (23)$$

where C is the carbonaceous deposit. At low temperature, Eqs. (22) and (23) are favorable, while Eqs. (17)–(21) are thermodynamically not favored [50]. The Boudouard reaction (Eq. (21)) and the decomposition of hydrocarbons (Eqs. (17)–(20) are the major pathways for carbon formation at such a high temperature as they show the largest change in Gibbs free energy [51]. Because of the high temperature employed in this study (700–900 °C), carbon formation via the decomposition of hydrocarbons and Boudouard reactions is possible. With the increase in steam to carbon ratio, the equilibrium of the water-gas shift reaction moves forward and produces more CO_2 rather than CO. Therefore, a high steam feed can avoid carbon deposition via the Boudouard reaction. However, a significant amount of carbon still forms due to the decomposition of hydrocarbons.

The high resistance toward carbon deposition on CeO_2, especially on high surface area CeO_2, is mainly due to the high oxygen storage capacity (OSC) of this material. CeO_2 contains a high concentration of highly mobile oxygen vacancies and thus acts as a local source or sink for oxygen on its surface. It has been reported that at high temperature, the lattice oxygen (O_O^x) at the CeO_2 surface can oxidize gaseous hydrocarbons (e.g. methane [42,48,49]). By using CeO_2 (HSA) as the catalyst, the carbon deposition due to the decomposition of hydrocarbons could be inhibited by the gas–solid reactions between the hydrocarbons present in the system (C_4H_{10}, C_3H_8, C_2H_6, C_2H_4, CH_4) and the lattice-oxygen (O_O^x) at the CeO_2 surface (Eq. (24)) forming CO_2 and H_2 from which the formation of carbon is thermodynamically unfavorable at high temperature.

$$C_nH_m + O_O^x \Leftrightarrow nCO + m/2H_2 + V_O^{\bullet\bullet} + 2e' \quad (24)$$

After the reactions, the lattice oxygen (O_O^x) is regenerated by reaction with oxygen containing compounds (e.g. steam) present in the system.

$$H_2O + V_O^{\bullet\bullet} + 2e' \Leftrightarrow O_O^x + H_2 \quad (25)$$

The redox mechanism between the hydrocarbons present in the system and the lattice oxygen (O_O^x) are illustrated below.

$$C_4H_{10} + 4S_{Ce} \Leftrightarrow 2(CH_3{-}S_{Ce}) + 2(CH_2{-}S_{Ce}) \quad (26)$$

$$C_3H_8 + 3S_{Ce} \Leftrightarrow 2(CH_3{-}S_{Ce}) + CH_2{-}S_{Ce} \quad (27)$$

$$C_2H_6 + 2S_{Ce} \Leftrightarrow 2(CH_3{-}S_{Ce}) \quad (28)$$

$$C_2H_4 + 2S_{Ce} \Leftrightarrow 2(CH_2{-}S_{Ce}) \quad (29)$$

$$CH_4 + 2S_{Ce} \Leftrightarrow CH_3{-}S_{Ce} + H{-}S_{Ce} \quad (30)$$

$$CH_3{-}S_{Ce} + S_{Ce} \Leftrightarrow CH_2{-}S_{Ce} + H{-}S_{Ce} \quad (31)$$

$$CH_2{-}S_{Ce} + S_{Ce} \Leftrightarrow CH{-}S_{Ce} + H{-}S_{Ce} \quad (32)$$

$$CH{-}S_{Ce} + S_{Ce} \Leftrightarrow C{-}S_{Ce} + H{-}S_{Ce} \quad (33)$$

$$C{-}S_{Ce} + O_O^x \Leftrightarrow CO + V_O^{\bullet\bullet} + 2e' + S_{Ce} \quad (34)$$

$$2H{-}S_{Ce} \Leftrightarrow H_2 + 2S_{Ce} \quad (35)$$

where S_{Ce} is the CeO_2 surface site and $CH_x{-}S_{Ce}$ is an intermediate surface hydrocarbon species. S_{Ce} can be considered to be a unique site, or the same site as the lattice oxygen (O_O^x). Steele and Floyd [52] reported that the measured value of the oxygen diffusion coefficient for ceria is high and the reaction rate is controlled by a surface reaction rather than by diffusion of oxygen from the bulk of the solid particles to ceria surfaces [52]. During the reaction, hydrocarbons are adsorbed on either a unique site (S_{Ce}) or the lattice oxygen (O_O^x).

Although conventional CeO_2 (CeO_2 (LSA)) has also been reported to provide a high resistance toward carbon formation, the major drawbacks of CeO_2 (LSA) are the low specific surface area and large size reduction due to the thermal sintering, resulting in a significant drop in the redox properties compared to CeO_2 (HSA), as presented in Section 3.1, and consequently low steam reforming reactivity. The corresponding post-reaction specific surface area for CeO_2 (LSA) after exposure in reforming conditions was 7.1 $m^2\,g^{-1}$, and the observed size reduction percentage was 17%, whereas the post-reaction specific surface area for CeO_2 (HSA) was 22 $m^2\,g^{-1}$, and the observed size reduction percentage was 9%. The low redox properties of CeO_2 (LSA) also resulted in a significantly lower resistance toward carbon deposition of this material compared to CeO_2 (HSA). As described earlier, the redox reaction (Eq. (25)) between the lattice oxygen (O_O^x) at the CeO_2 surface and the hydrocarbons present in the system (C_4H_{10}, C_3H_8, C_2H_6, C_2H_4, CH_4) can prevent the formation of carbon by the decomposition of these hydrocarbon components.

It was observed from the study that the addition of oxygen along with LPG and steam in the autothermal reforming reaction reduced the degree of carbon deposition and improved the product selectivities by eliminating the formation of C_2H_6 and C_2H_4. Theoretically, oxygen prevents the formation of high hydrocarbons (i.e. C_2H_6 and C_2H_4) and subsequent carbon deposition from the decomposition reactions (Eqs. (16)–(18)) by oxidizing these hydrocarbons producing the elements that are unfavored to form carbon. The presence of oxygen also helps steam regenerate the lattice oxygen (O_O^x) on the CeO_2 surface ($O_2 + V_O^{\bullet\bullet} + 2e' + S_{Ce} \rightarrow O_O^x$). The major consideration of the autothermal reforming operation is a suitable O_2/LPG ratio. The presence of too high an oxygen concentration could oxidize the hydrogen and carbon monoxide produced from the steam reforming to steam and carbon dioxide.

5. Conclusion

High surface area ceria (CeO_2 (HSA)), synthesized in a surfactant-assisted approach, is a good catalyst for the reforming of LPG (butane and propane) at SOFC temperatures (700–900 °C) due to a high resistance towards the deactivation from carbon formation. During the reforming process, the gas–solid reactions between the hydrocarbons present in the system (i.e. propane, butane, ethane, ethylene, and methane) and the lattice oxygen (O_O^x) take place on the ceria surface, reducing the degree of carbon deposition on the catalyst surface (from hydrocarbons decomposition and Boudouard reactions). At 700–900 °C, the main products from the steam reforming of LPG over CeO_2 (HSA) were H_2, CO, CO_2, and CH_4, whereas a small amount of C_2H_4 was also observed, particularly at low temperatures. By increasing the inlet steam content, hydrogen and carbon dioxide selectivities increased, whereas carbon monoxide selectivity decreased. Moreover, the conversions of methane and ethylene were found to increase with increasing steam content in the system.

The addition of oxygen in autothermal reforming can reduce the degree of carbon deposition and eliminate the formation of higher hydrocarbons (i.e. C_2H_6 and C_2H_4). The major consideration in the autothermal reforming operation is the inlet O_2/LPG molar ratio, as the presence of too high an oxygen concentration could oxidize hydrogen and carbon monoxide, produced from the steam reforming, to steam and carbon dioxide. A suitable O/C molar ratio for autothermal reforming on CeO_2 (HSA) was observed to be 0.6.

Acknowledgement

Financial support from The Thailand Research Fund (TRF) throughout this project is gratefully acknowledged.

References

[1] P. Aguiar, D. Chadwick, L. Kershenbaum, Chem. Eng. Sci. 57 (2002) 1665.
[2] K. Ahmed, J. Gamman, K. Föger, Solid State Ion. 152–153 (2002) 485–492.
[3] T. Suzuki, H.-i. Iwanami, O. Iwamoto, T. Kitahara, Int. J. Hydrogen Energy 26 (9) (2001) 935–940.
[4] A.K. Avci, D.L. Trimm, A.E. Aksoylu, Z.I. Önsan, Catal. Lett. 88 (2003) 17–22.
[5] A.F. Ghenciu, Curr. Opin. Solid State Mater. Sci. 6 (2002) 389–399.
[6] T. Rampe, A. Heinzel, B. Vogel, J. Power Sources 86 (2000) 536–541.
[7] F. Joensen, J.R. Rostrup-Nielsen, J. Power Sources 105 (2002) 195–201.
[8] V. Recupero, L. Pino, A. Vita, F. Cipiti, M. Cordaro, M. Laganà, Int. J. Hydrogen Energy 30 (9) (2005) 963–971.
[9] L.V. Mattos, E. Rodino, D.E. Resasco, F.B. Possos, F.B. Noronha, Fuel Proc. Technol. 83 (2003) 147.
[10] H.S. Roh, K.W. Jun, S.E. Park, Appl. Catal. A 251 (2003) 275.
[11] J.R. Rostrup-Nielsen, J.-H. Bak-Hansen, J. Catal. 144 (1993) 38.
[12] P. Fornasiero, G. Balducci, R.D. Monte, J. Kaspar, V. Sergo, G. Gubitosa, A. Ferrero, M. Graziani, J. Catal. 164 (1996) 173.
[13] T. Miki, T. Ogawa, M. Haneda, N. Kakuta, A. Ueno, S. Tateishi, S. Matsuura, M. Sato, J. Phys. Chem. 94 (1990) 339.
[14] C. Padeste, N.W. Cant, D.L. Trimm, Catal. Lett. 18 (1993) 305.
[15] S. Kacimi, J. Barbier Jr., R. Taha, D. Duperz, Catal. Lett. 22 (1993) 343.
[16] G.S. Zafiris, R.J. Gorte, J. Catal. 143 (1993) 86.
[17] G.S. Zafiris, R.J. Gorte, J. Catal. 139 (1993) 561.
[18] S. Imamura, M. Shono, N. Okamoto, R. Hamada, S. Ishida, Appl. Catal. A 142 (1996) 279.
[19] L. Fan, K. Fujimoto, J. Catal. 172 (1997) 238.
[20] M. Pijolat, M. Prin, M. Soustelle, J. Chem. Soc., Faraday Trans. 91 (1995) 3941.
[21] S. Imamura, T. Higashihara, Y. Saito, H. Aritani, H. Kanai, Y. Matsumura, N. Tsuda, Catal. Today 50 (1999) 369.
[22] S. Imamura, K. Denpo, K. Utani, Y. Matsumura, H. Kanai, React. Kinet. Catal. Lett. 67 (1999) 163.
[23] S. Imamura, K. Denpo, K. Kanai, H. Yamane, Y. Saito, K. Utani, Y. Matsumura, Sekiyu Gakkaishi 44 (2001) 293.
[24] S. Imamura, H. Yamane, H. Kanai, T. Shibuta, K. Utani, K. Hamada, J. Jpn. Petrol. Inst. 45 (2002) 187.
[25] S. Imamura, Y. Taniguchi, Y. Ikeda, S. Hosokawa, H. Kanai, H. Ando, React. Kinet. Catal. Lett. 76 (2002) 201.
[26] H.S. Roh, K.W. Jun, W.S. Dong, J.S. Chang, S.E. Park, Y.I. Joe, J. Mol. Catal. A 181 (2002) 137–142.
[27] Q. Miao, G. Xiong, S. Sheng, W. Cui, L. Xu, X. Guo, Appl. Catal. A 154 (1987) 17–27.
[28] A.A. Lemonidou, M.A. Goula, I.A. Vasalos, Catal. Today 46 (1987) 175–183.
[29] W.S. Dong, H.S. Roh, K.W. Jun, S.E. Park, Y.S. Oh, Appl. Catal. A 226 (2002) 63–72.
[30] M. Mamak, N. Coombs, G. Ozin, Adv. Mater. 12 (2000) 198–202.
[31] M. Mamak, N. Coombs, G. Ozin, J. Am. Chem. Soc. 122 (2000) 8932.
[32] M. Mamak, N. Coombs, G.A. Ozin, Chem. Mater. 13 (2001) 3564.
[33] P. Bera, S. Mitra, S. Sampath, M.S. Hegde, Chem. Commun. (2001) 927.
[34] A. Martinez-Arias, J.M. Coronado, R. Cataluna, J.C. Conesa, J.C. Soria, J. Phys. Chem. B 102 (1998) 4357.
[35] D. Skarmoutsos, F. Tietz, P. Nikolopoulos, Fuel Cells 1 (2001) 243.
[36] T. Takeguchi, S.N. Furukawa, M. Inoue, J. Catal. 202 (2001) 14.
[37] J. Sfeir, P.A. Philippe, P. Moseki, N. Xanthopoulos, R. Vasquez, J.M. Hans, V.H. Jan, K.R. Thampi, J. Catal. 202 (2001) 229.
[38] N. Kiratzis, P. Holtappels, C.E. Hatchwell, M. Mogensen, J.T.S. Irvine, Fuel Cells 1 (2001) 211.
[39] H.S. Roh, W.S. Dong, K.W. Jun, S.E. Park, Chem. Lett. (2001) 88.
[40] E. Ramírez-Cabrera, A. Atkinson, D. Chadwick, Appl. Catal. B 47 (2004) 127–131.
[41] E. Ramírez-Cabrera, N. Laosiripojana, A. Atkinson, D. Chadwick, Catal. Today 78 (2003) 433–438.
[42] N. Laosiripojana, Reaction engineering of indirect internal steam reforming of methane for application in solid oxide fuel cells. Ph.D. Thesis, University of London, England, 2003.
[43] K. Otsuka, T. Ushiyama, I. Yamanaka, Chem. Lett. (1993) 1517.
[44] K. Otsuka, M. Hatano, A. Morikawa, J. Catal. 79 (1983) 493.
[45] K. Otsuka, M. Hatano, A. Morikawa, Inorg. Chim. Acta 109 (1985) 193.
[46] P.J. Gellings, J.M. Henny, Bouwmeester, Solid state aspects of oxidation catalysis, Catal. Today 58 (2000) 1–53.
[47] D. Terribile, A. Trovarelli, J. Llorca, C. de Leitenburg, G. Dolcetti, Catal. Today 43 (1998) 79–88.
[48] N. Laosiripojana, S. Assabumrungrat, Appl. Catal. B: Environ. 60 (2005) 107.
[49] E. Ramirez, A. Atkinson, D. Chadwick, Appl. Catal. B 36 (2002) 193–206.
[50] Y. Lwin, W.R.W. Daud, A.B. Mohamad, Z. Yaakob, Int. J. Hydrogen Energy 25 (1) (2000) 47–53.
[51] J.N. Amor, Appl. Catal. A 176 (1999) 159–176.
[52] B.C.H. Steele, J.M. Floyd, Proc. Br. Ceram. Soc. 19 (1971) 55.

N. Laosiripojana and S. Assabumrungrat

"The effect of specific surface area on the activity of nano-scale ceria catalysts for methanol decomposition with and without steam at SOFC operating temperatures"

Chemical Engineering Science, In Press

(IF-2004 = 1.65)

ARTICLE IN PRESS

ELSEVIER

Chemical Engineering Science ▮▮▮ (▮▮▮▮) ▮▮▮–▮▮▮

Chemical Engineering Science

www.elsevier.com/locate/ces

The effect of specific surface area on the activity of nano-scale ceria catalysts for methanol decomposition with and without steam at SOFC operating temperatures

N. Laosiripojana[a,*], S. Assabumrungrat[b]

[a]*The Joint Graduate School of Energy and Environment, King Mongkut's University of Technology Thonburi, Bangkok 10140, Thailand*

[b]*Center of Excellence on Catalysis and Catalytic Reaction Engineering, Department of Chemical Engineering, Chulalongkorn University, Bangkok 10330, Thailand*

Received 25 August 2005; received in revised form 14 November 2005; accepted 14 November 2005

Abstract

Nano-particulate high surface area CeO_2 was found to have a useful methanol decomposition activity producing H_2, CO, CO_2, and a small amount of CH_4 without the presence of steam being required under solid oxide fuel cell temperatures, 700–1000 °C. The catalyst provides high resistance toward carbon deposition even when no steam is present in the feed. It was observed that the conversion of methanol was close to 100% at 850 °C, and no carbon deposition was detected from the temperature programmed oxidation measurement.

The reactivity toward methanol decomposition for CeO_2 is due to the redox property of this material. During the decomposition process, the gas–solid reactions between the gaseous components, which are homogeneously generated from the methanol decomposition (i.e., CH_4, CO_2, CO, H_2O, and H_2), and the lattice oxygen (O_O^x) on ceria surface take place. The reactions of adsorbed surface hydrocarbons with the lattice oxygen ($C_nH_m + O_O^x \rightarrow nCO + m/2(H_2) + V_{O^{\cdot\cdot}} + 2e'$) can produce synthesis gas (CO and H_2) and also prevent the formation of carbon species from hydrocarbons decomposition reaction ($C_nH_m \Leftrightarrow nC + m/2H_2$). $V_{O^{\cdot\cdot}}$ denotes an oxygen vacancy with an effective charge 2^+. Moreover, the formation of carbon via Boudouard reaction ($2CO \Leftrightarrow CO_2 + C$) is also reduced by the gas–solid reaction of carbon monoxide with the lattice oxygen ($CO + O_O^x \Leftrightarrow CO_2 + V_{O^{\cdot\cdot}} + 2e'$).

At steady state, the rate of methanol decomposition over high surface area CeO_2 was considerably higher than that over low surface area CeO_2 due to the significantly higher oxygen storage capacity of high surface area CeO_2, which also results in the high resistance toward carbon deposition for this material. In particular, it was observed that the methanol decomposition rate is proportional to the methanol partial pressure but independent of the steam partial pressure at 700–800 °C. The addition of hydrogen to the inlet stream was found to have a significant inhibitory effect on the rate of methanol decomposition.

Keywords: Methanol; Internal reforming; Hydrogen; SOFC; CeO_2

1. Introduction

A fuel cell is an energy conversion unit that produces electrical energy and heat with greater energy efficiency and lower pollutant emission than conventional processes (Minh and Takahashi, 1995). Among the various types of fuel cell, the solid oxide fuel cell (SOFCs) has attracted considerable interest as it offers a wide range of applications, flexibility in the choice of fuel, and high-system efficiency. The waste heat can also be utilized in co-generation applications and bottoming cycles. Moreover, unlike the low-temperature fuel cells, the SOFC anode is not affected by carbon monoxide poisoning.

Hydrogen is the major fuel for SOFCs. Nevertheless, the use of other fuels such as methane, methanol, ethanol, gasoline and other oil derivatives is also possible when operated as an internal or in-stack reforming. As SOFCs are operated at such a high temperature, these hydrocarbons can be internally reformed to produce a H_2/CO rich gas, which is eventually used to generate the electrical energy and heat.

* Corresponding author. Tel.: +66 2 8729014; fax: +66 2 8726736.
E-mail address: navadol_l@jgsee.kmutt.ac.th (N. Laosiripojana).

0009-2509/$ - see front matter © 2005 Published by Elsevier Ltd.
doi:10.1016/j.ces.2005.11.024

This operation, called indirect internal reforming (IIR-SOFC), is expected to simplify the overall system design (Aguiar et al., 2001). Douvartzides et al. (2003), applied a thermodynamic analysis to evaluate the feasibility of different fuels, i.e., methane, methanol, ethanol and gasoline, for SOFCs. The results obtained in terms of electromotive force output and efficiency show that ethanol and methanol are very promising alternatives to hydrogen. Among them, methanol is favourable due to its ready availability, high-specific energy and storage transportation convenience (Emonts et al., 1998; Ledjeff-Hey et al., 1998).

Several researchers have studied the catalytic decomposition of methanol with steam (Lwin et al., 2000; Brown, 2001; Maggio et al., 1998). The well known reactions involved in this process can be represented by the decomposition-shift mechanism

$$CH_3OH = 2H_2 + CO \quad \text{(methanol decomposition)}, \tag{1}$$

$$CO + H_2O = H_2 + CO_2 \quad \text{(water gas shift reaction)}, \tag{2}$$

$$CO + 3H_2 = CH_4 + H_2O \quad \text{(methanation)}. \tag{3}$$

Firstly, methanol can be directly converted to hydrogen and carbon monoxide by the decomposition process (Eq. (1)). In the presence of steam, the water–gas shift reaction (Eq. (2)) takes place to produce carbon dioxide and more hydrogen. Methane can be formed by the methanation reaction (Eq. (3)). It should be noted that the formations of higher molecular weight compounds such as formaldehyde, methyl formate and formic acid were found to be negligible (Lwin et al., 2000).

A major concern of the methanol decomposition is catalyst deactivation by carbon formation which, consequently, leads to the loss of system performance and poor durability (Dicks, 1996). The following are the most probable carbon formation reactions:

$$2CO = CO_2 + C, \tag{4}$$

$$CH_4 = 2H_2 + C, \tag{5}$$

$$CO + H_2 = H_2O + C, \tag{6}$$

$$CO_2 + 2H_2 = 2H_2O + C. \tag{7}$$

At low temperature, reactions (6)–(7) are favourable while reaction (5) is thermodynamically unfavoured. The Boudouard reaction (Eq. (4)) and the decomposition of methane (Eq. (5)) are the major pathways for carbon formation at high temperature as they show the largest change in Gibbs energy (Amor, 1999). Regarding the IIR-SOFC operation, the reforming temperatures are in the range of 700–1000 °C (Aguiar et al., 2001). The potential formation of carbon species on the surface of catalyst therefore arises from the decomposition and Boudouard reactions.

In order to maximize hydrogen production from the decomposition of methanol and to reduce the amount of carbon deposition, selection of catalyst is an important issue as it has been evident that the degree of carbon formation strongly depends on the type of catalyst used (Rostrup-Nielsen and Bak-Hansen, 1993). It is well established that cerium oxide is a useful catalyst for a wide variety of reactions involving the oxidation or partial oxidation of hydrocarbons (e.g. automotive catalysis). This material contains a high concentration of highly mobile oxygen vacancies and thus acts as a local source or sink for oxygen involved in reactions taking place on the ceria surface. There is now increasing interest in using ceria in more severe reducing conditions, such as in methane reforming at the anodes of SOFC, where the possibility of deactivation through carbon deposition is much higher (Marina et al., 1998). The excellent resistance toward carbon formation from methane cracking reaction over CeO_2 under SOFC conditions was reported (Laosiripojana, 2003). Recently, the successful use of ceria as a key constituent of the anode for a SOFC operated directly with 'dry' methane has also been presented. Furthermore, successful developments of the direct internal reforming (DIR-SOFC), in which the hydrocarbons can be reformed internally at the anode side of SOFC, using copper–ceria-based anodes (i.e., Cu–CeO_2, and Cu–CeO_2-YSZ) fueled by several hydrocarbon and oxyhydrocarbon compounds (i.e., C_4H_{10} and CH_3OH) were also reported (Kim et al., 2005; Jung et al., 2005; Costa-Nunes et al., 2005; Gorte et al., 2004; An et al., 2004; Brett et al., 2005). It was demonstrated that the addition of ceria at the anode can provide a stable operation and reasonable performance with a wide variety of hydrocarbon fuels (Jung et al., 2005; Costa-Nunes et al., 2005).

The gas–solid reaction between CeO_2 and CH_4 produces synthesis gas with a H_2/CO ratio of two, according to the following reaction (Otsuka et al., 1983):

$$CH_4 + O_O^x = 2H_2 + CO + V_{O^{\cdot\cdot}} + 2e'. \tag{8}$$

$V_{O^{\cdot\cdot}}$ denotes an oxygen vacancy with an effective charge 2^+, e' is an electron which can either be more or less localized on a cerium ion or delocalized in a conduction band. Moreover, it was also demonstrated that the reactions of the reduced ceria with CO_2 and steam produced CO and H_2, respectively, and regenerated the CeO_2 surface (Otsuka et al., 1985; Gellings and Bouwmeester, 2000)

$$V_{O^{\cdot\cdot}} + 2e' + CO_2 = O_O^x + CO, \tag{9}$$

$$V_{O^{\cdot\cdot}} + 2e' + H_2O = O_O^x + H_2. \tag{10}$$

The major limitation for the application of ceria to high temperature applications is its low specific surface area due to the significant size reduction by thermal sintering (Laosiripojana, 2003). It was reported that the corresponding post-reaction specific surface area for CeO_2 after exposure in methane steam reforming conditions at 900 °C for 10 h was 1.9 $m^2\,g^{-1}$, and the observed size reduction percentage was 23% (Laosiripojana, 2003). Therefore, the use of nano-particulate high surface area ceria would be a promising procedure to improve its catalytic performance at high operating temperatures.

The present work is focused on the study of hydrogen production from methanol decomposition at SOFC operating temperature of 700–1000 °C. The decomposition of methanol with and without steam presence over nano-particulate high surface area CeO_2 (CeO_2 (HSA)), synthesized by Nanophase Technologies Corporation, was investigated. The reactivity toward this reaction and the resistance toward carbon formation of this

material were compared to CeO_2 prepared by a precipitation method (CeO_2 (LSA)). At steady state, the influences of temperature and inlet components on the product selectivities were determined.

2. Experimental

2.1. Catalyst preparation and characterization

Nano-particulate high surface area CeO_2 powder (CeO_2 (HSA)) (NanoArc Cerium Oxide SGH grade with the average particle size of 11 nm) was supplied by Nanophase Technologies Corporation, USA. This material is prepared by the patent-pending NanoArc^{TM} Synthesis (NAS) process, using arc energy to produce nanoparticles. The nanomaterials produced by the NAS process consist of discrete, fully-dense particles of defined crystallinity. This method has been used to produce particles with average sizes ranging from 7 to 45 nm (http://www.nanophase.com). CeO_2 (HSA) was dried in an oven and calcined in air at 1000 °C for 6 h in order to minimize sintering at the maximum reaction temperature used in subsequent experiments (Ramírez-Cabrera et al., 2002). For comparison, a synthesized CeO_2 (CeO_2 (LSA)) was also prepared by precipitation of cerium chloride ($CeCl_3 \cdot 7H_2O$) from Aldrich. The starting solution was prepared by mixing 0.1 M of this metal salt solution with 0.4 M of ammonia at a 2:1 volumetric ratio. The mixture was stirred by a magnetic stirrer (100 rpm) and then aqueous ammonia was slowly added with the constant rate of 0.165 $cm^3\ min^{-1}$ until the pH was 11.5. We found that the rate of ammonia doping has a significant impact on the particle size and specific surface area of the synthesized CeO_2. This solution was stirred for 3 h, then sealed and placed in a thermostatic bath maintained at 90 °C for three days. The precipitate was filtered and washed with deionized water and acetone to remove the free surfactant. It was dried overnight in an oven at 110 °C, and then calcined in air at 1000 °C for 6 h. BET measurements of CeO_2 were carried out before and after the calcinations in order to determine the specific surface area. As presented in Table 1, after drying in the oven, surface areas of 82 and 55 $m^2\ g^{-1}$ were observed for CeO_2 (HSA) and CeO_2 (LSA), respectively, and as expected, the surface area dramatically decreased at high calcination temperatures. However, the value for CeO_2 (HSA) is still appreciable after calcination at 1000 °C and it is almost 3 times of that for the CeO_2 (LSA). The average mean particle sizes of CeO_2 (HSA) and CeO_2 (LSA) after calcination at 1000 °C were 60–90 and 135–160 nm, respectively.

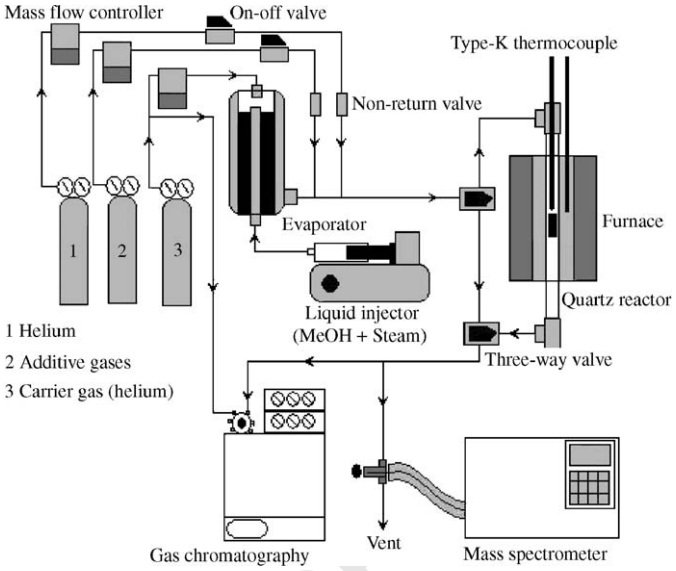

Fig. 1. Schematic diagram of the experimental set-up.

The redox properties and redox reversibilities of CeO_2 (HSA) and CeO_2 (LSA) were compared by the temperature programmed reduction (TPR-1) at high temperature and the temperature programmed oxidation (TPO) following with the second time temperature programmed reduction (TPR-2), respectively. In these experiments, 5% hydrogen and 10% oxygen in helium were used for the TPR and TPO, respectively, while the temperature of the system increased from room temperature to 900 °C by the rate of 8 °C/ min for both experiments.

2.2. Apparatus and procedures

An experimental reactor system was constructed as shown in Fig. 1. The feed gases including the components of interest (methanol and steam from the evaporator) and the carrier gas (helium) were introduced to the reaction section, in which 10-mm diameter quartz reactor was mounted vertically inside a furnace. The inlet methanol concentration was 5% (5 kPa), while the inlet steam concentrations were varied depending on the inlet H_2O/CH_3OH molar ratio requirement for each experiment (0, 1, and 3). The total gas pressure was always kept constant at 101.3 kPa. The catalyst (50 mg) was loaded in the quartz reactor, which was packed with a small amount of quartz wool to prevent the catalyst from moving. A Type-K thermocouple was placed into the annular space between the reactor and the furnace. This thermocouple was mounted on the tubular

Table 1
Specific surface area of the catalysts after drying and calcinations at different temperatures

Catalyst	BET surface area ($m^2\ g^{-1}$) after drying and calcination at						
	100 °C	200 °C	400 °C	600 °C	800 °C	900 °C	1000 °C
CeO_2 (LSA)	55	49	36	21	15	11	8.1
CeO_2 (HSA)	82	79	68	56	43	35	24

reactor in close contact with the catalyst bed to minimize the temperature difference between the catalyst bed and the thermocouple. Another Type-K thermocouple was inserted in the middle of the quartz tube in order to re-check the possible temperature gradient. The record showed that the maximum temperature fluctuation during the reaction was always ±0.75 °C or less from the temperature specified for the reaction.

After the reactions, the exit gas mixture was transferred via trace-heated lines to the analysis section, which consists of a Porapak Q column Shimadzu 14B gas chromatograph (GC) and a mass spectrometer (MS). The gas chromatography was applied in order to investigate the steady state condition experiments, whereas the mass spectrometer in which the sampling of the exit gas was done by a quartz capillary and differential pumping was used for the transient carbon formation experiment. In the present work, the outlet of the GC column was directly connected to a thermal conductivity detector (TCD) and a frame ionization detector (FID). In order to satisfactorily separate CH_3OH, CH_4, CO, CO_2, and H_2, the temperature setting inside the GC column was programmed varying with time. In the first 3 min, the column temperature was constant at 60 °C, it was then increased steadily by the rate of 15 °C/ min until 120 °C. Finally, the temperature was decreased to 60 °C. The analytical method applied is an internal standardization in which the peak area is related to the molar concentration through the response factor (RF)

$$\mathrm{RF} = \frac{\text{concentration (ppm)}}{\text{peak area}}. \tag{11}$$

In order to study the formation of carbon species on catalyst surface, TPO was applied by introducing 10% oxygen in helium into the system, after purging with helium. The operating temperature increased from room temperature to 1000 °C by a rate of 20 °C/min. The calibrations of CO and CO_2 productions were performed by injecting a known amount of these calibration gases from a loop, in an injection valve in the bypass line. The response factors were obtained by dividing the number of moles for each component over the respective areas under peaks. The amount of carbon formation on the surface of catalysts were determined by measuring the CO and CO_2 yields from the TPO results (using Microcal Origin Software) assuming a value of 0.026 nm^2 for the area occupied by a carbon atom in a surface monolayer of the basal plane in graphite (Ramírez-Cabrera et al., 2004). In addition to the TPO method, the amount of carbon deposition was confirmed by the calculation of carbon balance in the system. The amount of carbon deposited on the surface of catalyst would theoretically be equal to the difference between the inlet carbon containing components (CH_3OH) and the outlet carbon containing components (CO, CO_2, and CH_4). The amount of carbon deposited per gram of catalyst is given by the following equation:

$$C_{\text{deposition}} = \frac{\text{mole}_{\text{carbon(in)}} - \text{mole}_{\text{carbon(out)}}}{m_{\text{catalyst}}}. \tag{12}$$

2.3. Kinetic parameters formulae

The rate of methanol decomposition was defined in term of the turnover frequencies (N) which is calculated from the following equation. It was assumed that all surface sites accessible by nitrogen adsorption were active

$$N = \frac{r N_A A_{N_2}}{m_c S}, \tag{13}$$

where r is the reaction rate (moles of CH_3OH per unit time), N_A is the Avagadro's number, A_{N_2} is the area occupied by an adsorbed nitrogen molecule (16.2×10^{-20} m^2 $molecule^{-1}$ (Ramírez-Cabrera et al., 2004)), m_c is the mass of catalyst (50 mg), and S is the specific surface area of the catalyst.

Methanol conversions denoted as X_{Methanol}, and the product selectivities (hydrogen, carbon monoxide, carbon dioxide, and methane), denoted as S_{Product}, are calculated according to

$$X_{\text{Method}} = \frac{100(\text{Methanol}_{\text{in}} - \text{Methanol}_{\text{out}})}{\text{Methanol}_{\text{in}}}, \tag{14}$$

$$S_{\text{Product}} = \frac{100(\text{Mole of a specific product})}{(\text{Total moles of all products})}. \tag{15}$$

3. Results

3.1. Preliminary tests

In order to avoid any limitations by intraparticle diffusion, we checked the impact of the total flow rate at the minimum (700 °C) and maximum operating temperature (1000 °C) before the formal investigations. The total flow rate was changed between 20 and 200 cm^3 min^{-1} under the same residence time of 5×10^{-4} g min cm^{-3}. From Fig. 2, when the total flow rate was below 60 cm^3 min^{-1}, the methanol conversion and the hydrogen selectivity increased with increasing the gas flow rate, suggesting that the mass transfer between the bulk gas and the catalyst particles is the rate-determining step. The steady state

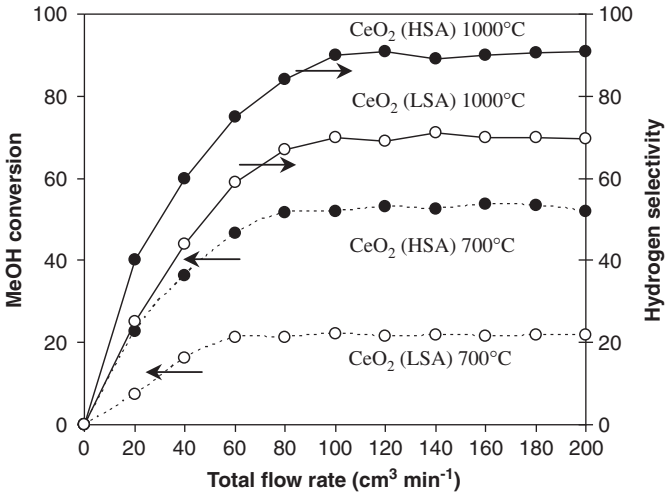

Fig. 2. Effect of the total gas flow rate on the methanol conversion over CeO_2 (LSA) and CeO_2 (HSA) at 700 °C (1 kPa MeOH, and 3 kPa H_2O).

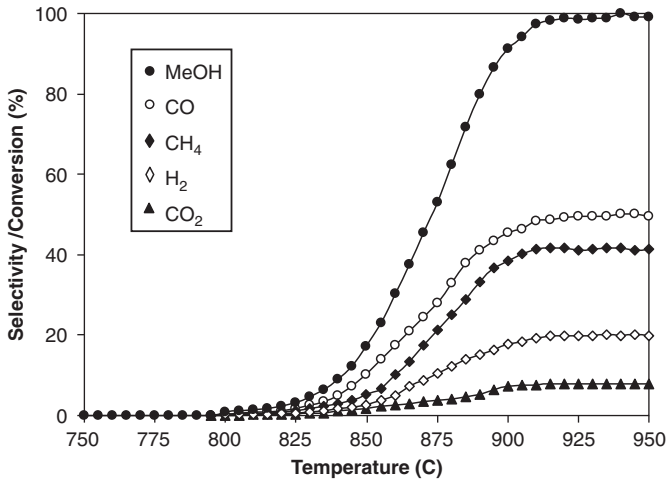

Fig. 3. Homogeneous (in the absence of catalyst) reactivity of methanol decomposition (1 kPa MeOH, and 3 kPa H_2O).

reforming rate was almost constant in the range where the gas flow rate was higher than 80 $cm^3\,min^{-1}$, indicating that the mass transfer effect is unimportant in this flow rate range. Consequently, the mass of catalyst loading was 50 mg, while the total gas flow was kept constant at 100 $cm^3\,min^{-1}$ in all experiments.

3.2. Homogeneous (non catalytic) reaction

Before studying the catalyst performance, homogeneous (non-catalytic) decomposition of methanol was investigated. Inlet H_2O/CH_3OH in helium with the molar ratio of 3 was introduced to the system, while the temperature increased from room temperature to 950 °C. From Fig. 3, it was observed that methanol was converted to methane, carbon monoxide, carbon dioxide, and hydrogen at the temperature above 800 °C. These components were formed via the decomposition of methanol, water–gas shift and methanation reactions.

3.3. Redox properties and redox reversibility of CeO_2

The oxygen storage capacities (OSC) and the degree of redox properties for fresh CeO_2 (both LSA and HSA) after calcinations were investigated using TPR-1, which was performed by heating the reduced catalysts up to 900 °C in 5% H_2 in helium. As shown in Fig. 4, hydrogen uptakes are detected from both CeO_2 at the temperature above 650 °C. The amount of hydrogen uptake over CeO_2 (HSA) is significantly higher than that over CeO_2 (LSA), suggesting that the OSC and the redox properties depend on the specific surface area of CeO_2. The benefit of the redox property on the reforming of methanol will be later presented in Section 3.4 and the discussion section. After purged with helium, the redox reversibilities for both CeO_2were then determined by applying TPO followed by TPR-2. The TPO was carried out by heating the catalyst up to 900 °C in 10% O_2 in helium; the amounts of oxygen chemisorbed were then measured, Fig. 5 and Table 2. Regarding the TPR-2 results as

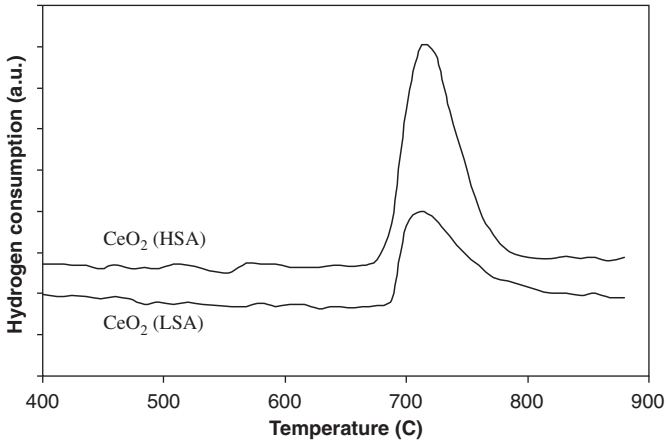

Fig. 4. TPR-1 of fresh ceria after reduction.

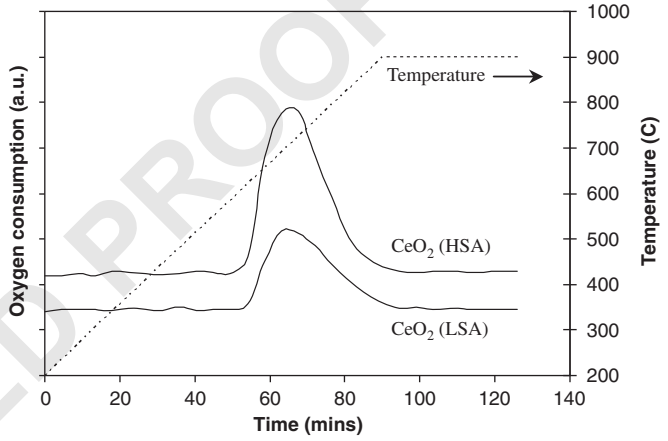

Fig. 5. TPO of CeO_2 (HSA, LSA) after TPR-1.

shown in Fig. 6 and Table 2, the amount of hydrogen uptakes for CeO_2 (both LSA and HSA) were approximately similar to those from TPR-1, indicating the redox reversibility for the synthesized CeO_2.

3.4. Reactivity toward methanol decomposition

The decomposition of methanol with and without steam over CeO_2 (HSA) and CeO_2 (LSA) were studied at 900 °C. The feed was H_2O/CH_3OH in helium with the molar ratios of 0, 1, and 3. The variations in hydrogen selectivities (%) with time at 900 °C for different catalysts and different inlet H_2O/CH_3OH ratio are shown in Fig. 7. After being operated for 100 h, the hydrogen selectivities for CeO_2 (HSA) were significantly higher than those for CeO_2 (LSA) in all conditions. However, the deactivations were also observed in all catalysts. Catalyst stabilities expressed as deactivation percentages are given in Table 3.

The post-reaction TPO experiments were carried out after a helium purge by introduction of 10% oxygen in helium in order to determine whether the observed deactivation is due to the carbon formation. From the TPO results shown in Fig. 8, small peaks of carbon dioxide and carbon monoxide were observed

Table 2
Results of TPR-1, TPO, TPR-2 analyses of CeO_2

Catalyst	Total H_2 uptake from TPR(1)[a] ($\mu mol/g_{cat}$)	Total O_2 uptake from TPO[b] ($\mu mol/g_{cat}$)	Total H_2 uptake from TPR(2)[c] ($\mu mol/g_{cat}$)
CeO_2 (LSA)	1784	867	1781
CeO_2 (HSA)	2076	989	2070

[a]Temperature Programmed Reduction of the reduced catalysts (Relative Standard Deviation = ±3%).
[b]Temperature Programmed Oxidation after TPR (1) (Relative Standard Deviation = ±1%).
[c]Re-Temperature Programmed Reduction after TPO (Relative Standard Deviation = ±2%).

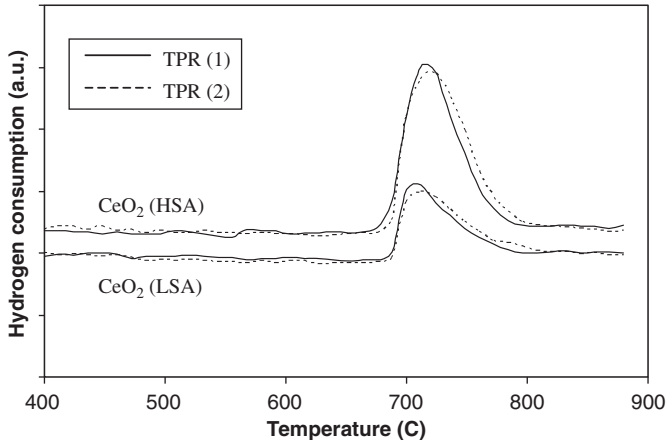

Fig. 6. TPR-2 of CeO_2 (HSA and LSA) compared to that of TPR-1.

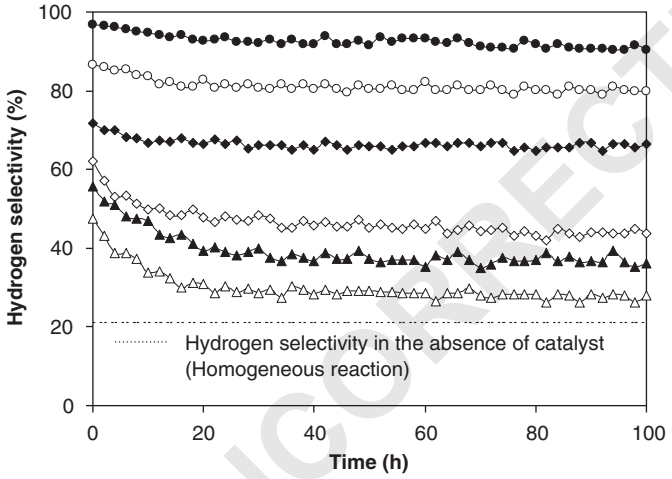

Fig. 7. Hydrogen selectivities from methanol decomposition at 900 °C for CeO_2 (HSA) with H_2O/CH_3OH of 3 (●), CeO_2 (HSA) with H_2O/CH_3OH of 1 (○), CeO_2 (HSA) with H_2O/CH_3OH of 0 (♦), CeO_2 (LSA) with H_2O/CH_3OH of 3 (◇), CeO_2 (LSA) with H_2O/CH_3OH of 1 (▲), and CeO_2 (LSA) with H_2O/CH_3OH of 0 (△).

for CeO_2 (LSA), whereas no peak of either carbon dioxide or carbon monoxide was detected for CeO_2 (HSA). The amount of carbon formations on the surface of CeO_2 (LSA) with different inlet H_2O/CH_3OH ratios were determined by measuring the CO and CO_2 yields from the TPO results. Using a value of 0.026 nm^2 for the area occupied by a carbon atom in a surface monolayer of the basal plane in graphite (Ramírez-Cabrera et al., 2004), the quantities of carbon deposited over this catalyst were observed to be approximately 0.35, 0.17, and 0.06 monolayer for the inlet H_2O/CH_3OH ratios of 0, 1, and 3, respectively. The total amounts of carbon deposited were ensured by the calculation of carbon balance in the system. Regarding the calculation, for the inlet H_2O/CH_3OH ratios of 0, 1, and 3, the moles of carbon deposited per gram of CeO_2 (LSA) were 0.39, 0.21, and 0.07 mmol g^{-1}. By the same assumption for the area occupied by a carbon atom (Ramírez-Cabrera et al., 2004), these values are equal to 0.33, 0.18, and 0.06 monolayer, respectively, which are in good agreement with the values observed from the TPO method described above. The TPO results clearly indicated the excellent resistance toward carbon formation for CeO_2 (HSA).

The BET measurement, as presented in Table 3, suggested that the deactivations of ceria are also due to the thermal sintering. Regarding the BET results, the surface area reduction percentage of CeO_2 (HSA) is lower than that of CeO_2 (LSA), indicating its better stability toward the thermal sintering.

3.5. Effects of temperature and inlet reactants

At steady state, the main products from this reaction over CeO_2 (HSA) were H_2, CO, and CO_2, with small amount of CH_4 depending on the operating conditions. The influences of operating temperature and the inlet steam content on the product selectivities and methanol conversion were studied by varying temperature from 700 to 1000 °C and changing the inlet steam to methanol ratio from 0.0 to 3.0.

As seen from Fig. 9, hydrogen and carbon monoxide selectivities increased with increasing temperature, whereas carbon dioxide and methane production selectivities decreased. Regarding the effect of steam, the conversion of methanol and the methane selectivity seem to be independent of the inlet steam content. However, hydrogen and carbon dioxide selectivities increased with increasing inlet steam concentration, whereas carbon monoxide selectivity decreased. Table 4 presents the comparison of product selectivities from methanol steam reforming at 900 °C between CeO_2 (HSA), and CeO_2 (LSA). It should be noted that the product selectivities from the homogeneous reaction (Fig. 6) and the product selectivities at equilibrium level, which were calculated by AspenPlus10.2 simulation program, are also shown in the table for comparison. Clearly, hydrogen and carbon monoxide selectivities from this reaction over CeO_2

Table 3
Deactivation percentages, steady state hydrogen selectivities, specific surface area, and amount of carbon deposition on the surface of catalysts after exposure in methanol decomposition conditions (various inlet H_2O/CH_3OH ratios) at 900 °C for 100 h

Catalyst	H_2O/CH_3OH ratio	Deactivation (%)	Hydrogen selectivity (%) at steady state	C formation[a] (monolayers)	BET surface ($m^2\ g^{-1}$)
CeO_2 (LSA)	0	40.9	28.0	0.35	6.0
	1	34.9	36.2	0.17	6.0
	3	29.7	43.6	0.06	6.1
CeO_2 (HSA)	0	7.4	66.5	~ 0	22.0
	1	7.6	80.0	~ 0	22.2
	3	6.5	90.4	~ 0	22.1

[a]Calculated using CO and CO_2 yields from temperature-programmed oxidation (TPO) with 10% oxygen.

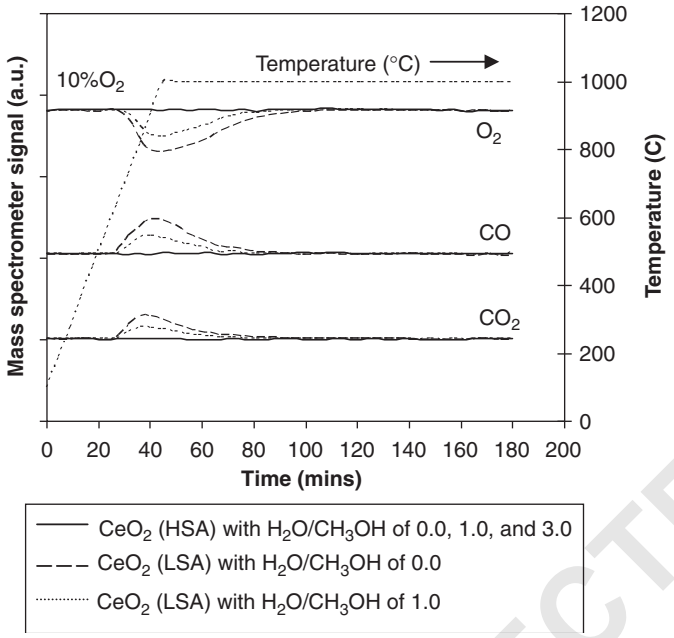

Fig. 8. TPO of CeO_2 (LSA) and CeO_2 (HSA) (10 kPa O_2) after exposure in methanol decomposition reaction at various inlet H_2O/CH_3OH ratios for 100 h.

(HSA) are higher and closer to their equilibrium levels than those over CeO_2 (LSA) in all conditions.

Without inlet steam, the effect of methanol concentration on the rate of decomposition at different temperatures was also studied by varying inlet methanol partial pressure from 1.0 to 4.0 kPa. The operating temperature range was between 700 and 800 °C in order to prevent the influence of homogeneous (non-catalytic) reaction. Fig. 10 presents the Arrhenius plots of the turnover frequencies at various inlet methanol concentrations. The results show that the decomposition rate is proportional to the methanol concentration and the temperature. The reaction order in methanol for CeO_2 (HSA) was observed to be between 0.37 and 0.68, independent of the steam partial pressure, for the range of conditions studied. These values were obtained experimentally by plotting $\ln(N)$ versus $\ln P_{CH_3OH}$ (where P_{CH_3OH} is the partial pressure of methanol; kPa). The reaction orders in other components (H_2O, and H_2) were achieved using the same approach by varying the inlet partial pressure of the component of interest while keeping the other inlet component partial pressures constant. Regarding the independence of inlet steam partial pressure on the rate of methanol decomposition, the reaction order in steam is therefore 0.

According to the post-reaction TPO, no carbon formation was observed on the surface of catalysts. In addition, the oxygen balance calculation was carried out during the stability testing to confirm the role of CeO_2. It was found from the calculation that the mole of oxygen (from methanol) fed into the system is almost similar to that in the products (CO, and CO_2) in all testing times, which indicates the unchanged state of CeO_2 (to Ce_2O_3) during the experiments. Furthermore, the TPO result for CeO_2 (HSA) in Fig. 8 also proves the unchanged state of spent CeO_2, as no oxygen uptakes were detected from the TPO of CeO_2 (HSA) after exposure in methanol decomposition conditions.

The influence of hydrogen on the rate of methanol decomposition was also investigated by adding various concentrations of hydrogen (1–3 kPa) in the feed. As shown in Fig. 11, the methanol conversion was significantly inhibited by the presence of hydrogen in the feed. The reaction order in hydrogen was between −0.29 and −0.17 in the range of conditions studied.

4. Discussion

CeO_2 (HSA) has a high reactivity for methanol decomposition and an excellent resistance toward carbon deposition without steam having to be present in the gas. This high resistance toward carbon deposition has been reported by several investigators (Laosiripojana, 2003; Ramírez-Cabrera et al., 2003, 2004; Laosiripojana and Assabumrungrat, 2005) and is mainly due to the high oxygen storage capacity of this material. CeO_2 contains a high concentration of highly mobile oxygen vacancies and thus acts as a local source or sink for oxygen on its surface. It has been reported that at high temperature the lattice oxygen (O_O^x) at the CeO_2 surface can oxidize gaseous hydrocarbons (methane, Ramírez-Cabrera et al., 2003, 2004; ethane and propane, Laosiripojana and Assabumrungrat, 2005) and also carbon monoxide (Laosiripojana, 2003).

In the decomposition of methanol at high temperature the presence of steam is normally required as it minimizes the carbon deposition on the catalyst surface, which is due to

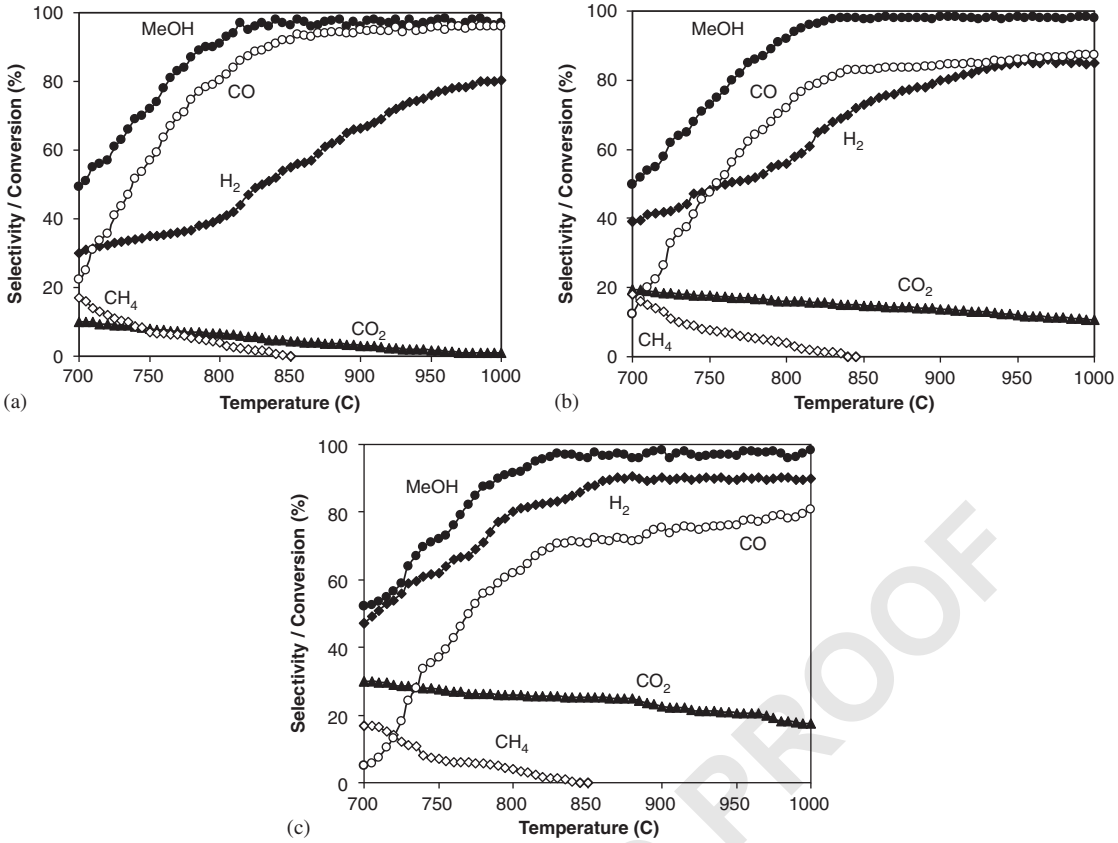

Fig. 9. Effects of reaction temperature and inlet H_2O/CH_3OH ratio on methanol conversion and product selectivities (H_2, CO, CO_2, and CH_4) from methanol decomposition over CeO_2 (HSA): (a) inlet H_2O/CH_3OH ratio of 0; (b) inlet H_2O/CH_3OH ratio of 1; (c) inlet H_2O/CH_3OH ratio of 3.

Table 4
Methanol conversion and product selectivities from the decomposition of methanol at various inlet H_2O/CH_3OH molar ratios (at isothermal condition, 900 °C)

Catalyst	H_2O/CH_3OH	Conversion and product selectivities at 900 °C				
	ratio	CH_3OH	H_2	CO	CO_2	CH_4
CeO_2 (LSA)	0	93.1	22.4	58.6	4.2	30.3
	1	94.2	27.1	55.0	11.0	28.2
	3	93.8	33.2	52.9	18.1	22.8
CeO_2 (HSA)	0	98.1	66.5	92.0	6.1	0
	1	98.2	80.0	84.4	13.7	0
	3	98.1	90.4	75.5	22.6	0
Homogeneous[a]	0	92.1	13.5	49.9	0	41.2
	1	92.4	17.4	49.1	3.4	39.9
	3	92.9	20.8	48.1	5.6	39.2
Equilibrium[b]	0	100	71.1	93.4	6.6	0
	1	100	89.4	85.2	14.8	0
	3	100	95.0	76.1	23.9	0

[a]Homogeneous (non-catalytic) reaction.
[b]Calculated by AspenPlus 10.2 simulation program.

reactions (4) and (5) mentioned in Section 1. By using CeO_2 as the catalyst, the carbon deposition from these reactions could be inhibited by the gas–solid reactions between CO and CH_4 formed with the lattice-oxygen (O_O^x) at the CeO_2 surface forming CO_2 and hydrogen from which the formation of carbon is thermodynamically unfavourable at high temperature. The reactions taken place can be summarized as follows:

$$C_nH_m + O_O^x = nCO + m/2H_2 + V_{O^{\cdot\cdot}} + 2e', \quad (16)$$

$$CO + O_O^x = 2CO_2 + V_{O^{\cdot\cdot}} + 2e'. \quad (17)$$

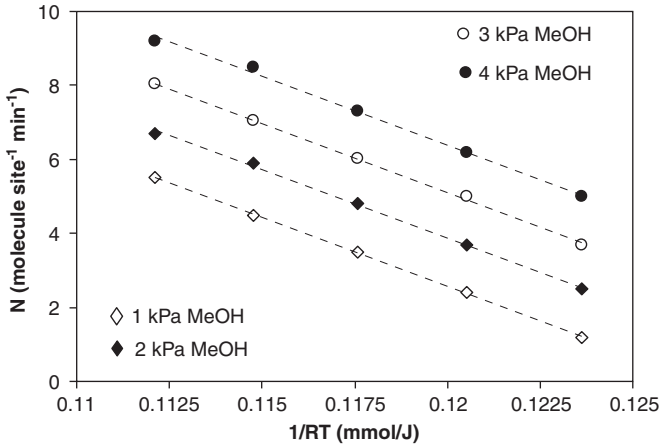

Fig. 10. Arrhenius plot of turnover frequencies (N) for methanol decomposition without steam over CeO_2 (HSA) with different inlet methanol partial pressures (1–4 kPa) at 700–800 °C.

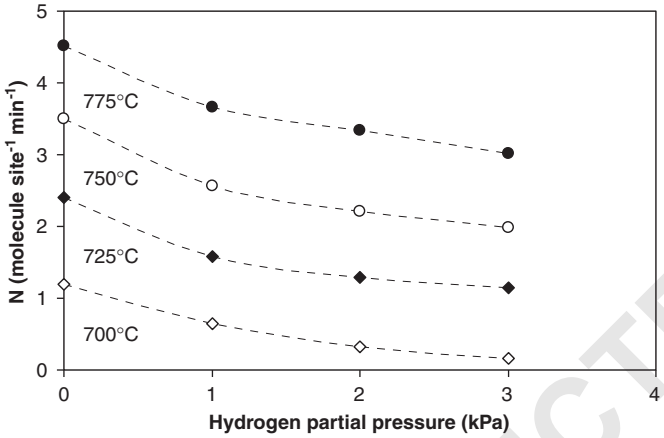

Fig. 11. Effect of hydrogen partial pressure on the turnover frequencies (N) for methanol decomposition over CeO_2 (HSA) at different temperatures (1 kPa MeOH and 3 kPa H_2O).

The lattice oxygen (O_O^x) is regenerated by reactions with oxygen containing compounds (methanol, steam) present in the system. The strong linear dependence of the methanol decomposition rate on methanol partial pressure and its independence of the steam partial pressure indicate that the lattice oxygen (O_O^x) is replenished by a sufficiently rapid reaction of the partially reduced CeO_2 with the oxygen containing molecules in the system, whereas the inhibitory effect of hydrogen could be due to the reverse of the methanol decomposition. According to the studies on the effect of temperature, hydrogen and carbon monoxide selectivities increased with increasing temperature, whereas carbon dioxide and methane production selectivities decreased. The changes of hydrogen, carbon monoxide, and carbon dioxide selectivities are mainly due to the influence of the mildly exothermic water–gas shift reaction ($CO + H_2O \rightarrow CO_2 + H_2$), whereas the decrease in methane production selectivity could be due to the further reforming to carbon monoxide and hydrogen.

Although the CeO_2 (LSA) can decompose methanol producing synthesis gas (CO and H_2), the major weaknesses of CeO_2 (LSA) are its nature, low specific surface area and its high size reduction due to the thermal sintering, which resulted in its low OSC as presented in Section 3.3. The low OSC for CeO_2 (LSA) results in its lower redox property (Eqs. (16) and (17)) and consequently caused the low reforming reactivity (almost three times lower than CeO_2 (HSA)) and low product selectivities (i.e., H_2 and CO). The comparative reforming reactivities between CeO_2 (HSA) and CeO_2 (LSA) are in good agreement with the results from the characterizations (i.e., BET and TPR)—the specific surface area of CeO_2 (HSA) and the amount of hydrogen uptakes from the temperature programmed reduction (TPR-1 and TPR-2) were significantly higher than those over the CeO_2 (LSA). By the same reason, the higher resistance toward carbon deposition for CeO_2 (HSA) compared to CeO_2 (LSA) is mainly due to the higher lattice oxygen (O_O^x) on its surface, which promotes the gas–solid reactions (Eqs. (16) and (17)) and consequently prevents the formation of carbon species via the methane decomposition and Boudouard reactions.

Due to the good performance of CeO_2 (HSA) in terms of high resistance toward carbon deposition and good product selectivities (producing only H_2, CO, and CO_2) at high temperature, this catalyst would be a good candidate to be applied as the internal or in-stack reforming catalyst for IIR-SOFC. Also, this material could be a promising option for application in the anode of SOFC (DIR-SOFC) compared to the CeO_2 (LSA), as it presents higher resistance toward carbon deposition and lower sintering rate. Importantly, without the presence of steam being required to reform methanol, the consideration of water management in SOFC system is negligible. Regarding the above benefits, the use of CeO_2 (HSA) is expected to simplify the overall SOFC system design (i.e., DIR and IIR), making SOFCs more attractive to be used commercially.

5. Conclusion

Nano-particulate high surface area CeO_2 (CeO_2 (HSA)) has a useful methanol decomposition activity at SOFC temperatures producing H_2, CO, CO_2, and small amount of CH_4 without the presence of steam being required. The conversion of methanol from the decomposition process over this catalyst was close to 100% at 850 °C, and no carbon deposition was observed on the surface of CeO_2 according to the TPO results. Hydrogen selectivities up to 90% can be produced. Regarding the influences of inlet components on the rate of methanol decomposition, the decomposition rate over CeO_2 (HSA) is proportional to the methanol partial pressure and independent of the steam partial pressure at 700–800 °C. Hydrogen was found to have a significant inhibitory effect on the rate of methanol decomposition.

Due to the good performance of CeO_2 (HSA) toward methanol decomposition in terms of high resistance toward carbon deposition and good product selectivities at SOFC temperature, this catalyst is a good candidate to be applied as the internal or in-stack reforming catalyst for solid oxide fuel cell application (IIR-SOFC).

Acknowledgements

The financial support from The Thailand Research Fund (TRF) throughout this project is gratefully acknowledged. The first author would like to acknowledge Professor David Chadwick from Department of Chemical Engineering and Chemical Technology, Imperial College London for his valuable suggestion.

References

Aguiar, P., Lapena-Rey, N., Chadwick, D., Kershenbaum, L., 2001. Improving catalyst structures and reactor configurations for autothermal reaction systems: application to solid oxide fuel cells. Chemical Engineering Science 56, 652.

Amor, J.N., 1999. The multiple roles for catalysis in the production of H_2. Applied Catalysis A 176, 159–176.

An, S., Lu, C., Worrell, W.L., Gorte, R.J., Vohs, J.M., 2004. Characterization of Cu–CeO_2 direct hydrocarbon anodes in a solid oxide fuel cell with lanthanum gallate electrolyte. Solid State Ionics 175 (1–4), 135–138.

Brett, D.J.L., Atkinson, A., Cumming, D., Ramírez-Cabrera, E., Rudkin, R., Brandon, N.P., 2005. Methanol as a direct fuel in intermediate temperature (500–600 °C) solid oxide fuel cells with copper based anodes. Chemical Engineering Science 60 (21), 5649–5662.

Brown, L.F., 2001. A comparative study of fuels for on-board hydrogen production for fuel-cell-powered automobiles. International Journal of Hydrogen Energy 26, 381–397.

Costa-Nunes, O., Gorte, R.J., Vohs, J.M., 2005. Comparison of the performance of Cu–CeO_2–YSZ and Ni–YSZ composite SOFC anodes with H_2, CO, and syngas. Journal of Power Sources 141 (2), 241–249.

Dicks, A.L., 1996. Hydrogen generation from natural gas for the fuel cell systems of tomorrow. Journal of Power Sources 61 (1–2), 113–124.

Douvartzides, S.L., Coutelieris, F.A., Demin, K., Tsiakaras, P.E., 2003. Fuel options for solid oxide fuel cells: a thermodynamic analysis. A.I.Ch.E. 49, 248–257.

Emonts, B., Hansen, J.B., Jorgensen, S.L., Hohlein, B., Peters, R., 1998. Compact methanol reformer test for fuel-cell powered light-duty vehicles. Journal of Power Sources 71, 288.

Gellings, P.J., Bouwmeester, H.J.M., 2000. Solid state aspects of oxidation catalysis. Catalysis Today 58, 1–53.

Gorte, R.J., Vohs, J.M., McIntosh, S., 2004. Recent developments on anodes for direct fuel utilization in SOFC. Solid State Ionics 175 (1–4), 1–6.

Jung, S., Lu, C., He, H., Ahn, K., Gorte, R.J., Vohs, J.M., 2005. Influence of composition and Cu impregnation method on the performance of Cu/CeO_2/YSZ SOFC anodes. Journal of Power Sources, in press.

Kim, T., Liu, G., Boaro, M., Lee, S.-I., Vohs, J.M., Gorte, R.J., Al-Madhi, O.H., Dabbousi, B.O., 2005. A study of carbon formation and prevention in hydrocarbon-fueled SOFC. Journal of Power Sources, in press.

Laosiripojana, N., 2003. Reaction engineering of indirect internal steam reforming of methane for application in solid oxide fuel cells. Ph.D. Thesis, University of London, England.

Laosiripojana, N., Assabumrungrat, S., 2005. Catalytic steam reforming of ethane and propane over CeO_2-doped Ni/Al_2O_3 at SOFC temperature: improvement of resistance toward carbon formation by the redox property of doping CeO_2. Fuel, in press.

Ledjeff-Hey, K., Formanski, V., Kalk, T., Roes, J., 1998. Compact hydrogen production systems for solid polymer fuel cells. Journal of Power Sources 71 (1–2), 199–207.

Lwin, Y., Daud, W.R.W., Mohamad, A.B., Yaakob, Z., 2000. Hydrogen production from steam-methanol reforming: thermodynamic analysis. International Journal of Hydrogen Energy 25 (1), 47–53.

Maggio, G., Freni, S., Cavallaro, S., 1998. Light alcohols/methane fuelled molten carbonate fuel cells: a comparative study. Journal of Power Sources 74, 17–23.

Marina, O.A., Bagger, C., Primdahl, S., Mogensen, M., 1998. In: Stevens, P., Bossell, U. (Eds.), Proceedings of Third European SOFC Forum, Oberrohrdorf, Nantes, Switzerland, p. 427.

Minh, N.Q., Takahashi, T., 1995. Science and Technology of Ceramic Fuel Cells. Elsevier, Amsterdam.

Otsuka, K., Hatano, M., Morikawa, A., 1983. Hydrogen from water by reduced cerium oxide. Journal of Catalysis 79, 493.

Otsuka, K., Hatano, M., Morikawa, A., 1985. Decomposition of water by cerium oxide of δ-phase. Inorganica Chimica Acta 109, 193.

Ramírez-Cabrera, E., Atkinson, A., Chadwick, D., 2002. Reactivity of ceria, Gd- and Nb-doped ceria to methane. Applied Catalysis B 36, 193.

Ramírez-Cabrera, E., Laosiripojana, N., Atkinson, A., Chadwick, D., 2003. Methane conversion over Nb-doped ceria. Catalysis Today 78, 433–438.

Ramírez-Cabrera, E., Atkinson, A., Chadwick, D., 2004. Catalytic steam reforming of methane over $Ce_{0.9}Gd_{0.1}O_{2-x}$. Applied Catalysis B 47, 127–131.

Rostrup-Nielsen, J.R., Bak-Hansen, J.-H., 1993. CO_2-reforming of methane over transition metals. Journal of Catalysis 144, 38.

N. Laosiripojana and S. Assabumrungrat

"Catalytic steam reforming of ethanol over high surface area CeO_2: The role of CeO_2 as an internal pre-reforming catalyst"

Applied Catalysis B: Environmental, revised

(IF-2004 = 4.06)

Submitted to Applied Catalysis B: Environmental (Revised)
Type of Contribution: Research Paper

Catalytic steam reforming of ethanol over high surface area CeO_2: The role of CeO_2 as an internal pre-reforming catalyst

N. Laosiripojana[1,*] and S. Assabumrungrat[2]

[1] The Joint Graduate School of Energy and Environment,
King Mongkut's University of Technology Thonburi, Bangkok, 10140, Thailand
[2] Center of Excellence on Catalysis and Catalytic Reaction Engineering,
Department of Chemical Engineering, Faculty of Engineering, Chulalongkorn University, Bangkok, Thailand

[*] Corresponding author (navadol_l@jgsee.kmutt.ac.th)

Abstract

In the present work, it was found that high surface area ceria (CeO_2 (HSA)), synthesized by a surfactant-assisted approach, have useful ethanol steam reforming activity under Solid Oxide Fuel Cells (SOFCs) temperatures. The catalyst provides good reforming reactivity and high resistance toward carbon deposition compared to Ni/Al_2O_3 and conventional low surface area ceria (CeO_2 (LSA)). Although the hydrogen selectivity at steady state from the ethanol steam reforming over CeO_2 (HSA) was lower than Rh/Al_2O_3, the resistance toward carbon deposition of CeO_2 (HSA) was considerably higher. The good reactivity toward the steam reforming of ethanol for CeO_2 (HSA) is due to the high redox property of this material. During the reforming process, the gas-solid reactions between the gaseous hydrocarbon components and the lattice oxygen (O_O^x) on CeO_2 surface take place ($C_nH_m + O_O^x \rightarrow nCO + m/2(H_2) + V_O^{\bullet\bullet} + 2\ e'$) forming synthesis gas and also preventing the formation of carbon species from hydrocarbon decomposition reactions ($C_nH_m \rightarrow nC + m/2H_2$).

At the temperature of 900ºC, the main products from the steam reforming of ethanol over CeO_2 (HSA) (with inlet C_2H_5OH/H_2O molar ratio of 1.0/3.0) were 67.5% H_2, 37.9%CH_4, 50.5%CO, and 11.6%CO_2. In contrast, the formations of C_2H_4 (5.8-15.8%) and C_2H_6 (1.2-8.5%) were also observed from the steam reforming of ethanol

over Ni/Al_2O_3 and CeO_2 (LSA). The combination use of CeO_2 and Ni/Al_2O_3 was studied in an annular ceramic reactor by applying CeO_2 as an internal pre-reforming catalyst. The main purpose of CeO_2 is to convert all ethanol and other high hydrocarbon compounds (e.g. C_2H_4 and C_2H_6) forming CH_4, CO, CO_2, and H_2, while Ni/Al_2O_3 is applied to reform all CH_4 left from the pre-reforming section and maximize the yield of hydrogen production. After operated at 900ºC for 100 h, this combination pattern offers high hydrogen selectivity (87.0-91.4%) and good resistance toward carbon deposition. This successful development eliminates the requirement of expensive noble metal catalysts or the installation of an external pre-reformer in order to reform ethanol internally (IIR-SOFC).

Keywords: Ethanol**,** internal reforming, ceria, redox, solid oxide fuel cell

1. Introduction

Solid Oxide Fuel Cell (SOFC) with an indirect internal reforming operation (IIR), called IIR-SOFC, is expected to be an important technology for energy generation in the near future due to the high efficiency and its lower pollutant emission. Regarding this operation, the endothermic reforming reaction takes place at the reformer, which is in close thermal contact with the anode side of fuel cell where the exothermic electrochemical reaction occurs, Fig. 1 [1]. The aim of the reformer unit is to reform and maximize the yield of hydrogen production, which can be generated from several sources such as natural gas, bio-ethanol, coal, biomass, and biogas, and supply this component to the anode side of SOFC. IIR-SOFC gives the advantage on eliminating the requirement for a separate fuel reformer and providing good heat transfer between the reformer and the fuel cell. In addition, the reformer part and the anode side for IIR operation can be operated separately. Therefore, the catalyst for reforming reaction at the reformer part and the material for electrochemical reactions at the anode side of fuel cell can be different and optimized individually. This operation is expected to simplify the overall SOFC system design, making SOFC more attractive and efficient for producing electrical power [1].

Regarding the current oil crisis and the shortage of fossil fuels, the development of the biomass-based fuels therefore attracts much attention. Among various resources, bio-ethanol is a promising candidate for hydrogen for SOFC, since it is readily produced by renewable resources (e.g., fermentation of biomasses) and has reasonably high

hydrogen content [2,3]. The major difficulty to reform ethanol is the deactivation of the reforming catalyst due to the possible carbon deposition from the ethanol decomposition. It has widely been reported that ethanol can homogenously decompose to several hydrocarbon elements (e.g. acetaldehyde, methane, carbon monoxide, carbon dioxide, ethylene, and ethane) without the requirement of catalyst [4]. The formations of ethylene and ethane are the major problem, as these components act as very strong promoters for carbon formation. When ethanol is reformed internally (IIR-SOFC) without any pre-treatments, the carbon formation can be easily formed on the catalyst surface.

SOFC fueled by high organic compounds (e.g. natural gas, DME, LPG, and bio-ethanol) normally requires a small external preliminary reforming unit (pre-reformer), where these high hydrocarbons are reformed readily forming low hydrocarbon compounds (e.g. methane) before introducing to the main part of the SOFC system [5]. The pre-reforming unit is normally operated at relatively lower temperatures, 300-500ºC, in which the carbon formation problem is less severe, but the disadvantage of this installation is the extra-requirement of the heat supplied into this unit, which can reduce the fuel cell efficiency.

The approach in this work is developing of an alternative catalytic reforming operation that is enabling to reform ethanol with low degree of carbon deposition at SOFC temperatures, 800-1000ºC. The successful development of this operation would help eliminate the requirement of the external pre-reformer. Previously, hydrogen production from the reforming of ethanol has been studied by several researchers [6-27], most of them have investigated the reforming of ethanol over noble metal catalysts (e.g. Rh, Ru, Pt, Pd) on several oxide supports (e.g. Al_2O_3, MgO, SiO_2, TiO_2) [11,13,14,17,24,25,26]. Freni et al. [11, 14, 16, 25] presented that Rh/Al_2O_3 provides the highest reforming reactivity among these noble metal catalysts. Burch and coworkers [19] found that the order of the ethanol steam reforming reactivity of the metals is Rh > Pd > Ni = Pt. In the present work, Ni/Al_2O_3 was selected as a based catalyst rather than these precious metals. Although the precious metals have been reported to be active for the ethanol steam reforming and provide high resistance to the carbon formation than Ni based catalysts [28, 29], the current prices of these metals are very high for commercial uses, and the availability of some precious metals such as ruthenium was too low to have a major impact on the total reforming catalyst market [30]. The main procedure to improve the ethanol steam reforming reactivity in this work is to investigate the use of

cerium oxide (CeO_2), as the reforming catalyst, together with the conventional Ni/Al_2O_3 in a single unit.

Cerium oxide (CeO_2) has been commonly reported to apply as catalysts in a wide variety of reactions involving oxidation or partial oxidation of hydrocarbons (e.g. automotive catalysis). A high oxygen mobility (redox property) [31], high oxygen storage capacity [32-37], strong interaction with the supported metal (strong metal–support interaction) [38] and the modifiable ability [39] render this material very interesting for catalysis. Recently, the high resistance toward carbon deposition over ceria has been widely observed [40-43]. Importantly, CeO_2 has been reported to have the reactivity toward the methane steam reforming reaction at such a high temperature (800-1000ºC) [40]. It was demonstrated that the gas–solid reaction between CeO_2 and CH_4 produces H_2 and CO, according to reaction (1). In addition, the reaction of the reduced ceria with H_2O and CO_2 produces more H_2 and CO, respectively, and regenerates a lattice oxygen in CeO_2 [44-45]:

$$CH_4 + O_O^x = 2\,H_2 + CO + V_O^{\bullet\bullet} + 2\,e' \quad (1)$$

$$V_O^{\bullet\bullet} + 2\,e' + H_2O = O_O^x + H_2 \quad (2)$$

$$V_O^{\bullet\bullet} + 2\,e' + CO_2 = O_O^x + CO \quad (3)$$

O_O^x denotes a lattice oxygen in CeO_2, $V_O^{\bullet\bullet}$ is an oxygen vacancy with an effective charge 2^+, e' is an electron which can either be more or less localized on a cerium ion or delocalized in a conduction band [46].

Unfortunately, the steam reforming reactivity over CeO_2 was too low compared to the conventional metallic catalysts [40]. This is mainly due to its low specific surface area, and its high sintering rate at high temperature [40, 43]. It was reported that the methane conversion of the methane steam reforming over CeO_2 was less than 10% [40]. In the present work, we therefore investigated the use of cerium oxide as either a preliminary reforming (pre-reforming) or a combined reforming (co-reforming) element instead.

It should be noted that, in order to minimise the weakness of CeO_2 in term of its low specific surface area, CeO_2 applied in this work was the high surface area CeO_2 (CeO_2 (HSA)). Several methods have recently been described for the preparation of CeO_2 (HSA) solid solution. Among these methods, the surfactant-assisted approach was employed to prepare high surface area CeO_2 with improved textural, structural, and

chemical properties [47-53]. Our previous publication [40] also presented the achievement of CeO_2 with high surface area and good stability after thermal treatment by this preparation method. Regarding the surfactant-assisted method, CeO_2 (HSA) is prepared by reacting a cationic surfactant with a hydrous oxide produced by co-precipitation under basic conditions. At high pH value, conducting the precipitation of hydrous oxide in the presence of cationic surfactant allows the cation exchange process between H^+ and the surfactant to take place, resulting in a developed pore structure with an increase in surface area [53]. The achievement of high thermal stability for CeO_2 (HSA) is due to the incorporation of surfactants during preparation, which can reduce the interfacial energy and eventually decrease the surface tension of water contained in the pores. This could reduce the shrinkage and collapse of the catalyst during heating up, which consequently help the catalyst maintaining high surface area after calcination [53].

In the present work, the first approach was to study the reactivity of CeO_2, especially the high surface area one, toward the steam reforming of ethanol. The effects of temperature, inlet C_2H_5OH/H_2O molar ratio, and C_2H_5OH concentration on the reforming rate and product selectivities were also determined. The benefit of applying CeO_2 together with conventional Ni/Al_2O_3 was then presented. It should be noted that the ethanol steam reforming over Rh/Al_2O_3 was also investigated in the present work for the comparison purpose. All experiments described above were carried out at the SOFC temperature range (800-1000ºC) for later application in IIR-SOFC system.

2. Experimental

2.1. Catalyst preparation and characterization

The conventional low surface area CeO_2 (CeO_2 (LSA)) was prepared by the precipitation method. The starting solution was prepared by mixing 0.1 M of cerium chloride ($CeCl_3 \cdot 7H_2O$) salt solution with 0.4 M of ammonia at a 2:1 volumetric ratio. This solution was stirred by magnetic stirring (100 rpm) for 3 h, then sealed and placed in a thermostatic bath maintained at 90°C for 3 days. The precipitate was filtered and washed with deionised water and acetone. It was dried overnight in an oven at 110°C, and then calcined in air at 1000°C for 6 h.

High surface area CeO_2 support (CeO_2 (HSA)) was prepared by adding an aqueous solution of the appropriate cationic surfactant, 0.1 M cetyltrimethylammonium

bromide solution from Aldrich, to a 0.1 M cerium chloride. The molar ratio of ([Ce])/ [cetyltrimethylammonium bromide] was kept constant at 0.8. The mixture was stirred and then aqueous ammonia was slowly added with the constant rate of 0.165 cm^3 min^{-1} until the pH was 11.5. We found that the rate of ammonia doping have a significant impact on the specific surface area of synthesis CeO_2, Table 1. According to our experiments, this flow rate of ammonia can provide solid CeO_2 with the highest specific surface area. The mixture was continually stirred for 3 h, then sealed and placed in the thermostatic bath maintained at 90°C for 3 days. After that, the mixture was cooled and the resulting precipitate was filtered and washed repeatedly with water and acetone. The filtered powder was then treated under the same procedures as CeO_2 (LSA). BET measurements of CeO_2 (both LSA and HSA) were carried out at different calcination temperatures in order to determine the decrease of specific surface area due to the thermal sintering. As presented in Table 1, after drying, surface areas of 308 and 55 m^2 g^{-1} were observed for CeO_2 (HSA) and conventional CeO_2, respectively and, as expected, the surface area dramatically decreased at high calcination temperatures. However, the value for CeO_2 (HSA) is still appreciable after calcination at 1000°C, Table 1. The homogeneity and morphology of CeO_2 (HSA) was also investigated. All samples have a similar morphology and exhibit a very narrow particle-size histogram. As expected, samples treated at 1000°C showed a larger particle size than those treated at lower temperatures. The redox properties and redox reversibilities of these synthesized CeO_2 (both LSA and HSA) were compared by the temperature programmed reduction (TPR) and the temperature programmed oxidation (TPO). In these experiments, 5% H_2/helium and 5% O_2/helium were used for the TPR and TPO respectively, while the temperature of the system increased from 100ºC to 900ºC with the rate of 12ºC/min for both experiments.

For comparison, Ni/Al_2O_3 and Rh/Al_2O_3 (5wt% Ni and Rh) were prepared by impregnating α-Al_2O_3 (from Aldrich) with $NiCl_3$ and $RhCl_3$ solutions, respectively. After stirring, the solution was dried and calcined at 1000°C for 6 h. Ni/Al_2O_3 was reduced with 10% hydrogen in helium at 700ºC for 6 h before use, while Rh/Al_2O_3 was reduced with 10% hydrogen + 5% steam in helium at 700ºC for 6 h. It should be noted that the adding of steam during the reduction of Rh/Al_2O_3 is to prevent the phenomenon of Strong Metal-Support Interaction (SMSI), which has been widely reported by several researchers [54-57]. After reduction, the catalysts were characterized by several physicochemical methods. The weight contents of Ni and Rh in Ni/Al_2O_3 and Rh/Al_2O_3 were determined by X-ray fluorescence (XRF) analysis. The reducibility and dispersion percentages of

nickel and rhodium were measured from temperature-programmed reduction (TPR) with 5% H_2 in Ar and temperature-programmed desorption (TPD) respectively. The catalyst specific surface areas were obtained from BET measurements. All physicochemical properties of the synthesized catalysts are presented in Table 2.

2.2. Apparatus and Procedures

An experimental reactor system was constructed as shown in Fig. 2. The feed gases including the components of interest (ethanol and steam from the evaporator) and the carrier gas (helium) were introduced to the reaction section, in which a 10-mm diameter quartz reactor was mounted vertically inside a furnace. The reactivities of catalyst toward the ethanol steam reforming were determined by loading each selected catalyst (e.g., CeO_2, Ni/Al_2O_3, and Rh/Al_2O_3) in this quartz reactor, which was packed with a small amount of quartz wool to prevent the catalyst from moving. Regarding the results in our previous publications [40-42], to avoid any limitations by intraparticle diffusion, the total gas flow was 1000 cm^3 min^{-1} under a constant residence time of 5 x 10^{-4} g min cm^{-3} in all experiments. A Type-K thermocouple was placed into the annular space between the reactor and the furnace. This thermocouple was mounted on the tubular reactor in close contact with the catalyst bed to minimize the temperature difference between the catalyst bed and the thermocouple. Another Type-K thermocouple was inserted in the middle of the quartz tube in order to re-check the possible temperature gradient. The record showed that the maximum temperature fluctuation during the reaction was always ±0.75ºC or less from the temperature specified for the reaction.

After the reactions, the exit gas mixture was transferred via trace-heated lines to the analysis section, which consists of a Porapak Q column Shimadzu 14B gas chromatograph (GC) and a mass spectrometer (MS). The gas chromatography with TCD and FID detectors was applied in order to investigate the reforming reactivity, whereas the mass spectrometer in which the sampling of the exit gas was done by a quartz capillery and differential pumping was used for the transient carbon formation experiment. In order to study the formation of carbon species on catalyst surface, Temperature programmed Oxidation (TPO) was applied by introducing 10% oxygen in helium into the system, after purged the system with helium. The operating temperature increased from 100ºC to 1000ºC by the rate of 20ºC/min. The amount of carbon formations on the surface of catalysts were determined by measuring the CO and CO_2 yields from the TPO results (using Microcal Origin Software) assuming a value of 0.026

nm^2 for the area occupied by a carbon atom in a surface monolayer of the basal plane in graphite [58]. The calibrations of CO and CO_2 productions were performed by injecting a known amount of these calibration gases from a loop, in an injection valve in the bypass line. The response factors were obtained by dividing the number of moles for each component over the respective areas under peaks.

In addition to the TPO method, the amount of carbon deposition was confirmed by the calculation of carbon balance in the system. The amount of carbon deposited on the surface of catalyst would theoretically be equal to the difference between the inlet carbon containing components (C_2H_5OH) and the outlet carbon containing components (CO, CO_2, CH_4, C_2H_6, C_2H_4, and CH_3CHO). The amount of carbon deposited per gram of catalyst is given by the following equation:

$$C_{deposition} = \frac{mole_{carbon(in)} - mole_{carbon(out)}}{m_{catalyst}} \tag{4}$$

The rate of ethanol decomposition was defined in term of conversion denoted as X_{Ethanol}, whereas the product selectivities (hydrogen, carbon monoxide, carbon dioxide, methane, ethane, ethylene, and acetaldehyde), denoted as S_{product}, are calculated according to Eqs. (5) – (12):

$$X_{Ethanol} = \frac{100(\%Ethanol_{in} - \%Ethanol_{out})}{\%Ethanol_{in}} \tag{5}$$

$$S_{H_2} = \frac{100(\%H_2)}{3(\%Ethanol_{in} - \%Ethanol_{out})} \tag{6}$$

$$S_{CO} = \frac{100(\%CO)}{2(\%Ethanol_{in} - \%Ethanol_{out})} \tag{7}$$

$$S_{CO_2} = \frac{100(\%CO_2)}{2(\%Ethanol_{in} - \%Ethanol_{out})} \tag{8}$$

$$S_{CH_4} = \frac{100(\%CH_4)}{2(\%Ethanol_{in} - \%Ethanol_{out})} \tag{9}$$

$$S_{C_2H_6} = \frac{100(\%C_2H_6)}{(\%Ethanol_{in} - \%Ethanol_{out})} \tag{10}$$

$$S_{C_2H_4} = \frac{100(\%C_2H_4)}{(\%Ethanol_{in} - \%Ethanol_{out})} \quad (11)$$

$$S_{CH_3CHO} = \frac{100(\%CH_3CHO)}{(\%Ethanol_{in} - \%Ethanol_{out})} \quad (12)$$

It should be noted that, from Eq. 6, three H_2 molecules from ethanol represent 100% H_2 selectivity. However, from the steam reforming of ethanol, H_2 selectivity can exceed 100%. This is possible because water is consumed as well as ethanol in the process, therefore, H atoms from H_2O can also be converted into H_2.

2.3 Catalytic reactor configuration

After testing the catalyst reactivity in the packed bed reactor as described above, the annular ceramic reactor was constructed in order to study the combination of CeO_2 (both LSA and HSA) with Ni/Al_2O_3 as a single reforming unit, Fig. 3. By this configuration, 200 mg of CeO_2 (with SiC), as an internal pre-reforming catalyst, was packed at the inner side of the annular reactor, where the inlet gas was firstly introduced. At the end of the inner tube, all gas components flowed backward through the outer side of this annular reactor, where 300 mg of Ni/Al_2O_3 (with SiC) was packed. The main purpose of Ni/Al_2O_3 is to convert all hydrocarbons left from the pre-reforming section and maximize the yield of hydrogen production.

For comparison of the combination method, CeO_2 was mixed together with Ni/Al_2O_3 and acted as the co-reforming catalyst. The ethanol steam reforming reactivities for these two methods were determined and compared to the use of single catalysts (e.g. Ni/Al_2O_3, and Rh/Al_2O_3). The effects of temperature, inlet C_2H_5OH/H_2O molar ratios, and inlet C_2H_5OH concentration on the product selectivity and amount of carbon deposition for each operation were also studied.

3. Results

3.1 Redox properties and redox reversibility of the synthesized CeO_2

The oxygen storage capacities (OSC) and the degree of redox properties for CeO_2 (both LSA and HSA) were investigated using temperature programmed reduction (TPR-1), which was performed by heating the reduced catalysts up to 900°C in 5%H_2 in

helium. The tests over Ni/Al_2O_3 and Rh/Al_2O_3 were also performed for comparison. As shown in Fig. 4, hydrogen uptakes are detected from both CeO_2 at the temperature above 750°C. The amount of hydrogen uptake over CeO_2 (HSA) is about 2.6 times higher than that over CeO_2 (LSA), suggesting the OSC and the redox properties strongly depend on the specific surface area of CeO_2. In contrast, no hydrogen consumption was observed from the TPR over Ni/Al_2O_3 and Rh/Al_2O_3, indicating that no occurrence of redox properties for these catalysts. The benefit of redox property on the reforming of ethanol will be presented later in the discussion section. After purged with helium, the redox reversibility for each CeO_2 was then determined by performing temperature programmed oxidation (TPO) followed by the second temperature programmed reduction (TPR-2). The TPO was carried out by heating the catalyst up to 900°C in $10\%O_2$ in helium; the amounts of oxygen chemisorbed were then measured, Fig. 5 and Table 3. Regarding the TPR-2 results as shown in Fig. 6 and Table 3, the amount of hydrogen uptakes for CeO_2 (both LSA and HSA) were approximately similar to those from TPR-1, indicating the redox reversibility for these synthesis CeO_2.

3.2 Homogenous (non catalytic) reaction

Before studying the catalyst performance, the homogeneous (non-catalytic) steam reforming of ethanol was primarily investigated. The inlet C_2H_5OH/H_2O in helium with the molar ratio of 1.0/3.0 was introduced to the system, while the temperature increased from 100ºC to 1000ºC. As shown in Fig. 7, it was observed that ethanol converted to acetaldehyde, and hydrogen at the temperature above 200°C. Methane and carbon monoxide productions were initially observed at the temperature of 250-300°C. When the temperature increased up to 550°C, the selectivity of acetaldehyde significantly decreased, while the hydrogen, carbon monoxide, and carbon dioxide selectivities remained increasing. In this range of temperature, the formations of ethane and ethylene were also observed.

3.3 Stability and activity toward the ethanol steam reforming

The synthesized CeO_2 (HSA), CeO_2 (LSA), Ni/Al_2O_3, and Rh/Al_2O_3 were tested for the ethanol steam reforming at 900°C with the inlet C_2H_5OH/H_2O molar ratio of 1.0/3.0 (inlet C_2H_5OH of 3.0 kPa). The reforming rate was measured as a function of time in order to indicate the stability and the deactivation rate. The variations in the hydrogen

selectivity with time at 900°C are shown in Fig. 8. Significant deactivations were detected for Ni/Al_2O_3 catalyst, whereas much lower deactivations were observed over CeO_2 (HSA), CeO_2 (LSA), and Rh/Al_2O_3. At steady state, the ethanol steam reforming over CeO_2 (HSA) showed the best performance in terms of stability, while Rh/Al_2O_3 presented the best activity at steady state. Catalyst stabilities expressed as deactivation percentages are given in Table 4. It should be noted that, in order to determine whether the observed deactivation is due to the carbon formation, the post-reaction temperature-programmed oxidation (TPO) experiments were carried out.

From the TPO results shown in Fig. 9, the huge amounts of carbon deposition were observed for Ni/Al_2O_3, whereas significant lower carbon formations were detected for CeO_2 (LSA) and Rh/Al_2O_3. No formation of carbon species was detected for CeO_2 (HSA) in all conditions. The values of carbon formations (monolayer) on the surface of catalysts were determined by measuring these CO and CO_2 yields (using Microcal Origin Software). Using a value of 0.026 nm^2 for the area occupied by a carbon atom in a surface monolayer of the basal plane in graphite [58], the quantities of carbon deposited for each catalyst were observed as also presented in Table 4. The total amounts of carbon deposited were also ensured by calculating the carbon balance of the system. Regarding the calculations, the moles of carbon deposited per gram of Ni/Al_2O_3, CeO_2 (LSA), and Rh/Al_2O_3 were 4.55, 0.70, and 1.46 mmol g^{-1}. By the same assumption for the area occupied by a carbon atom [58], these values are equal to 4.54, 0.69, and 1.44 monolayers respectively, which are in good agreement with the values observed from the TPO method described above. The results clearly indicated that the deactivations observed for Ni/Al_2O_3 were mainly due to the carbon deposition on the surface of catalyst. In addition, CeO_2 especially the high surface area one presented significantly stronger resistance toward carbon formation compared to Ni/Al_2O_3. The BET measurements were carried out to observe the surface area reduction percentages of all catalysts. As shown in Table 4, it was suggested that the deactivations of ceria are mainly due to the thermal sintering. However, the surface area reduction percentage of CeO_2 (HSA) is much lower than CeO_2 (LSA), indicating its better stability toward the thermal sintering.

3.4 Effects of temperature and inlet compositions

The influences of operating temperature and the inlet steam content on the ethanol conversion and product selectivities from the ethanol steam reforming over CeO_2 (HSA), CeO_2 (LSA), Ni/Al_2O_3, and Rh/Al_2O_3 were studied by varying temperature from 700°C to 1000°C for three different inlet C_2H_5OH/H_2O molar ratios (1.0/3.0, 1.0/4.0, and 1.0/5.0).

Fig. 10 (a, b, and c) presents the influences of temperature and the inlet C_2H_5OH/H_2O molar ratio on the ethanol conversion and product selectivities from the ethanol steam reforming over CeO_2 (HSA). At the temperature above 900°C, the products from this reaction over CeO_2 (HSA) were CH_4, H_2 and CO with some CO_2. The formations of ethylene and ethane were slightly observed at the lower temperatures. These formations decreased with increasing temperature and inlet steam concentration. Hydrogen and carbon monoxide selectivities increased with increasing temperature, whereas carbon dioxide and methane production selectivities decreased. Regarding the effect of steam, the conversion of ethanol and the methane selectivity seem to be independent of the inlet steam content. However, hydrogen and carbon dioxide selectivities increased with increasing inlet steam concentration, whereas carbon monoxide selectivity decreased. The yield of methane production was non-monotonic. It increased with increasing temperature until ~850°C, oppositely, the yield of methane production reduced at higher temperature.

The changes of hydrogen, carbon monoxide, and carbon dioxide selectivities are mainly due to the influence of mildly exothermic water-gas shift reaction ($CO + H_2O \rightarrow CO_2 + H_2$). The increase of methane production at low temperature (700-850°C) comes from the decomposition of ethanol, whereas the decrease at high temperature (>850°C) could be due to the further reforming to carbon monoxide and hydrogen. Table 5 summarizes the influence of the inlet steam content on the product selectivities at 900°C for all catalysts with the additional information regarding the characterization (e.g. TPO) over these spent catalysts.

According to the good performance of CeO_2 (HSA) in terms of product selectivities and resistance toward carbon formation, the effect of inlet ethanol concentration on the degree of carbon deposition over this catalyst was further studied by increase the inlet ethanol partial pressure from 3.0 to 15.0 kPa while keep the inlet C_2H_5OH/H_2O ratio constant at 1.0/3.0. At 900°C, no carbon formation was detected

when the inlet ethanol partial pressure was lower than 12 kPa. Small amounts of ethylene and ethane were observed when the inlet ethanol partial pressures were 12 and 15 kPa, Table 6.

3.5 The combination of CeO_2 and Ni/Al_2O_3 in the single unit

As the main approach of this work, CeO_2 (both LSA and HSA) were applied as the internal pre-reforming catalysts together with the conventional Ni/Al_2O_3 in the single unit (CeO_2(HSA)-Ni/Al_2O_3 and CeO_2(LSA)-Ni/Al_2O_3). Fig. 11 shows the variations in the hydrogen selectivity with time at 900°C over this configuration compared to the use of CeO_2 as the co-reforming catalyst (mixture of CeO_2 and Ni/Al_2O_3, CeO_2 (HSA)+Ni/Al_2O_3 and CeO_2(LSA)+Ni/Al_2O_3), and the use of single Ni/Al_2O_3 or Rh/Al_2O_3 in the system. The feed was C_2H_5OH/H_2O in helium with the inlet C_2H_5OH/H_2O molar ratio of 1.0/3.0 (with the inlet C_2H_5OH of 3 kPa). The initial yield of hydrogen production over CeO_2(HSA)-Ni/Al_2O_3 was significantly higher than that over CeO_2 (LSA)-Ni/Al_2O_3, CeO_2(HSA)+Ni/Al_2O_3, CeO_2(LSA)+Ni/Al_2O_3, and Ni/Al_2O_3. In addition, after exposure in this condition for 100 h, it was observed that the stability over CeO_2(HSA)-Ni/Al_2O_3 was higher than that over Rh/Al_2O_3, consequently, the long term hydrogen yield over CeO_2(HSA)-Ni/Al_2O_3 was the highest among these catalyst systems. The stabilities expressed as deactivation percentages and steady state activities over each operation are given in Table 7. Similarly, in order to determine the degree of carbon formation, the post-reaction temperature-programmed oxidation (TPO) experiments were carried out. Fig. 12 presents the quantities of carbon deposited observed from each operation. Significant amounts of carbon deposition were observed for CeO_2(LSA)-Ni/Al_2O_3, CeO_2(HSA)+Ni/Al_2O_3, CeO_2(LSA)+Ni/Al_2O_3, and Ni/Al_2O_3 (Fig. 9), whereas lower carbon formations were detected for CeO_2(HSA)-Ni/Al_2O_3 and Rh/Al_2O_3. Clearly, the deposition of carbon species over CeO_2(HSA)-Ni/Al_2O_3 was the lowest for all conditions.

The influences of operating temperature and the inlet C_2H_5OH/H_2O molar ratio on the ethanol conversion and product selectivities from the ethanol steam reforming over CeO_2(HSA)-Ni/Al_2O_3 and CeO_2(LSA)-Ni/Al_2O_3 were then studied. As shown in Fig. 13, the products from this reaction over CeO_2(HSA)-Ni/Al_2O_3 above 900°C were mainly H_2 and CO with some CO_2. Small amount of methane was detected at the temperature less than 900°C, whereas no formation of either ethylene or ethane was observed from the

system in all conditions. In contrast, significant amounts of ethylene and ethane were observed from the ethanol steam reforming over CeO_2(LSA)-Ni/Al_2O_3 even at high temperature (1000°C) and high inlet steam content, Fig. 14.

The effect of inlet ethanol concentration on the degree of carbon deposition over CeO_2(HSA)-Ni/Al_2O_3 system was then studied by increase the inlet ethanol partial pressure from 3.0 to 15.0 kPa at 900°C. Significant amount of carbon formation was observed over Ni/Al_2O_3 when the inlet ethanol partial pressure was higher than 12 kPa, moreover, ethylene formation was also found, Table 8.

4. Discussion

According to the homogeneous (non-catalytic) ethanol steam reforming, the dehydrogenation of ethanol and simultaneous fast decomposition of acetaldehyde first occur at relative low temperature (Eqs. 13 and 14), while the methane steam reforming and water-gas shift reactions (Eqs. 15 and 16) take place at higher temperature. Also, ethylene and ethane are formed by the dehydration of ethanol (Eq. 17) following with the production of ethane by ethylene hydrogenation (Eq. 18).

$$C_2H_5OH \rightarrow C_2H_4O + H_2 \quad (13)$$

$$C_2H_4O \rightarrow CH_4 + CO \quad (14)$$

$$CH_4 + H_2O \rightarrow CO + 3H_2 \quad (15)$$

$$CO + H_2O \rightarrow CO_2 + H_2 \quad (16)$$

$$C_2H_5OH \rightarrow C_2H_4 + H_2O \quad (17)$$

$$C_2H_4 + H_2 \rightarrow C_2H_6 \quad (18)$$

The formations of ethylene and ethane are the major difficulties for the catalytic steam reforming of ethanol, as these components act as very strong promoters for carbon formation. Eqs. 19-24 below present the most probable reactions that could lead to carbon deposition from the system of the steam reforming of ethanol:

$$C_2H_6 \Leftrightarrow 3H_2 + 2C \quad (19)$$

$$C_2H_4 \Leftrightarrow 2H_2 + 2C \quad (20)$$

$$CH_4 \Leftrightarrow 2H_2 + C \quad (21)$$

$$2CO \Leftrightarrow CO_2 + C \quad (22)$$

$$CO + H_2 \Leftrightarrow H_2O + C \quad (23)$$

$$CO_2 + 2H_2 \Leftrightarrow 2H_2O + C \quad (24)$$

C is the carbonaceous deposits. At low temperature, Eqs. (23-24) are favorable, while Eqs. (19-22) are thermodynamically unflavored [59]. The Boudouard reaction (Eq. 22) and the decomposition of hydrocarbons (Eqs. 19-21) are the major pathways for carbon formation at such a high temperature as they show the largest change in Gibbs energy [60]. According to the range of temperature in this study, carbon formation would be formed via the decomposition of hydrocarbons and Boudouard reactions.

From the present work, high surface area ceria (CeO_2 (HSA)), synthesized by a surfactant-assisted approach, was found to have useful ethanol steam reforming activity producing H_2 and CO under Solid Oxide Fuel Cells (SOFCs) conditions. As described, it has been reported that the gas-solid reaction between CeO_2 and CH_4 can generate CO and H_2 at high temperature [44, 45]. In addition, the reduced state of CeO_2 can react with CO_2 to produce CO [46]. By applying CeO_2 as the ethanol steam reforming catalyst at high temperature (800-1000°C), the gas-solid reactions between the hydrocarbons produced from the homogenous ethanol steam reforming reaction (ethylene, ethane, and methane) and the lattice oxygen (O_O^x) at CeO_2 surface occurs forming hydrogen and carbon monoxide. The redox mechanism between ethanol, ethylene, ethane, and methane with the lattice oxygen (O_O^x) could be derived as illustrated below.

$$C_2H_5OH + 2S_{Ce} \Leftrightarrow 2(CH_2\text{-}S_{Ce}) + H_2O \quad (25)$$

$$C_2H_6 + 2S_{Ce} \Leftrightarrow 2(CH_3\text{-}S_{Ce}) \quad (26)$$

$$C_2H_4 + 2S_{Ce} \Leftrightarrow 2(CH_2\text{-}S_{Ce}) \quad (27)$$

$$CH_4 + 2S_{Ce} \Leftrightarrow CH_3\text{-}S_{Ce} + H\text{-}S_{Ce} \quad (28)$$

$$CH_3\text{-}S_{Ce} + S_{Ce} \Leftrightarrow CH_2\text{-}S_{Ce} + H\text{-}S_{Ce} \quad (29)$$

$$CH_2\text{-}S_{Ce} + S_{Ce} \Leftrightarrow CH\text{-}S_{Ce} + H\text{-}S_{Ce} \quad (30)$$

$$CH\text{-}S_{Ce} + S_{Ce} \Leftrightarrow C\text{-}S_{Ce} + H\text{-}S_{Ce} \quad (31)$$

$$C\text{-}S_{Ce} + O_O^x \Leftrightarrow CO + V_O^{\bullet\bullet} + 2\,e' + S_{Ce} \quad (32)$$

$$2H\text{-}S_{Ce} \Leftrightarrow H_2 + 2S_{Ce} \quad (33)$$

S_{Ce} is the CeO_2 surface site and $CH_x\text{-}S_{Ce}$ is an intermediate surface hydrocarbon species. S_{Ce} can be considered to be a unique site, or the same site as the lattice oxygen

(O_O^x). During the reaction, hydrocarbons are adsorbed on either a unique site (S_{Ce}) or the lattice oxygen (O_O^x). The lattice oxygen is then regenerated by reaction with oxygen containing compounds (i.e. steam) present in the system, Eq. 34.

$$H_2O + + V_O^{\bullet\bullet} + 2\,e' \Leftrightarrow H_2 + O_O^x \quad (34)$$

It should be noted that the measured value of the oxygen diffusion coefficient for ceria is high and the reaction rate is controlled by a surface reaction, not by diffusion of oxygen from the bulk of the solid particles to ceria surfaces [61]. Regarding the above redox mechanism, the carbon formation from Eqs. 19-22 could be inhibited by the gas-solid reactions between gaseous components (ethylene, ethane, and methane produced from the decomposition of ethanol) with the lattice oxygen on CeO_2 surface, Eqs. 35 and 36.

$$C_nH_m + O_O^x = nCO + m/2\,H_2 + V_O^{\bullet\bullet} + 2\,e' \quad (35)$$

$$CO + O_O^x = 2CO_2 + V_O^{\bullet\bullet} + 2\,e' \quad (36)$$

Although conventional CeO_2 (LSA) also provides high resistance toward carbon formation, the major weaknesses of CeO_2 (LSA) are its nature low specific surface area and also high size reduction due to the thermal sintering impact, resulting in its low redox properties as presented in section 3.1. Consequently, the low ethanol steam reforming reactivity was observed over this catalyst. The comparative reforming reactivities between CeO_2 (HSA) and CeO_2 (LSA) are in good agreement with the results from characterizations (i.e. BET and TPR); the specific surface area of CeO_2 (HSA) and the amounts of hydrogen and oxygen uptakes from the temperature programmed reduction (TPR-1 and TPR-2) and the temperature programmed oxidation (TPO) were significantly higher than those observed over the conventional one.

In order to prove the above redox mechanism (Eqs. 25-34), the reactivities of CeO_2 (HSA) toward the steam reforming of ethane and ethylene were also carried out. Either ethane or ethylene was fed together with steam (with the inlet molar ratio of 1.0/1.0) to the catalytic reactor instead of ethanol. Figs. 15 and 16 show the product selectivities from the steam reforming of ethane and ethylene over CeO_2 (HSA) at different temperatures. Clearly, ethane and ethylene were converted mainly to methane,

carbon monoxide, carbon dioxide, and hydrogen. It was found that the conversions of ethane and ethylene were almost 100% when the temperature reached 900ºC, which supports the ethanol steam reforming mechanism of CeO_2 as described above.

According to the use of CeO_2 (HSA) as the pre-reforming catalyst in the annular design reactor, the main purpose of CeO_2 is to convert all high hydrocarbons from the homogenous decomposition of ethanol such as ethylene and ethane to methane, carbon monoxide, and hydrogen before these components reach the surface of Ni/Al_2O_3 at the outer side of the annular reactor. Therefore, the main reaction over this section is the steam reforming of methane instead of the steam reforming of ethane and ethylene, which is thermodynamically unflavored to form carbon deposition. The significant deactivation observed over the use of CeO_2 (LSA) as the pre-reforming catalyst (CeO_2(LSA)-Ni/Al_2O_3) is due to the low reforming reactivity of CeO_2 (LSA), thus the remaining ethylene and ethane from the ethanol steam reforming over CeO_2 (LSA) pass through the outer side of the annular reactor reacting with Ni/Al_2O_3 and form the carbonaceous deposits on Ni surface. Similarly, the use of CeO_2 (HSA) as the co-reforming catalyst (CeO_2(HSA)+Ni/Al_2O_3) also results in the high degree of carbon deposition. This is possibly due to the faster decomposition of ethylene and ethane on the surface of Ni (Eqs. 19 and 20) compared to the adsorption of these components on the surface of CeO_2 (Eqs. 26 and 27).

Lastly, it should be noted that the limitation of CeO_2(HSA)-Ni/Al_2O_3 annular system in the present work is the introducing of high ethanol concentration (higher than 12 kPa), which resulted in the presenting of ethylene and ethane at the end of the pre-reforming section due to the incomplete reforming reaction. Although CeO_2 (HSA) was found to have high resistance toward carbon deposition in the present of ethylene and ethane, these hydrocarbon components left from the pre-reforming unit can decompose and formed the carbon species on Ni/Al_2O_3 surface at the main reforming section. One solution to minimize this problem is to enlarge the pre-reforming part, but the size of the reformer system for IIR-SOFC operation must be concerned. The use of autothermal reforming instead of the steam reforming is another alternative method to solve this problem. The additional of oxygen together with ethanol and steam will oxidize the hydrocarbon elements in the system and also help steam to regenerate the lattice oxygen (O_O^x) on CeO_2 surface ($O_2 + V_O^{\bullet\bullet} + 2\,e' + S_{Ce} \rightarrow O_O^x$), however, the possible formation of NiO due to the reaction between oxygen adding and Ni catalyst at this high temperature

must be aware. The autothermal reforming operation is now under investigated in our group.

5. Conclusion

High surface area ceria (CeO_2 (HSA)) has useful ethanol steam reforming activity producing H_2, CH_4, CO, and CO_2 under Solid Oxide Fuel Cells (SOFCs) conditions. The catalyst provides excellent reforming reactivity and high resistance toward carbon deposition compared to Ni/Al_2O_3 and conventional low surface area ceria (CeO_2 (LSA)). At the temperature above 800°C, neither C_2H_4 nor C_2H_6 was observed from the reforming over CeO_2 (HSA), whereas significant amounts of these hydrocarbons were formed over Ni/Al_2O_3 and CeO_2 (LSA). These benefits of CeO_2 (HSA) are mainly due to the high redox property of this material, according to the temperature programmed reduction experiments (TPR). In addition, it was also proven that the redox of CeO_2 is reversible, according to the second temperature programmed reduction results after the temperature programmed oxidation (TPO).

By applying CeO_2 as the internal pre-reforming catalyst together with Ni/Al_2O_3, this reforming pattern provided excellent hydrogen selectivity comparable to Rh/Al_2O_3 and high resistance toward carbon deposition in a single unit. CeO_2 (HSA) converts all ethanol and forms CH_4, CO, CO_2, and H_2, while Ni/Al_2O_3 reforms all hydrocarbons left from the pre-reforming section and maximize the yield of hydrogen production. This successful development can improve the efficiency of the indirect internal reforming operation Solid Oxide Fuel Cells (IIR-SOFC) fueled by ethanol by eliminate the requirement of expensive noble metal catalysts or the installation of an external pre-reforming unit.

Acknowledgement

The financial support from The Thailand Research Fund (TRF) throughout this project is gratefully acknowledged.

References

[1] P. Aguiar, D. Chadwick and L. Kershenbaum, Chem. Eng. Sci. 57 (2002) 1665.

[2] S. Cavallaro, S. Freni, Int. J. Hydrogen Energy 21 (6) (1996) 465–469.

[3] N.F. Athanasio, X.E. Verykios, J. Catal. 225 (4) (2004) 39–452.

[4] V. Fierro, O. Akdim, H. Provendier and C. Mirodatos, Journal of Power Sources, 145 (2005) 659–666

[5] R. Peters, R. Dahl, U. Kluttgen, C. Palm, D. Stolten, J. Power Sources, 106, (2002), 238.

[6] J.R. Salge, G.A. Deluga and L.D. Schmidt, J. Catal. 235 (1) (2005) 69-78.

[7] L. Garcia, R. French, S. Czernik and E. Chornet. Appl. Catal. A: Gen. 201 (2000) 225.

[8] I. Fishtik, A. Alexander, R. Datta and D. Geana. Int. J. Hydrogen Energy 25 (2000) 31.

[9] S. Freni, G. Maggio and S. Cavallaro. J. Power Sour. 62 (1996) 67.

[10] K. Vasudera, N. Mitra, P. Umasankar and S.C. Dhinga. Int. J. Hydrogen Energy 21 (1996) 13.

[11] S. Cavallaro and S. Freni. Int. J. Hydrogen Energy 21 (1996) 465.

[12] F. Marino, E.G. Cerrella, S. Duhalde, M. Jobbagy and M.A. Laborde. Int. J. Hydrogen Energy 23 (1998) 1095.

[13] S. Cavallaro. Energy and Fuels 14 (2000) 1195.

[14] S. Freni. J. Power Sour. 94 (2001) 14.

[15] A. Fatsikostas, D. Kondarides and X. Verykios. Catal. Today 75 (2002) 145.

[16] S. Freni, S. Cavallaro, N. Mondello, L. Spadaro and F. Frusteri. J. Power Sour. 108 (2002) 53.

[17] A. Fatsikostas, D. Kondarides and X. Verykios. Catal. Today 75 (2002) 145.

[18] F. Marino, G. Baronetti, M. Jobbagy and M. Laborde. Appl. Catal. A: Gen. 6043 (2002) 1.

[19] J.P. Breen, R. Burch and H.M. Coleman. Appl. Catal. B: Environ. 39 (2002) 65.

[20] J. Llorca, N. Homs, J. Sales and P. Ramirez de la Piscina. J. Catal. 209 (2002) 306.

[21] V. Fierro, V. Klouz, O. Akdim and C. Mirodatos. Catal. Today 75 (2002) 141.

[22] D. Liguras, D. Kondarides and X. Verykios. Appl. Catal. B: Environ. 43 (2003) 345.

[23] J. Llorca, P. Ramirez de la Piscina, J.-A. Dalmon, J. Sales and N. Homs. Appl. Catal. B: Environ. 43 (2003) 355.

[24] S. Cavallaro, V. Chiodo, S. Freni, N. Mondello and F. Frusteri. Appl. Catal. A: Gen. 249 (2003) 119.

[25] S. Freni, S. Cavallaro, N. Mondello, L. Sadaro and F. Frusteri. Catal. Commun. 4 (2003) 259.

[26] S. Cavallaro, V. Chiodo, A. Vita and S. Freni. J. Power Sour. 123 (2003) 10.

[27] D. Srinivas, C.V.V. Satyanarayana, H.S. Potdar and P. Ratnasamy. Appl. Catal. A: Gen. 243 (2003) 261.

[28] L.V. Mattos, E. Rodino, D.E. Resasco, F.B. Possos and F.B. Noronha, Fuel Proc. Technol. 83 (2003) 147.

[29] H.S. Roh, K.W. Jun and S.E. Park, Appl. Catal. A 251 (2003) 275.

[30] J.R. Rostrup-Nielsen and J.-H. Bak-Hansen, J. Catal. 144 (1993) 38.

[31] P. Fornasiero, G. Balducci, R.D. Monte, J. Kaspar, V. Sergo, G. Gubitosa, A. Ferrero and M. Graziani. J. Catal. 164 (1996) 173.

[32] T. Miki, T. Ogawa, M. Haneda, N. Kakuta, A. Ueno, S. Tateishi, S. Matsuura and M. Sato, J. Phys. Chem. 94 (1990) 339.

[33] C. Padeste, N.W. Cant and D.L. Trimm, Catal. Lett. 18 (1993) 305.

[34] S. Kacimi, J. Barbier Jr., R. Taha and D. Duperz, Catal. Lett. 22 (1993) 343.

[35] G.S. Zafiris and R.J. Gorte, J. Catal. 143 (1993) 86.

[36] G.S. Zafiris and R.J. Gorte, J. Catal. 139 (1993) 561.

[37] S. Imamura, M. Shono, N. Okamoto, R. Hamada and S. Ishida, Appl. Catal. A 142 (1996) 279.

[38] L. Fan and K. Fujimoto. J. Catal. 172 (1997) 238.

[39] M. Pijolat, M. Prin and M. Soustelle. J. Chem. Soc., Faraday Trans. 91 (1995) 3941.

[40] N. Laosiripojana and S. Assabumrungrat, Appl. Catal. B: Environ, 60 (2005) 107.

[41] N. Laosiripojana, W. Sutthisripok, and S. Assabumrungrat, Chem. Eng. Journal 112 (2005) 13-22.

[42] N. Laosiripojana, W. Sangtongkitcharoen, and S. Assabumrungrat, Fuel, In Press

[43] N. Laosiripojana and S. Assabumrungrat, Appl. Catal. A: General, 290 (2005) 200.

[44] K. Otsuka, T. Ushiyama and I. Yamanaka, Chemistry Letters, (1993), 1517

[45] K. Otsuka, M. Hatano and A. Morikawa, J. Catalysis, 79, (1983), 493

[46] P.J. Gellings and Henny J. M. Bouwmeester, Solid state aspects of oxidation catalysis, Catalysis Today, 58, (2000) 1-53

[47] C.T. Kresge, M.E. Leonowicz, W.J. Roth, J.C. Vartuli and J.S. Beck, Nature, 359 (1992) 710.

[48] Q. Huo, D.I. Margolese, U. Ciesla, P. Feng, T.E. Gier, P. Sieger, R. Leon, P.M. Petroff, B. Schüth and G.D. Stucky, Nature 368 (1994) 317.

[49] P.T. Tanev and T.J. Pinnavaia, Science 267 (1995) 865.

[50] U. Ciesla, S. Schacht, G.D. Stucky, K.K. Unger and F. Schüth. Angew. Chem. Int. Ed. Engl. 35 (1996) 541.

[51] D.M. Antonelli and J.Y. Ying. Angew. Chem. Int. Ed. Engl. 35 (1996) 426.

[52] Q. Huo, D.I. Margolese, U. Ciesla, D.G. Demuth, P. Feng, T.E. Gier, P. Sieger, A. Firouzi, B.F. Chmelka, B. Schüth and G.D. Stucky, Chem. Mater. 6 (1994) 1176.

[53] D. Terribile, A. Trovarelli, J. Llorca, C. de Leitenburg and G. Dolcetti, Catal. Today 43 (1998) 79–88

[54] J.A Cairns, J.E.E. Baglin, G.J. Clark, and J.F. Ziegler, J. Cat., 83, (1983) 301-314

[55] G.J. Den Otter, and F.M. Dautzenberg, J. Catal., 53, (1978) 116-125

[56] T. Ren-Yuan, W. Rong-An, and L. Li-Wu, Appl. Catal. A, 10, (1984) 163-172

[57] J.E.E. Baglin, G.J. Clark, and J.F. Ziegler, Nuclear Instruments and Methods in Physic Research, 218, (1983) 445-450

[58] E. Ramirez, A. Atkinson and D. Chadwick, Appl. Catal. B 36 (2002) 193–206.

[59] Y. Lwin, W.R.W. Daud and A.B. Mohamad, Z. Yaakob, Int. J. Hydrogen Energy 25 (2000) (1) 47–53.

[60] J.N. Amor, Appl. Catal. A 176 (1999) 159–176.

[61] B.C.H. Steele and J.M. Floyd. Proc. Br. Ceram. Soc. 19 (1971) 55.

List of figures

List of Tables

Table 7 Yield of H_2 production (%), deactivation percentages, and the amount of carbon formation after exposure in ethanol steam reforming at 900ºC

Table 8 Effect of inlet ethanol concentration on the formations of ethane and ethylene and the amount of carbon deposition from the ethanol steam reforming over CeO_2(HSA)-Ni/Al_2O_3 at 900ºC (with the inlet C_2H_5OH/H_2O molar ratio of 1.0/3.0)

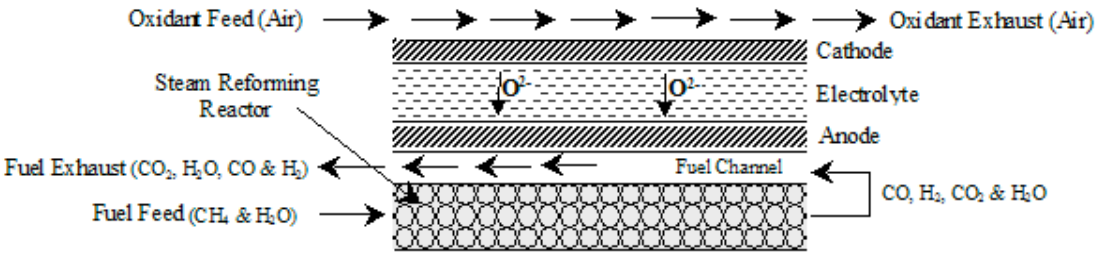

Fig. 1 Schematic diagram of SOFC with indirect internal reformer

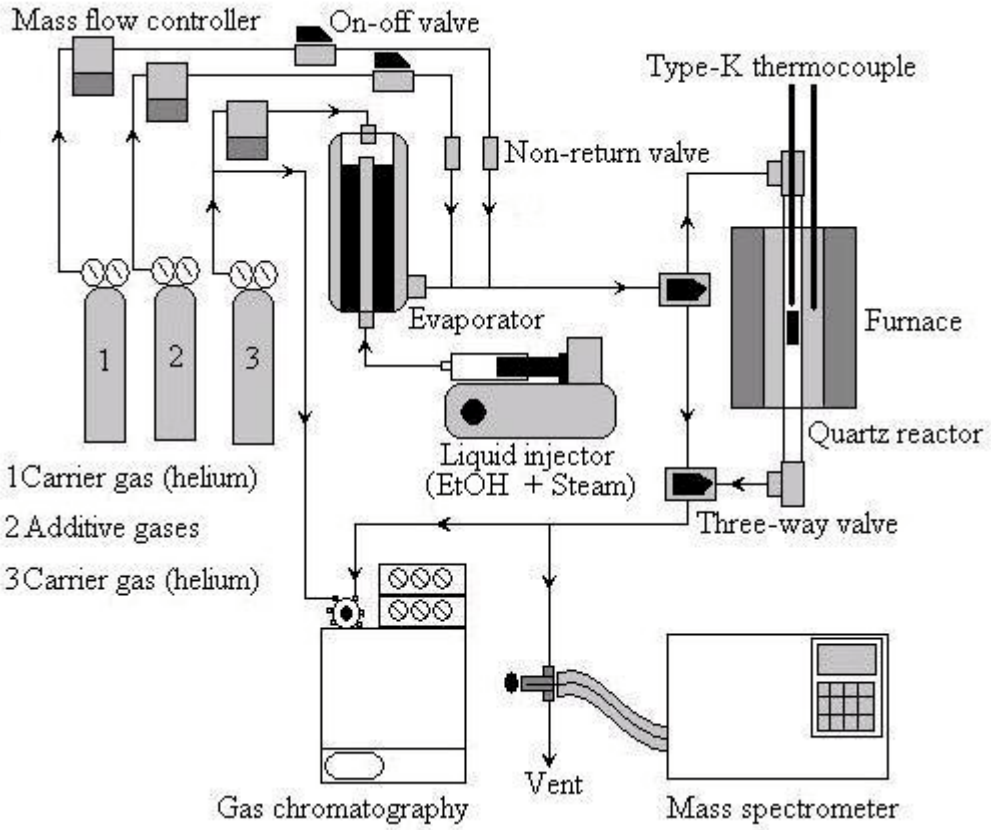

Fig. 2 Schematic diagram of the experimental set-up

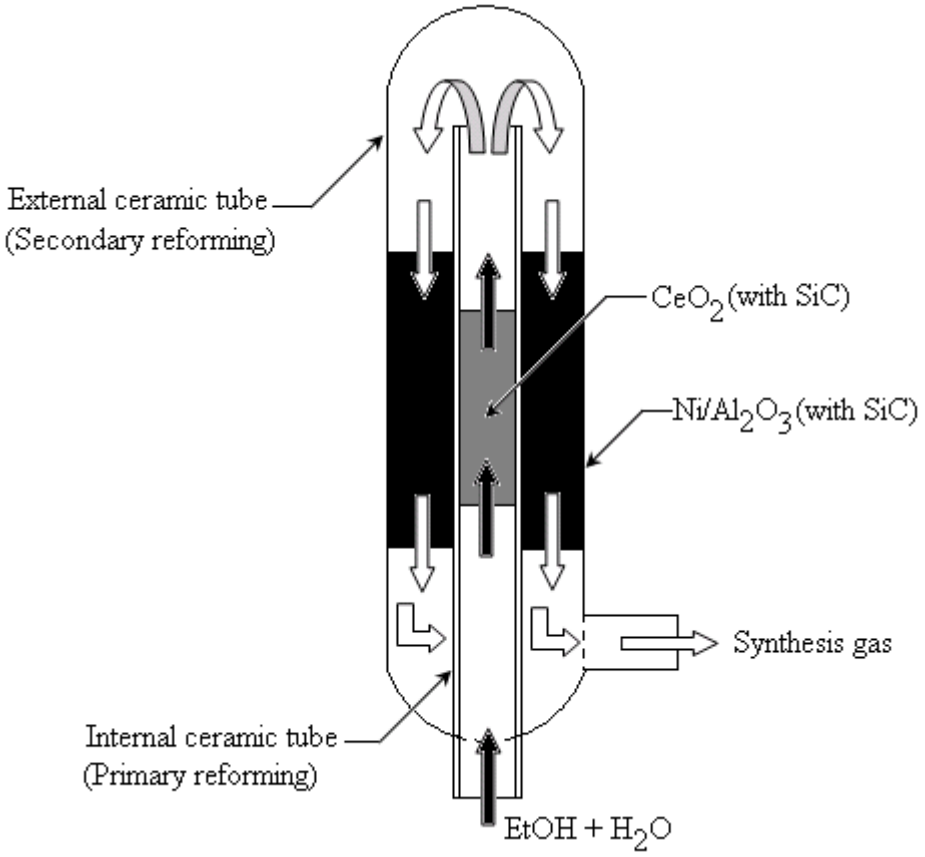

Fig. 3 Configuration of the catalytic testing unit with the pre-reforming catalyst

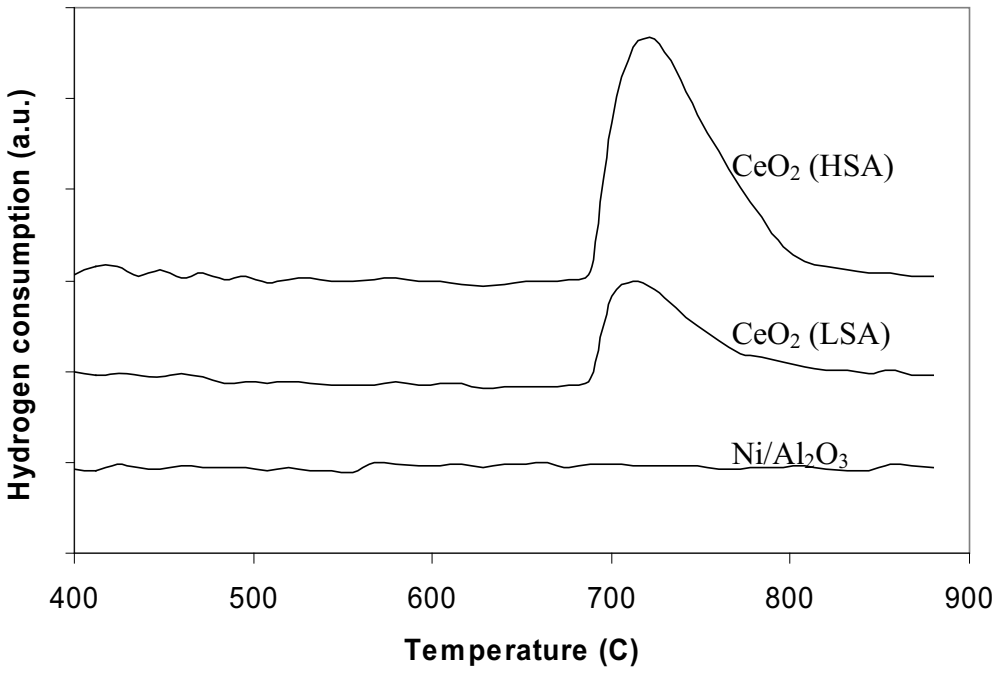

Fig. 4 Temperature Programmed Reduction (TPR-1) of fresh catalysts after reduction

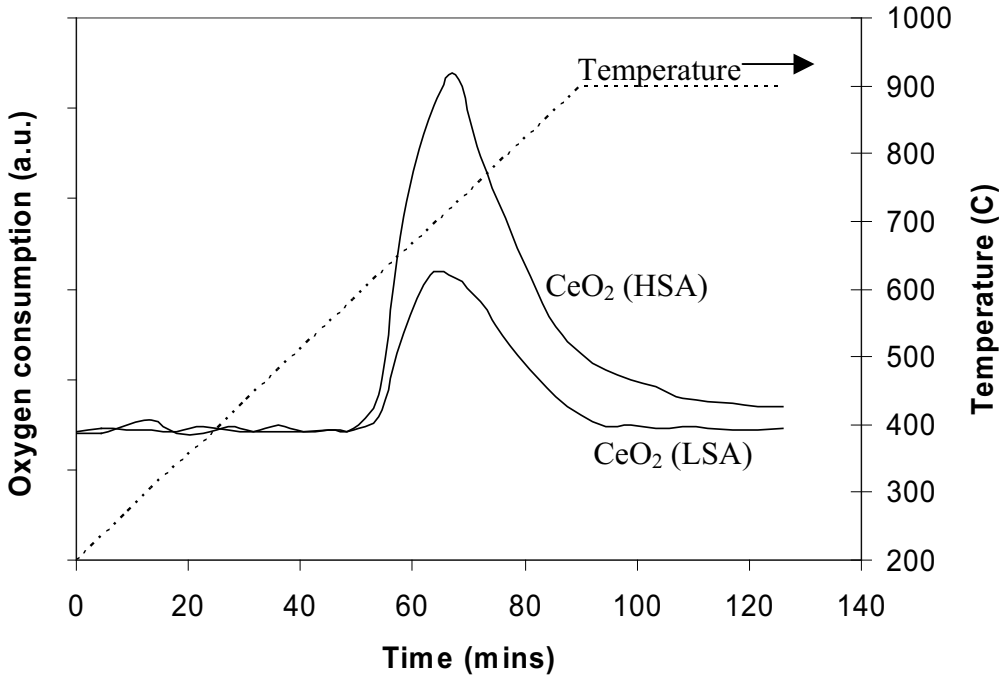

Fig. 5 Temperature Programmed Oxidation (TPO) of CeO_2 (HSA, LSA) after TPR-1

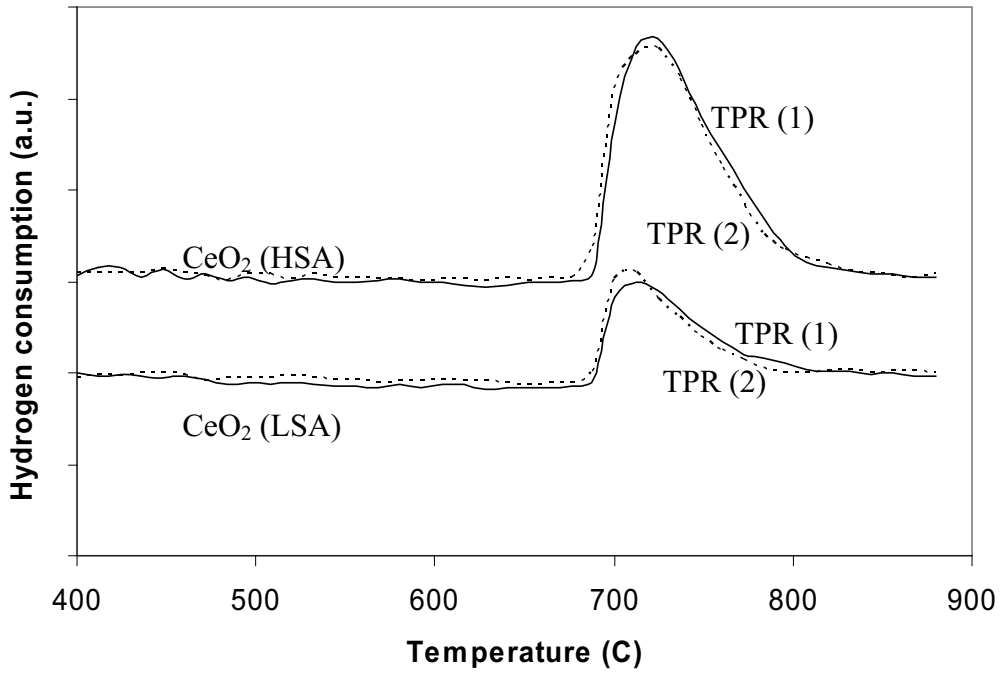

Fig. 6 Second time Temperature Programmed Reduction (TPR-2) of CeO_2 (HSA and LSA) compared to that of TPR-1

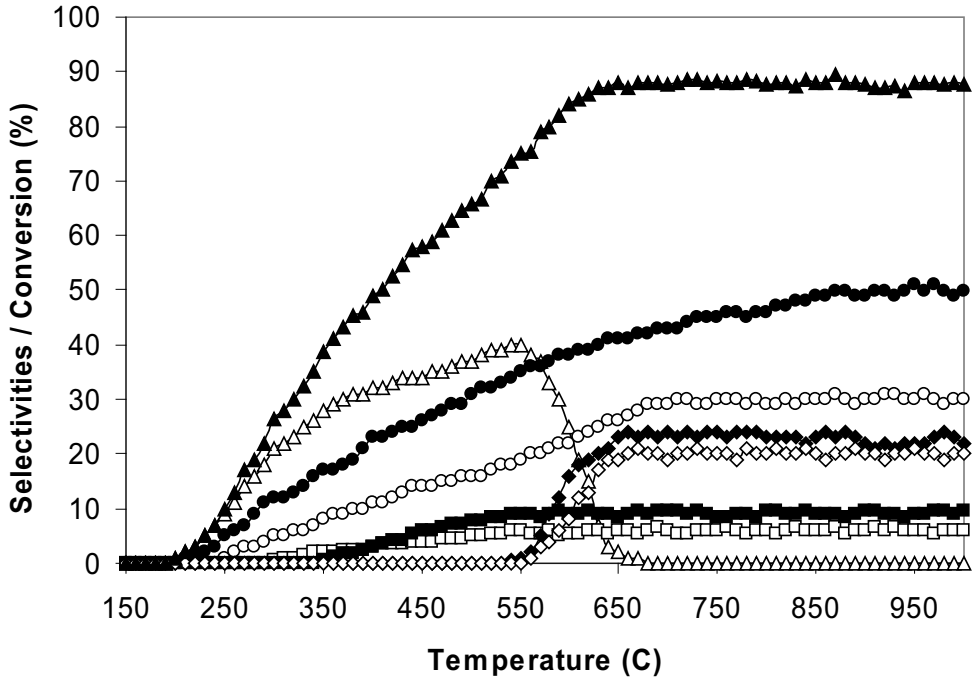

Fig. 7 Homogenous (in the absence of catalyst) reactivity of ethanol steam reforming (4 kPa C_2H_5OH, and 12 kPa H_2O) (EtOH (▲), H_2 (●), CO (○), CO_2 (■), CH_4 (□), CH_3CHO (△), C_2H_6 (◇), and C_2H_4 (◆))

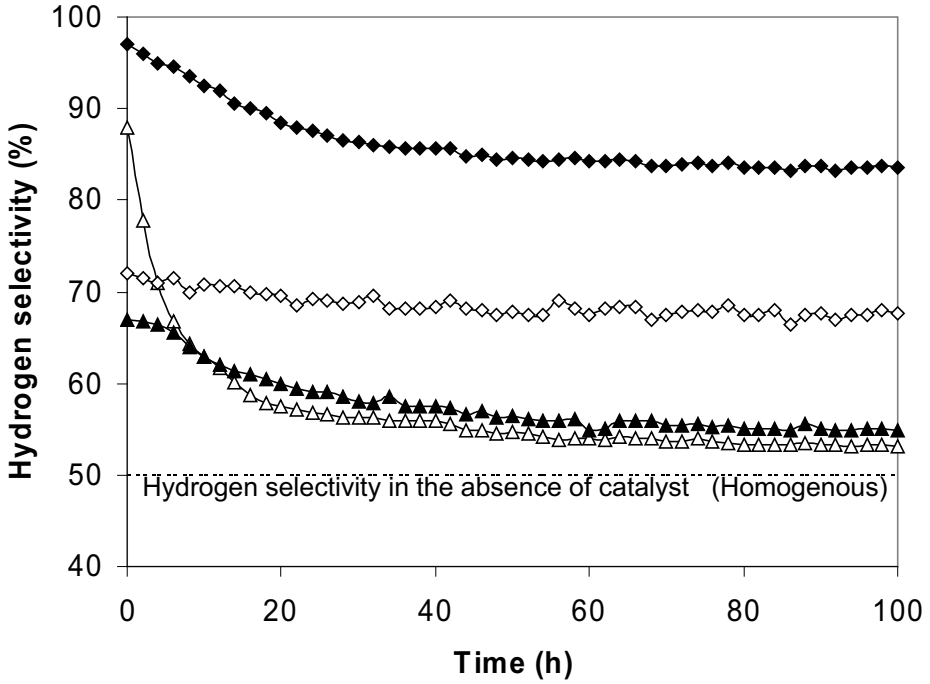

Fig. 8 Steam reforming of ethanol at 900°C for Rh/Al_2O_3 (◆), CeO_2 (HSA) (◇), CeO_2 (LSA) (▲),Ni/Al_2O_3 (△) (4 kPa C_2H_5OH, and 12 kPa H_2O)

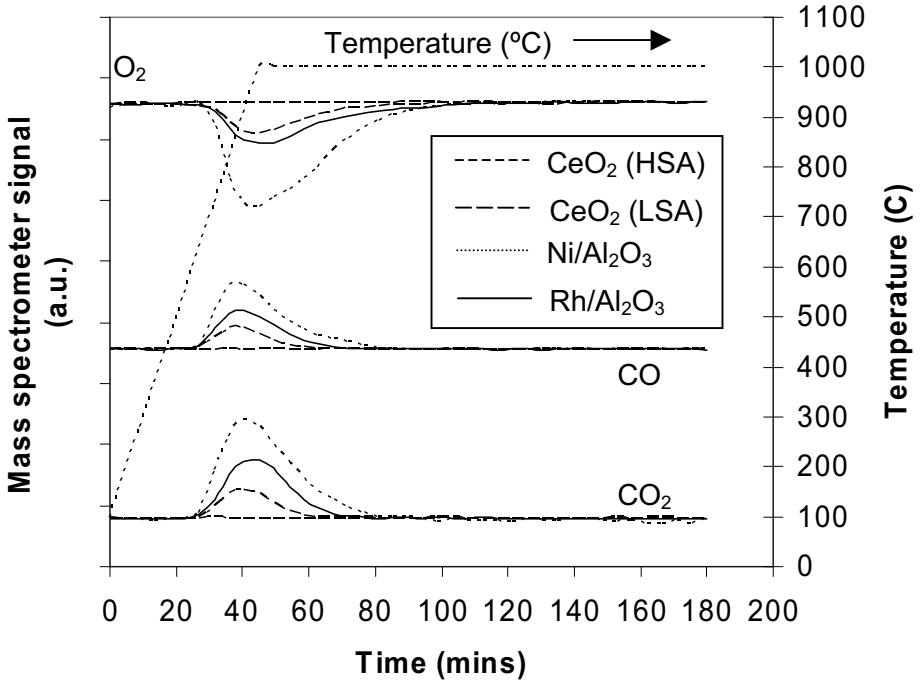

Fig. 9 Temperature Programmed Oxidation (TPO) of Rh/Al_2O_3, CeO_2 (HSA), CeO_2 (LSA), and Ni/Al_2O_3 after exposure in steam reforming of ethanol (4 kPa C_2H_5OH, and 12 kPa H_2O) for 100 h

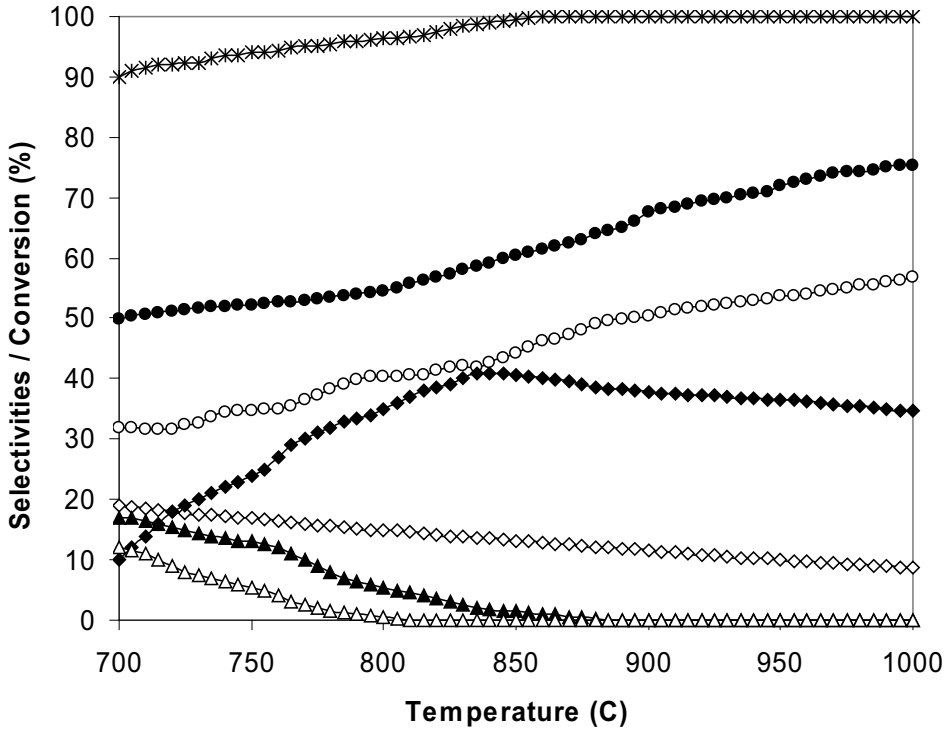

Fig. 10a

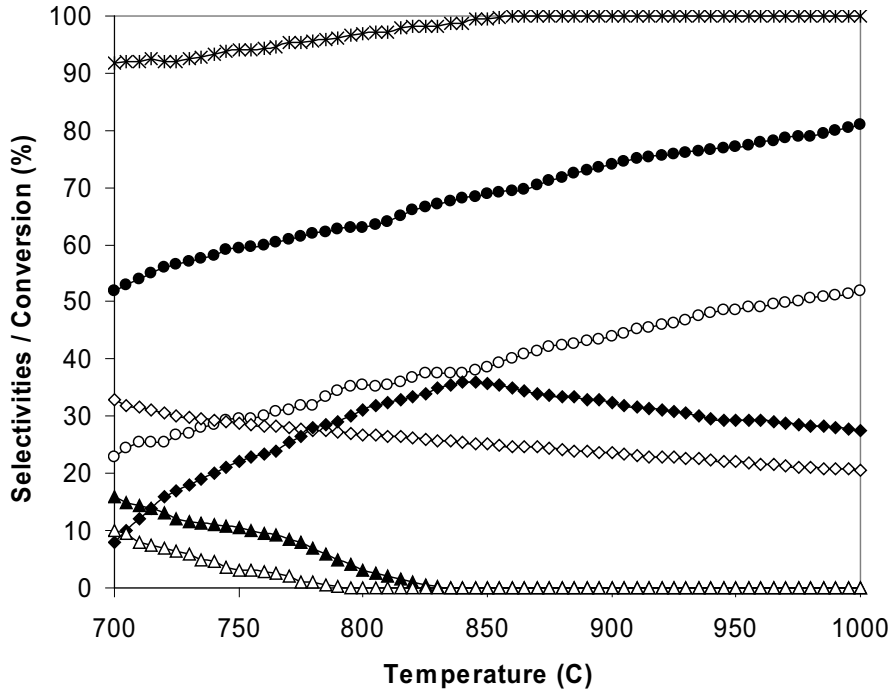

Fig. 10b

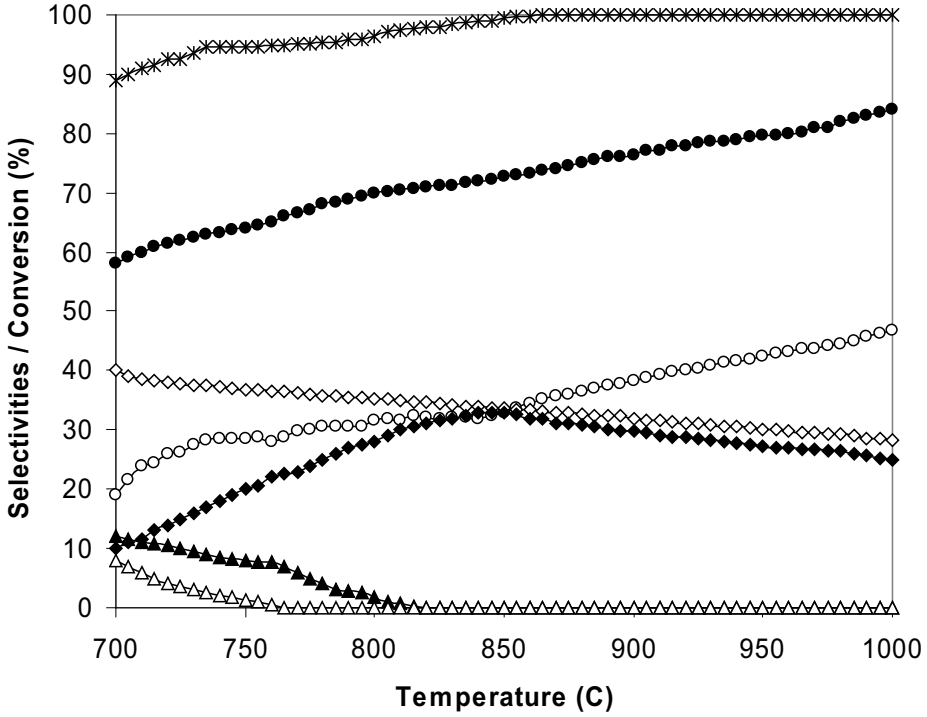

Fig. 10c

Fig. 10 Effect of temperature on the conversion and product selectivities (EtOH (×), H_2 (●), CO (○), CO_2 (◇), CH_4 (◆), C_2H_6 (△), and C_2H_4 (▲)) from ethanol steam reforming over CeO_2 (HSA) with EtOH/H_2O ratios of 1/3 (Fig. 10a), 1/4 (Fig. 10b), and 1/5 (Fig. 10c)

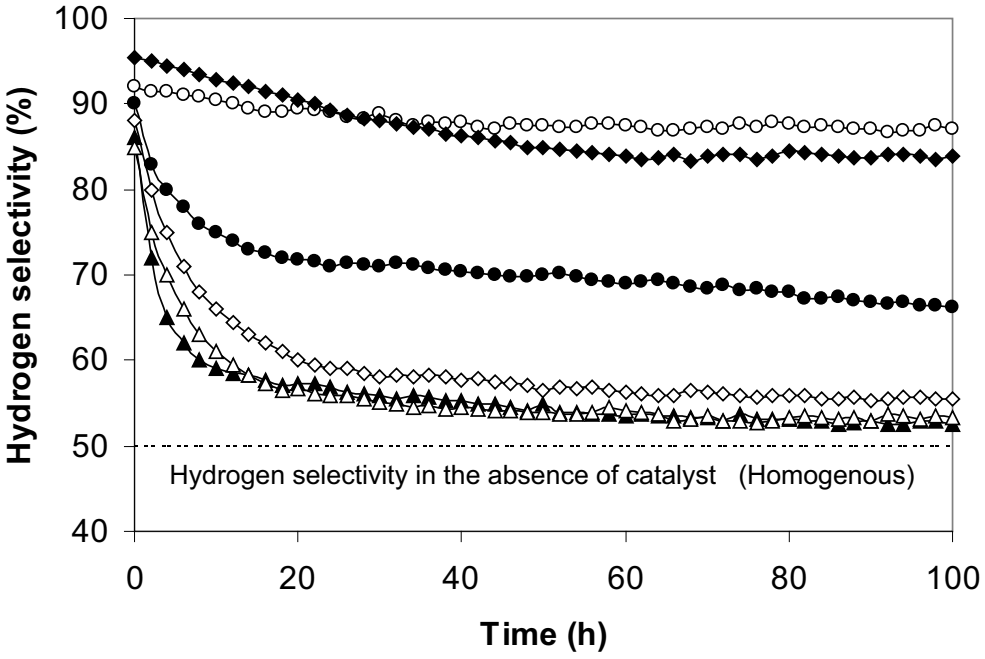

Fig. 11 Steam reforming of ethanol at 900°C for CeO_2(HSA)-Ni/Al_2O_3 (○), Rh/Al_2O_3 (◆), CeO_2(LSA)-Ni/Al_2O_3 (●), CeO_2(HSA)+Ni/Al_2O_3 (◇), CeO_2(LSA)+Ni/Al_2O_3 (△),Ni/Al_2O_3 (▲) (4 kPa C_2H_5OH, and 12 kPa H_2O)

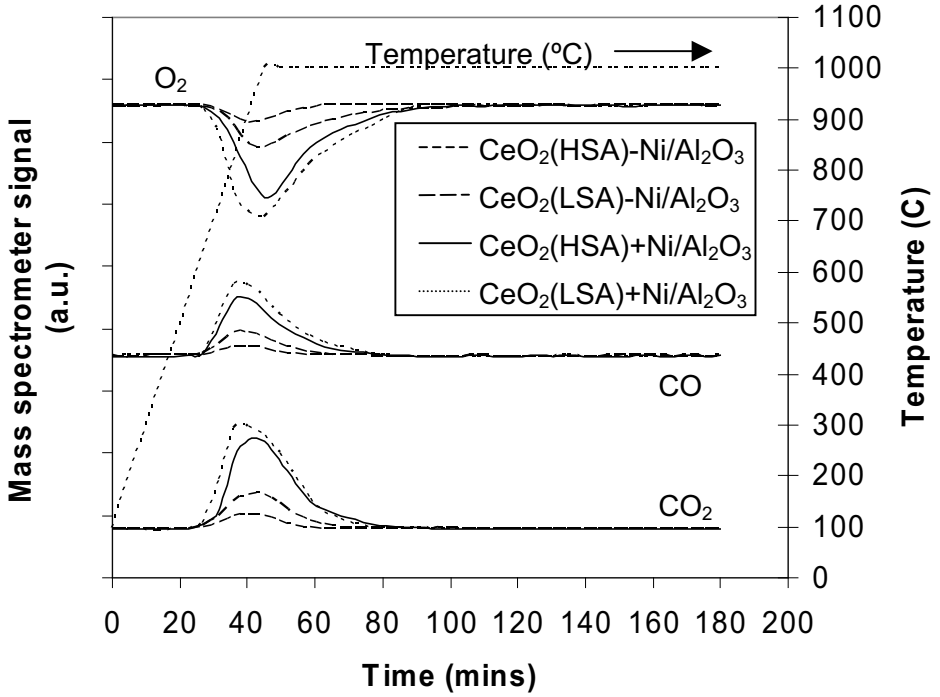

Fig. 12 Temperature Programmed Oxidation (TPO) of CeO_2(HSA)-Ni/Al_2O_3, CeO_2(LSA)-Ni/Al_2O_3, CeO_2(HSA)+Ni/Al_2O_3, and CeO_2(LSA)+Ni/Al_2O_3 after exposure in steam reforming of ethanol (4 kPa C_2H_5OH, and 12 kPa H_2O) for 100 h

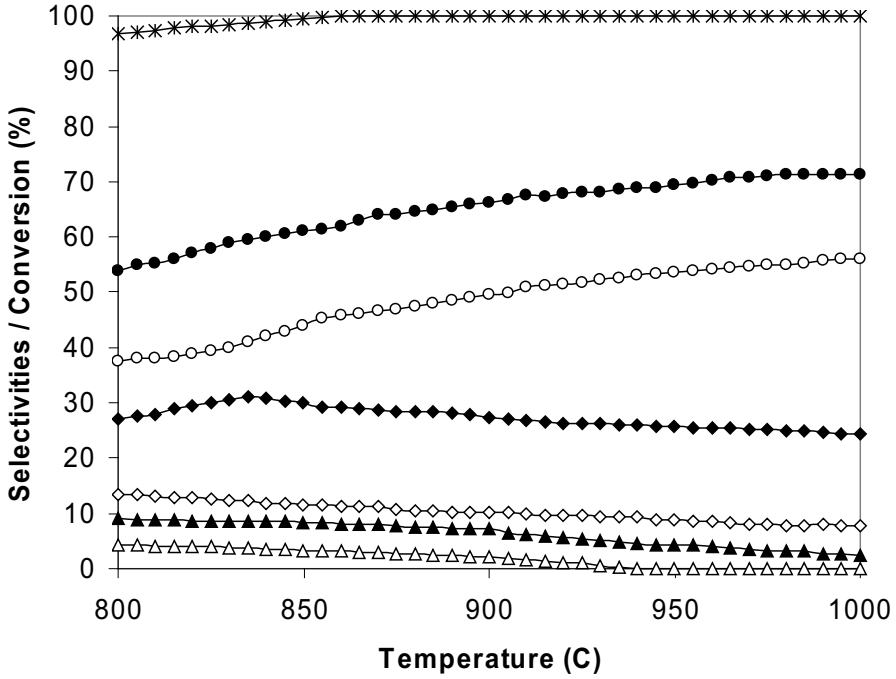

Fig. 13a

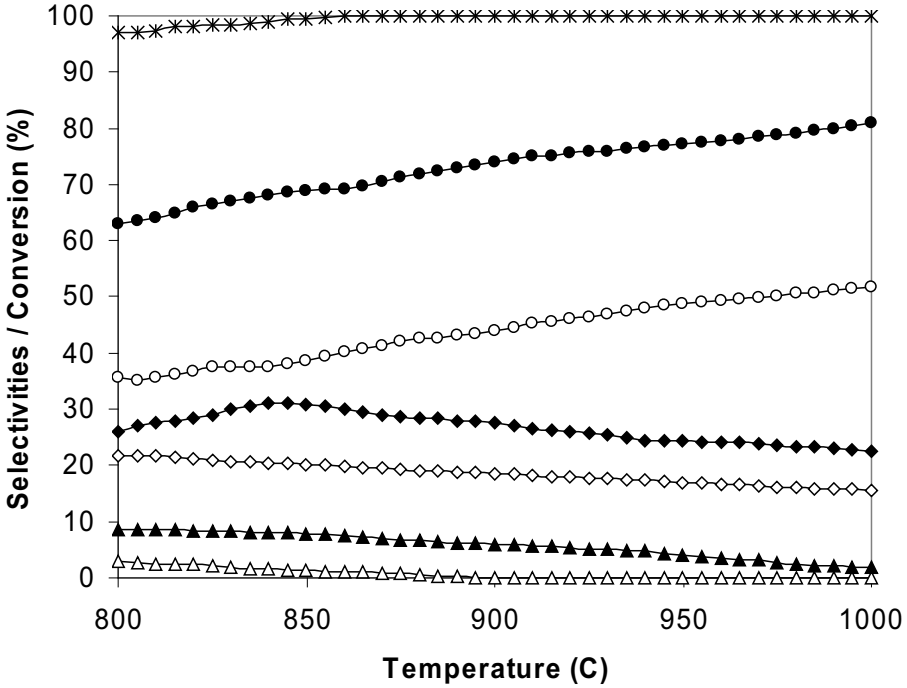

Fig. 13b

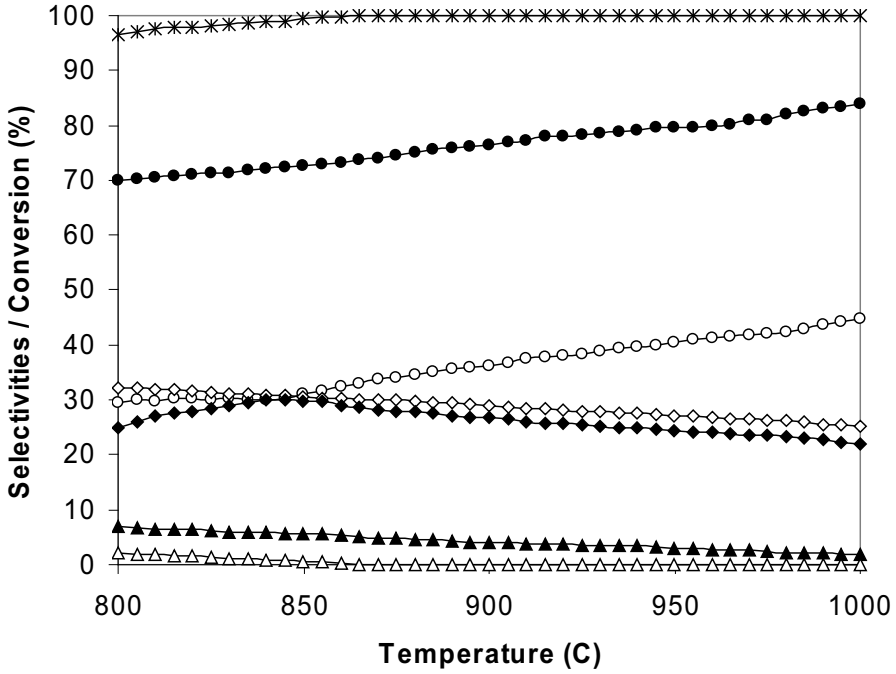

Fig. 13c

Fig. 13 Effect of temperature on the conversion and product selectivities (EtOH (×), H_2 (●), CO (○), CO_2 (◇), CH_4 (◆), C_2H_6 (△), and C_2H_4 (▲)) from ethanol steam reforming over CeO_2(LSA)-Ni/Al_2O_3 with EtOH/H_2O ratios of 1/3 (Fig. 13a), 1/4 (Fig. 13b), and 1/5 (Fig. 13c)

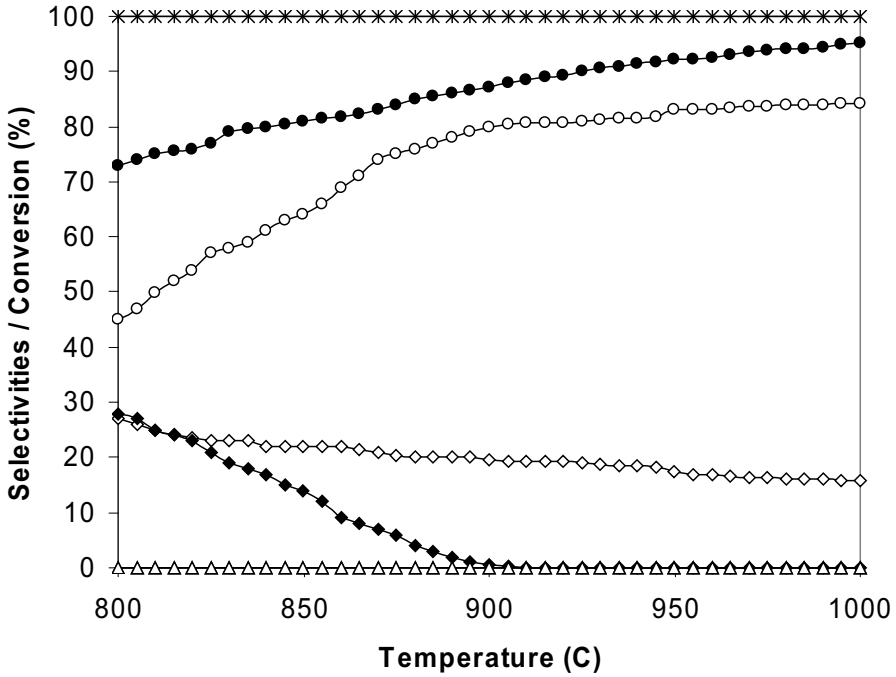

Fig. 14a

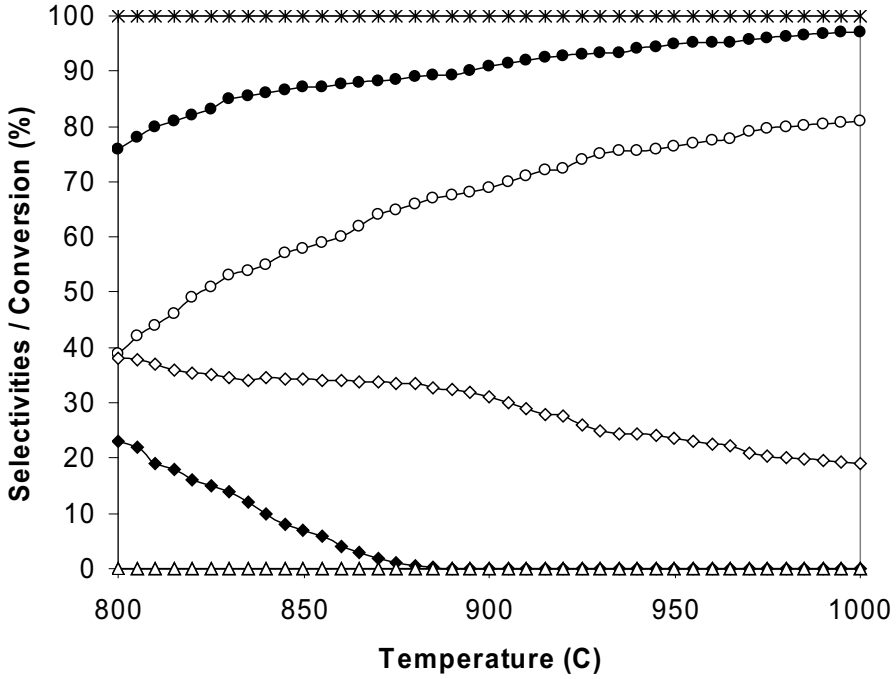

Fig. 14b

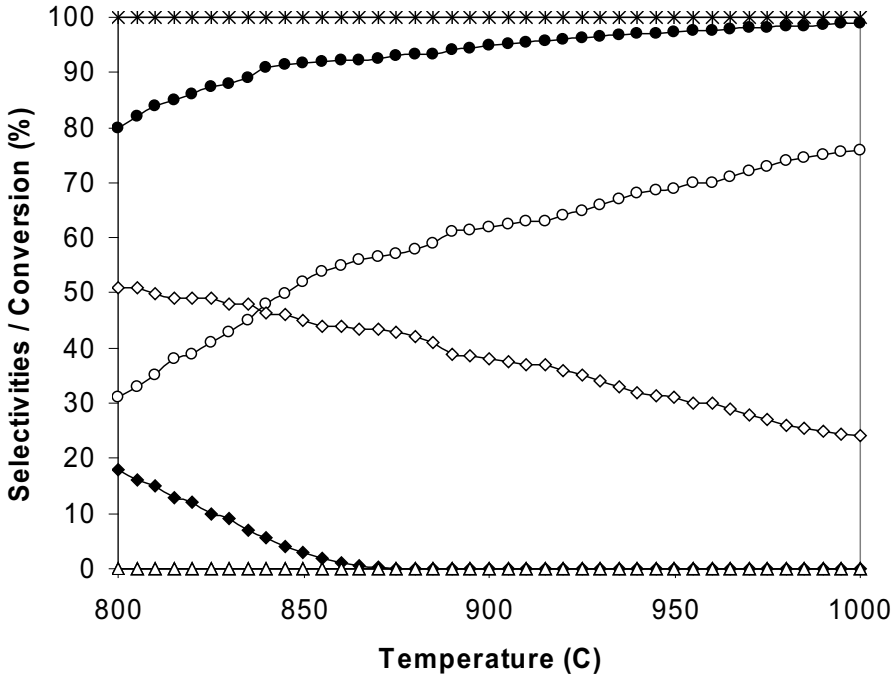

Fig. 14c

Fig. 14 Effect of temperature on the conversion and product selectivities (EtOH (×), H_2 (●), CO (○), CO_2 (◇), CH_4 (◆), C_2H_6 (△), and C_2H_4 (▲)) from ethanol steam reforming over CeO_2(HSA)-Ni/Al_2O_3 with EtOH/H_2O ratios of 1/3 (Fig. 14a), 1/4 (Fig. 14b), and 1/5 (Fig. 14c)

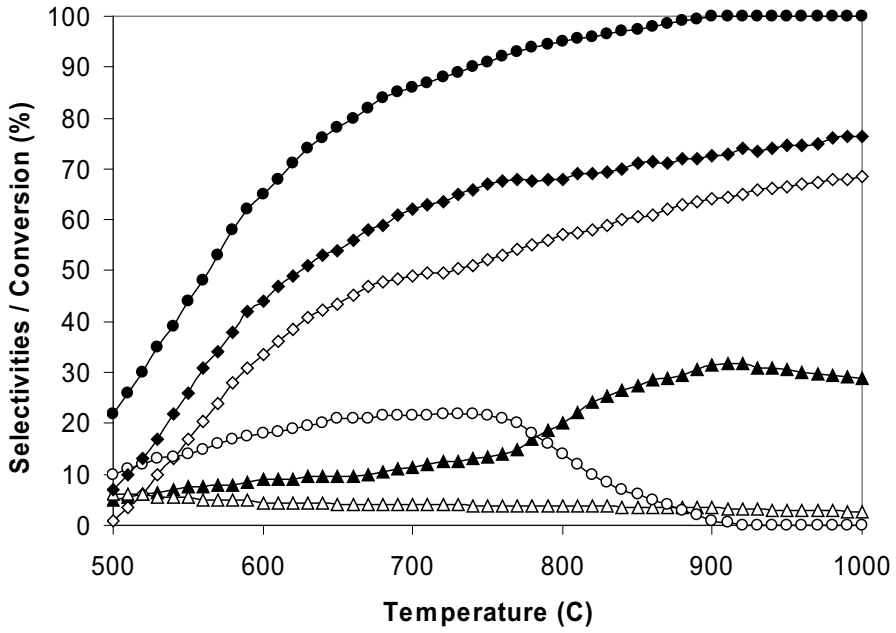

Fig. 15 Steam reforming of ethane over CeO_2 (HSA) (4 kPa C_2H_6, and 12 kPa H_2O) (C_2H_6 (●), H_2 (◆), CO (◇), CO_2 (△), CH_4 (▲), and C_2H_4 (○))

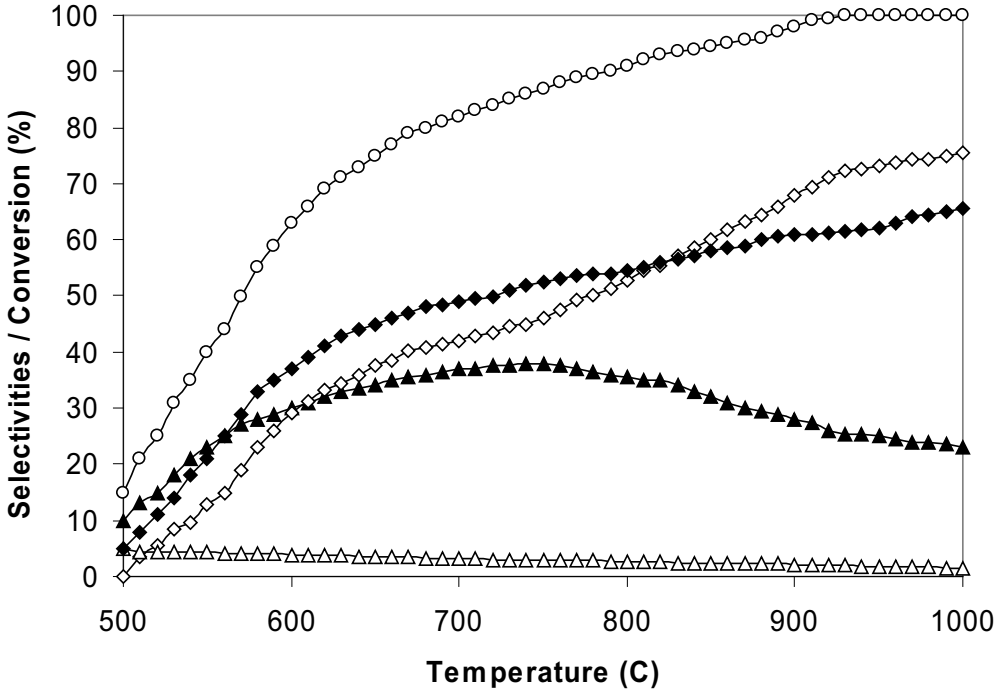

Fig. 16 Steam reforming of ethylene over CeO_2 (HSA) (4 kPa C_2H_4, and 12 kPa H_2O) (C_2H_4 (○), H_2 (◆), CO (◇), CO_2 (△), and CH_4 (▲))

Table 1
Specific surface area of the catalysts after drying and calcinations at different temperatures

Catalyst	BET surface area (m^2 g^{-1}) after drying or calcination at						
	100ºC	200ºC	400ºC	600ºC	800ºC	900ºC	1000ºC
CeO_2 (LSA.)[a]	55	49	36	21	15	11	8.5
CeO_2 (HSA-1)[b]	308	289	208	141	100	89	72
CeO_2 (HSA-2)[b]	189	177	136	97	72	55	43
CeO_2 (HSA-3)[b]	105	97	69	48	35	29	22

[a] conventional low surface area CeO_2 prepared by the precipitation method
[b] high surface area CeO_2 prepared by the surfactant-assisted approach with different flow rate of ammonia (1=0.165 cm^3 min^{-1}, 2=0.613 cm^3 min^{-1}, and 3=1.06 cm^3 min^{-1})

Table 2
Physicochemical properties of the catalysts after reduction

Catalyst	Metal-load[a] (wt.%)	BET Surface Area (m^2 g^{-1})	Metal-reducibility[b] (%)	Metal-dispersion[c] (%)
Ni/Al_2O_3	4.9	40	92.1	4.87
Rh/Al_2O_3	5.1	42	94.8	5.04

[a] Measured from X-ray fluorescence analysis.
[b] Measured from temperature-programmed reduction (TPR) with 5%hydrogen.
[c] Measured from temperature-programmed desorption (TPD) of hydrogen after TPR measurement.

Table 3
Results of TPR(1), TPO, TPR(2) analyses of CeO_2 (both HSA and LSA)

Catalyst	Total H_2 Uptake from TPR(1)[a] (μmol/g_{cat})	Total O_2 Uptake from TPO[b] (μmol/g_{cat})	Total H_2 Uptake from TPR(2)[c] (μmol/g_{cat})
CeO_2 (HSA)	2159	1044	2155
CeO_2 (LSA)	830	401	828

[a] Temperature Programmed Reduction of the reduced catalysts (Relative Standard Deviation = ± 3%)
[b] Temperature Programmed Oxidation after TPR (1) (Relative Standard Deviation = ± 1%)
[c] Re-Temperature Programmed Reduction after TPO (Relative Standard Deviation = ± 2%)

Table 4
Physicochemical properties of the catalysts after exposure in ethanol steam reforming at 900ºC for 100 h

Catalyst	Deactivation (%)	C formation (monolayers)	BET surface (m^2 g^{-1})	Metal-load [a] (wt.%)	Metal-red.[b] (Ni%)	Metal-disp.[c] (Ni%)
CeO_2 (HSA)	6.1	~0[d] (~0)[e]	66.9	-	-	-
CeO_2 (LSA)	17.9	0.67 (0.69)	7.3	-	-	-
Rh/Al_2O_3	13.8	1.47 (1.44)	~40.0	5.0	94.6	5.01
Ni/Al_2O_3	39.5	4.52 (4.54)	~40.0	4.9	92.0	4.85

[a] Measured from X-ray fluorescence analysis
[b] Nickel and rhodium reducibility
[c] Nickel and rhodium dispersion
[d] Calculated using CO and CO_2 yields from temperature-programmed oxidation (TPO) with 10% oxygen.
[e] Calculated from the balance of carbon in the system

Table 5
Product selectivities and the amount of carbon deposition from the catalysts after exposure in ethanol steam reforming at different inlet $EtOH/H_2O$ ratios

Catalyst	C_2H_5OH/H_2O ratio	Product Selectivities at 900°C						C formation (monolayers)
		H_2	CO	CO_2	CH_4	C_2H_6	C_2H_4	
CeO_2 (HSA)	1.0/3.0	67.5	50.5	11.6	37.9	0	0	~0[a] (~0)[b]
	1.0/4.0	74.0	43.9	23.6	32.5	0	0	0 (0)
	1.0/5.0	76.4	38.3	32	29.7	0	0	0 (0)
CeO_2 (LSA)	1.0/3.0	54.9	44.0	10.9	37.4	1.2	5.8	0.67 (0.69)
	1.0/4.0	59.7	40.1	19.1	35.1	1	4.1	0.61 (0.60)
	1.0/5.0	61.3	37.4	24.7	34.0	0.5	2.9	0.58 (0.58)
Rh/Al_2O_3	1.0/3.0	83.5	61.3	16.3	19.4	0.3	1.3	1.47 (1.44)
	1.0/4.0	85.1	55.6	25.4	17.2	0	0.5	1.32 (1.35)
	1.0/5.0	86.3	50.1	33.7	14.7	0	0.3	1.20 (1.18)
Ni/Al_2O_3	1.0/3.0	53.2	39.5	7.1	24.7	8.5	15.8	4.52 (4.54)
	1.0/4.0	55.4	38.1	13.7	22.6	6.1	14.1	4.47 (4.45)
	1.0/5.0	58.6	35.7	20.1	20.9	5.4	13.5	4.41 (4.42)

[a] Calculated using CO and CO_2 yields from temperature-programmed oxidation (TPO) with 10% oxygen.
[b] Calculated from the balance of carbon in the system

Table 6
Effect of inlet ethanol concentration on the formations of ethane and ethylene and the amount of carbon deposition from the ethanol steam reforming over CeO_2 (HSA) at 900ºC (with the inlet C_2H_5OH/H_2O molar ratio of 1.0/3.0)

Inlet C_2H_5OH (kPa)	Selectivities at 900ºC		C formation (monolayers)
	C_2H_6	C_2H_4	
3.0	0	0	~0[a] (~0)[b]
6.0	0	0	0 (0)
9.0	0	0	0 (0)
12.0	0.4	2.7	0.28 (0.22)
15.0	0.6	3.1	0.47 (0.47)

[a] Calculated using CO and CO_2 yields from temperature-programmed oxidation (TPO) with 10% oxygen.
[b] Calculated from the balance of carbon in the system

Table 7
Yield of H_2 production (%), deactivation percentages, and the amount of carbon formation after exposure in ethanol steam reforming at 900ºC

Type of operation	C_2H_5OH/H_2O ratio	Yield of H_2 (%) at steady state	Deactivation (%)	Total amount of carbon formation (monolayers)
CeO_2(HSA)-Ni/Al_2O_3	1.0/3.0	87.0	5.4	0.92[a] (0.92)[b]
	1.0/4.0	89.5	5.1	0.87 (0.84)
	1.0/5.0	91.4	4.8	0.79 (0.80)
CeO_2(LSA)-Ni/Al_2O_3	1.0/3.0	66.3	17.9	2.01 (1.98)
	1.0/4.0	67.7	16.4	1.95 (1.95)
	1.0/5.0	68.4	15.2	1.88 (1.91)
CeO_2(HSA)+Ni/Al_2O_3	1.0/3.0	55.5	26.3	3.42 (3.41)
	1.0/4.0	58.1	26.0	3.37 (3.36)
	1.0/5.0	60.2	25.4	3.31 (3.32)
CeO_2(LSA)+Ni/Al_2O_3	1.0/3.0	53.4	36.9	4.19 (4.20)
	1.0/4.0	56.0	35.8	4.12 (4.10)
	1.0/5.0	58.9	35.1	4.07 (4.08)
Rh/Al_2O_3	1.0/3.0	83.9	12.1	1.41 (1.39)
	1.0/4.0	85.7	10.7	1.34 (1.30)
	1.0/5.0	86.9	9.9	1.27 (1.28)
Ni/Al_2O_3	1.0/3.0	52.6	38.8	4.47 (4.49)
	1.0/4.0	55.2	37.4	4.36 (4.38)
	1.0/5.0	58.7	36.1	4.24 (4.28)

[a] Calculated using CO and CO_2 yields from temperature-programmed oxidation (TPO) with 10% oxygen.
[b] Calculated from the balance of carbon in the system

Table 8
Effect of inlet ethanol concentration on the formations of ethane and ethylene and the amount of carbon deposition from the ethanol steam reforming over CeO_2(HSA)-Ni/Al_2O_3 at 900ºC (with the inlet C_2H_5OH/H_2O molar ratio of 1.0/3.0)

Inlet C_2H_5OH (kPa)	Selectivities at 900ºC		C formation (monolayers)
	C_2H_6	C_2H_4	
3.0	0	0	0.92[a] (0.92)[b]
6.0	0	0	0.99 (1.01)
9.0	0	0	0.97 (0.97)
12.0	0	1.8	1.35 (1.33)
15.0	0.3	2.2	1.94 (1.89)

[a] Calculated using CO and CO_2 yields from temperature-programmed oxidation (TPO) with 10% oxygen.
[b] Calculated from the balance of carbon in the system

N. Laosiripojana and S. Assabumrungrat

"Reactivity of high surface area CeO_2 synthesized by surfactant-assisted method to ethanol decomposition with and without steam"

Submitted to Chemical Engineering Journal

(IF-2004 = 1.38)

Submitted to Chemical Engineering Journal
Type of Contribution: Research Article

Reactivity of high surface area CeO_2 synthesized by surfactant-assisted method to ethanol decomposition with and without steam

N. Laosiripojana[1,*] and S. Assabumrungrat[2]

[1] The Joint Graduate School of Energy and Environment,
King Mongkut's University of Technology Thonburi, Bangkok, 10140, Thailand
[2] Center of Excellence in Catalysis and Catalytic Reaction Engineering,
Department of Chemical Engineering, Faculty of Engineering, Chulalongkorn University, Bangkok 10330, Thailand
[*] Corresponding author (navadol_l@jgsee.kmutt.ac.th)

Abstract

High surface area CeO_2 (CeO_2 (HSA)) synthesized by surfactant-assisted method was found to have useful ethanol decomposition activity producing H_2, CO, CO_2, and CH_4 even when operated without the presence of steam. The catalyst provides high resistance toward carbon deposition compared to Ni/Al_2O_3 and the conventional low surface area CeO_2 (CeO_2 (LSA)). Neither ethane nor ethylene formation was observed at the temperature above 900ºC. Hydrogen selectivity up to 75% was achieved at 1000ºC, while no carbon deposition was detected at this temperature. The reactivity toward ethanol decomposition for CeO_2 is due to its high oxygen storage capacity (OSC). During the decomposition process, the gas-solid reactions between the gaseous components, which are homogenously generated from the ethanol decomposition, i.e. C_2H_6, C_2H_4, CH_4, CO_2, CO, H_2O, and H_2, and the lattice oxygen (O_O^x) on CeO_2 surface take place. The reactions of surface adsorbed hydrocarbons with the lattice oxygen ($C_nH_m + O_O^x \rightarrow nCO + m/2(H_2) + V_O^{\bullet\bullet} + 2\ e'$) can produce synthesis gas (CO and H_2) and prevent the formation of carbon species from hydrocarbon decomposition reactions ($C_nH_m \rightarrow nC + m/2H_2$).

In particular, it was observed that the ethanol decomposition rate over CeO_2 (HSA) is proportional to the inlet ethanol partial pressure but independent of the inlet steam partial pressure. This result suggests that the rate of ethanol decomposition is

governed by the slow reaction of adsorbed ethanol or surface hydrocarbon species with lattice oxygen in CeO_2, and a rapid gas-solid reaction between oxygen source in the system and the reduced ceria to replenish the oxygen.

Keywords: Ethanol, internal reforming, hydrogen, SOFC, and CeO_2

1. Introduction

Hydrogen is one of the most promising fuels in the near future. It could be produced efficiently from the catalytic reforming of several fuels such as methane, methanol, bio-ethanol, gasoline and other oil derivatives. According to the current oil crisis and the shortage of fossil fuels, the development of the biomass-based fuels attracts much attention. Among renewable resources, bio-ethanol is a promising candidate for converting to hydrogen-rich gas, since it is readily produced by renewable resources (e.g. fermentation of biomasses) and has reasonably high hydrogen content [1,2].

Previously, the reforming of ethanol has been studied by several researchers [3-23]. Most of them reported that the major difficulty to reform ethanol is the possible degradation of the catalyst due to the carbon deposition. It has been widely proposed that, at the temperature above 250ºC, ethanol homogeneously decomposes and forms several products (e.g. acetaldehyde, methane, carbon monoxide, carbon dioxide, ethylene, and ethane) without the requirement of catalyst. The formations of ethylene and ethane are the major difficulties for the catalytic reforming of ethanol, as it has been established that ethane and ethylene act as very strong promoters of carbon formation. Most of the recent works on the reforming of ethanol have been based on the noble metal catalysts (e.g. Rh, Ru, Pt, Pd) over several oxide supports (e.g. Al_2O_3, MgO, SiO_2, TiO_2) [7, 9, 10, 12, 20, 21, 22], as these precious metals were reported to provide high resistance to the carbon formation compared to the conventional catalysts (i.e. Ni based catalyst). Verykios and coworkers [11,13,18] reported that Rh based catalyst provides significantly higher activity and stability toward the steam reforming of ethanol compared to Ru, Pt, Pd, and also Ni. Similarly, Freni et al. [7, 10, 12, 21] presented that Rh/Al_2O_3 provides the highest reforming reactivity among these noble metal catalysts. Burch and coworkers [15] found that the order of ethanol steam reforming reactivity of the metals was Rh > Pd > Ni = Pt.

Unfortunately, although these precious metals were active for the ethanol steam reforming and provide high resistance to the carbon formation, the current prices of these metals are very high for commercial uses, and the availability of some precious metals such as ruthenium was too low to have a major impact on the total reforming catalyst market [24]. Adding some oxygen together with ethanol and steam as the inlet feed, called an autothermal reforming, was also widely reported as an attractive operation to reduce the degree of carbon formation on the catalyst surface. However, this reaction requires the air separation unit to separate oxygen from air, which is a costly process and makes fuel cell more expensive for operation. The use of air instead of oxygen could eliminate this problem; however, the hydrogen concentration obtained from the reaction will be significantly lower due to the high content of nitrogen in the feed.

In the present work, it is aimed at the development of an alternative catalyst that is cheaper than the noble metal materials and enables to decompose ethanol with high resistance toward carbon deposition. It is well established that cerium oxide (CeO_2) is used as a catalyst in a wide variety of reactions involving the oxidation, or partial oxidation, of hydrocarbons (e.g. automotive catalysis) [25, 26]. This material contains a high concentration of highly mobile oxygen vacancies, which act as a local source or sink for oxygen involved in reactions taking place on the surface [27-33]. There is now increasing interest in using ceria in more reducing conditions, such as in methane reforming at the anodes of solid oxide fuel cells (SOFC), where the potential deactivation through carbon deposition is much greater [34, 35]. The excellent resistance toward carbon formation from methane cracking reaction over CeO_2 under SOFC conditions was reported [36]. Recently, the successful use of ceria as a key constituent of the anode for a SOFC operating directly on "dry" methane has also been presented [37, 38, 39].

Importantly, at the temperature above 700ºC, the gas–solid reaction between CeO_2 and CH_4 produces synthesis gas with a H_2/CO ratio of two. It was also demonstrated that the reaction of the reduced ceria with CO_2 and steam produced CO and H_2, respectively, and regenerating the CeO_2 surface [40, 41, 42]; according to the following reactions:

$$CH_4 + O_O^x = 2\,H_2 + CO + V_O^{\bullet\bullet} + 2\,e' \quad (1)$$

$$V_O^{\bullet\bullet} + 2\,e' + CO_2 = O_O^x + CO \quad (2)$$

$$V_O^{\bullet\bullet} + 2\,e' + H_2O = O_O^x + H_2 \quad (3)$$

O_O^x denotes a lattice oxygen in CeO_2, $V_O^{\bullet\bullet}$ is an oxygen vacancy with an effective charge 2^+, e' is an electron which can either be more or less localized on a cerium ion or delocalized in a conduction band [43].

The major limitation to apply ceria for high temperature applications is its low specific surface area due to the significant size reduction by thermal sintering [44]. It was reported that the corresponding post-reaction specific surface area for CeO_2 after exposure in methane steam reforming conditions at 900ºC for 10 h was 1.9 $m^2\ g^{-1}$, and the observed size reduction percentage was 23% [39]. Therefore, the use of high surface area (HSA) ceria would be a good procedure to improve its catalytic performance at high operating temperatures. Several methods have recently been described for the preparation of CeO_2 (HSA) solid solution. Among these methods, the surfactant-assisted approach was employed to prepare high surface area CeO_2 with improved textural, structural, and chemical properties [44]. Our previous publication [45] also presented the achievement of CeO_2 with high surface area and good stability after thermal treatment by this preparation method. Regarding the surfactant-assisted method, CeO_2 (HSA) is prepared by reacting a cationic surfactant with a hydrous oxide produced by co-precipitation under basic conditions. At high pH value, conducting the precipitation of hydrous oxide in the presence of cationic surfactant allows the cation exchange process between H^+ and the surfactant, resulting in a developed pore structure with an increase in surface area [44]. The achievement of high thermal stability for CeO_2 (HSA) is due to the incorporation of surfactants during preparation, which can reduce the interfacial energy and eventually decrease the surface tension of water contained in the pores. This could reduce the shrinkage and collapse of the catalyst during heating up, which consequently help the catalyst maintain high surface area after calcination [44].

In this work, high surface area CeO_2 (CeO_2 (HSA)) was first synthesized by the surfactant-assisted method. The reactivity toward decomposition of ethanol, the effect of inlet steam content, and the resistance toward carbon formation of this material were investigated at 700-1000ºC, compared to those of conventional CeO_2 (CeO_2 (LSA)) prepared by precipitation method and Ni/Al_2O_3. At steady state, the influences of temperature and inlet components on the product selectivities from the decomposition of ethanol over CeO_2 (HSA) were then determined. At the end of this

article, the gas-solid redox mechanism between the hydrocarbons present in the system and the lattice oxygen (O_O^x) on the surface of CeO_2 (HSA) was discussed.

2. Experimental

2.1. Catalyst preparation and characterization

CeO_2 (HSA) was prepared by mixing an aqueous solution of the appropriate cationic surfactant, 0.1 M cetyltrimethylammonium bromide solution from Aldrich, to a 0.1 M cerium chloride. The molar ratio of ([Ce])/[cetyltrimethylammonium bromide] was kept constant at 0.8. The mixture was stirred and then aqueous ammonia was slowly added with the constant rate of 0.165 cm^3 min^{-1} until the pH was 11.5. We found that the rate of ammonia doping have a significant impact on the specific surface area of synthesis CeO_2. According to our experiments, this flow rate of ammonia can provide solid CeO_2 with the highest specific surface area. The mixture was continually stirred for 3 h, then sealed and placed in the thermostatic bath maintained at 90°C for 3 days. After that, the mixture was cooled and the resulting precipitate was filtered and washed repeatedly with water and acetone to remove the free surfactant. It was dried overnight in an oven at 110°C, and then calcined in air at 1000°C for 6 h.

CeO_2 (LSA) was prepared by the precipitation of cerium chloride ($CeCl_3 \cdot 7H_2O$) from Aldrich. The starting solution was prepared by mixing 0.1 M of this metal salt solution with 0.4 M of ammonia at a 2:1 volumetric ratio. This solution was stirred by magnetic stirring (100 rpm) for 3 h, then sealed and placed in a thermostatic bath maintained at 90°C for 3 days. The precipitate was filtered and washed with deionised water and acetone. The filtered powder was then treated under the same procedures as CeO_2 (HSA). BET measurements of CeO_2 (both LSA and HSA) were carried out at different calcination temperatures in order to determine the decreasing in specific surface area due to the thermal sintering. As presented in Fig. 1, after drying, surface areas of 308 and 55 m^2 g^{-1} were observed for CeO_2 (HSA) and conventional CeO_2, respectively and, as expected, the surface area dramatically decreased at high calcination temperatures. However, the value for CeO_2 (HSA) is still appreciable after calcination at 1000°C. The redox properties and redox reversibilities of these calcined CeO_2 (both LSA and HSA) were then determined by

the temperature programmed reduction (TPR) and the temperature programmed oxidation (TPO). Regarding these experiments, 5% H_2/He and 5% O_2/He were used for the TPR and TPO respectively, while the temperature of the system increased from 100ºC to 900ºC with the rate of 12ºC/min for both experiments. Details of these characterizations and experiments are presented in the result section.

For comparison, conventional Ni/Al_2O_3 (5wt% Ni) was also prepared by impregnating α-Al_2O_3 (from Aldrich) with $NiCl_3$. After stirring, the solution was dried and calcined at 1000°C for 6 h. The catalysts were also reduced with 10%H_2/He at 700ºC for 6 h before use.

2.2. Apparatus and Procedures

An experimental reactor system was constructed as shown in Fig. 2. The feed gases including the components of interest (ethanol and steam from the evaporator) and the carrier gas (helium) were introduced to the reaction section, in which a 10-mm diameter quartz reactor was mounted vertically inside a furnace. The catalyst was loaded in the quartz reactor, which was packed with a small amount of quartz wool to prevent the catalyst from moving. Regarding the results in our previous publications [46], in order to avoid any limitations by intraparticle diffusion, the weight of catalyst loading was kept constant at 50 mg, while the total gas flow was 100 cm^3 min^{-1} under a constant residence time of 5 x 10^{-4} g min cm^{-3} in all experiments. A type-K thermocouple was placed into the annular space between the reactor and the furnace. This thermocouple was mounted on the tubular reactor in close contact with the catalyst bed to minimize the temperature difference between the catalyst bed and the thermocouple. Another type-K thermocouple was inserted in the middle of the quartz tube in order to re-check the possible temperature gradient. The record showed that the maximum temperature fluctuation during the reaction was always ±0.75ºC or less from the temperature specified for the reaction.

After the reactions, the exit gas mixture was transferred via trace-heated lines to the analysis section, which consists of a Porapak Q column Shimadzu 14B gas chromatograph (GC) and a mass spectrometer (MS). The gas chromatography was applied in order to investigate the steady state condition experiments, whereas the mass spectrometer in which the sampling of the exit gas was done by a quartz capillery and differential pumping was used for the transient carbon formation experiment. In order to study the formation of carbon species on catalyst surface,

Temperature programmed Oxidation (TPO) was applied by introducing 10% oxygen in helium into the system, after purged the system with helium. The operating temperature increased from 100ºC to 1000ºC by the rate of 20ºC/min. The amount of carbon formation on the surface of catalysts was determined by measuring the CO and CO_2 yields from the TPO results (using Microcal Origin Software) assuming a value of 0.026 nm^2 for the area occupied by a carbon atom in a surface monolayer of the basal plane in graphite [38]. The calibrations of CO and CO_2 productions were performed by injecting a known amount of these calibration gases from a loop, in an injection valve in the bypass line. The response factors were obtained by dividing the number of moles for each component over the respective areas under peaks. In addition to the TPO method, the amount of carbon deposition was confirmed by the calculation of carbon balance in the system. The amount of carbon deposited on the surface of catalyst would theoretically be equal to the difference between the inlet carbon containing components (C_2H_5OH) and the outlet carbon containing components (CO, CO_2, CH_3CHO, C_2H_6, C_2H_4, and CH_4). The amount of carbon deposited per gram of catalyst is given by the following equation:

$$C_{deposition} = \frac{mole_{carbon(in)} - mole_{carbon(out)}}{m_{catalyst}} \tag{4}$$

The performances of the reforming of ethanol were defined in terms of conversion ($X_{Ethanol}$) and the product selectivities of hydrogen, carbon monoxide, carbon dioxide, methane, ethane, ethylene, and acetaldehyde ($S_{product}$) which are calculated according to Eqs. (5) – (12):

$$X_{Ethanol} = \frac{100(\%Ethanol_{in} - \%Ethanol_{out})}{\%Ethanol_{in}} \tag{5}$$

$$S_{H_2} = \frac{100(\%H_2)}{3(\%Ethanol_{in} - \%Ethanol_{out})} \tag{6}$$

$$S_{CO} = \frac{100(\%CO)}{2(\%Ethanol_{in} - \%Ethanol_{out})} \tag{7}$$

$$S_{CO_2} = \frac{100(\%CO_2)}{2(\%Ethanol_{in} - \%Ethanol_{out})} \tag{8}$$

$$S_{CH_4} = \frac{100(\%CH_4)}{2(\%Ethanol_{in} - \%Ethanol_{out})} \quad (9)$$

$$S_{C_2H_6} = \frac{100(\%C_2H_6)}{(\%Ethanol_{in} - \%Ethanol_{out})} \quad (10)$$

$$S_{C_2H_4} = \frac{100(\%C_2H_4)}{(\%Ethanol_{in} - \%Ethanol_{out})} \quad (11)$$

$$S_{CH_3CHO} = \frac{100(\%CH_3CHO)}{(\%Ethanol_{in} - \%Ethanol_{out})} \quad (12)$$

It should be noted that, from Eq. 6, three H_2 molecules from ethanol represent 100% H_2 selectivity. However, from the steam reforming of ethanol, H_2 selectivity can exceed 100%. This is possible because water is consumed as well as ethanol in the process, therefore, H atoms from H_2O can also be converted into H_2.

3. Results

3.1 Redox properties and redox reversibility of the synthesized catalysts

Firstly, the oxygen storage capacities (OSC) and the degree of redox properties for CeO_2 (both LSA and HSA) and Ni/Al_2O_3 were characterized using temperature programmed reduction (TPR-1), which was performed by heating the reduced catalysts up to 900°C in 5%H_2 in helium. As shown in Fig. 3, hydrogen consumptions of CeO_2 are detected at the temperature above 650°C. The amount of hydrogen uptake over CeO_2 (HSA) is significantly higher than that over CeO_2 (LSA), suggesting that the OSC strongly depends on the specific surface area of CeO_2. In contrast, no hydrogen consumption was observed from the TPR over Ni/Al_2O_3, indicating that no OSC for this catalyst.

After purged with helium, the redox reversibility for each catalyst was then determined by applying temperature programmed oxidation (TPO-1) followed by the second temperature programmed reduction (TPR-2). Regarding the TPR-2 results, the amount of hydrogen uptakes for CeO_2 (both LSA and HSA) were approximately similar to those from TPR-1, indicating the redox reversibility for these CeO_2. The second temperature programmed oxidation (TPO-2) and the third temperature programmed reduction (TPR-3) were also performed in order to reconfirm the redox

reversibility. The amounts of oxygen and hydrogen consumptions almost similar to those from TPO-1 and TPR-1 and 2 as shown in Figs. 4 and 5, and in Table 1.

3.2 Homogenous (non catalytic) reaction

Before studying the catalyst performance, homogeneous (non-catalytic) decomposition of ethanol was primarily investigated. Inlet H_2O/C_2H_5OH in helium with the molar ratios of 0.0 and 3.0 (inlet C_2H_5OH of 3.0 kPa) was introduced to the system, while the temperature increased from room temperature to 1000ºC. As shown in Figs. 6 and 7, it was observed that ethanol was converted to acetaldehyde, and hydrogen at the temperature above 200°C. Methane and carbon dioxide productions were initially observed at the temperature of 250-300°C. When the temperature increased up to 550°C, the selectivity of acetaldehyde significantly decreased, while those of hydrogen, carbon monoxide, and carbon dioxide selectivities remained increased. In this range of temperature, the formations of ethane and ethylene were also observed. At the same condition, hydrogen and carbon dioxide selectivities from ethanol decomposition with inlet H_2O/C_2H_5OH of 3.0 are higher than those with inlet H_2O/C_2H_5OH of 0.0, whereas the carbon monoxide selectivity is lower. These are simply due to the impact of the water-gas shift reaction.

3.3 Catalytic reactivity toward ethanol decomposition

The decomposition of ethanol with and without steam over CeO_2 (HSA), conventional CeO_2, and Ni/Al_2O_3 were first studied at 900°C. The feed at different inlet H_2O/C_2H_5OH molar ratios of 0.0, 1.0, and 3.0 (inlet C_2H_5OH of 3.0 kPa) was introduced to the system. The variations in hydrogen selectivities (%) with time at 900°C over different catalysts and different inlet H_2O/C_2H_5OH ratios are shown in Fig. 8. After operated for 10 h, the hydrogen selectivities for CeO_2 (HSA) were significantly higher than those for conventional CeO_2 and Ni/Al_2O_3; however, the deactivations were also observed for all catalysts. Catalyst stabilities expressed as deactivation percentages are given in Table 2. The post-reaction temperature-programmed oxidation (TPO) experiments over the spent catalysts were then carried out after a helium purge by introducing 5% oxygen in helium in order to determine whether the observed deactivation is due to the carbon formation. From the TPO results shown in Fig. 9, the huge amounts of carbon deposition were observed for

Ni/Al_2O_3, whereas significantly lower carbon formations were detected for CeO_2 (LSA). No formation of carbon species was detected over CeO_2 (HSA) in all conditions. The values of carbon formations (monolayer) on the surface of catalysts were determined by measuring these CO and CO_2 yields (using Microcal Origin Software). Using a value of 0.026 nm^2 for the area occupied by a carbon atom in a surface monolayer of the basal plane in graphite [38], the quantities of carbon deposited on each catalyst were observed as also presented in Table 2. The total amounts of carbon deposited were then ensured by calculating the carbon balance of the system. Regarding the calculations, for the inlet H_2O/C_2H_5OH ratios of 0.0, 1.0, and 3.0, the moles of carbon deposited per gram of CeO_2 (LSA) were 0.84, 0.79, and 0.73 mmol g^{-1}. By the same assumption for the area occupied by a carbon atom [38], these values are equal to 0.80, 0.74, and 0.69 monolayers respectively, which are in good agreement with the values observed from the TPO method described above. The results clearly indicated that the deactivations observed for Ni/Al_2O_3 were mainly due to the carbon deposition on the surface of catalyst, and CeO_2 especially the high surface area one presented significantly stronger resistance toward carbon formation compared to Ni/Al_2O_3. The BET measurements were carried out to observe the surface area reduction percentages of all catalysts. As shown in Table 2, it was suggested that the deactivations of ceria are also due to the thermal sintering. Clearly, the surface area reduction percentage of CeO_2 (HSA) is much lower than CeO_2 (LSA), indicating its better stability toward the thermal sintering.

3.4 Effects of temperature and inlet reactants

The influences of operating temperature and the inlet steam content on the product selectivities and ethanol conversion over CeO_2 (both HSA and LSA) were further studied by varying temperature from 700°C to 1000°C and changing the inlet H_2O/C_2H_5OH molar ratios from 0.0 to 1.0, and 3.0, Figs. 10 and 11.

From the study, in the range of temperature between 700-850ºC, it was found that H_2, CO, and CH_4 selectivities increased with increasing temperature, whereas C_2H_4, C_2H_6, and CO_2 selectivities decreased. At the temperature above 850ºC, the yield of CH_4 production starts level off, which is due to the strong endothermic steam reforming of CH_4 at high temperature. By considering the effect of steam, H_2 and CO_2 selectivities increased with increasing inlet steam concentration, whereas CO

selectivity decreased. These are mainly due to the influence of mildly exothermic water-gas shift reaction ($CO + H_2O \rightarrow CO_2 + H_2$). It should be noted that C_2H_4 and C_2H_6 selectivities decreased with increasing temperature and inlet steam content. In addition, compared between CeO_2 (HSA) and CeO_2 (LSA) in Figs. 10 and 11, no formation of C_2H_4 and C_2H_6 was detected at the temperature above 900ºC for CeO_2 (HSA), whereas appreciable amount of C_2H_4 was remains observed from the ethanol steam reforming over CeO_2 (LSA) even at 1000ºC.

The ethanol conversions and the product selectivities from the steam reforming of ethanol over both CeO_2 (HSA) and CeO_2 (LSA) were also compared to those values at equilibrium state, which were calculated using AspenPlus10.2 simulation program. As presented in Table 3, according to the simulation, the conversions of ethanol at equilibrium level are 100% in the range of temperature studied, 700-1000ºC. The yields of hydrogen production at equilibrium are higher than those achieved over CeO_2. In addition, neither C_2H_6 nor C_2H_4 formation was observed in all conditions due to the complete reforming of this component to CH_4, CO, and CO_2.

Without inlet steam, the effect of ethanol concentration on the rate of decomposition over CeO_2 (HSA) was further studied by varying inlet ethanol partial pressure from 1.0 to 4.0 kPa at the temperature between 700-900°C. Fig. 12 presents the Arrhenius plots of the ethanol conversion at various inlet ethanol concentrations. The results show that the conversion of ethanol is proportional to the ethanol concentration and the temperature. Regarding the post-reaction TPO, no carbon formation was observed on the surface of catalysts in all conditions.

In addition, several inlet steam partial pressures were then introduced to the feed with constant ethanol partial pressure in order to investigate the influence of steam on the rate of ethanol decomposition (H_2O/C_2H_5OH of 0.0, 1.0, 2.0, 3.0, 4.0, and 5.0). The ethanol conversion seems to be independent of the inlet steam partial pressure for the range of conditions studied as shown in Fig. 13.

4. Discussion

According to the homogeneous (non-catalytic) ethanol steam reforming in this study, ethanol is firstly converts to acetaldehyde, hydrogen, methane, and carbon

monoxide via the dehydrogenation of ethanol and simultaneous fast decomposition of acetaldehyde at relative low temperature (300-500ºC) (Eqs. 13 and 14).

$$C_2H_5OH \rightarrow C_2H_4O + H_2 \quad (13)$$

$$C_2H_4O \rightarrow CH_4 + CO \quad (14)$$

When the temperature increases, methane steam reforming and water gas shift reactions (Eqs. 15 and 16) take place. Also, ethylene and ethane are formed by the dehydration of ethanol (Eq. 17) following with the ethylene hydrogenation (Eq. 18).

$$CH_4 + H_2O \rightarrow CO + 3H_2 \quad (15)$$

$$CO + H_2O \rightarrow CO_2 + H_2 \quad (16)$$

$$C_2H_5OH \rightarrow C_2H_4 + H_2O \quad (17)$$

$$C_2H_4 + H_2 \rightarrow C_2H_6 \quad (18)$$

In the present work, it was found that the decomposition of ethanol at high temperature on the surface of CeO_2 (HSA) produced H_2, CH_4, CO, and CO_2. This reactivity is due to the containing of the lattice oxygen (O_O^x) in CeO_2, as the hydrocarbons present in the system (i.e. ethanol, ethane, ethylene, and methane) adsorbs and decomposes on the surface of CeO_2 (S_{ce}), and eventually reacts with the lattice oxygen (O_O^x). The gas-solid redox mechanism between these hydrocarbons and the lattice oxygen (O_O^x) on the surface of CeO_2 (HSA) could be derived as illustrated below.

$$C_2H_5OH + 2S_{Ce} = 2(CH_2\text{-}S_{Ce}) + H_2O \quad (27)$$

$$C_2H_6 + 2S_{Ce} = 2(CH_3\text{-}S_{Ce}) \quad (28)$$

$$C_2H_4 + 2S_{Ce} = 2(CH_2\text{-}S_{Ce}) \quad (29)$$

$$CH_4 + 2S_{Ce} = CH_3\text{-}S_{Ce} + H\text{-}S_{Ce} \quad (30)$$

$$CH_3\text{-}S_{Ce} + S_{Ce} = CH_2\text{-}S_{Ce} + H\text{-}S_{Ce} \quad (31)$$

$$CH_2\text{-}S_{Ce} + S_{Ce} = CH\text{-}S_{Ce} + H\text{-}S_{Ce} \quad (32)$$

$$CH\text{-}S_{Ce} + S_{Ce} = C\text{-}S_{Ce} + H\text{-}S_{Ce} \quad (33)$$

$$C\text{-}S_{Ce} + O_O^x = CO + V_O^{\bullet\bullet} + 2\,e' + S_{Ce} \quad (34)$$

$$2H\text{-}S_{Ce} = H_2 + 2S_{Ce} \quad (35)$$

S_{Ce} is the CeO_2 surface site and CH_x-S_{Ce} is an intermediate surface hydrocarbon species. S_{Ce} can be considered to be a unique site, or the same site as the lattice oxygen (O_O^x). Therefore, during the reaction, hydrocarbons are adsorbed on either a unique site (S_{Ce}) or the lattice oxygen (O_O^x). The lattice oxygen (O_O^x) can be regenerated by the inlet steam and also the steam that generated from ethanol dehydration (Eq. 27). Normally, the inlet steam is always required during the decomposition of ethanol over conventional metallic catalyst to prevent the formation of carbon species on catalyst surface. However, it was proven from this study that CeO_2 (HSA) can decompose ethanol efficiently without the presence of inlet steam being required (H_2O/C_2H_5OH = 0.0). This could be due to the significant rapid surface reaction of the reduced state CeO_2 with steam generated from the dehydration of ethanol during the decomposition reactions to replenish the lattice oxygen, Eq. 36.

$$H_2O + + V_O^{\bullet\bullet} + 2\,e' = H_2 + O_O^x \quad (36)$$

It should be noted that the measured value of the oxygen diffusion coefficient for ceria is high and the reaction rate is controlled by a surface reaction, not by diffusion of oxygen from the bulk of the solid particles to ceria surfaces [49]. The strong linear dependence of the inlet ethanol partial pressure and the independent of steam on ethanol decomposition rate also support the idea that the lattice oxygen is replenished by a significant rapid surface reaction of the reduced state CeO_2 with oxygen sources in the system.

In order to prove the gas-solid mechanism in Eqs. 27-36, three sets of experiments were carried out over CeO_2 (HSA). Ethane, ethylene, or methane was fed instead of ethanol to the catalytic reactor. Small amount of steam was also added (H_2O/C_nH_m molar ratio of 1.0/1.0) in order to replenish the lattice oxygen. Tables 4, 5, and 6 present the conversions and product selectivities from the steam reforming of ethane, ethylene, and methane at different temperatures. Clearly, CeO_2 (HSA) can convert ethane and ethylene to methane, carbon monoxide, carbon dioxide, and hydrogen in this range of temperature, while the steam reforming of methane over this catalyst produces H_2, CO, and small amount of CO_2. The conversions of ethane and ethylene were about 100% when the temperature reached 900ºC.

Theoretically, the formations of ethylene and ethane are the major difficulties for the catalytic reforming of ethanol, as it has been established that ethane and

ethylene act as a very strong promoter of carbon formation. Eqs. 19-24 below present the most probable reactions that could lead to carbon deposition from the steam reforming of ethanol:

$$C_2H_6 = 3H_2 + 2C \quad (19)$$

$$C_2H_4 = 2H_2 + 2C \quad (20)$$

$$CH_4 = 2H_2 + C \quad (21)$$

$$2CO = CO_2 + C \quad (22)$$

$$CO + H_2 = H_2O + C \quad (23)$$

$$CO_2 + 2H_2 = 2H_2O + C \quad (24)$$

C is the carbonaceous deposits. At low temperature, Eqs. (23-24) are favorable, while Eqs. (19-22) are thermodynamically unflavored [47]. The Boudard reaction (Eq. 22) and the decomposition of hydrocarbons (Eqs. 19-21) are the major pathways for carbon formation at such a high temperature as they show the largest change in Gibbs energy [48]. According to the operating temperature in this study (700-1000ºC), carbon formation would be formed via the decomposition of hydrocarbons and Boudard reactions. By applying CeO_2 (HSA) as the catalyst, the carbon decomposition from both reactions could be inhibited by the gas-solid reactions between gaseous components (ethylene, ethane, and methane produced from the decomposition of ethanol) with the lattice oxygen (O_O^x) on CeO_2 surface, Eqs. 25 and 26.

$$C_nH_m + O_O^x = nCO + m/2\ H_2 + V_O^{\bullet\bullet} + 2\ e' \quad (25)$$

$$CO + O_O^x = 2CO_2 + V_O^{\bullet\bullet} + 2\ e' \quad (26)$$

Although CeO_2 (LSA) also provides high resistance toward carbon formation, the major weaknesses of CeO_2 (LSA) are its nature low specific surface area and its high size reduction due to the thermal sintering, which result in its low oxygen storage capacity and consequently caused the low reforming reactivity. The comparative reforming reactivities between CeO_2 (HSA) and CeO_2 (LSA) are in good agreement with the results from characterizations (i.e. BET and TPR-1, 2 and 3).

According to the good performance of CeO_2 (HSA) in terms of high resistance toward carbon deposition and good product selectivities at high temperature, this

catalyst would be a good candidate to be applied as the internal or in-stack reforming catalyst for solid oxide fuel cell application (IIR-SOFC), eliminating the requirement of expensive noble metal catalysts or an external pre-reforming installation. In addition, without the inlet steam requirement to decompose ethanol, the consideration of water management in SOFC system can be negligible. Regarding the above benefits, the use of CeO_2 (HSA) as the reforming catalyst for IIR-SOFC fueled by ethanol is expected to simplify the overall system design, making SOFC more attractive to be used commercially.

5. Conclusion

High surface area ceria (CeO_2 (HSA)) has useful ethanol decomposition activity producing H_2, CH_4, CO, and CO_2 under Solid Oxide Fuel Cells (SOFCs) conditions without the presence of steam being required. The catalyst provides excellent reactivity and high resistance toward carbon deposition compared to Ni/Al_2O_3 and conventional low surface area ceria (CeO_2 (LSA)). At the temperature above 900°C, neither C_2H_4 nor C_2H_6 was observed from the reforming over CeO_2 (HSA), whereas significant amounts of these hydrocarbons were formed over Ni/Al_2O_3 and CeO_2 (LSA). These benefits of CeO_2 (HSA) are mainly due to the high redox property of this material.

According to the great benefits of CeO_2 (HSA) in terms of high resistance toward carbon deposition, no inlet steam requirement, and good product selectivities at SOFC temperature, this catalyst would be a good candidate to be applied as the internal or in-stack reforming catalyst (IIR-SOFC).

Acknowledgement

The financial support from The Thailand Research Fund (TRF) throughout this project is gratefully acknowledged.

References

[1] S. Cavallaro, S. Freni, Int. J. Hydrogen Energy 21 (6) (1996) 465–469.

[2] N.F. Athanasio, X.E. Verykios, J. Catal. 225 (4) (2004) 39–452.

[3] L. Garcia, R. French, S. Czernik and E. Chornet. Appl. Catal. A: Gen. 201 (2000), 225.

[4] I. Fishtik, A. Alexander, R. Datta and D. Geana. Int. J. Hydrogen Energy 25 (2000) 31.

[5] S. Freni, G. Maggio and S. Cavallaro. J. Power Sour. 62 (1996) 67.

[6] K. Vasudera, N. Mitra, P. Umasankar and S.C. Dhinga. Int. J. Hydrogen Energy 21 (1996) 13.

[7] S. Cavallaro and S. Freni. Int. J. Hydrogen Energy 21 (1996) 465.

[8] F. Marino, E.G. Cerrella, S. Duhalde, M. Jobbagy and M.A. Laborde. Int. J. Hydrogen Energy 23 (1998) 1095.

[9] S. Cavallaro. Energy and Fuels 14 (2000) 1195.

[10] S. Freni. J. Power Sour. 94 (2001) 14.

[11] A. Fatsikostas, D. Kondarides and X. Verykios. Catal. Today 75 (2002) 145.

[12] S. Freni, S. Cavallaro, N. Mondello, L. Spadaro and F. Frusteri. J. Power Sour. 108 (2002) 53.

[13] A. Fatsikostas, D. Kondarides and X. Verykios. Catal. Today 75 (2002) 145.

[14] F. Marino, G. Baronetti, M. Jobbagy and M. Laborde. Appl. Catal. A: Gen. 6043 (2002) 1.

[15] J.P. Breen, R. Burch and H.M. Coleman. Appl. Catal. B: Environ. 39 (2002) 65.

[16] J. Llorca, N. Homs, J. Sales and P. Ramirez de la Piscina. J. Catal. 209 (2002), 306.

[17] V. Fierro, V. Klouz, O. Akdim and C. Mirodatos. Catal. Today 75 (2002) 141.

[18] D. Liguras, D. Kondarides and X. Verykios. Appl. Catal. B: Environ. 43 (2003) 345.

[19] J. Llorca, P. Ramirez de la Piscina, J.-A. Dalmon, J. Sales and N. Homs. Appl. Catal. B: Environ. 43 (2003) 355.

[20] S. Cavallaro, V. Chiodo, S. Freni, N. Mondello and F. Frusteri. Appl. Catal. A: Gen. 249 (2003) 119.

[21] S. Freni, S. Cavallaro, N. Mondello, L. Sadaro and F. Frusteri. Catal. Commun. 4 (2003) 259.

[22] S. Cavallaro, V. Chiodo, A. Vita and S. Freni. J. Power Sour. 123 (2003) 10.

[23] D. Srinivas, C.V.V. Satyanarayana, H.S. Potdar and P. Ratnasamy. Appl. Catal. A: Gen. 243 (2003) 261.

[24] J.R. Rostrup-Nielsen and J.-H. Bak-Hansen, J. Catal. 144 (1993) 38.

[25] E. Ramirez, A. Atkinson, D. Chadwick, Appl. Catal. B, 36 (2002) 193-206

[26] A. Trovareli, C. Leitenburg, G. Dolcetti, Chemtech, (1997) 32.

[27] P. Fornasiero, G. Balducci, R.D. Monte, J. Kaspar, V. Sergo, G. Gubitosa, A. Ferrero and M. Graziani. J. Catal. 164 (1996) 173.

[28] T. Miki, T. Ogawa, M. Haneda, N. Kakuta, A. Ueno, S. Tateishi, S. Matsuura and M. Sato, J. Phys. Chem. 94 (1990) 339.

[29] C. Padeste, N.W. Cant and D.L. Trimm, Catal. Lett. 18 (1993) 305.

[30] S. Kacimi, J. Barbier Jr., R. Taha and D. Duperz, Catal. Lett. 22 (1993) 343.

[31] G.S. Zafiris and R.J. Gorte, J. Catal. 143 (1993) 86.

[32] G.S. Zafiris and R.J. Gorte, J. Catal. 139 (1993) 561.

[33] S. Imamura, M. Shono, N. Okamoto, R. Hamada and S. Ishida, Appl. Catal. A 142 (1996) 279.

[34] B.C.H. Steele, P.H. Middleton and R.A. Rudkin. Solid State Ionics 28 (1990) 388.

[35] O.A. Marina, C. Bagger, S. Primdahl, M. Mogensen, in: P. Stevens, U. Bossell (Eds.), Proceedings of Third European SOFC Forum, Oberrohrdorf, Nantes, Switzerland, 1998, 427.

[36] E. Ramirez, A. Atkinson, D. Chadwick, Applied Catalysis B, 36, (2002) 193-206.

[37] E. P Murray, T. Tsai and S.A. Barnett. Nature 400 (1999) 649.

[38] E. Ramírez-Cabrera, A. Atkinson and D. Chadwick, Applied Catalysis B, 47 (2004) 127-131.

[39] E. Ramírez-Cabrera, N. Laosiripojana, A. Atkinson and D. Chadwick, Catalysis Today, 78 (2003) 433-438.

[40] K. Otsuka, T. Ushiyama and I. Yamanaka, Chemistry Letters, (1993) 1517

[41] K. Otsuka, M. Hatano and A. Morikawa, J. Catalysis, 79, (1983) 493

[42] K. Otsuka, M. Hatano and A. Morikawa, Inorganica Chimica Acta, 109, (1985) 193

[43] P.J. Gellings and Henny J. M. Bouwmeester, Solid state aspects of oxidation catalysis, Catalysis Today, 58, (2000) 1-53

[44] D. Terribile, A. Trovarelli, J. Llorca, Carla de Leitenburg and G. Dolcetti, Catal. Today 43 (1998) 79-88.

[45] N. Laosiripojana, S. Assabumrungrat, Applied Catalysis B, 60 (1-2) 107-116.

[46] N. Laosiripojana, and S. Assabumrungrat, Fuel, in press

[47] Y. Lwin, W.R.W. Daud, A.B. Mohamad and Z. Yaakob, Int. J. Hydrogen Energy 25(1) (2000) 47-53.

[48] J.N. Amor, Appl. Catal. A 176 (1999) 159-176.

[49] B.C.H. Steele and J.M. Floyd. Proc. Br. Ceram. Soc. 19 (1971) 55.

List of figures

List of Tables

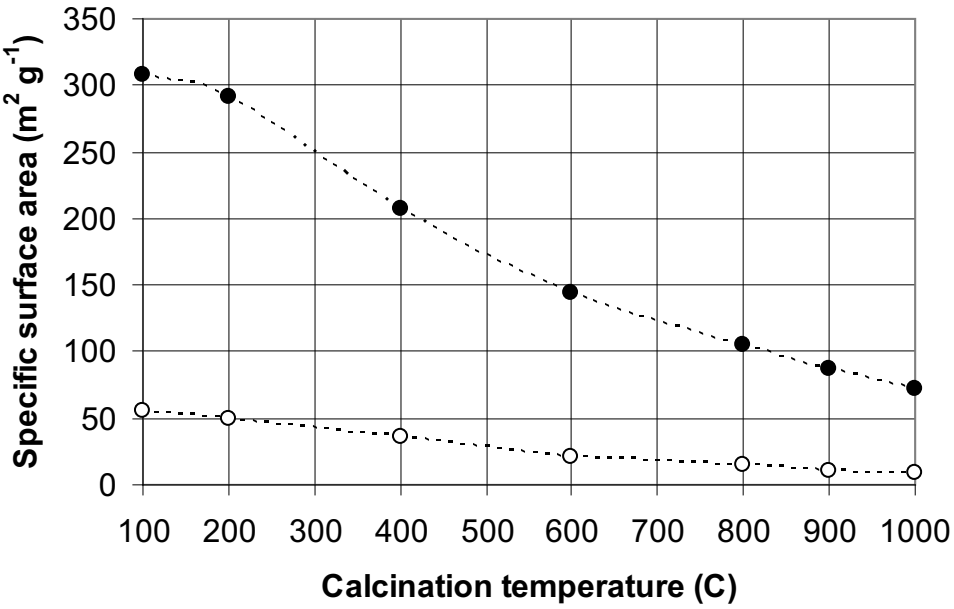

Fig. 1 Specific surface area of CeO_2 (HSA) (●) and CeO_2 (LSA) (○) after drying and calcinations at different temperatures

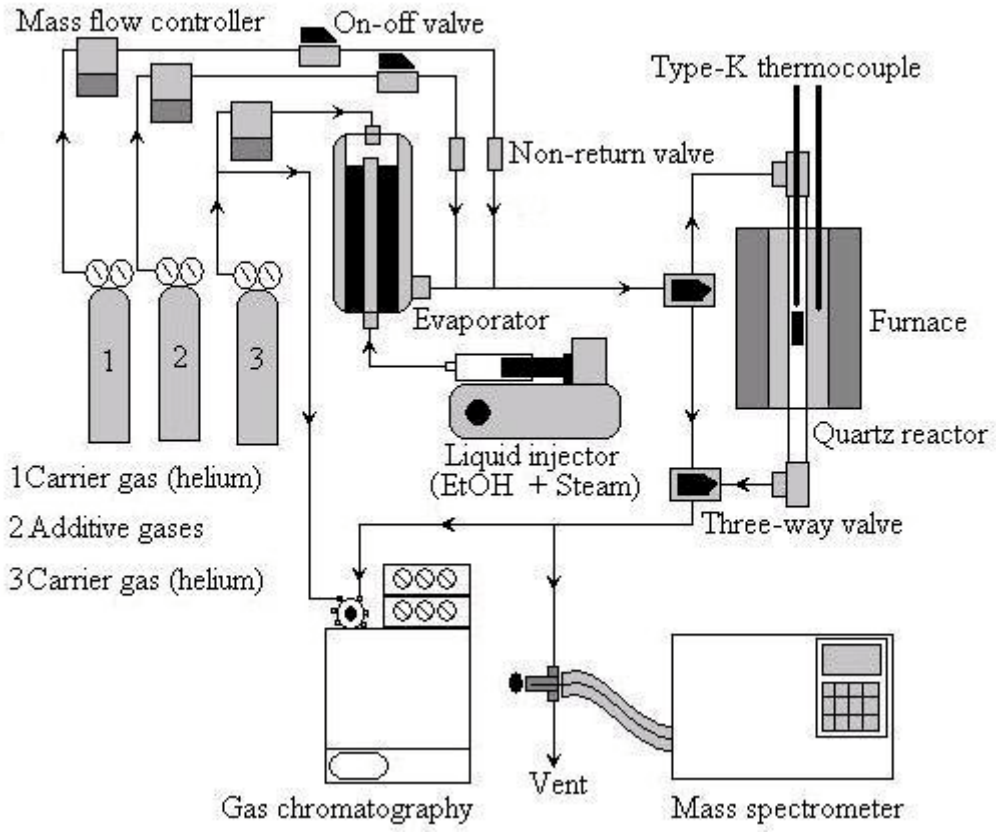

Fig. 2 Schematic diagram of the experimental set-up

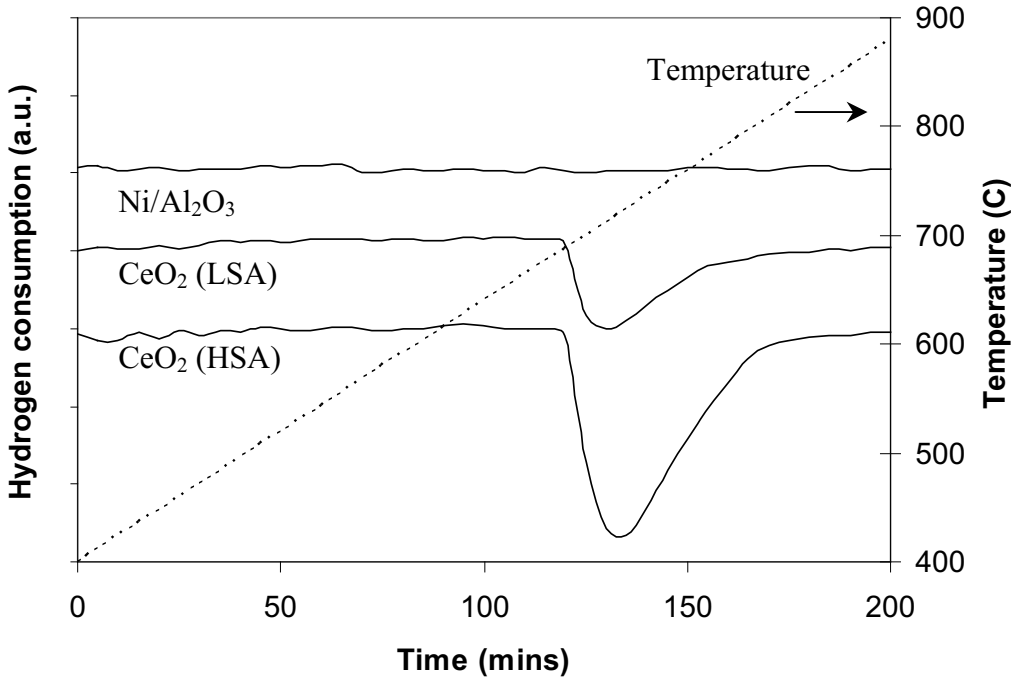

Fig. 3 Temperature Programmed Reduction (TPR-1) of fresh catalysts after reduction

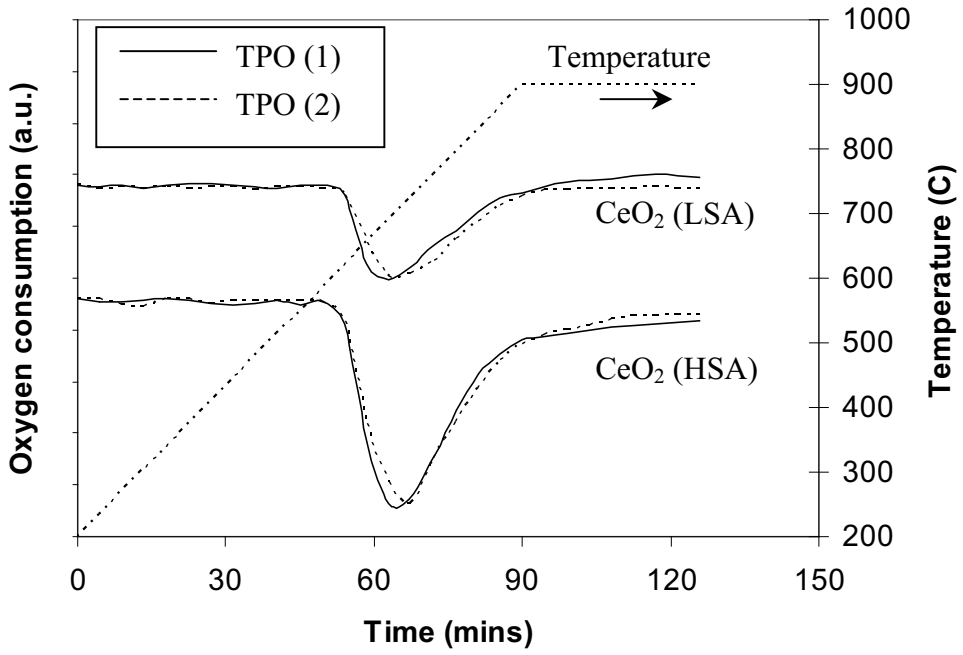

Fig. 4 Temperature Programmed Oxidation (TPO-1 and -2) of CeO_2 (HSA, LSA) after TPR-1 and TPR-2 respectively

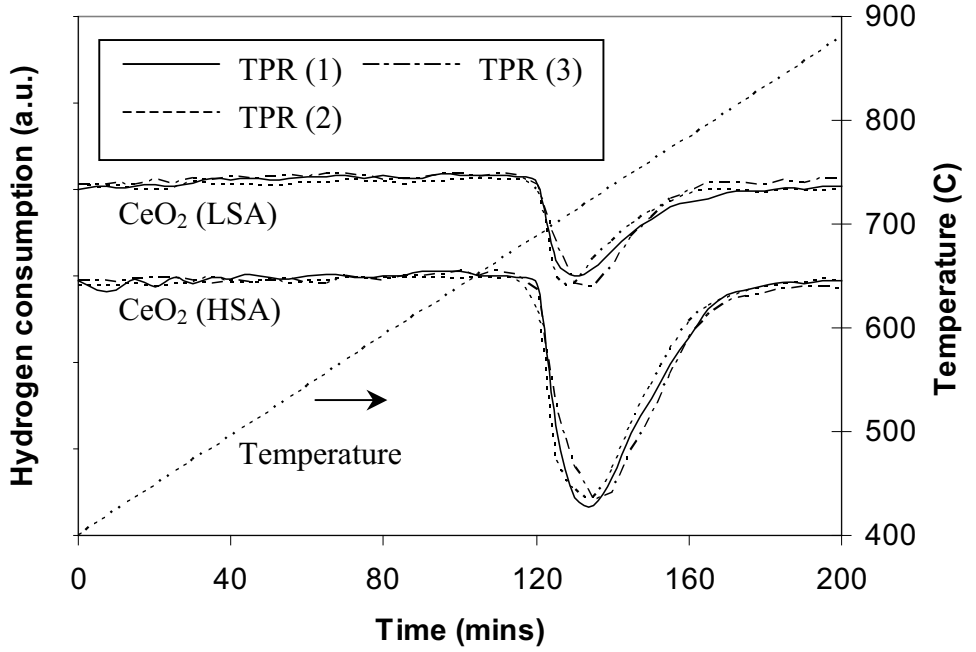

Fig. 5 Second and third times Temperature Programmed Reduction (TPR-2 and -3) of CeO_2 (HSA and LSA) compared to that of TPR-1

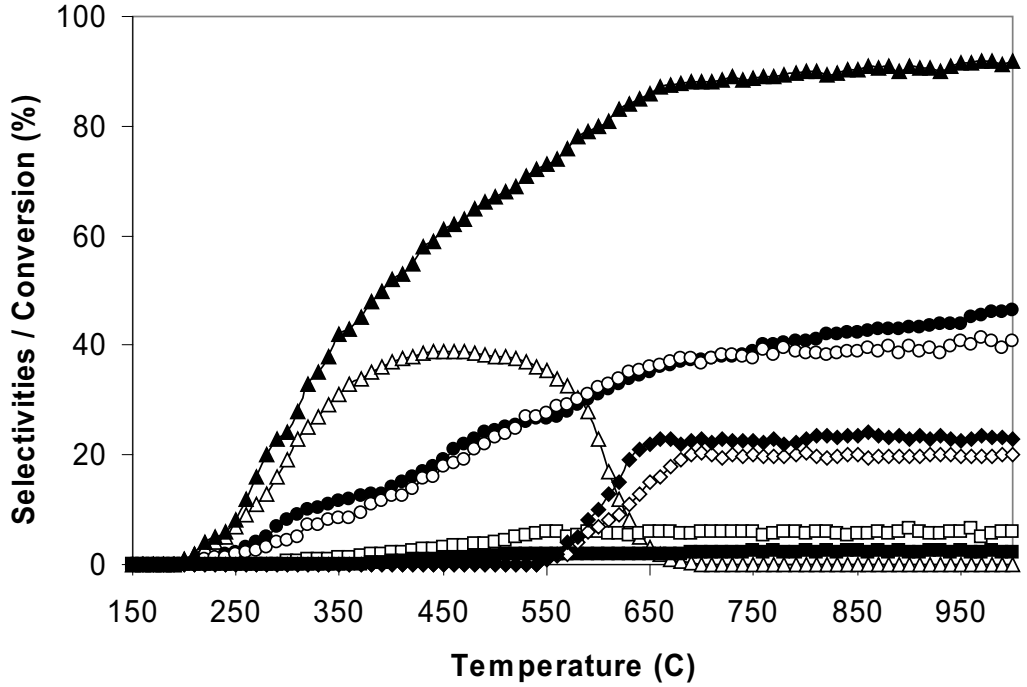

Fig. 6 Homogenous (in the absence of catalyst) reactivity of ethanol decomposition (4 kPa C_2H_5OH) (EtOH (▲), H_2 (●), CO (○), CO_2 (■), CH_4 (□), CH_3CHO (△), C_2H_6 (◇), and C_2H_4 (◆))

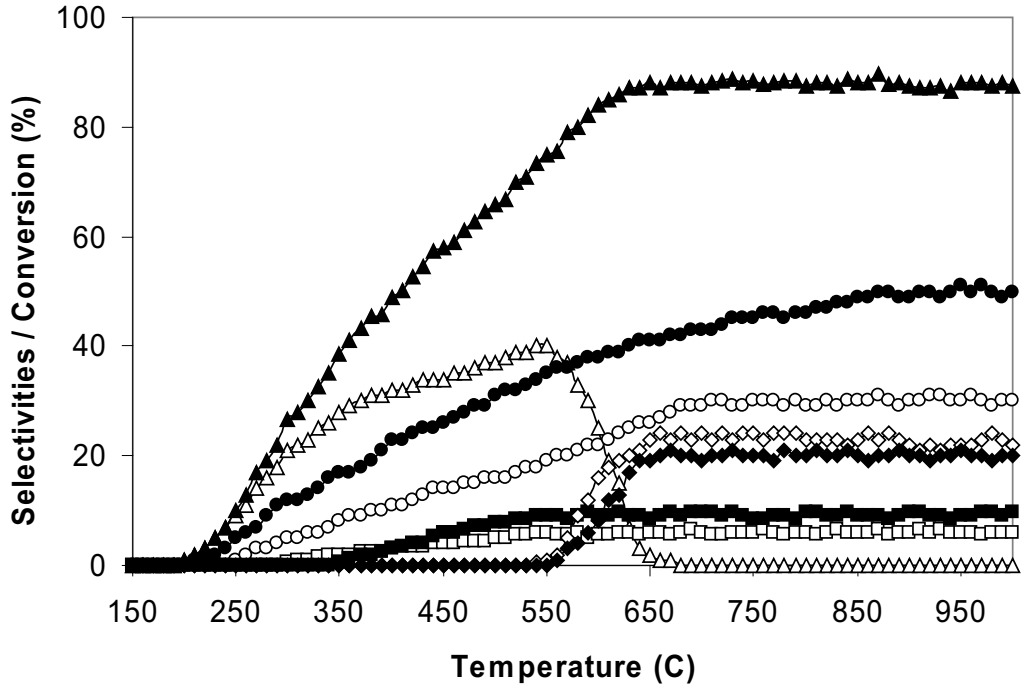

Fig. 7 Homogenous (in the absence of catalyst) reactivity of ethanol steam reforming (4 kPa C_2H_5OH, and 12 kPa H_2O) (EtOH (▲), H_2 (●), CO (○), CO_2 (■), CH_4 (□), CH_3CHO (△), C_2H_6 (◇), and C_2H_4 (◆))

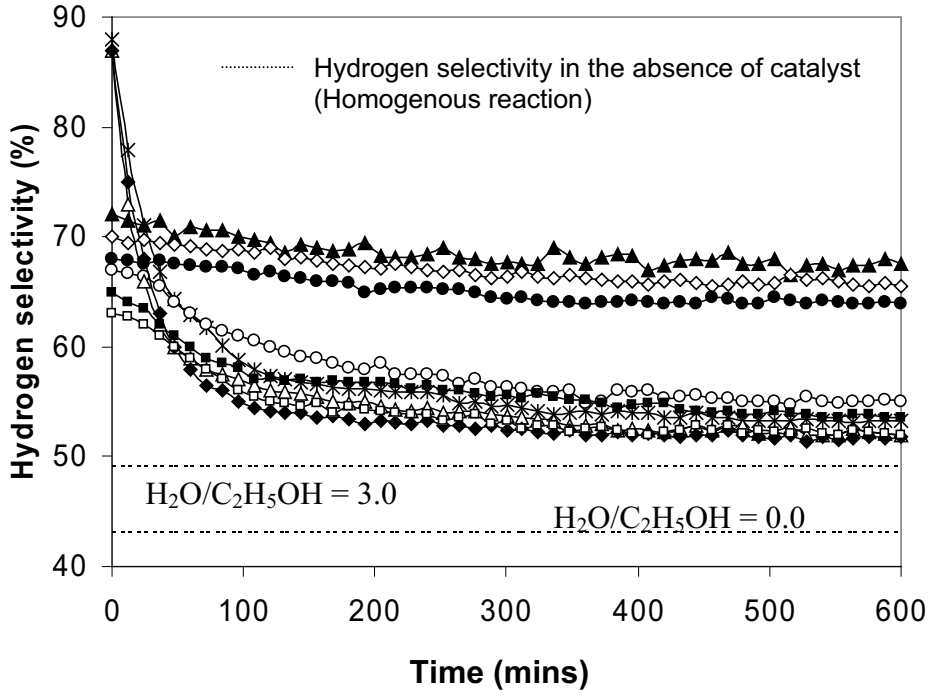

Fig. 8 Decomposition of ethanol (with and without steam) at 900°C for several catalysts and various inlet H_2O/C_2H_5OH ratios (CeO_2 (HSA) with H_2O/C_2H_5OH of 3.0 (▲), CeO_2 (HSA)

with H_2O/C_2H_5OH of 1.0 (◇), CeO_2 (HSA) with H_2O/C_2H_5OH of 0.0 (●), CeO_2 (LSA) with H_2O/C_2H_5OH of 3.0 (○), CeO_2 (LSA) with H_2O/C_2H_5OH of 1.0 (■), CeO_2 (LSA) with H_2O/C_2H_5OH of 0.0 (□), Ni/Al_2O_3 with H_2O/C_2H_5OH of 3.0 (×), Ni/Al_2O_3 with H_2O/C_2H_5OH of 1.0 (△), and Ni/Al_2O_3 with H_2O/C_2H_5OH of 0.0 (◆).

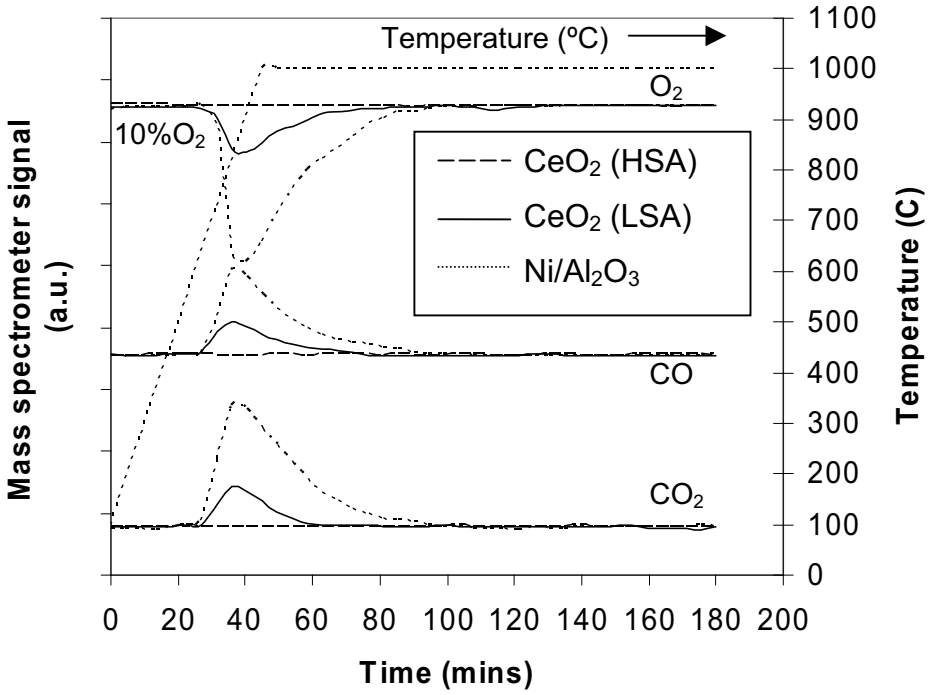

Fig. 9 Temperature Programmed Oxidation (TPO) of CeO_2 (HSA), CeO_2 (LSA), and Ni/Al_2O_3 after exposure in the decomposition of ethanol for 10 h (4 kPa C_2H_5OH)

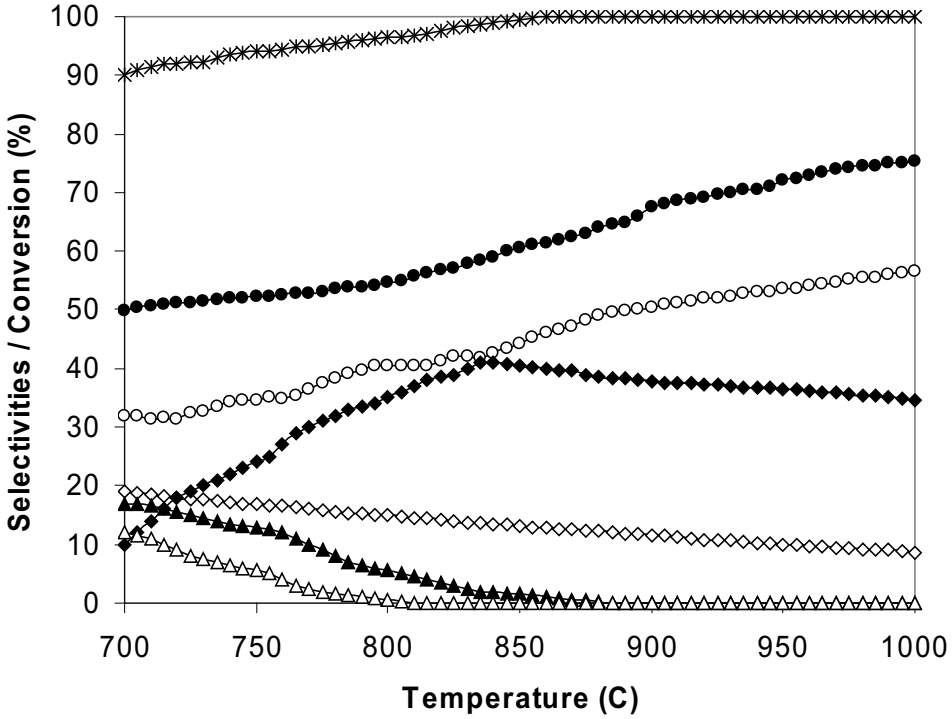

Fig. 10a

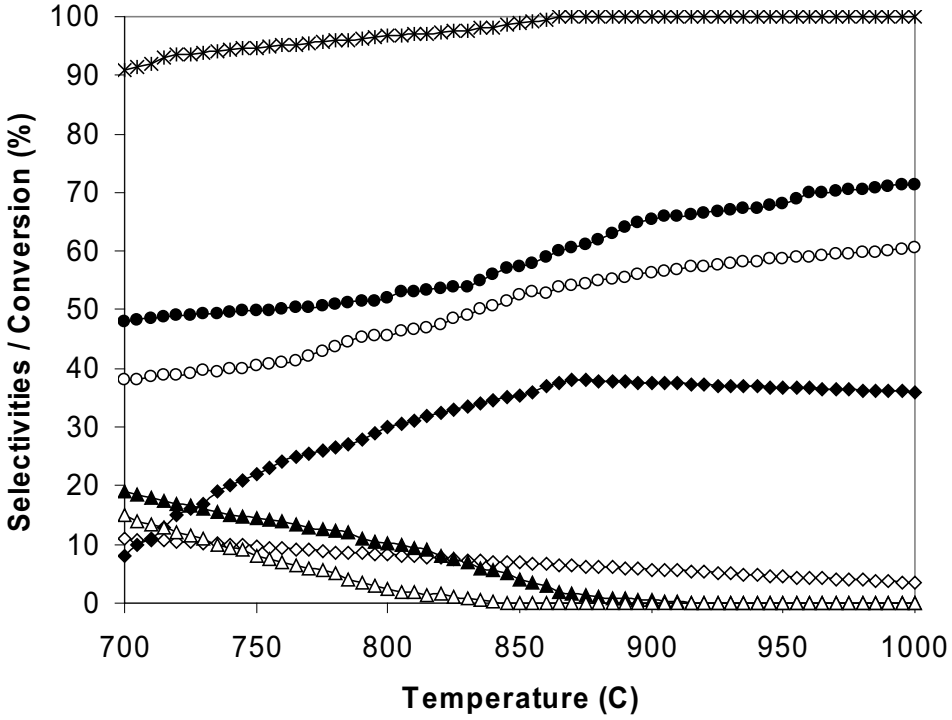

Fig. 10b

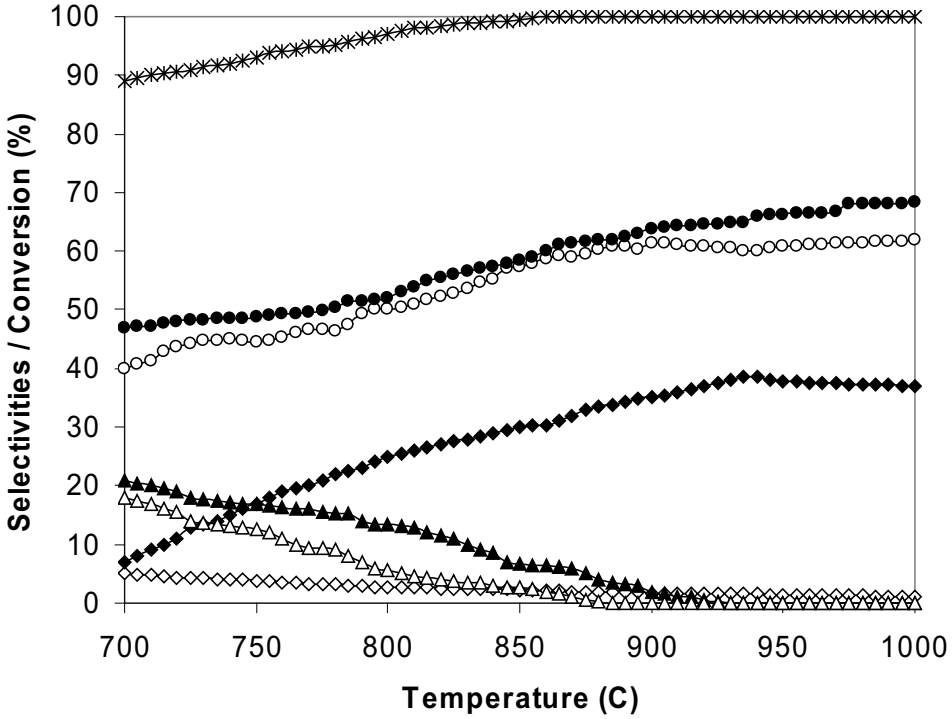

Fig. 10c

Fig. 10 Effect of temperature on the conversion and product selectivities (EtOH (×), H_2 (●), CO (○), CO_2 (◇), CH_4 (◆), C_2H_6 (△), and C_2H_4 (▲)) from ethanol steam reforming over CeO_2 (HSA) with H_2O/C_2H_5OH ratios of 3.0 (Fig. 10a), 1.0 (Fig. 10b), and 0.0 (Fig. 10c)

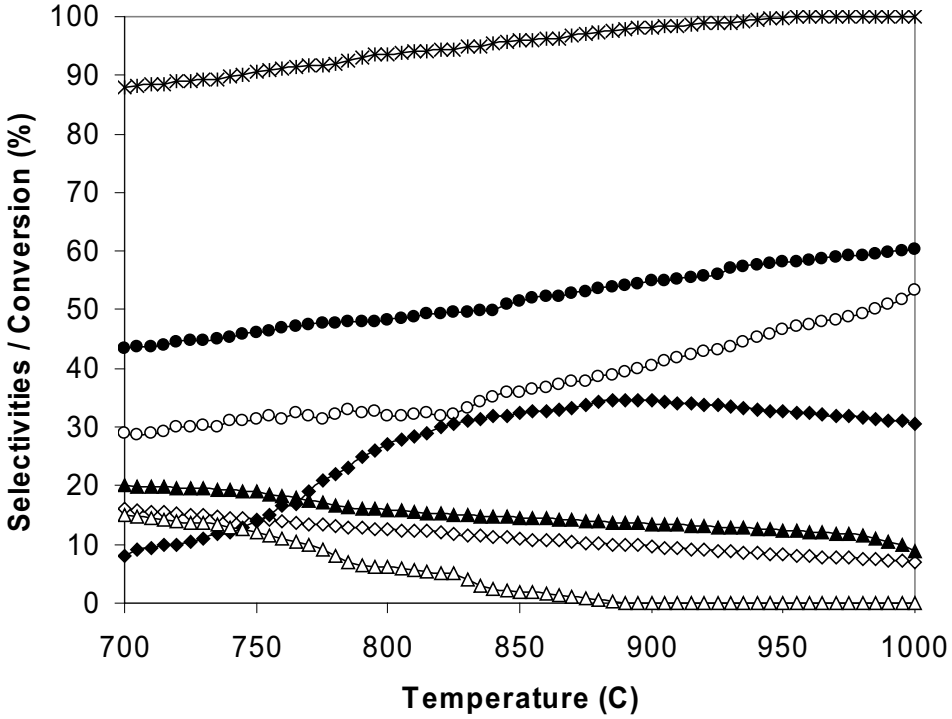

Fig. 11a

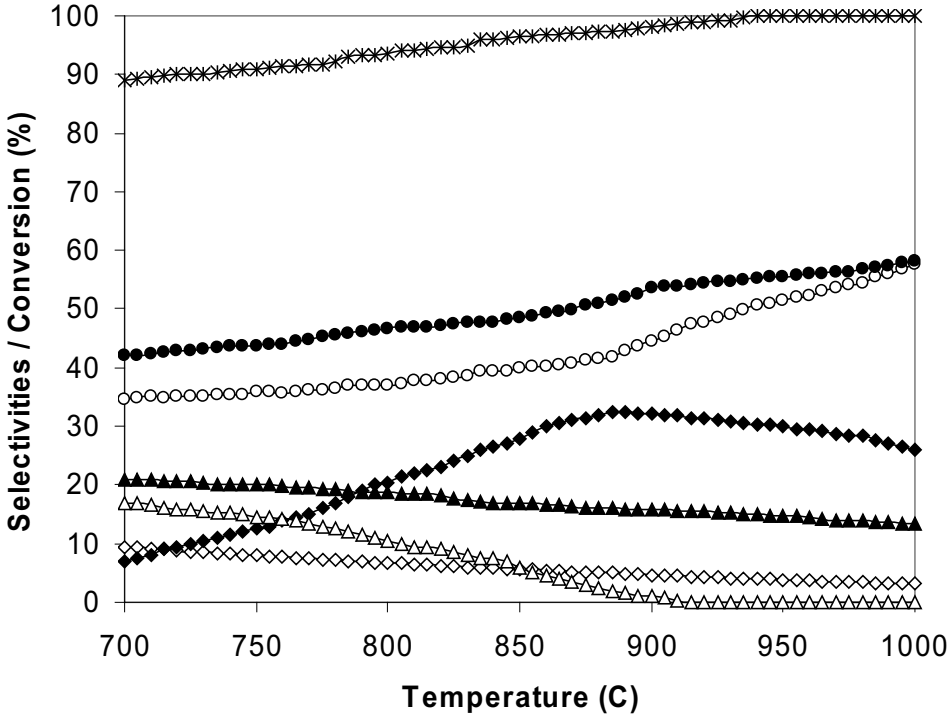

Fig. 11b

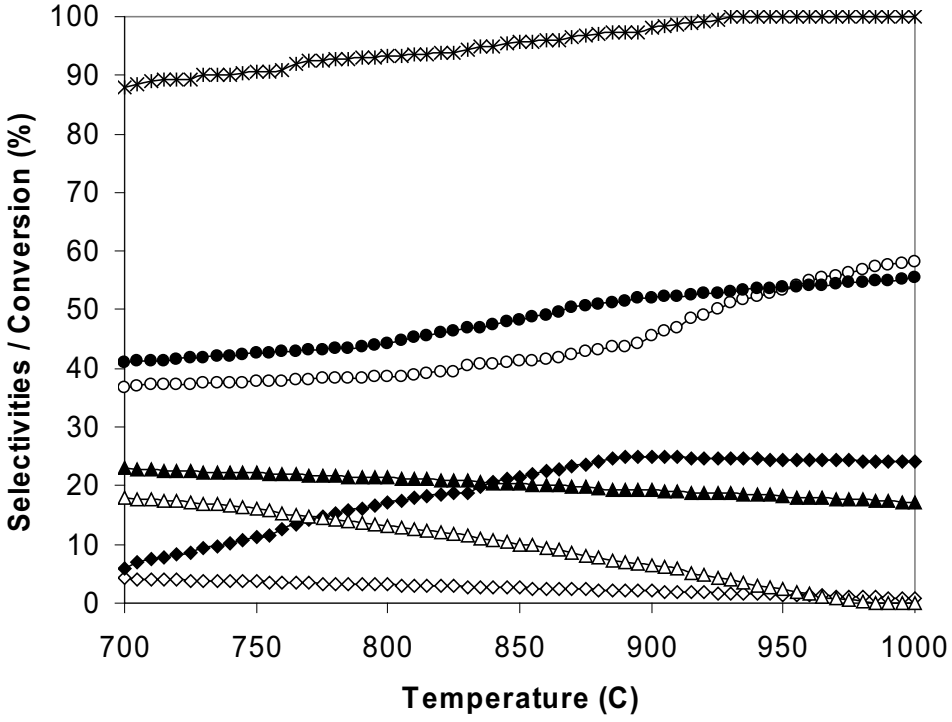

Fig. 11c

Fig. 11 Effect of temperature on the conversion and product selectivities (EtOH (×), H_2 (●), CO (○), CO_2 (◇), CH_4 (◆), C_2H_6 (△), and C_2H_4 (▲)) from ethanol steam reforming over CeO_2 (LSA) with H_2O/C_2H_5OH ratios of 3.0 (Fig. 11a), 1.0 (Fig. 11b), and 0.0 (Fig. 11c)

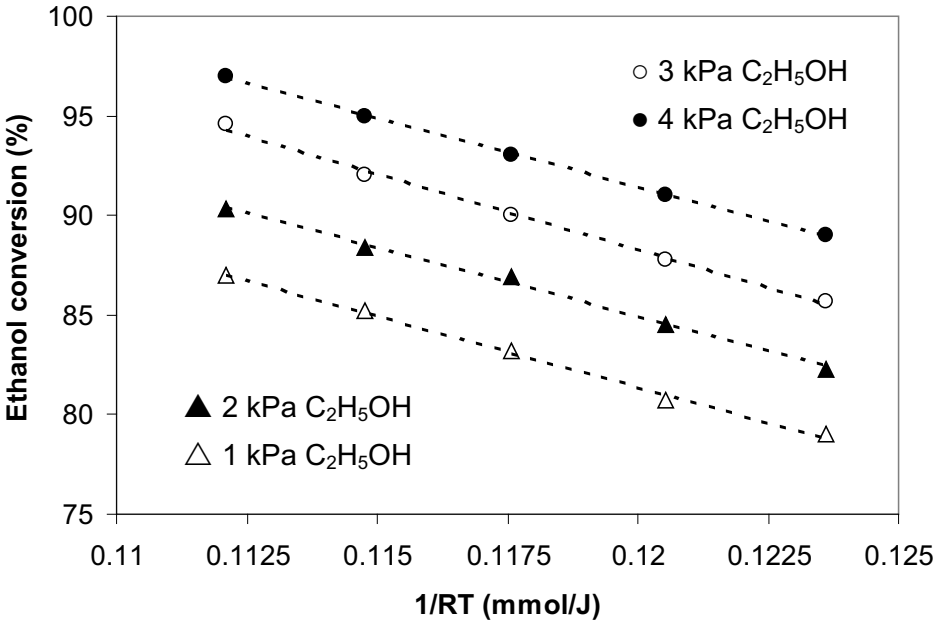

Fig. 12 Arrhenius plot of ethanol conversion from the decomposition of ethanol without steam over CeO_2 (HSA) with different inlet ethanol partial pressures (1-4 kPa) at 700-900 ºC

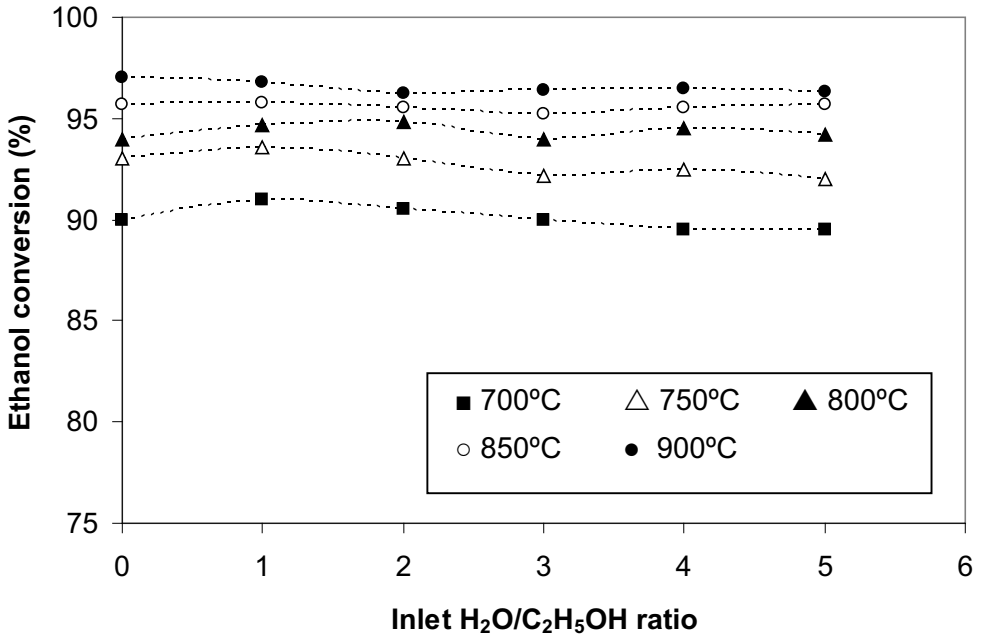

Fig. 13 Effect of steam partial pressure on the conversion of ethanol over CeO_2 (HSA) at different temperatures (4 kPa C_2H_5OH)

Table 1
Results of TPR(1), (2), and (3), and TPO(1) and (2) for CeO_2 (both HSA and LSA)

Catalyst	Total H_2 Uptake from TPR[a] ($\mu mol/g_{cat}$)			Total O_2 Uptake from TPO[b] ($\mu mol/g_{cat}$)	
	TPR(1)	TPR(2)[c]	TPR(3)	TPO(1)	TPO(2)
CeO_2 (HSA)	2159	2155	2158	1044	1047
CeO_2 (LSA)	830	828	830	401	403

[a] Temperature Programmed Reduction of the reduced catalysts (Relative Standard Deviation = ± 3%)
[b] Temperature Programmed Oxidation after TPR (1) (Relative Standard Deviation = ± 1%)
[c] Re-Temperature Programmed Reduction after TPO (Relative Standard Deviation = ± 2%)

Table 2
Physicochemical properties of the catalysts after exposure in ethanol decomposition with and without steam at 900ºC for 10 h

Catalyst	C_2H_5OH/H_2O ratio	Yield of H_2 (%) at steady state	Deactivation (%)	BET surface ($m^2\ g^{-1}$)	C formation (monolayers)
CeO_2 (HSA)	1.0/0.0	63.9	6.0	22.6	~0[a] (~0)[b]
	1.0/1.0	65.5	6.4	22.5	0 (0)
	1.0/3.0	67.9	6.1	22.5	0 (0)
CeO_2 (LSA)	1.0/0.0	52.0	18.1	7.2	0.81 (0.80)
	1.0/1.0	53.9	17.6	7.4	0.74 (0.74)
	1.0/3.0	54.5	17.4	7.4	0.67 (0.69)
Ni/Al_2O_3	1.0/0.0	51.8	40.4	39.0	4.64 (4.66)
	1.0/1.0	52.0	40.2	~ 40.0	4.59 (4.58)
	1.0/3.0	53.2	39.5	~ 40.0	4.52 (4.54)

[a] Measured from X-ray fluorescence analysis
[b] Nickel reducibility (measured from temperature-programmed reduction (TPR) with 5%hydrogen)
[c] Nickel dispersion (measured from temperature-programmed desorption (TPD) after TPR)

Table 3
Ethanol conversion and the product selectivities from ethanol steam reforming over CeO_2 (HSA) and CeO_2 (LSA) (with the inlet H_2O/C_2H_5OH of 3.0) at 900ºC compared to those from the homogeneous reaction and the equilibrium level at the same conditions

Catalyst	Conversion and Product selectivities						
	C_2H_5OH	C_2H_6	C_2H_4	CH_4	H_2	CO	CO_2
CeO_2 (HSA)	100	0	0	37.9	67.9	50.5	11.6
CeO_2 (LSA)	98.1	0	13.5	34.6	54.5	40.3	9.65
Homogeneous	87.6	20.1	21.9	5.9	49.0	30.1	9.6
Equilibrium	100	0	0	0	~100	76.9	23.1

Table 4
The conversion and the product selectivities from the steam reforming of ethane over CeO_2 (HSA) (with the inlet H_2O/C_2H_6 of 1.0) at different temperatures

Temperature (^oC)	Conversion and Product selectivities					
	C_2H_6	C_2H_4	H_2	CO	CO_2	CH_4
800	95.3	14.0	68.1	57.1	3.76	20.4
825	96.2	9.2	69.2	58.4	3.69	24.9
850	97.5	6.1	71.4	60.5	3.48	27.4
875	98.7	3.5	71.5	63.0	3.44	30.0
900	~100	0.2	72.5	64.7	3.39	31.7
925	~100	0	73.7	65.4	3.24	31.3
950	~100	0	74.5	66.9	2.95	30.1
975	~100	0	75.5	67.5	2.83	29.6
1000	~100	0	76.5	68.3	2.78	28.9

Table 5
The conversion and the product selectivities from the steam reforming of ethylene over CeO_2 (HSA) (with the inlet H_2O/C_2H_4 of 1.0) at different temperatures

Temperature (^oC)	Conversion and Product selectivities				
	C_2H_4	H_2	CO	CO_2	CH_4
800	91.0	54.5	52.9	2.61	35.4
825	93.2	56.2	56.4	2.45	34.5
850	94.5	58.0	60.1	2.4	32.0
875	95.7	59.5	63.7	2.25	29.7
900	99.1	60.8	68.8	2.19	28.1
925	99.8	61.4	71.7	2.03	25.9
950	~100	62.0	73.3	1.79	24.8
975	~100	64.2	74.6	1.58	23.8
1000	~100	65.5	75.6	1.49	22.9

Table 6
The conversion and the product selectivities from the steam reforming of methane over CeO_2 (HSA) (with the inlet H_2O/CH_4 of 1.0) at different temperatures

Temperature (^oC)	Conversion and Product selectivities			
	CH_4	H_2	CO	CO_2
800	11.2	17.4	9.91	1.27
825	16.8	19.7	15.5	1.25
850	23.1	25.8	21.8	1.24
875	28.3	31.0	27.1	1.22
900	34.7	36.6	33.5	1.19
925	39.6	40.7	38.4	1.17
950	44.2	44.1	43.1	1.14
975	51.0	48.8	49.9	1.09
1000	58.4	54.3	57.3	1.02

Submitted to Applied Catalysis B: Environmental (Revised)
Type of Contribution: Research Paper

Catalytic steam reforming of ethanol over high surface area CeO_2: The role of CeO_2 as an internal pre-reforming catalyst

N. Laosiripojana[1,*] and S. Assabumrungrat[2]

[1] The Joint Graduate School of Energy and Environment,
King Mongkut's University of Technology Thonburi, Bangkok, 10140, Thailand
[2] Center of Excellence on Catalysis and Catalytic Reaction Engineering,
Department of Chemical Engineering, Faculty of Engineering, Chulalongkorn University, Bangkok, Thailand

[*] Corresponding author (navadol_l@jgsee.kmutt.ac.th)

Abstract

In the present work, it was found that high surface area ceria (CeO_2 (HSA)), synthesized by a surfactant-assisted approach, have useful ethanol steam reforming activity under Solid Oxide Fuel Cells (SOFCs) temperatures. The catalyst provides good reforming reactivity and high resistance toward carbon deposition compared to Ni/Al_2O_3 and conventional low surface area ceria (CeO_2 (LSA)). Although the hydrogen selectivity at steady state from the ethanol steam reforming over CeO_2 (HSA) was lower than Rh/Al_2O_3, the resistance toward carbon deposition of CeO_2 (HSA) was considerably higher. The good reactivity toward the steam reforming of ethanol for CeO_2 (HSA) is due to the high redox property of this material. During the reforming process, the gas-solid reactions between the gaseous hydrocarbon components and the lattice oxygen (O_O^x) on CeO_2 surface take place ($C_nH_m + O_O^x \rightarrow nCO + m/2(H_2) + V_O^{\bullet\bullet} + 2\ e'$) forming synthesis gas and also preventing the formation of carbon species from hydrocarbon decomposition reactions ($C_nH_m \rightarrow nC + m/2H_2$).

At the temperature of 900ºC, the main products from the steam reforming of ethanol over CeO_2 (HSA) (with inlet C_2H_5OH/H_2O molar ratio of 1.0/3.0) were 67.5% H_2, 37.9%CH_4, 50.5%CO, and 11.6%CO_2. In contrast, the formations of C_2H_4 (5.8-15.8%) and C_2H_6 (1.2-8.5%) were also observed from the steam reforming of ethanol

over Ni/Al_2O_3 and CeO_2 (LSA). The combination use of CeO_2 and Ni/Al_2O_3 was studied in an annular ceramic reactor by applying CeO_2 as an internal pre-reforming catalyst. The main purpose of CeO_2 is to convert all ethanol and other high hydrocarbon compounds (e.g. C_2H_4 and C_2H_6) forming CH_4, CO, CO_2, and H_2, while Ni/Al_2O_3 is applied to reform all CH_4 left from the pre-reforming section and maximize the yield of hydrogen production. After operated at 900ºC for 100 h, this combination pattern offers high hydrogen selectivity (87.0-91.4%) and good resistance toward carbon deposition. This successful development eliminates the requirement of expensive noble metal catalysts or the installation of an external pre-reformer in order to reform ethanol internally (IIR-SOFC).

Keywords: Ethanol**,** internal reforming, ceria, redox, solid oxide fuel cell

1. Introduction

Solid Oxide Fuel Cell (SOFC) with an indirect internal reforming operation (IIR), called IIR-SOFC, is expected to be an important technology for energy generation in the near future due to the high efficiency and its lower pollutant emission. Regarding this operation, the endothermic reforming reaction takes place at the reformer, which is in close thermal contact with the anode side of fuel cell where the exothermic electrochemical reaction occurs, Fig. 1 [1]. The aim of the reformer unit is to reform and maximize the yield of hydrogen production, which can be generated from several sources such as natural gas, bio-ethanol, coal, biomass, and biogas, and supply this component to the anode side of SOFC. IIR-SOFC gives the advantage on eliminating the requirement for a separate fuel reformer and providing good heat transfer between the reformer and the fuel cell. In addition, the reformer part and the anode side for IIR operation can be operated separately. Therefore, the catalyst for reforming reaction at the reformer part and the material for electrochemical reactions at the anode side of fuel cell can be different and optimized individually. This operation is expected to simplify the overall SOFC system design, making SOFC more attractive and efficient for producing electrical power [1].

Regarding the current oil crisis and the shortage of fossil fuels, the development of the biomass-based fuels therefore attracts much attention. Among various resources, bio-ethanol is a promising candidate for hydrogen for SOFC, since it is readily produced by renewable resources (e.g., fermentation of biomasses) and has reasonably high

hydrogen content [2,3]. The major difficulty to reform ethanol is the deactivation of the reforming catalyst due to the possible carbon deposition from the ethanol decomposition. It has widely been reported that ethanol can homogenously decompose to several hydrocarbon elements (e.g. acetaldehyde, methane, carbon monoxide, carbon dioxide, ethylene, and ethane) without the requirement of catalyst [4]. The formations of ethylene and ethane are the major problem, as these components act as very strong promoters for carbon formation. When ethanol is reformed internally (IIR-SOFC) without any pre-treatments, the carbon formation can be easily formed on the catalyst surface.

SOFC fueled by high organic compounds (e.g. natural gas, DME, LPG, and bio-ethanol) normally requires a small external preliminary reforming unit (pre-reformer), where these high hydrocarbons are reformed readily forming low hydrocarbon compounds (e.g. methane) before introducing to the main part of the SOFC system [5]. The pre-reforming unit is normally operated at relatively lower temperatures, 300-500ºC, in which the carbon formation problem is less severe, but the disadvantage of this installation is the extra-requirement of the heat supplied into this unit, which can reduce the fuel cell efficiency.

The approach in this work is developing of an alternative catalytic reforming operation that is enabling to reform ethanol with low degree of carbon deposition at SOFC temperatures, 800-1000ºC. The successful development of this operation would help eliminate the requirement of the external pre-reformer. Previously, hydrogen production from the reforming of ethanol has been studied by several researchers [6-27], most of them have investigated the reforming of ethanol over noble metal catalysts (e.g. Rh, Ru, Pt, Pd) on several oxide supports (e.g. Al_2O_3, MgO, SiO_2, TiO_2) [11,13,14,17,24,25,26]. Freni et al. [11, 14, 16, 25] presented that Rh/Al_2O_3 provides the highest reforming reactivity among these noble metal catalysts. Burch and coworkers [19] found that the order of the ethanol steam reforming reactivity of the metals is Rh > Pd > Ni = Pt. In the present work, Ni/Al_2O_3 was selected as a based catalyst rather than these precious metals. Although the precious metals have been reported to be active for the ethanol steam reforming and provide high resistance to the carbon formation than Ni based catalysts [28, 29], the current prices of these metals are very high for commercial uses, and the availability of some precious metals such as ruthenium was too low to have a major impact on the total reforming catalyst market [30]. The main procedure to improve the ethanol steam reforming reactivity in this work is to investigate the use of

cerium oxide (CeO_2), as the reforming catalyst, together with the conventional Ni/Al_2O_3 in a single unit.

Cerium oxide (CeO_2) has been commonly reported to apply as catalysts in a wide variety of reactions involving oxidation or partial oxidation of hydrocarbons (e.g. automotive catalysis). A high oxygen mobility (redox property) [31], high oxygen storage capacity [32-37], strong interaction with the supported metal (strong metal–support interaction) [38] and the modifiable ability [39] render this material very interesting for catalysis. Recently, the high resistance toward carbon deposition over ceria has been widely observed [40-43]. Importantly, CeO_2 has been reported to have the reactivity toward the methane steam reforming reaction at such a high temperature (800-1000ºC) [40]. It was demonstrated that the gas–solid reaction between CeO_2 and CH_4 produces H_2 and CO, according to reaction (1). In addition, the reaction of the reduced ceria with H_2O and CO_2 produces more H_2 and CO, respectively, and regenerates a lattice oxygen in CeO_2 [44-45]:

$$CH_4 + O_O^x = 2\,H_2 + CO + V_O^{\bullet\bullet} + 2\,e' \quad (1)$$

$$V_O^{\bullet\bullet} + 2\,e' + H_2O = O_O^x + H_2 \quad (2)$$

$$V_O^{\bullet\bullet} + 2\,e' + CO_2 = O_O^x + CO \quad (3)$$

O_O^x denotes a lattice oxygen in CeO_2, $V_O^{\bullet\bullet}$ is an oxygen vacancy with an effective charge 2^+, e' is an electron which can either be more or less localized on a cerium ion or delocalized in a conduction band [46].

Unfortunately, the steam reforming reactivity over CeO_2 was too low compared to the conventional metallic catalysts [40]. This is mainly due to its low specific surface area, and its high sintering rate at high temperature [40, 43]. It was reported that the methane conversion of the methane steam reforming over CeO_2 was less than 10% [40]. In the present work, we therefore investigated the use of cerium oxide as either a preliminary reforming (pre-reforming) or a combined reforming (co-reforming) element instead.

It should be noted that, in order to minimise the weakness of CeO_2 in term of its low specific surface area, CeO_2 applied in this work was the high surface area CeO_2 (CeO_2 (HSA)). Several methods have recently been described for the preparation of CeO_2 (HSA) solid solution. Among these methods, the surfactant-assisted approach was employed to prepare high surface area CeO_2 with improved textural, structural, and

chemical properties [47-53]. Our previous publication [40] also presented the achievement of CeO_2 with high surface area and good stability after thermal treatment by this preparation method. Regarding the surfactant-assisted method, CeO_2 (HSA) is prepared by reacting a cationic surfactant with a hydrous oxide produced by co-precipitation under basic conditions. At high pH value, conducting the precipitation of hydrous oxide in the presence of cationic surfactant allows the cation exchange process between H^+ and the surfactant to take place, resulting in a developed pore structure with an increase in surface area [53]. The achievement of high thermal stability for CeO_2 (HSA) is due to the incorporation of surfactants during preparation, which can reduce the interfacial energy and eventually decrease the surface tension of water contained in the pores. This could reduce the shrinkage and collapse of the catalyst during heating up, which consequently help the catalyst maintaining high surface area after calcination [53].

In the present work, the first approach was to study the reactivity of CeO_2, especially the high surface area one, toward the steam reforming of ethanol. The effects of temperature, inlet C_2H_5OH/H_2O molar ratio, and C_2H_5OH concentration on the reforming rate and product selectivities were also determined. The benefit of applying CeO_2 together with conventional Ni/Al_2O_3 was then presented. It should be noted that the ethanol steam reforming over Rh/Al_2O_3 was also investigated in the present work for the comparison purpose. All experiments described above were carried out at the SOFC temperature range (800-1000ºC) for later application in IIR-SOFC system.

2. Experimental

2.1. Catalyst preparation and characterization

The conventional low surface area CeO_2 (CeO_2 (LSA)) was prepared by the precipitation method. The starting solution was prepared by mixing 0.1 M of cerium chloride ($CeCl_3 \cdot 7H_2O$) salt solution with 0.4 M of ammonia at a 2:1 volumetric ratio. This solution was stirred by magnetic stirring (100 rpm) for 3 h, then sealed and placed in a thermostatic bath maintained at 90°C for 3 days. The precipitate was filtered and washed with deionised water and acetone. It was dried overnight in an oven at 110°C, and then calcined in air at 1000°C for 6 h.

High surface area CeO_2 support (CeO_2 (HSA)) was prepared by adding an aqueous solution of the appropriate cationic surfactant, 0.1 M cetyltrimethylammonium

bromide solution from Aldrich, to a 0.1 M cerium chloride. The molar ratio of ([Ce])/[cetyltrimethylammonium bromide] was kept constant at 0.8. The mixture was stirred and then aqueous ammonia was slowly added with the constant rate of 0.165 cm^3 min^{-1} until the pH was 11.5. We found that the rate of ammonia doping have a significant impact on the specific surface area of synthesis CeO_2, Table 1. According to our experiments, this flow rate of ammonia can provide solid CeO_2 with the highest specific surface area. The mixture was continually stirred for 3 h, then sealed and placed in the thermostatic bath maintained at 90°C for 3 days. After that, the mixture was cooled and the resulting precipitate was filtered and washed repeatedly with water and acetone. The filtered powder was then treated under the same procedures as CeO_2 (LSA). BET measurements of CeO_2 (both LSA and HSA) were carried out at different calcination temperatures in order to determine the decrease of specific surface area due to the thermal sintering. As presented in Table 1, after drying, surface areas of 308 and 55 m^2 g^{-1} were observed for CeO_2 (HSA) and conventional CeO_2, respectively and, as expected, the surface area dramatically decreased at high calcination temperatures. However, the value for CeO_2 (HSA) is still appreciable after calcination at 1000°C, Table 1. The homogeneity and morphology of CeO_2 (HSA) was also investigated. All samples have a similar morphology and exhibit a very narrow particle-size histogram. As expected, samples treated at 1000°C showed a larger particle size than those treated at lower temperatures. The redox properties and redox reversibilities of these synthesized CeO_2 (both LSA and HSA) were compared by the temperature programmed reduction (TPR) and the temperature programmed oxidation (TPO). In these experiments, 5% H_2/helium and 5% O_2/helium were used for the TPR and TPO respectively, while the temperature of the system increased from 100ºC to 900ºC with the rate of 12ºC/min for both experiments.

For comparison, Ni/Al_2O_3 and Rh/Al_2O_3 (5wt% Ni and Rh) were prepared by impregnating α-Al_2O_3 (from Aldrich) with $NiCl_3$ and $RhCl_3$ solutions, respectively. After stirring, the solution was dried and calcined at 1000°C for 6 h. Ni/Al_2O_3 was reduced with 10% hydrogen in helium at 700ºC for 6 h before use, while Rh/Al_2O_3 was reduced with 10% hydrogen + 5% steam in helium at 700ºC for 6 h. It should be noted that the adding of steam during the reduction of Rh/Al_2O_3 is to prevent the phenomenon of Strong Metal-Support Interaction (SMSI), which has been widely reported by several researchers [54-57]. After reduction, the catalysts were characterized by several physicochemical methods. The weight contents of Ni and Rh in Ni/Al_2O_3 and Rh/Al_2O_3 were determined

by X-ray fluorescence (XRF) analysis. The reducibility and dispersion percentages of nickel and rhodium were measured from temperature-programmed reduction (TPR) with 5% H_2 in Ar and temperature-programmed desorption (TPD) respectively. The catalyst specific surface areas were obtained from BET measurements. All physicochemical properties of the synthesized catalysts are presented in Table 2.

2.2. Apparatus and Procedures

An experimental reactor system was constructed as shown in Fig. 2. The feed gases including the components of interest (ethanol and steam from the evaporator) and the carrier gas (helium) were introduced to the reaction section, in which a 10-mm diameter quartz reactor was mounted vertically inside a furnace. The reactivities of catalyst toward the ethanol steam reforming were determined by loading each selected catalyst (e.g., CeO_2, Ni/Al_2O_3, and Rh/Al_2O_3) in this quartz reactor, which was packed with a small amount of quartz wool to prevent the catalyst from moving. Regarding the results in our previous publications [40-42], to avoid any limitations by intraparticle diffusion, the total gas flow was 1000 cm^3 min^{-1} under a constant residence time of 5 x 10^{-4} g min cm^{-3} in all experiments. A Type-K thermocouple was placed into the annular space between the reactor and the furnace. This thermocouple was mounted on the tubular reactor in close contact with the catalyst bed to minimize the temperature difference between the catalyst bed and the thermocouple. Another Type-K thermocouple was inserted in the middle of the quartz tube in order to re-check the possible temperature gradient. The record showed that the maximum temperature fluctuation during the reaction was always ±0.75ºC or less from the temperature specified for the reaction.

After the reactions, the exit gas mixture was transferred via trace-heated lines to the analysis section, which consists of a Porapak Q column Shimadzu 14B gas chromatograph (GC) and a mass spectrometer (MS). The gas chromatography with TCD and FID detectors was applied in order to investigate the reforming reactivity, whereas the mass spectrometer in which the sampling of the exit gas was done by a quartz capillery and differential pumping was used for the transient carbon formation experiment. In order to study the formation of carbon species on catalyst surface, Temperature programmed Oxidation (TPO) was applied by introducing 10% oxygen in helium into the system, after purged the system with helium. The operating temperature increased from 100ºC to 1000ºC by the rate of 20ºC/min. The amount of carbon formations on the surface of catalysts were determined by measuring the CO and CO_2

yields from the TPO results (using Microcal Origin Software) assuming a value of 0.026 nm^2 for the area occupied by a carbon atom in a surface monolayer of the basal plane in graphite [58]. The calibrations of CO and CO_2 productions were performed by injecting a known amount of these calibration gases from a loop, in an injection valve in the bypass line. The response factors were obtained by dividing the number of moles for each component over the respective areas under peaks.

In addition to the TPO method, the amount of carbon deposition was confirmed by the calculation of carbon balance in the system. The amount of carbon deposited on the surface of catalyst would theoretically be equal to the difference between the inlet carbon containing components (C_2H_5OH) and the outlet carbon containing components (CO, CO_2, CH_4, C_2H_6, C_2H_4, and CH_3CHO). The amount of carbon deposited per gram of catalyst is given by the following equation:

$$C_{deposition} = \frac{mole_{carbon(in)} - mole_{carbon(out)}}{m_{catalyst}} \tag{4}$$

The rate of ethanol decomposition was defined in term of conversion denoted as X_{Ethanol}, whereas the product selectivities (hydrogen, carbon monoxide, carbon dioxide, methane, ethane, ethylene, and acetaldehyde), denoted as S_{product}, are calculated according to Eqs. (5) – (12):

$$X_{Ethanol} = \frac{100(\%Ethanol_{in} - \%Ethanol_{out})}{\%Ethanol_{in}} \tag{5}$$

$$S_{H_2} = \frac{100(\%H_2)}{3(\%Ethanol_{in} - \%Ethanol_{out})} \tag{6}$$

$$S_{CO} = \frac{100(\%CO)}{2(\%Ethanol_{in} - \%Ethanol_{out})} \tag{7}$$

$$S_{CO_2} = \frac{100(\%CO_2)}{2(\%Ethanol_{in} - \%Ethanol_{out})} \tag{8}$$

$$S_{CH_4} = \frac{100(\%CH_4)}{2(\%Ethanol_{in} - \%Ethanol_{out})} \tag{9}$$

$$S_{C_2H_6} = \frac{100(\%C_2H_6)}{(\%Ethanol_{in} - \%Ethanol_{out})} \tag{10}$$

$$S_{C_2H_4} = \frac{100(\%C_2H_4)}{(\%Ethanol_{in} - \%Ethanol_{out})} \quad (11)$$

$$S_{CH_3CHO} = \frac{100(\%CH_3CHO)}{(\%Ethanol_{in} - \%Ethanol_{out})} \quad (12)$$

It should be noted that, from Eq. 6, three H_2 molecules from ethanol represent 100% H_2 selectivity. However, from the steam reforming of ethanol, H_2 selectivity can exceed 100%. This is possible because water is consumed as well as ethanol in the process, therefore, H atoms from H_2O can also be converted into H_2.

2.3 Catalytic reactor configuration

After testing the catalyst reactivity in the packed bed reactor as described above, the annular ceramic reactor was constructed in order to study the combination of CeO_2 (both LSA and HSA) with Ni/Al_2O_3 as a single reforming unit, Fig. 3. By this configuration, 200 mg of CeO_2 (with SiC), as an internal pre-reforming catalyst, was packed at the inner side of the annular reactor, where the inlet gas was firstly introduced. At the end of the inner tube, all gas components flowed backward through the outer side of this annular reactor, where 300 mg of Ni/Al_2O_3 (with SiC) was packed. The main purpose of Ni/Al_2O_3 is to convert all hydrocarbons left from the pre-reforming section and maximize the yield of hydrogen production.

For comparison of the combination method, CeO_2 was mixed together with Ni/Al_2O_3 and acted as the co-reforming catalyst. The ethanol steam reforming reactivities for these two methods were determined and compared to the use of single catalysts (e.g. Ni/Al_2O_3, and Rh/Al_2O_3). The effects of temperature, inlet C_2H_5OH/H_2O molar ratios, and inlet C_2H_5OH concentration on the product selectivity and amount of carbon deposition for each operation were also studied.

3. Results

3.1 Redox properties and redox reversibility of the synthesized CeO_2

The oxygen storage capacities (OSC) and the degree of redox properties for CeO_2 (both LSA and HSA) were investigated using temperature programmed reduction (TPR-1), which was performed by heating the reduced catalysts up to 900°C in 5%H_2 in

helium. The tests over Ni/Al_2O_3 and Rh/Al_2O_3 were also performed for comparison. As shown in Fig. 4, hydrogen uptakes are detected from both CeO_2 at the temperature above 750°C. The amount of hydrogen uptake over CeO_2 (HSA) is about 2.6 times higher than that over CeO_2 (LSA), suggesting the OSC and the redox properties strongly depend on the specific surface area of CeO_2. In contrast, no hydrogen consumption was observed from the TPR over Ni/Al_2O_3 and Rh/Al_2O_3, indicating that no occurrence of redox properties for these catalysts. The benefit of redox property on the reforming of ethanol will be presented later in the discussion section. After purged with helium, the redox reversibility for each CeO_2 was then determined by performing temperature programmed oxidation (TPO) followed by the second temperature programmed reduction (TPR-2). The TPO was carried out by heating the catalyst up to 900°C in $10\%O_2$ in helium; the amounts of oxygen chemisorbed were then measured, Fig. 5 and Table 3. Regarding the TPR-2 results as shown in Fig. 6 and Table 3, the amount of hydrogen uptakes for CeO_2 (both LSA and HSA) were approximately similar to those from TPR-1, indicating the redox reversibility for these synthesis CeO_2.

3.2 Homogenous (non catalytic) reaction

Before studying the catalyst performance, the homogeneous (non-catalytic) steam reforming of ethanol was primarily investigated. The inlet C_2H_5OH/H_2O in helium with the molar ratio of 1.0/3.0 was introduced to the system, while the temperature increased from 100ºC to 1000ºC. As shown in Fig. 7, it was observed that ethanol converted to acetaldehyde, and hydrogen at the temperature above 200°C. Methane and carbon monoxide productions were initially observed at the temperature of 250-300°C. When the temperature increased up to 550°C, the selectivity of acetaldehyde significantly decreased, while the hydrogen, carbon monoxide, and carbon dioxide selectivities remained increasing. In this range of temperature, the formations of ethane and ethylene were also observed.

3.3 Stability and activity toward the ethanol steam reforming

The synthesized CeO_2 (HSA), CeO_2 (LSA), Ni/Al_2O_3, and Rh/Al_2O_3 were tested for the ethanol steam reforming at 900°C with the inlet C_2H_5OH/H_2O molar ratio of 1.0/3.0 (inlet C_2H_5OH of 3.0 kPa). The reforming rate was measured as a function of time in order to indicate the stability and the deactivation rate. The variations in the hydrogen

selectivity with time at 900°C are shown in Fig. 8. Significant deactivations were detected for Ni/Al_2O_3 catalyst, whereas much lower deactivations were observed over CeO_2 (HSA), CeO_2 (LSA), and Rh/Al_2O_3. At steady state, the ethanol steam reforming over CeO_2 (HSA) showed the best performance in terms of stability, while Rh/Al_2O_3 presented the best activity at steady state. Catalyst stabilities expressed as deactivation percentages are given in Table 4. It should be noted that, in order to determine whether the observed deactivation is due to the carbon formation, the post-reaction temperature-programmed oxidation (TPO) experiments were carried out.

From the TPO results shown in Fig. 9, the huge amounts of carbon deposition were observed for Ni/Al_2O_3, whereas significant lower carbon formations were detected for CeO_2 (LSA) and Rh/Al_2O_3. No formation of carbon species was detected for CeO_2 (HSA) in all conditions. The values of carbon formations (monolayer) on the surface of catalysts were determined by measuring these CO and CO_2 yields (using Microcal Origin Software). Using a value of 0.026 nm^2 for the area occupied by a carbon atom in a surface monolayer of the basal plane in graphite [58], the quantities of carbon deposited for each catalyst were observed as also presented in Table 4. The total amounts of carbon deposited were also ensured by calculating the carbon balance of the system. Regarding the calculations, the moles of carbon deposited per gram of Ni/Al_2O_3, CeO_2 (LSA), and Rh/Al_2O_3 were 4.55, 0.70, and 1.46 mmol g^{-1}. By the same assumption for the area occupied by a carbon atom [58], these values are equal to 4.54, 0.69, and 1.44 monolayers respectively, which are in good agreement with the values observed from the TPO method described above. The results clearly indicated that the deactivations observed for Ni/Al_2O_3 were mainly due to the carbon deposition on the surface of catalyst. In addition, CeO_2 especially the high surface area one presented significantly stronger resistance toward carbon formation compared to Ni/Al_2O_3. The BET measurements were carried out to observe the surface area reduction percentages of all catalysts. As shown in Table 4, it was suggested that the deactivations of ceria are mainly due to the thermal sintering. However, the surface area reduction percentage of CeO_2 (HSA) is much lower than CeO_2 (LSA), indicating its better stability toward the thermal sintering.

3.4 Effects of temperature and inlet compositions

The influences of operating temperature and the inlet steam content on the ethanol conversion and product selectivities from the ethanol steam reforming over CeO_2 (HSA), CeO_2 (LSA), Ni/Al_2O_3, and Rh/Al_2O_3 were studied by varying temperature from 700°C to 1000°C for three different inlet C_2H_5OH/H_2O molar ratios (1.0/3.0, 1.0/4.0, and 1.0/5.0).

Fig. 10 (a, b, and c) presents the influences of temperature and the inlet C_2H_5OH/H_2O molar ratio on the ethanol conversion and product selectivities from the ethanol steam reforming over CeO_2 (HSA). At the temperature above 900°C, the products from this reaction over CeO_2 (HSA) were CH_4, H_2 and CO with some CO_2. The formations of ethylene and ethane were slightly observed at the lower temperatures. These formations decreased with increasing temperature and inlet steam concentration. Hydrogen and carbon monoxide selectivities increased with increasing temperature, whereas carbon dioxide and methane production selectivities decreased. Regarding the effect of steam, the conversion of ethanol and the methane selectivity seem to be independent of the inlet steam content. However, hydrogen and carbon dioxide selectivities increased with increasing inlet steam concentration, whereas carbon monoxide selectivity decreased. The yield of methane production was non-monotonic. It increased with increasing temperature until ~850°C, oppositely, the yield of methane production reduced at higher temperature.

The changes of hydrogen, carbon monoxide, and carbon dioxide selectivities are mainly due to the influence of mildly exothermic water-gas shift reaction ($CO + H_2O \rightarrow CO_2 + H_2$). The increase of methane production at low temperature (700-850°C) comes from the decomposition of ethanol, whereas the decrease at high temperature (>850°C) could be due to the further reforming to carbon monoxide and hydrogen. Table 5 summarizes the influence of the inlet steam content on the product selectivities at 900°C for all catalysts with the additional information regarding the characterization (e.g. TPO) over these spent catalysts.

According to the good performance of CeO_2 (HSA) in terms of product selectivities and resistance toward carbon formation, the effect of inlet ethanol concentration on the degree of carbon deposition over this catalyst was further studied by increase the inlet ethanol partial pressure from 3.0 to 15.0 kPa while keep the inlet C_2H_5OH/H_2O ratio constant at 1.0/3.0. At 900°C, no carbon formation was detected

when the inlet ethanol partial pressure was lower than 12 kPa. Small amounts of ethylene and ethane were observed when the inlet ethanol partial pressures were 12 and 15 kPa, Table 6.

3.5 The combination of CeO_2 and Ni/Al_2O_3 in the single unit

As the main approach of this work, CeO_2 (both LSA and HSA) were applied as the internal pre-reforming catalysts together with the conventional Ni/Al_2O_3 in the single unit (CeO_2(HSA)-Ni/Al_2O_3 and CeO_2(LSA)-Ni/Al_2O_3). Fig. 11 shows the variations in the hydrogen selectivity with time at 900°C over this configuration compared to the use of CeO_2 as the co-reforming catalyst (mixture of CeO_2 and Ni/Al_2O_3, CeO_2(HSA)+Ni/Al_2O_3 and CeO_2(LSA)+Ni/Al_2O_3), and the use of single Ni/Al_2O_3 or Rh/Al_2O_3 in the system. The feed was C_2H_5OH/H_2O in helium with the inlet C_2H_5OH/H_2O molar ratio of 1.0/3.0 (with the inlet C_2H_5OH of 3 kPa). The initial yield of hydrogen production over CeO_2(HSA)-Ni/Al_2O_3 was significantly higher than that over CeO_2(LSA)-Ni/Al_2O_3, CeO_2(HSA)+Ni/Al_2O_3, CeO_2(LSA)+Ni/Al_2O_3, and Ni/Al_2O_3. In addition, after exposure in this condition for 100 h, it was observed that the stability over CeO_2(HSA)-Ni/Al_2O_3 was higher than that over Rh/Al_2O_3, consequently, the long term hydrogen yield over CeO_2(HSA)-Ni/Al_2O_3 was the highest among these catalyst systems. The stabilities expressed as deactivation percentages and steady state activities over each operation are given in Table 7. Similarly, in order to determine the degree of carbon formation, the post-reaction temperature-programmed oxidation (TPO) experiments were carried out. Fig. 12 presents the quantities of carbon deposited observed from each operation. Significant amounts of carbon deposition were observed for CeO_2(LSA)-Ni/Al_2O_3, CeO_2(HSA)+Ni/Al_2O_3, CeO_2(LSA)+Ni/Al_2O_3, and Ni/Al_2O_3 (Fig. 9), whereas lower carbon formations were detected for CeO_2(HSA)-Ni/Al_2O_3 and Rh/Al_2O_3. Clearly, the deposition of carbon species over CeO_2(HSA)-Ni/Al_2O_3 was the lowest for all conditions.

The influences of operating temperature and the inlet C_2H_5OH/H_2O molar ratio on the ethanol conversion and product selectivities from the ethanol steam reforming over CeO_2(HSA)-Ni/Al_2O_3 and CeO_2(LSA)-Ni/Al_2O_3 were then studied. As shown in Fig. 13, the products from this reaction over CeO_2(HSA)-Ni/Al_2O_3 above 900°C were mainly H_2 and CO with some CO_2. Small amount of methane was detected at the temperature less than 900°C, whereas no formation of either ethylene or ethane was observed from the

system in all conditions. In contrast, significant amounts of ethylene and ethane were observed from the ethanol steam reforming over CeO_2(LSA)-Ni/Al_2O_3 even at high temperature (1000°C) and high inlet steam content, Fig. 14.

The effect of inlet ethanol concentration on the degree of carbon deposition over CeO_2(HSA)-Ni/Al_2O_3 system was then studied by increase the inlet ethanol partial pressure from 3.0 to 15.0 kPa at 900°C. Significant amount of carbon formation was observed over Ni/Al_2O_3 when the inlet ethanol partial pressure was higher than 12 kPa, moreover, ethylene formation was also found, Table 8.

4. Discussion

According to the homogeneous (non-catalytic) ethanol steam reforming, the dehydrogenation of ethanol and simultaneous fast decomposition of acetaldehyde first occur at relative low temperature (Eqs. 13 and 14), while the methane steam reforming and water-gas shift reactions (Eqs. 15 and 16) take place at higher temperature. Also, ethylene and ethane are formed by the dehydration of ethanol (Eq. 17) following with the production of ethane by ethylene hydrogenation (Eq. 18).

$$C_2H_5OH \rightarrow C_2H_4O + H_2 \quad (13)$$

$$C_2H_4O \rightarrow CH_4 + CO \quad (14)$$

$$CH_4 + H_2O \rightarrow CO + 3H_2 \quad (15)$$

$$CO + H_2O \rightarrow CO_2 + H_2 \quad (16)$$

$$C_2H_5OH \rightarrow C_2H_4 + H_2O \quad (17)$$

$$C_2H_4 + H_2 \rightarrow C_2H_6 \quad (18)$$

The formations of ethylene and ethane are the major difficulties for the catalytic steam reforming of ethanol, as these components act as very strong promoters for carbon formation. Eqs. 19-24 below present the most probable reactions that could lead to carbon deposition from the system of the steam reforming of ethanol:

$$C_2H_6 \Leftrightarrow 3H_2 + 2C \quad (19)$$

$$C_2H_4 \Leftrightarrow 2H_2 + 2C \quad (20)$$

$$CH_4 \Leftrightarrow 2H_2 + C \quad (21)$$

$$2CO \Leftrightarrow CO_2 + C \quad (22)$$

$$CO + H_2 \Leftrightarrow H_2O + C \quad (23)$$

$$CO_2 + 2H_2 \Leftrightarrow 2H_2O + C \quad (24)$$

C is the carbonaceous deposits. At low temperature, Eqs. (23-24) are favorable, while Eqs. (19-22) are thermodynamically unflavored [59]. The Boudouard reaction (Eq. 22) and the decomposition of hydrocarbons (Eqs. 19-21) are the major pathways for carbon formation at such a high temperature as they show the largest change in Gibbs energy [60]. According to the range of temperature in this study, carbon formation would be formed via the decomposition of hydrocarbons and Boudouard reactions.

From the present work, high surface area ceria (CeO_2 (HSA)), synthesized by a surfactant-assisted approach, was found to have useful ethanol steam reforming activity producing H_2 and CO under Solid Oxide Fuel Cells (SOFCs) conditions. As described, it has been reported that the gas-solid reaction between CeO_2 and CH_4 can generate CO and H_2 at high temperature [44, 45]. In addition, the reduced state of CeO_2 can react with CO_2 to produce CO [46]. By applying CeO_2 as the ethanol steam reforming catalyst at high temperature (800-1000°C), the gas-solid reactions between the hydrocarbons produced from the homogenous ethanol steam reforming reaction (ethylene, ethane, and methane) and the lattice oxygen (O_O^x) at CeO_2 surface occurs forming hydrogen and carbon monoxide. The redox mechanism between ethanol, ethylene, ethane, and methane with the lattice oxygen (O_O^x) could be derived as illustrated below.

$$C_2H_5OH + 2S_{Ce} \Leftrightarrow 2(CH_2\text{-}S_{Ce}) + H_2O \quad (25)$$

$$C_2H_6 + 2S_{Ce} \Leftrightarrow 2(CH_3\text{-}S_{Ce}) \quad (26)$$

$$C_2H_4 + 2S_{Ce} \Leftrightarrow 2(CH_2\text{-}S_{Ce}) \quad (27)$$

$$CH_4 + 2S_{Ce} \Leftrightarrow CH_3\text{-}S_{Ce} + H\text{-}S_{Ce} \quad (28)$$

$$CH_3\text{-}S_{Ce} + S_{Ce} \Leftrightarrow CH_2\text{-}S_{Ce} + H\text{-}S_{Ce} \quad (29)$$

$$CH_2\text{-}S_{Ce} + S_{Ce} \Leftrightarrow CH\text{-}S_{Ce} + H\text{-}S_{Ce} \quad (30)$$

$$CH\text{-}S_{Ce} + S_{Ce} \Leftrightarrow C\text{-}S_{Ce} + H\text{-}S_{Ce} \quad (31)$$

$$C\text{-}S_{Ce} + O_O^x \Leftrightarrow CO + V_O^{\bullet\bullet} + 2\,e' + S_{Ce} \quad (32)$$

$$2H\text{-}S_{Ce} \Leftrightarrow H_2 + 2S_{Ce} \quad (33)$$

S_{Ce} is the CeO_2 surface site and CH_x-S_{Ce} is an intermediate surface hydrocarbon species. S_{Ce} can be considered to be a unique site, or the same site as the lattice oxygen

(O_O^x). During the reaction, hydrocarbons are adsorbed on either a unique site (S_{Ce}) or the lattice oxygen (O_O^x). The lattice oxygen is then regenerated by reaction with oxygen containing compounds (i.e. steam) present in the system, Eq. 34.

$$H_2O + + V_O^{\bullet\bullet} + 2\,e' \Leftrightarrow H_2 + O_O^x \quad (34)$$

It should be noted that the measured value of the oxygen diffusion coefficient for ceria is high and the reaction rate is controlled by a surface reaction, not by diffusion of oxygen from the bulk of the solid particles to ceria surfaces [61]. Regarding the above redox mechanism, the carbon formation from Eqs. 19-22 could be inhibited by the gas-solid reactions between gaseous components (ethylene, ethane, and methane produced from the decomposition of ethanol) with the lattice oxygen on CeO_2 surface, Eqs. 35 and 36.

$$C_nH_m + O_O^x = nCO + m/2\,H_2 + V_O^{\bullet\bullet} + 2\,e' \quad (35)$$

$$CO + O_O^x = 2CO_2 + V_O^{\bullet\bullet} + 2\,e' \quad (36)$$

Although conventional CeO_2 (LSA) also provides high resistance toward carbon formation, the major weaknesses of CeO_2 (LSA) are its nature low specific surface area and also high size reduction due to the thermal sintering impact, resulting in its low redox properties as presented in section 3.1. Consequently, the low ethanol steam reforming reactivity was observed over this catalyst. The comparative reforming reactivities between CeO_2 (HSA) and CeO_2 (LSA) are in good agreement with the results from characterizations (i.e. BET and TPR); the specific surface area of CeO_2 (HSA) and the amounts of hydrogen and oxygen uptakes from the temperature programmed reduction (TPR-1 and TPR-2) and the temperature programmed oxidation (TPO) were significantly higher than those observed over the conventional one.

In order to prove the above redox mechanism (Eqs. 25-34), the reactivities of CeO_2 (HSA) toward the steam reforming of ethane and ethylene were also carried out. Either ethane or ethylene was fed together with steam (with the inlet molar ratio of 1.0/1.0) to the catalytic reactor instead of ethanol. Figs. 15 and 16 show the product selectivities from the steam reforming of ethane and ethylene over CeO_2 (HSA) at different temperatures. Clearly, ethane and ethylene were converted mainly to methane,

carbon monoxide, carbon dioxide, and hydrogen. It was found that the conversions of ethane and ethylene were almost 100% when the temperature reached 900ºC, which supports the ethanol steam reforming mechanism of CeO_2 as described above.

According to the use of CeO_2 (HSA) as the pre-reforming catalyst in the annular design reactor, the main purpose of CeO_2 is to convert all high hydrocarbons from the homogenous decomposition of ethanol such as ethylene and ethane to methane, carbon monoxide, and hydrogen before these components reach the surface of Ni/Al_2O_3 at the outer side of the annular reactor. Therefore, the main reaction over this section is the steam reforming of methane instead of the steam reforming of ethane and ethylene, which is thermodynamically unflavored to form carbon deposition. The significant deactivation observed over the use of CeO_2 (LSA) as the pre-reforming catalyst (CeO_2(LSA)-Ni/Al_2O_3) is due to the low reforming reactivity of CeO_2 (LSA), thus the remaining ethylene and ethane from the ethanol steam reforming over CeO_2 (LSA) pass through the outer side of the annular reactor reacting with Ni/Al_2O_3 and form the carbonaceous deposits on Ni surface. Similarly, the use of CeO_2 (HSA) as the co-reforming catalyst (CeO_2(HSA)+Ni/Al_2O_3) also results in the high degree of carbon deposition. This is possibly due to the faster decomposition of ethylene and ethane on the surface of Ni (Eqs. 19 and 20) compared to the adsorption of these components on the surface of CeO_2 (Eqs. 26 and 27).

Lastly, it should be noted that the limitation of CeO_2(HSA)-Ni/Al_2O_3 annular system in the present work is the introducing of high ethanol concentration (higher than 12 kPa), which resulted in the presenting of ethylene and ethane at the end of the pre-reforming section due to the incomplete reforming reaction. Although CeO_2 (HSA) was found to have high resistance toward carbon deposition in the present of ethylene and ethane, these hydrocarbon components left from the pre-reforming unit can decompose and formed the carbon species on Ni/Al_2O_3 surface at the main reforming section. One solution to minimize this problem is to enlarge the pre-reforming part, but the size of the reformer system for IIR-SOFC operation must be concerned. The use of autothermal reforming instead of the steam reforming is another alternative method to solve this problem. The additional of oxygen together with ethanol and steam will oxidize the hydrocarbon elements in the system and also help steam to regenerate the lattice oxygen (O_O^x) on CeO_2 surface ($O_2 + V_O^{\bullet\bullet} + 2\,e' + S_{Ce} \rightarrow O_O^x$), however, the possible formation of NiO due to the reaction between oxygen adding and Ni catalyst at this high temperature

must be aware. The autothermal reforming operation is now under investigated in our group.

5. Conclusion

High surface area ceria (CeO_2 (HSA)) has useful ethanol steam reforming activity producing H_2, CH_4, CO, and CO_2 under Solid Oxide Fuel Cells (SOFCs) conditions. The catalyst provides excellent reforming reactivity and high resistance toward carbon deposition compared to Ni/Al_2O_3 and conventional low surface area ceria (CeO_2 (LSA)). At the temperature above 800°C, neither C_2H_4 nor C_2H_6 was observed from the reforming over CeO_2 (HSA), whereas significant amounts of these hydrocarbons were formed over Ni/Al_2O_3 and CeO_2 (LSA). These benefits of CeO_2 (HSA) are mainly due to the high redox property of this material, according to the temperature programmed reduction experiments (TPR). In addition, it was also proven that the redox of CeO_2 is reversible, according to the second temperature programmed reduction results after the temperature programmed oxidation (TPO).

By applying CeO_2 as the internal pre-reforming catalyst together with Ni/Al_2O_3, this reforming pattern provided excellent hydrogen selectivity comparable to Rh/Al_2O_3 and high resistance toward carbon deposition in a single unit. CeO_2 (HSA) converts all ethanol and forms CH_4, CO, CO_2, and H_2, while Ni/Al_2O_3 reforms all hydrocarbons left from the pre-reforming section and maximize the yield of hydrogen production. This successful development can improve the efficiency of the indirect internal reforming operation Solid Oxide Fuel Cells (IIR-SOFC) fueled by ethanol by eliminate the requirement of expensive noble metal catalysts or the installation of an external pre-reforming unit.

Acknowledgement

The financial support from The Thailand Research Fund (TRF) throughout this project is gratefully acknowledged.

References

[1] P. Aguiar, D. Chadwick and L. Kershenbaum, Chem. Eng. Sci. 57 (2002) 1665.

[2] S. Cavallaro, S. Freni, Int. J. Hydrogen Energy 21 (6) (1996) 465–469.

[3] N.F. Athanasio, X.E. Verykios, J. Catal. 225 (4) (2004) 39–452.

[4] V. Fierro, O. Akdim, H. Provendier and C. Mirodatos, Journal of Power Sources, 145 (2005) 659–666

[5] R. Peters, R. Dahl, U. Kluttgen, C. Palm, D. Stolten, J. Power Sources, 106, (2002), 238.

[6] J.R. Salge, G.A. Deluga and L.D. Schmidt, J. Catal. 235 (1) (2005) 69-78.

[7] L. Garcia, R. French, S. Czernik and E. Chornet. Appl. Catal. A: Gen. 201 (2000) 225.

[8] I. Fishtik, A. Alexander, R. Datta and D. Geana. Int. J. Hydrogen Energy 25 (2000) 31.

[9] S. Freni, G. Maggio and S. Cavallaro. J. Power Sour. 62 (1996) 67.

[10] K. Vasudera, N. Mitra, P. Umasankar and S.C. Dhinga. Int. J. Hydrogen Energy 21 (1996) 13.

[11] S. Cavallaro and S. Freni. Int. J. Hydrogen Energy 21 (1996) 465.

[12] F. Marino, E.G. Cerrella, S. Duhalde, M. Jobbagy and M.A. Laborde. Int. J. Hydrogen Energy 23 (1998) 1095.

[13] S. Cavallaro. Energy and Fuels 14 (2000) 1195.

[14] S. Freni. J. Power Sour. 94 (2001) 14.

[15] A. Fatsikostas, D. Kondarides and X. Verykios. Catal. Today 75 (2002) 145.

[16] S. Freni, S. Cavallaro, N. Mondello, L. Spadaro and F. Frusteri. J. Power Sour. 108 (2002) 53.

[17] A. Fatsikostas, D. Kondarides and X. Verykios. Catal. Today 75 (2002) 145.

[18] F. Marino, G. Baronetti, M. Jobbagy and M. Laborde. Appl. Catal. A: Gen. 6043 (2002) 1.

[19] J.P. Breen, R. Burch and H.M. Coleman. Appl. Catal. B: Environ. 39 (2002) 65.

[20] J. Llorca, N. Homs, J. Sales and P. Ramirez de la Piscina. J. Catal. 209 (2002) 306.

[21] V. Fierro, V. Klouz, O. Akdim and C. Mirodatos. Catal. Today 75 (2002) 141.

[22] D. Liguras, D. Kondarides and X. Verykios. Appl. Catal. B: Environ. 43 (2003) 345.

[23] J. Llorca, P. Ramirez de la Piscina, J.-A. Dalmon, J. Sales and N. Homs. Appl. Catal. B: Environ. 43 (2003) 355.

[24] S. Cavallaro, V. Chiodo, S. Freni, N. Mondello and F. Frusteri. Appl. Catal. A: Gen. 249 (2003) 119.

[25] S. Freni, S. Cavallaro, N. Mondello, L. Sadaro and F. Frusteri. Catal. Commun. 4 (2003) 259.

[26] S. Cavallaro, V. Chiodo, A. Vita and S. Freni. J. Power Sour. 123 (2003) 10.

[27] D. Srinivas, C.V.V. Satyanarayana, H.S. Potdar and P. Ratnasamy. Appl. Catal. A: Gen. 243 (2003) 261.

[28] L.V. Mattos, E. Rodino, D.E. Resasco, F.B. Possos and F.B. Noronha, Fuel Proc. Technol. 83 (2003) 147.

[29] H.S. Roh, K.W. Jun and S.E. Park, Appl. Catal. A 251 (2003) 275.

[30] J.R. Rostrup-Nielsen and J.-H. Bak-Hansen, J. Catal. 144 (1993) 38.

[31] P. Fornasiero, G. Balducci, R.D. Monte, J. Kaspar, V. Sergo, G. Gubitosa, A. Ferrero and M. Graziani. J. Catal. 164 (1996) 173.

[32] T. Miki, T. Ogawa, M. Haneda, N. Kakuta, A. Ueno, S. Tateishi, S. Matsuura and M. Sato, J. Phys. Chem. 94 (1990) 339.

[33] C. Padeste, N.W. Cant and D.L. Trimm, Catal. Lett. 18 (1993) 305.

[34] S. Kacimi, J. Barbier Jr., R. Taha and D. Duperz, Catal. Lett. 22 (1993) 343.

[35] G.S. Zafiris and R.J. Gorte, J. Catal. 143 (1993) 86.

[36] G.S. Zafiris and R.J. Gorte, J. Catal. 139 (1993) 561.

[37] S. Imamura, M. Shono, N. Okamoto, R. Hamada and S. Ishida, Appl. Catal. A 142 (1996) 279.

[38] L. Fan and K. Fujimoto. J. Catal. 172 (1997) 238.

[39] M. Pijolat, M. Prin and M. Soustelle. J. Chem. Soc., Faraday Trans. 91 (1995) 3941.

[40] N. Laosiripojana and S. Assabumrungrat, Appl. Catal. B: Environ, 60 (2005) 107.

[41] N. Laosiripojana, W. Sutthisripok, and S. Assabumrungrat, Chem. Eng. Journal 112 (2005) 13-22.

[42] N. Laosiripojana, W. Sangtongkitcharoen, and S. Assabumrungrat, Fuel, In Press

[43] N. Laosiripojana and S. Assabumrungrat, Appl. Catal. A: General, 290 (2005) 200.

[44] K. Otsuka, T. Ushiyama and I. Yamanaka, Chemistry Letters, (1993), 1517

[45] K. Otsuka, M. Hatano and A. Morikawa, J. Catalysis, 79, (1983), 493

[46] P.J. Gellings and Henny J. M. Bouwmeester, Solid state aspects of oxidation catalysis, Catalysis Today, 58, (2000) 1-53

[47] C.T. Kresge, M.E. Leonowicz, W.J. Roth, J.C. Vartuli and J.S. Beck, Nature, 359 (1992) 710.

[48] Q. Huo, D.I. Margolese, U. Ciesla, P. Feng, T.E. Gier, P. Sieger, R. Leon, P.M. Petroff, B. Schüth and G.D. Stucky, Nature 368 (1994) 317.

[49] P.T. Tanev and T.J. Pinnavaia, Science 267 (1995) 865.

[50] U. Ciesla, S. Schacht, G.D. Stucky, K.K. Unger and F. Schüth. Angew. Chem. Int. Ed. Engl. 35 (1996) 541.

[51] D.M. Antonelli and J.Y. Ying. Angew. Chem. Int. Ed. Engl. 35 (1996) 426.

[52] Q. Huo, D.I. Margolese, U. Ciesla, D.G. Demuth, P. Feng, T.E. Gier, P. Sieger, A. Firouzi, B.F. Chmelka, B. Schüth and G.D. Stucky, Chem. Mater. 6 (1994) 1176.

[53] D. Terribile, A. Trovarelli, J. Llorca, C. de Leitenburg and G. Dolcetti, Catal. Today 43 (1998) 79–88

[54] J.A Cairns, J.E.E. Baglin, G.J. Clark, and J.F. Ziegler, J. Cat., 83, (1983) 301-314

[55] G.J. Den Otter, and F.M. Dautzenberg, J. Catal., 53, (1978) 116-125

[56] T. Ren-Yuan, W. Rong-An, and L. Li-Wu, Appl. Catal. A, 10, (1984) 163-172

[57] J.E.E. Baglin, G.J. Clark, and J.F. Ziegler, Nuclear Instruments and Methods in Physic Research, 218, (1983) 445-450

[58] E. Ramirez, A. Atkinson and D. Chadwick, Appl. Catal. B 36 (2002) 193–206.

[59] Y. Lwin, W.R.W. Daud and A.B. Mohamad, Z. Yaakob, Int. J. Hydrogen Energy 25 (2000) (1) 47–53.

[60] J.N. Amor, Appl. Catal. A 176 (1999) 159–176.

[61] B.C.H. Steele and J.M. Floyd. Proc. Br. Ceram. Soc. 19 (1971) 55.

List of figures

List of Tables

Table 7 Yield of H_2 production (%), deactivation percentages, and the amount of carbon formation after exposure in ethanol steam reforming at 900ºC

Table 8 Effect of inlet ethanol concentration on the formations of ethane and ethylene and the amount of carbon deposition from the ethanol steam reforming over CeO_2(HSA)-Ni/Al_2O_3 at 900ºC (with the inlet C_2H_5OH/H_2O molar ratio of 1.0/3.0)

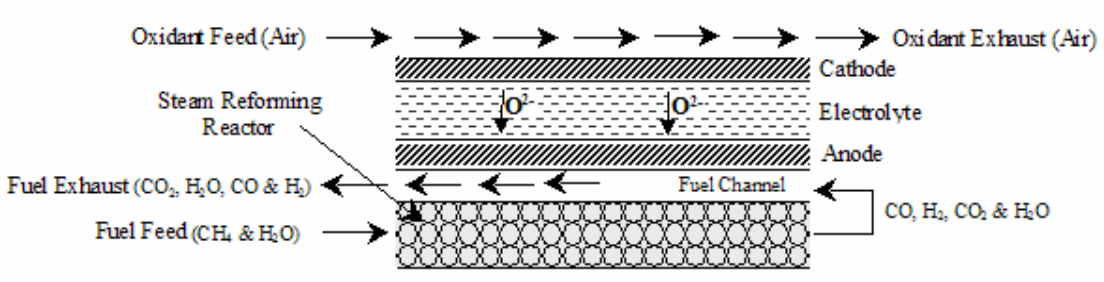

Fig. 1 Schematic diagram of SOFC with indirect internal reformer

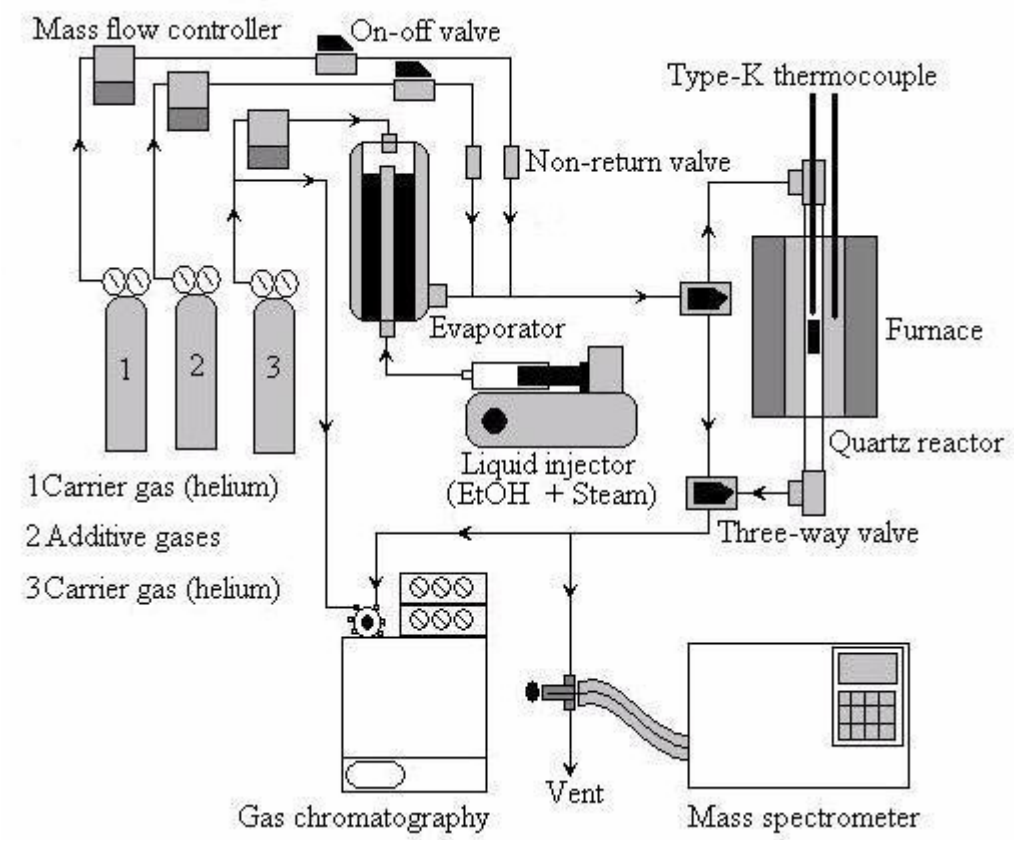

Fig. 2 Schematic diagram of the experimental set-up

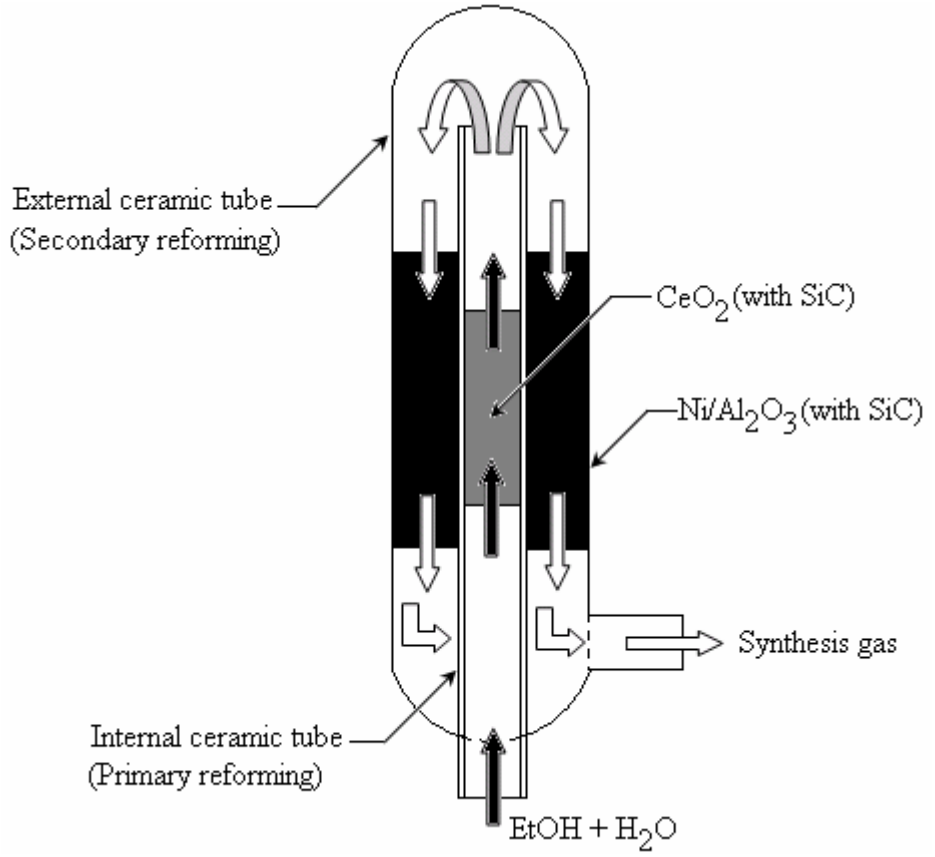

Fig. 3 Configuration of the catalytic testing unit with the pre-reforming catalyst

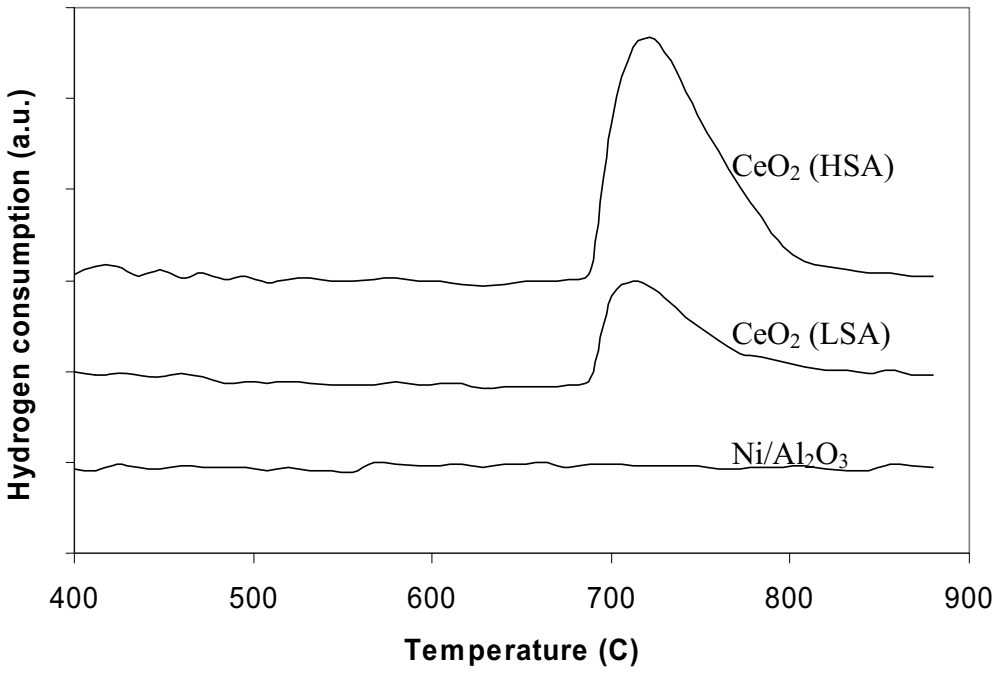

Fig. 4 Temperature Programmed Reduction (TPR-1) of fresh catalysts after reduction

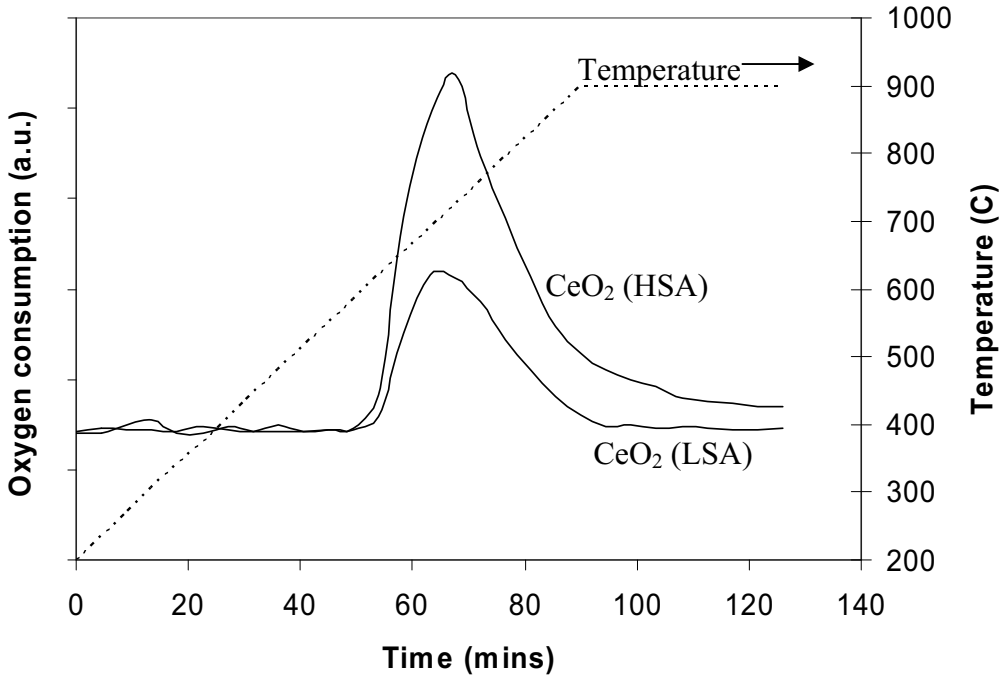

Fig. 5 Temperature Programmed Oxidation (TPO) of CeO_2 (HSA, LSA) after TPR-1

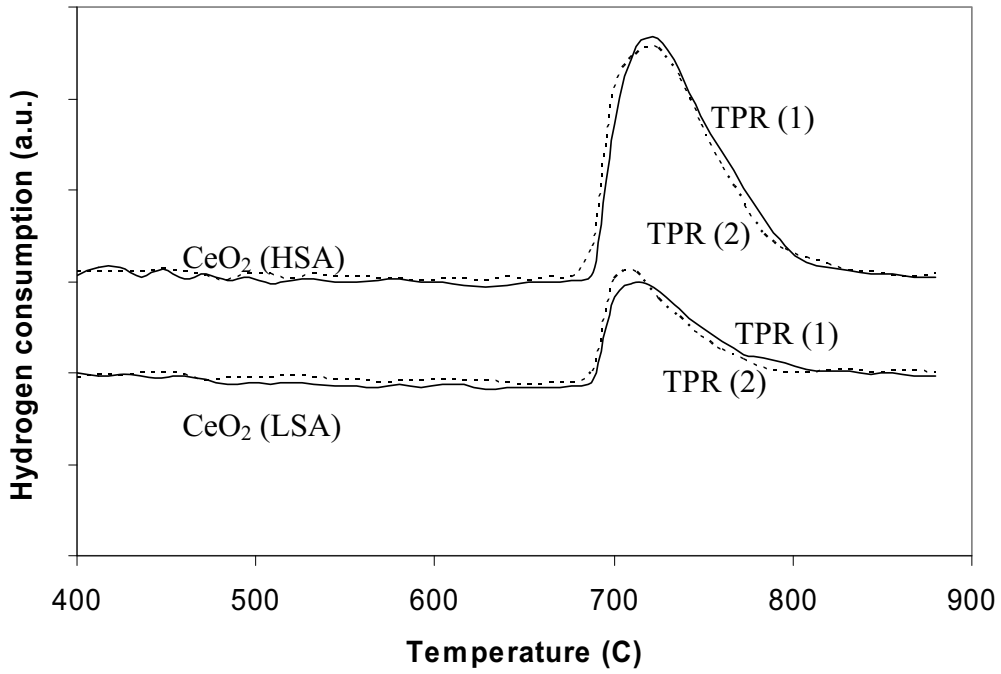

Fig. 6 Second time Temperature Programmed Reduction (TPR-2) of CeO_2 (HSA and LSA) compared to that of TPR-1

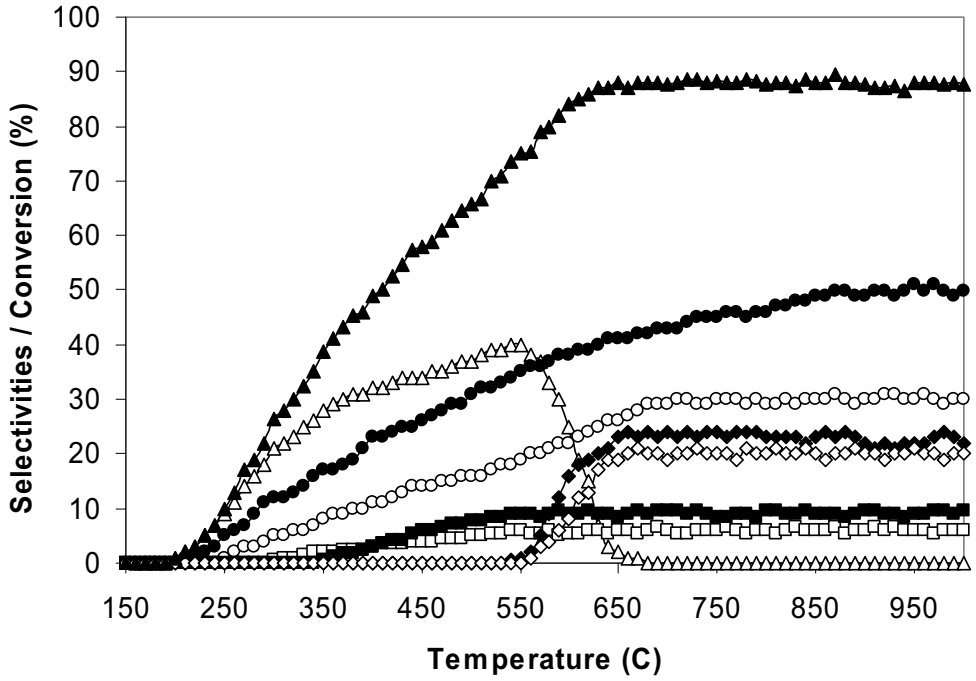

Fig. 7 Homogenous (in the absence of catalyst) reactivity of ethanol steam reforming (4 kPa C_2H_5OH, and 12 kPa H_2O) (EtOH (▲), H_2 (●), CO (○), CO_2 (■), CH_4 (□), CH_3CHO (△), C_2H_6 (◇), and C_2H_4 (◆))

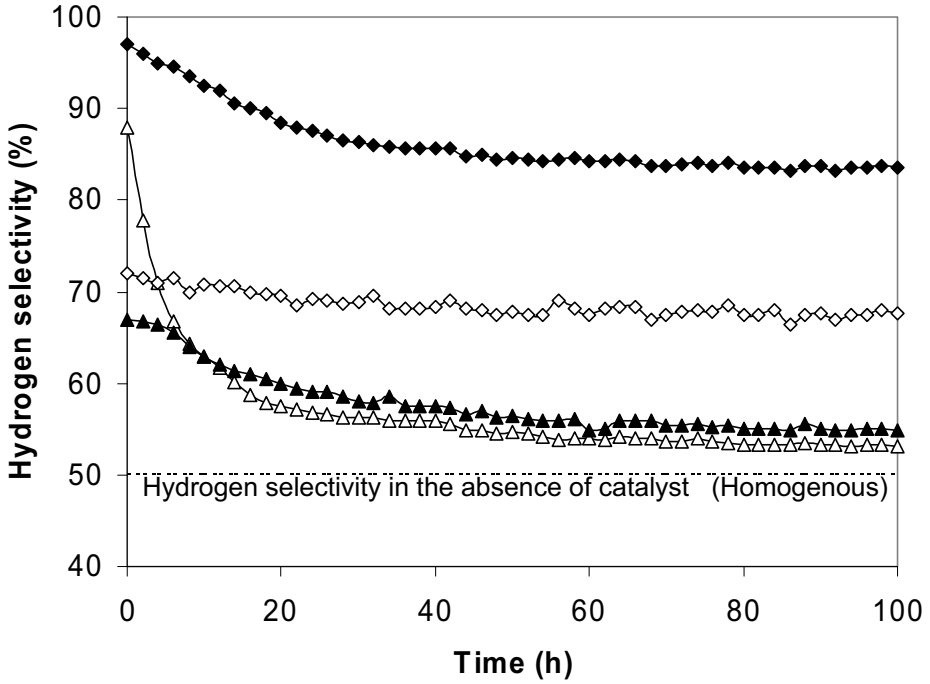

Fig. 8 Steam reforming of ethanol at 900°C for Rh/Al_2O_3 (◆), CeO_2 (HSA) (◇), CeO_2 (LSA) (▲),Ni/Al_2O_3 (△) (4 kPa C_2H_5OH, and 12 kPa H_2O)

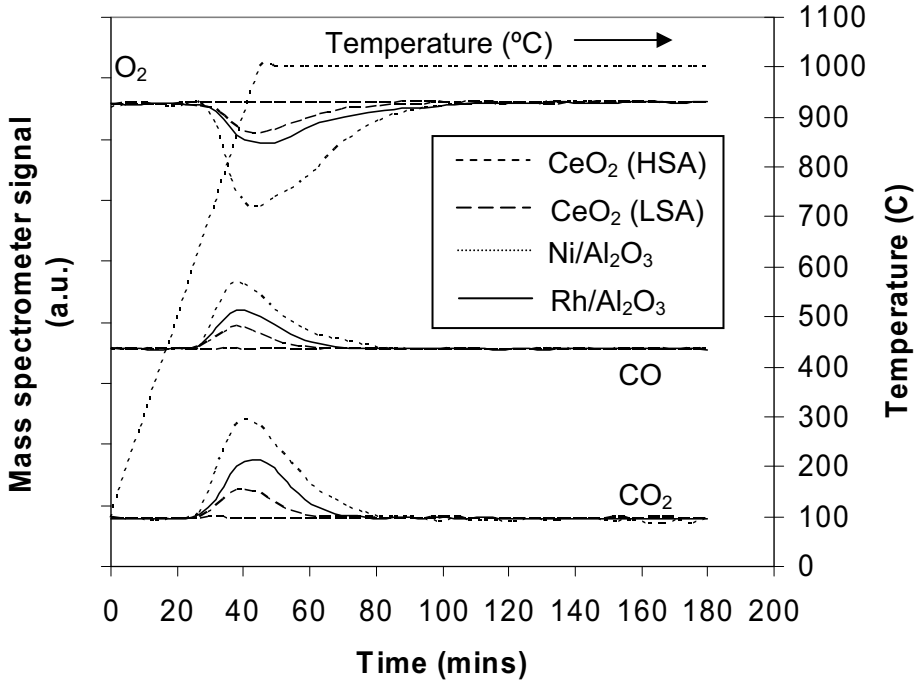

Fig. 9 Temperature Programmed Oxidation (TPO) of Rh/Al_2O_3, CeO_2 (HSA), CeO_2 (LSA), and Ni/Al_2O_3 after exposure in steam reforming of ethanol (4 kPa C_2H_5OH, and 12 kPa H_2O) for 100 h

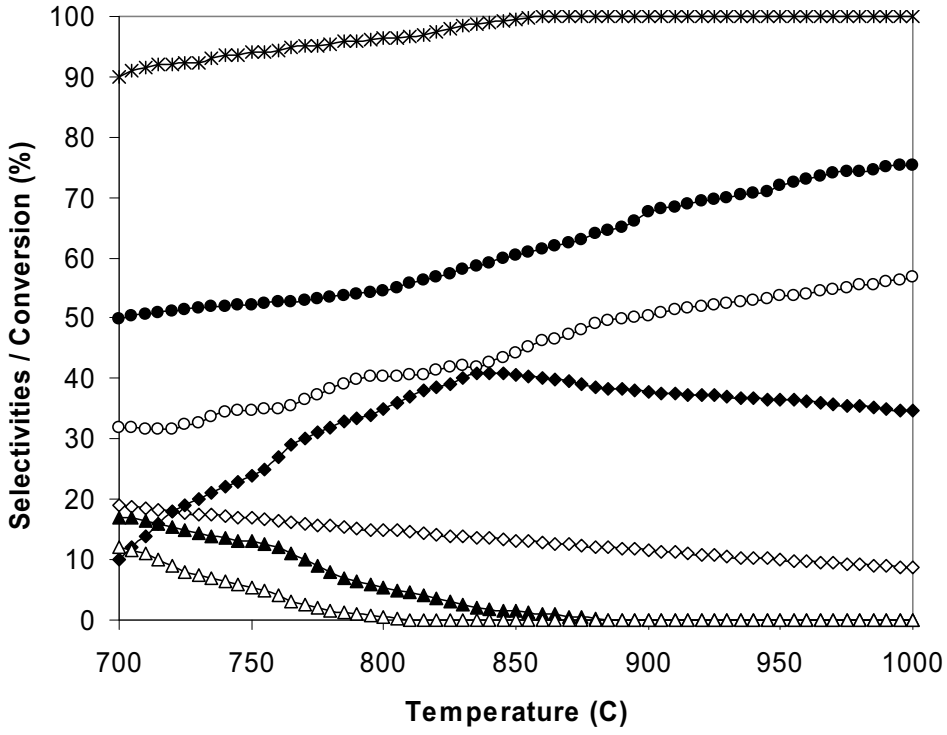

Fig. 10a

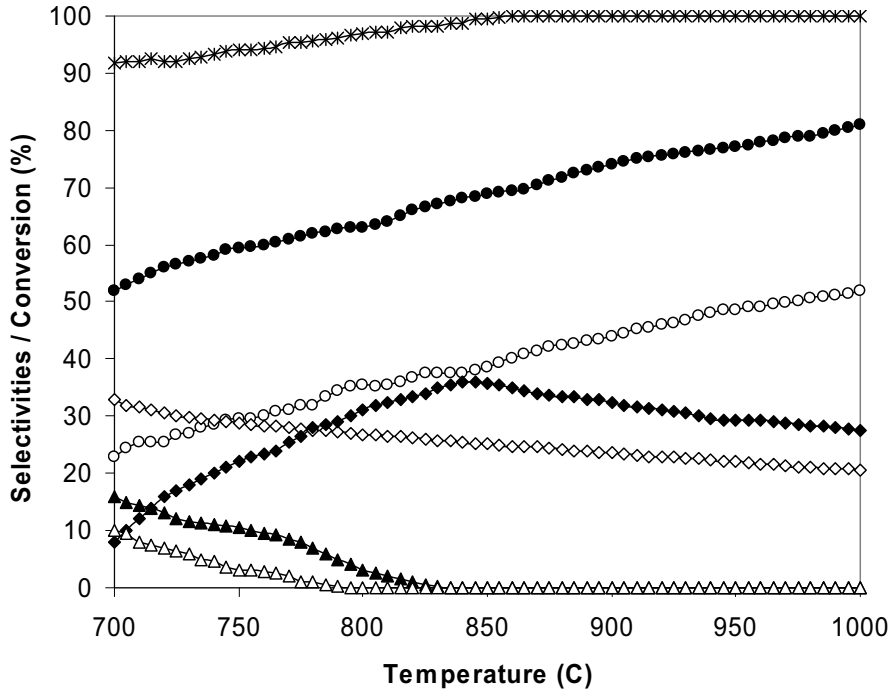

Fig. 10b

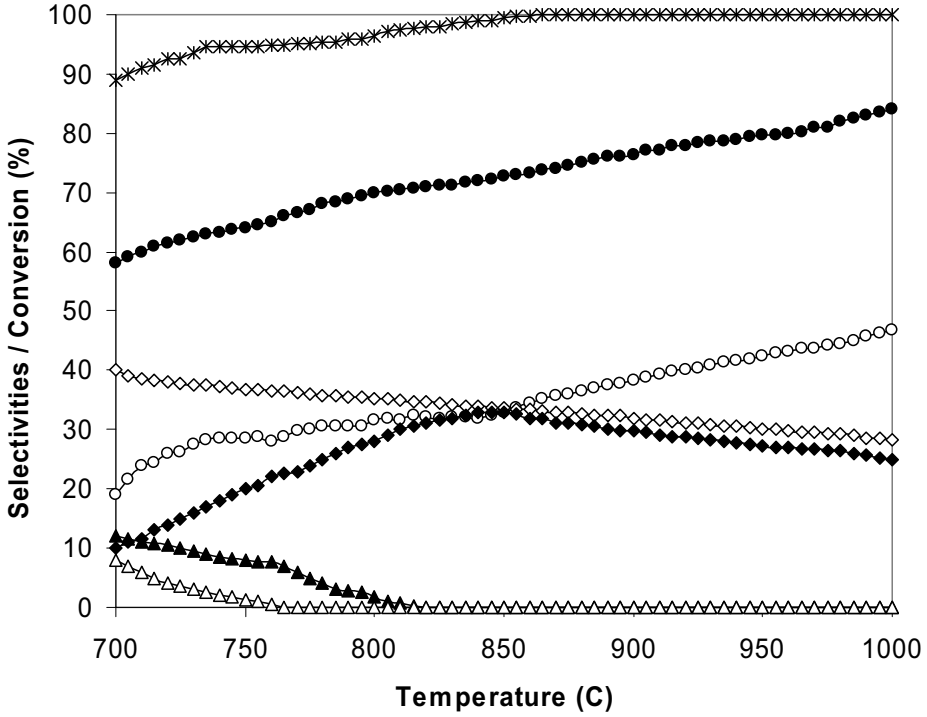

Fig. 10c

Fig. 10 Effect of temperature on the conversion and product selectivities (EtOH (×), H_2 (●), CO (○), CO_2 (◇), CH_4 (◆), C_2H_6 (△), and C_2H_4 (▲)) from ethanol steam reforming over CeO_2 (HSA) with EtOH/H_2O ratios of 1/3 (Fig. 10a), 1/4 (Fig. 10b), and 1/5 (Fig. 10c)

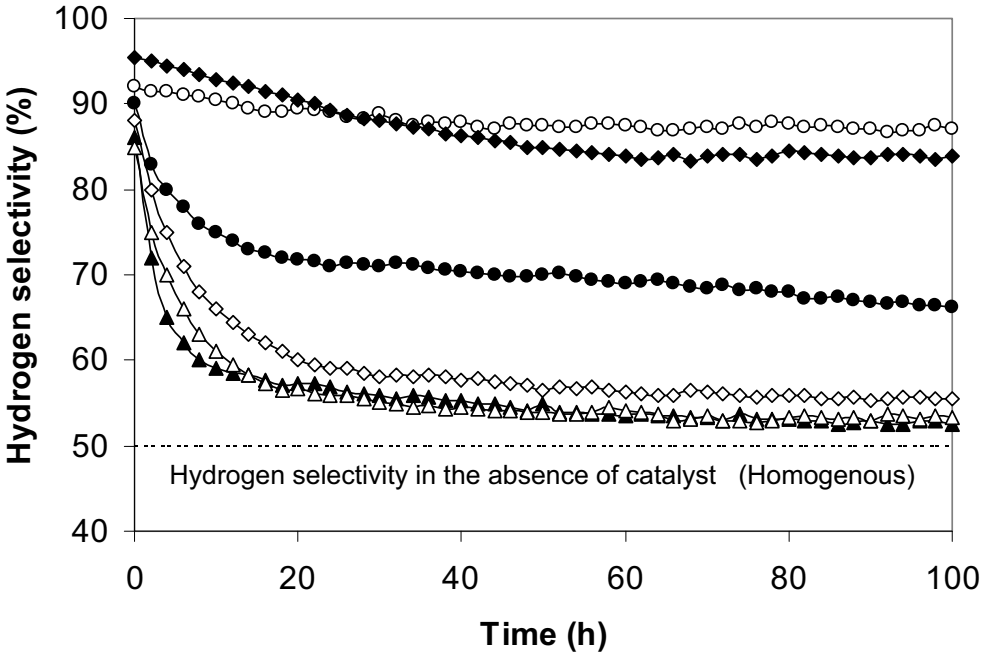

Fig. 11 Steam reforming of ethanol at 900°C for CeO_2(HSA)-Ni/Al_2O_3 (○), Rh/Al_2O_3 (◆), CeO_2(LSA)-Ni/Al_2O_3 (●), CeO_2(HSA)+Ni/Al_2O_3 (◇), CeO_2(LSA)+Ni/Al_2O_3 (△),Ni/Al_2O_3 (▲) (4 kPa C_2H_5OH, and 12 kPa H_2O)

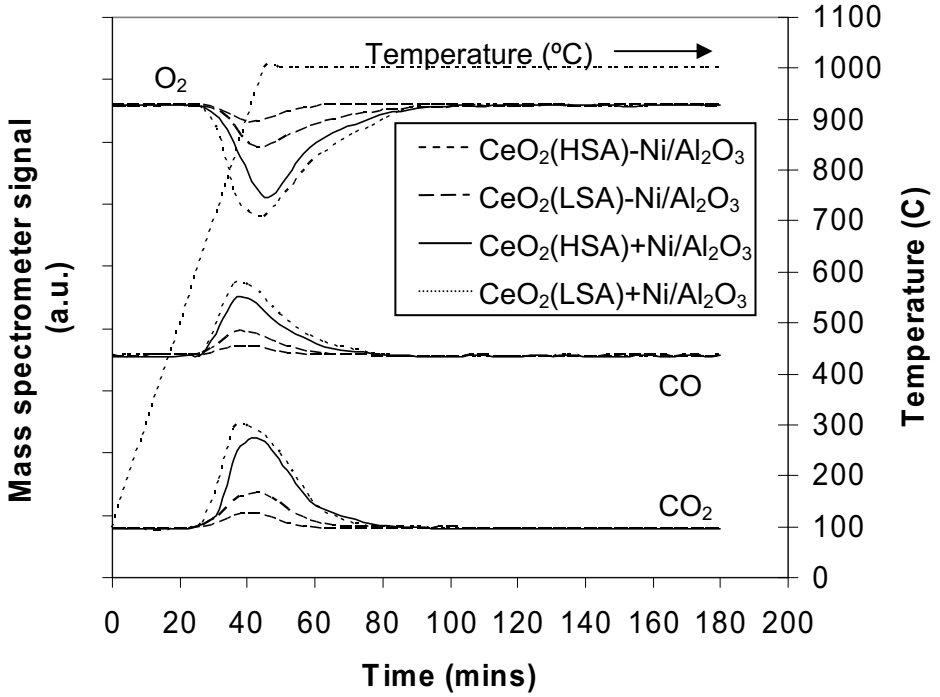

Fig. 12 Temperature Programmed Oxidation (TPO) of CeO_2(HSA)-Ni/Al_2O_3, CeO_2(LSA)-Ni/Al_2O_3, CeO_2(HSA)+Ni/Al_2O_3, and CeO_2(LSA)+Ni/Al_2O_3 after exposure in steam reforming of ethanol (4 kPa C_2H_5OH, and 12 kPa H_2O) for 100 h

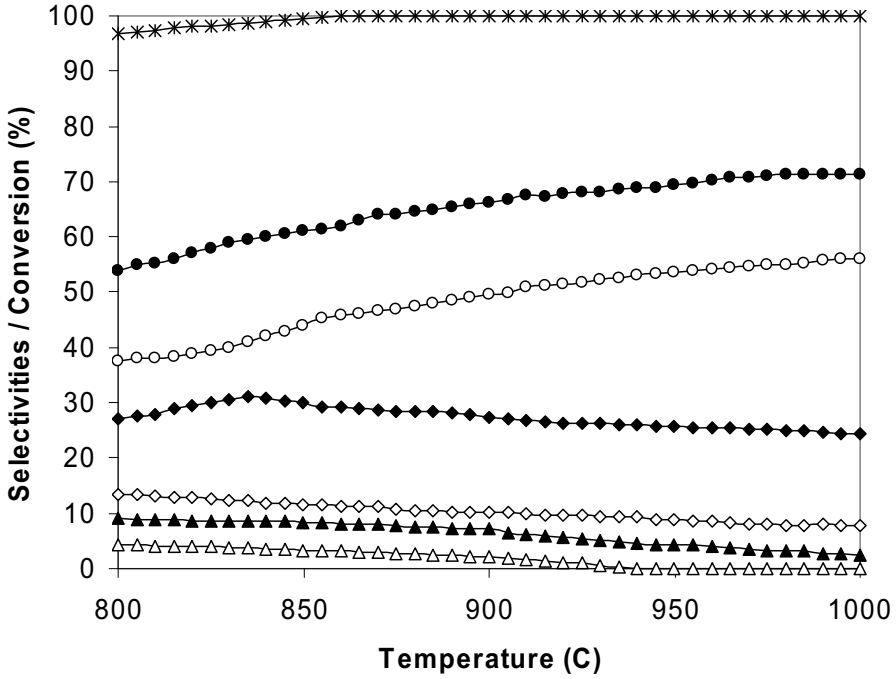

Fig. 13a

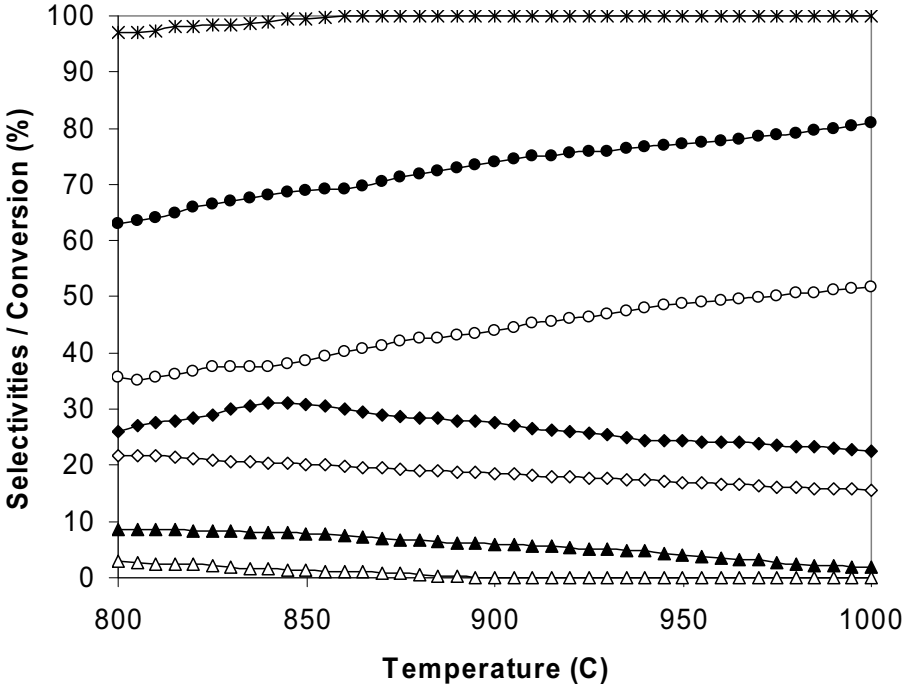

Fig. 13b

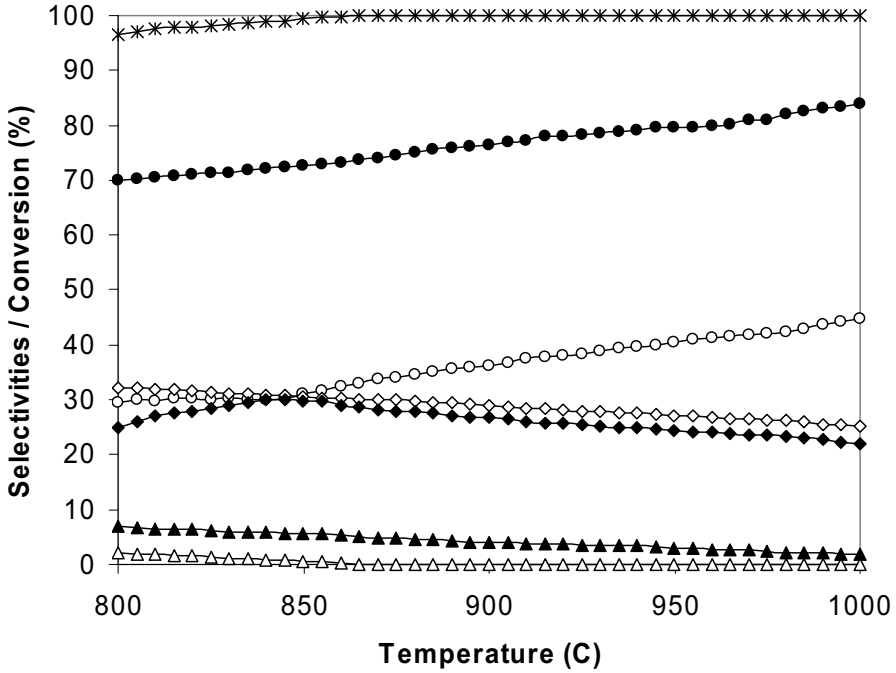

Fig. 13c

Fig. 13 Effect of temperature on the conversion and product selectivities (EtOH (×), H_2 (●), CO (○), CO_2 (◇), CH_4 (◆), C_2H_6 (△), and C_2H_4 (▲)) from ethanol steam reforming over CeO_2(LSA)-Ni/Al_2O_3 with EtOH/H_2O ratios of 1/3 (Fig. 13a), 1/4 (Fig. 13b), and 1/5 (Fig. 13c)

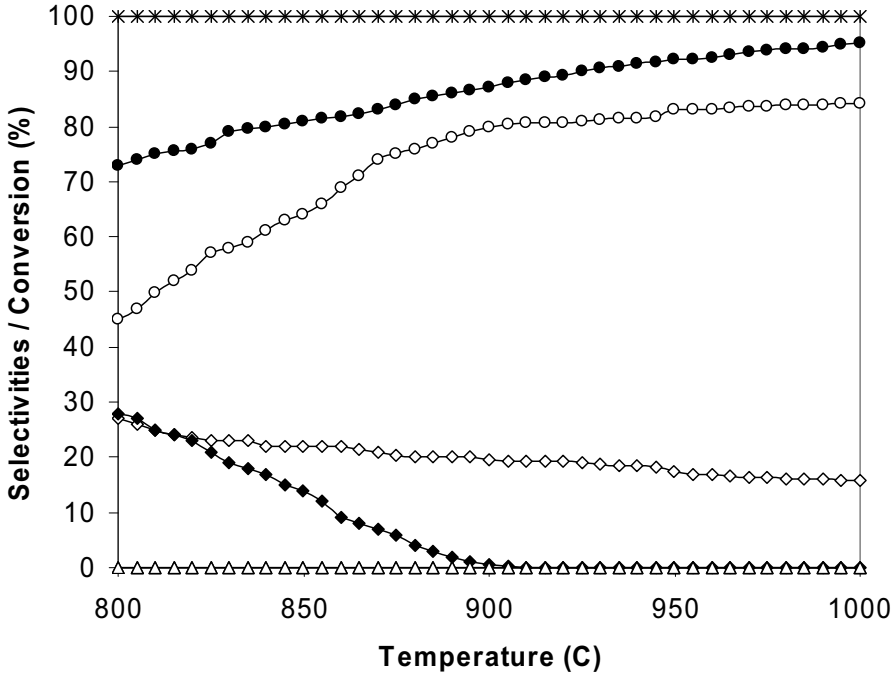

Fig. 14a

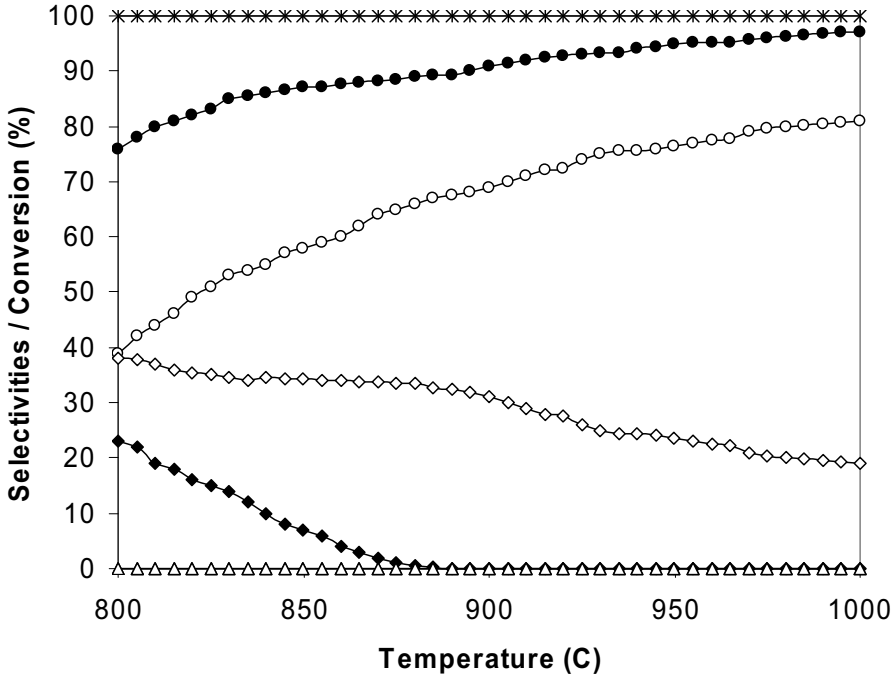

Fig. 14b

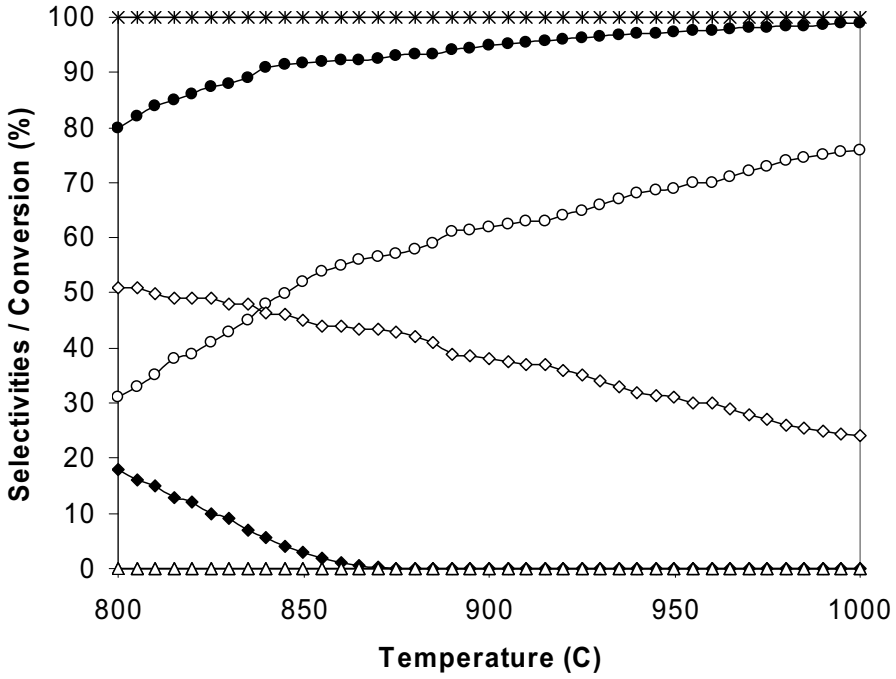

Fig. 14c

Fig. 14 Effect of temperature on the conversion and product selectivities (EtOH (×), H_2 (●), CO (○), CO_2 (◇), CH_4 (◆), C_2H_6 (△), and C_2H_4 (▲)) from ethanol steam reforming over CeO_2(HSA)-Ni/Al_2O_3 with EtOH/H_2O ratios of 1/3 (Fig. 14a), 1/4 (Fig. 14b), and 1/5 (Fig. 14c)

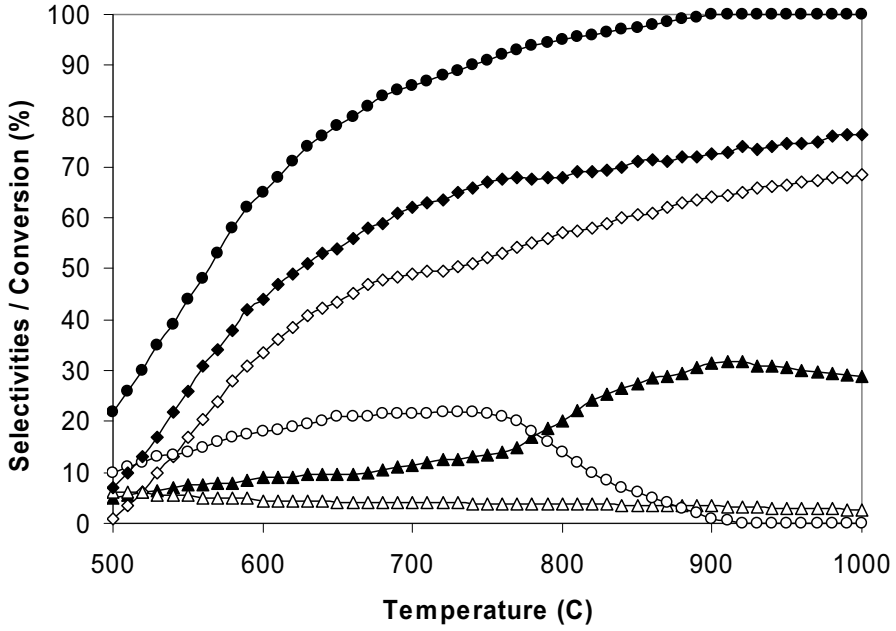

Fig. 15 Steam reforming of ethane over CeO_2 (HSA) (4 kPa C_2H_6, and 12 kPa H_2O) (C_2H_6 (●), H_2 (◆), CO (◇), CO_2 (△), CH_4 (▲), and C_2H_4 (○))

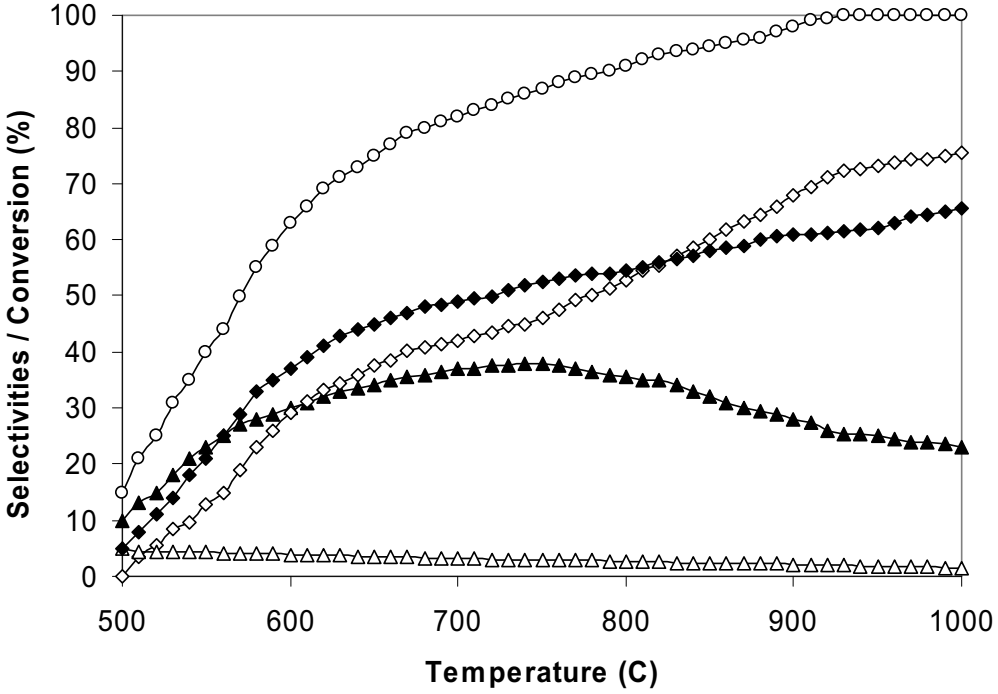

Fig. 16 Steam reforming of ethylene over CeO_2 (HSA) (4 kPa C_2H_4, and 12 kPa H_2O) (C_2H_4 (○), H_2 (◆), CO (◇), CO_2 (△), and CH_4 (▲))

Table 1
Specific surface area of the catalysts after drying and calcinations at different temperatures

Catalyst	BET surface area (m^2 g^{-1}) after drying or calcination at						
	100ºC	200ºC	400ºC	600ºC	800ºC	900ºC	1000ºC
CeO_2 (LSA.)[a]	55	49	36	21	15	11	8.5
CeO_2 (HSA-1)[b]	308	289	208	141	100	89	72
CeO_2 (HSA-2)[b]	189	177	136	97	72	55	43
CeO_2 (HSA-3)[b]	105	97	69	48	35	29	22

[a] conventional low surface area CeO_2 prepared by the precipitation method
[b] high surface area CeO_2 prepared by the surfactant-assisted approach with different flow rate of ammonia (1=0.165 cm^3 min^{-1}, 2=0.613 cm^3 min^{-1}, and 3=1.06 cm^3 min^{-1})

Table 2
Physicochemical properties of the catalysts after reduction

Catalyst	Metal-load[a] (wt.%)	BET Surface Area (m^2 g^{-1})	Metal-reducibility[b] (%)	Metal-dispersion[c] (%)
Ni/Al_2O_3	4.9	40	92.1	4.87
Rh/Al_2O_3	5.1	42	94.8	5.04

[a] Measured from X-ray fluorescence analysis.
[b] Measured from temperature-programmed reduction (TPR) with 5%hydrogen.
[c] Measured from temperature-programmed desorption (TPD) of hydrogen after TPR measurement.

Table 3
Results of TPR(1), TPO, TPR(2) analyses of CeO_2 (both HSA and LSA)

Catalyst	Total H_2 Uptake from TPR(1)[a] (μmol/g_{cat})	Total O_2 Uptake from TPO[b] (μmol/g_{cat})	Total H_2 Uptake from TPR(2)[c] (μmol/g_{cat})
CeO_2 (HSA)	2159	1044	2155
CeO_2 (LSA)	830	401	828

[a] Temperature Programmed Reduction of the reduced catalysts (Relative Standard Deviation = ± 3%)
[b] Temperature Programmed Oxidation after TPR (1) (Relative Standard Deviation = ± 1%)
[c] Re-Temperature Programmed Reduction after TPO (Relative Standard Deviation = ± 2%)

Table 4
Physicochemical properties of the catalysts after exposure in ethanol steam reforming at 900ºC for 100 h

Catalyst	Deactivation (%)	C formation (monolayers)	BET surface (m^2 g^{-1})	Metal-load [a] (wt.%)	Metal-red.[b] (Ni%)	Metal-disp.[c] (Ni%)
CeO_2 (HSA)	6.1	~0[d] (~0)[e]	66.9	-	-	-
CeO_2 (LSA)	17.9	0.67 (0.69)	7.3	-	-	-
Rh/Al_2O_3	13.8	1.47 (1.44)	~40.0	5.0	94.6	5.01
Ni/Al_2O_3	39.5	4.52 (4.54)	~40.0	4.9	92.0	4.85

[a] Measured from X-ray fluorescence analysis
[b] Nickel and rhodium reducibility
[c] Nickel and rhodium dispersion
[d] Calculated using CO and CO_2 yields from temperature-programmed oxidation (TPO) with 10% oxygen.
[e] Calculated from the balance of carbon in the system

Table 5
Product selectivities and the amount of carbon deposition from the catalysts after exposure in ethanol steam reforming at different inlet $EtOH/H_2O$ ratios

Catalyst	C_2H_5OH/H_2O ratio	Product Selectivities at 900°C						C formation (monolayers)
		H_2	CO	CO_2	CH_4	C_2H_6	C_2H_4	
CeO_2 (HSA)	1.0/3.0	67.5	50.5	11.6	37.9	0	0	~0[a] (~0)[b]
	1.0/4.0	74.0	43.9	23.6	32.5	0	0	0 (0)
	1.0/5.0	76.4	38.3	32	29.7	0	0	0 (0)
CeO_2 (LSA)	1.0/3.0	54.9	44.0	10.9	37.4	1.2	5.8	0.67 (0.69)
	1.0/4.0	59.7	40.1	19.1	35.1	1	4.1	0.61 (0.60)
	1.0/5.0	61.3	37.4	24.7	34.0	0.5	2.9	0.58 (0.58)
Rh/Al_2O_3	1.0/3.0	83.5	61.3	16.3	19.4	0.3	1.3	1.47 (1.44)
	1.0/4.0	85.1	55.6	25.4	17.2	0	0.5	1.32 (1.35)
	1.0/5.0	86.3	50.1	33.7	14.7	0	0.3	1.20 (1.18)
Ni/Al_2O_3	1.0/3.0	53.2	39.5	7.1	24.7	8.5	15.8	4.52 (4.54)
	1.0/4.0	55.4	38.1	13.7	22.6	6.1	14.1	4.47 (4.45)
	1.0/5.0	58.6	35.7	20.1	20.9	5.4	13.5	4.41 (4.42)

[a] Calculated using CO and CO_2 yields from temperature-programmed oxidation (TPO) with 10% oxygen.
[b] Calculated from the balance of carbon in the system

Table 6
Effect of inlet ethanol concentration on the formations of ethane and ethylene and the amount of carbon deposition from the ethanol steam reforming over CeO_2 (HSA) at 900ºC (with the inlet C_2H_5OH/H_2O molar ratio of 1.0/3.0)

Inlet C_2H_5OH (kPa)	Selectivities at 900ºC		C formation (monolayers)
	C_2H_6	C_2H_4	
3.0	0	0	~0[a] (~0)[b]
6.0	0	0	0 (0)
9.0	0	0	0 (0)
12.0	0.4	2.7	0.28 (0.22)
15.0	0.6	3.1	0.47 (0.47)

[a] Calculated using CO and CO_2 yields from temperature-programmed oxidation (TPO) with 10% oxygen.
[b] Calculated from the balance of carbon in the system

Table 7
Yield of H_2 production (%), deactivation percentages, and the amount of carbon formation after exposure in ethanol steam reforming at 900ºC

Type of operation	C_2H_5OH/H_2O ratio	Yield of H_2 (%) at steady state	Deactivation (%)	Total amount of carbon formation (monolayers)
CeO_2(HSA)-Ni/Al_2O_3	1.0/3.0	87.0	5.4	0.92[a] (0.92)[b]
	1.0/4.0	89.5	5.1	0.87 (0.84)
	1.0/5.0	91.4	4.8	0.79 (0.80)
CeO_2(LSA)-Ni/Al_2O_3	1.0/3.0	66.3	17.9	2.01 (1.98)
	1.0/4.0	67.7	16.4	1.95 (1.95)
	1.0/5.0	68.4	15.2	1.88 (1.91)
CeO_2(HSA)+Ni/Al_2O_3	1.0/3.0	55.5	26.3	3.42 (3.41)
	1.0/4.0	58.1	26.0	3.37 (3.36)
	1.0/5.0	60.2	25.4	3.31 (3.32)
CeO_2(LSA)+Ni/Al_2O_3	1.0/3.0	53.4	36.9	4.19 (4.20)
	1.0/4.0	56.0	35.8	4.12 (4.10)
	1.0/5.0	58.9	35.1	4.07 (4.08)
Rh/Al_2O_3	1.0/3.0	83.9	12.1	1.41 (1.39)
	1.0/4.0	85.7	10.7	1.34 (1.30)
	1.0/5.0	86.9	9.9	1.27 (1.28)
Ni/Al_2O_3	1.0/3.0	52.6	38.8	4.47 (4.49)
	1.0/4.0	55.2	37.4	4.36 (4.38)
	1.0/5.0	58.7	36.1	4.24 (4.28)

[a] Calculated using CO and CO_2 yields from temperature-programmed oxidation (TPO) with 10% oxygen.
[b] Calculated from the balance of carbon in the system

Table 8
Effect of inlet ethanol concentration on the formations of ethane and ethylene and the amount of carbon deposition from the ethanol steam reforming over CeO_2(HSA)-Ni/Al_2O_3 at 900ºC (with the inlet C_2H_5OH/H_2O molar ratio of 1.0/3.0)

Inlet C_2H_5OH (kPa)	Selectivities at 900ºC		C formation (monolayers)
	C_2H_6	C_2H_4	
3.0	0	0	0.92[a] (0.92)[b]
6.0	0	0	0.99 (1.01)
9.0	0	0	0.97 (0.97)
12.0	0	1.8	1.35 (1.33)
15.0	0.3	2.2	1.94 (1.89)

[a] Calculated using CO and CO_2 yields from temperature-programmed oxidation (TPO) with 10% oxygen.
[b] Calculated from the balance of carbon in the system

Available online at www.sciencedirect.com
SCIENCE DIRECT®
Applied Catalysis A: General 290 (2005) 200–211
APPLIED CATALYSIS A: GENERAL
www.elsevier.com/locate/apcata

Methane steam reforming over Ni/Ce–ZrO_2 catalyst: Influences of Ce–ZrO_2 support on reactivity, resistance toward carbon formation, and intrinsic reaction kinetics

N. Laosiripojana [a,*], S. Assabumrungrat [b]

[a] *The Joint Graduate School of Energy and Environment, King Mongkut's University of Technology Thonburi, 91 Prachauthit Road, Bangmod, Tungkru, Bangkok 10140, Thailand*
[b] *Center of Excellence on Catalysis and Catalytic Reaction Engineering, Department of Chemical Engineering, Faculty of Engineering, Chulalongkorn University, Bangkok 10330, Thailand*

Received 21 December 2004; received in revised form 17 May 2005; accepted 25 May 2005
Available online 6 July 2005

Abstract

Ni/Ce–ZrO_2 showed good methane steam reforming performance in term of stability toward the deactivation by carbon deposition. It was first observed that the catalyst with Ce/Zr ratio of 3/1 showed the best activity among Ni/Ce–ZrO_2 samples with the Ce/Zr ratios of 1/0, 1/1, 1/3, and 3/1. Temperature-programmed oxidation (TPO) experiments indicated the excellent resistance toward carbon formation for this catalyst, compared to conventional Ni/Al_2O_3; the requirement of inlet H_2O/CH_4 to operate without the formation of carbon species is much lower. These benefits are related to the high oxygen storage capacity (OSC) of Ce–ZrO_2. During the steam reforming process, in addition to the reactions on Ni surface (*), the redox reactions between the gaseous components present in the system and the lattice oxygen (O_x) on Ce–ZrO_2 surface also take place. Among these reactions, the redox reactions between the high carbon formation potential compounds (CH_4, CH_x-*n and CO) and the lattice oxygen (O_x) can prevent the formation of carbon species from the methane decomposition and Boudard reactions, even at low inlet H_2O/CH_4 ratio (1.0/1.0).

Regarding the intrinsic kinetic studies in the present work, the reaction order in methane over Ni/Ce–ZrO_2 was observed to be approximately 1.0 in all conditions. The dependence of steam on the rate was non-monotonic, whereas addition of oxygen as an autothermal reforming promoted the rate but reduced CO and H_2 production selectivities. The addition of a small amount of hydrogen increased the conversion of methane, however, this positive effect became less pronounced and the methane conversion was eventually inhibited when high hydrogen concentration was added. Ni/Ce–ZrO_2 showed significantly stronger negative impact of hydrogen than Ni/Al_2O_3. The redox mechanism on ceria proposed by Otsuka et al. [K. Otsuka, T. Ushiyama, I. Yamanaka, Chem. Lett. (1993) 1517; K. Otsuka, M. Hatano, A. Morikawa, J. Catal. 79 (1983) 493; K. Otsuka, M. Hatano, A. Morikawa, Inorg. Chim. Acta 109 (1985) 193] can explain this high inhibition.

1. Introduction

The methane steam reforming is a widely practiced technology for production of hydrogen or synthesis gas for later utilization in fuel cells. Three main reactions are always carried out as presented in the following equations:

$$CH_4 + H_2O \Leftrightarrow CO + 3H_2 \quad (1)$$

$$CO + H_2O \Leftrightarrow CO_2 + H_2 \quad (2)$$

$$CH_4 + 2H_2O \Leftrightarrow CO_2 + 4H_2 \quad (3)$$

Both water–gas shift reaction (Eq. (2)) and reverse methanation (Eq. (3)) are associated with the steam reforming over a catalyst at elevated temperatures. The reverse methanation (Eq. (3)) is thermodynamically linearly dependent on methane steam reforming and water–gas shift reaction, but it is kinetically independent [4–8]. Due to the

* Corresponding author. Tel.: +662 8729014; fax: +662 8726736.
E-mail address: navadol_1@jgsee.kmutt.ac.th (N. Laosiripojana).

0926-860X/$ – see front matter © 2005 Elsevier B.V. All rights reserved.
doi:10.1016/j.apcata.2005.05.026

overall high endothermic nature of the reactions, they are carried out at high temperature (700–900 °C). In recent years, many researchers have also investigated the addition of oxygen together with methane and steam in a single process, calling an autothermal reforming. This reaction is an economical process, in which the steam reforming of methane (1) is combined with the partial oxidation of methane, as presented in the following equation:

$$CH_4 + (1/2)\,O_2 \Leftrightarrow CO + 2H_2 \quad (4)$$

By this combination, exothermic heat from the partial oxidation can directly supply the energy required for the endothermic steam reforming reaction. Therefore, it is considered to be thermally self-sustaining and consequently more attractive than the steam reforming. However, the main disadvantage of this reaction is the lower production of synthesis gas (H_2 and CO) from this reaction compared to the steam reforming. Currently, the commercial process for the production of hydrogen and synthesis gas is still based on the steam reforming reaction using nickel catalyst on supports such as Al_2O_3, MgO, $MgAl_2O_4$ or their mixtures. Worldwide efforts are in progress to develop a novel catalyst with higher activity and stability for the reforming reactions. Various precious metals such as Pt, Rh and Ru have been reported to be active for the reforming reactions and resistant to the carbon formation [9,10]. However, the current prices of these metals are very high for commercial uses, and the availability of some precious metals such as ruthenium was too low to have a major impact on the total reforming catalyst market [11].

Selection of a support material is another important issue as there was some evidence that metal catalysts are not very active for the steam reforming when supported on inert oxides [12]. Various supports have been investigated, for example, α-Al_2O_3 [13], γ-Al_2O_3 and γ-Al_2O_3 with alkali metal oxide and rare earth metal oxide [14], $CaAl_2O_4$ [15] and Ce–ZrO_2 [16]. A promising catalyst system for the reforming reactions appeared to be a metal on Ce–ZrO_2 support, where the metal can be Ni, Pt or Pd [17–25]. Ni/Ce–ZrO_2 has been successfully applied to the partial oxidation and the autothermal reforming of methane [26]. It is well established that ceria and metal oxide (e.g. Gd, Nb, and Zr) doped cerias provide high oxygen storage capacity, which is beneficial in oxidation processes [27]. Moreover, it has been reported that the gas–solid reaction between CeO_2 and CH_4 produces synthesis gas with a H_2/CO ratio of two, while the reduced ceria, CeO_{2-n}, can react with CO_2 and H_2O to produce CO and H_2, respectively, according to the following reactions [1–3]:

$$CeO_2 + nCH_4 \rightarrow CeO_{2-n} + nCO + 2nH_2 \quad (5)$$

$$CeO_{2-n} + CO_2 \Leftrightarrow CeO_2 + CO \quad (6)$$

$$CeO_{2-n} + H_2O \Leftrightarrow CeO_2 + H_2 \quad (7)$$

The addition of zirconium oxide (ZrO_2) to cerium oxide (CeO_2) has been reported to improve the oxygen storage capacity, redox property, thermal stability and catalytic activity [28–37]. This high oxygen storage capacity was associated with enhanced reducibility of cerium(IV) in Ce–ZrO_2, which is a consequence of the high O^{2-} mobility inside the fluorite lattice. One possible reason for the increasing mobility might be related to the lattice strain, which is generated by the introduction of a smaller isovalent Zr cation into the CeO_2 lattice (Zr^{4+} has a crystal ionic radius of 0.84 Å, which is smaller than 0.97 Å for Ce^{4+} in the same co-ordination enviroment) [38]. Due to the high thermal stability of this material, Ce–ZrO_2 would be a good candidate to be used as the catalyst support for high temperature steam reforming reactions.

Apart from the efforts devoted to catalyst selection, a number of works have been focused on the kinetic study of methane steam reforming. There is a general agreement that the reaction order in methane is always 1.0. However, there is less agreement with the other kinetic parameters, such as dependence on H_2O, and H_2. This could be due to the use of different catalysts and experimental conditions. Moreover, the impact of diffusion limitation could affect the experimental results also. In a study at conditions similar to SOFC, Dicks et al. [39] observed that the product partial pressures from the methane steam reforming on Ni/ZrO_2 could significantly affect the reforming rate, in particular that of hydrogen. The first order reaction in methane was obtained, while a positive effect of hydrogen partial pressure and a negative effect of steam partial pressure on the rate of reforming were observed. The researchers also indicated that hydrogen must be added as the feed gas together with methane and steam, because the steam reforming rate in pure methane/steam gas mixture was low. Xu and Froment [4–6] presented a rate model for the methane steam reforming together with the water–gas shift reaction over Ni/$MgAl_2O_4$ catalyst and also derived intrinsic rate equations. They reported the non-monotonic dependence of steam on the rate of reforming due to the competition of the catalyst active sites. A similar result was observed by Elnashaie et al. [7,8]. Xu and Froment [4–6] also presented the inhibitory effect of hydrogen on the methane steam reforming rate due to the promotion of the reverse reactions of Eqs. (1)–(3).

In the present work, we aimed to study the intrinsic reaction kinetics of an alternative reforming catalyst, which provides high methane steam reforming activity and high resistance toward carbon formation. According to the economical point of view, Ni was selected as a catalyst rather than other precious metals such as Pt, Rh and Ru although Ni is more sensitive to carbon formation. Ni/Ce–ZrO_2 catalysts with different ratios of Ce/Zr were first investigated to determine a suitable ratio. The intrinsic reaction kinetics for the selected catalyst were then studied by varying inlet CH_4, and H_2O concentrations, and by adding H_2, and O_2 in order to evaluate the possible use of Ni/Ce–ZrO_2 industrially.

2. Experimental

2.1. Catalyst preparations and characterizations

$Ce_{1-x}Zr_xO_2$ supports with different Ce/Zr molar ratios were prepared by co-precipitation of cerium nitrate ($Ce(NO_3)_3{\cdot}H_2O$), and zirconium oxychloride ($ZrOCl_2{\cdot}H_2O$) H_2O) (from Aldrich). The starting solution was prepared by mixing 0.1 M of metal salt solution with 0.4 M of urea at a 2/1 volumetric ratio. The ratio between each metal salt was altered to achieve nominal Ce/Zr molar ratios: $Ce_{1-x}Zr_xO_2$, where $x = 0.25$, 0.50, and 0.75, respectively. This solution was stirred by magnetic stirring (100 rpm) for 3 h, and the precipitate was filtered and washed with deionised water and ethanol to prevent an agglomeration of the particles. It was dried overnight in an oven at 110 °C, and then calcined in air at 1000 °C for 6 h.

Ni/Ce–ZrO_2 was prepared by impregnating Ce–ZrO_2 with a $Ni(NO_3)_2$ solution (from Aldrich). The catalyst was reduced with 10%H_2/Ar for 6 h before use. For comparison, Ni/Al_2O_3 and Ni/CeO_2 (5 wt.% Ni) were also prepared by impregnating α-Al_2O_3 (from Aldrich) and CeO_2 with $Ni(NO_3)_2$. After reduction, the catalysts were characterized by several physicochemical methods. The weight content of Ni in Ni/Al_2O_3, Ni/Ce–ZrO_2 (with different Ce/Zr ratio), and Ni/CeO_2 were determined by X-ray fluorescence (XRF) analysis. The reducibility and dispersion percentages of nickel were measured from temperature-programmed reduction (TPR) with 5% H_2 in Ar and temperature-programmed desorption (TPD), respectively. The catalyst specific surface areas were obtained from BET measurement. All physicochemical properties of the synthesized catalysts are presented in Table 1.

2.2. Apparatus and procedures

In order to investigate the methane steam reforming and its associated reactions, we constructed an experimental reactor system as shown in Fig. 1. The feed gases including the components of interest such as CH_4, H_2O, H_2, or O_2 were introduced to the reaction section, in which an 8 mm internal diameter and 40 cm length quartz reactor was mounted vertically inside a furnace. The catalyst was loaded in the quartz reactor, which was packed with a small amount of quartz wool to prevent the catalyst from moving. The weight of catalyst loading was 50 mg, while a typical range of total gas flow was 20–200 $cm^3\ min^{-1}$ depending on the desired space velocity. A type-K thermocouple was placed into the annular space between the reactor and the furnace. This thermocouple was mounted on the tubular reactor in close contact with the catalyst bed to minimize the temperature difference between the catalyst bed and the thermocouple. Another type-K thermocouple was inserted in the middle of the quartz tube in order to re-check the possible temperature gradient, especially when O_2 was added along with CH_4 and H_2O as the autothermal reforming. The record showed that the maximum temperature fluctuation during the reaction was always ± 0.75 °C or less from the temperature specified for the reaction.

After the reactions, the exit gas mixture was transferred via trace-heated lines to the analysis section, which consists of a Porapak Q column Shimadzu 14B gas chromatograph (GC) and a mass spectrometer (MS). The gas chromatography was applied in order to investigate the steady state condition experiments, whereas the mass spectrometer in which the sampling of the exit gas was done by a quartz capillery and differential pumping was used for the transient and carbon formation experiments.

A temperature-programmed technique (TP) was applied in order to study the formation of carbon species on catalyst surface. Temperature-programmed methane adsorption (TPMA) was firstly carried out in order to investigate the reaction of methane with the surface of catalyst and to form the carbon species on catalyst surface. A 5% methane in helium was introduced into the system, while the operating temperature was increased from room temperature to 1000 °C at the rate of 10 °C/min. After the system was purged with helium, TPMA was followed by temperature-programmed oxidation (TPO) in order to quantify the deposited carbon on the catalyst surface. A 10% oxygen in helium was introduced into the system and, similar to TPMA, the temperature was increased from room temperature to 1000 °C at the rate of 10 °C/min. The calibrations of CO and CO_2 productions were performed by injecting a known amount of these calibration gases from a loop, in an injection valve in the bypass line. The response factors were obtained by dividing the number of moles for each component over the respective areas under the peaks. This process was performed before each experiment to achieve maximal accuracy in the quantitative carbon analysis. In

Table 1
Physicochemical properties of the catalysts after reduction

Catalyst	Ce/Zr ratio	Ni-load[a] (wt.%)	BET surface area ($m^2\ g^{-1}$)	Ni-reducibility[b] (Ni%)	Ni-dispersion[c] (Ni%)
Ni/CeO_2		4.8	8.5	84.7	3.17
Ni/Ce–ZrO_2	1/3	5.0	20	90.4	4.24
Ni/Ce–ZrO_2	1/1	4.7	18	89.8	4.13
Ni/Ce–ZrO_2	3/1	4.8	19	88.1	4.37
Ni/Al_2O_3		4.9	40	92.1	4.87

[a] Measured from X-ray fluorescence analysis.
[b] Measured from temperature-programmed reduction (TPR) with 5% hydrogen.
[c] Measured from temperature-programmed desorption (TPD) of hydrogen after TPR measurement.

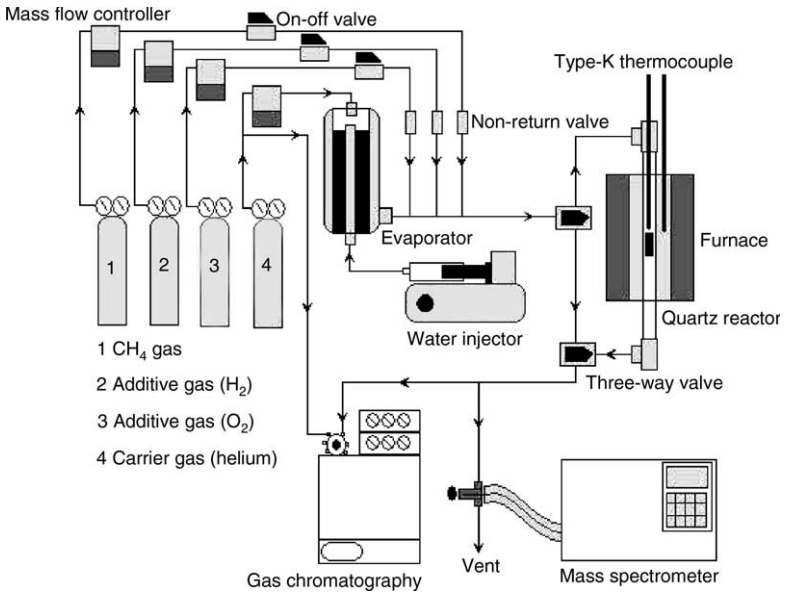

Fig. 1. Schematic diagram of the experimental set-up.

addition to the TPO method, the amount of carbon deposition was confirmed by calculating the carbon balance of the system. The amount of carbon formation would theoretically be equal to the difference between the inlet carbon containing component (CH_4) and the outlet carbon containing components (CO, CH_4, and CO_2). The amount of carbon deposited per gram of catalyst is calculated by the following equation:

$$C_{\text{deposition}} = \frac{\text{mole}_{\text{carbon(in)}} - \text{mole}_{\text{carbon(out)}}}{m_{\text{catalyst}}} \quad (8)$$

3. Results

3.1. Preliminary testing

In order to avoid any limitations by intraparticle diffusion, we checked the impact of the total flow rate before the formal investigations. The total flow rate was varied between 20 and 200 $cm^3\,min^{-1}$ under a constant residence time of 5×10^{-4} g min cm^{-3}. When the total flow rate was below 60 $cm^3\,min^{-1}$, the methane steam reforming rate increased with increasing the gas flow rate, suggesting that the mass transfer between the bulk gas and the catalyst particles is the rate-determining step. The steam reforming rate was almost constant in the range where the gas flow rate was higher than 80 $cm^3\,min^{-1}$, indicating that the mass transfer effect is unimportant in this flow rate range. The total flow rate was therefore kept constant at 100 $cm^3\,min^{-1}$ in all experiments. Fig. 2 shows the effect of the total gas flow rate on the reforming rate over Ni/Ce–ZrO_2.

The reactions on different average sizes (from 100 to 500 μm) of catalysts were carried out in order to guarantee that the experiments were carried out within the region of intrinsic kinetics. It was observed that there were no significant changes in the methane conversion for the catalyst with the particle size between 100 and 200 μm, which indicated that the intraparticle diffusion limitation was negligible in this range of operating conditions. Consequently, the catalyst diameter was kept between 100 and 200 μm in all experiments. Using these conditions, the steam reforming rate observed from the experiments should represent the intrinsic kinetics.

3.2. Stability and activity of Ni/Ce–ZrO_2 with different Ce/Zr ratios toward methane steam reforming

The steam reforming of methane over Ni/CeO_2 and Ni/Ce–ZrO_2 (with different Ce/Zr ratios) were studied at 900 °C by introducing CH_4/H_2O in helium with the inlet ratio of 1.0/1.0 in order to select the most suitable catalyst for further studies. The variations in methane conversion with time at

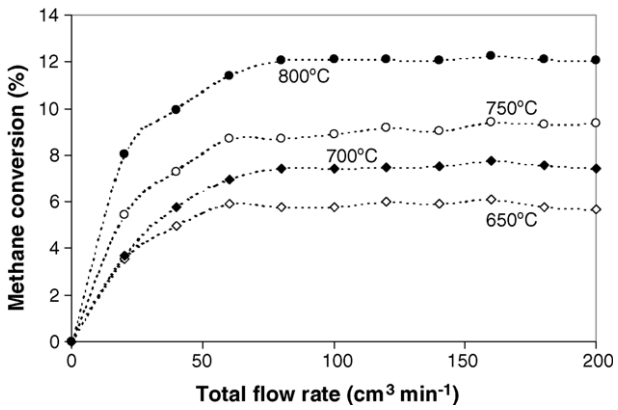

Fig. 2. Effect of the total gas flow rate on the reforming rate over Ni/Ce–ZrO_2 at different temperatures (3 kPa CH_4, 3 kPa H_2O).

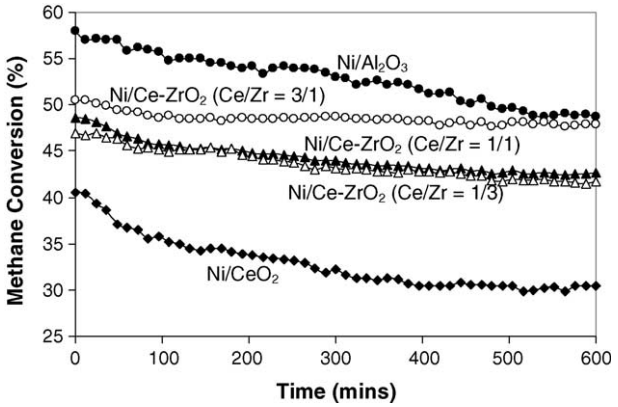

Fig. 3. Steam reforming of methane at 900 °C for different catalysts (3 kPa CH_4, 3 kPa H_2O).

900 °C for different catalysts are shown in Fig. 3. At steady state, the Ni/Ce–ZrO_2 with Ce/Zr ratio of 3/1 shows the best activity among Ni on ceria-based supports, its activity on a weight basis was slightly lower than that over Ni/Al_2O_3 due to the lower specific surface area. The steady state reforming rates of Ni/Ce–ZrO_2 (Ce/Zr = 3/1) and Ni/Al_2O_3 at 900 °C were 81.31 and 82.77 mol kg^{-1} h^{-1}, respectively.

As one can see from Fig. 3, the activities of Ni/Al_2O_3 and Ni/CeO_2 declined with time before reaching a significantly lower steady-state rate, while the activity of Ni/Ce–ZrO_2 declined slightly. Catalyst stabilities expressed as a deactivation percentage are given in Table 2. The post-reaction temperature-programmed oxidation (TPO) experiments were carried out after a helium purge by introducing 10% oxygen in helium in order to determine whether the observed deactivation is due to the carbon formation. TPO experiments detected no carbon formation on the surface of Ni on ceria-based supports. In contrast, the carbon species were observed on the surface of Ni/Al_2O_3. Using a value of 0.026 nm^2 for the area occupied by a carbon atom in a surface monolayer of the basal plane in graphite [27], the total quantities of carbon deposited formed on Ni/Al_2O_3 were 1.39 monolayers. This amount of carbon deposited was ensured by calculating the carbon balance of the system. Regarding the calculations, the molar amount of carbon deposited per gram of Ni/Al_2O_3 was 1.62 mmol g^{-1}. By the same assumption for the area occupied by a carbon atom [18], these values are equal to 1.37 monolayers, which is in good agreement with the value observed from the TPO method. More investigations about resistance toward carbon formation will be presented in the next section.

The BET measurement results as shown in Table 2 suggest that the deactivation of Ni on ceria-based supports could be mainly due to the sintering and the slight decrease of the catalyst dispersion. The % size reduction of these catalysts agreed well with the degree of catalyst deactivation. Regarding these experimental results, Ni/Ce–ZrO_2 with a Ce/Zr ratio of 3/1 was selected for further investigations.

3.3. Resistance toward carbon formation

The resistance of Ni/Ce–ZrO_2 (with Ce/Zr ratio of 3/1) toward the formation of carbon species was investigated and compared to that of Ni/Al_2O_3. Carbon species were firstly formed on the catalyst surface by introducing 5% methane in helium (TPMA). The amount of carbon formation on the surface of each catalyst was then investigated by temperature-programmed oxidation (TPO). Figs. 4 and 5 present the comparison of TPMA and TPO respectively over both Ni/Ce–ZrO_2 and Ni/Al_2O_3.

According to Fig. 4, only hydrogen was produced from the cracking of methane on Ni/Al_2O_3, whereas carbon monoxide and carbon dioxide were also generated along with hydrogen from the cracking of methane on Ni/Ce–ZrO_2. The formations of CO and CO_2 are due to the gas-solid reaction of CH_4 on Ce–ZrO_2 surface (Eq. (5)). After the system was purged with helium, the amount of carbon formation on the surface of each catalyst can be determined by measuring the CO and CO_2 yield from TPO experiment (Fig. 5). Using a value of 0.026 nm^2 for the area occupied by a carbon atom in a surface monolayer of the basal plane in graphite [27], the quantities of carbon deposited on the surface of Ni/Ce–ZrO_2 were approximately 1.29 monolayers, whereas the quantities of carbon deposited over Ni/Al_2O_3 were 2.35 monolayers. Regarding the calculation of carbon balance, the values of carbon deposited from the calculation are also in good agreement with the values observed from the TPO (1.31 monolayers for Ni/Ce–ZrO_2, and 2.34 monolayers for Ni/Al_2O_3).

When a small amount of steam was added during TPMA, the amount of carbon formation was observed to decrease significantly as the steam reforming takes place. The requirements of inlet steam to eliminate all carbon formation on the surface of Ni/Ce–ZrO_2 and Ni/Al_2O_3 were compared, as presented in Table 3. Ni/Ce–ZrO_2 required inlet H_2O/CH_4 ratio of 1.0 in order to prevent the formation of carbon species on catalyst surface, whereas Ni/Al_2O_3 required a higher H_2O/

Table 2
Catalyst deactivations and some characterization results after running the reaction at 900 °C for 10 h

Catalyst	Ce/Zr ratio	Deactivation (%)	BET after reaction (m^2 g^{-1})	Surface area reduction (%)	Ni-load (wt.%)	Ni-dispersion (Ni%)
Ni/CeO_2		24	6.2	27	4.8	3.02
Ni/Ce–ZrO_2	1/3	11	18	10	4.9	4.21
Ni/Ce–ZrO_2	1/1	12	15	13	4.7	4.12
Ni/Ce–ZrO_2	3/1	5.1	18	4.5	4.8	4.32
Ni/Al_2O_3		16	40	~0	4.8	4.80

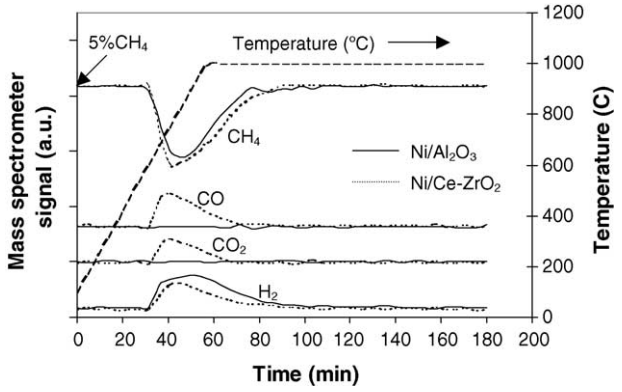

Fig. 4. Temperature-programmed methane adsorption (TPMA) of Ni/Ce–ZrO_2 (5 kPa CH_4).

CH_4 ratio to reduce the carbon formation. According to the table, the minimum requirement of inlet H_2O/CH_4 ratio to avoid the carbon formation for Ni/Al_2O_3 is 3.0.

3.4. Intrinsic reaction kinetic studies

3.4.1. Effects of temperature and methane

The inlet methane partial pressure was varied from 1 to 4 kPa, while the inlet steam was kept constant at 9 kPa. The operating temperature range was 650–850 °C. At steady state, the main products from this reaction were H_2 and CO with a small amount of CO_2, indicating a small contribution from the water–gas shift reaction, Eq. (2), and the reverse methanation (Eq. (3)). Fig. 6 showed the influences of temperature on the $CO/(CO + CO_2)$ production selectivity for both Ni/Ce–ZrO_2 and Ni/Al_2O_3. This selectivity increased with increasing operating temperature. At the same temperature, this selectivity for Ni/Al_2O_3 was observed to be higher than that over Ni/Ce–ZrO_2, which is due to the lower reactivity toward the water–gas shift reaction of Ni/Al_2O_3. The water–gas shift reaction (WGS) for each support was tested in order to ensure the influence of this reaction by using TPRx in CO/H_2O/He gas mixture (5 kPa CO, and 10 kPa H_2O). Fig. 7 shows the activities of

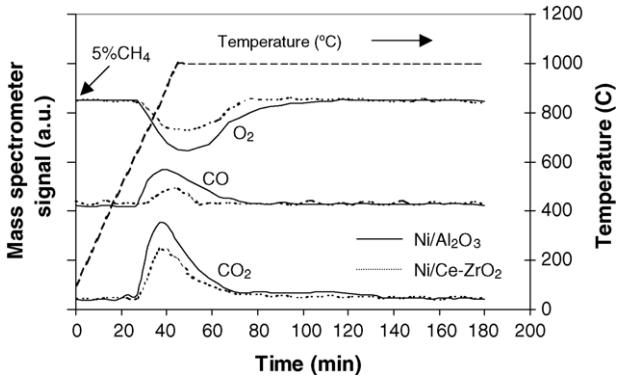

Fig. 5. Temperature-programmed oxidation (TPO) of Ni/Ce–ZrO_2 (10 kPa O_2).

Table 3
The dependence of inlet H_2O/CH_4 ratio on the amount of carbon formation remaining on the catalyst surface (calculated from CO and CO_2 yields during TPO)

H_2O/CH_4 ratio	Total carbon formation (monolayers)	
	Ni/Ce–ZrO_2	Ni/Al_2O_3
0	1.29[a] (1.31)[b]	2.35 (2.34)
0.2	0.47 (0.45)	2.26 (2.28)
0.4	0.39 (0.39)	1.97 (1.99)
0.6	0.21 (0.24)	1.66 (1.61)
0.8	0.11 (0.09)	1.33 (1.30)
1.0	~0 (0.005)	0.79 (0.81)
2.0	~0 (~0)	0.30 (0.27)
3.0	~0 (~0)	~0 (0.01)

[a] Calculated using CO and CO_2 yields from temperature-programmed oxidation (TPO) with 10% oxygen.
[b] Calculated from the balance of carbon in the system.

both supports toward this reaction. Clearly, the activity toward this reaction over Ce–ZrO_2 was significantly higher than that over Al_2O_3 at the same operating conditions.

Fig. 8 illustrates the influence of the inlet methane partial pressure on the turnover frequencies (N) for methane steam reforming over Ni/Ce–ZrO_2 at different operating temperatures. Turnover frequencies were calculated from the methane conversion following the given equation by assuming that all surface sites accessible by nitrogen adsorption (area per molecule 16.2×10^{-20} m^2 [40]) were active:

$$N = \frac{rN_A A_{N_2}}{m_c S} \tag{9}$$

Here r is the moles CH_4 per unit time, N_A the Avogadro's number, A_{N_2} the area occupied by an adsorbed nitrogen molecule (16.2×10^{-20} m^2), m_c the weight of catalyst used (50 mg), and S is the specific surface area of the catalyst (18 m^2 g^{-1}). The activities of each catalyst increased with increasing inlet methane partial pressure as well as operating temperature. Fig. 9 shows an Arrhenius-type plot for methane steam reforming over Ni/Ce–ZrO_2 with various

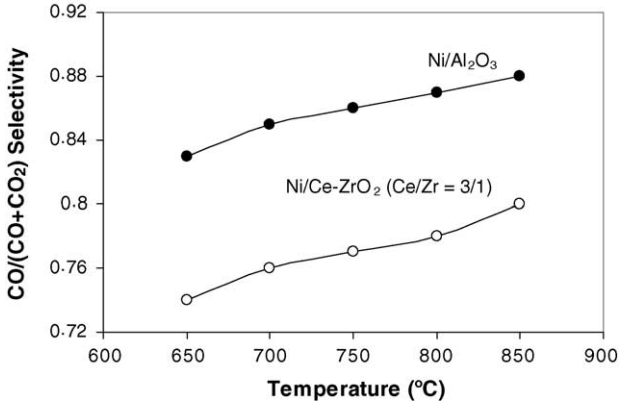

Fig. 6. Influence of temperature on $CO/(CO + CO_2)$ selectivity from methane steam reforming over Ni/Ce–ZrO_2 and Ni/Al_2O_3 (3 kPa CH_4, 9 kPa H_2O).

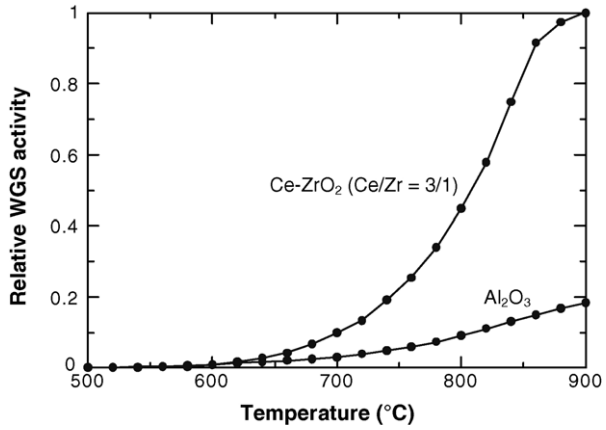

Fig. 7. The activities of Ce–ZrO_2 and Al_2O_3 toward the water-gas shift reaction using TPRx in CO/H_2O/He gas mixture (5 kPa CO, and 10 kPa H_2O).

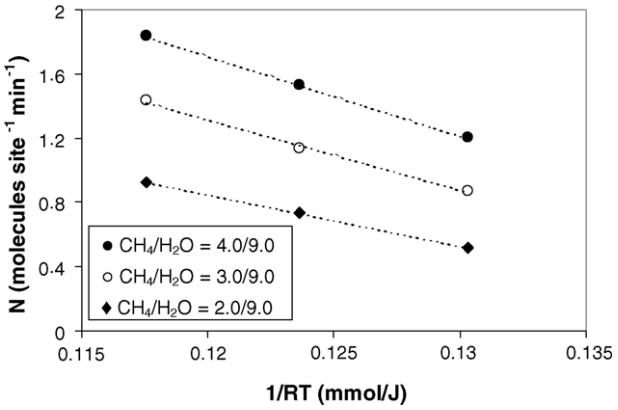

Fig. 9. Arrhenius plot of turnover frequencies (N) for methane steam reforming over Ni/Ce–ZrO_2 (Ce/Zr = 3/1) with different inlet methane/steam ratios.

methane/steam ratios over the temperature range of 650–750 °C. The corresponding activation energy observed for this catalyst is 142 ± 15 kJ mol^{-1}, slightly depending on the gas composition. The composition-dependence of activation energies from the Arrhenius plots has often been observed. The literature values, reviewed by Pointon [41] and Dicks et al. [39], were reported to be 35–287 and 154–253 kJ mol^{-1}, respectively.

The reaction orders in methane for both catalysts were observed to be 1.0 in all conditions. These values (n) were obtained experimentally by plotting $\ln(N)$ versus $\ln P_{CH_4}$ according to the equation below:

$$\ln(N) = \ln(k) + n(\ln P_{CH_4}) \quad (10)$$

The reaction order in methane seemed to be independent of the operating temperature in the range of conditions studied. By varying inlet steam partial pressure (9, 12, and 15 kPa) and adding hydrogen (1, 3, and 5 kPa), we found that the reaction order in methane was also independent of both components in this range of conditions.

3.4.2. Effect of hydrogen

Several inlet hydrogen concentrations (1–18 kPa) were added to the methane/steam in order to investigate the influence of this component on the steam reforming rate. Firstly, the inlet hydrogen partial pressure was varied from 0 to 5 kPa, while the inlet methane and steam partial pressure were kept constant at 3 and 9 kPa, respectively. In this range of conditions, hydrogen promoted the methane conversion as shown in Fig. 10. The reaction orders in hydrogen for Ni/Ce–ZrO_2 at this range of conditions studied were observed to be positive values between 0.18 and 0.20, while the reaction order in hydrogen for Ni/Al_2O_3 was in the range of 0.28–0.34. These values seemed to be independent of the inlet methane partial pressure and the operating temperature. However, they depended on the inlet steam partial pressure. The reaction order in hydrogen became slightly higher with increasing inlet steam partial pressure. This result is in good agreement with Dicks et al. [39] Fig. 11 showed the influences of hydrogen on the CO/(CO + CO_2) production selectivity. This selectivity increased with increasing inlet hydrogen partial pressure due to the promotion of the reverse water–gas shift reaction.

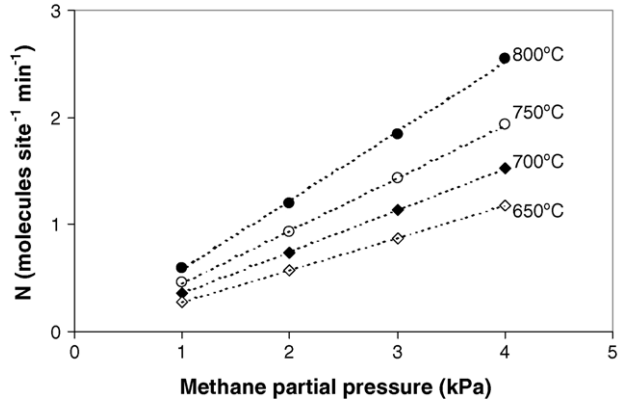

Fig. 8. Effect of methane partial pressure on the turnover frequencies (N) for steam reforming over Ni/Ce–ZrO_2 (Ce/Zr = 3/1) at different temperatures (9 kPa inlet H_2O).

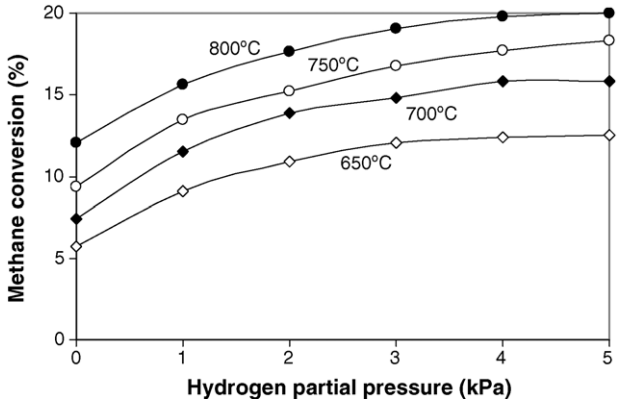

Fig. 10. Effect of hydrogen partial pressure on steam reforming rate over Ni/Ce–ZrO_2 (Ce/Zr = 3/1) at different temperatures (3 kPa CH_4, 9 kPa H_2O).

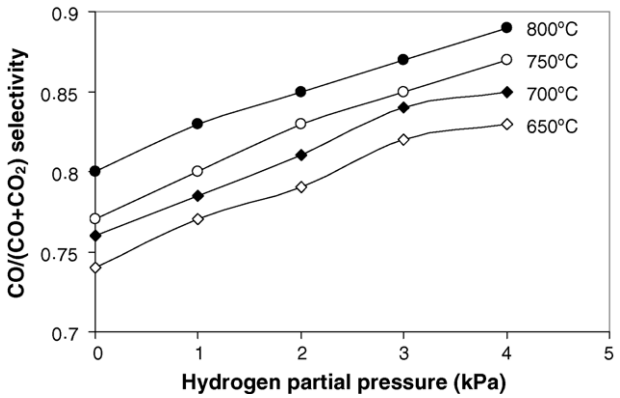

Fig. 11. Influence of hydrogen addition on CO/(CO + CO_2) selectivity from methane steam reforming over Ni/Ce–ZrO_2 at different temperatures (3 kPa CH_4, 9 kPa H_2O).

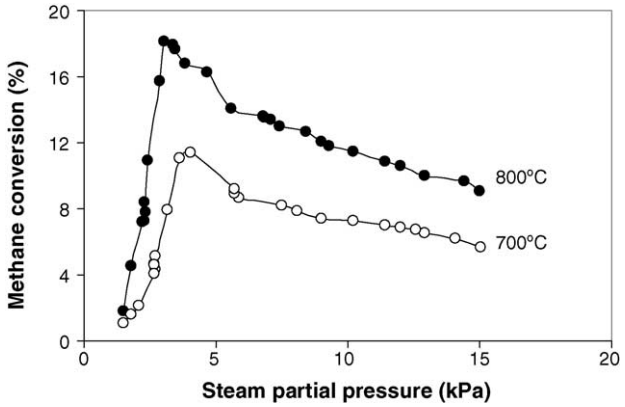

Fig. 13. Effect of steam partial pressure on steam reforming rate over Ni/Ce–ZrO_2 (Ce/Zr = 3/1) at 700 and 800 °C (3 kPa CH_4).

The steam reforming rates at higher inlet hydrogen partial pressures were then measured. The experiments yielded a non-linear positive hydrogen trend. When the inlet hydrogen partial pressure was greater than 8 kPa, the hydrogen influence on the steam reforming rate became much less pronounced. Moreover, the decrease in methane conversion was observed when the inlet hydrogen partial pressure was greater than 10 kPa (Fig. 12). Clearly, the negative effect of hydrogen for Ni/Ce–ZrO_2 was observed to be much stronger than that over Ni/Al_2O_3.

3.4.3. Effect of steam

In order to investigate the effect of inlet H_2O/CH_4 ratio on the steam reforming rate, this ratio was varied from 0.5 to 5.0 by changing the inlet steam partial pressure from 1.5 to 15 kPa. Two temperature levels of 700 and 800 °C were considered. As shown in Fig. 13, the dependence of steam on the rate of reforming is non-monotonic. The steam reforming rate increased with increasing inlet H_2O/CH_4 ratio until this ratio reached approximately 1.0–2.0. Then, steam presented a negative effect on the reforming rate at higher inlet H_2O/CH_4 ratio values. At the inlet H_2O partial pressure of 5–15 kPa, the reaction order related to steam decreased from −0.40 to −0.31 and −0.25 when the inlet hydrogen partial pressure increased from 0 to 1 and 2 kPa, respectively. This could be due to the decrease in the catalyst's oxidized state caused by a small addition of inlet hydrogen.

Unlike the effect of hydrogen, the reaction order in steam for the methane steam reforming over Ni/Al_2O_3 was close to that over Ni/Ce–ZrO_2 at the same operating conditions, indicating the same influence of steam on both Al_2O_3 and Ce–ZrO_2. This result was supported by the works of Laosiripojana [42], who reported the independence of inlet steam partial pressure on the methane steam reforming rate over ceria-based materials. Fig. 14 shows the influences of steam on the CO/(CO + CO_2) production selectivity. This selectivity decreased with increasing inlet steam partial pressure due to the promotion of the water–gas shift reaction in the forward direction. Table 4 presents the summary of observed reaction orders in each component (CH_4, H_2O, and H_2) for both Ni/Ce–ZrO_2 and Ni/Al_2O_3 at different temperatures and inlet compositions.

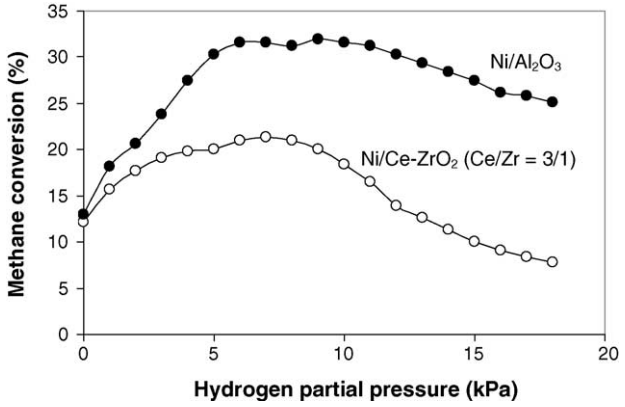

Fig. 12. Effect of hydrogen partial pressure on steam reforming rate over Ni/Ce–ZrO_2 (Ce/Zr = 3/1) and Ni/Al_2O_3 at high presence of hydrogen (0–18 kPa) at 800 °C.

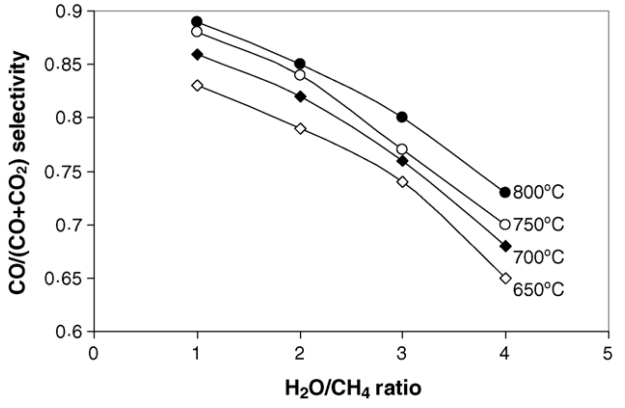

Fig. 14. Influence of inlet steam/methane ratio on CO/(CO + CO_2) selectivity from methane steam reforming over Ni/Ce–ZrO_2 at different temperatures (3 kPa CH_4).

Table 4
Reaction orders for the components of interest (CH_4, H_2O, and H_2) from methane steam reforming over Ni/Ce–ZrO_2 (Ce/Zr = 3/1) and Ni/Al_2O_3 at different operating conditions

Components of interest	Temperature (°C)	Other inlet compositions	Reaction order for components of interest	
			Ni/Ce–ZrO_2 (Ce/Zr = 3/1)	Ni/Al_2O_3
Methane (1–4 kPa)	650–800	9 kPaH_2O/0 kPaH_2	1.0 ± 0.04	1.0 ± 0.01
		12 kPa H_2O/0 kPa H_2	1.0 ± 0.05	1.0 ± 0.01
		15 kPaH_2O/0 kPa H_2	1.0 ± 0.02	1.0 ± 0.02
		9 kPaH_2O/1 kPa H_2	1.0 ± 0.02	1.0 ± 0.01
		9 kPa H_2O/3 kPa H_2	1.0 ± 0.01	1.0 ± 0.03
		9 kPaH_2O/5 kPa H_2	1.0 ± 0.03	1.0 ± 0.01
Hydrogen (1–4 kPa)	650	9 kPa H_2O/3 kPa CH_4	0.18	0.31
	700	9 kPa H_2O/3 kPa CH_4	0.20	0.28
	750	9 kPaH_2O/3 kPa CH_4	0.18	0.34
	800	9 kPa H_2O/3 kPa CH_4	0.19	0.33
	700	9 kPaH_2O/1 kPa CH_4	0.18	0.29
	700	9 kPa H_2O/5 kPa CH_4	0.20	0.32
	700	12 kPa H_2O/3 kPa CH_4	0.25	0.39
	700	15 kPa H_2O/3 kPa CH_4	0.28	0.42
Hydrogen (12–18 kPa)	650	9 kPaH_2 O/3 kPa CH_4	−0.31	−0.15
	700	9 kPa H_2O/3 kPa CH_4	−0.30	−0.16
	800	9 kPa H_2O/3 kPaCH_4	−0.34	−0.15
Steam (5–15 kPa)	650	0 kPa H_2/3 kPaCH_4	−0.39	−0.37
	700	0 kPa H_2/3 kPa CH_4	−0.40	−0.39
	750	0 kPa H_2/3 kPa CH_4	−0.38	−0.41
	800	0 kPaH_2/3 kPaCH_4	−0.42	−0.40
	700	1 kPa H_2/3 kPaCH_4	−0.31	−0.31
	700	2 kPaH_2/3 kPaCH_4	−0.25	−0.24
	700	3 kPa H_2/3 kPa CH_4	−0.22	−0.19

3.4.4. *Effect of oxygen*

As described earlier, autothermal reforming seems to be a promising reaction in order to produce hydrogen in the near future, as it is currently the most economical process. Methane steam reforming in the presence of oxygen or the autothermal reforming was then carried out by adding different oxygen partial pressures into the feed gas at several operating temperatures. The inlet methane and steam partial pressures were kept constant at 3 and 9 kPa, respectively, while the inlet oxygen partial pressure was varied from 0 to 4 kPa. At steady state, the methane steam reforming rate increased with increasing the inlet oxygen partial pressure as shown in Fig. 15. However, the CO/(CO + CO_2) production selectivity strongly decreased with increasing oxygen concentration due to the CO oxidation by O_2, as shown in Fig. 16. Hydrogen production also decreased with increasing oxygen concentration as shown in Fig. 17, which could be due to the inhibition of steam adsorption on the catalyst surface active sites by this component and also due to the combustion of H_2 production by inlet O_2.

4. Discussion

The steam reforming of methane over synthesized Ni/Ce–ZrO_2 was compared to conventional Ni/Al_2O_3 in the conditions where the influences of mass and heat transfer limitations could be considered negligible. Improvement of methane steam reforming performance in term of stability toward the deactivation by carbon deposition was achieved for Ni/Ce–ZrO_2. Compared to conventional Ni/Al_2O_3, Ni on Ce–ZrO_2 support provided higher resistance toward carbon formation and required significantly lower inlet H_2O/CH_4 ratio to prevent the formation of carbon species. These improvements are mainly related to the high redox property of Ce–ZrO_2 support.

Regarding the well known methane steam reforming mechanism over conventional Ni catalyst proposed by Dicks et al. [39], methane only adsorbs on the active surface site of Ni (*) and forms CH_x-*n. Simultaneously, the adsorption of

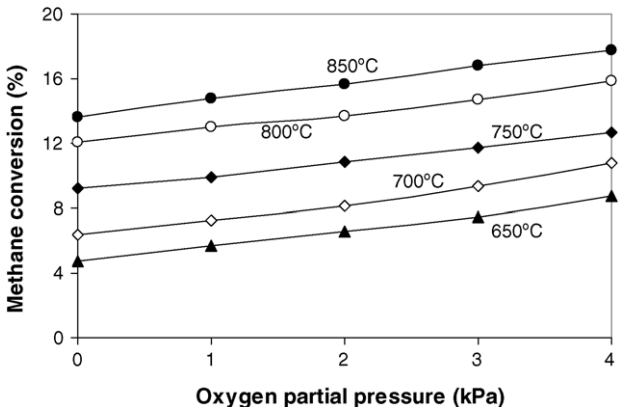

Fig. 15. Effect of oxygen partial pressure on steam reforming rate over Ni/Ce–ZrO_2 (Ce/Zr = 3/1) at different temperatures (3 kPa CH_4, 9 kPa H_2O).

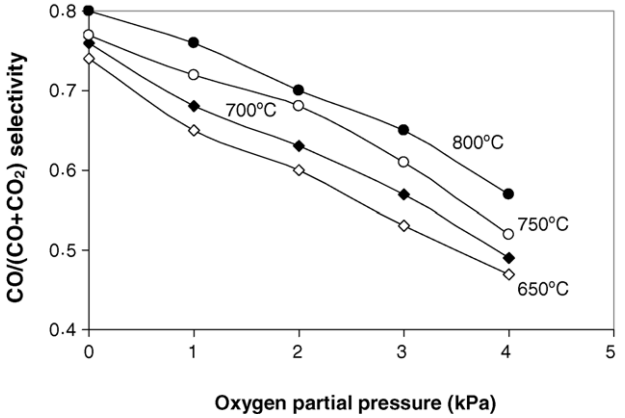

Fig. 16. Influence of oxygen addition on CO/(CO + CO_2) selectivity from methane steam reforming over Ni/Ce–ZrO_2 at different temperatures (3 kPa CH_4, 9 kPa H_2O).

inlet steam also takes place on the surface sites of Ni catalyst, forming O-*. These elements, O-* and CH_x-*n, eventually react with each other, producing CO and H_2, and the active surface site of Ni (*) also recovers as illustrated below:

$$CH_4 + n^* \rightarrow CH_x\text{-}*n + (4-x)/2H_2 \quad (11)$$

$$H_2O + * \Leftrightarrow O\text{-}* + H_2 \quad (12)$$

$$CH_x\text{-}*n + O\text{-}* \rightarrow CO + (x/2)H_2 + (n+1)^* \quad (13)$$

For the steam reforming of methane over Ni/Ce–ZrO_2, in addition to the reactions on Ni surface, the redox reaction between inlet CH_4 and the lattice oxygen (O_x) on Ce–ZrO_2 surface also takes place, producing H_2 and CO (Eq. (5)). Moreover, the reduced Ce–ZrO_2 can react with inlet H_2O to produce more H_2 and to recover O_x [42]. The proposed mechanism for these redox reactions, involving the reactions between methane and/or an intermediate surface hydrocarbon species with the lattice oxygen (O_x) on Ce–ZrO_2 surface and the recovery of O_x by steam, is presented

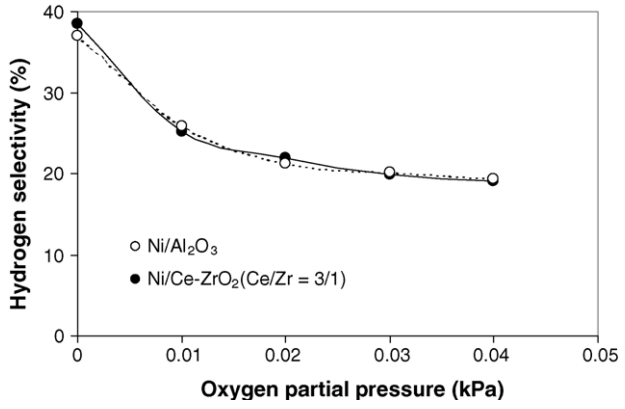

Fig. 17. Effect of oxygen on hydrogen selectivity (%) from methane steam reforming over Ni/Ce–ZrO_2 at 800 °C (3 kPa CH_4, 9 kPa H_2O).

schematically below:

$$CH_4 + 2S \Leftrightarrow CH_3\text{–}S + H\text{–}S \quad (14)$$

$$CH_3\text{–}S + S \Leftrightarrow CH_2\text{–}S + H\text{–}S \quad (15)$$

$$CH_2\text{–}S + S \Leftrightarrow CH\text{–}S + H\text{–}S \quad (16)$$

$$CH\text{–}S + S \Leftrightarrow C\text{–}S + H\text{–}S \quad (17)$$

$$C\text{–}S + O_x \Leftrightarrow CO + O_{x-1} + S \quad (18)$$

$$CO + O_x \Leftrightarrow CO_2 + O_{x-1} \quad (19)$$

$$2H\text{–}S \Leftrightarrow H_2 + 2S \quad (20)$$

$$H_2O + O_{x-1} \Leftrightarrow O_x + H_2 \quad (21)$$

The surface site (S) can be either a unique site, or it can also be considered to be the same site as the catalyst-oxidised site (O_x) [42]. It has been reported [43] that the controlling step of these redox reactions is the reaction of methane on the Ce–ZrO_2 surface; in addition, the lattice oxygen is replenished by a significant rapid surface reaction of the reduced state Ce–ZrO_2 with H_2O.

According to the possible formation of carbon species on the surface of catalyst during the steam reforming process, the following reactions are theoretically the most probable reactions that could lead to carbon formation:

$$2CO = CO_2 + C \quad (22)$$

$$CH_4 = 2H_2 + C \quad (23)$$

$$CO + H_2 = H_2O + C \quad (24)$$

$$CO_2 + 2H_2 = 2H_2O + C \quad (25)$$

C is the carbonaceous deposits. Reactions (24) and (25) are favorable at low temperature, while reaction (22) is thermodynamically unfavored [44]. At such a high temperature, the Boudard reaction (Eq. (22)) and the decomposition of methane (Eq. (23)) are the major pathways for carbon formation, as they show the largest change in Gibbs energy [45]. According to the range of temperature in this study, carbon formation would be formed via the decomposition of methane and Boudard reactions, especially at low inlet H_2O/CH_4 ratio. In the present work, we also observed a high amount of carbon formation on the surface of Ni/Al_2O_3 after exposure in methane steam reforming condition with the inlet H_2O/CH_4 ratio less than 3.0. By applying Ce–ZrO_2 as support, the formation of carbon species via Eqs. (22) and (23) could be inhibited by the redox reactions of methane and carbon monoxide (produced during the steam reforming process) with the lattice oxygen (O_x) at Ce–ZrO_2 surface (Eqs. (14)–(19)) forming hydrogen and carbon dioxide, which is thermodynamically unfavored to form carbon species in this range of conditions. Therefore, significant lower amounts of carbon deposition were consequently observed for Ni/Ce–ZrO_2 even at low inlet H_2O/CH_4 ratios. In addition, the reaction between the lattice oxygen (O_x) at

Ce–ZrO_2 surface with the adsorbed methane on Ni surface (CH_x-*n) and the rapid recovery of the lattice oxygen by the simultaneous supply of oxygen from H_2O also result in the higher resistance toward carbon formation and less inlet H_2O/CH_4 requirement for Ni/Ce–ZrO_2:

$$CH_x\text{-}*n + O_x \rightarrow CO + (x/2)H_2 + n^* + O_{x-1} \quad (26)$$

Many previous researchers have reported the excellent resistance toward carbon formation from methane cracking at high temperature for ceria-based materials including CeO_2 [27], Gd-doped CeO_2 [27], Nb-CeO_2 [46], and CeO_2-ZrO_2 [42]. One of them [42] also proposed that the addition of a small amount of H_2O to the inlet feed can eliminate all carbon species on the surface of CeO_2. The previous reports therefore agree well with the results in this work.

Regarding the kinetic studies over Ni/Ce–ZrO_2 in the present work, similar to the general metal catalysts as reported by previous researchers, the reaction orders in methane were observed to be approximately 1.0 in all conditions. The experiments yielded a non-linear positive hydrogen trend over this catalyst (Fig. 12). The positive effect at the low hydrogen appearance could be due to the reduction of oxidized state on the surface active site of nickel ($H_2 + O\text{-}* \Leftrightarrow H_2O + *$), while the inhibitory effect at high hydrogen partial pressure could be due to the promotion of the methanation, the reverse water–gas shift reactions and the reverse methane steam reforming [4-6]. In addition, the occupying of hydrogen atoms on some active sites of nickel particles ($H_2 + 2^* \Leftrightarrow 2H\text{-}*$) could also lead to the decrease in methane conversion, as explained by Xu and Froment [4–6].

Clearly, the negative effect of hydrogen for Ni/Ce–ZrO_2 was observed to be much stronger than that over Ni/Al_2O_3. This is due to the reduction of lattice oxygen (O_x) by hydrogen via the reverse of Eq. (21) ($O_x + H_2 \Leftrightarrow H_2O + O_{x-1}$) and consequently inhibits the reaction of the lattice oxygen (O_x) with the surface hydrocarbon species (both C–S and CH_x-n) in Eqs. (18) and (26) (C–S + $O_x \Leftrightarrow$ CO + O_{x-1} + S and CH_x-*n + $O_x \rightarrow$ CO + (x/2)H_2 + n^* + O_{x-1}). This explanation is in good agreement with the previous studies [42,43,46] which studied kinetics parameters for the methane steam reforming on ceria-based materials and reported the negative effect of hydrogen on methane conversion over these materials due to the change of Ce^{4+} to Ce^{3+}.

The dependence of steam on the rate of reforming is non-monotonic due to adsorption competition between CH_4 and H_2O on the catalyst active sites. Previous works [4,5] also reported the same results and explanation on Ni/ZrO_2. Furthermore, the study of autothermal reforming over this catalyst found that methane steam reforming rate increased with increasing the inlet oxygen partial pressure. However, the CO/(CO + CO_2) production selectivity and hydrogen production rates strongly decreased with increasing oxygen partial pressure. This is due to the inhibition of steam adsorption on the catalyst surface active sites and the oxidation of hydrogen by oxygen in the feed.

5. Conclusion

Methane steam reforming over Ni catalyst supported on Ce–ZrO_2 was studied at 650–900 °C in the conditions where the influence of mass transfer limitations could be considered negligible. At 900 °C, Ni/Ce–ZrO_2 with Ce/Zr ratio of 3/1 showed the best performance in term of activity and stability. The resistance toward carbon formation over this catalyst was higher than that over conventional Ni/Al_2O_3 at the same operating conditions regarding its high redox property; however, slight deactivation due to the sintering was observed over Ni/Ce–ZrO_2 at these high temperature conditions.

Similar to the conventional Ni/Al_2O_3, the reaction order in methane for Ni/Ce–ZrO_2 was always observed to be 1.0. The dependence of steam on the rate was non-monotonic, and the addition of oxygen promoted the rate but reduced CO and H_2 production selectivity. At high hydrogen appearance, Ni/Ce–ZrO_2 showed a stronger negative impact of hydrogen compared to Ni/Al_2O_3, due to the possible reduction of Ce–ZrO_2. This strong negative effect of hydrogen would be a major concern in applying Ni/Ce–ZrO_2 industrially. Although Ni/Ce–ZrO_2 is a good reforming catalyst in term of the high resistance toward the carbon formation, methane conversion could be significantly reduced at high hydrogen appearance, and the removal of hydrogen during the reforming process might be required.

Acknowledgements

The financial support from The Thailand Research Fund (TRF) throughout this project is gratefully acknowledged. The first author would like to acknowledge Professor David Chadwick from the Department of Chemical Engineering and Chemical Technology, Imperial College London, for his valuable suggestions.

References

[1] K. Otsuka, T. Ushiyama, I. Yamanaka, Chem. Lett. (1993) 1517.
[2] K. Otsuka, M. Hatano, A. Morikawa, J. Catal. 79 (1983) 493.
[3] K. Otsuka, M. Hatano, A. Morikawa, Inorg. Chim. Acta 109 (1985) 193.
[4] J. Xu, PhD Thesis, Laboratorium Voor Petrochemische Techniek, Rijkuniversiteit, Gent, Belgium, 1986.
[5] J. Xu, G.F. Froment, AIChE 35 (1989) 88.
[6] J. Xu, G.F. Froment, AIChE 35 (1989) 97.
[7] S.S.E.H. Elnashaie, A.M. Adris, A.S. Al-Ubaid, M.A. Soliman, Chem. Eng. Sci. 45 (1990) 491.
[8] S.S.E.H. Elnashaie, S.S. Elshishini, Modeling, Simulation and Optimization of Industrial Fixed Bed Catalytic Reactors, Gordon and Breach Science Publishers, UK, 1993.
[9] L.V. Mattos, E. Rodino, D.E. Resasco, F.B. Possos, F.B. Noronha, Fuel Proc. Technol. 83 (2003) 147.
[10] H.S. Roh, K.W. Jun, S.E. Park, Appl. Catal. A 251 (2003) 275.
[11] J.R. Rostrup-Nielsen, J.-H. Bak-Hansen, J. Catal. 144 (1993) 38.
[12] X. Wang, R.J. Gorte, Appl. Catal. A 224 (2002) 209.

[13] H.S. Roh, K.W. Jun, W.S. Dong, J.S. Chang, S.E. Park, Y.I. Joe, J. Mol. Catal. A 181 (2002) 137.
[14] Q. Miao, G. Xiong, S. Sheng, W. Cui, L. Xu, X. Guo, Appl. Catal. A 154 (1987) 17.
[15] A.A. Lemonidou, M.A. Goula, I.A. Vasalos, Catal. Today 46 (1987) 175.
[16] W.S. Dong, H.S. Roh, K.W. Jun, S.E. Park, Y.S. Oh, Appl. Catal. A 226 (2002) 63.
[17] M. Mamak, N. Coombs, G. Ozin, Adv. Mater. 12 (2000) 198.
[18] M. Mamak, N. Coombs, G. Ozin, J. Am. Chem. Soc. 122 (2000) 8932.
[19] M. Mamak, N. Coombs, G.A. Ozin, Chem. Mater. 13 (2001) 3564.
[20] P. Bera, S. Mitra, S. Sampath, M.S. Hegde, Chem. Commun. (2001) 927.
[21] A. Martinez-Arias, J.M. Coronado, R. Cataluna, J.C. Conesa, J.C. Soria, J. Phys. Chem. B 102 (1998) 4357.
[22] D. Skarmoutsos, F. Tietz, P. Nikolopoulos, Fuel Cells 1 (2001) 243.
[23] T. Takeguchi, S.N. Furukawa, M. Inoue, J. Catal. 202 (2001) 14.
[24] J. Sfeir, P.A. Philippe, P. Moseki, N. Xanthopoulos, R. Vasquez, J.M. Hans, V.H. Jan, K.R. Thampi, J. Catal. 202 (2001) 229.
[25] N. Kiratzis, P. Holtappels, C.E. Hatchwell, M. Mogensen, J.T.S. Irvine, Fuel Cells 1 (2001) 211.
[26] H.S. Roh, W.S. Dong, K.W. Jun, S.E. Park, Chem. Lett. 88 (2001).
[27] E. Ramirez, A. Atkinson, D. Chadwick, Appl. Catal. B 36 (2002) 193.
[28] M. Ozawa, M. Kimura, A. Isogai, J. Alloys Compd. 193 (1993) 73.
[29] G. Balducci, J. Kaspar, P. Fornasiero, M. Graziani, M.S. Islam, J. Phys. Chem. B 102 (1998) 557.
[30] G. Vlaic, P. Fornasiero, S. Geremia, J. Kaspar, M. Graziani, J. Catal. 168 (1997) 386.
[31] G.R. Rao, J. Kaspar, S. Meriani, R. Dimonte, M. Graziani, Catal. Lett. 24 (1994) 107.
[32] P. Fornasiero, R. Dimonte, G.R. Rao, J. Kaspar, S. Meriani, A. Trovarelli, M. Graziani, J. Catal. 151 (1995) 168.
[33] M. Haneda, K. Miki, N. Kakuta, A. Ueno, S. Tani, S. Matsura, M. Sato, Nihon Kagaku Kaishi (1990) 820.
[34] T. Ohata, Rare Earths 17 (1990) 37.
[35] J.G. Nunan, W.B. Williamson, H.J. Robota, SAE Paper 960768, 1996.
[36] S. Otsuka-Yao, H. Morikawa, N. Izu, K. Okuda, J. Jpn. Inst. Met. 59 (1995) 1237.
[37] M.H. Yao, T.E. Hoost, R.J. Baird, F.W. Kunz, J. Catal. 166 (1997) 67.
[38] D. Kim, J. Am. Ceram. Soc. 72 (1989) 1415.
[39] A.L. Dicks, K.D. Pointon, A. Siddle, J. Power Sources 86 (2000) 523.
[40] P.A. Webb, C. Orr, Analytical Methods in Fine Particle Technology, Micromeritics Instrument Corporation, USA, 1997.
[41] K.D. Pointon, Review of Work on Internal Reforming in the Solid Oxide Fuel Cell, ETSU Report F/01/00121/REP, 1997.
[42] N. Laosiripojana, Reaction engineering of indirect internal steam reforming of methane for application in solid oxide fuel cells, PhD Thesis, University of London, UK, 2003.
[43] E. Ramírez-Cabrera, A. Atkinson, D. Chadwick, Appl. Catal. B 47 (2004) 127.
[44] Y. Lwin, W.R.W. Daud, A.B. Mohamad, Z. Yaakob, Int. J. Hydrogen Energy 25 (1) (2000) 47.
[45] J.N. Amor, Appl. Catal. A 176 (1999) 159.
[46] E. Ramírez-Cabrera, N. Laosiripojana, A. Atkinson, D. Chadwick, Catal. Today 78 (2003) 433.

Available online at www.sciencedirect.com
SCIENCE DIRECT
Applied Catalysis B: Environmental 60 (2005) 107–116
APPLIED CATALYSIS B: ENVIRONMENTAL
www.elsevier.com/locate/apcatb

Catalytic dry reforming of methane over high surface area ceria

N. Laosiripojana [a,*], S. Assabumrungrat [b]

[a] *The Joint Graduate School of Energy and Environment, King Mongkut's University of Technology Thonburi, Bangkok 10140, Thailand*

[b] *Center of Excellence on Catalysis and Catalytic Reaction Engineering, Department of Chemical Engineering, Chulalongkorn University, Bangkok 10330, Thailand*

Received 6 October 2004; received in revised form 28 February 2005; accepted 1 March 2005
Available online 31 March 2005

Abstract

High surface area ceria (CeO_2 (HSA)), synthesized by a surfactant-assisted approach, was found to have useful dry reforming activity for H_2 and CO production under solid oxide fuel cells (SOFCs) conditions. The catalyst provides significantly higher reforming reactivity and excellent resistance toward carbon deposition compared to Ni/Al_2O_3 and conventional low surface area ceria (CeO_2 (LSA)) under dry reforming conditions. These enhancements are due to the high redox property of CeO_2 (HSA). During the dry reforming process, the redox reactions between the gaseous components in the system and the lattice oxygen (O_x) take place on ceria surface. Among these reactions, the rapid redox reactions of carbon compounds such as CH_4, and CO with lattice oxygen ($CH_4 + O_x \rightarrow CO + H_2 + O_{x-1}$ and $CO + O_x = CO_2 + O_{x-1}$) can prevent the formation of carbon species from the methane decomposition and Boudard reactions even at low inlet carbon dioxide concentration.

In particular, the dry reforming rate over CeO_2 (HSA) is proportional to the methane partial pressure and the operating temperature. Carbon dioxide presents weak positive impact on the methane conversion, whereas both carbon monoxide and hydrogen inhibit the reforming rate. The activation energies and reforming rates under the same methane concentration for CeO_2 toward the dry reforming are almost equal to the steam reforming as previously reported [1–4]. This result suggests the similar reaction mechanisms for both the steam reforming and the dry reforming over CeO_2; i.e., the dry reforming rate is governed by the slow reaction of adsorbed methane, or surface hydrocarbon species, with oxygen in CeO_2, and a rapid gas–solid reaction between CO_2 and CeO_2 to replenish the oxygen.

Keywords: Ceria; Dry reforming; High surface area; Hydrogen; SOFC

1. Introduction

Cerium oxide or ceria is an important material for a variety of catalytic reactions involving oxidation of hydrocarbons (e.g., automobile exhaust catalysts). This material contains a high concentration of highly mobile oxygen vacancies, which act as local sources or sinks for oxygen involved in reactions taking place on its surface.

Nowadays, a potential application of ceria is in solid oxide fuel cells (SOFCs) application as a reforming catalyst for in-stack (called indirect internal) reforming of methane [1]. Conventional Ni catalysts have been reported to provide too high endothermic reforming reactivity for in-stack reforming in SOFCs [5]. The rapid endothermic reaction can lead to local temperature gradients especially close to the entrance of the reformer, which consequently cause the possible mechanical failure due to thermally induced stresses [6,7]. In addition, the carbon deposition was easily formed on the surface of Ni catalyst under SOFC operating conditions, resulting in the rapid catalyst deactivation [8]. Thus, a less active and high resistant toward carbon formation catalyst is desirable to give better control of the coupled heat flows and chemical reactions. Ceria is a candidate catalyst for this application since it is much less active and more resistant toward carbon deposition

* Corresponding author. Tel.: +66 2 8729014; fax: +66 2 8726736.
E-mail address: navadol_l@jgsee.kmutt.ac.th (N. Laosiripojana).

0926-3373/$ – see front matter © 2005 Elsevier B.V. All rights reserved.
doi:10.1016/j.apcatb.2005.03.001

compared to Ni [3]. Recently, the successful tests of ceria for the 'dry methane' and 'methane steam reforming' reactions have been reported [1–3].

Due to the high resistance toward carbon formation, ceria should also be a good candidate for use in the dry reforming process. Both the steam and dry reforming reactions have similar thermodynamic characteristics except that the carbon formation in the dry reforming is more severe than in the steam reforming due to the lower H/C ratio of this reaction [9]. The attractive feature of the dry reforming reaction is the utilization of CO_2, which is a greenhouse effect gas. In general, the dry reforming reaction (Eq. (1)) is typically accompanied by the simultaneous occurrence of the reverse water–gas shift reaction (RWGS) (Eq. (2)).

$$CH_4 + CO_2 = 2CO + 2H_2 \Delta H = 247\text{kJ/mol} \quad (1)$$

$$CO_2 + H_2 = CO + H_2O \Delta H = 41.1\text{kJ/mol} \quad (2)$$

The hydrogen to carbon monoxide production ratio from the dry reforming reaction is, therefore, less than 1. Sodesawa et al. [10] studied the dry reforming reaction at a stoichiometric feed ratio over several catalysts. They found that the activities of most catalysts deactivated rapidly due to the carbon deposition. Previously, no researcher has investigated the dry reforming over ceria before.

As described, ceria has a great potential to be used as the reforming catalyst for the indirect internal reforming solid oxide fuel cells (IIR-SOFCs); however, the main weaknesses of this material are its low specific surface area and high deactivation due to the thermal sintering when operated under SOFC stack conditions. It was reported that after exposure in methane steam reforming conditions at 900 °C for 18 h, the reforming reactivity over ceria deactivated 30% and the steady-state methane conversion was less than 10% [3]. The use of high surface area ceria (CeO_2 (HSA)) would be a good alternative method to minimize the sintering impact and consequently improve the stability and steady-state activity. Several methods have recently been described for the preparation of CeO_2 (HSA) solid solution. Most interest is focused on the preparation via templating pathways [11–13]. Several meso-structured surfactant–oxide composites have been synthesized by this approach. However, a few of these composites showed a regular pore structure after calcination [14–16]. Terribile et al. [17] synthesized CeO_2 (HSA) with improved textural, structural and chemical properties for environmental applications by using a surfactant-assisted approach. The materials with good homogeneity and stability especially after thermal treatments were achieved.

In the present work, CeO_2 (HSA) was synthesized by the surfactant-assisted approach. The stability and activity toward the dry reforming of CeO_2 (HSA) were studied and compared to the conventional low surface area ceria (CeO_2 (LSA)), and Ni/Al_2O_3. The resistance toward carbon formation and the kinetics of the reactions on CeO_2 (HSA) were also determined.

2. Experimental

2.1. Catalyst preparations and characterizations

CeO_2 (LSA) was prepared by the precipitation of cerium chloride ($CeCl_3 \cdot 7H_2O$) from Aldrich. The starting solution was prepared by mixing 0.1 M of this metal salt solution with 0.4 M of ammonia at a 2:1 volumetric ratio. This solution was stirred by magnetic stirring (100 rpm) for 3 h, then sealed and placed in a thermostatic bath maintained at 90 °C for 3 days. The precipitate was filtered and washed with deionised water and acetone to remove the free surfactant. It was dried overnight in an oven at 110 °C, and then calcined in air at 1000 °C for 6 h.

Following to the work from Terribile et al. [17], CeO_2 (HSA) were prepared by adding an aqueous solution of the appropriate cationic surfactant, 0.1 M cetyltrimethylammonium bromide solution from Aldrich, to a 0.1 M cerium chloride. The molar ratio of ([Ce])/[cetyltrimethylammonium bromide] was kept constant at 0.8. The mixture was stirred and then aqueous ammonia was slowly added with vigorous stirring until the pH was 11.5 [17]. The mixture was continually stirred for 3 h, then sealed and placed in the thermostatic bath maintained at 90 °C for 3 days. After that, the mixture was cooled and the resulting precipitate was filtered and washed repeatedly with water and acetone. The filtered powder was then treated under the same procedures as CeO_2 (LSA). For comparison, Ni/Al_2O_3 (5 wt.% Ni) was also prepared by impregnating α-Al_2O_3 (from Aldrich) with $NiCl_3$. After stirring, the solution was dried and calcined at 1000 °C for 6 h. The catalyst powder was reduced with 10%H_2/Ar at 700 °C for 6 h before use.

BET measurements of CeO_2 were carried out before and after calcination at different temperatures in order to determine the decrease in surface area by the thermal sintering. As presented in Table 1, after drying in the oven, surface areas of 105 and 55 $m^2\ g^{-1}$ were observed for CeO_2 (HSA) and CeO_2 (LSA), respectively and, as expected, the surface area decreased at high calcination temperatures. However, the value for CeO_2 (HSA) is still appreciable after calcination at 1000 °C and it is almost three times of that for the general CeO_2 (LSA). The homogeneity and morphology of CeO_2 (HSA) was also investigated. All samples have a

Table 1
Specific surface area of the catalysts after drying and calcinations at different temperatures

Catalyst	BET surface area ($m^2\ g^{-1}$) after drying or calcination at (°C)						
	100	200	400	600	800	900	1000
CeO_2 (LSA)[a]	55	49	36	21	15	11	8.5
CeO_2 (HSA)[b]	105	97	69	48	35	29	24

[a] Conventional low surface area CeO_2 prepared by the precipitation method.
[b] Nanocomposite high surface area CeO_2 prepared by the surfactant-assisted approach.

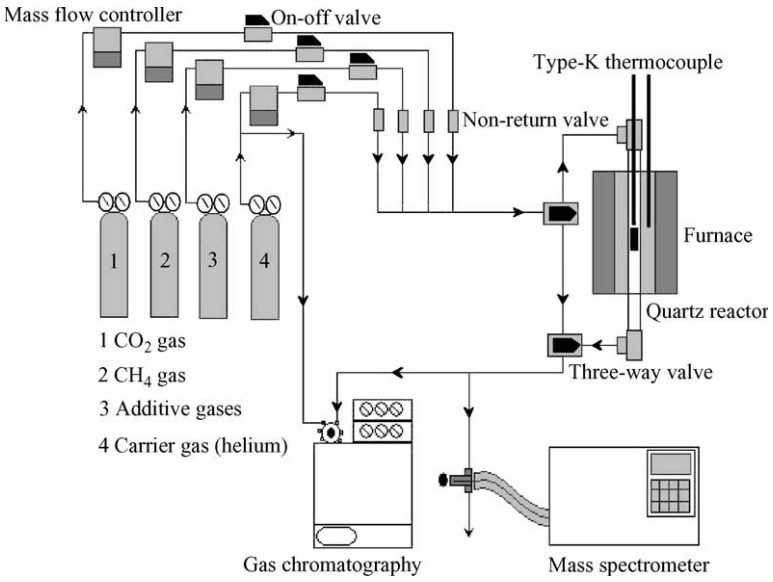

Fig. 1. Schematic diagram of the experimental set-up.

similar morphology and exhibit a very narrow particle-size histogram. As expected, samples treated at 1000 °C showed a larger particle size than those treated at lower temperatures. The mean particle size for CeO_2 (HSA) after calcination at 1000 °C was 30–100 nm.

2.2. Experimental set-up

In order to investigate the dry reforming reaction, an experimental reactor system was constructed as shown in Fig. 1. This system consists of three main sections: feed, reaction, and analysis sections. The main obligation of the feed section is to supply the components of interest including CH_4, CO_2, H_2, and CO to the reaction section, where an 8 mm internal diameter and 40 cm length quartz reactor was mounted vertically inside a furnace. The gas mixture was flowed though this quartz reactor, in which the catalyst was filled inside. A small amount of quartz wool was used to prevent the catalyst from moving. The weight of catalyst loading was 50 mg, while a typical range of total gas flow was 20–200 $cm^3\ min^{-1}$ depending on the desired space velocity. A Type-K thermocouple was placed into the annular space between the reactor and the furnace. This thermocouple was mounted on the tubular reactor in close contact with the catalyst bed to minimize the temperature difference between the catalyst bed and the thermocouple. Another Type-K thermocouple was inserted in the middle of the quartz tube in order to re-check the possible temperature gradient. The record showed that the maximum temperature fluctuation during the reaction was always within ±0.75 °C or less from the temperature specified for the reaction.

After reaction, the gas mixture was transferred via trace-heated lines to the analysis section, which consists of a Porapak Q column Shimadzu 14B gas chromatograph (GC) and a mass spectrometer (MS). The gas chromatography was applied in order to investigate the steady-state condition experiments, whereas the mass spectrometer was used for the transient carbon formation experiments.

In the present work, the outlet of the GC column was directly connected to a thermal conductivity detector (TCD). In order to satisfactorily separate CH_4, CO, CO_2, and H_2, the temperature setting inside the GC column was programmed varying with time. In the first 3 min, the column temperature was constant at 60 °C, it was then increased steadily by the rate of 15 °C per min until 120 °C. Finally, the temperature was decreased to 60 °C. The analytical method applied is an internal standardization in which the peak area is related to the molar concentration through the response factor (RF).

$$\mathrm{RF} = \frac{\text{concentration (ppm)}}{\text{peak area}} \tag{3}$$

Table 2 presents the absolute response factor (RF) for all components concerned in this research. In order to study the formation of carbon species on catalyst surface, the transient exhaust gas from the catalytic reactor was analyzed using the mass spectrometer. Sampling of the exhaust gas was done by a quartz capillary and differential pumping. The calibration of CO and CO_2 were performed by injecting a known amount of these calibration gases from a loop, in an injection valve in the bypass line. The response factors were obtained by dividing the number of moles for each component over the respective areas under peaks. This process was

Table 2
Absolute response factors and retention time of each component

Gas	Response factor (RF)	Retention time (min)
H_2	0.35	0.70
CO	0.19	1.15
CH_4	0.09	1.59
CO_2	0.21	2.65

performed before each experiment to achieve maximum accuracy in the quantitative carbon analysis.

2.3. Temperature programmed techniques (TP)

Temperature programmed technique (TP) was applied for studying the resistance toward carbon formation. The temperature programmed oxidation (TPO) was carried out by introducing 10% oxygen in helium with the total flow rate of 100 $cm^3\ min^{-1}$ into the system. The temperature was increased from room temperature to 900 °C at the rate of 10 °C/min. The amount of carbon formations on the surface of catalysts were determined by measuring the CO and CO_2 yields from the TPO results and assuming a value of 0.026 nm^2 for the area occupied by a carbon atom in a surface monolayer of the basal plane in graphite [18]. In addition to the TPO method, the amount of carbon deposition was confirmed by calculating carbon balance of the system. The amount of carbon deposited on the surface of catalyst would theoretically be equal to the difference between the inlet carbon containing components (CH_4 and CO_2) and the outlet carbon containing components (CO, CH_4, and CO_2). The amount of carbon deposited per gram of catalyst is given by the following equation:

$$C_{deposition} = \frac{mole_{carbon(in)} - mole_{carbon(out)}}{m_{catalyst}} \quad (4)$$

3. Results

3.1. Preliminary test

Preliminary experiments were carried out to find a suitable condition in which internal and external mass transfer effects are not predominant. Considering the effect of external mass transfer, the total gas flow rate was varied between 10 and 200 $cm^3\ min^{-1}$ under a constant residence time of 5×10^{-4} g min cm^{-3}. As shown in Fig. 2, the

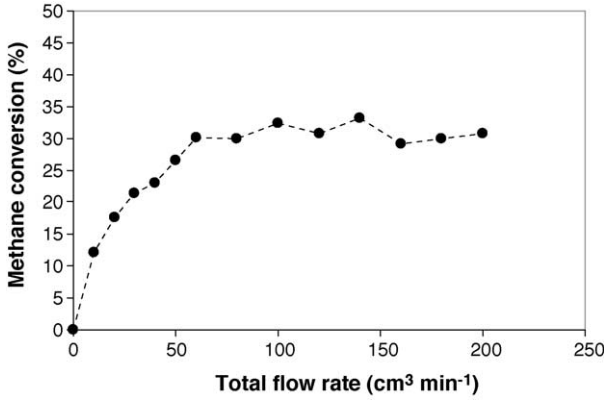

Fig. 2. Effect of the total gas flow rate on the methane conversion from the dry reforming (CH_4/CO_2 = 1.0/3.0) at 900 °C with the constant resident time of 5×10^{-4} g min cm^{-3}.

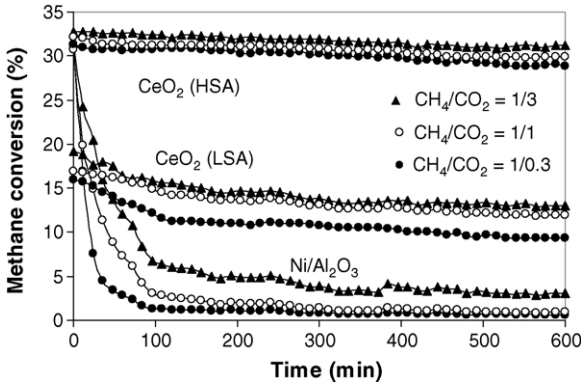

Fig. 3. Dry reforming of methane at 900 °C for different catalysts using different inlet CH_4/CO_2 ratios.

reforming rate was found to be independent of the gas velocity when the gas flow rate was higher than 60 $cm^3\ min^{-1}$, indicating the absence of external mass transfer effects at this high velocity.

The reaction on different average sizes of catalysts (up to 500 μm) were carried out in order to confirm that the experiments were performed within the region of intrinsic kinetics. It was observed that the catalysts with the particle size less than 200 μm showed no intraparticle diffusion limitation in the range of conditions studied. Therefore, in the following studies, the total flow rate was kept constant at 100 $cm^3\ min^{-1}$ whereas the catalyst diameters were kept within the above-mentioned range in all experiments.

3.2. Stability and activity toward the dry reforming

Synthesized CeO_2 (HSA), CeO_2 (LSA), and 5% Ni/Al_2O_3 were studied in the dry reforming at 900 °C. The feed was CH_4/CO_2 in helium with different CH_4/CO_2 molar ratios of 1.0/0.3, 1.0/1.0, and 1.0/3.0. The main products from this reaction were H_2 and CO with some H_2O. The observed H_2/CO production ratios were less than 1.0 in all conditions indicating a contribution from the reverse water–gas shift reaction at this operating temperature. The reforming rate was measured as a function of time in order to indicate the stability and the deactivation rate. The variations in the methane conversion with time at 900 °C for the different inlet CH_4/CO_2 ratios are shown in Fig. 3.

Significant deactivations were detected for Ni/Al_2O_3 catalyst in all conditions especially at high inlet CH_4/CO_2 ratio, whereas much lower deactivations were detected for both CeO_2 (HSA), and CeO_2 (LSA). At steady-state, the dry reforming over CeO_2 (HSA) with inlet CH_4/CO_2 of 1.0/3.0 showed the best performance in terms of stability, and activity. Catalyst stabilities expressed as deactivation percentages are given in Table 3. It should be noted that, in order to determine whether the observed deactivation is due to the carbon formation, the post-reaction temperature-programmed oxidation (TPO) experiments were carried out. From the TPO results shown in Fig. 4, the huge peaks of

Table 3
Deactivation percentages, specific surface area, and the amount of carbon deposition on the surface of catalysts after exposure in dry reforming conditions (various inlet CH_4/CO_2 ratios) at 900 °C for 10 h

Catalyst	CH_4/CO_2 ratio	Deactivation (%)	BET surface ($m^2\ g^{-1}$)	Surface area reduction (%)	C formation[a] (monolayers)
CeO_2 (HSA)[b]	1.0/3.0	4.5	23	4.2	~0
	1.0/1.0	6.9	22	8.3	~0
	1.0/0.3	7.7	22	8.3	~0
CeO_2 (LSA)[c]	1.0/3.0	28	6.2	27	0.08
	1.0/1.0	30	6.2	27	0.11
	1.0/0.3	41	6.0	30	0.15
Ni/Al_2O_3[d]	1.0/3.0	90	~40	~0	3.9
	1.0/1.0	96	~40	~0	5.2
	1.0/0.3	97	~40	~0	5.8

[a] Calculated using CO and CO_2 yields from temperature-programmed oxidation (TPO) with 10% oxygen.
[b] High surface area CeO_2 prepared by surfactant-assisted approach.
[c] Conventional low surface area CeO_2 prepared by precipitation method.
[d] Ni/Al_2O_3 prepared by impregnation method with the specific surface area of 40 $m^2\ g^{-1}$ after calcinations.

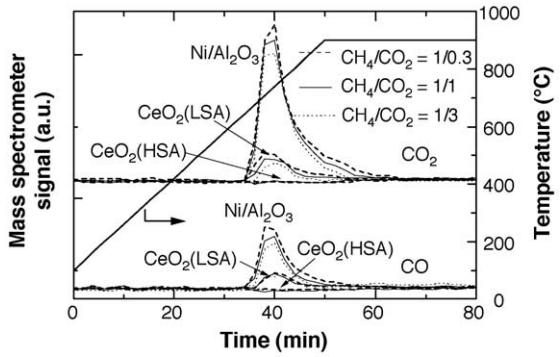

Fig. 4. Temperature programmed oxidation (TPO) over several catalysts after exposure in dry reforming conditions.

carbon dioxide and carbon monoxide were observed for Ni/Al_2O_3 at 600 °C, while small peaks of carbon dioxide and carbon monoxide were detected for CeO_2 (LSA). No peak of either carbon dioxide or carbon monoxide was detected for CeO_2 (HSA) in all conditions. The amount of carbon formations on the surface of Ni/Al_2O_3 with different inlet CH_4/CO_2 ratios were determined by measuring the CO and CO_2 yields from the TPO results (using Microcal Origin Software). Using a value of 0.026 nm^2 for the area occupied by a carbon atom in a surface monolayer of the basal plane in graphite [18], the quantities of carbon deposited over Ni/Al_2O_3 were observed to be approximately 5.8, 5.2, and 3.9 monolayers, while those over CeO_2 (LSA) were 0.15, 0.11, and 0.08 monolayers for the inlet CH_4/CO_2 ratios of 1.0/0.3, 1.0/1.0, and 1.0/3.0, respectively. The total amounts of carbon deposited were ensured by calculating the carbon balance of the system. Regarding the calculations, for the inlet CH_4/CO_2 ratios of 1.0/0.3, 1.0/1.0, and 1.0/3.0, the moles of carbon deposited per gram of CeO_2 (LSA) were 0.19, 0.12, and 0.09 mmol g^{-1}. By the same assumption for the area occupied by a carbon atom [18], these values are equal to 0.16, 0.10, and 0.07 monolayers, respectively, which is in good agreement with the values observed from the TPO method described above. The results clearly indicated that the deactivations observed for Ni/Al_2O_3 were mainly due to the carbon deposition on the surface of catalyst, and CeO_2 presented significantly stronger resistance toward carbon formation compared to Ni/Al_2O_3.

The BET measurements were carried out to observe the surface area reduction percentages of all catalysts. As shown in Table 3, it was suggested that the deactivations of ceria are mainly due to the thermal sintering. In addition, the surface area reduction percentage of CeO_2 (HSA) is much lower than CeO_2 (LSA), indicating its better stability toward the thermal sintering.

3.3. Kinetics of the dry reforming on CeO_2 (HSA)

The kinetics of the dry reforming over CeO_2 (HSA) was studied by varying inlet CH_4, and CO_2 partial pressures at different operating temperatures. The effects of CO and H_2 in feed on the reforming rate over this catalyst were also investigated, as both components are the main products from the dry reforming.

The inlet methane partial pressure was varied from 0.01 to 0.04 atm, while the operating temperature range was 900–1000 °C. The activity of CeO_2 (HSA) increased with increasing methane partial pressure as well as the operating temperature as shown in Fig. 5. In the present work, the dry reforming rate was represented in term of the turnover frequencies (N), calculated from the below equation [1].

$$N = \frac{rN_A A_{N_2}}{m_c S} \quad (5)$$

It is assumed that all surface sites accessible by nitrogen adsorption (area per molecule 16.2×10^{-20} m^2 [1,18]) were active. Here, r is the moles of CH_4 changing per unit time ($mol_{CH_4}\ min^{-1}$), N_A the Avagadro's number, A_{N_2} the area occupied by an adsorbed nitrogen molecule (16.2×10^{-20} m^2), m_c the weight of catalyst used (0.05 g), and S the specific surface area of the catalyst ($m^2\ g^{-1}$).

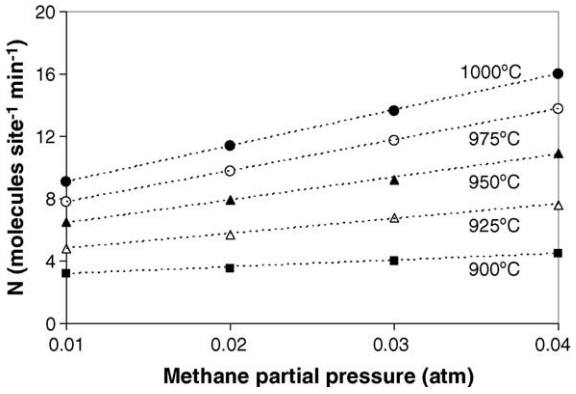

Fig. 5. Effect of methane partial pressure on the turnover frequencies (N) for CeO_2 (HSA) at different temperatures (inlet CO_2 = 0.05 atm).

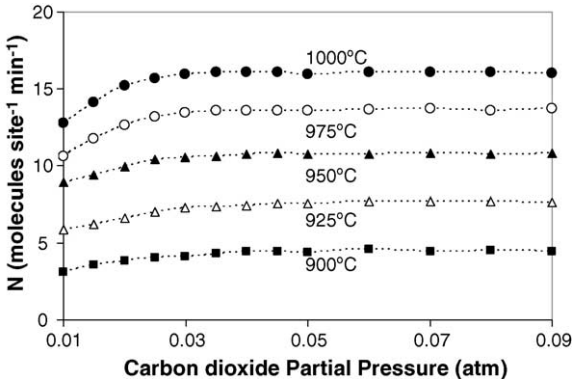

Fig. 6. Effect of carbon dioxide partial pressure on the turnover frequencies (N) for CeO_2 (HSA) at different temperatures (inlet CH_4 of 0.04 atm).

The reaction order in methane (n) for this catalyst was observed to be between 0.50 and 0.55, and seemed to be essentially independent of the operating temperature and carbon dioxide partial pressure for the range of conditions studied. These values n were obtained experimentally by plotting ln(N) versus ln P_{CH_4}. The reaction orders in other components (CO_2, H_2, and CO) were achieved using the same approach by varying the inlet partial pressure of the component of interest while keeping other inlet component partial pressures constant.

The H_2/CO ratio in the products increased with increasing inlet CH_4/CO_2 ratio, whereas it strongly decreased with increasing temperature, as presented in Table 4.

Several inlet carbon dioxide partial pressures, from 0.01 to 0.09 atm, were then introduced to the feed with constant methane partial pressure in order to investigate the influence of CO_2 on the dry reforming rate. Carbon dioxide presented slight positive effect on the dry reforming rate at high inlet CH_4/CO_2 ratios as shown in Fig. 6. The experiments yielded non-linear positive carbon dioxide trend. When the inlet carbon dioxide partial pressure was greater than 0.03 atm, the carbon dioxide influence on the dry reforming rate became less pronounced. At high inlet CH_4/CO_2 ratios, the reaction order in carbon dioxide for this catalyst was observed to be a small positive value between 0.08 and 0.12, and seemed to be independent of the inlet methane partial pressure and the operating temperature for the range of conditions studied. The proportion of H_2/CO in the products reduced from 0.94 to 0.89 as the CH_4/CO_2 ratio was decreased from 3.0/1.0 to 3.0/5.0 (Table 4). This is as expected from an increasing contribution from the RWGS reaction.

Table 4
Effect of inlet compositions on H_2/CO ratio from the dry reforming over CeO_2 (HSA) at different temperatures

Temperature (°C)	Inlet compositions (atm)	H_2/CO production ratio from the dry reforming over CeO_2 (HSA)
900	0.03 CH_4/0.03 CO_2	0.93
925	0.03 CH_4/0.03 CO_2	0.90
950	0.03 CH_4/0.03 CO_2	0.88
975	0.03 CH_4/0.03 CO_2	0.85
1000	0.03 CH_4/0.03 CO_2	0.81
900	0.01 CH_4/0.03 CO_2	0.90
	0.02 CH_4/0.03 CO_2	0.91
	0.03 CH_4/0.03 CO_2	0.93
	0.04 CH_4/0.03 CO_2	0.95
	0.05 CH_4/0.03 CO_2	0.96
900	0.03 CH_4/0.01 CO_2	0.94
	0.03 CH_4/0.02 CO_2	0.93
	0.03 CH_4/0.03 CO_2	0.93
	0.03 CH_4/0.04 CO_2	0.91
	0.03 CH_4/0.05 CO_2	0.89

The dry reforming in the presences of carbon monoxide and hydrogen were then investigated by adding either carbon monoxide or hydrogen to the feed gas at several operating temperatures. The results show that the reforming rates are also dependent on both carbon monoxide and hydrogen concentrations. Unlike CH_4 and CO_2, both components inhibited the dry reforming rate over CeO_2 as shown in Figs. 7 and 8. The reaction order in carbon monoxide was in the range of −0.15 to −0.10, while the reaction order in hydrogen was between −0.34 to −0.28 in the range of

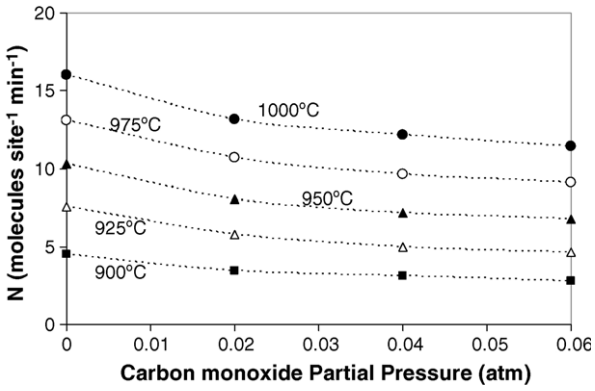

Fig. 7. Effect of carbon monoxide partial pressure on the turnover frequencies (N) for CeO_2 (HSA) at different temperatures (inlet CH_4 of 0.04 atm).

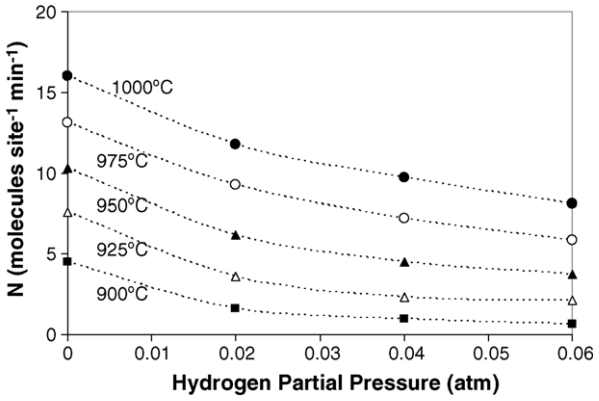

Fig. 8. Effect of hydrogen partial pressure the turnover frequencies (N) for CeO_2 (HSA) at different temperatures (inlet CH_4 of 0.04 atm).

conditions studied. These negative impacts are due to the inhibition of redox property on ceria surface, which will be discussed in the next section. Table 5 presents the summary of observed reaction orders in each component (CH_4, CO_2, CO, and H_2) for CeO_2 (HSA) at different inlet conditions.

According to the influences of CH_4, CO_2, CO, and H_2 as described above, the experimental data can be fitted well to a simple rate Eq. (6), which captures the essential features and could also easily be used in the simulation of indirect internal reforming over CeO_2 (HSA) in SOFCs.

$$-r_{CH_4} = \frac{k(T)(P_{CH_4})^n}{1 + K_1 \frac{P_{CO}}{P_{CO_2}} + K_2(P_{H_2})^m} \quad k(T) = A\exp\left(\frac{-E}{RT}\right)$$

$$\text{and} \quad K_i(T) = B_i \exp\left(\frac{-\Delta H_i}{RT}\right) \tag{6}$$

where P_i is the partial pressure of chemical component i, and K_1 and K_2 are adsorption parameters, obtained from Van't Hoff equation. The positive effect of methane on the dry reforming rate was a consequence of the presence of the $k(T)(P_{CH_4})^n$ term, whereas both positive and negative effects of carbon dioxide and carbon monoxide were a consequence of the $K_1(T)P_{CO}/P_{CO_2}$ term in the denominator. According to the fitting, when n and m were taken as 0.5, a good fit to the data was observed in the range of conditions studied. The value of $k(T)$ increased from 23.98 molecules site^{-1} min^{-1} atm$^{-0.5}$ at 900 °C to 83.76 molecules site^{-1} min^{-1} atm$^{-0.5}$ at 1000 °C, while $K_1(T)$ and $K_2(T)$, also temperature dependent parameters, were in the range of 0.35–0.50 and 8.5–15.2 atm$^{-0.5}$, respectively. The parameters of the rate expression can be summarized in Table 6. It should be noted that the activation energy for this reaction, which were achieved by the Arrhenius plots as shown in Fig. 9, was approximately 154 kJ/mol.

4. Discussion

It has been widely reported that the gas–solid reaction between ceria and CH_4 can generate CO and H_2 at high temperature [19,20]. In addition, the reduced state, CeO_{2-n}, can react with CO_2 to produce CO [21]. Therefore, the dry reforming of methane over CeO_2 can be presented as follows:

$$CeO_2 + nCH_4 \rightarrow CeO_{2-n} + nCO + 2nH_2 \tag{7}$$

$$CeO_{2-n} + nCO_2 = CeO_2 + nCO \tag{8}$$

$$CeO_2 + nH_2 = CeO_{2-n} + nH_2O \tag{9}$$

The positive effect of CH_4 and CO_2 on the dry reforming reactivity is due to the forward of Eqs. (7) and (8), respectively, while the reverse of Eq. (8) results in the negative effect of CO. Hydrogen presented negative effect on the dry

Table 5
Reaction orders for the components of interest (CH_4, CO_2, CO, and H_2) from the dry reforming over CeO_2 (HSA) at different operating conditions

Components of interest	Temperature (°C)	Other inlet compositions (atm)				Reaction order for components of interest
		CH_4	CO_2	H_2	CO	
CH_4 (0.01–0.04 atm)	900–1000		0.05	0	0	0.52 ± 0.02
	900		0.10	0	0	0.50
	900		0.15	0	0	0.51
	900–950		0.05	0.02	0	0.54 ± 0.01
	900–950		0.05	0	0.02	0.53 ± 0.02
CO_2 (0.01–0.09 atm)	900–1000	0.04		0	0	0.10 ± 0.02
	900	0.02		0	0	0.10
	900	0.07		0	0	0.08
	900–925	0.04		0.02	0	0.10 ± 0.02
	900–950	0.04		0	0.02	0.11 ± 0.01
H_2 (0.02–0.06 atm)	900–1000	0.04	0.05		0	−0.31 ± 0.03
	900	0.04	0.10		0	−0.28
	900	0.02	0.05		0	−0.34
	900	0.04	0.05		0.02	−0.30
CO (0.02–0.06 atm)	900–1000	0.04	0.05	0		−0.11 ± 0.01
	900	0.04	0.10	0		−0.12
	900	0.02	0.05	0		−0.15
	900	0.04	0.05	0.02		−0.10

Table 6
Summary of Pre-exponential factors for Arrhenius and Van't Hoff equations for dry reforming over CeO_2 (HSA)

A (molecules site^{-1} min^{-1} atm$^{-0.5}$)	E (kJ mol^{-1})	B_1	ΔH_1 (kJ mol^{-1})	B_2 (atm$^{-0.5}$)	ΔH_2 (kJ mol^{-1})
1.9×10^8	154	5.3×10^{-3}	−44.28	9.29×10^{-3}	−72.15

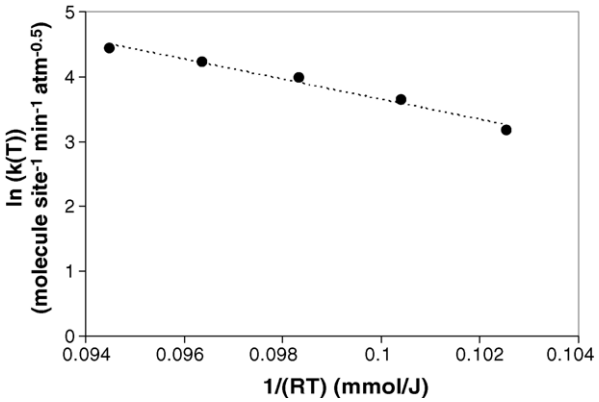

Fig. 9. The Arrhenius-type plot for dry reforming reaction over CeO_2 (HSA).

reforming, as this component reduced Ce^{4+} to Ce^{3+} via Eq. (9) and, consequently, results in the inhibition of methane conversion via Eq. (7). It should be noted that the inhibitory effect of hydrogen is the main disadvantage of using CeO_2 industrially, therefore, the removal of hydrogen during the reforming process might be required.

In the present work, the observed activation energy for the dry reforming over CeO_2 (HSA) is 154 kJ mol^{-1}. This value is in the same range as the activation energies previously observed for the methane steam reforming over CeO_2 (HSA) [4], CeO_2 (LSA) [3], and Gd–CeO_2 (LSA) [1]. Aguiar et al. [22] reported the methane steam reforming rate equation over conventional CeO_2 (LSA) in the form of $-r_{CH_4} = k(T)P_{CH_4}^{0.5}/(1 + K_H P_{H_2}^{0.5})$. The activation energy obtained by the Arrhenius plots of $k(T)$ was 133 kJ mol^{-1}. Laosiripojana and Chadwick [4] studied the methane steam reforming over CeO_2 (HSA) and presented the well-fitting of their experimental data to this form of rate equation. Their corresponding activation energy was 150 kJ mol^{-1}. Ramirez-Cabrera et al. [1] studied the methane steam reforming reaction over Gd–CeO_2 and compared the results with the dry methane reaction over the same catalyst. They reported that the observed activation energies from both reactions are in the same range of 153–165 kJ mol^{-1}. In addition, in the excess of inlet CO_2, the observed methane conversion for the dry reforming of 5% methane at 900 °C in the present work is approximately equal to that for the steam reforming of 5% methane [4]. These observations indicate that the rate-controlling step for the steam and dry reforming reactions for CeO_2 is similar. Hence, the methane steam reforming reaction mechanism for CeO_2 as proposed by Ramirez-Cabrera et al. [1] should also be applied to explain the dry reforming of methane over this material. The dry reforming mechanism for CeO_2 involves the reaction between methane, or an intermediate surface hydrocarbon species, with the lattice oxygen (O_x) at CeO_2 surface, as illustrated schematically below.

$$CH_4 + 2S_{Ce} = CH_3{-}S_{Ce} + H{-}S_{Ce} \quad (10)$$

$$CH_3{-}S_{Ce} + S_{Ce} = CH_2{-}S_{Ce} + H{-}S_{Ce} \quad (11)$$

$$CH_2{-}S_{Ce} + S_{Ce} = CH{-}S_{Ce} + H{-}S_{Ce} \quad (12)$$

$$CH{-}S_{Ce} + S_{Ce} = C{-}S_{Ce} + H{-}S_{Ce} \quad (13)$$

$$C{-}S_{Ce} + O_x = CO + O_{x-1} + S_{Ce} \quad (14)$$

$$CO_2 + O_{x-1} = O_x + CO \quad (15)$$

$$H_2 + O_x = O_{x-1} + H_2O \quad (16)$$

$$2H{-}S_{Ce} = H_2 + 2S_{Ce} \quad (17)$$

There are two possibilities for this scheme depending on what is assumed for the catalyst surface site, S_{Ce}. It can be a unique site, or can also be considered to be the same site as the catalyst oxidised site (O_x) [3]. During the dry reforming, methane is adsorbed on either a unique site, S_{Ce}, or the catalyst oxidized site, O_x, whereas CO_2 is always reacted with the catalyst reduced site, O_{x-1}. The steady-state reforming rate is mainly due to the continuous supply of the oxygen source by CO_2. It should be noted that the measured value of the oxygen diffusion coefficient for ceria is high and the reaction rate is controlled by a surface reaction and not by diffusion of oxygen from the bulk of the solid particles to ceria surfaces [23]. The stronger linear dependence of the reforming rate on methane partial pressure, and the weaker positive of CO_2 provide the evidence that the controlling step is the reaction of methane with the CeO_2 surface, and that oxygen is replenished by a significantly rapid surface reaction of the reduced state CeO_2 with CO_2.

The high resistance toward carbon deposition for ceria, which has been widely reported by several researchers [1–5,24], is mainly due to the high oxygen storage capacity (OSC) of this material. As described, carbon formation is one major problem for the dry reforming of methane. We also observed high amount of carbon formation on the surface of Ni/Al_2O_3 after exposure in a dry reforming condition. Regarding the possible carbon formation during the reforming processes, the following reactions are theoretically the most probable reactions that could lead to carbon formation:

$$2CO = CO_2 + C \quad (18)$$

$$CH_4 = 2H_2 + C \quad (19)$$

$$CO + H_2 = H_2O + C \quad (20)$$

$$CO_2 + 2H_2 = 2H_2O + C \quad (21)$$

At low temperature, reactions (20) and (21) are favorable, while reaction (18) is thermodynamically unflavored [25]. The Boudard reaction (Eq. (18)) and the decomposition of methane (Eq. (19)) are the major pathways for carbon formation at such a high temperature as they show the largest change in Gibbs energy [26]. According to the range of temperature in this study, carbon formation would be formed via the decomposition of methane and Boudard reactions especially at high inlet CH_4/CO_2 ratio (1.0/0.3 and 1.0/1.0). By applying CeO_2, both reactions (Eqs. (20) and (21)) could be inhibited by the redox reactions between methane and carbon monoxide (produced during the dry reforming process) with the lattice oxygen (O_x) at CeO_2 surface (Eqs. (22) and (23)) forming hydrogen and carbon dioxide, which is thermodynamically unflavored to form carbon species in this range of conditions. Therefore, significant lower amount of carbon deposition were observed for ceria even at low inlet carbon dioxide concentration.

$$CH_4 + O_x \rightarrow CO + H_2 + O_{x-1} \quad (22)$$

$$CO + O_x = CO_2 + O_{x-1} \quad (23)$$

Although CeO_2 (LSA) also provides high resistance toward carbon formation, the major weaknesses of CeO_2 (LSA) are its nature low specific surface area and also high size reduction due to the thermal sintering impact, resulting in its low redox property and consequently low reforming reactivity. In the present work, the specific surface area of CeO_2 (HSA) after calcination at 1000 °C was almost three times higher than the conventional one. Moreover, the size reduction percentage for CeO_2 (HSA) was significantly lower. These enhancements were also reported by Terrible et al. [17], who prepared Ce–ZrO_2 by the same procedure. They reported that the achievement of high surface area material by the surfactant-assisted procedure is mainly due to the interaction of hydrous oxide with cationic surfactants under basic conditions during the preparation [17]. At high pH value, conducting the precipitation of hydrous oxide in the presence of cationic surfactant allows the cation exchange process between H^+ and the surfactant, resulting in a developed pore structure with an increase in surface area [17]. Regarding the thermal stability at high temperature, Terrible et al. [17] explained that the incorporation of surfactants during preparation could reduce the interfacial energy and eventually decrease the surface tension of water contained in the pores. This could reduce the shrinkage and collapse of the catalyst during heating up, which consequently help the catalyst maintaining high surface area after calcination [17].

Our previous work on Ni/CeO_2 (HSA) and Ni/Ce–ZrO_2 (HSA) [24] for the steam reforming of methane also indicated the same improvement as described above. We previously studied the resistance of metal catalyst on ceria-based supports toward the carbon formation. Under methane steam reforming conditions with the H_2O/CH_4 ratio of 3.0, Ni/CeO_2 (HSA) exhibited high steady-state steam reforming activity and no carbon species was detected on the surface [24]. However, at steam to methane ratios less than 1, significant carbon deposition was formed. Thus, the use of Ni always increases the risk of carbon deposition even when CeO_2 (HSA) was applied as the support.

5. Conclusions

CeO_2 is a good candidate catalyst for the dry reforming of methane due to its extreme resistance toward the deactivation from carbon formation. The use of high surface area CeO_2 (CeO_2 (HSA)) significantly reduces the degree of deactivation by thermal sintering compared to general low surface area CeO_2.

The dry reforming rate over CeO_2 (HSA) is proportional to the methane partial pressure and the operating temperature. Carbon dioxide presents slight positive impact on the methane conversion, whereas carbon monoxide inhibits the reforming rate. Addition of hydrogen was found to have a significant inhibitory effect on the conversion of methane. This inhibitory effect is the main disadvantage of using CeO_2 as the dry reforming catalyst, and the removal of hydrogen during the reforming process might be required.

The activation energies and reforming rates at the same methane concentration for the dry reforming are equal to those for the steam reforming. These results suggest the similar reaction mechanisms for both the steam reforming and the dry reforming over CeO_2 in which the reforming rate is governed by the slow reaction of adsorbed methane, or surface hydrocarbon species, with oxygen in CeO_2, and a rapid gas–solid reaction between CO_2 and CeO_2 to replenish the oxygen.

Acknowledgement

The financial support from The Thailand Research Fund (TRF) throughout this project is gratefully acknowledged. The first author like to acknowledge Professor David Chadwick from Department of Chemical Engineering and Chemical Technology, Imperial College London for his valuable suggestion.

References

[1] E. Ramírez-Cabrera, A. Atkinson, D. Chadwick, Appl. Catal. B 47 (2004) 127–131.
[2] E. Ramírez-Cabrera, N. Laosiripojana, A. Atkinson, D. Chadwick, Catal. Today 78 (2003) 433–438.
[3] N. Laosiripojana 2003, Reaction engineering of indirect internal steam reforming of methane for application in solid oxide fuel cells. Ph.D. Thesis, University of London, England.

[4] N. Laosiripojana, D. Chadwick, Catalytic methane steam reforming of high surface area CeO_2, International Hydrogen Energy Congress & Exhibition 2005, in press.
[5] P. Aguiar, E. Ramírez-Cabrera, N. Laosiripojana, A. Atkinson, L.S. Kershenbaum, D. Chadwick, Stud. Surf. Sci. Catal. 145 (2003) 387.
[6] P. Aguiar, N. Lapena-Rey, D. Chadwick, L. Kershenbaum, Chem. Eng. Sci. 56 (2001) 652.
[7] P. Aguiar, D. Chadwick, L. Kershenbaum, Chem. Eng. Sci. 57 (2002) 1665.
[8] J.R. Rostrup-Nielsen, L.J. Christiansen, Appl. Catal. A 126 (2) (1995) 381–390.
[9] J.H. Edwards, A.M. Maitra, Fuel Process. Technol. 42 (1995) 269.
[10] T. Sodesawa, A. Dobashi, F. Nozaki, React. Kinet. Catal. Lett. 12 (1979) 107.
[11] C.T. Kresge, M.E. Leonowicz, W.J. Roth, J.C. Vartuli, J.S. Beck, Nature 359 (1992) 710.
[12] Q. Huo, D.I. Margolese, U. Ciesla, P. Feng, T.E. Gier, P. Sieger, R. Leon, P.M. Petroff, B. Schüth, G.D. Stucky, Nature 368 (1994) 317.
[13] P.T. Tanev, T.J. Pinnavaia, Science 267 (1995) 865.
[14] U. Ciesla, S. Schacht, G.D. Stucky, K.K. Unger, F. Schüth, Angew. Chem. Int. Ed. Engl. 35 (1996) 541.
[15] D.M. Antonelli, J.Y. Ying, Angew. Chem. Int. Ed. Engl. 35 (1996) 426.
[16] Q. Huo, D.I. Margolese, U. Ciesla, D.G. Demuth, P. Feng, T.E. Gier, P. Sieger, A. Firouzi, B.F. Chmelka, B. Schüth, G.D. Stucky, Chem. Mater. 6 (1994) 1176.
[17] D. Terribile, A. Trovarelli, J. Llorca, C. de Leitenburg, G. Dolcetti, Catal. Today 43 (1998) 79–88.
[18] E. Ramirez, A. Atkinson, D. Chadwick, Appl. Catal. B 36 (2002) 193–206.
[19] K. Otsuka, T. Ushiyama, I. Yamanaka, Chem. Lett. (1993) 1517.
[20] K. Otsuka, M. Hatano, A. Morikawa, J. Catal. 79 (1983) 493.
[21] K. Otsuka, M. Hatano, A. Morikawa, Inorganica Chim. Acta 109 (1985) 193.
[22] P. Aguiar, D. Chadwick, L. Kershenbaum, Chem. Eng. Sci. 59 (2004) 87–97.
[23] B.C.H. Steele, J.M. Floyd, Proc. Br. Ceram. Soc. 19 (1971) 55.
[24] N. Laosiripojana, S. Assabumrungrat, Catalytic steam reforming of methane over Ni on high surface area CeO_2 and Ce–ZrO_2 supports, PSU-UNS International Conference on Engineering and Environment (ICEE) 2005, in press.
[25] Y. Lwin, W.R.W. Daud, A.B. Mohamad, Z. Yaakob, Int. J. Hydrogen Energy 25 (1) (2000) 47–53.
[26] J.N. Amor, Appl. Catal. A 176 (1999) 159–176.

ELSEVIER

Chemical Engineering Journal 112 (2005) 13–22

Chemical Engineering Journal

www.elsevier.com/locate/cej

Synthesis gas production from dry reforming of methane over CeO_2 doped Ni/Al_2O_3: Influence of the doping ceria on the resistance toward carbon formation

N. Laosiripojana [a,*], W. Sutthisripok [b], S. Assabumrungrat [c]

[a] *The Joint Graduate School of Energy and Environment, King Mongkut's University of Technology Thonburi, Bangkok 10140, Thailand*
[b] *Department of Mining and Materials Engineering, Faculty of Engineering, Prince of Songkla University, Songkhla, Thailand*
[c] *Center of Excellence on Catalysis and Catalytic Reaction Engineering, Department of Chemical Engineering, Faculty of Engineering, Chulalongkorn University, Bangkok 10330, Thailand*

Received 17 January 2005; received in revised form 4 June 2005; accepted 9 June 2005

Abstract

Doping of CeO_2 as an additive promoter on Ni/Al_2O_3 was found to improve dry reforming activity for H_2 and CO productions at solid oxide fuel cell (SOFC) operating temperature (800–900 °C). The catalyst provides significantly higher reforming reactivity and resistance toward carbon deposition compared to conventional Ni/Al_2O_3. These enhancements are mainly due to the influence of the redox property of ceria. During dry reforming process, in addition to the reactions on Ni surface, the gas–solid reactions between the gaseous components presented in the system (CH_4, CO_2, CO, H_2O, and H_2) and the lattice oxygen (O_x) on ceria surface also take place. The reactions of adsorbed methane and carbon monoxide (produced during dry reforming process) with the lattice oxygen (O_x) on ceria surface ($CH_4 + O_x \rightarrow CO + H_2 + O_{x-1}$ and $CO + O_x \Leftrightarrow CO_2 + O_{x-1}$) can prevent the formation of carbon species on Ni surface from methane decomposition reaction and Boudard reaction.

In particular, CeO_2 doped Ni/Al_2O_3 with 8% ceria content showed the best reforming activity among those with the ceria content between 0 and 14%. The amount of carbon formation decreased with increasing Ce content. However, Ni was oxidized when more than 10% of ceria was doped. According to the post-XPS measurement, a small formation of Ce_2O_3 was observed after exposure in dry methane reforming conditions with low inlet CH_4/CO_2 ratio (1.0/0.3). The intrinsic reaction kinetics of 8% CeO_2 doped Ni/Al_2O_3 was studied by varying inlet CH_4 and CO_2 concentrations, and by adding H_2 and CO to the system at different temperatures. The dry reforming rate increased with increasing methane partial pressure and the operating temperature. The reaction orders in methane were always closed to 1.0 in all conditions. Carbon dioxide also presented weak positive impact on the methane conversion, whereas adding of carbon monoxide and hydrogen inhibited the reforming rate.

Keywords: Hydrogen; Synthesis gas; Carbon formation; Dry reforming; CeO_2

1. Introduction

Solid oxide fuel cell (SOFC) with an indirect internal reforming operation (IIR), called IIR-SOFC, is expected to be an important technology for energy generation in the near future due to the high efficiency and its low environmental impact. Regarding this operation, the endothermic reforming reaction takes place at the reformer, which is in close thermal contact with the anode side of fuel cell where the exothermic electrochemical reaction takes place (Fig. 1). IIR gives the advantage on eliminating the requirement for a separate fuel reformer and providing good heat transfer between the reformer and the fuel cell. In addition, the reformer part and the anode side for IIR operation can be operated separately. Therefore, the catalyst for reforming reaction at the reformer part and the material for electrochemical reactions at the anode side of fuel cell can be different

* Corresponding author.
E-mail address: navadol_l@jgsee.kmutt.ac.th (N. Laosiripojana).

1385-8947/$ – see front matter © 2005 Elsevier B.V. All rights reserved.
doi:10.1016/j.cej.2005.06.003

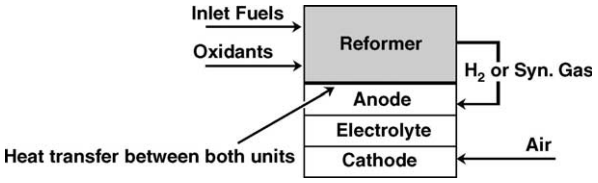

Fig. 1. Diagram of IIR-SOFC operation.

and optimized individually. This operation is expected to simplify the overall system design, making SOFC more attractive and efficient for producing electrical power [1].

The aim of the reformer unit is to reform and maximize the yield of hydrogen production and supply this component to the anode side of SOFC. Theoretically, hydrogen can be produced from several natural hydrocarbon sources including natural gas, bio-ethanol, coal, biomass, and biogas. Biogas consists mainly of methane and carbon dioxide is expected to be the attractive raw material for hydrogen production in the near future due to its economic availability. Due to the rich CO_2 for biogas, carbon dioxide (or dry) reforming reaction would be one of the most suitable processes to convert biogas to hydrogen or synthesis gas (CO and H_2). Compared to the steam reforming, both steam and dry reforming reactions have similar thermodynamic characteristics except that the carbon formation in the dry reforming is more severe than in the steam reforming due to the lower H/C ratio of this reaction [2]. The attractive feature of the dry reforming reaction is the utilisation of CO_2, which is a greenhouse effect gas. In general, the dry reforming reaction (Eq. (1)) is typically accompanied by the simultaneous occurrence of the reverse water-gas shift reaction (RWGS) (Eq. (2)).

$$CH_4 + CO_2 \Leftrightarrow 2CO + 2H_2 \qquad \Delta H = 247\,\text{kJ/mol} \qquad (1)$$

$$CO_2 + H_2 \Leftrightarrow CO + H_2O \qquad \Delta H = 41.1\,\text{kJ/mol} \qquad (2)$$

The hydrogen to carbon monoxide production ratio (H_2/CO ratio) from the dry reforming reaction is always less than 1. Vannice and Bradford [3] presented the apparent activation energies for the consumption of methane and carbon dioxide, as well as the production of carbon monoxide, hydrogen, and water in order to investigate the influence of the RWGS reaction. They observed that the apparent activation energy for hydrogen formation is greater than that for the formation of carbon monoxide, in which supported the influence of the reverse water-gas shift reaction on the reaction mechanism. Sodesawa et al. [4] studied the dry reforming reaction at a stoichiometric feed ratio over several catalysts. They found that the activities of most catalysts deactivated rapidly due to the carbon deposition. Topor et al. [5] suggested that the use of excess carbon dioxide could avoid carbon formation. Chubb et al. [6,7] studied the carbon dioxide reforming using an excess of carbon dioxide with carbon dioxide to methane ratios of 3:1 and 5:1 over Ni/Al_2O_3. They reported that the rate of disintegration is smaller for the higher one. Rostrup-Nielsen and Bak Hansen [8] investigated the activity toward dry reforming over several metals. Their order of reactivity for this reaction was Ru > Rh > Ni ∼ Ir > Pt > Pd, in which similar to their proposed order for steam reforming. They also observed that the replacing of steam with carbon dioxide gave similar activation energies, which indicated a similar rate-determining step in these two reactions. In addition, low levels or no carbon formation was detected from dry reforming over Rh metal at low temperature and CO_2 content [9]. Erdöhelyi et al. [10,11] studied the influence of the catalyst support on the dry reforming of rhodium-based catalyst, and reported that the support had no effect on the activity of Rh. In contrast, Nakamura et al. [12] and Zhang et al. [13] observed that the initial turnover frequency (specific activity) of Rh crystallities was significantly affected by their supports. Zhang et al. [13] also reported that the deactivation of Rh crystallities was strongly dependent on their supports.

In this present study, it is aimed at the development of an alternative catalyst for dry methane reforming reaction, which provided high stability, and activity toward this reaction at such a high temperature (800–900 °C) for later application in IIR-SOFC. According to the economical point of view, Ni/Al_2O_3 was selected as a based catalyst rather than the precious metals. Cerium oxide (CeO_2) was chosen as an additive promoter. This material (called ceria) is an important material for a variety of catalytic reactions involving oxidation of hydrocarbons (e.g. automobile exhaust catalysts). It contains a high concentration of highly mobile oxygen vacancies, which act as local sources or sinks for oxygen involved in reactions taking place on its surface. Nowadays, a potential application of ceria is in solid oxide fuel cells application as a reforming catalyst for in-stack (called indirect internal) reforming of methane, since it is high resistant toward carbon deposition compared to Ni [14]. Recently, the successful test of ceria for the methane steam reforming reaction has been reported [15–17]. Due to the high resistance toward carbon formation, ceria should be a good additive promoter for dry reforming process.

Recently, the use of ceria-based materials as the support and promoter for the catalytic reforming reaction has been reported by several researchers. As the support, it has been reported to be promising support among α-Al_2O_3 [18], γ-Al_2O_3, and γ-Al_2O_3 with alkali metal oxide and rare earth metal oxide [19] and $CaAl_2O_4$ [18–21], while the selected metals were Ni, Pt, or Pd [22–31]. As the promoter, ceria was also reported to be a good promoter for the dry methane reforming at intermediate temperature [32]. Wang and Lu [32] prepared CeO_2 doped Ni/Al_2O_3 by adding CeO_2 on γ-Al_2O_3 powder before impregnated Ni on CeO_2–Al_2O_3 support and tested the dry methane reforming reactivity at 500–800 °C. They found that the doping of CeO_2 significantly improved the resistance of catalyst toward the carbon deposition.

In this work, various amounts of cerium oxide were firstly doped on the surface of Ni/Al_2O_3 in order to determine the suitable doping ratio. The reactivity toward dry reforming and the resistance toward carbon formation over CeO_2 doped Ni/Al_2O_3 was studied and compared to conventional

Ni/Al_2O_3 at the temperature range of 800–900 °C. In addition, the intrinsic kinetics of the dry methane reforming reaction over this catalyst was also studied by varying inlet CH_4, CO_2, and by adding CO and H_2 at different temperatures. The reaction orders in each component and the possible rate isotherm with the fitting parameters were determined. These kinetic informations are important in order to determine the behavior of the catalyst toward this reaction for the large scale or industrial application. By fitting the rate isotherm and parameters in the modeling, the behavior of the whole reformer and the IIR-SOFC system can be predicted.

2. Experimental

2.1. Catalyst preparations

Ni/Al_2O_3 (5 wt.% Ni) was prepared by impregnating α-Al_2O_3 (from Aldrich) with $NiCl_3$ solution at room temperature. This solution was stirred by magnetic stirring (100 rpm) for 6 h, dried overnight in an oven at 110 °C, and calcined in air at 900 °C for 6 h. The catalyst powder was then reduced with 10% H_2/Ar at 700 °C for 6 h. CeO_2 doped Ni/Al_2O_3 was prepared by impregnate different concentration of cerium nitrate ($Ce(NO_3)_3{\cdot}6H_2O$ (99.0%), Fluka) on Ni/Al_2O_3 powder. Similarly, this solution was stirred by magnetic stirring (100 rpm) for 6 h before filtered and washed with deionised water and ethanol to prevent an agglomeration. The sample was dried and calcined in air at 1000 °C for 6 h. It was reduced with 10% H_2/Ar at 700 °C for 6 h before use.

2.2. Apparatus and procedures

In order to investigate the dry reforming and its associated reactions, an experimental reactor system was constructed. The feed gases including the components of interest such as CH_4, CO_2, H_2, or CO were introduced to the reaction section, in which an 8-mm internal diameter and 40-cm length quartz reactor was mounted vertically inside a furnace. The catalyst (50 mg) was loaded in the quartz reactor, which was packed with a small amount of quartz wool to prevent the catalyst from moving. In order to observe the intrinsic reaction kinetics, the methane conversions from dry reforming were always kept below 20% in all experiments.

In the present work, the desired space velocity and suitable catalyst particle size were achieved from several preliminary tests, which were carried out to avoid any limitations by intraparticle diffusion in the experiments. Regarding to these testing, the total flow rate was varied between 20 and 200 $cm^3\ min^{-1}$ under a constant residence time of 5×10^{-4} g min cm^{-3}. When the total flow rate was below 60 $cm^3\ min^{-1}$, the reforming rate increased with increasing the gas flow rate, suggesting that the mass transfer between the bulk gas and the catalyst particles is the rate-determining step. The reforming rate was almost constant in the range where the gas flow rate was higher than 80 $cm^3\ min^{-1}$, indicating that the mass transfer effect is unimportant in this flow rate range. Fig. 2 shows the effect of the total gas flow rate on the reforming rate over 8% CeO_2 doped Ni/Al_2O_3 at different temperatures. The reactions on different average sizes (from 100 to 500 μm) of catalysts were also carried out. It was observed that there were no significant changes in the methane conversion for the catalyst with the particle size between 100 and 200 μm, which indicated that the intraparticle diffusion limitation was negligible in this range of operating conditions. Consequently, the weight of catalyst loading was 50 mg, while the total gas flow was kept constant at 100 $cm^3\ min^{-1}$. The catalyst particle size diameter was between 100 and 200 μm in all experiments.

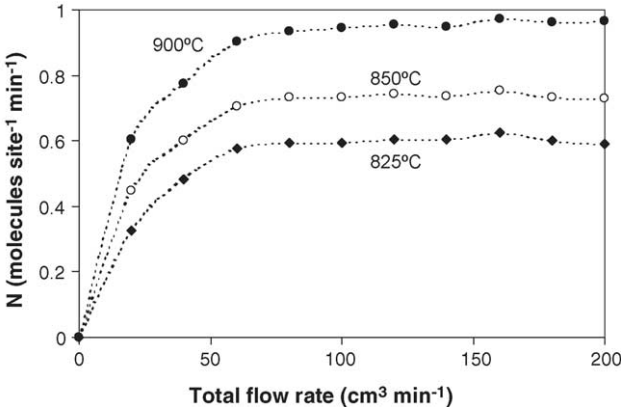

Fig. 2. Effect of the total gas flow rate on the turnover frequencies (*N*) for dry reforming over 8% CeO_2 doped Ni/Al_2O_3 at different temperatures (4 kPa CH_4 and 12 kPa CO_2).

A type-K thermocouple was placed into the annular space between the reactor and the furnace. This thermocouple was mounted on the tubular reactor in close contact with the catalyst bed to minimize the temperature difference between the catalyst bed and the thermocouple. Another type-K thermocouple was inserted in the middle of the quartz tube in order to re-check the possible temperature gradient. The record showed that the maximum temperature fluctuation during the reaction was always ±0.75 °C or less from the temperature specified for the reaction.

After the reactions, the exit gas mixture was transferred via trace-heated lines to the analysis section, which consists of a Porapak Q column Shimadzu 14B gas chromatograph (GC) and a mass spectrometer (MS). The gas chromatography was applied in order to investigate the steady state condition experiments, whereas the mass spectrometer in which the sampling of the exit gas was done by a quartz capillary and differential pumping was used for the transient and carbon formation experiments. In order to study the formation of carbon species on catalyst surface, temperature-programmed oxidation (TPO) was applied by introducing 10% oxygen in helium into the system, after purged with helium. The operating temperature increased from room temperature to 1000 °C by the rate of 10 °C/min. The calibrations of CO and CO_2 productions were performed by injecting a known amount of

these calibration gases from a loop, in an injection valve in the bypass line. The response factors were obtained by dividing the number of moles for each component over the respective areas under peaks. In addition to the TPO method, the amount of carbon deposition was confirmed by the calculation of carbon balance in the system. The amount of carbon deposited on the surface of catalyst would theoretically be equal to the difference between the inlet carbon containing components (CH_4 and CO_2) and the outlet carbon containing components (CO, CO_2, and CH_4). The amount of carbon deposited per gram of catalyst is given by the following equation:

$$C_{\text{deposition}} = \frac{\text{mole}_{\text{carbon (in)}} - \text{mole}_{\text{carbon (out)}}}{m_{\text{catalyst}}} \quad (3)$$

3. Results and discussion

3.1. Catalyst characterizations

After reduction, the catalysts were characterized with several physicochemical methods. The weights content of Ni and Ce loadings were determined by X-ray fluorescence (XRF) analysis. The reducibility and dispersion percentages of nickel were measured from temperature-programmed reduction (TPR) with 5% H_2 in Ar and temperature-programmed desorption (TPD), respectively. The catalyst specific surface areas were obtained from BET measurement. All physicochemical properties of the synthesized catalysts are presented in Table 1. The catalyst specific surface areas slightly increased by the doping of Ce.

3.2. Selection of suitable Ce doping content

After reduction, various Ce contents (from 2 to 14%) doped on Ni/Al_2O_3 were studied in dry reforming at 900 °C. The feed was CH_4/CO_2 in helium with the CH_4/CO_2 ratio of 1.0/0.3. Fig. 3 presents the steady state turnover frequencies (N) for CeO_2 doped Ni/Al_2O_3 with different CeO_2 contents. The turnover frequencies were calculated from the methane conversion following the below equation by assuming that all surface sites accessible by nitrogen adsorption (area per molecule 16.2×10^{-20} m^2 [14]) were active.

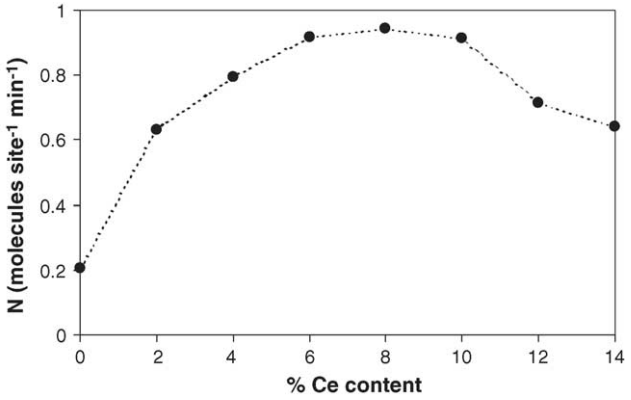

Fig. 3. Effect of Ce doping content on the turnover frequencies (N) for dry reforming (900 °C, 4 kPa CH_4, and 12 kPa CO_2).

$$N = \frac{rN_A A_{N_2}}{m_c S} \quad (4)$$

where r is the reaction rate (moles CH_4 per unit time), N_A the Avagadro's number, A_{N_2} the area occupied by an adsorbed nitrogen molecule (16.2×10^{-20} m^2), m_c the weight of catalyst used (50 mg), and S is the specific surface area of the catalyst. The figure indicates that 8% CeO_2 doping on Ni/Al_2O_3 presents the highest turnover frequencies.

The post-reaction temperature-programmed oxidation experiments were then carried out after a helium purge by introducing of 10% oxygen in helium in order to determine the degree of carbon deposition on the surface of each sample. Table 2 presents the important physicochemical properties of the spent catalysts after exposure in dry reforming conditions for 10 h. According to TPO, the amount of carbon formation decreased with increasing Ce content. No carbon species was observed when the Ce doping content was higher than 8%. The decreasing in the reactivity when more than 10% CeO_2 was doped could be due to the oxidized of Ni, as the reducibility of Ni reduced after exposure in dry reforming for 10 h, regarding to the TPR experiments.

It should also be noted that, at steady state, the main products from this reaction were H_2 and CO with H_2/CO always less than 1, indicating a contribution of the reverse water-

Table 1
Physicochemical properties of the catalysts after reduction at 700 °C

Catalyst	Ni load[a] (wt.%)	Ce load[a] (wt.%)	BET surface area ($m^2\ g^{-1}$)	Ni-reducibility[b] (Ni%)	Ni-dispersion[c] (Ni%)
Ni/Al_2O_3	4.91	0.0	40.2	92.1	4.87
2% Ce-Ni/Al_2O_3	4.84	1.87	40.8	93.5	4.54
4% Ce-Ni/Al_2O_3	4.93	4.02	42.7	91.4	5.12
6% Ce-Ni/Al_2O_3	5.01	5.94	46.5	90.6	4.54
8% Ce-Ni/Al_2O_3	4.96	8.03	49.1	91.1	4.65
10% Ce-Ni/Al_2O_3	4.88	9.86	49.8	89.9	4.77
12% Ce-Ni/Al_2O_3	4.93	12.1	50.4	90.3	4.64
14% Ce-Ni/Al_2O_3	4.92	13.9	50.9	91.0	4.20

[a] Measured from X-ray fluorescence analysis.
[b] Measured from temperature-programmed reduction (TPR) with 5% hydrogen.
[c] Measured from temperature-programmed desorption (TPD) of hydrogen after TPR measurement.

Table 2
Methane conversions, H_2/CO production ratio, and physicochemical properties of the catalysts after exposure in dry reforming (4 kPa CH_4 and 12 kPa CO_2) at 900 °C

Catalyst	CH_4 conversions (%) at steady state	H_2/CO ratio	Ni and Ce load[a] (wt.%)	Carbon formation[b] (monolayers)	BET surface ($m^2\ g^{-1}$)	Ni reducibility[c] (Ni%)	Ni dispersion[d] (Ni%)
Ni/Al_2O_3	3.32	0.89	4.89/0.0	3.48	40.0	92.1	4.84
2% Ce-Ni[e]	9.43	0.88	4.86/1.87	3.01	40.8	93.2	4.48
4% Ce-Ni	12.2	0.84	4.96/4.00	1.62	42.0	91.0	5.07
6% Ce-Ni	14.7	0.81	4.97/5.98	0.43	43.9	90.0	4.52
8% Ce-Ni	15.3	0.80	4.98/8.01	∼0	44.4	90.4	4.60
10% Ce-Ni	14.9	0.77	4.83/9.93	∼0	44.7	87.3	4.71
12% Ce-Ni	11.8	0.75	4.87/11.9	∼0	45.1	70.1	4.55
14% Ce-Ni	10.7	0.71	4.94/14.0	∼0	45.6	67.6	4.14

[a] Measured from X-ray fluorescence analysis.
[b] Calculated using CO and CO_2 yields from temperature-programmed oxidation (TPO) with 10% oxygen.
[c] Nickel reducibility (measured from temperature-programmed reduction (TPR) with 5% hydrogen).
[d] Nickel dispersion (measured from temperature-programmed desorption (TPD) after TPR).
[e] CeO_2 dopedNi/Al_2O_3.

gas shift reaction. Small amount of steam was also observed from the reaction. The H_2/CO ratio decreased with increasing Ce doping content indicated the high reactivity toward the reverse water-gas shift reaction of ceria (Table 2). The reactivities toward the reverse water-gas shift reaction for CeO_2 doped Ni/Al_2O_3 (with several Ce contents) and Ni/Al_2O_3 were tested in order to ensure the above explanation by using TPRx in CO_2/H_2/He gas mixture (5 kPa CO_2 and 10 kPa H_2). Fig. 4 shows the activities of all catalysts toward this reaction. Clearly, the activity toward the RWGS reaction over CeO_2 doped Ni/Al_2O_3 with high Ce content was significantly higher than that over Ni/Al_2O_3 at the same operating conditions.

3.3. Reactivity toward dry reforming

Ni/Al_2O_3 and 8% CeO_2 doped Ni/Al_2O_3 were further studied in dry reforming at 900 °C. The feed was CH_4/CO_2 in helium with different CH_4/CO_2 ratios of 1.0/0.3, 1.0/1.0, and 1.0/3.0. The reforming rate was measured as a function of time in order to indicate the stability and the deactivation rate.

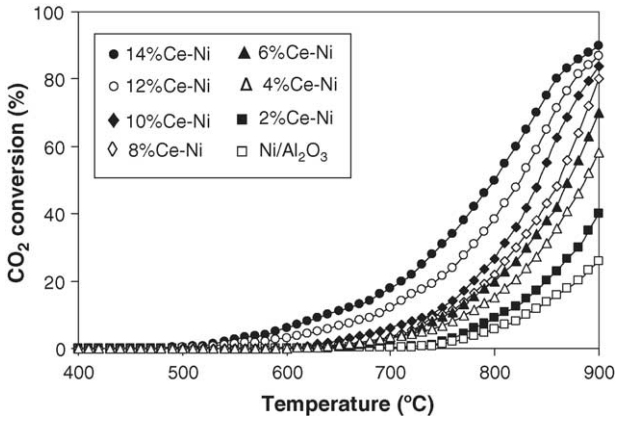

Fig. 4. The activities of Ni/Al_2O_3 and CeO_2 doped Ni/Al_2O_3 (with different Ce contents) toward the reverse water-gas shift reaction using TPRx in CO_2/H_2/He gas mixture (5 kPa CO_2 and 10 kPa H_2).

The variations in turnover frequencies (N) with time at 900 °C for different catalysts and different inlet CH_4/CO_2 ratio are shown in Fig. 5. The significant deactivations were detected for Ni/Al_2O_3 catalyst in all conditions especially at high inlet CH_4/CO_2 ratio, whereas considerable lower deactivations were detected for 8% CeO_2 doped Ni/Al_2O_3. At steady state, the dry reforming over 8% CeO_2 doped Ni/Al_2O_3 with inlet CH_4/CO_2 of 1.0/3.0 showed the best activity. Catalyst stabilities expressed as deactivation percentages are given in Table 3.

The characterization of these spent catalysts by X-ray diffraction (XRD) and X-ray photoelectron spectroscopy (XPS) were then carried out to determine the formation or the changing of chemical states in the spent catalysts, compared to the fresh one after reduction. X-ray diffraction was performed using X-ray defractometer with Cu Kα radiation (λ = 1.54060 Å) and operating parameters of 40 kV and 40 mA. Diffraction patterns were acquired by a step-scanning technique, using a step size ($\Delta 2\theta$) of 0.020°. The XPS spectra were acquired on spectrometer with a hemispherical electron analyser detector, operated in a constant threshold pass energy mode (50 eV), and using a non-monochromatic Al

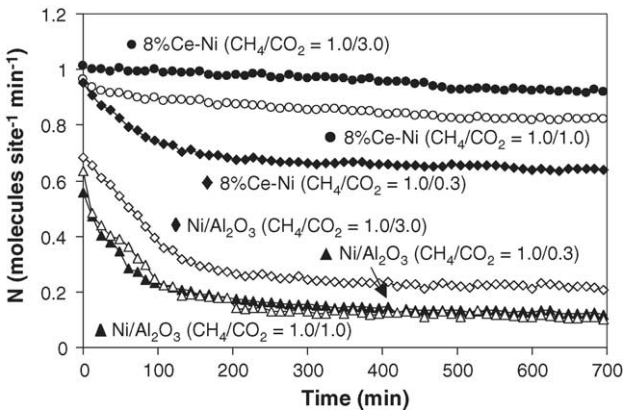

Fig. 5. Dry reforming of methane at 900 °C for several catalysts and various inlet CH_4/CO_2 ratios.

Table 3
Methane conversions, stabilities, and physicochemical properties of the catalysts after exposure in dry reforming conditions at 900 °C for 12 h

Catalyst	CH_4/CO_2 ratio	CH_4 conversions (%) at steady state	Deactivation (%)	Carbon formation[a] (monolayers)	BET after reaction ($m^2\ g^{-1}$)	Ni reducibility[b] (Ni%)
Ni/Al_2O_3	1.0/0.3	1.64	84.2	4.26	40.0	91.0
	1.0/1.0	2.01	78.4	3.97	39.5	93.2
	1.0/3.0	3.32	69.9	3.48	40.0	92.1
8% Ce-Ni[c]	1.0/0.3	10.6	33.1	0.85	44.0	90.0
	1.0/1.0	13.6	14.8	0.34	44.5	89.3
	1.0/3.0	15.3	9.08	~0	44.4	90.4

[a] Calculated using CO and CO_2 yields from temperature-programmed oxidation (TPO) with 10% oxygen.
[b] Nickel reducibility (measured from temperature-programmed reduction (TPR) with 5% hydrogen).
[c] CeO_2 doped Ni/Al_2O_3.

Kα (1.4866 eV) radiation source, which operated at 12 kV and 20 mA. Fig. 6 presents the XRD patterns of the spent and fresh Ni/Al_2O_3 and CeO_2 doped Ni/Al_2O_3. From the XRD results, Ni and $NiAl_2O_4$ reflectance were found in both Ni/Al_2O_3 and CeO_2 doped Ni/Al_2O_3. It is clearly seen that the intensities of $NiAl_2O_4$ peaks for CeO_2 doped Ni/Al_2O_3 were lower than that for Ni/Al_2O_3. This implies that the interaction between NiO and Al_2O_3 was prevented by the doping of CeO_2. A significant carbon peak was observed for the spent Ni/Al_2O_3, indicated the high formation of carbon species on the catalyst surface, whereas a smaller peak of carbon was detect for the spent CeO_2 doped Ni/Al_2O_3.

Table 4 presents the Ce^{3+}/Ce^{4+} ratio for CeO_2 doped Ni/Al_2O_3 before and after exposure in dry methane reforming conditions, determined from XPS. It is seen that no Ce^{3+} (Ce_2O_3) formation was observed for the fresh CeO_2 doped Ni/Al_2O_3 after reduction. Regarding the spent CeO_2 doped Ni/Al_2O_3, no Ce^{3+} formation was detect after exposure in dry methane reforming with the inlet CH_4/CO_2 ratios of 1.0/3.0 and 1.0/1.0, however, a small formation of Ce_2O_3 was observed over CeO_2 doped Ni/Al_2O_3 catalyst after exposure in dry methane reforming with the inlet CH_4/CO_2 ratio of 1.0/0.3. This Ce_2O_3 formation is obviously due to the remaining non-oxidation CeO_2, which will be explained at the end of this section.

Table 4
Ce^{3+}/Ce^{4+} ratio observed from the XPS measurement over CeO_2 doped Ni/Al_2O_3 after reduction and after exposure in dry methane reforming conditions

	Ce^{3+}/Ce^{4+} ratio
After reduction	0
After exposure in dry methane reforming; with CH_4/CO_2 of	
1.0/3.0	0
1.0/1.0	0
1.0/0.3	0.21

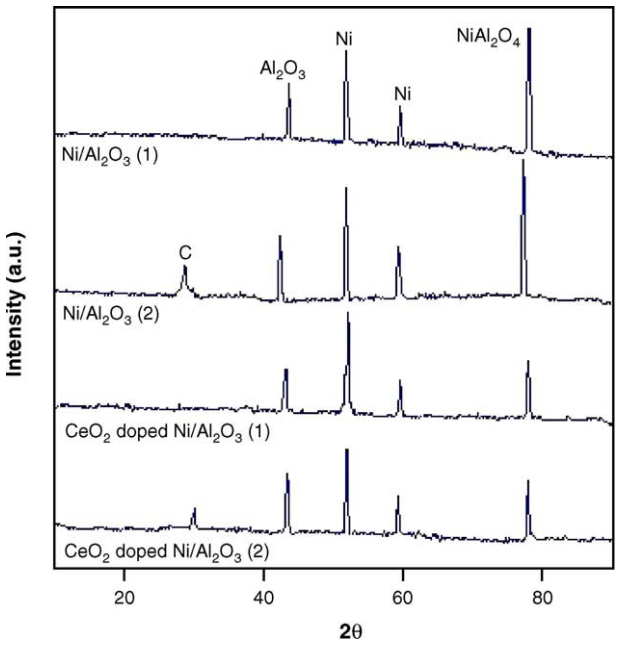

Fig. 6. XRD patterns of the catalysts after reduction (1) and after exposure in dry methane reforming at 900 °C with the inlet CH_4/CO_2 of 1.0/1.0 (2).

The post-reaction temperature-programmed oxidation experiments were then carried out after a helium purge by introducing of 10% oxygen in helium in order to determine whether the observed deactivation is due to the carbon formation. From the TPO results shown in Fig. 7, the huge peaks of carbon dioxide and carbon monoxide were observed for Ni/Al_2O_3 at 600 °C, while smaller peaks of both components were detected for 8% CeO_2 doped Ni/Al_2O_3. The amount of carbon formations on the surface of these catalysts with

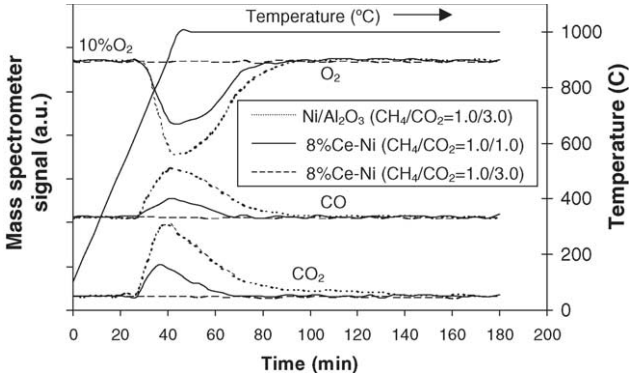

Fig. 7. Temperature-programmed oxidation (TPO) of Ni/Al_2O_3 and 8% CeO_2 doped Ni/Al_2O_3 (10 kPa O_2) after exposure in dry reforming conditions for 10 h.

different inlet CH_4/CO_2 ratios were determined by measuring the CO and CO_2 yields from the TPO results (using Microcal Origin Software). Using a value of 0.026 nm^2 for the area occupied by a carbon atom in a surface monolayer of the basal plane in graphite [17], the quantities of carbon deposited over Ni/Al_2O_3 were observed to be approximately 4.26, 3.97, and 3.48 monolayers, while those over 8% CeO_2 doped Ni/Al_2O_3 were 0.85, 0.34, and ~0 monolayers for the inlet CH_4/CO_2 ratios of 1.0/0.3, 1.0/1.0, and 1.0/3.0, respectively. The total amounts of carbon deposited were ensured by the calculation of carbon balance in the system. Regarding to the calculation for the inlet CH_4/CO_2 ratios of 1.0/0.3, 1.0/1.0, and 1.0/3.0, the moles of carbon deposited per gram of 8% CeO_2 doped Ni/Al_2O_3 were 1.34, 0.49, and ~0 mmol g^{-1}. By the same assumption for the area occupied by a carbon atom [17], these values are equal to 0.87, 0.32, and 0 monolayers, respectively, which is in good agreement with the values observed from the TPO method described above. The results clearly indicated the strong resistance toward carbon formation for 8% CeO_2 doped Ni/Al_2O_3 compared to Ni/Al_2O_3. The BET measurements, as presented in Table 3, indicated that deactivations of 8% CeO_2 doped Ni/Al_2O_3 are also due to the slight sintering of CeO_2. Several researchers also reported the high thermal sintering rate of ceria-based materials at high operating temperature [15,16].

The improvement of dry reforming reactivity and resistance toward carbon formation for CeO_2 doped Ni/Al_2O_3 could be mainly due to the redox property of ceria. During the dry reforming, in addition to the reactions on Ni surface, the solid–gas reaction between CeO_2 and CH_4 also produces synthesis gas with a H_2/CO ratio of two, while the reduced ceria, CeO_{2-x}, can react with CO_2 to produce CO [33–35]. This solid–gas mechanism involves the reactions between methane and/or an intermediate surface hydrocarbon species with the lattice oxygen (O_x) at CeO_2 surface, as illustrated schematically below [36].

$$CH_4 + 2S \Leftrightarrow CH_3{-}S + H{-}S \quad (5)$$

$$CH_3{-}S + S \Leftrightarrow CH_2{-}S + H{-}S \quad (6)$$

$$CH_2{-}S + S \Leftrightarrow CH{-}S + H{-}S \quad (7)$$

$$CH{-}S + S \Leftrightarrow C{-}S + H{-}S \quad (8)$$

$$C{-}S + O_x \Leftrightarrow CO + O_{x-1} + S \quad (9)$$

$$2H{-}S \Leftrightarrow H_2 + 2S \quad (10)$$

During the dry reforming, methane is adsorbed on either a unique site (S) or the lattice oxygen (O_x), whereas CO_2 can react with the reduced site of ceria, O_{x-1}. The steady state reforming rate is mainly due to the continuous supply of the oxygen source by CO_2 (Eq. (11)). Therefore, the Ce_2O_3 formation observed by XPS measurement in Table 4 over spent CeO_2 doped Ni/Al_2O_3 after exposure in dry methane reforming with high inlet CH_4/CO_2 ratio is due to the insufficient supply of inlet CO_2.

$$CO_2 + O_{x-1} \Leftrightarrow O_x + CO \quad (11)$$

Regarding the possible carbon formation during the reforming processes, the following reactions are the most probable reactions that could lead to carbon formation:

$$2CO \Leftrightarrow CO_2 + C \quad (12)$$

$$CH_4 \Leftrightarrow 2H_2 + C \quad (13)$$

$$CO + H_2 \Leftrightarrow H_2O + C \quad (14)$$

$$CO_2 + 2H_2 \Leftrightarrow 2H_2O + C \quad (15)$$

At low temperature, reactions (14) and (15) are favorable, while reaction (12) is thermodynamically unflavored [37]. The Boudard reaction (Eq. (12)) and the decomposition of methane (Eq. (13)) are the major pathways for carbon formation at such a high temperature as they show the largest change in Gibbs energy [38]. According to the range of temperature in this study, 800–900 °C, carbon formation would be formed via the decomposition of methane and Boudard reactions. By doping CeO_2 as the promoter, both reactions (Eqs. (12) and (13)) could be inhibited by the gas–solid reactions between methane and carbon monoxide with the lattice oxygen (O_x) at CeO_2 surface forming hydrogen and carbon dioxide, which is thermodynamically unflavored to form carbon species.

3.4. Effects of temperature and inlet components

The inlet methane partial pressure was varied from 1 to 4 kPa, while inlet carbon dioxide partial pressure was kept constant at 12 kPa. The operating temperature range was 825–900 °C. Fig. 8 illustrates the influence of the inlet methane partial pressure on the turnover frequencies (N) for dry reforming over 8% CeO_2 doped Ni/Al_2O_3 at different operating temperatures. The activities of catalyst increased with increasing inlet methane partial pressure as well as operating temperature. Fig. 9 shows an Arrhenius-type plot

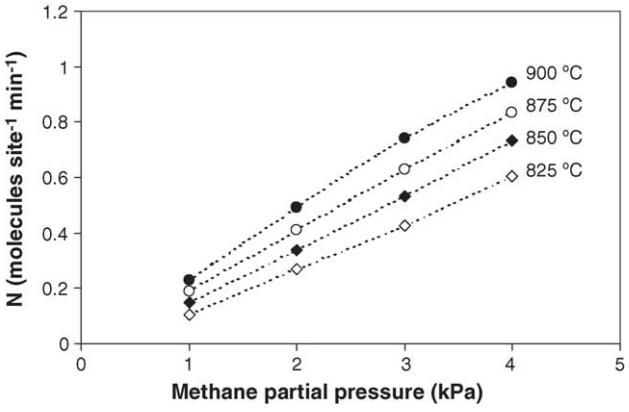

Fig. 8. Effect of methane partial pressure on the turnover frequencies (N) for dry reforming over 8% CeO_2 doped Ni/Al_2O_3 at different temperatures (12 kPa inlet CO_2).

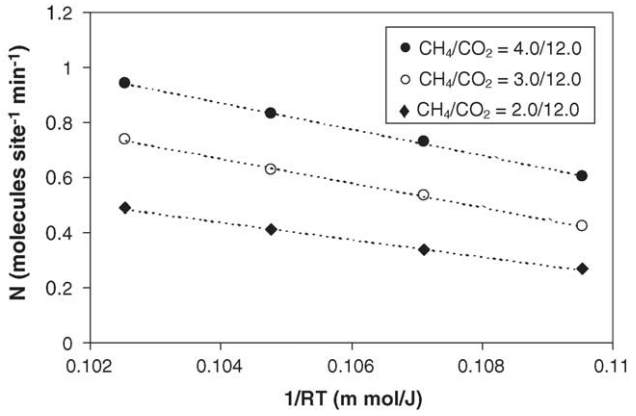

Fig. 9. Arrhenius plot of turnover frequencies (N) for dry reforming of methane over 8% CeO_2 doped Ni/Al_2O_3 with different inlet methane/carbon dioxide ratio.

for dry reforming over CeO_2 doped Ni/Al_2O_3 with various methane/carbon dioxide ratios over the temperature range 825–900 °C. The corresponding activation energy observed for this catalyst is 178 ± 9 kJ/mol, slightly depending on the gas composition.

The reaction order in methane (n) for CeO_2 doped Ni/Al_2O_3 was observed to be 0.96–1.04, and seemed to be essentially independent of the operating temperature and other inlet compositions in the range of conditions studied. These values n were obtained experimentally by plotting $\ln(-r_{CH_4})$ versus $\ln(P_{CH_4})$ according to the equation below.

$$\ln(-r_{CH_4}) = \ln(k) + n\ \ln(P_{CH_4}) \quad (16)$$

where $-r_{CH_4}$ is the dry reforming rate (mol kg_{cat}^{-1} h^{-1}), while P_{CH_4} the methane partial pressure. k is the apparent reaction rate constant and n is the reaction order in methane. The reaction orders in other components (CO_2, H_2, and CO) were achieved using the same approach by varying the inlet partial pressure of the component of interest and keeping other inlet component partial pressures constant.

In order to investigate the influence of CO_2 on the dry reforming rate, several inlet carbon dioxide partial pressures, from 9 to 12 kPa, were introduced to the feed with constant methane partial pressure (3 kPa). Carbon dioxide presented slight positive effect on the dry reforming rate as shown in Fig. 10. The reaction order in carbon dioxide was observed to be a positive value between 0.44 and 0.54, and seemed to be independent of the operating temperature for the range of conditions studied. At 900 °C, the proportion of H_2/CO in the products reduced from 0.80 to 0.67 as the CO_2/CH_4 ratio was increased from 3.0 to 12.0 (Fig. 11). This is as expected from an increasing contribution from the reverse water-gas shift (RWGS) reaction.

The dry reforming in the presences of carbon monoxide and hydrogen were then investigated by adding either carbon monoxide or hydrogen to the feed gas at several operating temperatures. The results show that the reforming rates are also dependent on both carbon monoxide and hydrogen

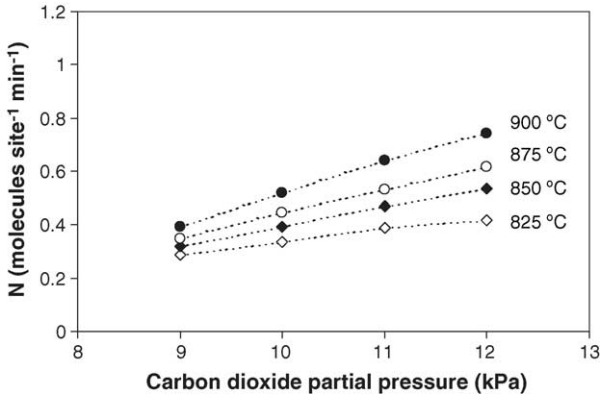

Fig. 10. Effect of carbon dioxide partial pressure on the turnover frequencies (N) for dry reforming over 8% CeO_2 doped Ni/Al_2O_3 at different temperatures (3 kPa CH_4).

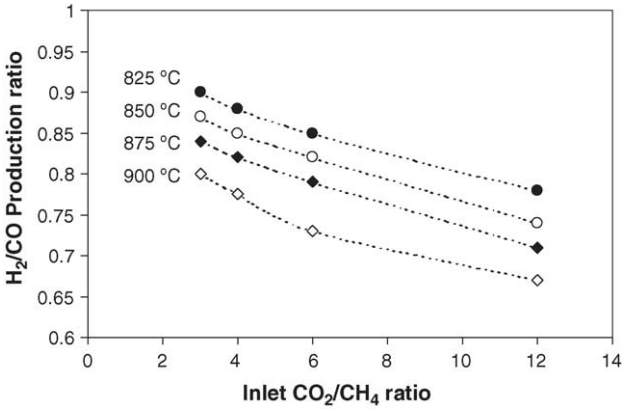

Fig. 11. Influence of inlet carbon dioxide/methane ratio on H_2/CO production ratio from dry reforming of methane over 8% CeO_2 doped Ni/Al_2O_3 at different temperatures (12 kPa CO_2).

concentrations. Unlike CH_4 and CO_2, both components inhibited the dry reforming rate as shown in Figs. 12 and 13. The reaction order in carbon monoxide was in the range of −0.42 to −0.37, while the reaction order in hydrogen was between −0.55 and −0.45 in the range of conditions studied.

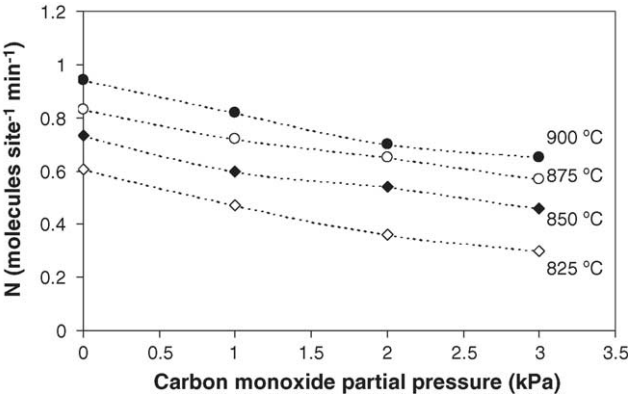

Fig. 12. Effect of carbon monoxide partial pressure on the turnover frequencies (N) for dry reforming of methane over 8% CeO_2 doped Ni/Al_2O_3 at different temperatures (4 kPa CH_4 and 12 kPa CO_2).

Table 5
Reaction orders for the components of interest (CH_4, CO_2, CO, and H_2) from dry reforming over 8% CeO_2 doped Ni/Al_2O_3 at different operating conditions

Components of interest	Temperature (°C)	Other inlet compositions	Reaction order for components of interest
Methane (1–4 kPa)	825	12 kPa CO_2	1.00
	850	12 kPa CO_2	0.97
	900	12 kPa CO_2	0.98
	850	15 kPa CO_2	1.01
	850	17 kPa CO_2	0.99
	825–900	12 kPa CO_2/1 kPa H_2	1.01 ± 0.03
	825–900	12 kPa CO_2/3 kPa H_2	0.98 ± 0.01
	825–900	12 kPa CO_2/1 kPa CO	0.99 ± 0.03
Carbon dioxide (9–12 kPa)	825	3 kPa CH_4	0.44
	850	3 kPa CH_4	0.54
	900	3 kPa CH_4	0.50
	850	3 kPa CH_4/3 kPa H_2	0.48
Hydrogen (1–3 kPa)	825–900	3 kPa CH_4/12 kPa CO_2	-0.49 ± 0.04
	825–850	1 kPa CH_4/12 kPa CO_2	-0.48 ± 0.03
	825–850	3 kPa CH_4/15 kPa CO_2	-0.52 ± 0.03
Carbon monoxide (1–3 kPa)	825–900	3 kPa CH_4/12 kPa CO_2	-0.40 ± 0.01
	825–850	3 kPa CH_4/15 kPa CO_2	-0.38 ± 0.01
	825–850	3 kPa CH_4/17 kPa CO_2	-0.40 ± 0.02

Table 5 presents the summary of observed reaction orders in each component (CH_4, CO_2, CO, and H_2) for CeO_2 doped Ni/Al_2O_3 at different inlet conditions.

Regarding to the above experiments, the experimental data can be fitted well to a simple relative rate coefficient, in which captures the essential features.

$$-r_{CH_4} = \frac{k(T)(P_{CH_4})^n(P_{CO_2})^m}{1 + K_1(T)P_{CO}^a + K_2(T)P_{H_2}^b} \quad (17)$$

where P_i is the partial pressure of chemical component i. The positive effects of methane and carbon dioxide on the dry reforming rate were a consequence of the presence of the $k(T)(P_{CH_4})^n(P_{CO_2})^m$ term, whereas negative effects of carbon monoxide and hydrogen were a consequence of the $K_1(T)P_{CO}^a$ and $K_2(T)P_{H_2}^b$ terms in the denominator. According to the fitting, when n, m, a, and b were taken as 1.0, 0.5, 0.4, and 0.5, a good fit to the data was observed in the range of conditions studied. $k(T)$ increased from 649.0 mol kg^{-1} h^{-1} atm$^{-1.5}$ at 825 °C to 954.3 mol kg^{-1} h^{-1} atm$^{-1.15}$ at 900 °C, while $K_1(T)$ and $K_2(T)$, also temperature dependent parameters, were in the range of 1.68–4.43 atm$^{-0.4}$ and 0.93–3.94 atm$^{-0.5}$, respectively. It should be noted that the apparent activation energy for this reaction, which were achieved by the Arrhenius plots, was approximately 150 kJ/mol.

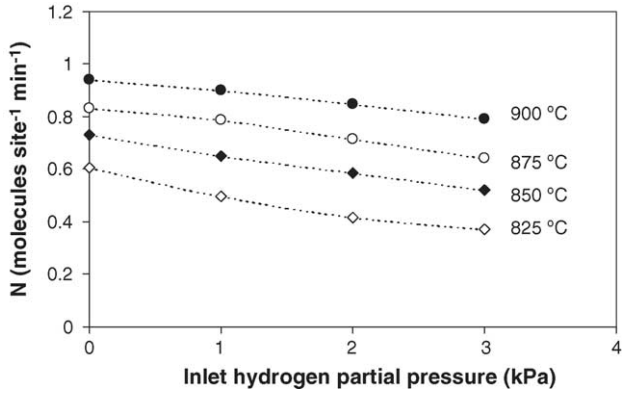

Fig. 13. Effect of hydrogen partial pressure on the turnover frequencies (N) for dry reforming of methane over 8% CeO_2 doped Ni/Al_2O_3 at different temperatures (4 kPa CH_4 and 12 kPa CO_2).

4. Conclusion

8% CeO_2 doped Ni/Al_2O_3 is a good candidate catalyst for the dry reforming of methane due to the high resistance toward the deactivation from carbon formation. During dry reforming process, the gas–solid reaction on ceria surface takes place simultaneously with the reactions on the surface of Ni, in which reduces the degree of carbon deposition on catalyst surface from methane decomposition and Boudard reactions. However, it should also be noted that the doping of too high ceria content results in the oxidation of Ni, which could reduce the reforming reactivity.

The intrinsic kinetic reaction of 8% CeO_2 doped Ni/Al_2O_3 was studied in the conditions where the intraparticle diffusion limitation was negligible. The dry reforming rate increased with increasing methane and carbon dioxide partial pressures as well as the operating temperature. In contrast, the methane conversion was inhibited when hydrogen and carbon monoxide were added to the system during dry reforming process. It can be concluded from the present work that CeO_2 doped Ni/Al_2O_3 seems to be a promise catalyst for the indirect internal reforming solid oxide fuel cells (IIR-SOFC) operation.

Acknowledgement

The financial support from The Thailand Research Fund (TRF) throughout this project is gratefully acknowledged.

References

[1] P. Aguiar, D. Chadwick, L. Kershenbaum, Chem. Eng. Sci. 57 (2002) 1665.
[2] J.H. Edwards, A.M. Maitra, Fuel Process. Technol. 42 (1995) 269.
[3] M.A. Vannice, M.C.J. Bradford, Appl. Catal. A: Gen. 142 (1) (1996) 97–122.
[4] T. Sodesawa, A. Dobashi, F. Nozaki, React. Kinet. Catal. Lett. 12 (1979) 107.
[5] L. Topor, L. Bejan, E. Ivana, N. Georgescu, Rev. Chim. Bucharest 30 (1979) 539.
[6] T.A. Chubb, Sol. Energy 24 (1980) 341.
[7] T.A. Chubb, J.H. McCrary, G.E. McCrary, J.J. Nemecek, D.E. Simmons, Proc. Meet. Am. Sect. Int. Sol. Eng. Soc. 4 (1981) 166.
[8] J.R. Rostrup-Nielsen, J.H. Bak Hansen, J. Catal. 144 (1993) 38.
[9] P. Gronchi, C. Mazzocchia, E. Tempesti, R. Del Rosso, in: G. Centi, et al. (Eds.), Enviromental Catalysis, SCI Publication, Roma, 1995, p. 627.
[10] A. Erdöhelyi, J. Cserényi, F. Solymosi, J. Catal. 141 (1993) 287.
[11] A. Erdöhelyi, J. Cserényi, E. Rapp, F. Solymosi, Appl. Catal. A: Gen. 108 (1994) 205.
[12] J. Nakamura, K. Aikawa, K. Sato, T. Uchijima, Catal. Lett. 25 (1994) 265.
[13] Z.L. Zhang, V.A. Tsipouriari, A.M. Efstathiou, X.E. Verykios, J. Catal. 158 (1996) 51.
[14] E. Ramírez-Cabrera, A. Atkinson, D. Chadwick, Appl. Catal. B 47 (2004) 127–131.
[15] E. Ramírez-Cabrera, N. Laosiripojana, A. Atkinson, D. Chadwick, Catal. Today 78 (2003) 433–438.
[16] N. Laosiripojana, Reaction engineering of indirect internal steam reforming of methane for application in solid oxide fuel cells, Ph.D. Thesis, University of London, England, 2003.
[17] E. Ramirez, A. Atkinson, D. Chadwick, Appl. Catal. B 36 (2002) 193–206.
[18] X. Wang, R.J. Gorte, Appl. Catal. A 224 (2002) 209–218.
[19] H.S. Roh, K.W. Jun, W.S. Dong, J.S. Chang, S.E. Park, Y.I. Joe, J. Mol. Catal. A 181 (2002) 137–142.
[20] Q. Miao, G. Xiong, S. Sheng, W. Cui, L. Xu, X. Guo, Appl. Catal. A 154 (1987) 17–27.
[21] A.A. Lemonidou, M.A. Goula, I.A. Vasalos, Catal. Today 46 (1987) 175–183.
[22] W.S. Dong, H.S. Roh, K.W. Jun, S.E. Park, Y.S. Oh, Appl. Catal. A 226 (2002) 63–72.
[23] M. Mamak, N. Coombs, G. Ozin, Adv. Mater. 12 (2000) 198–202.
[24] M. Mamak, N. Coombs, G. Ozin, J. Am. Chem. Soc. 122 (2000) 8932.
[25] M. Mamak, N. Coombs, G.A. Ozin, Chem. Mater. 13 (2001) 3564.
[26] P. Bera, S. Mitra, S. Sampath, M.S. Hegde, Chem. Commun. (2001) 927.
[27] A. Martinez-Arias, J.M. Coronado, R. Cataluna, J.C. Conesa, J.C. Soria, J. Phys. Chem. B 102 (1998) 4357.
[28] D. Skarmoutsos, F. Tietz, P. Nikolopoulos, Fuel Cells 1 (2001) 243.
[29] T. Takeguchi, S.N. Furukawa, M. Inoue, J. Catal. 202 (2001) 14.
[30] J. Sfeir, P.A. Philippe, P. Moseki, N. Xanthopoulos, R. Vasquez, J.M. Hans, V.H. Jan, K.R. Thampi, J. Catal. 202 (2001) 229.
[31] N. Kiratzis, P. Holtappels, C.E. Hatchwell, M. Mogensen, J.T.S. Irvine, Fuel Cells 1 (2001) 211.
[32] S. Wang, G.Q. Lu, Appl. Catal. B 19 (1998) 267.
[33] K. Otsuka, T. Ushiyama, I. Yamanaka, Chem. Lett. (1993) 1517.
[34] K. Otsuka, M. Hatano, A. Morikawa, J. Catal. 79 (1983) 493.
[35] K. Otsuka, M. Hatano, A. Morikawa, Inorg. Chim. Acta 109 (1985) 193.
[36] N. Laosiripojana, S. Assabumrungrat, Appl. Catal. B 60 (2005) 109–118.
[37] Y. Lwin, W.R.W. Daud, A.B. Mohamad, Z. Yaakob, Int. J. Hydrogen Energy 25 (1) (2000) 47–53.
[38] J.N. Amor, Appl. Catal. A 176 (1999) 159–176.

ARTICLE IN PRESS

ELSEVIER

Chemical Engineering Science ▮▮▮ (▮▮▮▮) ▮▮▮–▮▮▮

Chemical Engineering Science

www.elsevier.com/locate/ces

The effect of specific surface area on the activity of nano-scale ceria catalysts for methanol decomposition with and without steam at SOFC operating temperatures

N. Laosiripojana[a,*], S. Assabumrungrat[b]

[a]*The Joint Graduate School of Energy and Environment, King Mongkut's University of Technology Thonburi, Bangkok 10140, Thailand*

[b]*Center of Excellence on Catalysis and Catalytic Reaction Engineering, Department of Chemical Engineering, Chulalongkorn University, Bangkok 10330, Thailand*

Received 25 August 2005; received in revised form 14 November 2005; accepted 14 November 2005

Abstract

Nano-particulate high surface area CeO_2 was found to have a useful methanol decomposition activity producing H_2, CO, CO_2, and a small amount of CH_4 without the presence of steam being required under solid oxide fuel cell temperatures, 700–1000 °C. The catalyst provides high resistance toward carbon deposition even when no steam is present in the feed. It was observed that the conversion of methanol was close to 100% at 850 °C, and no carbon deposition was detected from the temperature programmed oxidation measurement.

The reactivity toward methanol decomposition for CeO_2 is due to the redox property of this material. During the decomposition process, the gas–solid reactions between the gaseous components, which are homogeneously generated from the methanol decomposition (i.e., CH_4, CO_2, CO, H_2O, and H_2), and the lattice oxygen (O_O^x) on ceria surface take place. The reactions of adsorbed surface hydrocarbons with the lattice oxygen ($C_nH_m + O_O^x \rightarrow nCO + m/2(H_2) + V_{O^{\cdot\cdot}} + 2e'$) can produce synthesis gas (CO and H_2) and also prevent the formation of carbon species from hydrocarbons decomposition reaction ($C_nH_m \Leftrightarrow nC + m/2H_2$). $V_{O^{\cdot\cdot}}$ denotes an oxygen vacancy with an effective charge 2^+. Moreover, the formation of carbon via Boudouard reaction ($2CO \Leftrightarrow CO_2 + C$) is also reduced by the gas–solid reaction of carbon monoxide with the lattice oxygen ($CO + O_O^x \Leftrightarrow CO_2 + V_{O^{\cdot\cdot}} + 2e'$).

At steady state, the rate of methanol decomposition over high surface area CeO_2 was considerably higher than that over low surface area CeO_2 due to the significantly higher oxygen storage capacity of high surface area CeO_2, which also results in the high resistance toward carbon deposition for this material. In particular, it was observed that the methanol decomposition rate is proportional to the methanol partial pressure but independent of the steam partial pressure at 700–800 °C. The addition of hydrogen to the inlet stream was found to have a significant inhibitory effect on the rate of methanol decomposition.

Keywords: Methanol; Internal reforming; Hydrogen; SOFC; CeO_2

1. Introduction

A fuel cell is an energy conversion unit that produces electrical energy and heat with greater energy efficiency and lower pollutant emission than conventional processes (Minh and Takahashi, 1995). Among the various types of fuel cell, the solid oxide fuel cell (SOFCs) has attracted considerable interest as it offers a wide range of applications, flexibility in the choice of fuel, and high-system efficiency. The waste heat can also be utilized in co-generation applications and bottoming cycles. Moreover, unlike the low-temperature fuel cells, the SOFC anode is not affected by carbon monoxide poisoning.

Hydrogen is the major fuel for SOFCs. Nevertheless, the use of other fuels such as methane, methanol, ethanol, gasoline and other oil derivatives is also possible when operated as an internal or in-stack reforming. As SOFCs are operated at such a high temperature, these hydrocarbons can be internally reformed to produce a H_2/CO rich gas, which is eventually used to generate the electrical energy and heat.

* Corresponding author. Tel.: +66 2 8729014; fax: +66 2 8726736.
E-mail address: navadol_l@jgsee.kmutt.ac.th (N. Laosiripojana).

0009-2509/$ - see front matter © 2005 Published by Elsevier Ltd.
doi:10.1016/j.ces.2005.11.024

This operation, called indirect internal reforming (IIR-SOFC), is expected to simplify the overall system design (Aguiar et al., 2001). Douvartzides et al. (2003), applied a thermodynamic analysis to evaluate the feasibility of different fuels, i.e., methane, methanol, ethanol and gasoline, for SOFCs. The results obtained in terms of electromotive force output and efficiency show that ethanol and methanol are very promising alternatives to hydrogen. Among them, methanol is favourable due to its ready availability, high-specific energy and storage transportation convenience (Emonts et al., 1998; Ledjeff-Hey et al., 1998).

Several researchers have studied the catalytic decomposition of methanol with steam (Lwin et al., 2000; Brown, 2001; Maggio et al., 1998). The well known reactions involved in this process can be represented by the decomposition-shift mechanism

$$CH_3OH = 2H_2 + CO \quad \text{(methanol decomposition)}, \tag{1}$$

$$CO + H_2O = H_2 + CO_2 \quad \text{(water gas shift reaction)}, \tag{2}$$

$$CO + 3H_2 = CH_4 + H_2O \quad \text{(methanation)}. \tag{3}$$

Firstly, methanol can be directly converted to hydrogen and carbon monoxide by the decomposition process (Eq. (1)). In the presence of steam, the water–gas shift reaction (Eq. (2)) takes place to produce carbon dioxide and more hydrogen. Methane can be formed by the methanation reaction (Eq. (3)). It should be noted that the formations of higher molecular weight compounds such as formaldehyde, methyl formate and formic acid were found to be negligible (Lwin et al., 2000).

A major concern of the methanol decomposition is catalyst deactivation by carbon formation which, consequently, leads to the loss of system performance and poor durability (Dicks, 1996). The following are the most probable carbon formation reactions:

$$2CO = CO_2 + C, \tag{4}$$

$$CH_4 = 2H_2 + C, \tag{5}$$

$$CO + H_2 = H_2O + C, \tag{6}$$

$$CO_2 + 2H_2 = 2H_2O + C. \tag{7}$$

At low temperature, reactions (6)–(7) are favourable while reaction (5) is thermodynamically unfavoured. The Boudouard reaction (Eq. (4)) and the decomposition of methane (Eq. (5)) are the major pathways for carbon formation at high temperature as they show the largest change in Gibbs energy (Amor, 1999). Regarding the IIR-SOFC operation, the reforming temperatures are in the range of 700–1000 °C (Aguiar et al., 2001). The potential formation of carbon species on the surface of catalyst therefore arises from the decomposition and Boudouard reactions.

In order to maximize hydrogen production from the decomposition of methanol and to reduce the amount of carbon deposition, selection of catalyst is an important issue as it has been evident that the degree of carbon formation strongly depends on the type of catalyst used (Rostrup-Nielsen and Bak-Hansen, 1993). It is well established that cerium oxide is a useful catalyst for a wide variety of reactions involving the oxidation or partial oxidation of hydrocarbons (e.g. automotive catalysis). This material contains a high concentration of highly mobile oxygen vacancies and thus acts as a local source or sink for oxygen involved in reactions taking place on the ceria surface. There is now increasing interest in using ceria in more severe reducing conditions, such as in methane reforming at the anodes of SOFC, where the possibility of deactivation through carbon deposition is much higher (Marina et al., 1998). The excellent resistance toward carbon formation from methane cracking reaction over CeO_2 under SOFC conditions was reported (Laosiripojana, 2003). Recently, the successful use of ceria as a key constituent of the anode for a SOFC operated directly with 'dry' methane has also been presented. Furthermore, successful developments of the direct internal reforming (DIR-SOFC), in which the hydrocarbons can be reformed internally at the anode side of SOFC, using copper–ceria-based anodes (i.e., Cu–CeO_2, and Cu–CeO_2-YSZ) fueled by several hydrocarbon and oxyhydrocarbon compounds (i.e., C_4H_{10} and CH_3OH) were also reported (Kim et al., 2005; Jung et al., 2005; Costa-Nunes et al., 2005; Gorte et al., 2004; An et al., 2004; Brett et al., 2005). It was demonstrated that the addition of ceria at the anode can provide a stable operation and reasonable performance with a wide variety of hydrocarbon fuels (Jung et al., 2005; Costa-Nunes et al., 2005).

The gas–solid reaction between CeO_2 and CH_4 produces synthesis gas with a H_2/CO ratio of two, according to the following reaction (Otsuka et al., 1983):

$$CH_4 + O_O^x = 2H_2 + CO + V_{O^{\cdot\cdot}} + 2e'. \tag{8}$$

$V_{O^{\cdot\cdot}}$ denotes an oxygen vacancy with an effective charge 2^+, e' is an electron which can either be more or less localized on a cerium ion or delocalized in a conduction band. Moreover, it was also demonstrated that the reactions of the reduced ceria with CO_2 and steam produced CO and H_2, respectively, and regenerated the CeO_2 surface (Otsuka et al., 1985; Gellings and Bouwmeester, 2000)

$$V_{O^{\cdot\cdot}} + 2e' + CO_2 = O_O^x + CO, \tag{9}$$

$$V_{O^{\cdot\cdot}} + 2e' + H_2O = O_O^x + H_2. \tag{10}$$

The major limitation for the application of ceria to high temperature applications is its low specific surface area due to the significant size reduction by thermal sintering (Laosiripojana, 2003). It was reported that the corresponding post-reaction specific surface area for CeO_2 after exposure in methane steam reforming conditions at 900 °C for 10 h was 1.9 $m^2\,g^{-1}$, and the observed size reduction percentage was 23% (Laosiripojana, 2003). Therefore, the use of nano-particulate high surface area ceria would be a promising procedure to improve its catalytic performance at high operating temperatures.

The present work is focused on the study of hydrogen production from methanol decomposition at SOFC operating temperature of 700–1000 °C. The decomposition of methanol with and without steam presence over nano-particulate high surface area CeO_2 (CeO_2 (HSA)), synthesized by Nanophase Technologies Corporation, was investigated. The reactivity toward this reaction and the resistance toward carbon formation of this

material were compared to CeO_2 prepared by a precipitation method (CeO_2 (LSA)). At steady state, the influences of temperature and inlet components on the product selectivities were determined.

2. Experimental

2.1. Catalyst preparation and characterization

Nano-particulate high surface area CeO_2 powder (CeO_2 (HSA)) (NanoArc Cerium Oxide SGH grade with the average particle size of 11 nm) was supplied by Nanophase Technologies Corporation, USA. This material is prepared by the patent-pending NanoArc^{TM} Synthesis (NAS) process, using arc energy to produce nanoparticles. The nanomaterials produced by the NAS process consist of discrete, fully-dense particles of defined crystallinity. This method has been used to produce particles with average sizes ranging from 7 to 45 nm (http://www.nanophase.com). CeO_2 (HSA) was dried in an oven and calcined in air at 1000 °C for 6 h in order to minimize sintering at the maximum reaction temperature used in subsequent experiments (Ramírez-Cabrera et al., 2002). For comparison, a synthesized CeO_2 (CeO_2 (LSA)) was also prepared by precipitation of cerium chloride ($CeCl_3 \cdot 7H_2O$) from Aldrich. The starting solution was prepared by mixing 0.1 M of this metal salt solution with 0.4 M of ammonia at a 2:1 volumetric ratio. The mixture was stirred by a magnetic stirrer (100 rpm) and then aqueous ammonia was slowly added with the constant rate of 0.165 $cm^3\ min^{-1}$ until the pH was 11.5. We found that the rate of ammonia doping has a significant impact on the particle size and specific surface area of the synthesized CeO_2. This solution was stirred for 3 h, then sealed and placed in a thermostatic bath maintained at 90 °C for three days. The precipitate was filtered and washed with deionized water and acetone to remove the free surfactant. It was dried overnight in an oven at 110 °C, and then calcined in air at 1000 °C for 6 h. BET measurements of CeO_2 were carried out before and after the calcinations in order to determine the specific surface area. As presented in Table 1, after drying in the oven, surface areas of 82 and 55 $m^2\ g^{-1}$ were observed for CeO_2 (HSA) and CeO_2 (LSA), respectively, and as expected, the surface area dramatically decreased at high calcination temperatures. However, the value for CeO_2 (HSA) is still appreciable after calcination at 1000 °C and it is almost 3 times of that for the CeO_2 (LSA). The average mean particle sizes of CeO_2 (HSA) and CeO_2 (LSA) after calcination at 1000 °C were 60–90 and 135–160 nm, respectively.

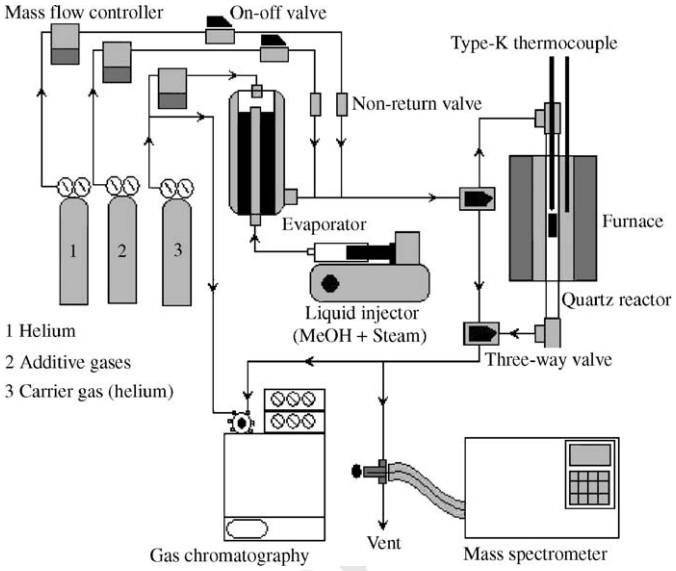

Fig. 1. Schematic diagram of the experimental set-up.

The redox properties and redox reversibilities of CeO_2 (HSA) and CeO_2 (LSA) were compared by the temperature programmed reduction (TPR-1) at high temperature and the temperature programmed oxidation (TPO) following with the second time temperature programmed reduction (TPR-2), respectively. In these experiments, 5% hydrogen and 10% oxygen in helium were used for the TPR and TPO, respectively, while the temperature of the system increased from room temperature to 900 °C by the rate of 8 °C/ min for both experiments.

2.2. Apparatus and procedures

An experimental reactor system was constructed as shown in Fig. 1. The feed gases including the components of interest (methanol and steam from the evaporator) and the carrier gas (helium) were introduced to the reaction section, in which 10-mm diameter quartz reactor was mounted vertically inside a furnace. The inlet methanol concentration was 5% (5 kPa), while the inlet steam concentrations were varied depending on the inlet H_2O/CH_3OH molar ratio requirement for each experiment (0, 1, and 3). The total gas pressure was always kept constant at 101.3 kPa. The catalyst (50 mg) was loaded in the quartz reactor, which was packed with a small amount of quartz wool to prevent the catalyst from moving. A Type-K thermocouple was placed into the annular space between the reactor and the furnace. This thermocouple was mounted on the tubular

Table 1
Specific surface area of the catalysts after drying and calcinations at different temperatures

Catalyst	BET surface area ($m^2\ g^{-1}$) after drying and calcination at						
	100 °C	200 °C	400 °C	600 °C	800 °C	900 °C	1000 °C
CeO_2 (LSA)	55	49	36	21	15	11	8.1
CeO_2 (HSA)	82	79	68	56	43	35	24

reactor in close contact with the catalyst bed to minimize the temperature difference between the catalyst bed and the thermocouple. Another Type-K thermocouple was inserted in the middle of the quartz tube in order to re-check the possible temperature gradient. The record showed that the maximum temperature fluctuation during the reaction was always ±0.75 °C or less from the temperature specified for the reaction.

After the reactions, the exit gas mixture was transferred via trace-heated lines to the analysis section, which consists of a Porapak Q column Shimadzu 14B gas chromatograph (GC) and a mass spectrometer (MS). The gas chromatography was applied in order to investigate the steady state condition experiments, whereas the mass spectrometer in which the sampling of the exit gas was done by a quartz capillary and differential pumping was used for the transient carbon formation experiment. In the present work, the outlet of the GC column was directly connected to a thermal conductivity detector (TCD) and a frame ionization detector (FID). In order to satisfactorily separate CH_3OH, CH_4, CO, CO_2, and H_2, the temperature setting inside the GC column was programmed varying with time. In the first 3 min, the column temperature was constant at 60 °C, it was then increased steadily by the rate of 15 °C/ min until 120 °C. Finally, the temperature was decreased to 60 °C. The analytical method applied is an internal standardization in which the peak area is related to the molar concentration through the response factor (RF)

$$\mathrm{RF} = \frac{\text{concentration (ppm)}}{\text{peak area}}. \tag{11}$$

In order to study the formation of carbon species on catalyst surface, TPO was applied by introducing 10% oxygen in helium into the system, after purging with helium. The operating temperature increased from room temperature to 1000 °C by a rate of 20 °C/min. The calibrations of CO and CO_2 productions were performed by injecting a known amount of these calibration gases from a loop, in an injection valve in the bypass line. The response factors were obtained by dividing the number of moles for each component over the respective areas under peaks. The amount of carbon formation on the surface of catalysts were determined by measuring the CO and CO_2 yields from the TPO results (using Microcal Origin Software) assuming a value of 0.026 nm^2 for the area occupied by a carbon atom in a surface monolayer of the basal plane in graphite (Ramírez-Cabrera et al., 2004). In addition to the TPO method, the amount of carbon deposition was confirmed by the calculation of carbon balance in the system. The amount of carbon deposited on the surface of catalyst would theoretically be equal to the difference between the inlet carbon containing components (CH_3OH) and the outlet carbon containing components (CO, CO_2, and CH_4). The amount of carbon deposited per gram of catalyst is given by the following equation:

$$C_{\text{deposition}} = \frac{\text{mole}_{\text{carbon(in)}} - \text{mole}_{\text{carbon(out)}}}{m_{\text{catalyst}}}. \tag{12}$$

2.3. Kinetic parameters formulae

The rate of methanol decomposition was defined in term of the turnover frequencies (N) which is calculated from the following equation. It was assumed that all surface sites accessible by nitrogen adsorption were active

$$N = \frac{r N_A A_{N_2}}{m_c S}, \tag{13}$$

where r is the reaction rate (moles of CH_3OH per unit time), N_A is the Avagadro's number, A_{N_2} is the area occupied by an adsorbed nitrogen molecule (16.2×10^{-20} m^2 $molecule^{-1}$ (Ramírez-Cabrera et al., 2004)), m_c is the mass of catalyst (50 mg), and S is the specific surface area of the catalyst.

Methanol conversions denoted as X_{Methanol}, and the product selectivities (hydrogen, carbon monoxide, carbon dioxide, and methane), denoted as S_{Product}, are calculated according to

$$X_{\text{Method}} = \frac{100(\text{Methanol}_{\text{in}} - \text{Methanol}_{\text{out}})}{\text{Methanol}_{\text{in}}}, \tag{14}$$

$$S_{\text{Product}} = \frac{100(\text{Mole of a specific product})}{(\text{Total moles of all products})}. \tag{15}$$

3. Results

3.1. Preliminary tests

In order to avoid any limitations by intraparticle diffusion, we checked the impact of the total flow rate at the minimum (700 °C) and maximum operating temperature (1000 °C) before the formal investigations. The total flow rate was changed between 20 and 200 cm^3 min^{-1} under the same residence time of 5×10^{-4} g min cm^{-3}. From Fig. 2, when the total flow rate was below 60 cm^3 min^{-1}, the methanol conversion and the hydrogen selectivity increased with increasing the gas flow rate, suggesting that the mass transfer between the bulk gas and the catalyst particles is the rate-determining step. The steady state

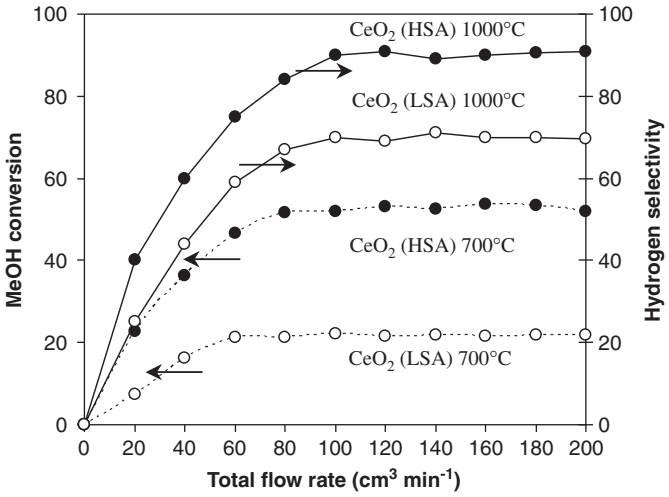

Fig. 2. Effect of the total gas flow rate on the methanol conversion over CeO_2 (LSA) and CeO_2 (HSA) at 700 °C (1 kPa MeOH, and 3 kPa H_2O).

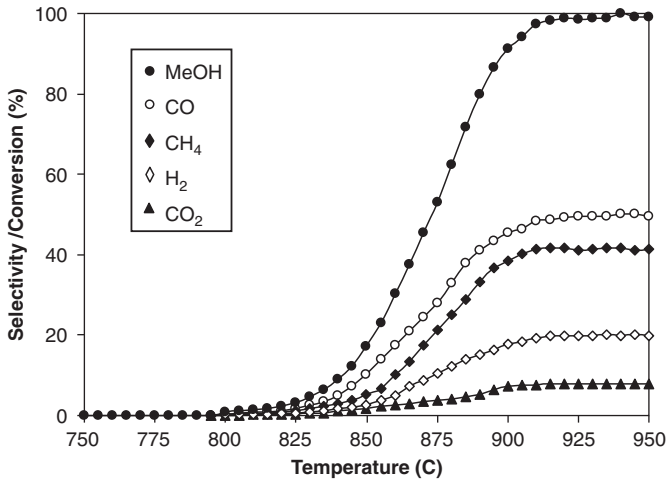

Fig. 3. Homogeneous (in the absence of catalyst) reactivity of methanol decomposition (1 kPa MeOH, and 3 kPa H_2O).

reforming rate was almost constant in the range where the gas flow rate was higher than 80 $cm^3\,min^{-1}$, indicating that the mass transfer effect is unimportant in this flow rate range. Consequently, the mass of catalyst loading was 50 mg, while the total gas flow was kept constant at 100 $cm^3\,min^{-1}$ in all experiments.

3.2. Homogeneous (non catalytic) reaction

Before studying the catalyst performance, homogeneous (non-catalytic) decomposition of methanol was investigated. Inlet H_2O/CH_3OH in helium with the molar ratio of 3 was introduced to the system, while the temperature increased from room temperature to 950 °C. From Fig. 3, it was observed that methanol was converted to methane, carbon monoxide, carbon dioxide, and hydrogen at the temperature above 800 °C. These components were formed via the decomposition of methanol, water–gas shift and methanation reactions.

3.3. Redox properties and redox reversibility of CeO_2

The oxygen storage capacities (OSC) and the degree of redox properties for fresh CeO_2 (both LSA and HSA) after calcinations were investigated using TPR-1, which was performed by heating the reduced catalysts up to 900 °C in 5% H_2 in helium. As shown in Fig. 4, hydrogen uptakes are detected from both CeO_2 at the temperature above 650 °C. The amount of hydrogen uptake over CeO_2 (HSA) is significantly higher than that over CeO_2 (LSA), suggesting that the OSC and the redox properties depend on the specific surface area of CeO_2. The benefit of the redox property on the reforming of methanol will be later presented in Section 3.4 and the discussion section. After purged with helium, the redox reversibilities for both CeO_2were then determined by applying TPO followed by TPR-2. The TPO was carried out by heating the catalyst up to 900 °C in 10% O_2 in helium; the amounts of oxygen chemisorbed were then measured, Fig. 5 and Table 2. Regarding the TPR-2 results as

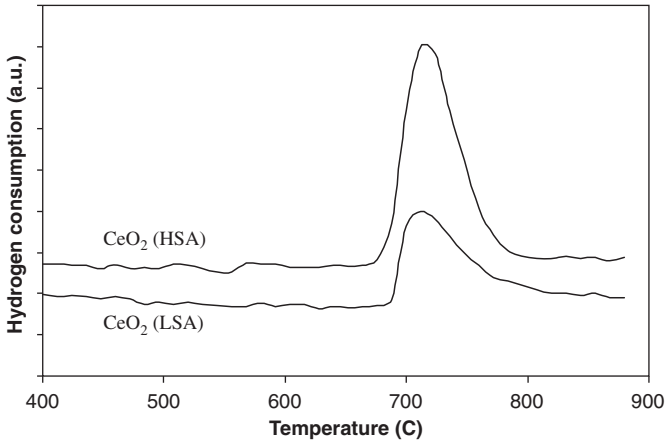

Fig. 4. TPR-1 of fresh ceria after reduction.

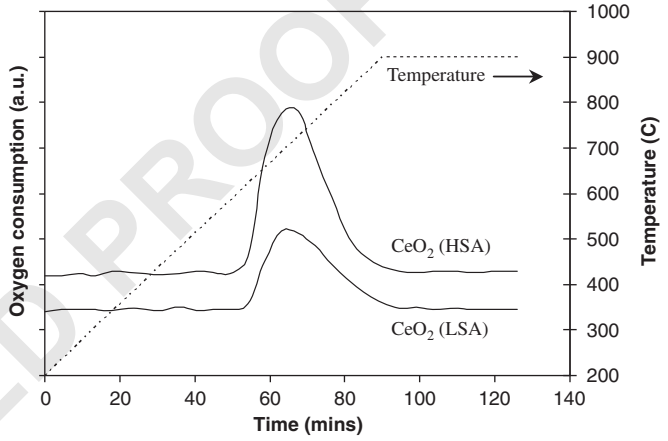

Fig. 5. TPO of CeO_2 (HSA, LSA) after TPR-1.

shown in Fig. 6 and Table 2, the amount of hydrogen uptakes for CeO_2 (both LSA and HSA) were approximately similar to those from TPR-1, indicating the redox reversibility for the synthesized CeO_2.

3.4. Reactivity toward methanol decomposition

The decomposition of methanol with and without steam over CeO_2 (HSA) and CeO_2 (LSA) were studied at 900 °C. The feed was H_2O/CH_3OH in helium with the molar ratios of 0, 1, and 3. The variations in hydrogen selectivities (%) with time at 900 °C for different catalysts and different inlet H_2O/CH_3OH ratio are shown in Fig. 7. After being operated for 100 h, the hydrogen selectivities for CeO_2 (HSA) were significantly higher than those for CeO_2 (LSA) in all conditions. However, the deactivations were also observed in all catalysts. Catalyst stabilities expressed as deactivation percentages are given in Table 3.

The post-reaction TPO experiments were carried out after a helium purge by introduction of 10% oxygen in helium in order to determine whether the observed deactivation is due to the carbon formation. From the TPO results shown in Fig. 8, small peaks of carbon dioxide and carbon monoxide were observed

Table 2
Results of TPR-1, TPO, TPR-2 analyses of CeO_2

Catalyst	Total H_2 uptake from TPR(1)[a] ($\mu mol/g_{cat}$)	Total O_2 uptake from TPO[b] ($\mu mol/g_{cat}$)	Total H_2 uptake from TPR(2)[c] ($\mu mol/g_{cat}$)
CeO_2 (LSA)	1784	867	1781
CeO_2 (HSA)	2076	989	2070

[a]Temperature Programmed Reduction of the reduced catalysts (Relative Standard Deviation = ±3%).
[b]Temperature Programmed Oxidation after TPR (1) (Relative Standard Deviation = ±1%).
[c]Re-Temperature Programmed Reduction after TPO (Relative Standard Deviation = ±2%).

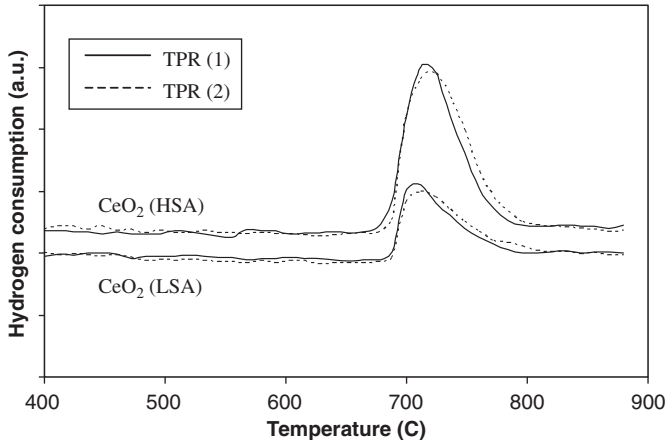

Fig. 6. TPR-2 of CeO_2 (HSA and LSA) compared to that of TPR-1.

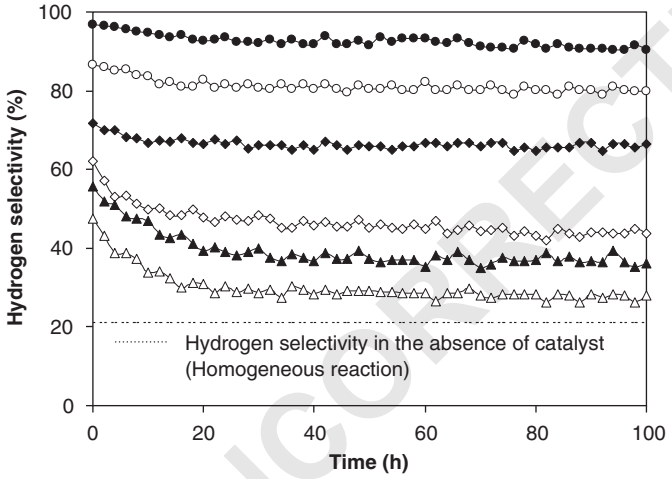

Fig. 7. Hydrogen selectivities from methanol decomposition at 900 °C for CeO_2 (HSA) with H_2O/CH_3OH of 3 (●), CeO_2 (HSA) with H_2O/CH_3OH of 1 (○), CeO_2 (HSA) with H_2O/CH_3OH of 0 (♦), CeO_2 (LSA) with H_2O/CH_3OH of 3 (◇), CeO_2 (LSA) with H_2O/CH_3OH of 1 (▲), and CeO_2 (LSA) with H_2O/CH_3OH of 0 (△).

for CeO_2 (LSA), whereas no peak of either carbon dioxide or carbon monoxide was detected for CeO_2 (HSA). The amount of carbon formations on the surface of CeO_2 (LSA) with different inlet H_2O/CH_3OH ratios were determined by measuring the CO and CO_2 yields from the TPO results. Using a value of 0.026 nm^2 for the area occupied by a carbon atom in a surface monolayer of the basal plane in graphite (Ramírez-Cabrera et al., 2004), the quantities of carbon deposited over this catalyst were observed to be approximately 0.35, 0.17, and 0.06 monolayer for the inlet H_2O/CH_3OH ratios of 0, 1, and 3, respectively. The total amounts of carbon deposited were ensured by the calculation of carbon balance in the system. Regarding the calculation, for the inlet H_2O/CH_3OH ratios of 0, 1, and 3, the moles of carbon deposited per gram of CeO_2 (LSA) were 0.39, 0.21, and 0.07 mmol g^{-1}. By the same assumption for the area occupied by a carbon atom (Ramírez-Cabrera et al., 2004), these values are equal to 0.33, 0.18, and 0.06 monolayer, respectively, which are in good agreement with the values observed from the TPO method described above. The TPO results clearly indicated the excellent resistance toward carbon formation for CeO_2 (HSA).

The BET measurement, as presented in Table 3, suggested that the deactivations of ceria are also due to the thermal sintering. Regarding the BET results, the surface area reduction percentage of CeO_2 (HSA) is lower than that of CeO_2 (LSA), indicating its better stability toward the thermal sintering.

3.5. Effects of temperature and inlet reactants

At steady state, the main products from this reaction over CeO_2 (HSA) were H_2, CO, and CO_2, with small amount of CH_4 depending on the operating conditions. The influences of operating temperature and the inlet steam content on the product selectivities and methanol conversion were studied by varying temperature from 700 to 1000 °C and changing the inlet steam to methanol ratio from 0.0 to 3.0.

As seen from Fig. 9, hydrogen and carbon monoxide selectivities increased with increasing temperature, whereas carbon dioxide and methane production selectivities decreased. Regarding the effect of steam, the conversion of methanol and the methane selectivity seem to be independent of the inlet steam content. However, hydrogen and carbon dioxide selectivities increased with increasing inlet steam concentration, whereas carbon monoxide selectivity decreased. Table 4 presents the comparison of product selectivities from methanol steam reforming at 900 °C between CeO_2 (HSA), and CeO_2 (LSA). It should be noted that the product selectivities from the homogeneous reaction (Fig. 6) and the product selectivities at equilibrium level, which were calculated by AspenPlus10.2 simulation program, are also shown in the table for comparison. Clearly, hydrogen and carbon monoxide selectivities from this reaction over CeO_2

Table 3
Deactivation percentages, steady state hydrogen selectivities, specific surface area, and amount of carbon deposition on the surface of catalysts after exposure in methanol decomposition conditions (various inlet H_2O/CH_3OH ratios) at 900 °C for 100 h

Catalyst	H_2O/CH_3OH ratio	Deactivation (%)	Hydrogen selectivity (%) at steady state	C formation[a] (monolayers)	BET surface ($m^2\ g^{-1}$)
CeO_2 (LSA)	0	40.9	28.0	0.35	6.0
	1	34.9	36.2	0.17	6.0
	3	29.7	43.6	0.06	6.1
CeO_2 (HSA)	0	7.4	66.5	~ 0	22.0
	1	7.6	80.0	~ 0	22.2
	3	6.5	90.4	~ 0	22.1

[a]Calculated using CO and CO_2 yields from temperature-programmed oxidation (TPO) with 10% oxygen.

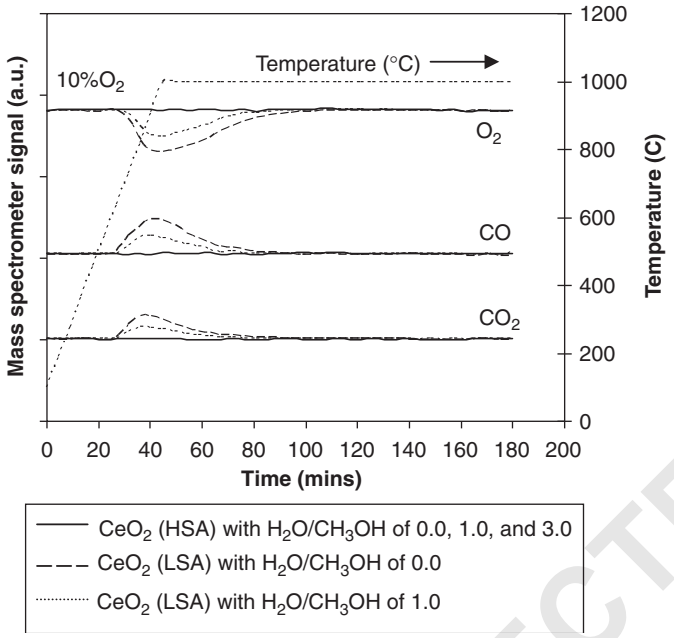

Fig. 8. TPO of CeO_2 (LSA) and CeO_2 (HSA) (10 kPa O_2) after exposure in methanol decomposition reaction at various inlet H_2O/CH_3OH ratios for 100 h.

(HSA) are higher and closer to their equilibrium levels than those over CeO_2 (LSA) in all conditions.

Without inlet steam, the effect of methanol concentration on the rate of decomposition at different temperatures was also studied by varying inlet methanol partial pressure from 1.0 to 4.0 kPa. The operating temperature range was between 700 and 800 °C in order to prevent the influence of homogeneous (non-catalytic) reaction. Fig. 10 presents the Arrhenius plots of the turnover frequencies at various inlet methanol concentrations. The results show that the decomposition rate is proportional to the methanol concentration and the temperature. The reaction order in methanol for CeO_2 (HSA) was observed to be between 0.37 and 0.68, independent of the steam partial pressure, for the range of conditions studied. These values were obtained experimentally by plotting $\ln(N)$ versus $\ln P_{CH_3OH}$ (where P_{CH_3OH} is the partial pressure of methanol; kPa). The reaction orders in other components (H_2O, and H_2) were achieved using the same approach by varying the inlet partial pressure of the component of interest while keeping the other inlet component partial pressures constant. Regarding the independence of inlet steam partial pressure on the rate of methanol decomposition, the reaction order in steam is therefore 0.

According to the post-reaction TPO, no carbon formation was observed on the surface of catalysts. In addition, the oxygen balance calculation was carried out during the stability testing to confirm the role of CeO_2. It was found from the calculation that the mole of oxygen (from methanol) fed into the system is almost similar to that in the products (CO, and CO_2) in all testing times, which indicates the unchanged state of CeO_2 (to Ce_2O_3) during the experiments. Furthermore, the TPO result for CeO_2 (HSA) in Fig. 8 also proves the unchanged state of spent CeO_2, as no oxygen uptakes were detected from the TPO of CeO_2 (HSA) after exposure in methanol decomposition conditions.

The influence of hydrogen on the rate of methanol decomposition was also investigated by adding various concentrations of hydrogen (1–3 kPa) in the feed. As shown in Fig. 11, the methanol conversion was significantly inhibited by the presence of hydrogen in the feed. The reaction order in hydrogen was between −0.29 and −0.17 in the range of conditions studied.

4. Discussion

CeO_2 (HSA) has a high reactivity for methanol decomposition and an excellent resistance toward carbon deposition without steam having to be present in the gas. This high resistance toward carbon deposition has been reported by several investigators (Laosiripojana, 2003; Ramírez-Cabrera et al., 2003, 2004; Laosiripojana and Assabumrungrat, 2005) and is mainly due to the high oxygen storage capacity of this material. CeO_2 contains a high concentration of highly mobile oxygen vacancies and thus acts as a local source or sink for oxygen on its surface. It has been reported that at high temperature the lattice oxygen (O_O^x) at the CeO_2 surface can oxidize gaseous hydrocarbons (methane, Ramírez-Cabrera et al., 2003, 2004; ethane and propane, Laosiripojana and Assabumrungrat, 2005) and also carbon monoxide (Laosiripojana, 2003).

In the decomposition of methanol at high temperature the presence of steam is normally required as it minimizes the carbon deposition on the catalyst surface, which is due to

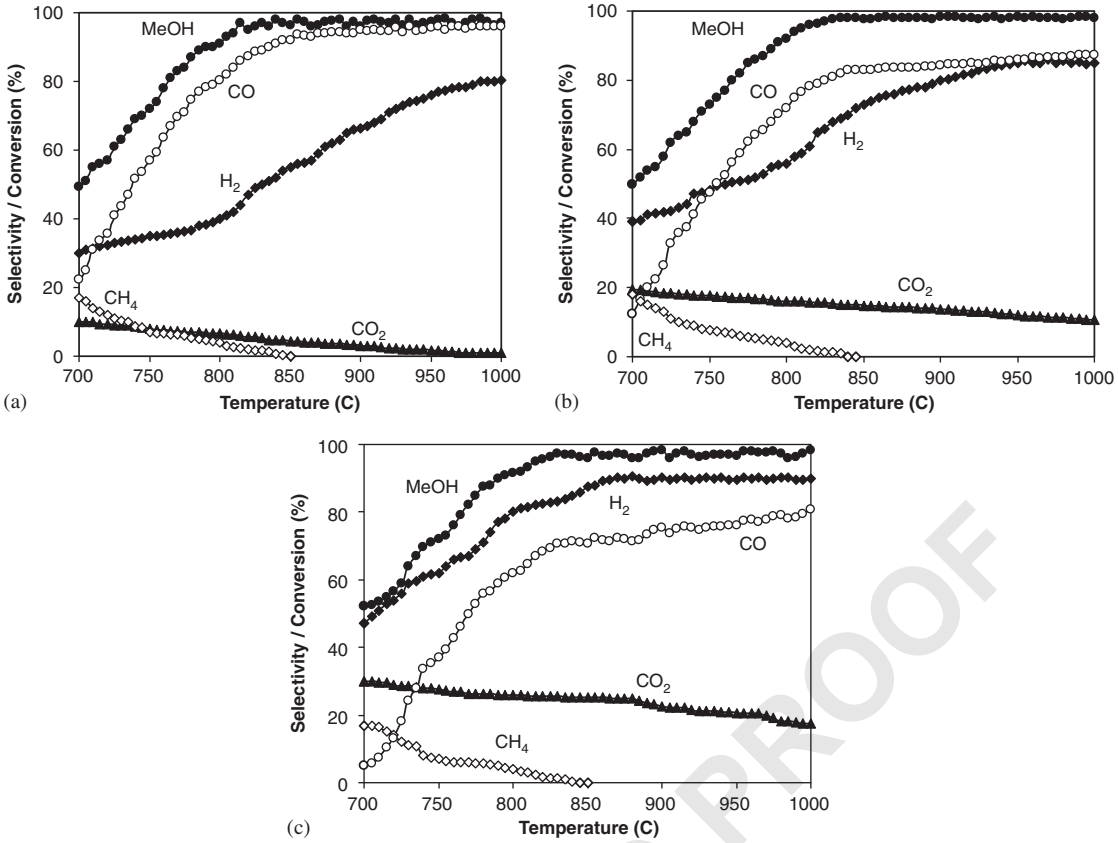

Fig. 9. Effects of reaction temperature and inlet H_2O/CH_3OH ratio on methanol conversion and product selectivities (H_2, CO, CO_2, and CH_4) from methanol decomposition over CeO_2 (HSA): (a) inlet H_2O/CH_3OH ratio of 0; (b) inlet H_2O/CH_3OH ratio of 1; (c) inlet H_2O/CH_3OH ratio of 3.

Table 4
Methanol conversion and product selectivities from the decomposition of methanol at various inlet H_2O/CH_3OH molar ratios (at isothermal condition, 900 °C)

Catalyst	H_2O/CH_3OH	Conversion and product selectivities at 900 °C				
	ratio	CH_3OH	H_2	CO	CO_2	CH_4
CeO_2 (LSA)	0	93.1	22.4	58.6	4.2	30.3
	1	94.2	27.1	55.0	11.0	28.2
	3	93.8	33.2	52.9	18.1	22.8
CeO_2 (HSA)	0	98.1	66.5	92.0	6.1	0
	1	98.2	80.0	84.4	13.7	0
	3	98.1	90.4	75.5	22.6	0
Homogeneous[a]	0	92.1	13.5	49.9	0	41.2
	1	92.4	17.4	49.1	3.4	39.9
	3	92.9	20.8	48.1	5.6	39.2
Equilibrium[b]	0	100	71.1	93.4	6.6	0
	1	100	89.4	85.2	14.8	0
	3	100	95.0	76.1	23.9	0

[a]Homogeneous (non-catalytic) reaction.
[b]Calculated by AspenPlus 10.2 simulation program.

reactions (4) and (5) mentioned in Section 1. By using CeO_2 as the catalyst, the carbon deposition from these reactions could be inhibited by the gas–solid reactions between CO and CH_4 formed with the lattice-oxygen (O_O^x) at the CeO_2 surface forming CO_2 and hydrogen from which the formation of carbon is thermodynamically unfavourable at high temperature. The reactions taken place can be summarized as follows:

$$C_nH_m + O_O^x = nCO + m/2H_2 + V_{O^{\cdot\cdot}} + 2e', \quad (16)$$

$$CO + O_O^x = 2CO_2 + V_{O^{\cdot\cdot}} + 2e'. \quad (17)$$

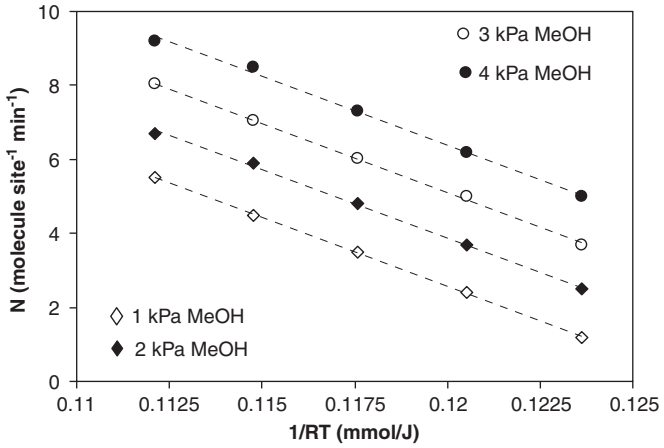

Fig. 10. Arrhenius plot of turnover frequencies (N) for methanol decomposition without steam over CeO_2 (HSA) with different inlet methanol partial pressures (1–4 kPa) at 700–800 °C.

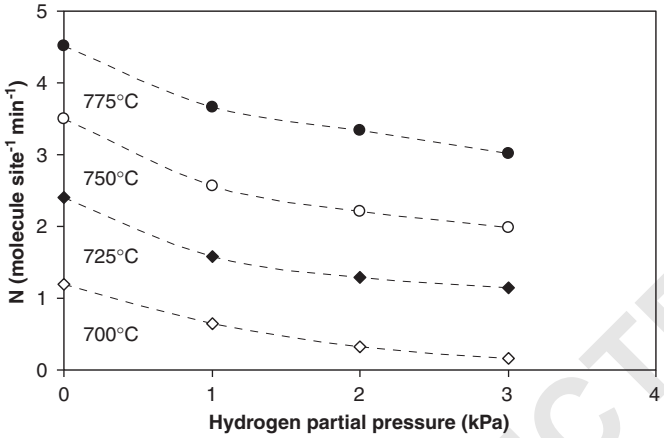

Fig. 11. Effect of hydrogen partial pressure on the turnover frequencies (N) for methanol decomposition over CeO_2 (HSA) at different temperatures (1 kPa MeOH and 3 kPa H_2O).

The lattice oxygen (O_O^x) is regenerated by reactions with oxygen containing compounds (methanol, steam) present in the system. The strong linear dependence of the methanol decomposition rate on methanol partial pressure and its independence of the steam partial pressure indicate that the lattice oxygen (O_O^x) is replenished by a sufficiently rapid reaction of the partially reduced CeO_2 with the oxygen containing molecules in the system, whereas the inhibitory effect of hydrogen could be due to the reverse of the methanol decomposition. According to the studies on the effect of temperature, hydrogen and carbon monoxide selectivities increased with increasing temperature, whereas carbon dioxide and methane production selectivities decreased. The changes of hydrogen, carbon monoxide, and carbon dioxide selectivities are mainly due to the influence of the mildly exothermic water–gas shift reaction ($CO + H_2O \rightarrow CO_2 + H_2$), whereas the decrease in methane production selectivity could be due to the further reforming to carbon monoxide and hydrogen.

Although the CeO_2 (LSA) can decompose methanol producing synthesis gas (CO and H_2), the major weaknesses of CeO_2 (LSA) are its nature, low specific surface area and its high size reduction due to the thermal sintering, which resulted in its low OSC as presented in Section 3.3. The low OSC for CeO_2 (LSA) results in its lower redox property (Eqs. (16) and (17)) and consequently caused the low reforming reactivity (almost three times lower than CeO_2 (HSA)) and low product selectivities (i.e., H_2 and CO). The comparative reforming reactivities between CeO_2 (HSA) and CeO_2 (LSA) are in good agreement with the results from the characterizations (i.e., BET and TPR)—the specific surface area of CeO_2 (HSA) and the amount of hydrogen uptakes from the temperature programmed reduction (TPR-1 and TPR-2) were significantly higher than those over the CeO_2 (LSA). By the same reason, the higher resistance toward carbon deposition for CeO_2 (HSA) compared to CeO_2 (LSA) is mainly due to the higher lattice oxygen (O_O^x) on its surface, which promotes the gas–solid reactions (Eqs. (16) and (17)) and consequently prevents the formation of carbon species via the methane decomposition and Boudouard reactions.

Due to the good performance of CeO_2 (HSA) in terms of high resistance toward carbon deposition and good product selectivities (producing only H_2, CO, and CO_2) at high temperature, this catalyst would be a good candidate to be applied as the internal or in-stack reforming catalyst for IIR-SOFC. Also, this material could be a promising option for application in the anode of SOFC (DIR-SOFC) compared to the CeO_2 (LSA), as it presents higher resistance toward carbon deposition and lower sintering rate. Importantly, without the presence of steam being required to reform methanol, the consideration of water management in SOFC system is negligible. Regarding the above benefits, the use of CeO_2 (HSA) is expected to simplify the overall SOFC system design (i.e., DIR and IIR), making SOFCs more attractive to be used commercially.

5. Conclusion

Nano-particulate high surface area CeO_2 (CeO_2 (HSA)) has a useful methanol decomposition activity at SOFC temperatures producing H_2, CO, CO_2, and small amount of CH_4 without the presence of steam being required. The conversion of methanol from the decomposition process over this catalyst was close to 100% at 850 °C, and no carbon deposition was observed on the surface of CeO_2 according to the TPO results. Hydrogen selectivities up to 90% can be produced. Regarding the influences of inlet components on the rate of methanol decomposition, the decomposition rate over CeO_2 (HSA) is proportional to the methanol partial pressure and independent of the steam partial pressure at 700–800 °C. Hydrogen was found to have a significant inhibitory effect on the rate of methanol decomposition.

Due to the good performance of CeO_2 (HSA) toward methanol decomposition in terms of high resistance toward carbon deposition and good product selectivities at SOFC temperature, this catalyst is a good candidate to be applied as the internal or in-stack reforming catalyst for solid oxide fuel cell application (IIR-SOFC).

Acknowledgements

The financial support from The Thailand Research Fund (TRF) throughout this project is gratefully acknowledged. The first author would like to acknowledge Professor David Chadwick from Department of Chemical Engineering and Chemical Technology, Imperial College London for his valuable suggestion.

References

Aguiar, P., Lapena-Rey, N., Chadwick, D., Kershenbaum, L., 2001. Improving catalyst structures and reactor configurations for autothermal reaction systems: application to solid oxide fuel cells. Chemical Engineering Science 56, 652.

Amor, J.N., 1999. The multiple roles for catalysis in the production of H_2. Applied Catalysis A 176, 159–176.

An, S., Lu, C., Worrell, W.L., Gorte, R.J., Vohs, J.M., 2004. Characterization of Cu–CeO_2 direct hydrocarbon anodes in a solid oxide fuel cell with lanthanum gallate electrolyte. Solid State Ionics 175 (1–4), 135–138.

Brett, D.J.L., Atkinson, A., Cumming, D., Ramírez-Cabrera, E., Rudkin, R., Brandon, N.P., 2005. Methanol as a direct fuel in intermediate temperature (500–600 °C) solid oxide fuel cells with copper based anodes. Chemical Engineering Science 60 (21), 5649–5662.

Brown, L.F., 2001. A comparative study of fuels for on-board hydrogen production for fuel-cell-powered automobiles. International Journal of Hydrogen Energy 26, 381–397.

Costa-Nunes, O., Gorte, R.J., Vohs, J.M., 2005. Comparison of the performance of Cu–CeO_2–YSZ and Ni–YSZ composite SOFC anodes with H_2, CO, and syngas. Journal of Power Sources 141 (2), 241–249.

Dicks, A.L., 1996. Hydrogen generation from natural gas for the fuel cell systems of tomorrow. Journal of Power Sources 61 (1–2), 113–124.

Douvartzides, S.L., Coutelieris, F.A., Demin, K., Tsiakaras, P.E., 2003. Fuel options for solid oxide fuel cells: a thermodynamic analysis. A.I.Ch.E. 49, 248–257.

Emonts, B., Hansen, J.B., Jorgensen, S.L., Hohlein, B., Peters, R., 1998. Compact methanol reformer test for fuel-cell powered light-duty vehicles. Journal of Power Sources 71, 288.

Gellings, P.J., Bouwmeester, H.J.M., 2000. Solid state aspects of oxidation catalysis. Catalysis Today 58, 1–53.

Gorte, R.J., Vohs, J.M., McIntosh, S., 2004. Recent developments on anodes for direct fuel utilization in SOFC. Solid State Ionics 175 (1–4), 1–6.

Jung, S., Lu, C., He, H., Ahn, K., Gorte, R.J., Vohs, J.M., 2005. Influence of composition and Cu impregnation method on the performance of Cu/CeO_2/YSZ SOFC anodes. Journal of Power Sources, in press.

Kim, T., Liu, G., Boaro, M., Lee, S.-I., Vohs, J.M., Gorte, R.J., Al-Madhi, O.H., Dabbousi, B.O., 2005. A study of carbon formation and prevention in hydrocarbon-fueled SOFC. Journal of Power Sources, in press.

Laosiripojana, N., 2003. Reaction engineering of indirect internal steam reforming of methane for application in solid oxide fuel cells. Ph.D. Thesis, University of London, England.

Laosiripojana, N., Assabumrungrat, S., 2005. Catalytic steam reforming of ethane and propane over CeO_2-doped Ni/Al_2O_3 at SOFC temperature: improvement of resistance toward carbon formation by the redox property of doping CeO_2. Fuel, in press.

Ledjeff-Hey, K., Formanski, V., Kalk, T., Roes, J., 1998. Compact hydrogen production systems for solid polymer fuel cells. Journal of Power Sources 71 (1–2), 199–207.

Lwin, Y., Daud, W.R.W., Mohamad, A.B., Yaakob, Z., 2000. Hydrogen production from steam-methanol reforming: thermodynamic analysis. International Journal of Hydrogen Energy 25 (1), 47–53.

Maggio, G., Freni, S., Cavallaro, S., 1998. Light alcohols/methane fuelled molten carbonate fuel cells: a comparative study. Journal of Power Sources 74, 17–23.

Marina, O.A., Bagger, C., Primdahl, S., Mogensen, M., 1998. In: Stevens, P., Bossell, U. (Eds.), Proceedings of Third European SOFC Forum, Oberrohrdorf, Nantes, Switzerland, p. 427.

Minh, N.Q., Takahashi, T., 1995. Science and Technology of Ceramic Fuel Cells. Elsevier, Amsterdam.

Otsuka, K., Hatano, M., Morikawa, A., 1983. Hydrogen from water by reduced cerium oxide. Journal of Catalysis 79, 493.

Otsuka, K., Hatano, M., Morikawa, A., 1985. Decomposition of water by cerium oxide of δ-phase. Inorganica Chimica Acta 109, 193.

Ramírez-Cabrera, E., Atkinson, A., Chadwick, D., 2002. Reactivity of ceria, Gd- and Nb-doped ceria to methane. Applied Catalysis B 36, 193.

Ramírez-Cabrera, E., Laosiripojana, N., Atkinson, A., Chadwick, D., 2003. Methane conversion over Nb-doped ceria. Catalysis Today 78, 433–438.

Ramírez-Cabrera, E., Atkinson, A., Chadwick, D., 2004. Catalytic steam reforming of methane over $Ce_{0.9}Gd_{0.1}O_{2-x}$. Applied Catalysis B 47, 127–131.

Rostrup-Nielsen, J.R., Bak-Hansen, J.-H., 1993. CO_2-reforming of methane over transition metals. Journal of Catalysis 144, 38.

Available online at www.sciencedirect.com
SCIENCE DIRECT
Fuel 85 (2006) 323–332
FUEL
www.fuelfirst.com

Catalytic steam reforming of ethane and propane over CeO_2-doped Ni/Al_2O_3 at SOFC temperature: Improvement of resistance toward carbon formation by the redox property of doping CeO_2

N. Laosiripojana[a,*], W. Sangtongkitcharoen[b], S. Assabumrungrat[b]

[a]*The Joint Graduate School of Energy and Environment, King Mongkut's University of Technology Thonburi, Bangkok 10140, Thailand*
[b]*Center of Excellence on Catalysis and Catalytic Reaction Engineering, Department of Chemical Engineering, Faculty of Engineering, Chulalongkorn University, Bangkok 10330, Thailand*

Received 21 January 2005; received in revised form 2 June 2005; accepted 28 June 2005
Available online 28 July 2005

Abstract

Ni/Al_2O_3 with the doping of CeO_2 was found to have useful activity to reform ethane and propane with steam under Solid Oxide Fuel Cells (SOFCs) conditions, 700–900 °C. CeO_2-doped Ni/Al_2O_3 with 14% ceria doping content showed the best reforming activity among those with the ceria content between 0 and 20%. The amount of carbon formation decreased with increasing Ce content. However, Ni was easily oxidized when more than 16% of ceria was doped. Compared to conventional Ni/Al_2O_3, 14%CeO_2-doped Ni/Al_2O_3 provides significantly higher reforming reactivity and resistance toward carbon deposition. These enhancements are mainly due to the influence of the redox properties of doped ceria. Regarding the temperature programmed reduction experiments (TPR-1), the redox properties and the oxygen storage capacity (OSC) for the catalysts increased with increasing Ce doping content. In addition, it was also proven in the present work that the redox of these catalysts are reversible, according to the temperature programmed oxidation (TPO) and the second time temperature programmed reduction (TPR-2) results.

During the reforming process, in addition to the reactions on Ni surface, the gas–solid reactions between the gaseous components presented in the system (C_2H_6, C_3H_8, C_2H_4, CH_4, CO_2, CO, H_2O, and H_2) and the lattice oxygen (O_x) on ceria surface also take place. The reactions of adsorbed surface hydrocarbons with the lattice oxygen (O_x) on ceria surface ($C_nH_m + O_x \rightarrow nCO + m/2(H_2) + O_{x-n}$) can prevent the formation of carbon species on Ni surface from hydrocarbons decomposition reaction ($C_nH_m \Leftrightarrow nC + m/2H_2$). Moreover, the formation of carbon via Boudard reaction ($2CO \Leftrightarrow CO_2 + C$) is also reduced by the gas–solid reaction of carbon monoxide (produced from steam reforming) with the lattice oxygen ($CO + O_x \Leftrightarrow CO_2 + O_{x-1}$).

Keywords: Hydrogen; Ethane; Propane; Carbon formation; Steam reforming; CeO_2

1. Introduction

Solid Oxide Fuel Cell (SOFC) is generally operated at high temperature between 700 and 1100 °C [1,2]. Due to its high-operating temperature, fuels such as methane can be in-stack or internal reformed by catalytic steam reforming to produce a H_2/CO rich gas, which is eventually used to generate electrical energy and heat. The operation, called indirect internal reforming (IIR), is expected to simplify the overall system design [3].

Currently, one of the most interesting fuels for SOFC is natural gas consisting mainly of methane. Normally, natural gas also contains significant amounts of higher hydrocarbons such as ethane and propane. When natural gas is reformed internally (IIR) without any pre-treatments, the carbon formation can be easily formed on the catalyst surface due to the decompositions of these hydrocarbons at high temperature. SOFC fueled by natural gas therefore requires a small external pre-reformer unit, where the high hydrocarbon components are reformed readily before introducing to the main part of the system [4]. The pre-reforming unit is normally operated at relatively lower temperature, 300–500 °C, in which the carbon formation is

* Corresponding author.
E-mail address: navadol_l@jgsee.kmutt.ac.th (N. Laosiripojana).

0016-2361/$ - see front matter © 2005 Elsevier Ltd. All rights reserved.
doi:10.1016/j.fuel.2005.06.013

thermodynamically unflavored. The disadvantage of this installation is the extra-requirement of the heat supplied into this unit, which can reduce the fuel cell efficiency [5].

The approach to this problem in this work is developing of an alternative catalyst that is enable to reform high hydrocarbon components with low degree of carbon deposition at SOFC temperature, 700–900 °C. The successful development of this catalyst would help eliminate the requirement of the external pre-reformer, as these high hydrocarbon elements can be simultaneously reformed together with methane at high temperature. In this study, ethane and propane were chosen as the inlet fuels, because they are the main high hydrocarbon components presented in natural gas. According to the economical point of view, Ni/Al_2O_3 was selected as a based catalyst rather than the precious metals such as Pt, Rh and Ru although it is more sensitive to carbon formation. Cerium oxide (CeO_2) was chosen as an additive promoter. This material (called ceria) is an important material for a variety of catalytic reactions involving oxidation of hydrocarbons (e.g. automobile exhaust catalysts). Recently, the use of ceria-based catalysts has shown a rapid increase [6]. A high oxygen mobility [7], high oxygen storage capacity [8–13], strong interaction with the supported metal (strong metal-support interaction) [14] and the modifiable ability [15] render the ceria-based materials very interesting for catalysis and as a support and promoter. It has widely been reported, regarding the above properties, that cerias can promote the action of various metals in the reactions in which hydrogen is involved as a reactant or product [16–20]. According to the catalytic steam reforming reaction, ceria-based materials have been reported by several researchers to be promising supports among α-Al_2O_3 [21], γ-Al_2O_3 and γ-Al_2O_3 with alkali metal oxide and rare earth metal oxide [22], and $CaAl_2O_4$ [21–24]. One of the most promising ceria-based supports for the reforming reactions appeared to be Ce-ZrO_2, where the metal can be Ni, Pt or Pd [25–34].

It has been reported that the gas–solid reaction between CeO_2 and CH_4 produces synthesis gas with a H_2/CO ratio of two according to the following reactions [35,36]. Moreover, the reduced ceria, CeO_{2-x}, can react with CO_2 and steam to produce CO and H_2, respectively [37].

$$CeO_2 + nCH_4 \rightarrow CeO_{2-n} + nCO + 2nH_2 \quad (1)$$

$$CeO_{2-x} + CO_2 \Leftrightarrow CeO_2 + CO \quad (2)$$

$$CeO_{2-x} + H_2O \Leftrightarrow CeO_2 + H_2 \quad (3)$$

Nowadays, a potential application of ceria is in Solid Oxide Fuel Cells (SOFCs) application as a reforming catalyst for in-stack (called indirect internal) reforming of methane, since it is high resistant toward carbon deposition compared to Ni [38]. Recently, the successful tests of ceria for the methane steam reforming reaction have been reported [39,40]. Due to the high resistance toward carbon formation, ceria should be a good additive promoter for the reforming of ethane and propane. In this work, various amounts of ceria were doped on the surface of Ni/Al_2O_3 in order to determine the suitable doping ratio. The reactivity toward steam reforming of ethane and propane, as well as the resistance toward carbon formation of CeO_2-doped Ni/Al_2O_3 were studied and compared to those of conventional Ni/Al_2O_3. The influence of inlet steam content on the product selectivity from this reaction at various temperatures was also determined.

2. Experimental

2.1. Catalyst preparations and characterizations

CeO_2-doped Ni/Al_2O_3 was prepared by impregnating different concentration of cerium nitrate ($Ce(NO_3)_3 \cdot 6H_2O$ (99.0%), Fluka) on Ni/Al_2O_3 powder. Ni/Al_2O_3 (10 wt% Ni) was prepared by impregnating α-Al_2O_3 (from Aldrich) with $NiCl_3$ solution at room temperature. This solution was stirred by magnetic stirring (100 rpm) for 6 h, dried overnight in an oven at 110 °C, and calcined in air at 900 °C for 6 h before use.

After reduction, the catalysts were characterized with several physicochemical methods. The weight contents of Ni and Ce loadings were determined by X-ray fluorescence (XRF) analysis. The reducibility and dispersion percentages of nickel were measured from temperature-programmed reduction (TPR) using 5% H_2 in Ar with the total flow rate of 100 $cm^3\ min^{-1}$ and temperature-programmed desorption (TPD) respectively. The catalyst specific surface areas were obtained from BET measurement. All physicochemical properties of the synthesized catalysts are presented in Table 1.

In addition to the above characterizations, the redox properties and redox reversibilities of the catalysts with different Ce doping contents were determined by the temperature programmed reduction (TPR-1) at high temperature and the temperature programmed oxidation (TPO) following with temperature programmed reduction (TPR-2), respectively. Regarding these experiments, 5% H_2/Ar and 5% O_2/He were used for the TPR and TPO, respectively, while the temperature of the system increased from room temperature to 900 °C and 1000°C, respectively.

2.2. Apparatus and procedures

An experimental reactor system was constructed as shown in Fig. 1. The feed gases including the components of interest (ethane, propane, and steam from the evaporator) and the carrier gas (helium) were introduced to the reaction section, in which a 10-mm diameter quartz reactor was mounted vertically inside a furnace. In the present work, the ethane/propane feed ratio was kept constant at 0.65/0.35, regarding to the approximate ratio of these components presented in natural gas (this information is based on the compositions of natural gas from PTT Company (Thailand)

Table 1
Physicochemical properties of the catalysts after reduction at 700 °C

Catalyst	Ni-load[a] (wt.%)	Ce-load[a] (wt.%)	BET Surface Area ($m^2\ g^{-1}$)	Ni-reducibility[b] (Ni%)	Ni-dispersion[c] (Ni%)
Ni/Al_2O_3	4.91	0.0	40.2	92.1	4.87
$2\%Ce\text{-}Ni/Al_2O_3$	4.84	1.87	40.8	93.5	4.54
$4\%Ce\text{-}Ni/Al_2O_3$	4.93	4.02	42.7	91.4	5.12
$6\%Ce\text{-}Ni/Al_2O_3$	5.01	5.94	46.5	90.6	4.54
$8\%Ce\text{-}Ni/Al_2O_3$	4.96	8.03	49.1	91.1	4.65
$10\%Ce\text{-}Ni/Al_2O_3$	4.88	9.86	49.8	89.9	4.77
$12\%Ce\text{-}Ni/Al_2O_3$	4.93	12.1	50.4	90.3	4.64
$14\%Ce\text{-}Ni/Al_2O_3$	4.92	13.9	50.9	91.0	4.20
$16\%Ce\text{-}Ni/Al_2O_3$	5.00	16.1	51.4	89.7	5.09
$18\%Ce\text{-}Ni/Al_2O_3$	4.94	17.9	51.0	90.1	4.13
$20\%Ce\text{-}Ni/Al_2O_3$	4.98	19.9	52.0	90.3	4.37

[a] Measured from X-ray fluorescence analysis.
[b] Measured from temperature-programmed reduction (TPR) with 5%hydrogen.
[c] Measured from temperature-programmed desorption (TPD) of hydrogen after TPR measurement.

containing 67%CH_4, 8.3%C_2H_6, 4.5%C_3H_8, 2.0%C_4H_{10}, 0.5%C_5H_{12}, and 14.5%CO_2). The catalyst was loaded in the quartz reactor, which was packed with a small amount of quartz wool to prevent the catalyst from moving. The weight of catalyst loading was 50 mg, while a typical range of total gas flow was 20–200 $cm^3\ min^{-1}$ depending on the desired space velocity. A Type-K thermocouple was placed into the annular space between the reactor and the furnace. This thermocouple was mounted on the tubular reactor in close contact with the catalyst bed to minimize the temperature difference between the catalyst bed and the thermocouple. Another Type-K thermocouple was inserted in the middle of the quartz tube in order to re-check the possible temperature gradient. The record showed that the maximum temperature fluctuation during the reaction was always ± 0.75 °C or less from the temperature specified for the reaction. Before the reaction, the catalyst was reduced under 5% H_2 in helium with the flow rate of 100 $cm^3\ min^{-1}$ for 6 h.

During the reactions, the exit gas mixture was transferred via trace-heated lines to the analysis section, which consists of a Porapak Q column Shimadzu 14B gas chromatograph (GC) and a mass spectrometer (MS). The gas chromatography was applied in order to investigate the steady state condition experiments, whereas the mass spectrometer in which the sampling of the exit gas was done by a quartz capillary and differential pumping was used for the transient and carbon formation experiments. In order to study the formation of carbon species on catalyst surface, Temperature programmed Oxidation (TPO) was applied by introducing 10% oxygen in helium into the system, after purged with helium. The operating temperature increased from room temperature to 1000 °C by the rate of 10 °C/min.

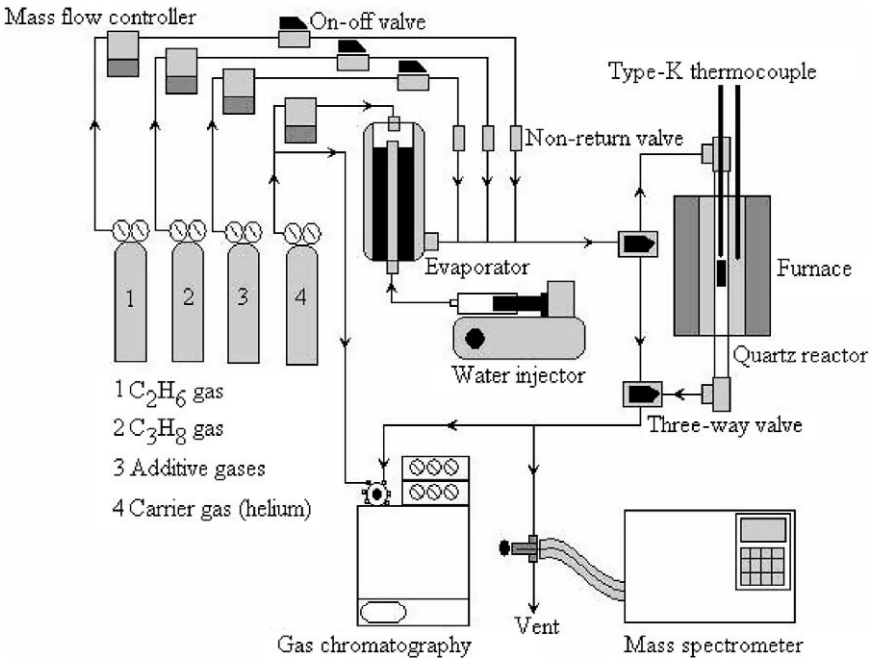

Fig. 1. Schematic diagram of the experimental set-up.

The calibrations of CO and CO_2 productions were performed by injecting a known amount of these calibration gases from a loop, in an injection valve in the bypass line. The response factors were obtained by dividing the number of moles for each component over the respective areas under peaks. The amount of carbon formations on the surface of catalysts were determined by measuring the CO and CO_2 yields from the TPO results (using Microcal Origin Software) assuming a value of 0.026 nm^2 for the area occupied by a carbon atom in a surface monolayer of the basal plane in graphite [38]. In addition to the TPO method, the amount of carbon deposition was confirmed by the calculation of carbon balance in the system. The amount of carbon deposited on the surface of catalyst would theoretically be equal to the difference between the inlet carbon containing components (C_2H_6, and C_3H_8) and the outlet carbon containing components (C_2H_6, C_3H_8, CO, CO_2, CH_4, and C_2H_4). The amount of carbon deposited per gram of catalyst is given by the following equation:

$$C_{\text{deposition}} = \frac{\text{mole}_{\text{carbon(in)}} - \text{mole}_{\text{carbon(out)}}}{m_{\text{catalyst}}} \quad (4)$$

The steam reforming reactivity was defined in terms of the conversions and selectivities. Hydrocarbon conversions (ethane and propane) denoted as $X_{\text{hydrocarbon}}$, and the products selectivity (hydrogen, carbon monoxide, carbon dioxide, methane, and ethylene), denoted as S_{product}, are calculated according to Eqs. (5)–(11):

$$X_{\text{Ethane}} = \frac{100(\%\text{Ethane}_{\text{in}} - \%\text{Ethane}_{\text{out}})}{\%\text{Ethane}_{\text{in}}} \quad (5)$$

$$X_{\text{Propane}} = \frac{100(\%\text{Propane}_{\text{in}} - \%\text{Propane}_{\text{out}})}{\%\text{Propane}_{\text{in}}} \quad (6)$$

$$S_{\text{H}_2} = \frac{100(\%\text{H}_2)}{3(\%\text{Ethane}_{\text{in}} - \%\text{Ethane}_{\text{out}}) + 4(\%\text{Propane}_{\text{in}} - \%\text{Propane}_{\text{out}}) + (\%\text{H}_2\text{O}_{\text{in}} - \%\text{H}_2\text{O}_{\text{out}})} \quad (7)$$

$$S_{\text{CO}} = \frac{100(\%\text{CO})}{2(\%\text{Ethane}_{\text{in}} - \%\text{Ethane}_{\text{out}}) + 3(\%\text{Propane}_{\text{in}} - \%\text{Propane}_{\text{out}})} \quad (8)$$

$$S_{\text{CO}_2} = \frac{100(\%\text{CO}_2)}{2(\%\text{Ethane}_{\text{in}} - \%\text{Ethane}_{\text{out}}) + 3(\%\text{Propane}_{\text{in}} - \%\text{Propane}_{\text{out}})} \quad (9)$$

$$S_{\text{CH}_4} = \frac{100(\%\text{CH}_4)}{2(\%\text{Ethane}_{\text{in}} - \%\text{Ethane}_{\text{out}}) + 3(\%\text{Propane}_{\text{in}} - \%\text{Propane}_{\text{out}})} \quad (10)$$

$$S_{\text{C}_2\text{H}_4} = \frac{100(\%\text{C}_2\text{H}_4)}{(\%\text{Ethane}_{\text{in}} - \%\text{Ethane}_{\text{out}}) + 1.5(\%\text{Propane}_{\text{in}} - \%\text{Propane}_{\text{out}})} \quad (11)$$

3. Results and discussion

3.1. Preliminary tests

The desired space velocity and suitable catalyst particle size were achieved from several preliminary tests, which were carried out to avoid any limitations by intraparticle diffusion in the experiments. The total flow rate was varied between 20 and 200 $cm^3\ min^{-1}$ under a constant residence time of 5×10^{-4} g $min\ cm^{-3}$. When the total flow rate was below 60 $cm^3\ min^{-1}$, the reforming rate increased with increasing the gas flow rate, suggesting that the mass transfer between the bulk gas and the catalyst particles is the rate-determining step. The reforming rate was almost constant in the range where the gas flow rate was higher than 80 $cm^3\ min^{-1}$, indicating that the mass transfer effect is unimportant in this flow rate range. Fig. 2 shows the effect of the total gas flow rate on the reforming rate over 14%CeO_2-doped Ni/Al_2O_3 at different temperatures. The reactions on different average sizes (from 100 to 500 μm) of catalysts were also carried out. It was observed that there were no significant changes in the methane conversion for the catalyst with the particle size between 100 and 200 μm, which indicated that the intraparticle diffusion limitation was negligible in this range. Consequently in this study, the weight of catalyst loading was 50 mg, while the total gas flow was kept constant at 100 $cm^3\ min^{-1}$. The catalyst particle size diameter was between 100 and 200 μm in all experiments.

Before studying the catalyst performance, homogeneous (non-catalytic) steam reforming of ethane and propane was investigated. Inlet $C_2H_6/C_3H_8/H_2O$ in helium with the molar ratio of 0.65/0.35/3.0 was introduced to the system, while the temperature increased from room temperature to 900 °C. From Fig. 3, it was observed that both ethane and propane were converted to methane, ethylene, and hydrogen at

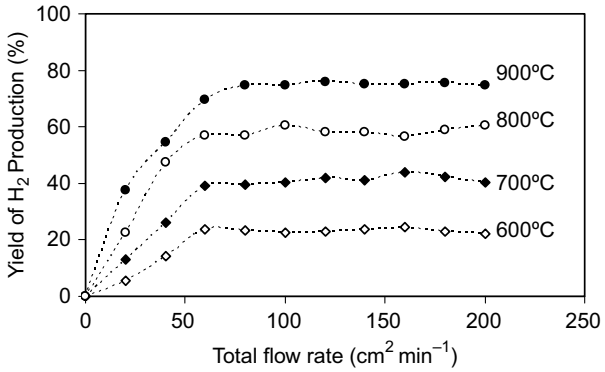

Fig. 2. Effect of the gas flow rate on the yield of H_2 production (%) for steam reforming over 14% CeO_2-doped Ni/Al_2O_3 at different temperatures (2.6 kPa C_2H_6, 1.4 kPa C_3H_8, 12 kPa H_2O).

the temperature above 700 °C. Significant amount of carbons was also detected in the blank reactor after exposure for 10 h. These components were formed via the decomposition of ethane and propane as shown in the equations below [41].

$$C_2H_6 \rightarrow C_2H_4 + H_2 \quad (12)$$

$$C_3H_8 \rightarrow 3/2(C_2H_4) + H_2 \quad (13)$$

$$C_2H_4 \rightarrow 2H_2 + 2C \quad (14)$$

$$C + 2H_2 \rightarrow CH_4 \quad (15)$$

There was no change in steam concentration, and no carbon monoxide and carbon dioxide was produced in the system, indicating that the non-homogenous reforming reaction between steam and hydrocarbon elements took place at this range of conditions studied.

3.2. Investigation of the redox properties and redox reversibility of the catalysts

As described earlier, the oxygen storage capacities and the degree of redox properties for catalysts with different Ce

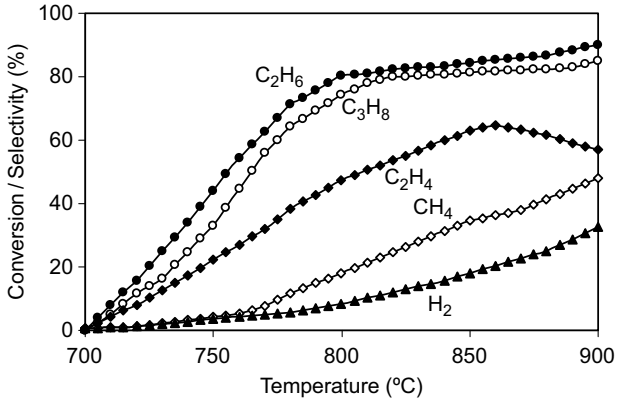

Fig. 3. Homogenous (in the absence of catalyst) reactivity of ethane and propane in the presence of steam (2.6 kPa C_2H_6, 1.4 kPa C_3H_8, and 12 kPa H_2O).

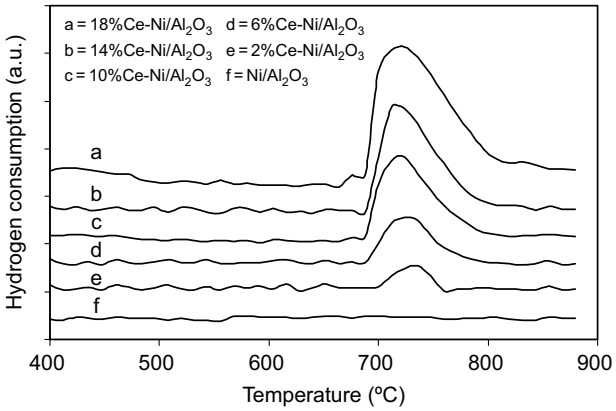

Fig. 4. Temperature Programmed Reduction (TPR-1) of the catalysts with different Ce doping content (0–18% Ce).

doping contents (0–18%) were investigated using temperature programmed reduction (TPR-1), in which performed by heating the reduced catalysts up to 900 °C in 5%H_2 in argon. As shown in Fig. 4, significant amount of hydrogen uptakes were detected from Ni/Al_2O_3 with the doping of CeO_2 at the temperature above 650 °C. The amount of hydrogen uptakes increased with increasing Ce doping content, suggesting the reduction of bulk oxygen ions on ceria surface. In contrast, no hydrogen consumption was observed from the TPR over conventional Ni/Al_2O_3. These results indicated the occurrence of redox properties for Ni/Al_2O_3 with CeO_2 doping at high temperature (650–900 °C), in which increased with increasing Ce content. This redox property provides a great benefit toward the reforming of ethane and propane, which will be presented in Section 3.4.

After purged with helium, the redox reversibility for each catalyst was then determined by applying temperature programmed oxidation (TPO) following with the second time temperature programmed reduction (TPR-2). The TPO was carried out by heating the catalyst up to 1000 °C in 10%O_2 in helium; the amounts of oxygen chemisorbed were then measured, Fig. 5 and Table 2. Regarding the TPR-2 results as shown in Fig. 6 and Table 2, the amount of

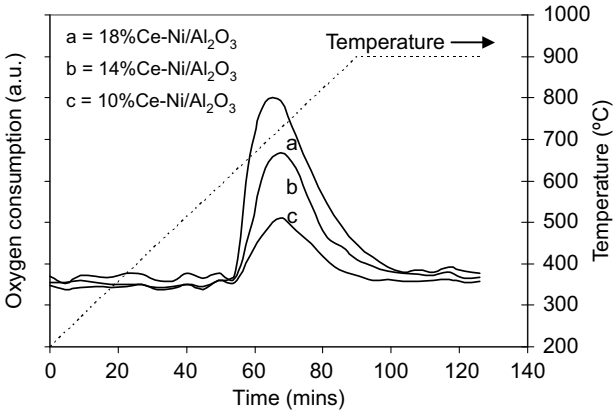

Fig. 5. Temperature Programmed Oxidation (TPO) of CeO_2-doped Ni/Al_2O_3 after TPR-1.

Table 2
Results of TPR(1), TPO, TPR(2) analyses of CeO_2 doped Ni/Al_2O_3 at high temperature

Catalyst	Total H_2 Uptake from TPR(1)[a] ($\mu mol/g_{cat}$)	Total O_2 Uptake from TPO[b] ($\mu mol/g_{cat}$)	Total H_2 Uptake from TPR(2)[c] ($\mu mol/g_{cat}$)
2%Ce-Ni/Al_2O_3	523	271	520
6%Ce-Ni/Al_2O_3	840	402	840
10%Ce-Ni/Al_2O_3	1078	540	1075
14%Ce-Ni/Al_2O_3	1350	691	1350
18%Ce-Ni/Al_2O_3	1505	784	1503

[a] Temperature Programmed Reduction of the reduced catalysts (Relative Standard Deviation = ±3%).
[b] Temperature Programmed Oxidation after TPR (1) (Relative Standard Deviation = ±1%).
[c] Re-Temperature Programmed Reduction after TPO (Relative Standard Deviation = ±2%).

hydrogen uptakes for each catalyst were approximately similar to those from TPR-1, indicated the redox reversibility for these catalysts.

3.3. Selection of suitable Ce doping content for the steam reforming of ethane/propane

After reduction of CeO_2-doped Ni/Al_2O_3, the steam reforming of ethane/propane was performed at 900 °C. The feed was $C_2H_6/C_3H_8/H_2O$ in helium with the molar ratio of 0.65/0.35/3.0. Fig. 7 presents the steady state yield of H_2 production (%) for CeO_2-doped Ni/Al_2O_3 with various CeO_2 contents (0–20%) at 900 °C. It was found that 14% CeO_2 doping on Ni/Al_2O_3 presents the highest hydrogen production yield.

The post-reaction temperature-programmed oxidation (TPO) experiments were then carried out after a helium purge by introducing 10% oxygen in helium in order to determine the degree of carbon deposition on the surface of each sample. Table 3 presents the important physicochemical properties of the spent catalysts after exposure in the steam reforming conditions for 10 h. According to TPO, the amount of carbon formation decreased with increasing Ce content. This is due to the increasing of redox properties by doping more CeO_2, which can inhibit the formation of carbon species on Ni surface. However, as seen from Fig. 7, slight decrease in reforming rate was observed when the Ce doping contents were higher than 14%. This decreasing in reactivity could be due to the possible oxidised of Ni because the reducibility of the catalysts (with 16, 18, and 20% Ce doping) reduced after exposure in the steam reforming for 10 h, according to the TPR experiment. Therefore, 14% CeO_2 doping on Ni/Al_2O_3 is the optimum content, which provides the highest resistance toward carbon deposition and is enable to operate without the oxidised of Ni.

3.4. Reactivity toward steam reforming of ethane/propane

The steam reforming of C_2H_6/C_3H_8 over Ni/Al_2O_3 and 14%CeO_2 doped Ni/Al_2O_3 were studied at 900 °C. After reducing with 5% hydrogen for 6 h, the catalysts were heated up under helium flow to 900 °C. At the isothermal condition, $C_2H_6/C_3H_8/H_2O$ in helium with different $C_2H_6/C_3H_8/H_2O$ molar ratios of 0.65/0.35/1.0, 0.65/0.35/2.0, and 0.65/0.35/3.0 were introduced in order to compare the reforming rates. The variations in hydrogen production yield with time at 900 °C for different catalysts and different inlet $C_2H_6/C_3H_8/H_2O$ ratio are shown in Fig. 8. The significant deactivations were detected for Ni/Al_2O_3 catalyst in all conditions especially at high inlet $C_2H_6/C_3H_8/H_2O$ ratio, whereas considerable lower deactivations were detected for 14%CeO_2 doped Ni/Al_2O_3. Catalyst stabilities expressed as deactivation percentages are given in Table 4.

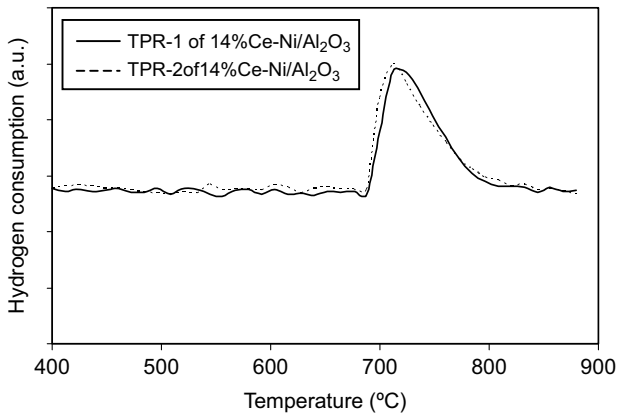

Fig. 6. Second time Temperature Programmed Reduction (TPR-2) of 14% CeO_2-doped Ni/Al_2O_3 compared to that of TPR-1.

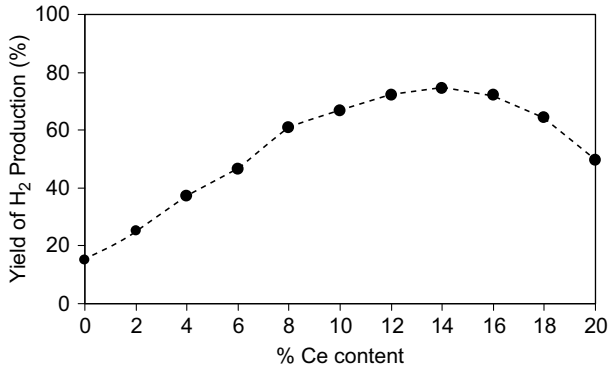

Fig. 7. Effect of Ce doping content on the yield of H_2 production (%) for steam reforming (900 °C, 2.6 kPa C_2H_6, 1.4 kPa C_3H_8, and 12 kPa H_2O).

Table 3
Yield of H_2 production (%), and physicochemical properties of the catalysts after exposure in steam reforming (2.6 kPa C_2H_6, 1.4 kPa C_3H_8, and 12 kPa H_2O) at 900 °C

Catalyst	Yield of H_2 production (%) at steady state	Ni and Ce load[a] (wt.%)	C formation[b] (monolayers)	BET surface ($m^2\ g^{-1}$)	Ni-red.[c] (Ni%)	Ni-disp.[d] (Ni%)
Ni/Al_2O_3	15.2	4.87/0.0	4.85	40.0	92.0	4.80
2%Ce-Ni/Al_2O_3	25.1	4.80/1.84	4.28	40.0	92.6	4.51
4%Ce-Ni/Al_2O_3	36.9	4.91/4.01	4.04	41.4	91.4	5.11
6%Ce-Ni/Al_2O_3	46.2	5.00/5.95	3.21	43.6	90.1	4.49
8%Ce-Ni/Al_2O_3	60.8	4.96/8.00	3.09	45.4	91.9	4.64
10%Ce-Ni/Al_2O_3	66.6	4.87/9.89	2.76	45.2	88.7	4.73
12%Ce-Ni/Al_2O_3	71.8	4.89/12.0	1.98	45.8	90.1	4.59
14%Ce-Ni/Al_2O_3	74.5	4.91/13.9	1.07	45.6	90.4	4.17
16%Ce-Ni/Al_2O_3	72.1	4.98/16.0	1.06	45.5	80.8	4.99
18%Ce-Ni/Al_2O_3	64.3	4.95/17.9	1.02	46.0	71.7	4.10
20%Ce-Ni/Al_2O_3	49.4	4.97/19.9	1.11	46.2	68.5	4.29

[a] Measured from X-ray fluorescence analysis.
[b] Calculated using CO and CO_2 yields from temperature-programmed oxidation (TPO) with 10% oxygen.
[c] Nickel reducibility (measured from temperature-programmed reduction (TPR) with 5%hydrogen).
[d] Nickel dispersion (measured from temperature-programmed desorption (TPD) after TPR).

After operated for 100 h, the steam reforming over 14%CeO_2 doped Ni/Al_2O_3 with inlet $C_2H_6/C_3H_8/H_2O$ of 0.65/0.35/3.0 showed the best activity. The influences of operating temperature and the inlet steam to ethane/propane ratio on the product selectivity were also studied by varying temperature from 700–900 °C and changing the inlet steam to carbon ratio from 1.0/1.0 to 5.0/1.0. As shown in Fig. 9, it was found that, at steady state, the main products from this reaction over 14%CeO_2 doped Ni/Al_2O_3 were H_2, CO, CO_2, and CH_4, with small amount of C_2H_4 depending on the operating temperature. For comparison, the conversions and the product selectivities at equilibrium level were calculated using AspenPlus10.2 simulation program, Fig. 10. Regarding the simulation, the conversions of C_2H_6 and C_3H_8 at equilibrium level are 100% in the range of temperature between 700 and 900 °C. The yields of hydrogen production at equilibrium are slightly higher than those achieved from the experiments, in addition, no C_2H_4 formation was observed at the equilibrium level in this range of temperature due to the complete reforming of this component to CH_4, CO, and CO_2.

Regarding the influence of inlet steam, hydrogen and carbon dioxide selectivity increased with increasing inlet steam concentration, whereas carbon monoxide selectivity decreased, Fig. 11. These are mainly due to the influence of water–gas shift reaction ($CO + H_2O \rightarrow CO_2 + H_2$). Moreover, the appearances of methane and ethylene in the system were found to decrease with increasing steam content, as these components were further reformed to CO, CO_2, and H_2 by the excess steam.

The post-reaction temperature-programmed oxidation (TPO) experiments were carried out after a helium purge by introducing of 10% oxygen in helium in order to determine whether the observed deactivation is due to the carbon formation. From the TPO results shown in Fig. 12, the huge peaks of carbon dioxide and carbon monoxide were observed for Ni/Al_2O_3, while smaller peaks of both components were detected for 14%CeO_2 doped Ni/Al_2O_3. The amount of carbon formations on the surface of these catalysts with different inlet $C_2H_6/C_3H_8/H_2O$ ratios were determined by measuring the CO and CO_2 yields from the TPO results. Using a value of 0.026 nm^2 for the area occupied by a carbon atom in a surface monolayer of the basal plane in graphite [38], the quantities of carbon deposited over Ni/Al_2O_3 were observed to be approximately 5.98, 5.41, and 4.85 monolayers, while those over 14%CeO_2 doped Ni/Al_2O_3 were 2.19, 1.48, and 1.07 monolayers for the inlet $C_2H_6/C_3H_8/H_2O$ ratios of 0.65/0.35/1.0, 0.65/0.35/2.0, and 0.65/0.35/3.0, respectively. The total amounts of carbon deposited were ensured by the calculation of carbon balance in the system. Regarding the calculations, for the inlet $C_2H_6/C_3H_8/H_2O$ ratios of 0.65/0.35/1.0, 0.65/0.35/2.0, and 0.65/0.35/3.0, the moles of carbon deposited per gram of 14%CeO_2 doped Ni/Al_2O_3 were 3.32, 2.33, and 1.68 mmol g^{-1}. By the same assumption for the area

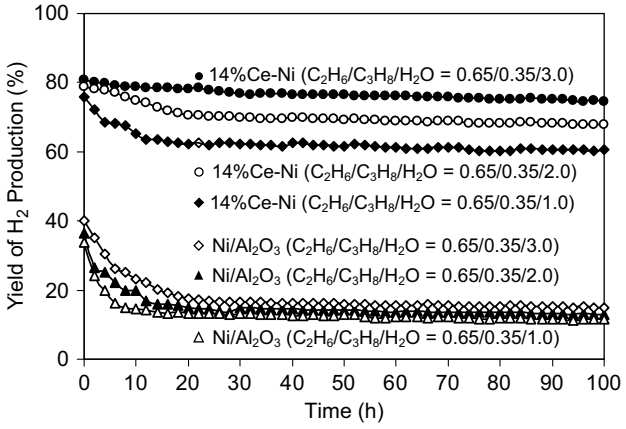

Fig. 8. Steam reforming of ethane/propane at 900 °C for several catalysts and various inlet $C_2H_6/C_3H_8/H_2O$ ratios.

Table 4
Yield of H_2 production (%), deactivation percentages, and physicochemical properties of the catalysts after exposure in steam reforming conditions (various inlet steam/carbon ratio) at 900 °C for 100 h

Catalyst	H_2O/C ratio	Yield of H_2 production (%) at steady state	Deactivation (%)	C formation[a] (monolayers)	BET surface (m^2 g^{-1})	Ni-red.[b] (Ni%)
Ni/Al_2O_3	1.0/1.0	11.5	65.8	5.98	40.0	91.9
	2.0/1.0	12.9	64.6	5.41	39.7	91.8
	3.0/1.0	15.1	62.5	4.85	40.0	92.0
14%Ce-Ni[c]	1.0/1.0	60.2	20.0	2.19	45.4	92.0
	2.0/1.0	67.8	13.6	1.48	45.1	91.8
	3.0/1.0	74.5	7.41	1.07	45.6	90.4

[a] Calculated using CO and CO_2 yields from temperature-programmed oxidation (TPO) with 10% oxygen.
[b] Nickel reducibility (measured from temperature-programmed reduction (TPR) with 5%hydrogen).
[c] CeO_2-doped Ni/Al_2O_3.

occupied by a carbon atom [38], these values are equal to 2.15, 1.51, and 1.09 monolayers, respectively, which are in good agreement with the values observed from the TPO method described above.

The results clearly indicated the strong resistance toward carbon formation for 14%CeO_2 doped Ni/Al_2O_3 compared to Ni/Al_2O_3. The BET measurements, as presented in Table 4, indicated that deactivations of 14%CeO_2 doped Ni/Al_2O_3 are also due to the slight sintering of CeO_2. The improvement of reforming reactivity and resistance toward carbon formation for CeO_2-doped Ni/Al_2O_3 could be mainly due to the redox property of ceria. During the reforming of C_2H_6/C_3H_8, the carbon formation could occur due to several reactions, the following reactions are the most probable reactions that could lead to carbon formation:

$$C_3H_8 \Leftrightarrow 4H_2 + 3C \quad (16)$$

$$C_2H_6 \Leftrightarrow 3H_2 + 2C \quad (17)$$

$$CH_4 \Leftrightarrow 2H_2 + C \quad (18)$$

$$C_2H_4 \Leftrightarrow 2H_2 + 2C \quad (19)$$

$$2CO \Leftrightarrow CO_2 + C \quad (20)$$

$$CO + H_2 \Leftrightarrow H_2O + C \quad (21)$$

$$CO_2 + 2H_2 \Leftrightarrow 2H_2O + C \quad (22)$$

where C is the carbonaceous deposits. At low temperature, Eqs. (21) and (22) are favorable, while Eqs. (16)–(19) are thermodynamically unflavored [42]. The Boudard reaction (Eq. (20)) and the decomposition of hydrocarbons (Eqs. (16)–(19)) are the major pathways for carbon formation at such a high temperature as they show the largest change in Gibbs energy [43]. According to the high temperature in this study, 900 °C, carbon formation would be formed via the decomposition of hydrocarbons and Boudard reactions. With the increase of steam to carbon ratio, the equilibrium of water-gas shift reaction moves forward and produces more CO_2 rather than CO. Therefore, high steam feed can avoid carbon deposition via the Boudouard reaction. However, significant amount of carbon remains detected on the surface of Ni/Al_2O_3 due to the decomposition of ethane, propane, ethylene, and methane (Eqs. (16)–(19)). By doping CeO_2 as the promoter, these reactions could be inhibited by the gas–solid reactions between hydrocarbons

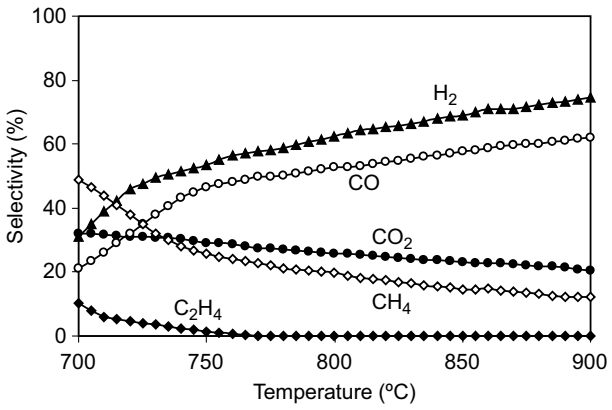

Fig. 9. Effect of reaction temperature on the selectivities of product elements (H_2, CO, CO_2, CH_4, and C_2H_4) from steam reforming over 14%CeO_2-doped Ni/Al_2O_3 (2.6 kPa C_2H_6, 1.4 kPa C_3H_8, and 12 kPa H_2O).

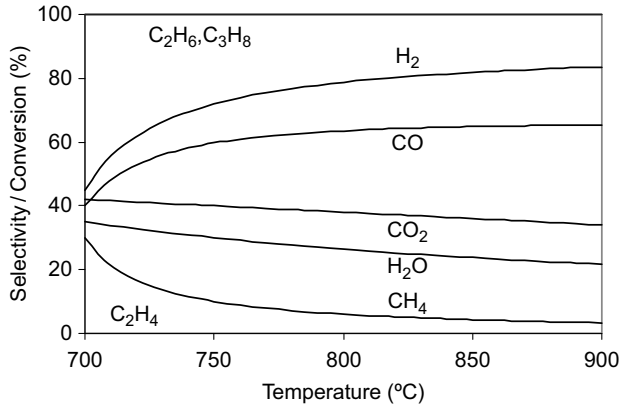

Fig. 10. Conversions of C_2H_6 and C_3H_8, and the selectivities of H_2, CO, CO_2, C_2H_4, and CH_4 at equilibrium level (Inlet conditions of 2.6 kPa C_2H_6, 1.4 kPa C_3H_8, and 12 kPa H_2O).

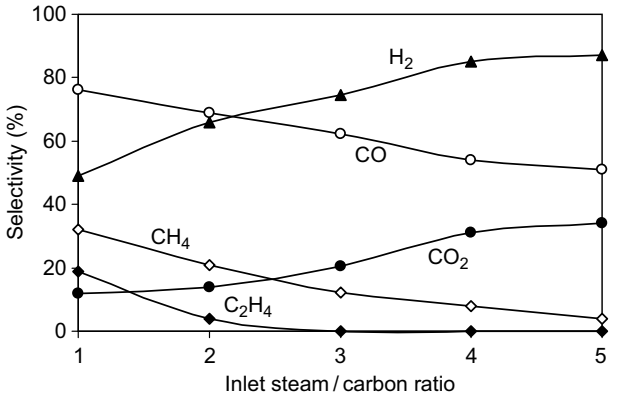

Fig. 11. Effect of inlet steam/carbon molar ratio on the selectivities of product elements (H_2, CO, CO_2, CH_4, and C_2H_4) from steam reforming over 14%CeO_2-doped Ni/Al2O_3 at 900 °C (2.6 kPa C_2H_6, 1.4 kPa C_3H_8, and 12 kPa H_2O).

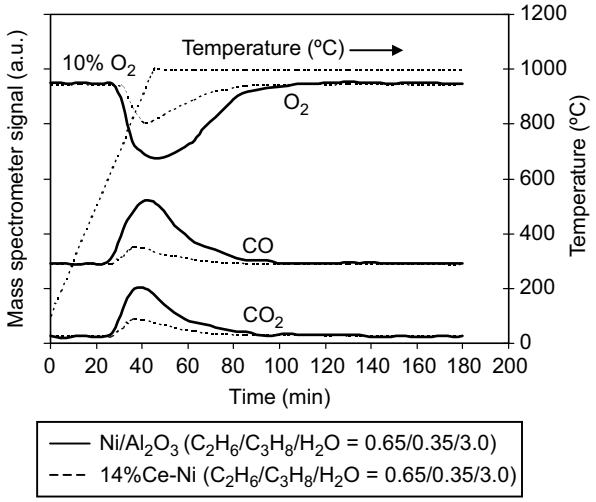

Fig. 12. Temperature Programmed Oxidation (TPO) of Ni/Al_2O_3 and 14%CeO_2-doped Ni/Al_2O_3 (10 kPa O_2) after exposure in steam reforming of ethane/propane (2.6 kPa C_2H_6, 1.4 kPa C_3H_8, and 12 kPa H_2O) for 100 h.

with the lattice oxygen (O_x) at CeO_2 surface forming hydrogen and carbon dioxide, which are thermodynamically unflavored to form carbon species.

Theoretically, the solid–gas reaction between CeO_2 and CH_4 produces synthesis gas, while the reduced ceria, CeO_{2-x}, can react with steam to produce H_2 [35–37]. In the present work, the solid–gas mechanism involves the reactions between hydrocarbons (C_2H_6, C_3H_8, CH_4, and C_2H_4) and/or an intermediate surface hydrocarbon species with the lattice oxygen (O_x) at CeO_2 surface, as illustrated schematically below.

$$C_3H_8 + 3S \Leftrightarrow 2(CH_3-S) + CH_2-S \quad (23)$$

$$C_2H_6 + 2S \Leftrightarrow 2(CH_3-S) \quad (24)$$

$$CH_4 + 2S \Leftrightarrow CH_3-S + H-S \quad (25)$$

$$C_2H_4 + 2S \Leftrightarrow 2(CH_2-S) \quad (26)$$

$$CH_3-S + S \Leftrightarrow CH_2-S + H-S \quad (27)$$

$$CH_2-S + S \Leftrightarrow CH-S + H-S \quad (28)$$

$$CH-S + S \Leftrightarrow C-S + H-S \quad (29)$$

$$C-S + O_x \Leftrightarrow CO + O_{x-1} + S \quad (30)$$

$$2H-S \Leftrightarrow H_2 + 2S \quad (31)$$

where *S* is the catalyst surface site. It can be considered to be a unique site, or the same site as the lattice oxygen (O_x) [40]. During the steam reforming, hydrocarbons are adsorbed on either a unique site (S) or the lattice oxygen (O_x), whereas H_2O can react with the reduced site of ceria, O_{x-1}. The steady state reforming rate is mainly due to the continuous supply of the oxygen source by H_2O.

$$H_2O + O_{x-1} \Leftrightarrow O_x + H_2 \quad (32)$$

It should be noted that the solid–gas reaction on the surface of ceria could also reduce the formation of carbon via Boudouard reaction, as carbon monoxide can adsorb and react with the lattice oxygen (O_x) on the surface of ceria forming carbon dioxide ($CO + O_x \Leftrightarrow O_{x-1} + CO_2$), which is less flavored to form carbon species at high temperature.

4. Conclusion

14%CeO_2-doped Ni/Al_2O_3 is a good candidate catalyst for the reforming of ethane and propane at SOFC temperature (900 °C) due to the high resistance toward the deactivation from carbon formation at high temperature. During reforming process, the gas–solid redox reactions on ceria surface take place simultaneously with the reforming reactions on the surface of Ni, and they reduce the degree of carbon deposition on catalyst surface from hydrocarbons decomposition and Boudard reactions. Regarding the TPR measurement, the redox properties increased with increasing Ce doping content. In addition, this oxygen storage property was proven to be reversible. However, it should also be noted that the doping of too high ceria content on the catalyst results in the oxidation of Ni, which could reduce the reforming reactivity.

In particular, at the temperature above 800 °C and the inlet steam/carbon ratio higher than 3.0, all ethylene formation in which occurs homogenously (non-catalytic) from the thermal cracking of ethane and propane was converted by the steam reforming over this catalyst. By increasing inlet steam content, hydrogen and carbon dioxide selectivities increased, whereas carbon monoxide selectivity decreased. Moreover, the conversions of methane and ethylene were found to increase with increasing steam content in the system.

Acknowledgements

The financial support from The Thailand Research Fund (TRF) throughout this project is gratefully acknowledged.

References

[1] W.L. Lundberg, S.E. Veyo, Conceptual design and performance analysis of a 300 MWel LNG-fuelled pressurised SOFC/Gas turbine power plant, in: Yokohawa, S.C. Singhal (Eds.), Proceeding of the 7th International Symposium Solid Oxide Fuel Cells VII, 2001, 78-87.
[2] Aguiar P, Chadwick D, Kershenbaum L. Chem. Eng. Sci. 2002;57: 1665.
[3] Aguiar P, Lapena-Rey N, Chadwick D, Kershenbaum L. Chemical Engineering Science 2001;56:652.
[4] Peters R, Dahl R, Kluttgen U, Palm C, Stolten D, Power J. Sources 2002;106:238.
[5] N. Laosiripojana, 6th European Solid Oxide Fuel Cell Forum, 28 June - 2 July 2004.
[6] Trovareli A, Leitenburg C, Dolcetti G. Chemtech 1997;32.
[7] Fornasiero P, Balducci G, Monte RD, Kaspar J, Sergo V, Gubitosa G, Ferrero A. M. Graziani. J. Catal. 1996;164:173.
[8] Miki T, Ogawa T, Haneda M, Kakuta N, Ueno A, Tateishi S, Matsuura S. M. Sato, J. Phys. Chem. 1990;94:339.
[9] Padeste C, Cant NW, Trimm L. Catal. Lett. 1993;18:305.
[10] Kacimi S, Barbier Jr. J, Taha R. D. Duperz, Catal. Lett. 1993;22:343.
[11] Zafiris GS, Gorte J. J. Catal. 1993;143:86.
[12] Zafiris GS, Gorte J. J. Catal. 1993;139:561.
[13] Imamura S, Shono M, Okamoto N, Hamada R. S. Ishida, Appl. Catal. A 1996;142:279.
[14] Fan L. K. Fujimoto. J. Catal. 1997;172:238.
[15] Pijolat M, Prin M. M. Soustelle. J. Chem. Soc., Faraday Trans. 1995; 91:3941.
[16] Imamura S, Higashihara T, Saito Y, Aritani H, Kanai H, Matsumura Y. N. Tsuda, Catal. Today 1999;50:369.
[17] Imamura S, Denpo K, Utani K, Matsumura Y. H. Kanai, React. Kinet. Catal. Lett. 1999;67:163.
[18] Imamura S, Denpo K, Kanai K, Yamane H, Saito Y, Utani K. Y. Matsumura, Sekiyu Gakkaishi 2001;44:293.
[19] Imamura S, Yamane H, Kanai H, Shibuta T, Utani K. K. Hamada, J. Jpn. Petrol. Inst. 2002;45:187.
[20] Imamura S, Taniguchi Y, Ikeda Y, Hosokawa S, Kanai H. H. Ando, React. Kinet. Catal. Lett. 2002;76:201.
[21] Roh HS, Jun KW, Dong WS, Chang JS, Park SE, Joe YI. J. Mol. Catal. A 2002;181:137–42.
[22] Miao Q, Xiong G, Sheng S, Cui W, Xu L. Guo. Appl. Catal. A 1987; 154:17–27.
[23] Lemonidou AA, Goula MA, Vasalos IA. Catal. Today 1987;46: 175–83.
[24] Dong WS, Roh HS, Jun KW, Park SE, Oh YS. Appl. Catal. A 2002; 226:63–72.
[25] Mamak M, Coombs N, Ozin G. Adv. Mater. 2000;12:198–202.
[26] Mamak M, Coombs N, Ozin G. J. Am. Chem. Soc. 2000;122:8932.
[27] Mamak M, Coombs N, Ozin GA. Chem. Mater. 2001;13:3564.
[28] Bera P, Mitra S, Sampath S, Hegde MS. Chem. Commun. 2001;927.
[29] Martinez-Arias A, Coronado JM, Cataluna R, Conesa JC, Soria JC. J. Phys. Chem. B 1998;102:4357.
[30] Skarmoutsos D, Tietz F, Nikolopoulos P. Fuel Cells 2001;1:243.
[31] Takeguchi T, Furukawa SN, Inoue M. J. Catal. 2001;202:14.
[32] Sfeir J, Philippe PA, Moseki P, Xanthopoulos N, Vasquez R, Hans JM, Jan VH, Thampi KR. J. Catal. 2001;202:229.
[33] Kiratzis N, Holtappels P, Hatchwell CE, Mogensen M, Irvine JTS. Fuel Cells 2001;1:211.
[34] Roh HS, Dong WS, Jun KW, Park SE. Chem. Lett. 2001;88.
[35] Otsuka K, Ushiyama T. I. Yamanaka, Chemistry Letters 1993;1517.
[36] Otsuka K, Hatano M. A. Morikawa, J. Catalysis 1983;79:493.
[37] Otsuka K, Hatano M. A. Morikawa, Inorganica Chimica Acta 1985; 109:193.
[38] Ramírez-Cabrera E, Atkinson A. D. Chadwick, Applied Catalysis B 2004;47:127–31.
[39] Ramírez-Cabrera E, Laosiripojana N, Atkinson A. D. Chadwick, Catalysis Today 2003;78:433–8.
[40] N. Laosiripojana 2003, Reaction engineering of indirect internal steam reforming of methane for application in solid oxide fuel cells. Ph.D. Thesis, University of London, England.
[41] M.V. Twigg, Catalyst Handbook, 2nd Edition, Wolfe Publishing, London, (1989).
[42] Lwin Y, Daud WRW, Mohamad AB. Z. Yaakob, Int. J. Hydrogen Energy 2000;25(1):47–53.
[43] Amor JN. Appl. Catal. A 1999;176:159–76.

Available online at www.sciencedirect.com
SCIENCE DIRECT®
Journal of Power Sources xxx (2005) xxx–xxx
JOURNAL OF POWER SOURCES
www.elsevier.com/locate/jpowsour

Hydrogen production from steam and autothermal reforming of LPG over high surface area ceria

N. Laosiripojana [a,*], S. Assabumrungrat [b]

[a] *The Joint Graduate School of Energy and Environment, King Mongkut's University of Technology Thonburi, Bangkok 10140, Thailand*
[b] *Center of Excellence in Catalysis and Catalytic Reaction Engineering, Department of Chemical Engineering, Faculty of Engineering, Chulalongkorn University, Bangkok 10330, Thailand*

Received 22 September 2005; received in revised form 18 October 2005; accepted 18 October 2005

Abstract

Steam and autothermal reforming reactions of LPG (propane/butane) over high surface area CeO_2 (CeO_2 (HSA)) synthesized by a surfactant-assisted approach were studied under solid oxide fuel cell (SOFC) operating conditions. The catalyst provides significantly higher reforming reactivity and excellent resistance toward carbon deposition compared to the conventional Ni/Al_2O_3. These benefits of CeO_2 are due to the redox property of this material. During the reforming process, the gas–solid reactions between the hydrocarbons present in the system (i.e. C_4H_{10}, C_3H_8, C_2H_6, C_2H_4, and CH_4) and the lattice oxygen (O_O^x) take place on the ceria surface. The reactions of these adsorbed surface hydrocarbons with the lattice oxygen ($C_nH_m + O_O^x \rightarrow nCO + m/2(H_2) + V_O^{\bullet\bullet} + 2e'$) can produce synthesis gas (CO and H_2) and also prevent the formation of carbon species from hydrocarbons decomposition reactions ($C_nH_m \Leftrightarrow nC + 2mH_2$). Afterwards, the lattice oxygen (O_O^x) can be regenerated by reaction with the steam present in the system ($H_2O + V_O^{\bullet\bullet} + 2e' \Leftrightarrow O_O^x + H_2$). It should be noted that $V_O^{\bullet\bullet}$ denotes as an oxygen vacancy with an effective charge 2^+.

At 900 °C, the main products from steam reforming over CeO_2 (HSA) were H_2, CO, CO_2, and CH_4 with a small amount of C_2H_4. The addition of oxygen in autothermal reforming was found to reduce the degree of carbon deposition and improve product selectivities by completely eliminating C_2H_4 formation. The major consideration in the autothermal reforming operation is the O_2/LPG (O/C molar ratio) ratio, as the presence of a too high oxygen concentration could oxidize the hydrogen and carbon monoxide produced from the steam reforming. A suitable O/C molar ratio for autothermal reforming of CeO_2 (HSA) was 0.6.

Keywords: LPG; Steam reforming; Autothermal reforming; Ceria; Solid oxide fuel cell

1. Introduction

A fuel cell is an energy conversion device that produces electrical energy with greater conversion efficiency and lower pollutant emissions than combustion processes. Among the various types of fuel cells, the solid oxide fuel cell (SOFC) has attracted considerable interest as it offers the widest range of applications, flexibility in the choice of fuel, and high system efficiency. The waste heat for SOFC can also be utilized in co-generation applications and bottoming cycles to improve the overall system efficiency. Moreover, unlike low-temperature fuel cells, the SOFC anode is not affected by carbon monoxide poisoning. Although, hydrogen is the major fuel for a SOFC, the use of other fuels such as methane, methanol, ethanol, liquefied petroleum gas (LPG), gasoline and other oil derivatives are also possible via internal or in-stack reforming. Since an SOFC is operated at such a high temperature, these hydrocarbons can be internally reformed producing a H_2/CO rich gas, which is eventually used to generate the electrical energy and heat. This operation, called indirect internal reforming (IIR-SOFC), is expected to simplify the overall SOFC system design [1].

Among the above hydrocarbon fuels, liquefied petroleum gas (LPG) is a commercial gas that is easily transported and stored on-site. This gas was proposed to be an attractive fuel for SOFC systems in remote areas where pipeline natural gas is not available [2]. LPG can also be used for auxiliary power units (APU) based on SOFC systems. Typically, the main components of

* Corresponding author. Tel.: +66 2 8729014; fax: +66 2 8726736.
E-mail address: navadol_l@jgsee.kmutt.ac.th (N. Laosiripojana).

0378-7753/$ – see front matter © 2005 Elsevier B.V. All rights reserved.
doi:10.1016/j.jpowsour.2005.10.058

LPG are propane and butane. According to the Australian LPG Association, the composition of LPG in Australia ranges from pure propane to a 40:60 mixture of propane and butane [2]. The steam reforming process has widely been used to produce hydrogen from LPG. The main products from the steam reforming of LPG are hydrogen, carbon monoxide, and carbon dioxide, however, the formation of ethane, ethylene, and methane are usually observed due to the decomposition of LPG and methanation reactions. The major difficulty in reforming LPG is the degradation of the reforming catalyst due to the possible carbon deposition from the decomposition of hydrocarbons, particularly at high temperature. Previously, steam reforming of LPG has been studied by a few researchers [2–8], and most of them have investigated the reforming of LPG over noble metal catalysts (e.g. Rh, Ru, and Pt) on oxide supports. Recupero et al. [8] reported that Pt/CeO_2 provides high reforming reactivity with low carbon formation. Suzuki et al. [3] found that Ru/CeO_2-Al_2O_3 can reform LPG with a low inlet steam requirement at 450 °C. Adding oxygen together with LPG and steam as an autothermal reforming process was reported to provide great benefits in terms of catalyst stability and low coke formation [4,5], however, the yield of hydrogen production could be reduced due to the oxidation of hydrogen by oxygen added. The attractive benefit of this operation is that the exothermic heat from the partial oxidation can directly supply the energy required for the endothermic steam reforming reaction, and so it is considered to be thermally self-sustaining process.

This work is aimed at the development of a catalyst for steam and autothermal reforming of LPG, which provides high stability and activity at a high temperature (700–900 °C) for later application in an IIR-SOFC. Although the precious metals such as Pt, Rh and Ru have been reported by several researchers to provide high activity for the reforming reactions and excellent resistant to carbon formation [9,10], the current prices of these metals are too high for commercial usage, and the availability of some precious metals such as ruthenium was too low to have a major impact on the total reforming catalyst market [11]. In view of these economical considerations, an alternative catalyst was developed and studied instead. Cerium oxide or ceria has been reported to be a catalyst in a wide variety of reactions involving oxidation or partial oxidation of hydrocarbons (e.g. automotive catalysis). A high oxygen mobility (redox property) [12], high oxygen storage capacity [13–18], strong interaction with the supported metal (strong metal–support interaction) [19] and a modifiable capability [20] render this material very interesting for catalysis. It has widely been reported, regarding the above properties, that ceria can promote the action of various metals in the reactions in which hydrogen is involved as a reactant or product [21–25]. According to the catalytic steam reforming reaction, ceria-based materials have been reported by several researchers to be promising supports among α-Al_2O_3 [26], γ-Al_2O_3 and γ-Al_2O_3 with alkali metal oxide and rare earth metal oxide [27], and $CaAl_2O_4$ [26–29]. One of the most promising ceria-based supports for the reforming reactions appeared to be Ce-ZrO_2, where the metal can be Ni, Pt or Pd [30–39]. Recently, a high resistance toward carbon deposition over ceria has been observed [40].

Importantly, CeO_2 has been reported to have reactivity toward methane decomposition at a high temperature (800–1000 °C) [41,42]. It was demonstrated that the gas–solid reaction between CeO_2 and CH_4 produces H_2 and CO, according to Eq. (1). Moreover, the reactions of the reduced ceria (CeO_{2-n}) with carbon dioxide and steam produce more CO and H_2 and regenerate the CeO_2 surface, Eqs. (2) and (3) [43–45]:

$$CH_4 + O_O{}^x = 2H_2 + CO + V_O{}^{\bullet\bullet} + 2e' \quad (1)$$

$$V_O{}^{\bullet\bullet} + 2e' + CO_2 = O_O{}^x + CO \quad (2)$$

$$V_O{}^{\bullet\bullet} + 2e' + H_2O = O_O{}^x + H_2 \quad (3)$$

$V_O{}^{\bullet\bullet}$ denotes an oxygen vacancy with an effective charge 2^+, $O_O{}^x$ is lattice oxygen, e′ is an electron which can either be more or less localized on a cerium ion or delocalized in a conduction band [46].

The major limitation for CeO_2 in high temperature applications is its low specific surface area due to the significant size reduction on thermal sintering [42] and, consequently, the reforming reactivity over CeO_2 was much lower than the conventional metallic catalysts [42]. It was reported that the methane conversion from CeO_2 after exposure in methane steam reforming conditions at 900 °C for 10 h was less than 10%. In addition, the corresponding post-reaction specific surface area for this material after exposure in methane steam reforming conditions was 1.9 $m^2\,g^{-1}$, and the observed size reduction percentage was 23% [42]. Therefore, the use of high surface area ceria (CeO_2 (HSA)) would be a good procedure to improve its catalytic performance at high operating temperatures. Several methods have recently been described for the preparation of a CeO_2 (HSA) solid solution. Among these methods, the surfactant-assisted approach was employed to prepare high surface area CeO_2 with improved textural, structural, and chemical properties [47]. Our previous publication [48] reported the achievement of CeO_2 with a high surface area and good stability after thermal treatment by this preparation method. Regarding the surfactant-assisted method, CeO_2 (HSA) is prepared by reacting a cationic surfactant with a hydrous oxide produced by co-precipitation under basic conditions. At a high pH value, conducting the precipitation of hydrous oxide in the presence of a cationic surfactant allows the cation exchange process between H^+ and the surfactant, resulting in a developed pore structure with an increase in surface area [47]. The achievement of high thermal stability for CeO_2 (HSA) is due to the incorporation of surfactants during preparation, which can reduce the interfacial energy and eventually decrease the surface tension of water contained in the pores. This could reduce the shrinkage and collapse of the catalyst during heating, which consequently helps the catalyst maintain a high surface area after calcination [47].

In the present work, the stability and activity toward steam reforming of LPG over high surface area CeO_2 (CeO_2 (HSA)) was studied and compared to those over the conventional low surface area CeO_2 (CeO_2 (LSA)), and also conventional Ni/Al_2O_3. The resistance towards carbon formation and the influence of the inlet H_2O/LPG molar ratio and temperature on product selectivities over these catalysts were determined. In

Table 1
Specific surface area of CeO_2 (HSA and LSA) after drying and calcinations at different temperatures

Catalyst	BET surface area ($m^2\ g^{-1}$) after drying or calcination at						
	100 °C	200 °C	400 °C	600 °C	800 °C	900 °C	1000 °C
CeO_2 (LSA)[a]	55	49	36	21	15	11	8.5
CeO_2 (HSA)[b]	105	97	69	48	35	29	24

[a] Conventional low surface area CeO_2 prepared by the precipitation method.
[b] Nanocomposite high surface area CeO_2 prepared by the surfactant-assisted approach.

addition, autothermal reforming of LPG was also investigated by adding oxygen at the inlet feed. The improvement in the resistance to carbon deposition by the presence of oxygen and a suitable inlet O_2/LPG molar ratio were determined. It should be noted that the contents of desulpherized LPG used in this work are 60% C_3H_8 and 40% C_4H_{10} (based on the compositions of LPG from PTT Company (Thailand)).

2. Experimental

2.1. Catalyst preparation and characterization

Conventional CeO_2 (CeO_2 (LSA)) was prepared by the precipitation of cerium chloride ($CeCl_3 \cdot 7H_2O$) from Aldrich. The starting solution was prepared by mixing 0.1 M of this metal salt solution with 0.4 M of ammonia in a 2:1 volumetric ratio. This solution was stirred by magnetic stirring (100 rpm) for 3 h, then sealed and placed in a thermostatic bath maintained at 90 °C for 3 days. The precipitate was filtered and washed with deionised water and acetone to remove the free surfactant. It was dried overnight in an oven at 110 °C, and then calcined in air at 1000 °C for 6 h.

High surface area CeO_2 (CeO_2 (HSA)) was prepared by adding an aqueous solution of the appropriate cationic surfactant, 0.1 M cetyltrimethylammonium bromide solution from Aldrich, to a 0.1 M cerium chloride. The molar ratio of ([Ce])/[cetyltrimethylammonium bromide] was kept constant at 0.8. The mixture was stirred and then aqueous ammonia was slowly added with vigorous stirring until the pH was 11.5 [47]. The mixture was continually stirred for 3 h, then sealed and placed in the thermostatic bath maintained at 90 °C for 3 days. After that, the mixture was cooled and the resulting precipitate was filtered and washed repeatedly with water and acetone. The filtered powder was then treated under the same procedures as CeO_2 (LSA). BET measurements of CeO_2 (both LSA and HSA) were carried out at different calcination temperatures in order to determine the loss of specific surface area due to the thermal sintering. As presented in Table 1, after drying, surface areas of 82 and 55 $m^2\ g^{-1}$ were observed for CeO_2 (HSA) and conventional CeO_2, respectively, and as expected, the surface area dramatically decreased at high calcination temperatures. However, the value for CeO_2 (HSA) is still appreciable after calcination at 1000 °C and it is almost three times that of the conventional CeO_2.

The redox properties and redox reversibilities of these synthesized CeO_2 (both LSA and HSA) were then determined by the temperature-programmed reduction (TPR) and temperature-programmed oxidation (TPO). TPR and TPO experiments were conducted in the presence of 5% H_2/Ar and 5% O_2/He, respectively, while the temperature of the system increased from room temperature to 900 °C for both experiments.

For comparison, Ni/Al_2O_3 (5 wt.% Ni) was also prepared by impregnating α-Al_2O_3 (from Aldrich) with $NiCl_3$. After stirring, the solution was dried and calcined at 1000 °C for 6 h. The catalysts were also reduced with 10%H_2/Ar at 500 °C for 6 h before use. After reduction, the catalysts were characterized by several physicochemical methods. The weight content of Ni in Ni/Al_2O_3 was determined by X-ray fluorescence (XRF) analysis. The reducibility and dispersion percentages of nickel were measured from temperature-programmed reduction (TPR) with 5% H_2 in helium and temperature-programmed desorption (TPD), respectively. The catalyst specific surface areas were obtained from BET measurement. All physicochemical properties of the synthesized Ni/Al_2O_3 are presented in Table 2.

2.2. Apparatus and procedures

An experimental reactor system was constructed as shown in Fig. 1. The feed gases including the components of interest (e.g. LPG, steam from the evaporator, and oxygen) and the carrier gas (helium) were introduced to the reaction section, in which a 10 mm diameter quartz reactor was mounted vertically inside a furnace. The reactivities of the catalyst toward steam reforming of LPG were determined by loading the catalyst in this quartz reactor, which was packed with a small amount of quartz wool to prevent the catalyst from moving. The inlet LPG concentration was kept constant at 5 kPa (C_3H_8/C_4H_{10} ratio of 0.6/0.4), while the inlet steam concentrations were varied depending on the inlet H_2O/LPG molar ratio requirement for each experiment (3.0, 4.0, 5.0, 6.0, and 7.0). Regarding the results in our previous publications [48], to avoid any limitations by intraparticle diffusion, the weight of catalyst was always kept constant at 50 mg, while the total gas flow was 100 $cm^3\ min^{-1}$ with a constant residence time of 5×10^{-4} g min cm^{-3} in all experiments. A Type-K

Table 2
Physicochemical properties of synthesized Ni/Al_2O_3 after reduction

Catalyst	Ni-load[a] (wt.%)	BET surface area ($m^2\ g^{-1}$)	Ni-reducibility[b] (Ni%)	Ni-dispersion[c] (Ni%)
Ni/Al_2O_3	4.9	40	92.1	4.87

[a] Measured from X-ray fluorescence analysis.
[b] Measured from temperature-programmed reduction (TPR) with 5% hydrogen.
[c] Measured from temperature-programmed desorption (TPD) of hydrogen after TPR measurement.

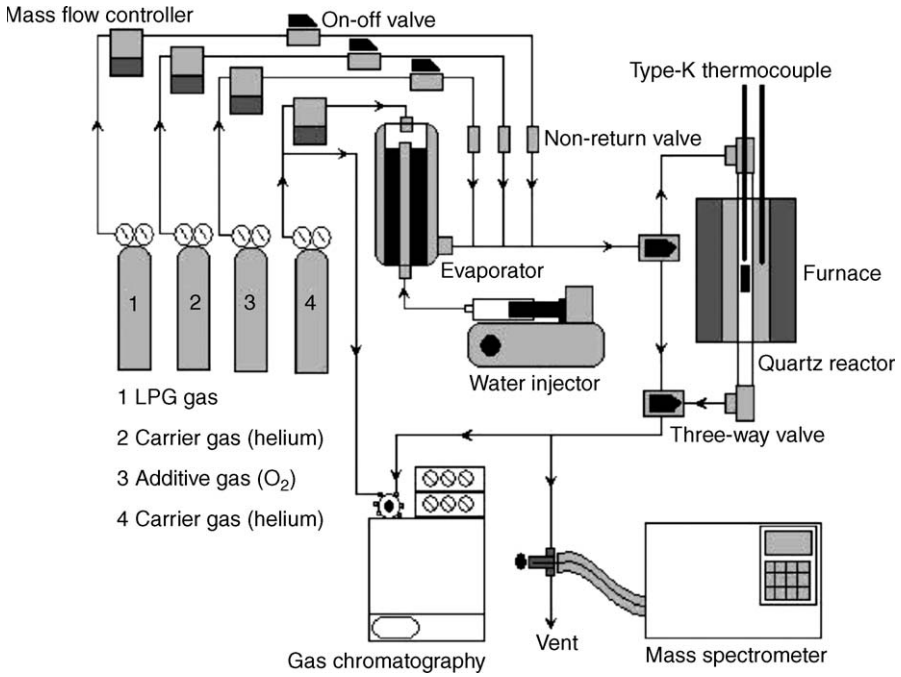

Fig. 1. Schematic diagram of the experimental set-up.

thermocouple was placed in the annular space between the reactor and the furnace. This thermocouple was mounted on the tubular reactor in close contact with the catalyst bed to minimize the temperature difference between the catalyst bed and the thermocouple. Another Type-K thermocouple was inserted in the middle of the quartz tube in order to re-check the possible temperature gradient, especially when O_2 was added along with LPG and H_2O in autothermal reforming. The recorded values showed that the maximum temperature fluctuation during the reaction was always $\pm 0.75\,^{\circ}C$ or less from the temperature specified for the reaction.

After the reactions, the exit gas mixture was transferred via trace-heated lines to the analysis section, which consisted of a Porapak Q column Shimadzu 14B gas chromatograph (GC) and a mass spectrometer (MS). Gas chromatography was used in order to investigate the steady state condition experiments, whereas the mass spectrometer, in which the sampling of the exit gas was done by a quartz capillary and differential pumping, was used in the transient carbon formation experiment. In order to study the formation of carbon species on catalyst surface, temperature-programmed oxidation (TPO) was applied by introducing 5% oxygen in helium into the system, after being purged with helium. The operating temperature was increased from room temperature to 900 °C at a rate of 10 °C min^{-1}. The calibration of CO and CO_2 were performed by injecting a known amount of the gases from a sample loop into an injection valve in the bypass line. The response factors were obtained by dividing the number of moles for each component over the respective areas under peaks. The amount of carbon formed on the surface of catalysts was determined by measuring the CO and CO_2 yields from the TPO results (using Microcal Origin Software) assuming a value of 0.026 nm^2 for the area occupied by a carbon atom in a surface monolayer of the basal plane in graphite [49]. In addition to the TPO method, the amount of carbon deposition was confirmed by the calculation of carbon balance in the system. The amount of carbon deposited on the surface of catalyst would theoretically be equal to the difference between the inlet carbon containing components (C_3H_8 and C_4H_{10}) and the outlet carbon containing components (CO, CO_2, CH_4, C_2H_6, and C_2H_4). The amount of carbon deposited per gram of catalyst is given by the following equation:

$$C_{\text{deposition}} = \frac{\text{mole}_{\text{carbon(in)}} - \text{mole}_{\text{carbon(out)}}}{m_{\text{catalyst}}} \tag{4}$$

The steam reforming reactivity was defined in terms of the conversions and selectivities. Hydrocarbon conversions (propane and butane) denoted as $X_{\text{hydrocarbon}}$, and the products selectivity (hydrogen, carbon monoxide, carbon dioxide, methane, and ethylene), denoted as S_{product}, are calculated according to Eqs. (5)–(12):

$$X_{\text{butane}} = \frac{100(\%\text{butane}_{\text{in}} - \%\text{butane}_{\text{out}})}{\%\text{butane}_{\text{in}}} \tag{5}$$

$$X_{\text{propane}} = \frac{100(\%\text{propane}_{\text{in}} - \%\text{propane}_{\text{out}})}{\%\text{propane}_{\text{in}}} \tag{6}$$

$$S_{H_2} = \frac{100(\%H_2)}{3(\%\text{butane}_{\text{in}} - \%\text{butane}_{\text{out}}) + 4(\%\text{propane}_{\text{in}} - \%\text{propane}_{\text{out}}) + (\%H_2O_{\text{in}} - \%H_2O_{\text{out}})} \tag{7}$$

$$S_{\text{CO}} = \frac{100(\%\text{CO})}{2(\%\text{butane}_{\text{in}} - \%\text{butane}_{\text{out}}) + 3(\%\text{propane}_{\text{in}} - \%\text{propane}_{\text{out}})} \tag{8}$$

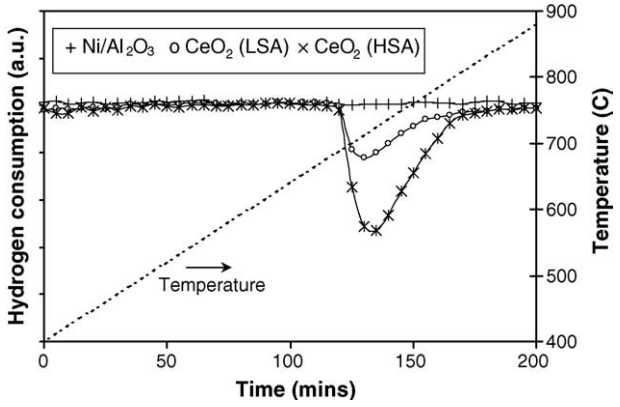

Fig. 2. Temperature-programmed reduction (TPR-1) of fresh catalysts after reduction.

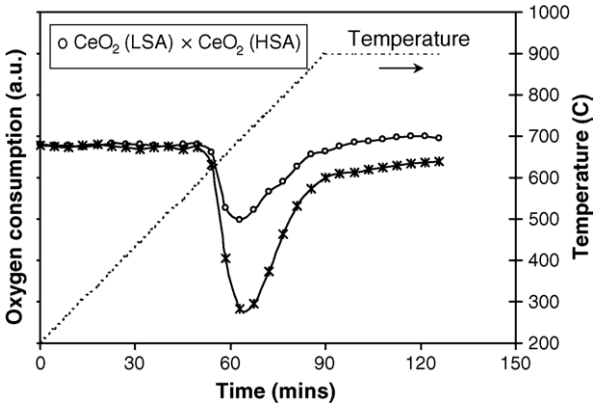

Fig. 3. Temperature-programmed oxidation (TPO) of CeO_2 (HSA and LSA) after TPR-1.

$$S_{CO_2} = \frac{100(\%CO_2)}{2(\%\text{butane}_{in} - \%\text{butane}_{out}) + 3(\%\text{propane}_{in} - \%\text{propane}_{out})} \quad (9)$$

$$S_{CH_4} = \frac{100(\%CH_4)}{2(\%\text{butane}_{in} - \%\text{butane}_{out}) + 3(\%\text{propane}_{in} - \%\text{propane}_{out})} \quad (10)$$

$$S_{C_2H_6} = \frac{100(\%C_2H_6)}{(\%\text{butane}_{in} - \%\text{butane}_{out}) + 1.5(\%\text{propane}_{in} - \%\text{propane}_{out})} \quad (11)$$

$$S_{C_2H_4} = \frac{100(\%C_2H_4)}{(\%\text{butane}_{in} - \%\text{butane}_{out}) + 1.5(\%\text{propane}_{in} - \%\text{propane}_{out})} \quad (12)$$

3. Results

3.1. Redox property and redox reversibility of the synthesized CeO_2

The oxygen storage capacities (OSC) and the redox properties of CeO_2 (both LSA and HSA) were investigated using temperature-programmed reduction (TPR-1) which was performed by heating the reduced catalysts up to 900 °C in 5%H_2 in argon. A test over Ni/Al_2O_3 was also performed for comparison. As shown in Fig. 2, hydrogen uptake was detected from both types of CeO_2 at the temperature above 650 °C. The amount of hydrogen uptake over CeO_2 (HSA) is significantly higher than that over CeO_2 (LSA), suggesting that the OSC and the redox properties strongly depend on the specific surface area of CeO_2. In contrast, no hydrogen consumption was observed from the TPR over Ni/Al_2O_3, indicating the absence of redox properties for this catalyst. The benefit of having a redox property in the reforming of LPG will be presented in Section 4. After being purged with helium, the redox reversibility for each type of CeO_2 was then determined by conducting temperature-programmed oxidation (TPO) following by a second temperature-programmed reduction (TPR-2). The TPO was carried out by heating the catalyst up to 900 °C in 5%O_2 in helium; the amount of oxygen chemisorbed was then measured, as shown in Fig. 3 and Table 3. Regarding the TPR-2 results as shown in Fig. 4 and Table 3, the amount of hydrogen uptake for CeO_2 (both LSA and HSA) were approximately similar to those from TPR-1, indicating the redox reversibility of these synthesized versions of CeO_2.

3.2. Homogenous (non-catalytic) reactions

Before studying the catalyst performance, homogeneous (non-catalytic) steam reforming of LPG was investigated. A

Table 3
Results of TPR(1), TPO, TPR(2) analyses of CeO_2 (both HSA and LSA)

Catalyst	Total H_2 uptake from TPR(1)[a] (μmol g_{cat}^{-1})	Total O_2 uptake from TPO[b] (μmol g_{cat}^{-1})	Total H_2 uptake from TPR(2)[c] (μmol g_{cat}^{-1})
CeO_2 (HSA)	2159	1044	2155
CeO_2 (LSA)	1784	867	1781

[a] Temperature-programmed reduction of the reduced catalysts (relative standard deviation = ±3%).
[b] Temperature-programmed oxidation after TPR(1) (relative standard deviation = ±1%).
[c] Re-temperature-programmed reduction after TPO (relative standard deviation = ±2%).

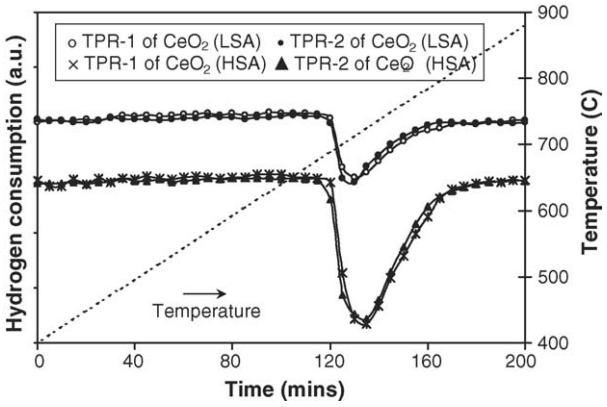

Fig. 4. Second time temperature-programmed reduction (TPR-2) of CeO_2 (HSA and LSA) compared to that of TPR-1.

feed stream consisting a LPG/H_2O at a molar ratio of 1.0/5.0 was introduced into the system, while the temperature increased from ambient to 900 °C. Both propane and butane were converted to methane, ethane, ethylene, and hydrogen at the temperature above 700 °C, as shown in Fig. 5. A significant amount of carbon was also detected in the blank reactor after exposure for 10 h. These components were formed via the decomposition of butane and propane as shown in the equations below.

$$C_4H_{10} \rightarrow C_2H_6 + C_2H_4 \quad (13)$$

$$C_3H_8 \rightarrow 3/2(C_2H_4) + H_2 \quad (14)$$

$$C_2H_6 \rightarrow C_2H_4 + H_2 \quad (15)$$

$$C_2H_4 \Leftrightarrow CH_4 + C \quad (16)$$

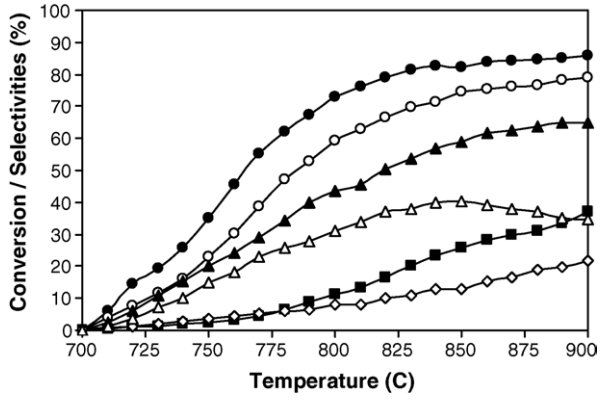

Fig. 5. Homogeneous (in the absence of a catalyst) reactivity of LPG in the presence of steam (with the inlet H_2O/LPG of 5.0) (C_4H_{10} (●), C_3H_8 (◯), C_2H_4 (▲), C_2H_6 (△), CH_4 (■), and H_2 (◇)).

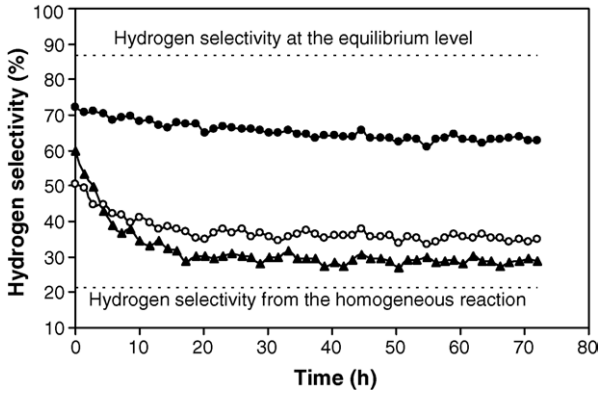

Fig. 6. Hydrogen selectivity from the steam reforming of LPG over CeO_2 (HSA) (●), CeO_2 (LSA) (◯), and Ni/Al_2O_3 (▲) at 900 °C compared to that from the homogeneous reaction and at the equilibrium level.

There was no change in the steam concentration, and no carbon monoxide and carbon dioxide were produced in the system, indicating that the non-homogenous reforming reaction between steam and hydrocarbons did not take place at this range of conditions studied.

3.3. Stability and activity toward the steam reforming of LPG

The synthesized CeO_2 (HSA), CeO_2 (LSA), and Ni/Al_2O_3 were studied in the steam reforming of C_3H_8/C_4H_{10} at 900 °C. The feed was H_2O/LPG in helium with the molar ratio of 5.0 (H_2O/C ratio of 1.45). The reforming rate was measured as a function of time in order to determine the stability and the deactivation rate. The variations in the hydrogen selectivity with time at 900 °C are shown in Fig. 6. Significant deactivation was detected with Ni/Al_2O_3 catalyst, whereas much lower deactivations were observed for CeO_2 (HSA). Catalyst stabilities expressed as deactivation percentages are given in Table 4. It should be noted that, in order to determine whether the observed deactivation is due to the carbon formation, the post-reaction temperature-programmed oxidation (TPO) experiments were carried out.

From the TPO results shown in Fig. 7, a huge amount of carbon deposition was observed on Ni/Al_2O_3, whereas significantly less carbon formation was detected on CeO_2 (LSA) and CeO_2 (HSA) after exposure to the steam reforming conditions for 72 h. The amount of carbon formation (monolayer) on the surface of catalysts was determined by measuring the CO and CO_2 yields (using Microcal Origin Software). Using a value of 0.026 nm^2 for the area occupied by a carbon atom in a surface mono-

Table 4
Physicochemical properties of catalysts after exposure in the steam reforming of LPG at 900 °C for 72 h.

Catalyst	Deactivation (%)	C formation (monolayers)	BET surface (m^2 g^{-1})	Ni-load (wt.%)	Ni-red. (Ni%)	Ni-disp. (Ni%)
CeO_2 (HSA)	12.8	0.51[a] (0.48)[b]	22.0	–	–	–
CeO_2 (LSA)	30.6	0.92 (0.92)	7.1	–	–	–
Ni/Al_2O_3	52.3	4.73 (4.71)	~40.0	4.9	92.1	4.82

[a] Calculated using CO and CO_2 yields from temperature-programmed oxidation (TPO) with 5% oxygen.
[b] Calculated from the balance of carbon in the system.

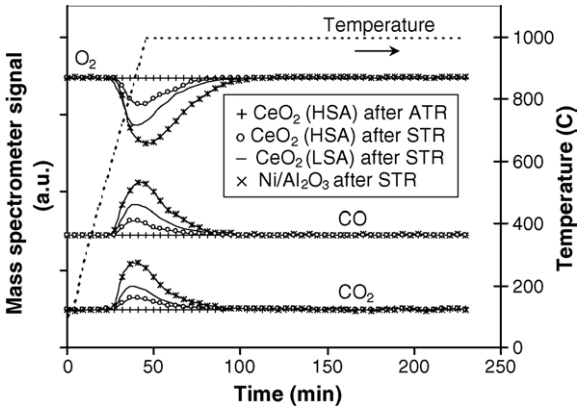

Fig. 7. Temperature-programmed oxidation (TPO) of CeO_2 (HSA), CeO_2 (LSA), and Ni/Al_2O_3 after exposure in the steam reforming (STR) and autothermal reforming (ATR) of LPG (H_2O/LPG of 5.0 for STR and O_2/LPG of 0.6 for ATR) for 72 h.

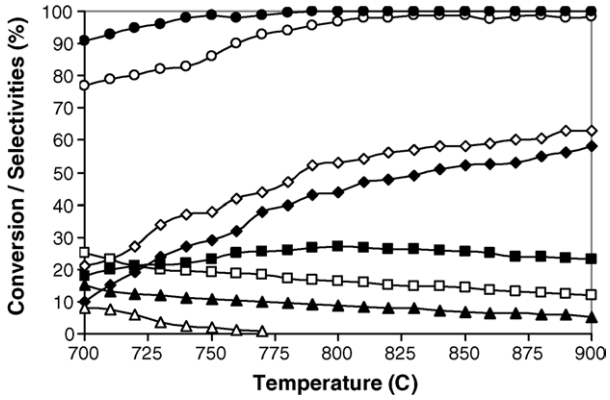

Fig. 8. Effect of reaction temperature on the conversions of C_4H_{10} (●) and C_3H_8 (○), and the selectivities of H_2 (◊), CO (♦), CO_2 (□), CH_4 (■), C_2H_6 (△), and C_2H_4 (▲) from steam reforming over CeO_2 (HSA) (with the inlet H_2O/LPG of 5.0).

layer of the basal plane in graphite [49], the quantities of carbon deposited for each catalyst were observed as in Table 4. The total amounts of carbon deposited were then verified by calculating the carbon balance of the system. Regarding the calculations, the moles of carbon deposited per gram of CeO_2 (HSA), CeO_2 (LSA), and Ni/Al_2O_3 were 0.54, 0.97, and 4.76 mmol g^{-1}. By the same assumption for the area occupied by a carbon atom [49], the values shown in Table 4 are in good agreement with the values observed from the TPO method described above. These results clearly indicate that the deactivation observed on Ni/Al_2O_3 was mainly due to carbon deposition on the surface of catalyst, and CeO_2 especially the high surface area had a significant resistance toward carbon formation as compared to Ni/Al_2O_3. BET measurements were then carried out to observe the percentage decrease in surface area of all catalysts. It should be noted that the BET measurement for Ni/Al_2O_3 was carried out after reducution of the catalyst (after TPO) with hydrogen in order to eliminate all NiO from the TRO experiment, which could affect the catalyst surface area. Results shown in Table 4 suggest that the deactivation of ceria is mainly due to the thermal sintering. However, the surface area reduction percentage of CeO_2 (HSA) is much lower than CeO_2 (LSA), indicating a higher stability toward the thermal sintering.

It should be noted that, the steady-state hydrogen selectivity observed from all catalysts (62.9% for CeO_2 (HSA), 35.0% for CeO_2 (LSA), and 28.6% for Ni/Al_2O_3) was lower than that at equilibrium state, which is approximately 87% (according to the simulation using AspenPlus 10.2), due to the incomplete decomposition of LPG to H_2, CO, and CO_2.

3.4. Effects of temperature and inlet reactants

The influences of operating temperature and the inlet steam content on the conversion of butane and propane, and the product selectivities from the steam reforming of LPG over CeO_2 (HSA) and CeO_2 (LSA) were studied by varying the operating temperature from 700 to 900 °C and changing the inlet H_2O/LPG ratio from 3.0 to 7.0 (H_2O/C ratio from 0.87 to 2.02) as represented in Figs. 8 and 9.

At 900 °C, the main products from the steam reforming reaction over CeO_2 (HSA) were CH_4, H_2 CO, and CO_2. Some formation of C_2H_4 was also observed. Hydrogen and carbon monoxide selectivities increased with increasing temperature, whereas carbon dioxide and ethylene production selectivities decreased. The dependence of methane selectivity on the operating temperature was non-monotonic, the maximum production of methane occurred at approximately 800 °C. Regarding the effect of steam, hydrogen and carbon dioxide selectivities increased with increasing inlet steam concentration, whereas carbon monoxide, methane, and ethylene selectivities decreased. These changes in product selectivities are due to the influence of the exothermic water-gas shift reaction ($CO + H_2O \rightarrow CO_2 + H_2$), whereas the decreased methane and ethylene selectivities could be due to further reforming which would generate more carbon monoxide and hydrogen. Temperature-programmed oxidations of CeO_2 (HSA) after exposure in steam reforming with different inlet H_2O/LPG ratios were then carried out to determine the effect of the inlet steam concentration on the degree of carbon formation. From the TPO results, the amount of carbon deposited slightly decreased with increasing inlet steam concentration, however, a

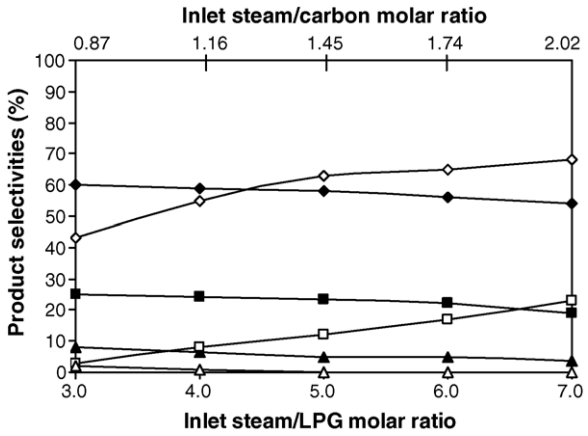

Fig. 9. Effect of inlet steam/LPG molar ratio on the selectivities of H_2 (◊), CO (♦), CO_2 (□), CH_4 (■), C_2H_6 (△), and C_2H_4 (▲) from the steam reforming of LPG over CeO_2 (HSA) at 900 °C.

Table 5
The dependence of hydrogen yield on the H_2O/LPG molar ratio and the amount of carbon formation on CeO_2 (HSA) after exposure in the steam reforming condition for 72 h

H_2O/LPG ratio	Hydrogen selectivity (%) at steady state	Total carbon formation (monolayers)
3.0	43.1	0.82[a] (0.84)[b]
4.0	55.0	0.67 (0.65)
5.0	62.9	0.51 (0.48)
6.0	65.3	0.44 (0.44)
7.0	68.0	0.41 (0.39)

[a] Calculated using CO and CO_2 yields from temperature-programmed oxidation (TPO) with 5% oxygen.
[b] Calculated from the balance of carbon in the system.

significant amount of carbon was detected even at a H_2O/LPG molar ratio of 7.0 (0.39–0.41 monolayers, Table 5).

3.5. Reactivity toward autothermal reforming

In order to reduce the degree of carbon formation and improve the product selectivities, autothermal reforming of LPG over CeO_2 (HSA) was studied by adding oxygen along with LPG and steam. The inlet H_2O/C molar ratio was kept constant at 1.45 (H_2O/LPG molar ratio of 5.0), while the inlet O/C molar ratios were varied at 0.2, 0.4, 0.6, 0.8 and 1.0. It should be noted that, while varying the ratios of H_2O/LPG and O_2/LPG, the overall space velocity was always maintained at a constant value by adjusting the flow rate of carrier gas (helium) to keep the total flow rate constant.

The effect of oxygen concentration on the product selectivities (%) at 900 °C is shown in Fig. 10. The effect of oxygen on the yields of hydrogen and carbon monoxide productions were non-monotonic. Hydrogen selectivity increased with increasing O/C molar ratio until the ratio reached 0.6. The positive effect of oxygen on the hydrogen selectivity in this range is due to the assistance of this component to reform hydrocarbons. However, higher O/C ratios showed a negative effect on the hydrogen selectivity, as too high an oxygen concentration resulted in the oxidation of the hydrogen produced from the steam reforming.

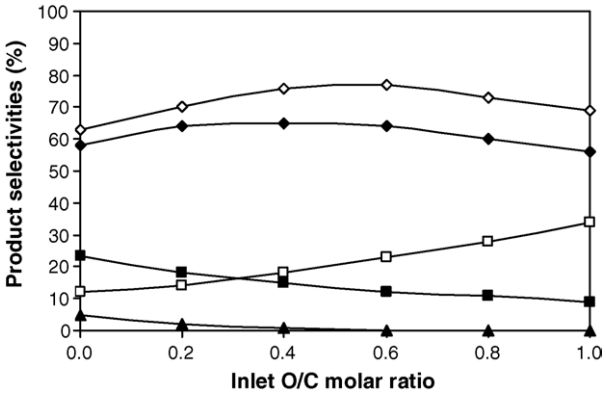

Fig. 10. Effect of inlet oxygen/carbon molar ratio on the selectivities of H_2 (◊), CO (♦), CO_2 (□), CH_4 (■), and C_2H_4 (▲) from the autothermal reforming of LPG over CeO_2 (HSA) at 900 °C.

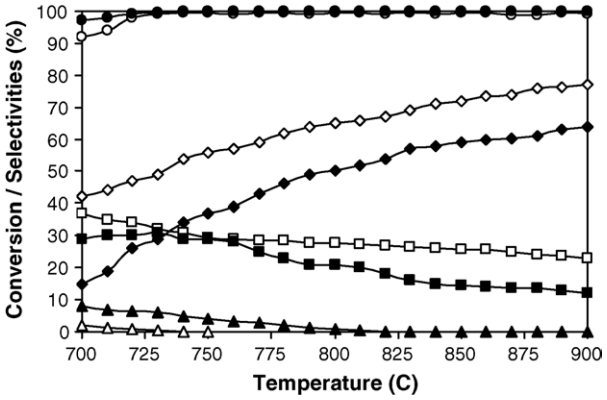

Fig. 11. Effect of reaction temperature on the conversions of C_4H_{10} (●) and C_3H_8 (●), and the selectivities of H_2 (◊), CO (♦), CO_2 (□), CH_4 (■), C_2H_6 (△), and C_2H_4 (▲) from the autothermal reforming over CeO_2 (HSA) (inlet O_2/C molar ratio of 0.6).

Table 6
The dependence of hydrogen yield on the O/C molar ratio and the amount of carbon formation on CeO_2 (HSA) after exposure in the reforming for 72 h

O/C ratio	Hydrogen selectivity (%) at steady state	Total carbon formation (monolayers)
0.0	62.9	0.51[a] (0.48)[b]
0.2	69.8	0.19 (0.21)
0.4	76.1	0.07 (0.06)
0.6	77.0	∼0.0 (∼0.0)
0.8	72.8	∼0.0 (∼0.0)
1.0	69.0	∼0.0 (∼0.0)

[a] Calculated using CO and CO_2 yields from temperature-programmed oxidation (TPO) with 5% oxygen.
[b] Calculated from the balance of carbon in the system.

Fig. 11 presents the product selectivities from the autothermal reforming of LPG (with the O/C molar ratio of 0.6) over CeO_2 (HSA) at different temperatures (700 °C to 900 °C). It was found that the main products from the autothermal reforming are similar to the steam reforming (e.g. H_2, CO, CO_2, and CH_4). Higher H_2, CO, and CO_2 selectivities were observed from autothermal reforming, whereas less CH_4, C_2H_6, and C_2H_4 were found compared to steam reforming under the same operating conditions. At 900 °C, neither C_2H_6 nor C_2H_4 formation was observed from the reaction due to the complete decomposition of these high hydrocarbons by the addition of oxygen. The benefits of the oxygen addition along with LPG and steam are presented in Section 4.

Temperature-programmed oxidation was carried out on the spent catalysts in order to determine the degree of carbon formation on the catalyst surface after exposure to the autothermal reforming reaction. From the TPO results, significantly lower quantities of deposited carbon was observed over CeO_2 (HSA) surface, and no carbon formation was detected when the inlet O/C molar ratio reached 0.6, shown in Fig. 7 and Table 6.

4. Discussion

High surface area ceria (CeO_2 (HSA)), synthesized by a surfactant-assisted approach, provided a high LPG reforming

reactivity and excellent resistance toward carbon deposition compared to conventional Ni/Al_2O_3. Carbon formation during LPG reforming could occur due to the reactions listed below:

$$C_4H_{10} \Leftrightarrow 5H_2 + 4C \quad (17)$$

$$C_3H_8 \Leftrightarrow 4H_2 + 3C \quad (18)$$

$$C_2H_4 \Leftrightarrow 2H_2 + 2C \quad (19)$$

$$CH_4 \Leftrightarrow 2H_2 + C \quad (20)$$

$$2CO \Leftrightarrow CO_2 + C \quad (21)$$

$$CO + H_2 \Leftrightarrow H_2O + C \quad (22)$$

$$CO_2 + 2H_2 \Leftrightarrow 2H_2O + C \quad (23)$$

where C is the carbonaceous deposit. At low temperature, Eqs. (22) and (23) are favorable, while Eqs. (17)–(21) are thermodynamically not favored [50]. The Boudouard reaction (Eq. (21)) and the decomposition of hydrocarbons (Eqs. (17)–(20) are the major pathways for carbon formation at such a high temperature as they show the largest change in Gibbs free energy [51]. Because of the high temperature employed in this study (700–900 °C), carbon formation via the decomposition of hydrocarbons and Boudouard reactions is possible. With the increase in steam to carbon ratio, the equilibrium of the water-gas shift reaction moves forward and produces more CO_2 rather than CO. Therefore, a high steam feed can avoid carbon deposition via the Boudouard reaction. However, a significant amount of carbon still forms due to the decomposition of hydrocarbons.

The high resistance toward carbon deposition on CeO_2, especially on high surface area CeO_2, is mainly due to the high oxygen storage capacity (OSC) of this material. CeO_2 contains a high concentration of highly mobile oxygen vacancies and thus acts as a local source or sink for oxygen on its surface. It has been reported that at high temperature, the lattice oxygen (O_O^x) at the CeO_2 surface can oxidize gaseous hydrocarbons (e.g. methane [42,48,49]). By using CeO_2 (HSA) as the catalyst, the carbon deposition due to the decomposition of hydrocarbons could be inhibited by the gas–solid reactions between the hydrocarbons present in the system (C_4H_{10}, C_3H_8, C_2H_6, C_2H_4, CH_4) and the lattice-oxygen (O_O^x) at the CeO_2 surface (Eq. (24)) forming CO_2 and H_2 from which the formation of carbon is thermodynamically unfavorable at high temperature.

$$C_nH_m + O_O^x \Leftrightarrow nCO + m/2H_2 + V_O^{\bullet\bullet} + 2e' \quad (24)$$

After the reactions, the lattice oxygen (O_O^x) is regenerated by reaction with oxygen containing compounds (e.g. steam) present in the system.

$$H_2O + V_O^{\bullet\bullet} + 2e' \Leftrightarrow O_O^x + H_2 \quad (25)$$

The redox mechanism between the hydrocarbons present in the system and the lattice oxygen (O_O^x) are illustrated below.

$$C_4H_{10} + 4S_{Ce} \Leftrightarrow 2(CH_3{-}S_{Ce}) + 2(CH_2{-}S_{Ce}) \quad (26)$$

$$C_3H_8 + 3S_{Ce} \Leftrightarrow 2(CH_3{-}S_{Ce}) + CH_2{-}S_{Ce} \quad (27)$$

$$C_2H_6 + 2S_{Ce} \Leftrightarrow 2(CH_3{-}S_{Ce}) \quad (28)$$

$$C_2H_4 + 2S_{Ce} \Leftrightarrow 2(CH_2{-}S_{Ce}) \quad (29)$$

$$CH_4 + 2S_{Ce} \Leftrightarrow CH_3{-}S_{Ce} + H{-}S_{Ce} \quad (30)$$

$$CH_3{-}S_{Ce} + S_{Ce} \Leftrightarrow CH_2{-}S_{Ce} + H{-}S_{Ce} \quad (31)$$

$$CH_2{-}S_{Ce} + S_{Ce} \Leftrightarrow CH{-}S_{Ce} + H{-}S_{Ce} \quad (32)$$

$$CH{-}S_{Ce} + S_{Ce} \Leftrightarrow C{-}S_{Ce} + H{-}S_{Ce} \quad (33)$$

$$C{-}S_{Ce} + O_O^x \Leftrightarrow CO + V_O^{\bullet\bullet} + 2e' + S_{Ce} \quad (34)$$

$$2H{-}S_{Ce} \Leftrightarrow H_2 + 2S_{Ce} \quad (35)$$

where S_{Ce} is the CeO_2 surface site and $CH_x{-}S_{Ce}$ is an intermediate surface hydrocarbon species. S_{Ce} can be considered to be a unique site, or the same site as the lattice oxygen (O_O^x). Steele and Floyd [52] reported that the measured value of the oxygen diffusion coefficient for ceria is high and the reaction rate is controlled by a surface reaction rather than by diffusion of oxygen from the bulk of the solid particles to ceria surfaces [52]. During the reaction, hydrocarbons are adsorbed on either a unique site (S_{Ce}) or the lattice oxygen (O_O^x).

Although conventional CeO_2 (CeO_2 (LSA)) has also been reported to provide a high resistance toward carbon formation, the major drawbacks of CeO_2 (LSA) are the low specific surface area and large size reduction due to the thermal sintering, resulting in a significant drop in the redox properties compared to CeO_2 (HSA), as presented in Section 3.1, and consequently low steam reforming reactivity. The corresponding post-reaction specific surface area for CeO_2 (LSA) after exposure in reforming conditions was 7.1 $m^2\,g^{-1}$, and the observed size reduction percentage was 17%, whereas the post-reaction specific surface area for CeO_2 (HSA) was 22 $m^2\,g^{-1}$, and the observed size reduction percentage was 9%. The low redox properties of CeO_2 (LSA) also resulted in a significantly lower resistance toward carbon deposition of this material compared to CeO_2 (HSA). As described earlier, the redox reaction (Eq. (25)) between the lattice oxygen (O_O^x) at the CeO_2 surface and the hydrocarbons present in the system (C_4H_{10}, C_3H_8, C_2H_6, C_2H_4, CH_4) can prevent the formation of carbon by the decomposition of these hydrocarbon components.

It was observed from the study that the addition of oxygen along with LPG and steam in the autothermal reforming reaction reduced the degree of carbon deposition and improved the product selectivities by eliminating the formation of C_2H_6 and C_2H_4. Theoretically, oxygen prevents the formation of high hydrocarbons (i.e. C_2H_6 and C_2H_4) and subsequent carbon deposition from the decomposition reactions (Eqs. (16)–(18)) by oxidizing these hydrocarbons producing the elements that are unfavored to form carbon. The presence of oxygen also helps steam regenerate the lattice oxygen (O_O^x) on the CeO_2 surface ($O_2 + V_O^{\bullet\bullet} + 2e' + S_{Ce} \rightarrow O_O^x$). The major consideration of the autothermal reforming operation is a suitable O_2/LPG ratio. The presence of too high an oxygen concentration could oxidize the hydrogen and carbon monoxide produced from the steam reforming to steam and carbon dioxide.

5. Conclusion

High surface area ceria (CeO_2 (HSA)), synthesized in a surfactant-assisted approach, is a good catalyst for the reforming of LPG (butane and propane) at SOFC temperatures (700–900 °C) due to a high resistance towards the deactivation from carbon formation. During the reforming process, the gas–solid reactions between the hydrocarbons present in the system (i.e. propane, butane, ethane, ethylene, and methane) and the lattice oxygen (O_O^x) take place on the ceria surface, reducing the degree of carbon deposition on the catalyst surface (from hydrocarbons decomposition and Boudouard reactions). At 700–900 °C, the main products from the steam reforming of LPG over CeO_2 (HSA) were H_2, CO, CO_2, and CH_4, whereas a small amount of C_2H_4 was also observed, particularly at low temperatures. By increasing the inlet steam content, hydrogen and carbon dioxide selectivities increased, whereas carbon monoxide selectivity decreased. Moreover, the conversions of methane and ethylene were found to increase with increasing steam content in the system.

The addition of oxygen in autothermal reforming can reduce the degree of carbon deposition and eliminate the formation of higher hydrocarbons (i.e. C_2H_6 and C_2H_4). The major consideration in the autothermal reforming operation is the inlet O_2/LPG molar ratio, as the presence of too high an oxygen concentration could oxidize hydrogen and carbon monoxide, produced from the steam reforming, to steam and carbon dioxide. A suitable O/C molar ratio for autothermal reforming on CeO_2 (HSA) was observed to be 0.6.

Acknowledgement

Financial support from The Thailand Research Fund (TRF) throughout this project is gratefully acknowledged.

References

[1] P. Aguiar, D. Chadwick, L. Kershenbaum, Chem. Eng. Sci. 57 (2002) 1665.
[2] K. Ahmed, J. Gamman, K. Föger, Solid State Ion. 152–153 (2002) 485–492.
[3] T. Suzuki, H.-i. Iwanami, O. Iwamoto, T. Kitahara, Int. J. Hydrogen Energy 26 (9) (2001) 935–940.
[4] A.K. Avci, D.L. Trimm, A.E. Aksoylu, Z.I. Önsan, Catal. Lett. 88 (2003) 17–22.
[5] A.F. Ghenciu, Curr. Opin. Solid State Mater. Sci. 6 (2002) 389–399.
[6] T. Rampe, A. Heinzel, B. Vogel, J. Power Sources 86 (2000) 536–541.
[7] F. Joensen, J.R. Rostrup-Nielsen, J. Power Sources 105 (2002) 195–201.
[8] V. Recupero, L. Pino, A. Vita, F. Cipiti, M. Cordaro, M. Laganà, Int. J. Hydrogen Energy 30 (9) (2005) 963–971.
[9] L.V. Mattos, E. Rodino, D.E. Resasco, F.B. Possos, F.B. Noronha, Fuel Proc. Technol. 83 (2003) 147.
[10] H.S. Roh, K.W. Jun, S.E. Park, Appl. Catal. A 251 (2003) 275.
[11] J.R. Rostrup-Nielsen, J.-H. Bak-Hansen, J. Catal. 144 (1993) 38.
[12] P. Fornasiero, G. Balducci, R.D. Monte, J. Kaspar, V. Sergo, G. Gubitosa, A. Ferrero, M. Graziani, J. Catal. 164 (1996) 173.
[13] T. Miki, T. Ogawa, M. Haneda, N. Kakuta, A. Ueno, S. Tateishi, S. Matsuura, M. Sato, J. Phys. Chem. 94 (1990) 339.
[14] C. Padeste, N.W. Cant, D.L. Trimm, Catal. Lett. 18 (1993) 305.
[15] S. Kacimi, J. Barbier Jr., R. Taha, D. Duperz, Catal. Lett. 22 (1993) 343.
[16] G.S. Zafiris, R.J. Gorte, J. Catal. 143 (1993) 86.
[17] G.S. Zafiris, R.J. Gorte, J. Catal. 139 (1993) 561.
[18] S. Imamura, M. Shono, N. Okamoto, R. Hamada, S. Ishida, Appl. Catal. A 142 (1996) 279.
[19] L. Fan, K. Fujimoto, J. Catal. 172 (1997) 238.
[20] M. Pijolat, M. Prin, M. Soustelle, J. Chem. Soc., Faraday Trans. 91 (1995) 3941.
[21] S. Imamura, T. Higashihara, Y. Saito, H. Aritani, H. Kanai, Y. Matsumura, N. Tsuda, Catal. Today 50 (1999) 369.
[22] S. Imamura, K. Denpo, K. Utani, Y. Matsumura, H. Kanai, React. Kinet. Catal. Lett. 67 (1999) 163.
[23] S. Imamura, K. Denpo, K. Kanai, H. Yamane, Y. Saito, K. Utani, Y. Matsumura, Sekiyu Gakkaishi 44 (2001) 293.
[24] S. Imamura, H. Yamane, H. Kanai, T. Shibuta, K. Utani, K. Hamada, J. Jpn. Petrol. Inst. 45 (2002) 187.
[25] S. Imamura, Y. Taniguchi, Y. Ikeda, S. Hosokawa, H. Kanai, H. Ando, React. Kinet. Catal. Lett. 76 (2002) 201.
[26] H.S. Roh, K.W. Jun, W.S. Dong, J.S. Chang, S.E. Park, Y.I. Joe, J. Mol. Catal. A 181 (2002) 137–142.
[27] Q. Miao, G. Xiong, S. Sheng, W. Cui, L. Xu, X. Guo, Appl. Catal. A 154 (1987) 17–27.
[28] A.A. Lemonidou, M.A. Goula, I.A. Vasalos, Catal. Today 46 (1987) 175–183.
[29] W.S. Dong, H.S. Roh, K.W. Jun, S.E. Park, Y.S. Oh, Appl. Catal. A 226 (2002) 63–72.
[30] M. Mamak, N. Coombs, G. Ozin, Adv. Mater. 12 (2000) 198–202.
[31] M. Mamak, N. Coombs, G. Ozin, J. Am. Chem. Soc. 122 (2000) 8932.
[32] M. Mamak, N. Coombs, G.A. Ozin, Chem. Mater. 13 (2001) 3564.
[33] P. Bera, S. Mitra, S. Sampath, M.S. Hegde, Chem. Commun. (2001) 927.
[34] A. Martinez-Arias, J.M. Coronado, R. Cataluna, J.C. Conesa, J.C. Soria, J. Phys. Chem. B 102 (1998) 4357.
[35] D. Skarmoutsos, F. Tietz, P. Nikolopoulos, Fuel Cells 1 (2001) 243.
[36] T. Takeguchi, S.N. Furukawa, M. Inoue, J. Catal. 202 (2001) 14.
[37] J. Sfeir, P.A. Philippe, P. Moseki, N. Xanthopoulos, R. Vasquez, J.M. Hans, V.H. Jan, K.R. Thampi, J. Catal. 202 (2001) 229.
[38] N. Kiratzis, P. Holtappels, C.E. Hatchwell, M. Mogensen, J.T.S. Irvine, Fuel Cells 1 (2001) 211.
[39] H.S. Roh, W.S. Dong, K.W. Jun, S.E. Park, Chem. Lett. (2001) 88.
[40] E. Ramírez-Cabrera, A. Atkinson, D. Chadwick, Appl. Catal. B 47 (2004) 127–131.
[41] E. Ramírez-Cabrera, N. Laosiripojana, A. Atkinson, D. Chadwick, Catal. Today 78 (2003) 433–438.
[42] N. Laosiripojana, Reaction engineering of indirect internal steam reforming of methane for application in solid oxide fuel cells. Ph.D. Thesis, University of London, England, 2003.
[43] K. Otsuka, T. Ushiyama, I. Yamanaka, Chem. Lett. (1993) 1517.
[44] K. Otsuka, M. Hatano, A. Morikawa, J. Catal. 79 (1983) 493.
[45] K. Otsuka, M. Hatano, A. Morikawa, Inorg. Chim. Acta 109 (1985) 193.
[46] P.J. Gellings, J.M. Henny, Bouwmeester, Solid state aspects of oxidation catalysis, Catal. Today 58 (2000) 1–53.
[47] D. Terribile, A. Trovarelli, J. Llorca, C. de Leitenburg, G. Dolcetti, Catal. Today 43 (1998) 79–88.
[48] N. Laosiripojana, S. Assabumrungrat, Appl. Catal. B: Environ. 60 (2005) 107.
[49] E. Ramirez, A. Atkinson, D. Chadwick, Appl. Catal. B 36 (2002) 193–206.
[50] Y. Lwin, W.R.W. Daud, A.B. Mohamad, Z. Yaakob, Int. J. Hydrogen Energy 25 (1) (2000) 47–53.
[51] J.N. Amor, Appl. Catal. A 176 (1999) 159–176.
[52] B.C.H. Steele, J.M. Floyd, Proc. Br. Ceram. Soc. 19 (1971) 55.